Nuclear Science
2011

OECD

Technology and Components of Accelerator-driven Systems

Workshop Proceedings
Karlsruhe, Germany
15–17 March 2010

NEA

NUCLEAR ENERGY AGENCY

Nuclear Science ISBN 978-92-64-11727-3

Technology and Components of Accelerator-driven Systems

Workshop Proceedings

Karlsruhe, Germany
15-17 March 2010

© OECD 2011
NEA No. 6897

NUCLEAR ENERGY AGENCY
Organisation for Economic Co-operation and Development

ORGANISATION FOR ECONOMIC CO-OPERATION AND DEVELOPMENT

The OECD is a unique forum where the governments of 34 democracies work together to address the economic, social and environmental challenges of globalisation. The OECD is also at the forefront of efforts to understand and to help governments respond to new developments and concerns, such as corporate governance, the information economy and the challenges of an ageing population. The Organisation provides a setting where governments can compare policy experiences, seek answers to common problems, identify good practice and work to co-ordinate domestic and international policies.

The OECD member countries are: Australia, Austria, Belgium, Canada, Chile, the Czech Republic, Denmark, Estonia, Finland, France, Germany, Greece, Hungary, Iceland, Ireland, Israel, Italy, Japan, Luxembourg, Mexico, the Netherlands, New Zealand, Norway, Poland, Portugal, the Republic of Korea, the Slovak Republic, Slovenia, Spain, Sweden, Switzerland, Turkey, the United Kingdom and the United States. The European Commission takes part in the work of the OECD.

OECD Publishing disseminates widely the results of the Organisation's statistics gathering and research on economic, social and environmental issues, as well as the conventions, guidelines and standards agreed by its members.

This work is published on the responsibility of the OECD Secretary-General.
The opinions expressed and arguments employed herein do not necessarily reflect the official views of the Organisation or of the governments of its member countries.

NUCLEAR ENERGY AGENCY

The OECD Nuclear Energy Agency (NEA) was established on 1 February 1958. Current NEA membership consists of 30 OECD member countries: Australia, Austria, Belgium, Canada, the Czech Republic, Denmark, Finland, France, Germany, Greece, Hungary, Iceland, Ireland, Italy, Japan, Luxembourg, Mexico, the Netherlands, Norway, Poland, Portugal, the Republic of Korea, the Slovak Republic, Slovenia, Spain, Sweden, Switzerland, Turkey, the United Kingdom and the United States. The European Commission also takes part in the work of the Agency.

The mission of the NEA is:

- to assist its member countries in maintaining and further developing, through international co-operation, the scientific, technological and legal bases required for a safe, environmentally friendly and economical use of nuclear energy for peaceful purposes, as well as
- to provide authoritative assessments and to forge common understandings on key issues, as input to government decisions on nuclear energy policy and to broader OECD policy analyses in areas such as energy and sustainable development.

Specific areas of competence of the NEA include the safety and regulation of nuclear activities, radioactive waste management, radiological protection, nuclear science, economic and technical analyses of the nuclear fuel cycle, nuclear law and liability, and public information.

The NEA Data Bank provides nuclear data and computer program services for participating countries. In these and related tasks, the NEA works in close collaboration with the International Atomic Energy Agency in Vienna, with which it has a Co-operation Agreement, as well as with other international organisations in the nuclear field.

Corrigenda to OECD publications may be found online at: *www.oecd.org/publishing/corrigenda*.
© OECD 2011

You can copy, download or print OECD content for your own use, and you can include excerpts from OECD publications, databases and multimedia products in your own documents, presentations, blogs, websites and teaching materials, provided that suitable acknowledgment of the OECD as source and copyright owner is given. All requests for public or commercial use and translation rights should be submitted to *rights@oecd.org*. Requests for permission to photocopy portions of this material for public or commercial use shall be addressed directly to the Copyright Clearance Center (CCC) at *info@copyright.com* or the Centre français d'exploitation du droit de copie (CFC) *contact@cfcopies.com*.

Foreword

The accelerator-driven system (ADS) is a potential transmutation system option as part of partitioning and transmutation strategies for radioactive waste in advanced nuclear fuel cycles. Following the success of the workshop series on the utilisation and reliability of high power proton accelerators (HPPA), the scope of this new workshop series has been extended to cover subcritical systems as well as the use of neutron sources.

The first workshop was organised on 15-17 March 2010 in Karlsruhe, Germany, and was hosted by the Karlsruhe Institute of Technology (KIT). It provided experts with a forum to present and discuss state-of-the-art developments in the field of ADS and neutron sources. A total of 62 papers was presented during the oral and poster sessions. Following presentations on the programmes of Belgium, Japan and the European Commission and a special session on EUROTRANS, four technical sessions were organised addressing current ADS experiments and test facilities, accelerators, neutron sources and subcritical systems.

These proceedings include all the papers presented at the workshop. The opinions expressed are those of the authors only, and do not necessarily reflect the views of the NEA, any national authority or any other international organisation.

Acknowledgements

The OECD Nuclear Energy Agency (NEA) gratefully acknowledges the Karlsruhe Institute of Technology (KIT) for hosting the first Workshop on Technology and Components of Accelerator-driven Systems.

Table of Contents

Foreword 3

Executive Summary 11

Opening and National ADS Programmes 17

Chair: C. Fazio

J.U. Knebel
KIT welcome address 19

Th.W. Tromm
NEA Nuclear Science Committee welcome address 21

P. Fritz
The Karlsruhe Institute of Technology: A unique institution in German research 23

K. Tsujimoto, H. Oigawa
Outline of check and review on partitioning and transmutation by Atomic Energy Commission of Japan and recommendation for R&D on ADS 25

H. Aït Abderrahim, P. Baeten, D. De Bruyn
The MYRRHA ADS programme in Belgium: A multi-national demonstration programme for incineration of spent nuclear fuel wastes 33

J.U. Knebel
The EUROTRANS Project: Partitioning and transmutation research in Europe* 43

Special Session: EUROTRANS 45

Chair: A.C. Müller

D. De Bruyn, H. Aït Abderrahim, G. Rimpault, L. Mansani, M. Reale, A.C. Müller, A. Guertin, J-L. Biarrotte, J. Wallenius, C. Angulo, A. Orden, A. Rolfe, D. Struwe, M. Schikorr, A. Woaye-Hune, C. Artioli
Achievements and lessons learnt within the Domain 1 "DESIGN" of the Integrated Project EUROTRANS 47

G. Granget, H. Aït Abderrahim, P. Baeten, C. Berglöf, A. Billebaud, E. González-Romero, F. Mellier, R. Rosa, M. Schikorr
EUROTRANS/ECATS or neutronic experiments for the validation of XT-ADS and EFIT monitoring 53

* The full paper being unavailable at the time of publication, only the abstract is included.

F. Delage, R. Belin, X-N. Chen, E. D'Agata, F. Klaassen, W. Maschek, J-P. Ottaviani, S. Pillon, A. Rineiski, V. Sobolev, J. Somers, D. Staicu, R. Thetford, J. Wallenius, B. Wernli
Minor actinide transmutation in the accelerator-driven system EFIT: Results from fuel developments in Domain AFTRA 69

C. Fazio, J. Van den Bosch, F. Javier Martin Muñoz, J. Henry, F. Roelofs, P. Turroni, L. Mansani, A. Weisenburger, D. Gorse, J. Abella, L. Brissonneau, Y. Dai, L. Magielsen, J. Neuhausen, P. Vladimirov, A. Class, H. Jeanmart, A. Ciampichetti, G. Gerbeth, T. Wetzel, A. Karbojian, K. Litfin, M. Tarantino, L. Zanini
Development and assessment of structural materials and heavy liquid metal technologies for transmutation systems (DEMETRA): Highlights on major results 81

E. González-Romero, A. Koning, S. Leray, A. Plompen, J. Sanz (on behalf of NUDATRA/IP-EUROTRANS)
NUDATRA/EUROTRANS nuclear data for nuclear waste transmutation* 107

Special Lecture 109

C. Rubbia
Subcritical thorium reactors* 111

Session I: Current ADS Experiments and Test Facilities 113

Chairs: Th. Wetzel, S. Monti

C-H. Pyeon, J-Y. Lim, T. Misawa, S. Shiroya
Experiments on injection of spallation neutrons by 100 MeV protons in the Kyoto University Critical Assembly 115

M. Fernández-Ordóñez, V. Bécares, C. Berglöf, D. Villamarín, M. Becker, V. Bournos, Y. Fokov, P. Gajda, V. Glivici, E.M. González-Romero, J. Janczyszyn, S. Mazanik, B. Merk, J.L. Muñoz-Cobo, W. Pohorecki
Experimental validation of the industrial ADS reactivity monitoring using the YALINA-Booster subcritical assembly 123

M. Tarantino, G. Benamati, P. Gaggini, V. Labanti
Integral Circulation Experiment: Thermal-hydraulic simulator of the ETD primary system 135

L. Mercatali, P. Baeten, A. Kochetkov, W. Uyttenhove, G. Vittiglio
The GUINEVERE experiments at the VENUS facility: Status and perspectives 149

Th. Wetzel, K. Litfin, R. Stieglitz, A.G. Class, M. Daubner, F. Fellmoser, A. Batta
Experimental investigation of turbulent flow distribution in a hexagonal rod bundle for ADS prototype application 159

F. Beauchamp, O. Morier, L. Brissonneau, J-L. Courouau, C. Chabert, F. Reyne
A review of lead-bismuth alloy purification systems with regard to the latest results achieved on STELLA loop 171

J-B. Vogt, I. Proriol-Serre, L. Martinelli, K. Ginestar
Reliability in liquid lead-bismuth of the 316L and T91 steels: Coupling effects between corrosion and fatigue 183

A. Weisenburger, M. del Giacco, A. Jianu, G. Müller
Compatibility of different steels and alloys with lead up to 750°C* 193

* The full paper being unavailable at the time of publication, only the abstract is included.

Session II: Accelerators 195

Chair: H. Klein

J-L. Biarrotte, A.C. Müller (on behalf of the EUROTRANS WP1.3 collaboration)
Accelerator reference design for the European ADS demonstrator 197

H. Podlech, M. Busch, F. Dziuba, U. Ratzinger, H. Klein, R. Tiede, C. Zhang
The 17 MeV injector for the EUROTRANS proton driver 209

F. Bouly, S. Bousson, J-L. Biarrotte, P. Blache, F. Chatelet, C. Commeaux, P. Duthil, C. Joly, J. Lesrel, G. Olry, E. Rampnoux, H. Saugnac, S. Barbanotti, A. Bosotti, R. Paparella, P. Pierini
Developments of 350 MHz and 700 MHz prototypical cryomodules for the EUROTRANS ADS proton linear accelerator 217

H. Takei, K. Nishihara, K. Tsujimoto, H. Oigawa
Estimation of acceptable beam trip frequencies of accelerators for ADS and comparison with performances of existing accelerators 231

S-H. Kim, J. Galambos
High-power operational experience at the Spallation Neutron Source (SNS) 243

M. Seidel, J. Grillenberger, A. Mezger
Experience with the production of a 1.3 MW proton beam in a cyclotron-based facility 251

Session III: Neutron Sources 261

Chair: M. Seidel

Ch. Latgé, M. Wolmuther, P. Agostini, M. Dierckx, C. Fazio, A. Guertin, Y. Kurata, G. Laffont, T. Song, K. Thomsen, W. Wagner, F. Groeschel, L. Zanini, Y. Dai, J. Henri, J. Konys, K. Woloshun
MEGAPIE spallation target: Irradiation of the first prototypical spallation target for future ADS 263

W. Wagner, H. Heyck, D. Kiselev, K. Thomsen, M. Wohlmuther, L. Zanini
PSI experience with high-power target design and operation 275

R.Ž. Milenković, K. Samec, S. Dementjevs, A. Kalt, C. Kharoua, E. Platacis, A. Zik, A. Flerov, L. Blumenfeld, F. Barbagallo, K. Thomsen, E. Manfrin, Y. Kadi
EURISOL compact liquid metal converter target: Representative prototype design and tests 283

O. Meusel, L.P. Chau, M. Heilmann, H. Klein, H. Podlech, U. Ratzinger, K. Volk, C. Wiesner
The Frankfurt Neutron Source – FRANZ 297

Session IV: Subcritical Systems 305

Chairs: K. Tsujimoto, E.M. González-Romero, J.U. Knebel

F. Mulhauser, P. Adelfang, R.M. Capote Noy, V. Inozemtsev, G. Mank, D. Ridikas, A. Stanculescu, A. Zeman
ADS-related activities at IAEA: From accelerators, neutron sources to fuel cycle and databases 307

L. Mansani, M. Reale, C. Artioli, D. De Bruyn
The designs of an experimental ADS facility (XT-ADS) and of a European Industrial Transmutation Demonstrator (EFIT) 321

A. Guertin, N. Thiollière, A. Cadiou, J.M. Buhour, O. Batrak, M. Dierckx, J. Heyse, K. Rosseel, P. Schuurmans, K. Van Tichelen, R. Stieglitz, A. Batta, A. Class, F. Roelofs, V.R. Gopala, H. Jeanmart, V. Moreau
XT-ADS windowless spallation target design and corresponding R&D topics 335

T. Sugawara, K. Nishihara, K. Tsujimoto, Y. Kurata, H. Oigawa
Investigation of safety for accelerator-driven system 347

V. Sobolev, W. Uyttenhove, W. Maschek, A. Rineiski, X-N. Chen, J. Wallenius, A. Fokau, F. Delage
Optimisation of the EFIT fuel design 359

X-N. Chen, W. Maschek, P. Liu, A. Rineiski, S. Wang, C. Matzerath Boccaccini, V. Sobolev, G. Rimpault
Design and safety studies of an EFIT core with cermet fuel 375

F. Agosti, P. Botazzoli, V. Di Marcello, L. Luzzi, G. Pastore
Fuel rod performance analysis for the Italian LBE-XADS: A comparison of two different cladding materials 385

D.J. Coates, G.T. Parks
Isotope equilibrium in fast thorium reactors 397

R.L. Sheffield, E.J. Pitcher
Subcritical minor actinide reduction through transmutation – SMART 407

A. Fokau, Y. Zhang, J. Wallenius, S. Ishida
A source-efficient ADS for minor actinide burning 417

Annex 1: Scientific Advisory Committee 427

Annex 2: List of participants 429

Posters

Poster session contributions can be consulted on the Nuclear Energy Agency website on the page dedicated to the TCADS workshop: www.oecd-nea.org/science/wpfc/tcads/1st/index.html.

Session I: Current ADS Experiments and Test Facilities

G. Bianchini, M. Carta, M. Frisoni, V. Peluso, F. Pisacane
GUINEVERE project pre-analysis by the French ERANOS code

R. Fernandez, Ph. Benoit
ASTIR: The development of irradiation experiments for ADS steel T91

Å. Strinning (on behalf of the MEGAPIE collaboration)
Dismantling and conditioning of the MEGAPIE target*

H. Yoshida, T. Misawa, K. Takase, T. Suzuki
Current status of development of thermal-hydraulic design method for accelerator-driven system in JAEA

L. Zanini, V. Boutellier, R. Brütsch, J. Eikenberg. D. Gavillet, H.P. Linder, M. Martin, J. Neuhausen, M. Rüthi, D. Schumann, J. Krbanjevic, A. Grimberg, I. Leya, E. Noah, T. Stora
Post-irradiation analysis of a Pb/Bi-filled Ta target irradiated at ISOLDE

* The full paper being unavailable at the time of publication, only the abstract is included.

Session II: Accelerators

R. Brucker
Integrated reliability analysis of the EUROTRANS accelerator*

S. Gordeev, R. Stieglitz, L. Stoppel, M. Daubner, F. Fellmoser
Validation of turbulence models for high-speed liquid metal target applications

P. McIntyre, A. Sattarov
Accelerator-driven thorium cycle fission using a flux-coupled isochronous cyclotron stack*

S.J. Steer, M-A. Cardin, W.J. Nuttall, G.T. Parks, L.V.N. Gonçalves
Assessing the economic value of constructing multiple accelerators for an accelerator-driven subcritical reactor

Session III: Neutron Sources

A.G. Class, A. Batta
XT-ADS windowless target: High resolution interface capturing simulations

R. Moormann, M. Medarde, E. Platacis, K. Thomsen
Lead-gold eutectics (LGE) as target material for ESS

J. Neuhausen, S. Heinitz, D. Schumann
Nuclear reaction product behaviour in liquid eutectic lead-bismuth alloy

J. Sved
High output line source gas-plasma target sealed tube neutron generator

Session IV: Subcritical Systems

F. Álvarez-Velarde, E.M. González-Romero
TR_EVOL, upgrading of EVOLCODE2 for transition scenario studies

J-L. Courouau, C. Chabert, L. Pignoly, L. Gicquel, K. Ginestar, L. Brissonneau
Demonstration of the effect of impurities on the long-term behaviour of electrochemical oxygen sensor during the STELLA 2006 tests

D. D'Andrea, X-N. Chen, C. Matzerath Boccaccini, W. Maschek, A. Rineiski
XT-ADS safety analysis with SIMMER-III

G.L. Khorasanov; A.I. Blokhin
Macroscopic cross-sections of neutron radiation capture by ^{nat}Pb, ^{208}Pb, ^{238}U and ^{99}Tc in neutron spectra of subcritical core cooled with natural and enriched lead

K. Nishihara
Effect of the minor actinide composition on the inert matrix fuel for the accelerator-driven system

H. Obayashi, M. Tezuka, K. Kikuchi
Flow measurement of LBE by using ultrasonic Doppler profiling

D. Pellini, W. Maschek, N. Forgione, F. Oriolo, A. Ciampichetti
Energy evaluation of the LBE-water interaction experiments in LIFUS 5

M. Polidori, G. Bandini, P. Meloni
Analysis of protected and unprotected transients in the EFIT reactor with RELAP5 and RELAP5/PARCS codes

* The full paper being unavailable at the time of publication, only the abstract is included.

S. Saito, D. Hamaguchi, K. Usami, S. Endo, K. Ono, H. Matsui, K. Kikuchi, M. Kawai, Y. Dai
Mechanical properties of austenitic stainless steels irradiated at SINQ Target 4

G. Van den Eynde, V. Sobolev, P. Baeten, D. De Bruyn, H. Aït Abderrahim, K. Nishihara
Core reshuffling scenarios and fuel behaviour in MYRRHA/XT-ADS

L.V.N. Gonçalves, A. Ahmad, G.T. Parks, W.J. Nuttall, S.J. Steer
A comparison of ADSR concepts for power generation

M. Yurechko, J. Konys
Creep-rupture behaviour of austenitic and martensitic steels containing 10-18 mass.%-Cr in air

Executive Summary

The main topics of the workshop covered: R&D status on ADS including accelerators, neutron sources and subcritical systems for current facilities and future experimental and power systems; technology, engineering and research aspects of the above components; system optimisation for reducing capital and operational costs; and the role of ADS in advanced fuel cycles.

The scope of the workshop covered:

- Specific aspects of ADS accelerators:
  - continuous mode and operational control;
  - reliabilities and fail safety;
  - high beam power and low losses;
  - safety systems.
- Neutron sources:
  - current and future intense neutron sources;
  - spallation and non-spallation targets;
  - design concepts and required technologies (e.g. coolant, materials, performance, instrumentation, etc.);
  - operational characteristics and related technical issues (e.g. window/windowless, solid/liquid, interface between accelerator and target, etc.).
- Subcritical systems:
  - design concepts and performance parameters (e.g. transmutation, energy production, etc.);
  - ADS fuel/target design options;
  - subcritical reactor physics (e.g. reactivity monitoring, etc.);
  - materials, coolant technology and thermal-hydraulics;
  - unique ADS auxiliary systems (e.g. target replacement, refuelling machine, etc.);
  - related safety issues.
- Current ADS experiments and test facilities:
  - low power coupling experiments;
  - zero power physics simulators.

A total of 109 participants from 17 countries and 3 international organisations participated. The number of participants by country was: Belgium (6), Bulgaria (1), Canada (1), Czech Republic (1), France (15), Germany (38), Greece (1), Italy (10), Japan (8), Portugal (1), the Russian Federation (1), Spain (2), Sweden (4), Switzerland (6), Turkey (1), the United Kingdom (6), the United States (3), CERN (2), NEA (1) and IAEA (1). The list of participants is provided in Annex 2.

The total number of presentations amounted to 64 (38 oral presentation and 26 posters). The number of presentations by session was:

- Opening session – KIT introduction, Japan, Belgium and EUROTRANS activities: four presentations;
- Special session – EUROTRANS: five presentations;
- Session I – Current ADS experiments and test facilities: eight presentations, five posters;
- Session II – Accelerators: six presentations, four posters;
- Session III – Neutron sources: four presentations, four posters;
- Session IV – Subcritical systems: ten presentations, thirteen posters.

Opening session

Chair: C. Fazio (KIT, Germany)

The workshop was opened by the welcome addresses from J.U. Knebel (KIT, Germany), the Chair of the workshop, and W. Tromm (KIT, Germany), the German member of the NEA Nuclear Science Committee.

P. Fritz (KIT, Germany) introduced the KIT and its role in education, research and innovation in the various sciences and technologies. K. Tsujimoto (JAEA, Japan) summarised a recent review on partitioning and transmutation by the atomic energy commission of Japan and provided R&D recommendations for ADS. The historical background for R&D of P&T, a review of the current state of the art and future R&D plans in JAEA were presented.

H. Aït Abderrahim (SCK•CEN, Belgium) presented "MYRRHA: ADS Programme in Belgium – A Multi-national Demonstration Programme for Incineration of Spent Nuclear Fuel Wastes". An introduction to the project was provided, and milestones and future work were summarised

J.U. Knebel discussed the history, current status and prospects of EUROTRANS, the Integrated Project for a European transmutation project.

Professor C. Rubbia, the Nobel Prize winner, gave a special lecture on subcritical thorium reactors. The Th/^{233}U option may have a practical potential for breeding over the whole neutron spectrum, while the U/^{239}Pu option is operable only with fast neutrons. Advantages and drawbacks as well as current status on thorium utilisation for nuclear systems were summarised.

Special Session on the EUROTRANS Programme

Chair: A.C. Müller (CNRS, France)

- D. De Bruyn (SCK•CEN, Belgium) gave an overview of the DM1: DESIGN. The conceptual design of the European Facility for Industrial Transmutation (EFIT) comprises 400 MWth, which is five times more than in PDS-XADS, Pb-cooled or He-cooled concepts. The XT-ADS has a more advanced design, starting from MYRRHA which is more suitable or simplified, and safety requirements are respected. Furthermore, accelerator component reliability has dramatically increased.
- G. Granget (CEA, France) summarised DM2: ECATS (Experiments on the Coupling of an Accelerator, a Target and a Subcritical Blanket). Qualification of subcriticality monitoring, validation of the core power/beam current relationship, start-up and shutdown procedures, instrumentation validation and specific dedicated experimentation, interpretation and validation of experimental data, benchmarking and code validation activities, and safety and licensing issues as well as the status of the GUINEVERE project were presented.

- F. Delage (CEA, France) addressed the current status of DM3: AFTRA and the activities concerning the fuel. The main concept of EFIT fuel is U-free fuel which is based on the oxide-based inert matrix fuels such as ceramic and metallic (cermet) fuels as a reference and nitride-based fuels as back-up. The current study focuses on the accuracy of data in the following areas: thermal properties, mechanical properties and chemical compatibility, phase diagrams and core, fuel element and safety analysis.
- The DM4: DEMETRA project was summarised by C. Fazio. Recent results were derived on the basis of EFIT and XT-ADS needs. Major achievements include: in terms of materials, application ranges of temperature, stresses and irradiation dose defined for T91 and AISI 316L; as per coolant chemistry, technologies to measure and adjust oxygen in HLM have been developed, and filter systems for aerosol and slag removal assessed; single rod, rod bundle and integral experiments have been set up to address thermal-hydraulics issues, and the first experimental results are available; for components, windowless spallation target design rules have been defined and performance assessed, window target (MEGAPIE) post-test analysis has been performed and lessons learnt; and in the safety area LBE/water experiments have been performed and the SIMMER code has been validated.
- E.M. González-Romero (CIEMAT, Spain) summarised the DM5: NUDATRA project and sensitivities for fuel cycle parameters on nuclear data. The data available are good for single recycling but better accuracy is needed for 31 cross-sections for multi-recycling. Very significant improvement has been made for critical Pb/Bi and minor actinide cross-sections for ADS and transmutation cycles. Very significant improvement has been achieved in terms of evaluation tools (TALYS-1.0), and much better evaluated files for all Pb and Bi isotopes now exist. Significant improvements on quality and completeness of nuclear data for gas and LCP production cross-sections have also been made. The improvements concerning absolute values for spallation cross-sections and the more predictive nature of high-energy models INCL+ABLA were also reported.

Session I: Current ADS Experiments and Test Facilities

Chairs: Th. Wetzel (KIT, Germany), S. Monti (ENEA, Italy)

- "Experiments on injection of spallation neutrons by 100 MeV protons into the Kyoto University Critical Assembly (KUCA)" was presented by J-Y. Lim (U. Kyoto, Japan). The presentation covered characteristics and features of KUCA, proton beam characteristics and a study on thorium-loaded ADS experiments.
- D. Villamarín (CIEMAT, Spain) presented "Experimental validation of the industrial ADS reactivity monitoring using the YALINA-Booster subcritical assembly". He summarised the YALINA-Booster set-up, PNS experiments and beam trip experiments.
- "Integral circulation experiment: The thermal-hydraulic simulator of the ETD primary system" was presented by M. Tarantino (ENEA, Italy). The test was performed under both natural and gas-enhanced circulation. The aims of the support tests run in the NACIE loop were to test and qualify the prototypical elements before installation in the ICE bundle.
- L. Mercatali (KIT, Germany) presented "The GUINEVERE experiments at the VENUS facility: Status and perspectives". The programme is oriented towards EUROTRANS DM2 ECATS. Recent studies and results as well as proposals to the FP7 were described.
- "Experimental investigation of turbulent flow distribution in a hexagonal rod bundle for ADS prototype applications" was presented by Th. Wetzel. The single rod experiment at the KALLA LBE loop THESYS2, the water rod bundle experiment at the KALLA H_2O loop and the LBE rod bundle experiment at the KALLA LBE loop THEADES were summarised.

- F. Beauchamp (CEA, France) gave "A review of lead-bismuth alloy purification systems with regard to the latest results achieved on STELLA loop". The presentation covered characterisation of impurities in LBE, a description of the STELLA loop and filter unit, liquid filtration tests in STELLA, recommendations for basic design of LBE filtration process and a proposal of a purification strategy in LBE.
- J-B. Vogt (CNRS, France) made a presentation on "Reliability in liquid lead-bismuth of the 316L and T91 steels: Coupling effects between corrosion and fatigue". The study aims to appreciate the combined effect of surface modification resulting from corrosion and cyclic stress and to increase basic knowledge on damage of structural materials for ADS.
- "Compatibility of different steels and alloys with lead and LBE up to 750°C" was presented by A. Weisenburger (KIT, Germany). The status of ADS structural material research in Europe (DEMETRA) was summarised, and materials, experimental matrix and results on alternative pump materials, Al-containing alloys and 1.4571 and Ni-based alloy (Alloy 800) were presented.

Session II: Accelerators

Chair: H. Klein (U. Frankfurt, Germany)

- J-L. Biarrotte (CNRS, France) presented "Accelerator reference design for the European ADS demonstrator". The XT-ADS linac 2010 reference design, the reliability issue and related R&D achievements were discussed. A new project, the "MAX" proposal (MYRRHA Accelerator Experiment R&D Programme) will be submitted to the FP7 and FISSION-2010.
- H. Podlech (U. Frankfurt, Germany) introduced "The 17 MeV injector for the EUROTRANS proton driver". Development of RF structures, experimental results and beam dynamics simulations were presented. The reference design based on CH cavities and prototype cavities was tested successfully. The beam dynamics simulations showed large safety margins and large current range.
- "Developments of 350 MHz and 700 MHz prototypical cryomodules for the EUROTRANS ADS proton linear accelerator" was summarised by F. Bouly (CNRS, France). For 352 MHz developments, spoke cavities and cryomodule, high RF power developments, power couplers tests and tuning system, and for 704 MHz developments, experimental area construction, five cell elliptical cavities, power coupler, cryomodule status and reliability aspects were presented.
- H. Takei (JAEA, Japan) presented the "Estimation of acceptable beam trip frequencies of accelerators for ADS and comparison with performances of existing accelerators". The design concept, acceptable frequency of beam trips, estimation of the beam trip frequency based on the current experimental data and comparison of beam trip frequencies were summarised.
- "High-power operational experience at the Spallation Neutron Source (SNS)" was presented by S-H. Kim (ORNL, USA). The SNS has finished the initial period of power ramp-up. The main interest is beam availability during neutron production. The SNS will provide various lessons for ADS R&D.
- M. Seidel (PSI, Switzerland) presented "Experience with the production of a 1.3 MW proton beam in a cyclotron-based facility". The presentation covered facility overview, introduction to sector cyclotrons, subsystems with relevance for high-intensity operation, operational experience and upgrade plans.

Session III: Neutron Sources

Chair: M. Seidel (PSI, Switzerland)

- Ch. Latgé (CEA, France) gave an overview of the "MEGAPIE spallation target: Irradiation of the first protypical spallation target for future ADS". The presentation focused on status of the programme as well as recent achievements and future work.
- "PSI experience with high-power target design and operation" was presented by W. Wagner (PSI, Switzerland). The status of the solid spallation targets for the 1 MW beam power ranges of SINQ and future aspects were summarised.
- R.Ž. Milenković (PSI, Switzerland) introduced "EURISOL compact liquid metal converter target: Representative prototype design and tests". "EURISOL" stands for "European Isotope Separation On-line Facility". Design concept and features were presented.
- O. Meusel (U. Goethe, Germany) introduced "The Frankfurt Neutron Source – FRANZ" (Frankfurt Neutron Source at the Stern-Gerlach-Zentrum). The design concept and characteristics, features and current tests were presented.

Session IV: Subcritical Systems

Chairs: K. Tsujimoto (JAEA, Japan), E.M. González-Romero (CIEMAT, Spain), J.U. Knebel (KIT, Germany)

- F. Mulhauser (IAEA) gave an overview of "ADS-related activities at IAEA: From accelerators, neutron sources to fuel cycle and database". The presentation gave a brief overview of the IAEA ADS-related activities, including materials science, research reactors, advanced nuclear fuel cycles, accelerators and spallation.
- L. Mansani (Ansaldo, Italy) presented "The designs of an experimental ADS facility (XT-ADS) and of a European Industrial Transmutation Demonstrator (EFIT)". Characteristics of XT-ADS and EFIT were compared, and R&D needs and future plans were presented.
- A. Guertin (CNRS, France) presented "XT-ADS windowless spallation target design and corresponding R&D topics". The results of the detailed design of EFIT and XT-ADS for primary systems as well as their cores, and the design of XT-ADS windowless spallation target and the status of corresponding R&D topics (thermo-mechanics, thermal-hydraulics, nuclear assessment) were presented.
- K. Tsujimoto (JAEA, Japan) presented "Investigation of safety for accelerator-driven system". The presentation mainly addressed the safety analysis of a JAEA concept for a 800 MWt ADS. The preliminary safety analysis of an unprotected transient over-power beam window breakage (UTOP-BWB) was mainly discussed.
- W. Uyttenhove (SCK•CEN) presented "Optimisation of the EFIT fuel design". The discussion mainly dealt with the performance comparison of cercer (MgO) versus cermet (Mo, light Mo) fuels after optimisation.
- "Fuel rod performance analysis for the Italian LBE-XADS: A comparison of two different cladding materials", was presented by P. Botazzoli (Pol. di Milano, Italy). A comparison of T91 and 316L as cladding materials for an LBE ADS under normal operation was made, showing the differences in swelling and performing a sensitivity analysis.

- D.J. Coates (U. Cambridge, UK) presented "Isotope equilibrium in fast thorium reactors". The presentation covered thorium ADS utilisation in the field of actinide production. The nuclide equilibrium and evolution methods and the mechanisms governing nuclide evolution within a nuclear reactor were summarised.
- R. Sheffield (LANL, USA) introduced "Subcritical minor actinide reduction through transmutation – SMART". Used fuel management – a major impediment to increasing nuclear power usage, and a path to increasing the public acceptance of used nuclear fuel – solving the americium problem and project SMART were presented.
- "A source-efficient ADS for minor actinide burning" was presented by A. Fokau (KTH, Sweden). The presentation covered the reference EFIT-MgO/Pb, which features lower source efficiency than XT-ADS, the EFIT-Mo/Pb core with cermet fuel proposed by KIT and a compact and more source-efficient EFIT core.

Summary Session

Each session chair summarised and presented the highlights of their sessions.

Some conclusions of the workshop are: the projects around the world are generally in good shape, e.g. EUROTRANS (EC), MYRRHA (Belgium), J-PARC (Japan), SNS (USA), MEGAPIE (Switzerland); technology on the beam stability, windowless target, spallation sources and materials has been improved; studies on subcritical system design such as fuel cycle issues, fuels and materials and system analysis have been increased; innovative use of ADS including ADS with Th fuels and ADS for Am/Cm burner are being studied. However, in order to maintain the current tendency, human resources should be expanded through various national and international education programmes.

The workshop was closed by J.U. Knebel, the Chair of the workshop.

Opening and National ADS Programmes

Chair: C. Fazio

KIT welcome address

Joachim U. Knebel
TCADS Technical Chair
Karlsruhe Institute of Technology, Germany

I would like to welcome all of you to this International Workshop on Technology and Components of Accelerator-driven Systems (TCADS) in Karlsruhe, which is jointly organised by the OECD/NEA, the EURATOM Integrated Project EUROTRANS and the Karlsruhe Institute of Technology (KIT).

Especially do I welcome you in this beautiful Garden Hall of Karlsruhe Castle. This allows me to give a brief introduction to the history of this historical site.

Some 300 years ago, Karlsruhe Castle was erected in 1715 by the High Duke Karl-Wilhelm of Baden-Durlach. For 200 years, until 1918, it was used as the residence of the Margraves and Grand Dukes of Baden. Friedrich II was the last noble to live here, until he resigned at the end of World War I. As you know, it is important to mention that this region here is called Baden and Karlsruhe is its residence.

Since 1919 until today, the castle has been used as the State Museum of Baden. Its collections represent more than 5 500 years of cultural history, covering selected parts of pre-history and proto-history over the middle ages up to the 20th century. Some rooms are home to parts of the Federal Constitutional Court which has its main building just nearby. To have this court in Karlsruhe is also the reason why Karlsruhe is named the German capital of justice.

The first building of the castle was made of wood and, due to humidity and fouling, had to be fully reconstructed in stone 30 years later. The castle has two floors with attics in the roof part, taking credit from the style of French castles. Sitting in the Garden Hall, right now, you are more or less below the central seven-storied tower which has a total height of 51 meters. If you like, you can climb up the tower and enjoy the 360 degree round view. Of special interest for a nuclear engineer are the cooling towers of the NPP Philippsburg (Block 1 being a 926 MWel BWR from 1979 and Block 2 being a 1 458 MWel PWR from 1984) which you can see in north direction.

In addition, when looking around from above, you will notice that the castle resembles a butterfly with two slender long wings. You will also notice that the city of Karlsruhe is built along the rays of a sun, the castle being right in the centre of the sun, and the roads following the rays. In the old days, these roads connected Karlsruhe castle with the well-known neighbouring castles in Durlach, Bruchsal and Rastatt. The nobles used them with their horse-drawn carriages. Even today, you can recognise that federal roads follow the old tracks.

Over the years, the castle was modified several times. The Grand Duke Karl Friedrich of Baden, you passed his statute while walking from Marktplatz to the Castle, hired the well-known baroque architect Balthasar Neumann and asked him to redecorate the castle so as to give it a more impressive look: larger windows and higher doors were added.

During World War II, the castle burnt down after heavy air strikes in 1944, but was successfully reconstructed in the years of 1955 to 1966, and again used as a museum. As you recognise today, the outer face of the building was kept in the original style, the interior however was designed in a modern and practical way to allow for exhibitions or meetings.

A beautiful feature of the castle is its huge garden spreading in the north of the building: the garden is separated from the forest by a circular wall, so that the nobles did not get lost in the surrounding forest during their Sunday strolls. Initially, the garden had been designed in a French baroque style which was very modern at this time. In later years, it was turned into an English garden with large lawn areas and a variety of old and precious trees which I personally like very much.

Students use the warm season to study books and discuss with fellow students in the shade of the huge trees. However, you are expected to follow a scientific workshop here, and the garden is unfortunately only for breaks and lunchtime.

Dear colleagues and friends, I wish you a successful meeting, challenging discussions and arguments, and a splendid time here in Karlsruhe.

TECHNOLOGY AND COMPONENTS OF ACCELERATOR-DRIVEN SYSTEMS, ISBN 978-92-64-11727-3, © OECD 2011

NEA Nuclear Science Committee welcome address

Th. Walter Tromm
NEA Nuclear Science Committee Member
Karlsruhe Institute of Technology, Germany

It is a great pleasure for me to welcome you to the first TCADS workshop on behalf of the Nuclear Science Committee of the OECD Nuclear Energy Agency.

The Nuclear Science Committee has a number of activities in the fields of reactor and fuel cycle physics, including activities in the area of partitioning and transmutation. Two reports were for example issued in 2005 on "Benchmark on Beam Interruptions in an Accelerator-driven System", and on "Accelerator and Spallation Target Technologies for ADS Applications" and in 2006 on "Physics and Safety of Transmutation Systems". In addition to these specific studies the NEA Nuclear Science Committee also organises a series of "Information Exchange Meetings on Partitioning and Transmutation", the last one held in October 2008 in Japan.

The first workshop on "Utilisation and Reliability of High-power Proton Accelerators" was organised by the Nuclear Science Committee in October 1998 in Japan. That workshop was one of the first with a structured discussion within the accelerator and reactor physics communities interested in accelerator-driven systems (ADS). These discussions were so successful that the series of workshops continued and we even have today the successor in place, the first international workshop on Technology and Components of Accelerator-driven Systems (TCADS-1), co-sponsored by the EU EUROTRANS project.

The scope of the new workshop series has been extended to cover subcritical systems as well as the use of neutron sources. We believe that this workshop with its technical sessions:

- current ADS experiments and test facilities;
- accelerators;
- neutron sources;
- subcritical systems;

will provide experts a forum to present and discuss state-of-the-art developments in the field of ADS and neutron sources.

ADS is a potential option of a transmutation system in terms of the partitioning and transmutation strategies for radioactive waste in the advanced nuclear fuel cycle.

And therefore, the organisation of workshops such as this one is very much in line with Nuclear Science Committee's role as an international committee to promote co-operation among scientists in all fields of nuclear energy, especially focusing on options and outlooks for the future of nuclear energy.

We hope and we are sure that these kind of workshops are very useful for scientists to get an overall picture of ongoing and planned research activities in this specific area and also to get the opportunity to meet and discuss face-to-face with other scientists with similar interests, which certainly will be demonstrated by your lively discussions during the coming days.

Finally, I think we all have to thank the Scientific Advisory Committee for the organisation of the workshop and especially Yong-Joon Choi for all his efforts that enable us to have a fruitful and perfectly organised workshop.

In this sense, I wish us all a very interesting meeting here at the Garden Hall in the Castle of Karlsruhe and thank you for your attention.

The Karlsruhe Institute of Technology: A unique institution in German research

Peter Fritz
Vice-President
Karlsruhe Institute of Technology, Germany

The Karlsruhe Institute of Technology – briefly called KIT – is the result of the merger of the Forschungszentrum Karlsruhe and the University of Karlsruhe. This merger results in one of the largest science institutions in Europe, which will have the potential to permanently assume a top position in selected fields of research world wide. Two partners of equal strength unite in KIT. The university and the research centre contribute about half of the roundabout 8 000 staff members and the annual budget of about EUR 700 million each. Co-operation of the Forschungszentrum and university has grown constantly for more than 50 years. Of the 31 heads of institutes, 26 of the Forschungszentrum are also lecturing at the university. They manage research teams, in which scientists of both institutions co-operate closely.

In October 2006, the University Karlsruhe succeeded in all three funding lines (graduate school, excellence cluster and concept for the future) of the first round of the Excellence Initiative launched by the Federal Republic of Germany and the federal states. As one of three universities, it was granted the elite status. This success was based largely on the concept for the future. The central element of this concept is the foundation of the Karlsruhe Institute of Technology (KIT) together with the Forschungszentrum Karlsruhe.

With a separate KIT law by the state of Baden-Württemberg the Karlsruhe Institute of Technology KIT, the merger of Forschungszentrum and University Karlsruhe was established on 1 October 2009.

KIT is an institution with two missions: research and education of a state university and programme-oriented preventative research of a large-scale research institution of the Helmholtz Association and KIT focuses on three columns: research, education and innovation.

Research

Research at the University Karlsruhe and the Forschungszentrum Karlsruhe is structured differently by tradition. Nevertheless, it has a common feature: it is based above all on the skills and knowledge of their scientific and technical staff. In KIT these scientists will work in fields of competence depending on their expert know-how. Related fields of competence are bundled in areas of competence. Fields of competence and areas of competence make up the competence portfolio of KIT. It is dynamic and will develop and take up new scientific topics. While the competence portfolio is the basis of KIT research, KIT centres and KIT focuses are organisational units that bundle research projects. These projects give KIT research its profile and allow for its strategic planning.

Education

Education and promotion of young scientists are central activities of KIT; the large joint competence portfolio creates a much larger basis of scientists and engineers, who will also be available for education purposes. Promotion of young scientists at KIT starts during the studies already. In research- and application-driven education modules, students are familiarised with (large-scale) research projects at a very early point in time. PhD students are also granted particular support. They are embedded in an attractive, high-performance environment that is characterised by excellent research in small working groups and research using large-scale devices. In this way, young scientists are instructed to accomplish independent research work in high-performance international research teams. Moreover, specific education is offered. These tasks are fulfilled mainly by the faculties and KIT graduate schools, of which the Karlsruhe School of Optics and Photonics was opened on 5 November 2007. Others will follow.

Two new establishments have been conceived especially for promoting young scientists at KIT: The Karlsruhe House of Young Scientists represents a social and cultural meeting point of PhD and post-doctoral students, offers specific help by grants and supports participation in international conferences. The House of Competence offers a number of advanced training activities related to complementary skills in order to convey general and job-oriented key qualifications to PhD students and young scientists.

Innovation

KIT innovation first comprises the classical transfer of research and development results to application and innovative products, for example, by co-operation with industry. In addition, the foundation of new enterprises is supported. In the past ten years, the Forschungszentrum and University Karlsruhe founded more than 250 start-ups, of which only 10% were not viable. Another major element is the career service, i.e. the transfer of persons with pertinent know-how from research to industry and *vice versa*.

Outline of check and review on partitioning and transmutation by Atomic Energy Commission of Japan and recommendation for R&D on ADS

Kazufumi Tsujimoto, Hiroyuki Oigawa
Japan Atomic Energy Research Institute, Japan

Abstract

The Atomic Energy Commission (AEC) of Japan conducted a check and review on partitioning and transmutation (P&T) technology by setting up a subcommittee in August 2008. The subcommittee compiled and submitted a final report to AEC in April 2009. As the basic policy for R&D of P&T technologies, the report presented that the R&D of double-strata concept should be undertaken as a part of the R&D for future nuclear power generation systems considering the transitional phase from light water reactor (LWR) cycle to FBR cycle as well as the equilibrium phase of FBR cycle. The report indicated that further R&D and the collaborations with foreign R&D activities are required for the ADS to proceed to next R&D phase where the feasibility study is to be performed from the engineering and economical viewpoints. The report also pointed out the importance of the integral experiments of the transmutation systems, especially the requirement of the critical experiments using MA, and the importance to prepare the facility to perform these experiments. Moreover, the report recommended that the Transmutation Physics Experimental Facility (TEF-P) planned in the second phase of the J-PARC project should be investigated as a part of the preparation for the facility.

Introduction

Partitioning and transmutation (P&T) technology is a radioactive waste management concept to separate elements and radioactive nuclides from high-level radioactive waste (HLW) depending on their half lives and recycling purposes, and to transmute long-lived radioactive nuclides to short-lived or stable ones in order to reduce the burden of the radioactive waste disposal and utilise radioactive waste as useful resources. In 1988, the Atomic Energy Commission (AEC) of Japan started a long-term programme for research and development (R&D) on P&T technology, called the "OMEGA" programme [1]. The programme was jointly carried out by three institutions, the Central Research Institute of Electric Power Industry (CRIEPI), the Power Reactor and Nuclear Fuel Development Co-operation [PNC, later re-formed as the Japan Nuclear Cycle Development Institute (JNC)], and the Japan Atomic Energy Research Institute (JAERI). Under the OMEGA programme, JAERI has been developing technologies for a dedicated partitioning process and transmutation system based on the concept of a double-strata fuel cycle, in which P&T is carried out in a dedicated and small-scale fuel cycle for P&T attached to the commercial fuel cycle. JNC has been devoting its major efforts to developing an advanced fuel recycling on PUREX and TRUEX processes for co-extraction of U, Pu and minor actinides (MA), as well as of MOX fuel fast breeder reactor (FBR) for transmutation. CRIEPI has been developing pyroprocessing recycling technologies for metallic fuel FBR. The R&D programme has been stimulated by the collaborative efforts of three institutes.

The progress of Step-I and Step-II of the OMEGA programme were reviewed in 1999 by the AEC's Advisory Committee on Nuclear Fuel Cycle Back-end Policy, and the report was issued in March 2000. In the report, the result of R&D was analysed and the steps on how to proceed with R&D in the future were recommended. Some of the conclusions of the report were as follows. Since the P&T technologies have the potential to be useful by decreasing long-tem radioactive inventory, it is appropriate to proceed with the R&D on P&T. The P&T systems based on the commercial FBR fuel cycle and the double-strata fuel cycle have specific features; R&D for both concepts is to be studied to establish the necessary basic technologies in the foreseeable future. Hereafter, implementation scenarios of P&T, including a co-existence scenario, are to be studied.

The Japan Atomic Energy Agency was founded by the integration of JAEA and JNC in 2005. In 2006, JAEA launched the Fast Reactor Cycle Technology Development (FaCT) project in which transmutation of MA was one of the development issues. In response to this situation, the AEC of Japan set up the subcommittee of P&T Technology under the Advisory Committee on Research and Development in August 2008. The subcommittee investigated the current status related to the R&D of P&T technologies, analysed the results and significance of the P&T technologies, discussed a way forward to promote their R&D and issued the report [2].

Significance of P&T technologies

The objective of P&T is oriented to removal and transmutation of mainly MA and fission products (FP). P&T technologies mainly consist of P&T of MA, partition and predisposal storage of FP such as ^{90}Sr and ^{137}Cs, P&T of long-lived FP such as ^{129}I and ^{99}Tc, and partitioning and utilisation of useful FP such as noble metals.

The subcommittee reviewed the study for the impact of P&T on HLW disposal by JAEA. In this study, potential hazard, effective dose rate of HLW, amount of waste form and repository area were investigated for four different scenarios: *i)* reference non-P&T; *ii)* transmutation process only (separation and transmutation of MA); *iii)* partitioning process only (separation of some FP); *iv)* both partitioning and transmutation. The subcommittee analysed the results of the study and concluded that the significances of the P&T technologies were as follows:

- *Reduction of the potential toxicity*. Implementation of P&T technologies will reduce the long-term potential toxicity of the HLW, keeping in mind that the degree of reducing the potential toxicity depends on the mixture ratio of MA.
- *Reduction of the requirement for the geological repository*. The MA by the implementation of P&T technologies will increase the time that is necessary to set up new disposal fields, or reduce the burden of managing waste forms.
- *Enhancement of a freedom for rational design of nuclear waste disposal systems*. Partitioning technologies of heat-generating fission product and transmutation technologies of MA have the possibility to improve the design of nuclear waste disposal systems. However, further studies of storage and disposal methods for each waste are required.

Review of R&D on P&T technologies

As for the previous C&R in 2000, P&T technologies were considered as future technologies different from the R&D of the commercial FBR fuel cycle. However, the Feasibility Study on Commercialised Fast Reactor Cycle Systems (1999-2005) concluded that the P&T of MA was considered as one of the objectives of commercialised FBR. Based on the conclusion of the Feasibility Study, in the FaCT project, the MOX-fuelled sodium-cooled FBR with advanced aqueous reprocessing was taken as the most viable technology option for commercialisation. As the runner-up concept, a metallic plutonium-uranium (U-Pu-Zr alloy) fuelled sodium-cooled FBR with pyrochemical reprocessing which was deemed equally viable for commercialisation but more uncertain in its social and technical aspects. In both concepts, MA are homogeneously recycled and mixed with plutonium-uranium fuel.

On the other hand, in the R&D for the double-strata concept, the system study of transmutation made it clear that an accelerator-driven system (ADS) is better than a dedicated critical reactor for MA transmutation from the safety viewpoint. Based on this result, transmutation study related to the double-strata concept has been concentrated on the development of ADS and related technology. The present reference design is a nitride-fuelled lead-bismuth-cooled ADS with a super-conducting proton linac. The lead-bismuth is used for both coolant and spallation target. In the double-strata fuel cycle, while an aqueous partitioning process is considered to be used for separating elements in HLW from the commercial fuel cycle, MA nitride fuel may be used and processed by a molten salt electrorefining technique in MA transmutation with ADS system.

Moreover, basic R&D for a concept with heterogeneous loading of MA target fuel in FBR, which is an intermediary concept with regard to the homogeneous MA recycling concept in the commercial FBR cycle and the double-strata concept, has been performed on a limited scale.

The concepts for P&T which were reviewed by the subcommittee are summarised as follows:

- commercial sodium-cooled FBR with MOX fuel, homogeneously mixed MA;
- commercial sodium-cooled FBR with metallic fuel, homogeneously mixed with MA;
- commercial sodium-cooled FBR with MOX fuel in which target MA fuel is loaded heterogeneously;
- double-strata fuel cycle concept with the lead-bismuth-cooled ADS with nitride fuel.

Conclusion of review results

Basic policy for R&D on P&T technologies

As the result of the review, in general, R&D for each P&T concept have been successfully developed from the basic research phase to feasibility studies at the industrial level. However, the information for making some decisions are not sufficient to judge the degree of attainment for performance targets required for the nuclear fuel cycle containing P&T technologies. For example, they have not had the engineering feasibility to be applicable as a practical technique, as the basic experimental data and benchmarks for the calculation tools are not enough, and proof of engineering feasibility for an elemental technique, which is the dominant one in engineering viability of some concepts, is not sufficient. Therefore, the subcommittee recommended that the enhancement of basic experimental data, which is common for all P&T concepts, must be expanded.

As the basic policy for R&D of P&T technologies, the R&D of P&T technologies based on the homogeneous and heterogeneous fuel cycle concept of FBR should be undertaken as a part of the R&D for practical application of FBR and its fuel cycle technologies. R&D of the double-strata concept should be undertaken as a part of the R&D for future nuclear power generation systems considering the transitional phase from a light water reactor cycle to a FBR cycle and the equilibrium phase of the FBR cycle. The progress of these R&D activities should be reviewed regularly and promoted reflecting the evaluation results under the strong co-operation between R&D for different concepts.

Promoting of R&D for each P&T concept

MOX fuel FBR technology supposing homogeneous/heterogeneous MA cycle

Concerning R&D on a homogeneous MA cycle, the following points will be important subjects in the future:

- to create partitioning/recovery systems for MA nuclides with high reliability using the aqueous reprocessing method;
- to create practical manufacturing process for the MOX fuel containing MA nuclides with high heat generation and high dose by MA nuclides;
- to realise the reactor core that launches the fuel containing up to 5% MA which satisfies the safety requirements;
- to manufacture a fuel that has high burn-up capability with high reliability under the prescribed conditions.

Future efforts should be processed by the development programme aiming to completion of the practical FBR with the target performance until 2050. Meanwhile, in R&D on heterogeneous MA cycle, the comprehensive assessment, including nuclear safety of heterogeneous reactor core with MA fuel containing Am, Np and Cm and performance of FBR as an electric power plant, is required.

Metal fuel FBR technology supposing homogeneous MA cycle

As concerns the development of each elemental technology for metal fuel, though some part of them are in the engineering research phase, most are considered to be in the semi-engineering research phase. It will be required to develop engineering scale apparatuses and their demonstration tests after this. As concerns the fundamental properties of metal fuel alloys containing MA, the fundamental data to design the practical fuel is insufficient. The most important subject is to construct a hot cell to obtain fundamental data on MA behaviour at high temperature.

The point of system design for MA transmutation by sodium-cooled FBR with metal fuel is to satisfy the design criteria for the safety and performance of the system through evaluation of MA effect on integral quantity. In the future, it will be necessary to improve the assessment precision of the important integral quantity through efforts to improve the precision of each nuclear data using differential experiments, nuclear data collection and integral experiments to verify the design code. MA containing ratio, nuclear safety and economy are in the trade-off relation. It should be optimised by considering the development risk to transmute MA by FBR power plant system.

Double-strata concept using the ADS

The technological issues for this concept are:

- to achieve the performance and cost of the accelerator not avoiding the total performance of the electric generation system;
- to confirm the engineering feasibility of the beam window;
- to reliably solve the reactor physics issues to control the subcritical system;
- to confirm the design and safety of the Pb-Bi-cooled reactor;
- to show the practicality of the fuel cycle system with the pyro-reprocessing for the nitride fuel;
- to confirm the capability to fabricate the nitride fuel attaining the required performance and the high burn-up under the prescribed conditions.

The authorisation of the development of the double-strata concept will be investigated when the homogenous MA recycle using FBR is judged to be unable to satisfy the prescribed performance, or when the development of the electric generation system introduced the partitioning and transmutation technology with the ADS is judged to have advantages in terms of the technological feasibility and the cost-to-benefit. Therefore, the efforts to solve each of the issues, or, to technologically and economically foresee the possibility to solve them should be substantially promoted. Moreover, along with the estimations for each achievement level of the fast breeder reactor's performance goal done as the occasion demands, similar estimations for the double-strata concept should be done, the relative status to the fast breeder reactor should be evaluated and the framework of the efforts should be investigated.

Framework of the efforts for the principal issues

Partitioning process

Although the partitioning process has been principally confirmed by the laboratory-scale experiment using the active liquid waste, a number of problems remain to start the engineering proof of the process. Moreover, the R&D for the advanced aqueous reprocessing keeping flexibility of the partitioning process in the transient times from the light water reactor to the fast breeder reactor is needed.

MA fuel

Although basic knowledge about the MA fuel has been obtained, the basic properties involving curium are not sufficiently known. Moreover, the technical capability of the fuel manufacture under the circumstance with high radiation and temperature cannot be judged. It is important to continuously obtain the basic data needed to design the facility, construct it and execute the assembly-scale experiments.

Transmutation system

For the transmutation systems, the basic data to estimate the safety or the performance of these systems are not enough, and the verification of the calculation code accuracy for the system design is also insufficient. For the hetero-loaded FR core, a design evaluation is required to verify its feasibility. It is necessary to accumulate the basic data of MA for the improvement of the reliability of these designs and estimations. For the differential and integral experiments of the MA nuclear data, the experiments at the existing facilities should have been carried on and both the enhancement of the nuclear data library and the sophistication of the numerical simulation methods should also have been performed. For the integral experiments of the transmutation systems in particular, the critical experiments using Am and Cm are required. Therefore, it is important to create the environment to perform these experiments. As part of the creation of the environment, the Transmutation Physics Experimental Facility (TEF-P) planned in the second phase of the J-PARC project should be investigated.

For the ADS, further R&D is necessary to proceed to the next phase, the feasibility of which is discussed from the engineering and economical viewpoints. R&D should be promoted with foreign R&D, development of neutron source by an accelerator and R&D of FBR. It is anticipated to perform a simulation experiment for a combination of the spallation neutron source and a fast subcritical core which has not been performed world wide. The utilisation of J-PARC or other facilities is anticipated for the combination experiment. The combination experiment should refer to experiments for a combination of an accelerator and a subcritical core performed at Kyoto University Research Reactor Institute.

System estimation

In the R&D of the FBR cycle technology, since the targets for safety, economic efficiency, environmental acceptability, effective utilisation of the resource and nuclear proliferation resistance have been given, it is necessary to provide feedback on the R&D results to adequately design and modify the issues for each component. Based on these situations, development of a system estimation tool which is able to estimate achievements for those targets should be carried out with the consideration that the FBR cycle technology will cover each concept of P&T.

Strengthening of co-operation with basic studies

Among the four concepts currently investigated – the homogeneous MA recycle with MOX FBR cycle, the homogeneous MA recycle with metal FBR cycle, the heterogeneous MA recycle with MOX FBR cycle and the double-strata concept with ADS – there are many common issues and essential data for these R&D and estimations. To obtain these essential data, it is necessary to collaborate between basic and application and between other fields. Additionally, international collaborations should be sought since the domestic facilities are not sufficient to obtain these data. These various collaborations permit to perform cross-cutting estimations for the current concepts and to investigate better combinations of each component. For instance, the estimation of the following combinations are anticipated: to employ metal or MOX fuel in the double-strata concept, to adapt various concepts to load the target assembly in the hetero-loaded FBR cycle and to investigate combinations between the wet separation of MA nuclides included in the high-level liquid waste from LWR and other separation concepts.

Recommendations

Around 2010, the government will review FBR and its fuel cycle technology including P&T technology, and will begin discussion of the second nuclear fuel reprocessing plant. Therefore, the subcommittee recommends that R&D organisations promote R&D activities in line with the aforementioned basic policy.

On the review and the discussion from around 2010, the R&D achievements for FBR and its fuel cycle technology will be evaluated from the view point of the possibility to satisfy performance criteria. At this review, the subcommittee recommends that the government should specify a more concrete R&D policy including enhancement, keeping and aborting R&D items to resolve the problems pointed out in this report. For the double-strata concept, the subcommittee also proposes that the government should indicate basic policy and specify a more concrete R&D policy. At this review, R&D organisations should present rational and R&D strategies including utilisation plans for domestic and overseas R&D facilities. After the next review around 2010, cross-cutting reviews for P&T technology must be continued. It is appropriate to evaluate achievement regarding R&D activities every five years.

Since the R&D activities for P&T technology are important from the view point of preserving capability of basic science and the development of human resources, R&D organisations should vigorously promote collaboration and co-operation with universities. They should steadily progress as concerns R&D activities for P&T technology in consideration of the following points:

- evaluation of the possibility to satisfy performance criteria from view point of increasing advantage of nuclear technology in the market, and reflection of the evaluated results in R&D plans and their implementation;
- reinforcement of the research activities to evaluate the characteristics as the nuclear power plant system consisting of “fuel cycle” and “radioactive waste management”;
- enhancement of the important fundamental science data and basic benchmarks;
- promotion of semi-engineering or engineering experiments for the system proved the feasibility;
- development of an outlook to indicate the possibility to overcome the problems by utilising international collaboration for unresolved issues toward the engineering feasibility;
- and exploring the possibility of a better combination of present technical concepts.

Conclusion

The subcommittee listened to explanations from relevant research and development institutions on their activities for the R&D of P&T technologies promoted in accordance with the policies given in the report entitled “Current Status and Future Plan of the Research and Development of Technologies for Partitioning and Transmutation of Long-lived Radioactive Nuclides”, which was issued by the AEC’s Advisory Committee on the Policy for the Back-end of Nuclear Fuel Cycle in March 2000. The subcommittee evaluated the progress of the R&D activities, analysed the results that may be brought about by the commercialisation of P&T technologies and discussed a way forward to promote their R&D. The report recommended that as P&T technologies will enhance freedom for rational design of nuclear waste disposal systems when they are realised, satisfying the design requirements specified for future nuclear power generation systems, the activities for the R&D of P&T technologies should be undertaken as a part of the activities for the R&D of FBR and its fuel cycle technologies, and pointed out problems and issues of each technology development activity on which effort and thought should be focused in accordance with the attainment level of their R&D.

The AEC considers this report to be appropriate and suggests the concerned administrative bodies to respect the substance of this report and steadily promote the activities for the R&D of P&T technologies [3]. Following the decision of the AEC, JAEA has started the discussion for rational R&D strategies including utilisation plans for domestic and overseas R&D facilities.

References

[1] Mukaiyama, T., *et al.*, "Review of Research and Development of Accelerator-driven System in Japan", P*rogress in Nuclear Energy*, Vol. 38, No. 1-2, pp. 107-134 (2001).

[2] "Current Status and a Way Forward to Promote the Research and Development of Partitioning and Transmutation Technologies", *www.aec.go.jp/jicst/NC/senmon/bunri/houkokusho-090428.pdf* [in Japanese].

[3] AEC decision, "Concerning the Report Entitled 'Current Status and a Way Forward to Promote the Research and Development of Partitioning and Transmutation Technologies'", *www.aec.go.jp/jicst/NC/about/kettei/kettei090428_e.pdf*.

The MYRRHA ADS programme in Belgium: A multi-national demonstration programme for incineration of spent nuclear fuel wastes

Hamid Aït Abderrahim, Peter Baeten, Didier De Bruyn
Belgian Nuclear Research Centre (SCK•CEN)
Mol, Belgium

Abstract

The coupling between an accelerator, a spallation target and a subcritical core has been studied for the first time at SCK•CEN in collaboration with Ion Beam Applications (IBA, Louvain-la-Neuve) in the framework of the ADONIS project (1995-1997). ADONIS was a small irradiation facility based on the ADS concept, having a dedicated objective to produce radioisotopes for medical purposes and more particularly ^{99}Mo as a fission product from highly enriched ^{235}U fissile targets. The ad hoc scientific advisory committee recommended extending the purpose of the ADONIS machine to become a Materials Testing Reactor (MTR) for material and fuel research, to study the feasibility of transmutation of the minor actinides and to demonstrate at a reasonable power scale the principle of the ADS. The project, since 1998 named MYRRHA, then evolved to a larger installation.

MYRRHA is now conceived as a flexible irradiation facility, able to work as an accelerator-driver (subcritical mode) and in critical mode. In this way, MYRRHA will allow fuel developments for innovative reactor systems, material developments for Gen-IV systems, material developments for fusion reactors, radioisotope production for medical and industrial applications and industrial applications, such as Si-doping.

MYRRHA will also demonstrate the ADS full concept by coupling the three components (accelerator, spallation target and subcritical reactor) at reasonable power level to allow operation feedback, scalable to an industrial demonstrator and allow the study of efficient transmutation of high-level nuclear waste.

Being based on the heavy liquid metal technology, the eutectic lead-bismuth, MYRRHA will be able to significantly contribute to the development of lead fast reactor technology. Since MYRRHA will also be operated in critical mode, it can even better play the role of European technology pilot plant in the roadmap for LFR.

Introduction

Since its creation in 1952, the Belgian Nuclear Research Centre (SCK•CEN) at Mol has always been heavily involved in the conception, design, realisation and operation of large nuclear infrastructures. The centre has even played a pioneering role at such infrastructures in Europe and world wide. SCK•CEN has successfully operated these facilities at all times thanks to the high degree of qualification and competence of its personnel and by inserting these facilities in European and international research networks, contributing to the development of crucial aspects of nuclear energy at the international level.

One of the flagships of the nuclear infrastructure of SCK•CEN is the BR2 reactor [1], a flexible irradiation facility known as a multi-purpose materials testing reactor. This reactor has been in operation since 1962 and has proven to be an excellent research tool, which has produced remarkable results for the international nuclear energy community in various fields such as materials research for fission and fusion reactors, fuel research, reactor safety, reactor technology and for the production of radioisotopes for medical and industrial applications.

BR2 has been refurbished twice, in the beginning of the 80s and in the mid-90s. The BR2 reactor is now licensed for operating until 2016 but around that period, it will have to be decided whether another refurbishment around 2020 will have to be done or whether BR2 will have to be replaced by another facility. Therefore, the Belgian Nuclear Research Centre at Mol has been working for several years on the pre- and conceptual design of MYRRHA (Multi-purpose hYbrid Research Reactor for High-tech Applications), a multi-purpose flexible irradiation facility that can replace BR2 and that is sufficiently innovative to support future-oriented research projects needed to sustain the future of the research centre.

Scope of MYRRHA

At the international level, there is a clear need to obtain a sustainable solution for the high-level, long-lived radioactive waste (HLLW) consisting of minor actinides (MA) and long-lived fission products (LLFP). These MA and LLFP stocks need to be managed in an appropriate way. Reprocessing of used fuel followed by geological disposal or direct geological disposal are today the envisaged solutions depending on national fuel cycle options and waste management policies. The required time scale for geological disposal exceeds the time span of profound historical knowledge and this creates problems of public acceptance. The partitioning and transmutation (P&T) concept has been pointed out in numerous studies in the past [2-4, see also Figure 1] and more recently in the framework of the Gen-IV initiative as the strategy that can relax the constraints on geological disposal and that can reduce the monitoring period to technological and manageable time scales.

The reduction of the volume and the half-life of HLLW and LLFP can be achieved conceptually by using a park of fast critical reactors that will simultaneously produce electricity and transmute the actinides, or by a “double strata” reactor park with a first stratum of reactors dedicated to electricity production using “clean fuel” containing only U and Pu and systems devoted to transmutation of HLLW and LLFP. These systems of the second stratum will be based on special fast critical reactors or more probably subcritical fast systems [accelerator-driven systems (ADS)] loaded with homogeneous fuels with high MA content.

Even when considering the phase out of nuclear energy, the combination of P&T and dedicated burner technologies such as ADS is needed to relax the constraints on the geological disposal and reduce the monitoring period to technological and manageable time scales for existing waste. Hence, since ADS represent a possible major component in the P&T framework, the demonstration of the subcritical dedicated burner concept is needed and this was indicated in the EU vision document [5] and in the strategic research agenda (SRA) [6].

Figure 1: Radiotoxicity as a function of time – with and without P&T

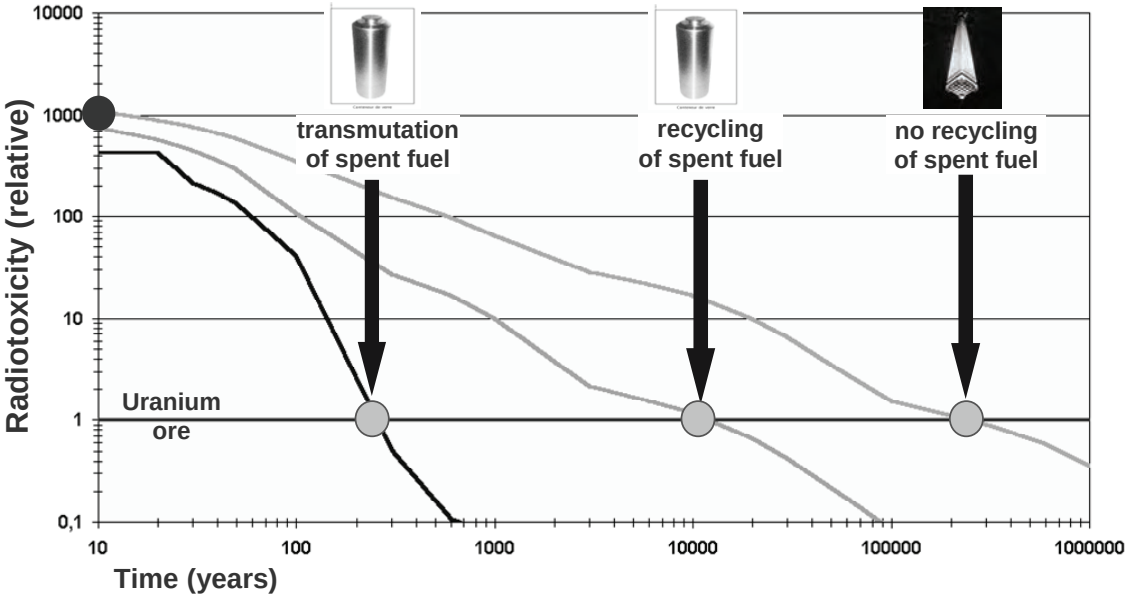

Since 2000, the Generation International Forum (GIF) [7] has selected six Generation IV (Gen-IV) concepts of which three are based on the fast spectrum technologies, namely: the sodium fast reactor (SFR), the lead-cooled fast reactor (LFR) and the gas-cooled fast reactor (GFR). The SNETP community has at present given a higher priority to the SFR technology but has also indicated the need for the development of an alternative coolant technology, weather lead or gas. The technological development of the fuel and materials of these concepts require the availability of a flexible fast spectrum irradiation facility. The vision document and the SRA of the SNETP have also stated that Europe should be at the forefront of Gen-IV reactor development.

Being based on the heavy liquid metal technology, the eutectic lead-bismuth, MYRRHA will be able to significantly contribute to the development of lead fast reactor technology. Since Europe no longer has a fast spectrum irradiation facility, there is a clear need for a flexible fast spectrum irradiation facility in support of the development of the different fast reactor systems: SFR, LFR and GFR. As it will also be operated in critical mode, MYRRHA can even better play the role of European technology pilot plant in the roadmap for LFR.

MYRRHA objectives

With the objectives described in the previous section, MYRRHA should therefore target the following applications catalogue:

- The demonstration of the ADS full concept by coupling the three components (accelerator, spallation target and subcritical reactor) at a reasonable power level to allow operation feedback, scalable to an industrial demonstrator.
- The study of efficient transmutation of high-level nuclear waste, in particular minor actinides that would request high fast flux intensity ($\Phi_{>0.75MeV} = 10^{15}$ n/cm^{2}s).
- To be operated as a flexible fast spectrum irradiation facility allowing for:
  - fuel developments for innovative reactor systems, which need irradiation rigs with a representative flux spectrum, a representative irradiation temperature and high total flux levels ($\Phi_{tot} = 5 \times 10^{14}$ to 10^{15} n/cm^{2}s) (the main target will be fast spectrum Gen-IV systems which require fast spectrum conditions);

  - material developments for Gen-IV systems, which need large irradiation volumes (3 000 cm^3) with high uniform fast flux level ($\Phi_{>1MeV}$ = 1 ~ 5 × 10^{14} n/cm^2s) in various irradiation positions, representative irradiation temperature and representative neutron spectrum conditions (the main target will be fast spectrum Gen-IV systems);
  - material developments for fusion reactors which also need large irradiation volumes (3 000 cm^3) with high constant fast flux level ($\Phi_{>1MeV}$ = 1 ~ 5 × 10^{14} n/cm^2s), representative irradiation temperature and a representative ratio appm He/dpa(Fe) = 10;
  - radioisotope production for medical and industrial applications by:
    - holding a back-up role for classical medical radioisotopes;
    - focusing on R&D and production of radioisotopes requesting very high thermal flux levels (Φ_{th} = 2 to 3 × 10^{15} n/cm^2s) due to double capture reactions;
  - industrial applications such as Si-doping need a thermal flux level depending on the desired irradiation time: for a flux level Φ_{th} = 10^{13} n/cm^2s an irradiation time in the order of days is needed and for a flux level of Φ_{th} = 10^{14} n/cm^2s an irradiation time in the order of hours is needed to obtain the required specifications;
  - the demonstration of LBE technology;
- To contribute to the demonstration of LFR technology and the critical mode operation of heavy liquid metal cooled reactor as an alternative technology to SFR.

Genesis of MYRRHA and its evolution

The ADONIS project (1995-1997)

The coupling between an accelerator, a spallation target and a subcritical core was studied for the first time at SCK•CEN in collaboration with Ion Beam Applications (IBA, Louvain-la-Neuve) in the framework of the ADONIS project (1995-1997). ADONIS was a small irradiation facility based on the ADS concept, having a dedicated objective to produce radioisotopes for medical purposes and more particularly ^{99}Mo as a fission product from highly enriched ^{235}U fissile targets. The proposed design was of limited size with an accelerator of 150 MeV and a core with a power of around 1.5 MWth. The subcritical core was made of the ^{235}U targets for production of the ^{99}Mo without other driver fuel. The system was a thermal spectrum machine and therefore water was used as coolant and moderator.

From ADONIS to MYRRHA (1998-2005)

The *ad hoc* scientific advisory committee recommended extending the purpose of the ADONIS machine to become a materials testing reactor for material and fuel research, to study the feasibility of transmutation of the minor actinides and to demonstrate at a reasonable power scale the principle of the ADS.

This decision was taken around the same time of the last BR2 refurbishment. It was then clear that a subsequent BR2 refurbishment would be compulsory around 2020. Even if such refurbishment remains technically possible, a new machine would be better adapted to the new needs, in particular for Gen-IV and fusion research. The project, since 1998 named MYRRHA, then evolved to a larger installation.

In mid-2002, a first pre-design file of MYRRHA, the "MYRRHA Draft – 1" file [8] with a core nominal power of 30 MWth, was submitted to an International Technical Guidance Committee for review. This international panel consisted of experts from research reactor designers, ADS development, reactor safety authorities and spallation target specialists. No show stopper was

identified in the project but some recommendations were made. The design was upgraded and the MYRRHA project team favoured as much as possible mature or less demanding technologies in terms of research and development. In its 2005 version, MYRRHA consisted of a proton accelerator delivering a 350 MeV * 5mA beam to a windowless liquid Pb-Bi spallation target that in turn couples to a Pb-Bi cooled, subcritical fast core of 50 MW thermal power. The so-called "Draft – 2" design, published early 2005 [9], is summarised in Ref. [10]. In addition, a business plan was written in 2007 and is updated on a regular basis [11].

Figure 2: MYRRHA "Draft – 2"

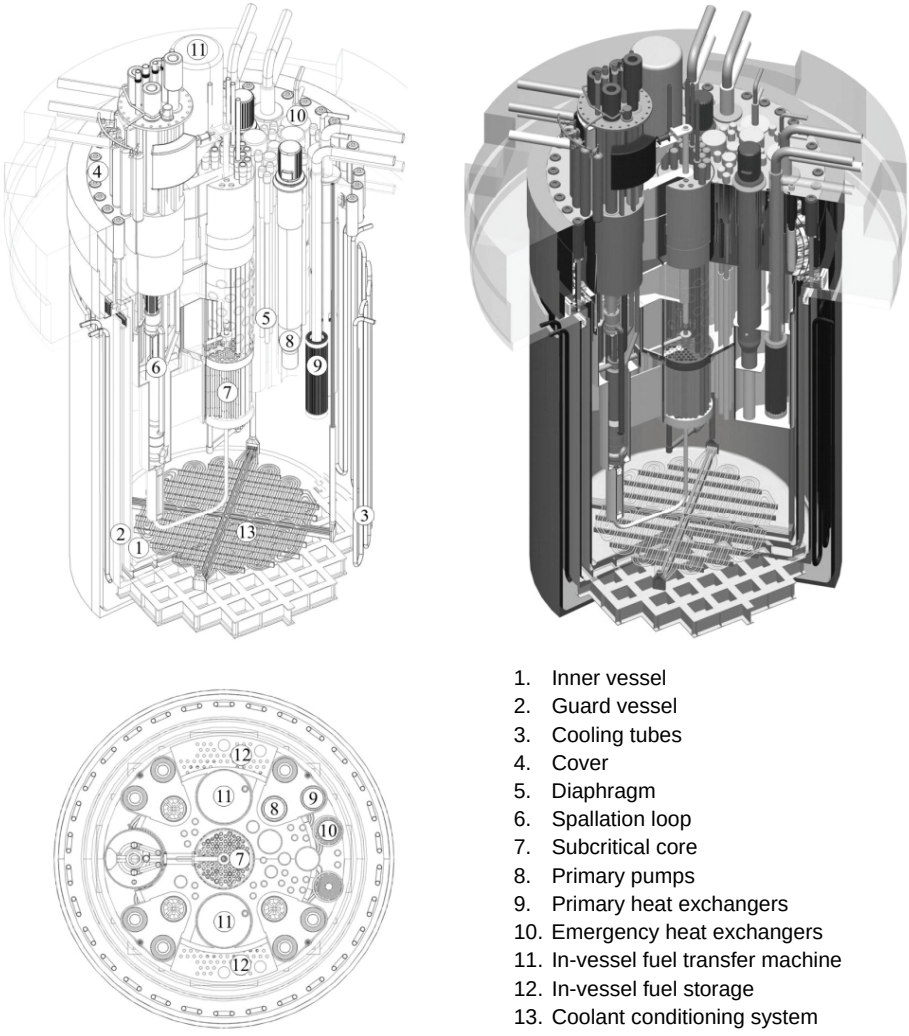

From MYRRHA to XT-ADS (2005-2009)

SCK•CEN offered to use the MYRRHA 2005 design file as a starting basis for the Experimental Facility Demonstrating the Technical Feasibility of Transmutation in an Accelerator-driven System (XT-ADS) design in the FP6 EUROTRANS Integrated Project. This allowed optimising an existing design towards the needs of XT-ADS and within the limits of the safety requirements instead of starting from a blank page. MYRRHA and XT-ADS differ however on several points such as the accelerator (600 MeV beam instead of 350 MeV), the temperature level, the plutonium vector in the fuel, the fuel pitch and the simplification of several major components resulting in a

lower power density core, an increased core power of 57 MW and a neutron flux of 7×10^{14} n/cm^{3}s instead of 1×10^{15} n/cm^{3}s (>0.75 MeV). XT-ADS is presented more in detail in another contribution to this workshop [12].

Figure 3: XT-ADS

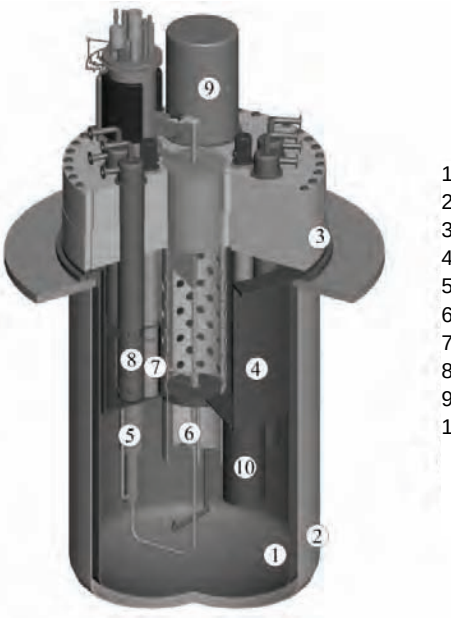

1. Inner vessel
2. Guard vessel
3. Cover
4. Diaphragm
5. Spallation loop
6. Subcritical core
7. Primary pumps
8. Primary heat exchangers
9. In-vessel fuel transfer machine
10. In-vessel fuel storage

From XT-ADS to FASTEF (2009-2011)

The performances of XT-ADS do not fully correspond to the objectives described in the previous section. Therefore, it is clear that future design work is needed to bring this design in line with the objectives and applications catalogue.

First of all, since the objective of MYRRHA is to operate both in a subcritical mode and a critical mode, an analysis will be performed to establish to which extent the design of XT-ADS (which only considers subcritical mode operation) needs to be modified to respond to the objective to operate also in critical mode. In this respect, it is clear that reactor control and scram systems have to be included in the design. A primary reactor shutdown system based on shutdown rods and a secondary shutdown system based on another type of system need to be incorporated to guarantee not only redundancy but also diversification. Control rods need to be foreseen as well. Also, an analysis will have to be performed to determine which further design changes might be induced by removing the spallation target, especially with regard to the operation of MYRRHA in critical mode as a flexible fast spectrum irradiation facility. Working in critical mode will significantly modify the safety characteristics of the facility and the impact of the safety feedback on the design needs to be implemented.

A second major topic for the update of the MYRRHA design is to obtain the targets set in the applications catalogue. The XT-ADS concept is able to reach the different targets in terms of irradiation conditions listed in the applications catalogue except for the targeted fast flux level above E = 0.75 MeV of 10^{15} n/cm^{2}s. In XT-ADS, this flux level reaches $\Phi_{>0.75MeV} = 0.7 \times 10^{15}$ n/cm^{2}s. To increase this flux level, it is obvious that the total power and power density will have to be increased. Therefore, already a preliminary study [13] was performed to investigate what would be the most optimal design changes to reach this target of $\Phi_{>0.75MeV} = 10^{15}$ n/cm^{2}s given the different design constraints. Preliminary conclusions of this study resulted in preserving the existing design choices of XT-ADS except for:

- an increase of the power from 57 MW_{th} to 85 MW_{th};
- an increase of the power density by decreasing the number of fuel assemblies from 72 to 64 for the equilibrium core;
- an increase of the allowable temperature increment over the core from 100°C to 130°C, resulting in a decrease of the inlet temperature from 300°C to 270°C (the outlet temperature remains at 400°C);
- an increase of the beam current from 2.2 mA to 3.0 mA for ADS operation (during normal operation);
- an increase of the Pu content from 33% in a depleted uranium matrix to 35% in a natural uranium matrix.

The study pointed out that the implications of these modifications can be accommodated by the design, but a detailed confirmation is still needed.

These aspects for the upgrade of the MYRRHA design, now called FASTEF, will together with a progress towards an advanced engineering design level for all components make up the work for the Central Design Team (CDT) within the FP7 project CDT that recently started [14].

Table 1: MYRRHA design evolution

Draft 2 2005	XT-ADS 2006-2009	XT-ADS-HF end 2009	FASTEF 2010
Linac 350 MeV	Linac 600 MeV	Linac 600 MeV	Subcritical design optimisation and critical operation
High-power density core → Safety "ULOF"	Low-power density core	Low-power density core	
Low core power 52 MW	Low core power 57 MW →	High core power 85 MW	
Neutron flux 10^{15} n/cm²s (>0.75 MeV)	Neutron flux $7 \cdot 10^{14}$ n/cm²s (>0.75 MeV)	Neutron flux 10^{15} n/cm²s (>0.75 MeV)	

Project schedule and budget

At the end of the EUROTRANS project, for which MYRRHA serves as the basis, in March 2010, the conceptual design of the machine and of its different components will be available. During the period 2010-2014, the following tasks will be accomplished in parallel:

- The detailed engineering design, part of this design work will be performed through the FP7 project, CDT and continued until 2014.
- Drafting of the technical specifications of the different procurement packages, publication of the call for tenders, comparison of the technical and financial proposals from the contractors and finally the awarding of the manufacturing contracts (2014-2015).
- Development and testing of key innovative components (for the accelerator and for the reactor) will run in parallel during the same time period.
- Licensing and permitting activities, namely the writing of a preliminary safety assessment report, the environment impact assessment report and the preliminary dismantling plan, the objective being to obtain the licensing permit and permit for construction at the end of 2014.

The construction of the components and the civil engineering work is to be accomplished over a three-year period (2016-2018), followed by one year of assembly (2019). Commissioning at progressive levels of power will be accomplished over a three-year period (2020-2022) with the final objective to be in full power operation by 2023.

In the design and licensing of MYRRHA both modes of operation are foreseen from the beginning. A minimum of three years preparatory period is considered for the progressive commissioning of the facility which will include both operation modes.

To obtain an answer concerning the viability of the ADS concept in an international context as soon as possible, thereby allowing evaluation of the realism of subcritical burners in a double strata fuel cycle approach, it was opted to start in MYRRHA with the demonstration of ADS and hence the full power coupling with an accelerator. The MYRRHA facility is thus projected to be initially operated as an ADS in subcritical mode for the demonstration of the full power ADS operation and the efficient transmutation of minor actinides (with available fuels). During this period, MYRRHA will also be used as a flexible fast spectrum irradiation facility with the applications catalogue as described previously. It is also envisaged to deflect a small part (about 5% of the nominal beam) for nuclear physics applications at the proton accelerator.

Up until now, all flexible irradiation facilities have been operated very efficiently in critical mode. Working efficiently and reliably in subcritical mode introduces heavy constraints on the accelerator. Since working in critical mode is not conditioned by this fact, it might be advantageous to work in critical mode. The facility will then be converted into a critical fast spectrum irradiation facility based on heavy liquid metal coolant technology by separating the accelerator from the reactor, by removing the spallation source and adding fuel assemblies to reach criticality. The entire accelerator facility can then be used for nuclear physics applications by the user club of Belgian and other universities.

In the central positions, which hosted the spallation source, an in-pile section with a maximum high flux can be inserted. MYRRHA will from then on be operated as a flexible fast spectrum irradiation facility with the applications catalogue as described in the previous paragraph, except for the demonstration of the ADS concept. Further study of the efficient demonstration of minor actinides can be pursued in the critical MYRRHA and new minor actinide fuels can be tested and qualified.

Presently nearly all major research facilities built world wide are being conceived as open user facilities. Even the existing facilities that were built as national infrastructures are moving towards open-user organisations. This means that the research facility proposed is of interest for the international research community and is unique or having characteristics making it very attractive to a large number of researchers and users. This leads to the formation of an owner consortium group that develops and later on operates the facility.

Apart from the traditional sources of funding, e.g. the contribution of the owner consortium group members during the investment phase of the project and the endowment for the operation phase, SCK•CEN management, as the promoter of the project, intends to call on the recent financing facility jointly developed by the European Commission (EC) and the European Investment Bank (EIB) in support of higher risk financing of research infrastructures such as the MYRRHA infrastructure.

The total investment costs (in EUR 2009) have been estimated [11] at EUR 960 M, including direct investment (civil engineering, equipments, components, instrumentation and control, spare parts), detailed design, installation co-ordination and licensing, project management costs, support R&D programme and about EUR 192 M of contingencies on the direct investment cost.

Similarly the operational costs (in EUR 2009) amount approximately to EUR 46.6 M including the direct operational costs (labour for operations, fuel, waste management, provisions for dismantling, other operation linked services, contingency, financial costs) and the experiments' costs (labour for scientific experiments). A supplementary amount of about EUR 14.6 M should be foreseen for providing full support for technology and services development (reinforcing of internal organisation).

Figure 4: Investment and operational budgets (in EUR 2009)

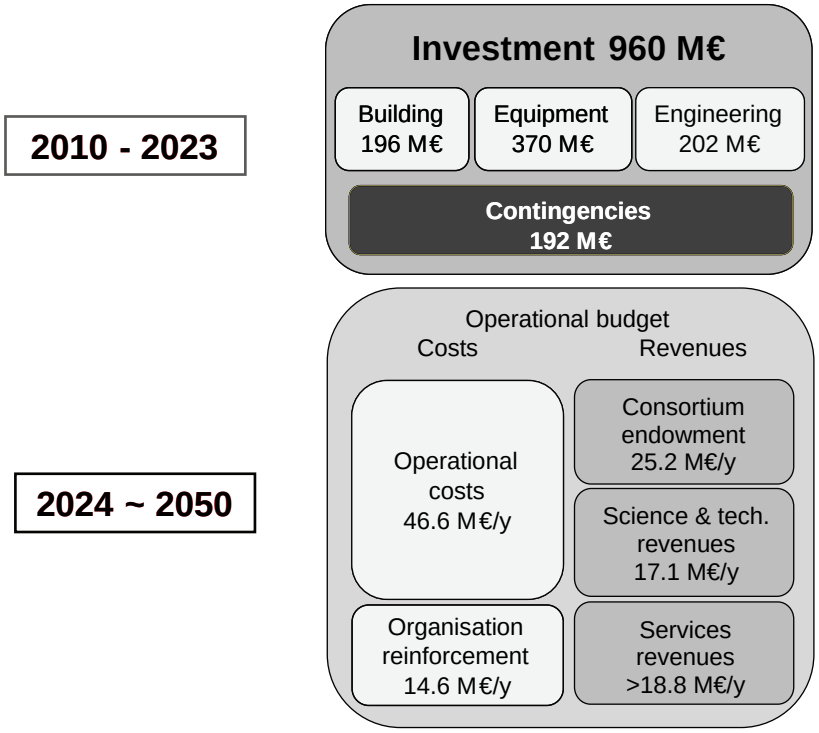

Conclusions

Europe aims to become the most competitive and dynamic knowledge-driven economy, as determined in Lisbon in March 2000, by encouraging and promoting research and innovation. In addition, Europe is also facing the challenges of its long-term sustainable development by use of non-CO_2 emitting energy technologies that can play a significant role in guaranteeing the energy independence of Europe.

SCK•CEN is proposing to replace its ageing flagship, the Material Testing Reactor BR2, with a new flexible irradiation facility MYRRHA. In view of its innovative character and its field of application MYRRHA contributes to the realisation of EU's goal towards a sustainable future.

MYRRHA is conceived as a flexible fast spectrum irradiation facility able to work in subcritical and critical mode. MYRRHA is foreseen to be in full operation by 2023 and it will be operated in the first years as an accelerator-driven system to demonstrate the ADS technology and the efficient demonstration of minor actinides in subcritical mode.

Afterwards it is intended to decouple the accelerator from the reactor and run MYRRHA as a critical flexible fast spectrum irradiation facility by removing the spallation target. As a fast spectrum irradiation facility, it will address fuel research for innovative reactor systems, materials research for Gen-IV systems and for fusion reactors, radioisotope production for medical and industrial applications, such as Si-doping. Being based on the heavy liquid metal technology, the eutectic lead-bismuth, MYRRHA will be able to significantly contribute to the development of lead fast reactor technology. Since MYRRHA will also be operated in critical mode, it can even better play the role of European technology pilot plant in the roadmap for LFR.

This project is intended to be organised as an international open user facility, constructed by an owner consortium made up of European and even larger research centres and European member states representative agencies or international bodies such as the European Commission.

Acknowledgements

The XT-ADS design work was performed under the Integrated Project EUROTRANS (Ref. FI6W-CT-2004-516520) co-funded by the European Union in its 6th Framework Programme. The FASTEF design work is being performed under the Collaborative Project CDT (Ref. FP7-232527) co-funded by the European Union in its 7th Framework Programme.

References

[1] BR2 reactor, *www.sckcen.be/en/Our-Research/Research-facilities/BR2-Belgian-Reactor-2*.

[2] Nuclear Energy Agency (NEA), *Accelerator-driven Systems (ADS) and Fast Reactors (FR) in Advanced Nuclear Fuel Cycles. A Comparative Study*, OECD/NEA, Paris (2002), ISBN 92-64-18482-1.

[3] NEA, *Physics and Safety of Transmutation Systems. A Status Report*, OECD/NEA, Paris (2006), ISBN 92-64-01082-3.

[4] PATEROS, Partitioning and Transmutation European Roadmap for Sustainable Nuclear Energy, FI6W – Contract Number 036418.

[5] European Commission (EC), *The Sustainable Nuclear Energy Technology Platform. A Vision Report*, EUR 22842.

[6] EC, "Strategic Research Agenda of the Sustainable Nuclear Energy Technology Platform", *www.snetp.eu* (2009).

[7] US DOE Nuclear Energy Research Advisory Committee, *A Technology Roadmap for Generation IV Nuclear Energy Systems*, GIF-002-00 (2002).

[8] Aït Abderrahim, H., P. Kupschus, *MYRRHA, A Multipurpose Accelerator Driven System (ADS) for Research & Development, March 2002 Pre-design Report*, Report prepared for reviewing of the project by the International Technical Guidance Committee, SCK•CEN Report R-3595, HAA-PK/svg.32.B043000 85/02-64, March (2002).

[9] Aït Abderrahim, H., *et al.*, *MYRRHA Pre-design File – Draft-2*, SCK•CEN Report R-4234 (2005).

[10] Aït Abderrahim, H., D. De Bruyn, *et al.*, *MYRRHA Project – Technical Description*, SCK•CEN Report ANS/HAA/DDB/3900.B043000/85/07-17bis, 57 pgs., April (2007).

[11] Aït Abderrahim, H., *et al.*, *The MYRRHA Project, Science Towards Sustainability, Business Plan 2010*, SCK•CEN report ANS/HAA/OVdB/3900.A0B043000-00/85/10-06.

[12] Mansani, L., *et al.*, "The Designs of an Experimental ADS Facility (XT-ADS) and of a European Industrial Transmutation Demonstrator (EFIT)", these proceedings.

[13] Nishihara, K., *et al.*, *MYRRHA Update for High Performance*, SCK•CEN internal report, ANS/KN/3910.B043000 85/08-19.

[14] Baeten, P., H. Aït Abderrahim, D. De Bruyn, "The Next Step for MYRRHA: The Central Design Team FP7 Project", *International Topical Meeting on Nuclear Research Applications and Utilization of Accelerators (AccApp09)*, Vienna, Austria, 4-8 May (2009).

The EUROTRANS Project: Partitioning and transmutation research in Europe*

Joachim U. Knebel
Karlsruhe Institute of Technology (KIT)
Programme Nuclear Safety Research (NUKLEAR)

Abstract

The Integrated Project EUROTRANS (European Research Programme for the Transmutation of High-level Nuclear Waste in an Accelerator-driven System) within the ongoing EURATOM 6th Framework Programme (FP6) is devoted to the study of transmutation of high-level waste from nuclear power plants. The work is focused on transmutation in an accelerator-driven system (ADS).

The objective of EUROTRANS is the assessment of the design and feasibility of an industrial ADS prototype dedicated to transmutation. The necessary R&D results in the areas of accelerator components, fuel development, structural materials, thermal-hydraulics, heavy liquid metal technology and nuclear data will be made available, together with the experimental demonstration of the ADS component coupling. The outcome of this work will allow to provide a fairly reliable assessment of technological feasibility and a cost estimate for ADS-based transmutation, and to possibly decide on the detailed design of an experimental ADS and its construction in the future.

EUROTRANS strengthens and consolidates the European research and development activities in transmutation. The involvement of universities strengthens education and training in nuclear technologies. The involvement of industries assures a market-oriented and economic design development and an effective dissemination of the results.

EUROTRANS is a five-year project which started in April 2005. The scientific and technical results produced by EUROTRANS are among others used by the FP6 Project ELSY (European Lead-cooled System), the FP7 Project CDT (Central Design Team for a Fast-spectrum Transmutation Experimental Facility) and the FP7 Project LEADER (Lead-cooled European Advanced Demonstration Reactor).

The paper gives selected results of the five scientific Domains of EUROTRANS, being:

- *A first advanced design of an Experimental Facility Demonstrating the Technical Feasibility of Transmutation in an Accelerator-driven System (XT-ADS), as well as a conceptual design of the European Facility for Industrial Transmutation (EFIT – realisation in the long term).*
- *Experimental results from experiments on the coupling of an accelerator, an external neutron and a subcritical blanket, being RACE and GUINEVERE.*
- *Achievements in linear accelerator components, fuels, structural materials at medium to high temperature and high radiation exposure conditions, thermal-hydraulics, heavy liquid metal technologies and measurement techniques, and nuclear data.*

* The full paper being unavailable at the time of publication, only the abstract is included.

Special Session

EUROTRANS

Chair: A.C. Müller

Achievements and lessons learnt within the Domain 1 "DESIGN" of the Integrated Project EUROTRANS

Didier De Bruyn[1], **Hamid Aït Abderrahim**[1], **Gérald Rimpault**[2], **Luigi Mansani**[3], **Marco Reale**[3], **Alex C. Müller**[4], **Arnaud Guertin**[4], **Jean-Luc Biarrotte**[4], **Janne Wallenius**[5], **Carmen Angulo**[6], **Alfredo Orden**[7], **Alan Rolfe**[8], **Dankward Struwe**[9], **Michaël Schikorr**[9], **Antony Woaye-Hune**[10], **Carlo Artioli**[11]

[1]Belgian Nuclear Research Centre, Mol, Belgium; [2]Commissariat à l'énergie atomique (CEA), Cadarache, France; [3]Ansaldo Nucleare, Genova, Italy; [4]Centre National de la Recherche Scientifique (CNRS), Paris, France; [5]Kungliga Tekniska Högskolan, Stockholm, Sweden; [6]Tractebel Engineering S.A., Brussels, Belgium; [7]Empresarios Agrupados, Madrid, Spain; [8]Oxford Technology Ltd, Abingdon, United Kingdom; [9]Karlsruher Institut für Technologie (KIT), Karlsruhe, Germany; [10]AREVA, Lyon, France; [11]Ente per le Nuove Technologie, l'Energia e l'Ambiente (ENEA), Italy

Abstract

The present communication focuses on the global achievements in the different sectors of the "DM1 DESIGN" domain of the Integrated Project EUROTRANS and on the remaining topics to be further developed. Special attention is paid to the lessons learnt from this large Integrated Project; as a total of 23 partners (from research centres but also industrial partners), coming from 10 different countries, participated in our domain "DM1 DESIGN".

Introduction

The implementation of partitioning and transmutation of a large part of the high-level nuclear wastes in Europe needs the demonstration of the feasibility of several installations at an "engineering" level. This is the general objective of the Integrated Project EUROTRANS. More in detail, the overall objectives of IP EUROTRANS, launched in April 2005 for a duration of five years, are:

1) to perform a first advanced design of a short-term, short-scale (50-100 MW_{th}) Experimental Facility Demonstrating the Technical Feasibility of Transmutation in an Accelerator-driven System (XT-ADS), as well as accomplish a generic conceptual design of the long-term, larger-scale (several hundreds MW_{th}) European Facility for Industrial Transmutation (EFIT);
2) to provide validated experimental input on the coupling of an accelerator, a spallation target and a subcritical blanket;
3) to develop and demonstrate the necessary associated technologies, especially reliable linear accelerator components, fuels development, heavy liquid metal (HLM) technologies and the required nuclear data;
4) to prove the overall technical feasibility of the transmutation facility;
5) to carry out an economic assessment of the whole system.

The project is integrating critical masses of resources and activities, including education and training efforts, within the industry, the national European research centres and the European universities. The technical works within the project have been divided into five sub-projects, also called "domains". The "DM1 DESIGN" domain is fully involved in objectives 1), 4) and 5) described above and is also involved in the accelerator components of objective 3).

The short-term XT-ADS machine uses lead-bismuth eutectic (LBE) as core coolant and target material, while the longer-term EFIT has a pure lead target and reactor coolant, gas being the back-up solution for the core cooling. Both systems are developed using the same principles in order to assess the scale effects regarding safety, performance and costs.

Domain organisation

The activities within the domain "DM1 DESIGN" have been divided into six work packages (WP):

- definition of reference design specifications, this work package also being in charge of submitting the synthesis report of the whole domain;
- primary systems, core designs and plant layout, also including remote handling;
- development of accelerator components, from the injector to the high-energy part;
- spallation target proof of feasibility;
- safety assessment, including containment and source term definition;
- cost estimate and planning issues.

Several of these activities are described more in detail in separate communications (oral or posters) during the present workshop.

We decided very early in the project to have only one annual meeting where all partners of the domain would be invited. The reporting from the work packages could be organised task by task, if the WP leader wishes. We also felt the necessity in such a project to have an intermediate meeting but for a limited group of individuals that we called the "Co-ordination Committee". All WP leaders were present, but also task leaders having a significant impact on the whole process of the domain.

Overview of the activities

The objective of "DM1 DESIGN" is to proceed by a significant jump towards the demonstration of the industrial transmutation through the ADS route. This is carried out with two interconnected activities that form together the strategy of European Transmutation Demonstration (ETD).

The first activity is to carry out an advanced design leading to the short-term XT-ADS, i.e. the construction of the facility starting at least within the next eight years. The total power level of the XT-ADS ranges between 50 and 100 MW_{th}. This facility is intended to be as much as possible a test bench for the main components and for the operation scheme of the longer-term EFIT, but at lower working temperatures thanks to the use of LBE as core coolant and spallation target material. The initial loading of XT-ADS is made with standard MOX fuel, but it is designed to handle a full minor actinide (MA) fuel assembly in representative irradiation conditions in terms of dpa and burn-up of the EFIT machine. Already in the beginning of the EUROTRANS project, SCK•CEN offered to use its MYRRHA 2005 design file, developed internally, as a starting basis for the XT-ADS design. This allowed optimising an existing design towards the needs of XT-ADS and within the limits of the safety requirements instead of starting from a blank page [1,2].

The second activity is the development of the conceptual design of the EFIT with a power of up to several hundreds MW_{th}. Design features are worked out to a level of detail which allows a parametric cost estimate of the machine and safety studies for the ADS-based transmutation. The reactor coolant and the spallation target material are pure lead [3-5]. Both designs (XT-ADS and EFIT) bear the same fundamental system characteristics in order to allow for scalability considerations between them [6]. Gas as coolant is chosen as a back-up solution for the core cooling of the EFIT. The gas back-up activity is however limited to core studies and safety analysis.

The development of the associated accelerator that will be serving for the XT-ADS as well as for the EFIT focuses on the improvement of the beam reliability as this is one of the key issues in order to achieve a high availability factor for the transmutation facility [7]. The work on the accelerator is dedicated to the experimental testing of the linear accelerator main components' reliability, being the "full scale" injector with a 1 MW proton beam, the intermediate energy section, and a "full scale" accelerating module of the high-energy section.

The design of the spallation source is concentrated on XT-ADS in terms of thermo-mechanical, thermal-hydraulic, nuclear assessment and vacuum designs [8]. Within this project, the windowless design is the option investigated. On the other hand, the spallation target design activity related to the EFIT is included in the generic primary system design and is based essentially on the work accomplished during previous projects.

For safety, the reassessment of the global safety approach for ADS developed during FP5 is carried forward, but is now applied to a core heavily loaded with MA in the EFIT case. In particular the design based conditions (DBC) and design extended conditions (DEC) transients analysis with emphasis on the XT-ADS core have been conducted. The assessments of the containment analysis taking into account the radiological source term are carried out for the XT-ADS as well as for EFIT. In the case of XT-ADS, polonium release is also taken into account. The development of the pertinent parts of the safety analysis report (SAR) and preparation of the inventory of the information required by the licensing authorities in view of licensing the XT-ADS is also included in the work to be done in this part of the project.

A cost estimate of the XT-ADS has been performed and consideration has been given to the scale effect for the larger EFIT in terms of investment, operational costs and needed R&D efforts.

Major achievements

Coherent designs have been obtained for both EFIT and XT-ADS. Both machines achieve, with a reasonably good level of performance, their own objectives with an improved level of safety [9].

The Pb-EFIT has been designed so as to accomplish its transmutation objective efficiently. Improving the design is bound to breakthrough in the cladding material technology. For instance, in order to deploy more easily these plants in double strata scenario for which it has been designed, reduction in heavy nuclide mass inventory is required. Also, increasing the U-free fuel burn-up (currently at 13.9% for MA and 0.7% for Pu) might be desirable to avoid frequent reprocessing and fabrication of the fuel.

The XT-ADS design has allowed reaching a flux level up to $\Phi_{>0.75MeV} = 0.66 \times 10^{15}$ n.cm^{-2}.s^{-1}, the best that could be achieved considering the design constraints: the core power has been limited to 57 MW_{th} and uses a reduced Pu content (30 wt.%), the LBE temperature increase across the core is rather small (100°C), as is the case for the core pressure loss across the core (this allows for a rather passive safety) and finally we have to take into account the presence of eight irradiation positions.

A reliability-oriented superconducting linac was identified as the reference solution for the European ADS concept, and an advanced design of the 600 MeV machine was proposed in the XT-ADS/MYRRHA case. It is composed of a 17 MeV injector, possibly doubled, followed by independently-phased modular superconducting cavities with fault tolerance capability. A huge R&D effort was performed during the project, with very successful results and conclusions [7].

In the reference design of the target, all active components (pumps, heat exchanger, chemistry control, vacuum system,…) are positioned away from the central axis of the core where radiation levels are lower and more space is available. Only the spallation zone itself is kept in the centre of the core. There is no structural material that separates the flowing LBE in the spallation zone and the vacuum of the beam line, hence the name "windowless spallation target". In the different design support studies that have been performed no showstopper was identified. These include the spallation target zone and spallation loop thermal-hydraulics, system dynamics, beam impact studies, neutronics, mechanical integration and safety analyses.

Results of consequence analyses of representative accidents belonging to DBC and DEC categories demonstrated that both EFIT and XT-ADS are a very robust and forgiving design ascribable to the unique combination of inherent and dedicated plant design features (HLM coolant properties, moderate linear rating, subcritical operation, excellent natural convection). Most unprotected transients allow sufficient grace time (~30 minutes) before manual corrective actions are required; this is a major improvement when compared to the previous PDS-XADS FP5 results.

The construction cost of the whole XT-ADS facility has been estimated and compared to the SCK•CEN internal exercise (the "MYRRHA Business Plan"); the figures obtained in both cases for the so-called "base price", being the sum of direct and indirect costs, without any contingency, are remarkably close (EUR 767 M for the Business Plan versus EUR 784 M in the EUROTRANS approach) and that the main difference lies on the contingency level.

Further developments and road ahead

At the end of this EUROTRANS project, we may conclude that both the EFIT conceptual design and the more advanced XT-ADS design have complied with the main project requirements. Nevertheless, some technical solutions for achieving them remain to be confirmed and this is particularly true for the short-term XT-ADS. Additional R&D studies and qualifications are requested before advancing to the writing of tender specifications [10]:

- Accelerator availability, where significant improvement has been obtained, needs to be confirmed to operate over a long duration.
- Qualification of the core and primary circuit materials under LBE environment needs to be validated.

- Oxidation by lead stability and control in the whole coolant circuit is an awkward issue. An oxide layer is necessary to protect components against corrosion/erosion. The thickness of this protective oxide layer on the PHX must be validated and the conductivity value confirmed since it can have a significant influence on the component size.
- Qualification of the plant control system, especially the control of the subcriticality level, should be done.
- Design tools (computing codes, design standards) need to be qualified.
- Qualification of in-service inspection devices LBE and the qualification of the remote handling system are still open issues.

From a safety point of view, the available results obtained on the first confinement barrier (clad) and on fuel when the plant is subjected to severe unprotected transient (such as the unprotected loss of flow), indicate that the current LBE-cooled XT-ADS design seems quite viable. But the simplified assumptions retained for the natural flow rate during the transient may lead to underestimate the thermo-mechanical stresses on structures. Analysis has to be completed by more accurate calculation evaluations.

Attention also needs to be placed on the operational control of the oxygen content in the LBE coolant in order to control chemical fouling and the build-up of the oxide layer. Analyses have to be completed and checks have to be made on core support equipment, internals, reactor vessel and other remaining confinement barriers, the behaviour of which are not yet fully assessed under transient situations.

Finally the early available results on material characterisation, within the "DM4 DEMETRA" part of the EUROTRANS programme, confirm that the environmental effects induced by both irradiation level and LBE coolant are issues that cannot be neglected since they may have a strong impact on the safety justification.

Domain organisation experience

It was not obvious in the beginning of the EUROTRANS project, to organise the DM1 work between the 23 partners. We therefore decided to limit the meetings where all partners were invited to only one annual meeting. This decision has been a successful one, since the work packages, and sometimes also the tasks, have been organised in dedicated working meetings with a limited number of partners being present.

The set-up of the Co-ordination Committee, as mentioned in the beginning of this communication, was in such a context the compulsory link between the work packages, where global coherency could be, and indeed has been, guaranteed.

Conclusions

Significant improvement has been obtained for both the long-term EFIT and the short-term XT-ADS. A more advanced design has been obtained for the accelerator components, with a clear focus on the expected reliability. The results obtained in DM1 DESIGN are a valuable set of data for further studies.

Acknowledgements

DM1 DESIGN work has been performed under the Integrated Project EUROTRANS (Ref. FI6W-CT-2004-516520) co-funded by the European Union in its 6th Framework Programme. Thanks are due to all the colleagues of the participant institutes for their contributions to many different topics.

References

[1] Aït Abderrahim, A., P. D'hondt, D. De Bruyn, "MYRRHA, a New Fast Spectrum Facility", *Seminar on Fission – Corsendonck Priorij*, 18-21 September 2007, Proceedings April 2008, World Scientific, ISBN 978-981-279-105-4, pp. 207-221 (2008).

[2] De Bruyn, D., *et al.*, "From MYRRHA to XT-ADS: The Design Evolution of an Experimental ADS System", *AccApp'07 Conference*, Pocatello, Idaho, 30 July-2 August 2007, pp. 848-854 (2007).

[3] Barbensi, A., *et al.*, "EFIT: The European Facility for Industrial Transmutation of Minor Actinides", *AccApp'07 Conference*, Pocatello, Idaho, 30 July-2 August 2007, pp. 885-892 (2007).

[4] Artioli, C., *et al.*, "Optimization of the Minor Actinides Transmutation in ADS: The European Facility for Industrial Transmutation EFIT-Pb Concept", *AccApp'07 Conference*, Pocatello, Idaho, 30 July-2 August 2007, pp. 560-567 (2007).

[5] Artioli, C., "Minor Actinides Burning in the 42-0 Concept: The EU 'EFIT' (European Facility for Industrial Transmutation) ADS", *International Conference on Peaceful Uses of Atomic Energy*, New Delhi, 29 September-1 October (2009).

[6] Mansani, L., "The Designs of an Experimental ADS Facility (XT-ADS) and of an European Industrial Transmutation Demonstrator (EFIT)", these proceedings.

[7] Biarrotte, J-L., A.C. Müller, "Accelerator Reference Design for the European ADS Demonstrator", these proceedings.

[8] Guertin, A., *et al.*, "XT-ADS Windowless Spallation Target Design and Corresponding R&D Topics", these proceedings.

[9] De Bruyn, D., *et al.*, "Accelerator Driven Systems for Transmutation: Main Design Achievements of the XT-ADS and EFIT Systems Within the FP6 IP-EUROTRANS Integrated Project", *International Congress on Advances in Nuclear Power Plants (ICAPP'10)*, San Diego, CA, USA, 13-17 June (2010).

[10] Baeten, P., H. Aït Abderrahim, D. De Bruyn, "From MYRRHA/XT-ADS to MYRRHA/FASTEF: The FP7 Central Design Team Project", *International Conference on Fast Reactors and Related Fuel Cycles: Challenges & Opportunities (FR09)*, Kyoto, Japan, 7-11 December (2009).

EUROTRANS/ECATS or neutronic experiments for the validation of XT-ADS and EFIT monitoring

G. Granget[1], H. Aït Abderrahim[2], P. Baeten[2], C. Berglöf[7], A. Billebaud[3], E. González-Romero[4], F. Mellier[1], R. Rosa[6], M. Schikorr[5]

[1]Commissariat à l'énergie atomique (CEA Cadarache), France; [2]Belgian Nuclear Research Centre (SCK•CEN), Belgium; [3]Centre National de la Recherche Scientifique (CNRS/IN2P3), Grenoble, France; [4]Centro de Investigaciones Energéticas, Medioambientales y Tecnológicas (CIEMAT), Spain; [5]Forschungszentrum Karlsruhe (FZK), Germany; [6]ENEA, Casaccia, Italy; [7]Department of Reactor Physics, Royal Institute of Technology, Stockholm, Sweden

Abstract

Within the 6th Framework Programme the Domain 2 "Experiments on the Coupling of an Accelerator, a Target and a Subcritical Blanket" (ECATS) of EUROTRANS is devoted to neutronic experiments for the demonstration of the conceptual feasibility of an accelerator-driven system (ADS).

The DM2 objectives were specified in full consultation with the design team of the "Domain 1 DESIGN" which is developing a reference design for a long-term European Facility for Industrial Transmutation (EFIT) together with a more detailed design for a short-term Experimental Demonstration of the Technical Feasibility of Transmutation in an Accelerator-driven Subcritical System (XT-ADS). After recollection of the ECATS objectives expected by DOMAIN 1, progress and first assessments coming from the RACE and YALINA results are presented and the first stage of the GUINEVERE experimental programme is also detailed.

Objectives of EUROTRANS/ECATS

Within the 6th Framework Programme, the Domain 2 "Experimental Activities on the Coupling of an Accelerator, a Target and a Subcritical Blanket" (ECATS) in the Integrated Project EUROTRANS, is devoted to neutronic experiments for the demonstration of the conceptual feasibility of an accelerator-driven system (ADS). The DM2 objectives were specified in full consultation with the design team of the "Domain 1 DESIGN" which is developing a reference design for a long-term European Facility for Industrial Transmutation (EFIT) 400 MWth, together with a more detailed design of a short-term Experimental Demonstration of the Technical Feasibility of Transmutation in an Accelerator driven Subcritical System (XT-ADS) 80 MWth [18].

As far as the reactivity control is concerned, the effective multiplication factor, K_{eff}, independent of the external neutron source strength, is a meaningful measure of the actual safety characteristic of the system. That is, $\rho = (K_{eff} - 1)/K_{eff}$, which is the reactivity of the system and the gauge of the distance from criticality. Hence, prevention of reactor power divergence is achieved if the effective multiplication factor is maintained below one. In fact during the refuelling period, regulatory rules are requiring that K_{eff} should not be larger than 0.95. This penalty is acceptable for the XT-ADS design (penalty reduced by the high importance of the source in this case) but not for the ETD/EFIT design because of adversary constraints associated to the size of the spallation module and to the size of the core. It is of prime importance to design a protocol in order to ensure that the reactivity limit in operation is never reached with an associated reliable and accurate measurement. Since two reactivity values are necessary, moving up from the low maximum reactivity used during the refuelling periods to the higher reactivity value used during the operating conditions should be performed by some means such as the removal of an absorbing element (either handled by the standard subassembly loading machine or by a dedicated mechanism). The 0.05 distance from criticality is currently judged to be adequate for the controlled and continuously monitored operations involved in refuelling of the reactor [21]. For an ADS, variations in the total power level can be considered as arising from two independent contributions which are the subcriticality level and the source strength. The absence of natural feedback effects between the subcritical core and the spallation source requires, in order to maintain the XT-ADS at a fixed power level, to compensate for the reactivity changes occurring in the core by equivalent interventions on the source strength. The actions for maintaining the pre-set power level shall be necessarily based on instrumentation readings from the core and the core cooling system. In order to avoid malfunction and/or overshooting of the source intensity control, which could trigger overpowers and/or oscillations in the core, the source controlling rate should be restricted below a maximum value. Also important and very much associated with the safety philosophy of an ADS (and furthermore to the experimental aspect of the XT-ADS) is the monitoring of the reactivity of the core. It is clear from the beginning that ADS with high minor actinide content has been promoted as being safe as concerns reactivity excursions significantly lower than the subcriticality level. On-line reactivity measurements are important in order to control and ensure that the subcriticality level is below the value considered for the safety analysis. The current-to-power relation can be used for monitoring but it must be normalised to give the reactivity level with the interim calibration techniques.

After the second feasibility study [1], five requirements coming from Domain 1 EUROTRANS/ DESIGN are expressed: qualification of subcriticality monitoring; validation of the core power/beam current relationship; start-up and shutdown procedures, instrumentation validation and specific dedicated experimentation; interpretation and validation of experimental data, benchmarking and code validation activities; safety and licensing issues of different components and for the integrated system. Different experiments were considered to validate these topics and the domain was established to take maximal advantage of the different experiments and displayed into Work Packages (WP). The results are surveyed according to the order of the WP: YALINA, RACE and GUINEVERE.

The YALINA experiments

Description of the YALINA-Booster facility and first reference

The YALINA-Booster is a subcritical fast thermal core coupled to a neutron generator [2]. The neutron generator uses a deuteron ion accelerator impinging on a Ti-T target to produce 14 MeV neutrons. The maximum beam current in quasi continuous mode is around 1.5 mA giving a maximum neutron yield of approximately 10^{11} n/s. A ^{252}Cf neutron source with intensity of 2.56×10^6 n/s was also available for the experiments. The central fast spectrum lead zone and the thermal spectrum polyethylene zone are separated by a so-called thermal neutron filter, or valve zone, consisting of one layer of metallic natural uranium and one layer of boron carbide (B_4C), which are located in the outermost two rows of the fast zone. Three B_4C-control rods can be inserted in the thermal zone for changing the reactivity of the system by about 0.5$. The fuel in the innermost part of the booster zone could be uranium oxide of 36% enrichment or metallic uranium of 90% enrichment, whereas the rest of the fast booster zone consisted of 36% enriched uranium oxide fuel. The thermal zone was loaded with uranium oxide of 10% enrichment.

Figure 1: Schematic view of the core

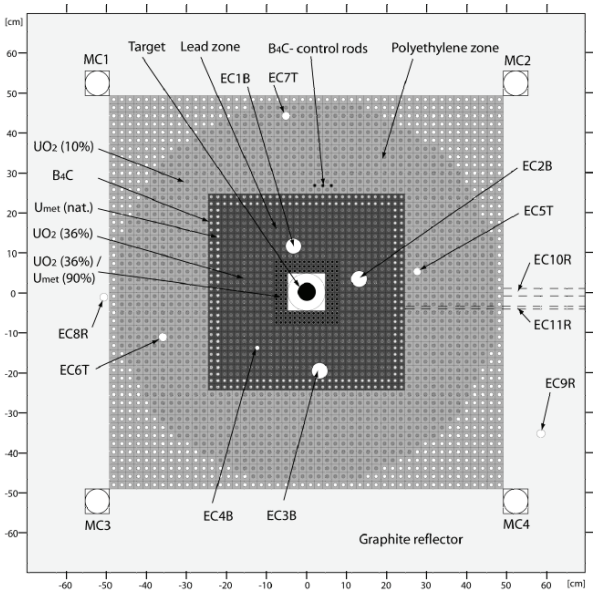

Table 1: Core configurations studied

	Zone and fuel enrichment				MCNP k_{eff}
	Inner booster 90%	Inner booster 36%	Outer booster 36%	Thermal zone 10%	
SC0	132	–	563	1 141	0.977
SC3a	–	132	563	1 077	0.950
SC6	–	132	563	726	0.850

The main neutronics parameters of this first reference assembly were measured. Among the measurements, spectral index $\overline{\sigma}_f\left(^{238}U\right)/\overline{\sigma}_f\left(^{235}U\right)$ along the fuel rod in the centre of the 36% zone was achieved with solid state track detector technique, exhibiting the filter shown in the figure and table below.

Figure 2: $\overline{\sigma}_f\left(^{238}U\right)/\overline{\sigma}_f\left(^{235}U\right)$

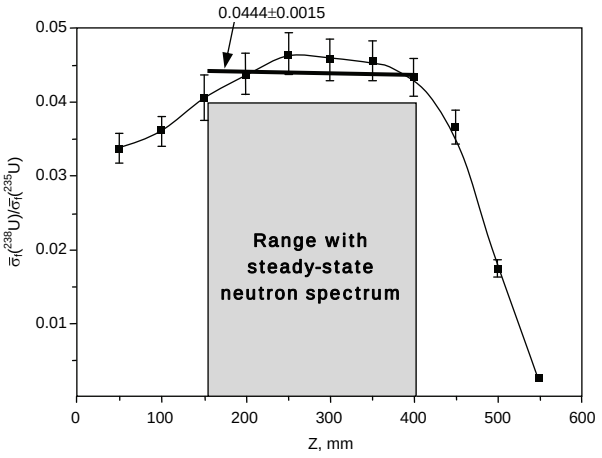

Table 2: Kinetic parameters of configuration SC0

Parameter	YALINA-Booster
K_{eff}	0.97943
α	-470 s^{-1}
Λ	56 μs
β_{eff}	738 pcm

YALINA results

Calibration techniques and current to flux measurements [8]

As mentioned above, during a beam trip, we can also apply the prompt decay constant method to determine the reactivity value. From the point kinetic model we can extract the following expression for the reactivity expressed in units of β:

$$\alpha = \frac{\rho - \beta}{\Lambda} \Rightarrow \frac{\rho}{\beta} = \frac{\beta}{\Lambda}\alpha + 1$$

where α is the prompt neutron decay constant that can be determined experimentally by fitting the decay of the prompt neutron population with an exponential. The values of Λ and β can be computed. The analysis of the prompt decay constant during a beam trip is complicated by the large fraction of delayed neutrons, and to the low statistics that can be achieved using small binning time.

Table 3: Prompt decay constant results for SC3a

Detector	Control rods extracted		Control rods inserted	
	α_{PNS} (s^{-1})	α (s^{-1})	α_{PNS} (s^{-1})	α (s^{-1})
EC1B	-1 039 ± 12	-1 055 ± 28	-1 103 ± 5	-1 155 ± 42
EC2B	–	-1 054 ± 19	-1 101 ± 3	-1 175 ± 29
EC5T	-1 061 ± 13	-930 ± 51	-1 101 ± 24	-1 146 ± 51

The prompt decay constant method with beam trips provided coherent results with the PNS and the agreement is even better than 10% and the effect of the control rods (~$/2) is well established. These values are not corrected for spatial effect of detector locations and of the

effect of the source intensity appeared in other results. The reactivity was also determined by the PNS techniques with reduced statistical uncertainties but with a reduced coherency due mainly to the spatial effect. The current mode of detection with beam trip was also tested with success to follow the reactivity effect of the control rods.

Neutron noise measurements Rossi-α and Feynman-α [9]

A set of neutron noise measurements was achieved in the three configurations mentioned above. The neutron noise measurements were performed with a ^{252}Cf neutron source located in the centre of the core with the neutron generator beam tube still in place. The neutron flux was measured by two ^{3}He-detectors located in EC5T and EC6T respectively. In the fitting procedure of the Rossi-α data, it was found that three exponentials are needed to obtain a good fit for configuration SC0 and SC3a and two exponentials for configuration SC6. The contribution of the delayed neutrons was found negligible. The results from the fittings are summarised in the table.

Table 4: Results from the fittings

Case	EC	Conf	CR	Source	α_2 [s^{-1}]	α_1 [s^{-1}]	α_0 [s^{-1}]
1	EC5T	SC0	Out	INK5	-11 340 ± 426	-2 442 ± 50	-674 ± 10
2				INK7			
3		SC3a	In	INK7			-1 094 ± 77
4			Out	INK5			-1 114 ± 8
5		SC6	Out	INK7		–	-3 094 ± 113
6	EC6T	SC0	Out	INK7	-6 821 ± 251	-2 656 ± 71	-746 ± 115
7		SC3a	In	INK7			-1 156 ± 86
8			Out	INK5			-1 163 ± 7
9		SC6	Out	INK7		–	-3 042 ± 62

In the Rossi-α analysis of the data, it was found that there exist two higher eigenmodes in addition to the fundamental mode. The higher eigenmodes made the fitting procedure cumbersome and obtaining good results of the fundamental mode was challenging. For the deepest subcritical configuration SC6 one higher eigenmode coincides with or is close to the fundamental mode, thus causing problems in obtaining a good value of the fundamental mode. Although long measurement times were spent giving low statistical uncertainties in the experimental data, the accuracy of the fundamental mode after fitting was not high enough to be able to observe a reactivity difference of 0.5$. Other coherent results were obtained according to the Feynman-α formula (as the ratio variation of the variance of the counts to the mean value); they present the same features in terms of alpha modes.

The RACE experiments

The RACE experiments at low power (LP) were operated in two different facilities: the TRIGA reactor of the ENEA Casaccia named "RACE-T" and the RACE LP/IAC subcritical assembly of the Idaho Accelerator Center named "RACE-LP/IAC".

The RACE-T experiments

Description of the RACE-T facility

The TRIGA Mark II nuclear reactor of the ENEA is a pool thermal reactor having a core contained in an aluminium vessel and placed inside a cylindrical graphite reflector, bounded with lead shielding. The European experimental teams performing the different experiments operated in the February 2004-February 2006 period, on different core configurations [17]. In that period the

reactor operation was exclusively in subcritical conditions, with the exception of the critical reference core assessment at the beginning of the campaign where the maximum power was 50 W. This ensures that the burn-up of each fuel was constant through all measurements, allowing a whole comparison in the experimental data analysis and correction factor calculations. Two different neutron sources were used during the experiments: a pulsed generator and a ^{252}Cf source (0.4 MBq). Source jerk measurements were performed using a Fast Rabbit instrumentation system. The pulsed neutron generator accelerates deuterium ions onto a tritium target and produced 10^8 n/s 14.3 MeV neutrons, at maximal frequency (150 Hz).

Figure 3: Top view of the ENEA/TRIGA

Figure 4: Reference critical (REG rod at 50% insertion)

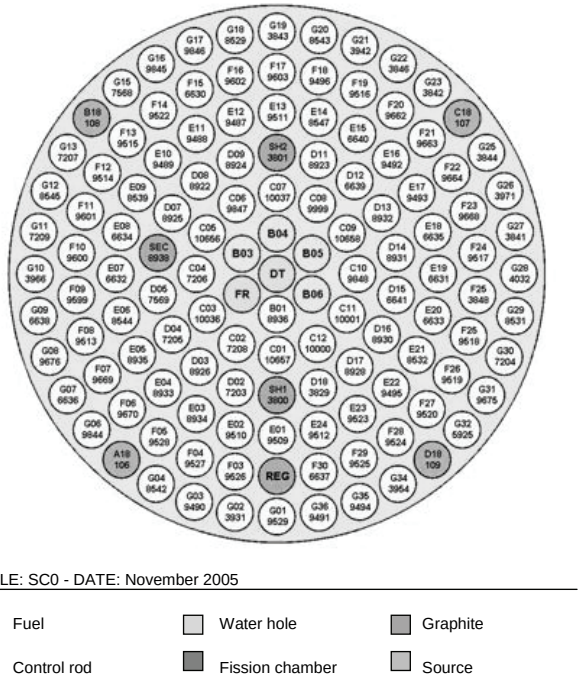

RACE-T results

The main RACE-T results reported in the EUROTRANS deliverables [3,5] are: the characterisation of the critical phase; the investigation of different subcritical configurations with D/T generator in the core centre and specific instrumentation and acquisition systems in order to determine the subcriticality and the relation current/power for ADS in a large scale of subcriticality were also tested in these experiments.

Characterisation of the critical phase performed by fission rate traverses

The radial traverses on the G13-G31 diagonal can be plotted on the same diagram, leading to the results displayed in the figure.

Figure 5: Normalised count rates on G13-G31 diagonal

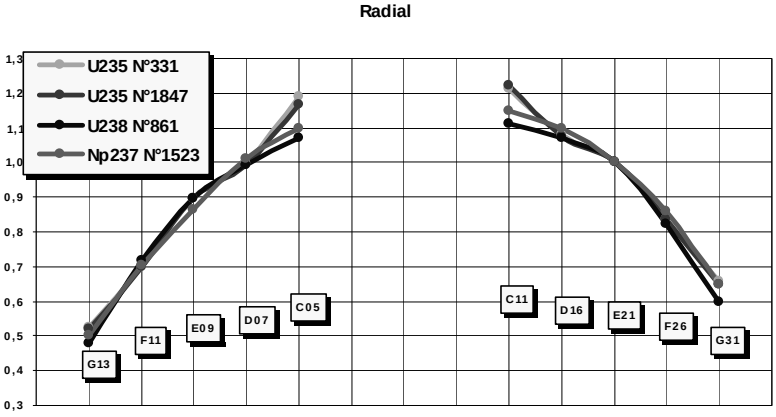

One observes the thermal flux tilt at the centre of the core, due to the local moderation from the water in the middle of the configuration and a strong dissymmetry in the diagonal for all the radial traverses, reaching up to 20% on the peripheral fuel pins due to the presence of a tangential voided beam tube in the reflector. Axial distribution were also extracted from Au and In foil measurements and the ratio of thermal and epithermal neutron fluxes were also measured by the technique of the cadmium ratio with Au and In samples. Fast neutron flux was measured with Al shuttles.

Experimental reactivity estimates of the three subcritical configurations of RACE-T

The efficiency of various experimental techniques for assessing a subcritical level was tested: the response to a pulsed neutron source; the transient due to a source jerk with ^{252}Cf (SJ-Cf) or by switching off the neutron generator (SJ-Gen); the transient due to a rod drop and MSA method. The reactivity was estimated with the various methods at four core locations and for the three different subcritical core configurations, namely SC0 (~ -500 pcm), SC2 (~ -2 500 pcm) and SC3 (~ -5 000 pcm).

Figure 6: Comparison of techniques for the SC0 configuration

PNS area-ratio method (PNS-Area), MSA method, source jerk method by switching off the neutron generator (SJ-Gen), source jerk method with ^{252}Cf source (SJ-Cf) (the error bars are for 95% of confidence)

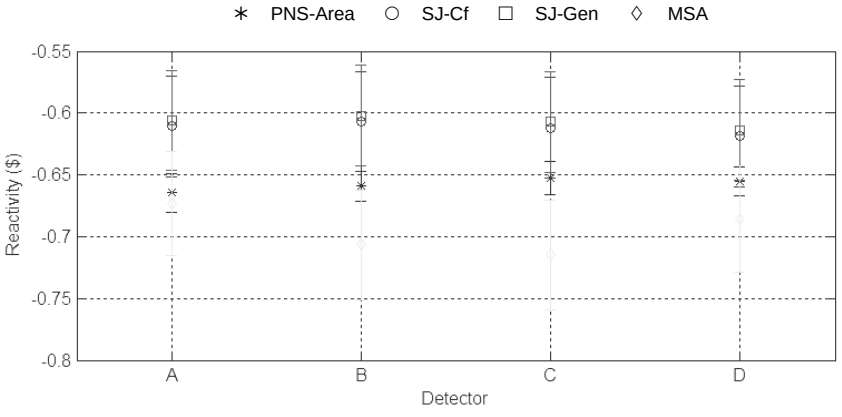

The area ratio method using a pulsed neutron source exhibits the best performance in terms of uncertainties and insensitivity to spatial effects (due to measurement or source location). Except the MSA, all the techniques agree in the range of 10% even for deeper subcriticality levels.

The source multiplication method, which requires for calibration critical state and therefore is not suitable for future ADS, is a well-established technique but needs large spatial correction factors far from criticality. The source jerk method (SJ-Cf) did not provide reliable results. A particular effort was sustained in the estimation of the TRIGA RC-1 fuel burn-up evaluation.

The RACE LP/IAC experiments

In the US, the first experiment of the RACE project was performed at the Idaho Accelerator Centre of the Idaho State University (ISU-IAC). The core of the ISU RACE subcritical assembly is constructed of 6 modular aluminium trays each containing 25 flat plates of 20% enriched uranium-aluminium alloy with aluminium-clad. The subcritical assembly is surrounded by a graphite reflector and water inside an aluminium tank that is ~1 m [6]. The K_{eff} of such a subassembly is typically in the range of 0.90.

The neutron source was created by electrons produced by a linac and impinging a water-cooled target (75% of W and 25% Cu). The neutron source intensity is ~ 10^9 n/s. The effective delayed neutron fraction was evaluated with MCNP by different methods, the best estimated value was equal to 768.4 ± 4.2 pcm. A methodology to calculate with MCNP the spatial correcting factors for the area ratio technique has been developed.

Figure 7: Horizontal view

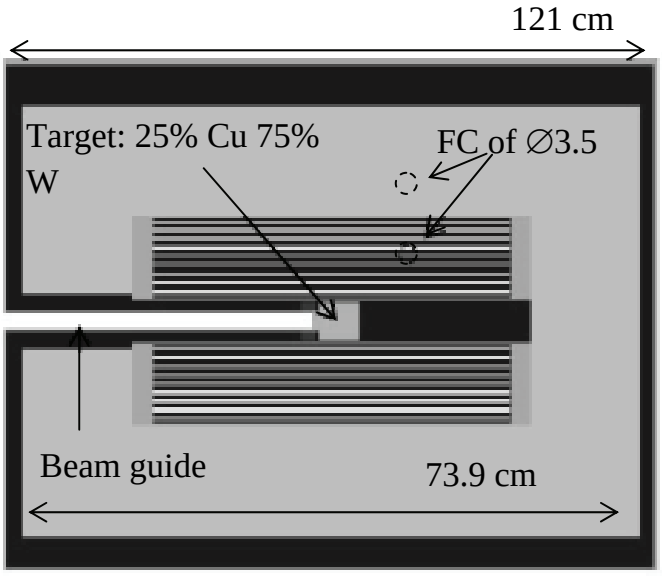

The transient techniques (inverse kinetic and non-linear fitting techniques) were also applied and corrected with MCNP, these corrective factors account for both source and spatial effects [7].

After corrections, the subassembly appears to be more subcritical than calculated. The area ratio method allowed obtaining smaller overall uncertainties of 2.5% at most after correction. The beam trip or transient techniques furnished less satisfactory results in terms of accuracy. That comes from the fact that the subassembly was so subcritical that the transient caused by the shutdown of the pulsed neutron source was too short to successfully perform a transient analysis with the inverse kinetics method.

Figure 8: Experimental reactivity estimates

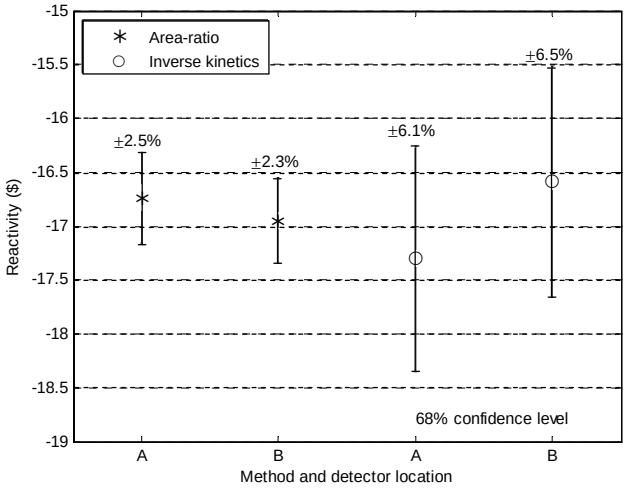

Survey of solid target design studies

Studies to design a target providing a neutron source of the order of ~10^{14} n/s, from a 20-25 MeV electron beam were also performed [4]. The objectives of the work were: the identification of the main design constraints (thermo-mechanics stresses); the guidelines to design a solid target based on a electron beam; the approach to the dimensioning of the target and cooling capability by calculations; the support to the RACE-ISU experiment (target at low power) by means of MCNPX calculations. These studies have permitted to clarify the main guidelines for the design of such targets.

The GUINEVERE experiments

In November 2006, the Scientific Consultancy Committee of EUROTRANS considered that the proposed GUINEVERE experiment would be an important added value concerning the validation of the monitoring of the ADS system. The final working plan of DOMAIN 2 was approved by the extraordinary Governing Council of EUROTRANS in December 2006. The necessary activities before the experiments concerned the modifications of VENUS, the construction of the GENEPI-3C accelerator and the safety considerations [19].

Figure 9: The GUINEVERE facility

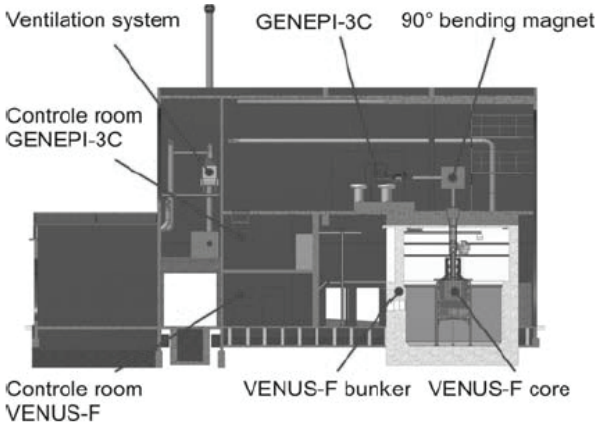

VENUS modifications

Two types of modifications were performed. First, modifications connected to the installation of the GENEPI-3C accelerator and its coupling to the core. The second type of modification is linked with the adaptation of the VENUS critical facility to host a fast lead core [10]. The licensing of the coupling was facilitated by the fact that the coupling of 14 MeV Pulsed Neutron Source has already been performed (1960-1970) at the VENUS reactor and the experience gained during the MUSE project.

Construction of GENEPI-3C

The GENEPI-3C neutron source is the third of a series of machines designed for reactor physics. It consists of a 250 keV deuteron accelerator producing neutrons by the $D(d,n)^3He$ or $T(d,n)^4He$ nuclear fusion reactions in a target.

The specifications are summed-up [11] in the table below.

Table 5: The GENEPI specifications

	Pulsed mode	Continuous mode
Beam energy	140 to 240 keV	140 to 240 keV
Peak current	40 mA	–
Mean current	190 μA at 4 700 Hz	160 μA to 1 mA
Pulse rate/beam trip rate	10 up to 4 700 Hz	0.1 Hz up to 100 Hz
Pulse FWHM/beat trip duration	700 ns	20 μs up 50 10 ms
Transition time on/off	–	1 μs
Spot size	20 mm in diameter	20 to 40 mm in diameter
Source intensity	8×10^9 n/s (4 kHz)	5×10^{10} n/s

The maximum beam intensity foreseen, in the continuous mode, is I_{max} = 1 mA. Higher current is not prohibited but it is limited by the target cooling capacity (to avoid fast tritium desorption and target support melting). The mean intensity commonly used during the MUSE experiment was 40 μA (pulsed mode at 1 kHz). The maximum continuous intensity foreseen is then 25 times higher. It will provide a source strength of about 5×10^{10} n/s (this value might vary in time as a function of the beam charge sent onto the target).

The intensity of the beam is adjustable in the range 160 μA-1 mA. For the purpose of the experimental programme, in the continuous mode, beam interruptions ("beam trips") can be performed. Two neutron source monitors will be installed: the first one is a silicone detector placed upstream from the target that will detect the alpha particles emitted in the T(d,n)4He reactions, the second will monitor directly the 14-MeV neutron at 180° thanks to a recoil proton telescope located above the vertical beam line.

Core specifications and experimental programme [12]

The effect of a lead buffer area, devoted to decrease the source neutron energy was investigated. Even if the effect of this buffer remains limited it was agreed to maintain the corresponding slowing-down of the neutron source. For the experimental programme [14], two configurations are foreseen: a clean critical core named CR0 without the accelerator and the corresponding subcritical configuration with the accelerator named SC1, obtained by the removal of the four central subassemblies. According to independent MCNP calculations the critical state will be reached with 88 assemblies with fuel corresponding to the pattern 5×5 with plates (82 fuels + 6 rods). The following measurements are planned to be carried out:

- Calibration of all control rod worths. These calibrations will be used to define the reference subcriticality for MSM method.
- Axial traverses by ^{235}U, ^{237}Np and ^{238}U fission chambers in dedicated channel of the experimental assembly. This experimental assembly will be placed in eight different co-ordinates of the layout.
- Radial traverses by $^{235}U/^{238}U$ foils.
- Spectral indices F238/F235, C238/F235, F239/F235, F237/F235, F240/F235, F242/F235 and F241/F235, in the core centre by activation foils and fission chambers simultaneously.
- β_{eff} measurements by CPSD and Rossi-α technique.

Figure 10: The final design and the main characteristics of the critical core

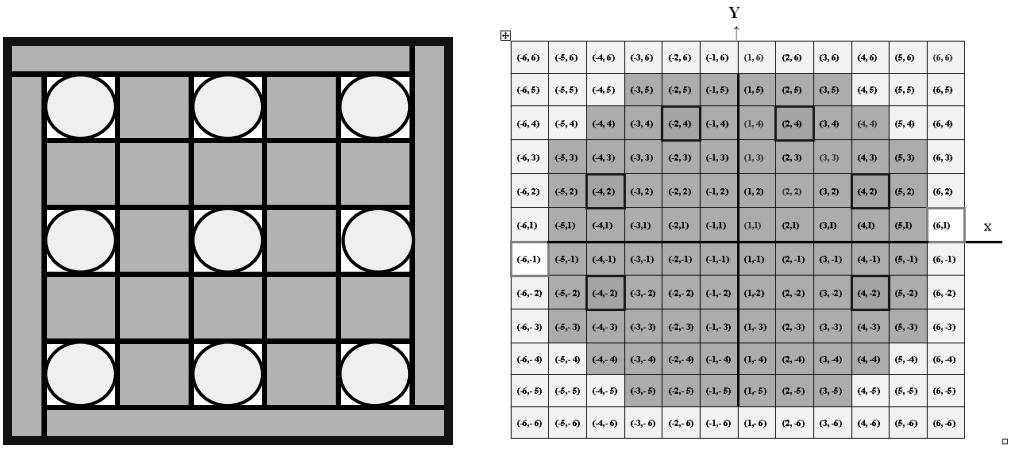

Fuel volumic content	17%
Spectrum hardness index	0.64
Critical mass	88 FA
Peripheral FA reactivity worth	248 pcm
K_{eff}	1.01031
β_{eff}	748 pcm
Λ (prompt neutron generation time)	$3.8 \cdot 10^{-7}$
Safety rod reactivity worth	14$
Control/pilot rod reactivity worth	1.2$

The SC1 configuration with a K_{eff} target value of ~0.97 will be driven by the GENEPI-3C accelerator source in pulsed, continuous wave and continuous wave with beam interruptions. The same measurements as for the CR0 will be performed concerning the calibration and the axial traverses. In addition, GENEPI-3C will be operated in the different modes for the experiments: PNS method, current-to-flux measurement and interim cross-checking techniques. Taking into account the time needed for fuel loading and changing the experimental devices, the necessary periods for fulfilling the experiments are 14 days for CR0 and 34 days for SC1.

Safety considerations

The GUINEVERE facility must satisfy the nuclear safety criteria required by the Belgian safety authorities to be licensed. The report [13] provides an overview of the GUINEVERE safety-related studies with emphasis on the safety aspects associated to the core physics, shielding, activation and thermal analyses.

A conservative scenario of reactivity insertions has been assumed and the reactivity coefficients relative to the envelope of core configurations have been calculated. Some configurations are hypothetical and not related to a realistic scenario, however they can serve as conservative guidance for the evaluation of a whole set of realistic scenarios.

Independent neutronic calculations have been performed by different institutions using the MCNPX Monte Carlo code and the deterministic ERANOS code package and one can conclude that the K_{eff} is estimated in a window of 2 000 pcm.

Different scenarios of reactivity insertions have been considered. These cases serve as a conservative envelope and it has been demonstrated that only the complete flooding of the core without integrity of the fuel assemblies cannot be compensated by the reactivity worth of the safety rods. However measures have been taken in the design of the fuel assemblies that should exclude water ingress and tests will be performed to show the effectiveness of such a design.

A physical model including thermal treatment and neutron point-kinetics calculations has been developed in order to evaluate the maximum rate of reactivity insertion that can be accepted in the GUINEVERE core. The temperature profiles in the VENUS-F core as well as in the reflector have been assessed both in steady state and transient conditions under the assumption that the cooling is provided by natural convection of the surrounding air. Results show that in both the cases of critical and subcritical core, the lead melting temperature will never be reached during all standard operating conditions, this being the most conservative safety criterion for the GUINEVERE analysis.

The complete neutron and photon dose mapping of the GUINEVERE building has been performed and results show that the modification of the VENUS-thermal into VENUS-F does not result in higher doses in the reactor and accelerator rooms. Also, the contributions to the total dose coming from the D-T and D-D reactions are negligible.

The calendar of the main milestones concerning the regulatory authority aspects of GUINEVERE is as follows:

- Derogation of the standard licensing procedures was obtained in May 2008.
- Positive preliminary advice from the Scientific Council to the FANC about the GUINEVERE project was obtained on June 2008.
- Positive final and definitive advice from the Scientific Council was obtained on 11 December 2009.

Conclusions

During the 6th FP, ECATS provided a large panel of results concerning the ADS monitoring but also the designs of facilities, accelerator and targets. New analysis methods and new results and theoretical considerations concerning the treatment of the harmonics with MCNP and deterministic neutronic codes can be noticed.

After MUSE [20], some guidelines were expressed:

- An on-line and continuous subcriticality monitoring should be established thanks to performing monitoring of the accelerator current, the intensity of the source and the power of the core.
- The comparison critical versus subcritical methods should be continued.
- The ability of different techniques for measuring the absolute subcriticality level should be confirmed. This ability should be robust and checked at different locations and different subcritical levels. The different correcting factors should be clarified (counter location, type of nuclear reaction used, with or without threshold). The uncertainties should be set.

The YALINA experiments allowed ensuring that techniques and analysis methods can be adapted to such complex core geometry. First experimental data with the current power technique were obtained and confirmed the interest of the approach. Nevertheless, more experiments would have been necessary for an uncertainty assessment. The main results are commented upon hereafter for the different techniques of reactivity measurements:

- *The pulsed neutron source area ratio technique*. The spatial spread was very large and reactivity results from different detectors could differ by a factor of two. A converged result could be obtained after applying Monte Carlo correction factors [8].
- *The beam trip technique*. The beam trip technique obeyed the same spatial dependence as the area ratio method. The major difference, however, is the mode of functionality. The beam trip method may be used as a reactivity monitoring method in a semi-continuous manner since the source is running in continuous mode with small interruptions for the reactivity measurement. This method gave the same results for detectors in pulsed and current mode operation.
- *The prompt decay fitting technique*. The prompt neutron decay measurements at various detector positions were found to be very close to one other. However, in the reflector a slightly slower decay was noticed. This effect became stronger at deep subcriticality.
- *The Rossi-alpha technique*. The neutron noise based Rossi-alpha method visualised the presence of two higher alpha-modes in addition to the fundamental mode. Most of the correlated events were occupied by the higher eigenmodes making the fundamental mode hard to obtain through fitting. As a result, the statistical accuracy in the fundamental mode was not high enough to be able to distinguish a reactivity difference of 0.5$. Consequently, to obtain good results when higher eigenmodes are present, an extremely long measurement time is needed, in particular at deep subcriticality.
- *The Feynman-alpha technique*. The Feynman-alpha method gave the same results as the related Rossi-alpha method, however, this method is much more sensitive to non-ideal circumstances such as non-stationary count rate and dead time effects. A consequence was that only one higher eigenmode could be obtained instead of two.
- *The current-to-flux technique*. This relative method is the only real monitoring technique since it can, in principle, be used at full power without beam interruptions. However, frequent beam interruptions will be necessary for intermediate calibrations. During the experiments, it was found that in addition to the beam current and the neutron flux, it is also necessary to monitor the neutron source strength and the position of the beam impact on the target to reach a full understanding of the process. The current mode electronic chain to monitor the neutron flux, the likely mode to be used in a power ADS, was also tested with success in YALINA.

During the RACE experiments consistent results with MUSE were encountered. In RACE-T, the area ratio method using a pulsed neutron source exhibits the best performance in terms of uncertainties and insensitivity to spatial effects (due to measurement or source location). The source multiplication method, which requires a calibration in a critical state and therefore is not suitable for future ADS is a well-established technique but necessitates a lot of heavy calculations for correcting factors often important far from criticality. In RACE-LP-ISU, the area ratio method allowed obtaining smaller overall statistical of 2.5% at most after correction and an appropriate work on statistical error treatment. The beam trip or transient techniques furnished less satisfactory results in terms of accuracy.

After the YALINA experiments, all the different subcritical methods for determining the reactivity can be managed. The first trials on the on-line monitoring are satisfactory and promising. An important step towards a better comprehension of the harmonics was reached and different correcting factors were produced with Monte Carlo codes. The discrepancies are

still of the same level as at MUSE, but a great part are due to the particular conditions: multi-region system and hard conditions of measurements. After the RACE experiments, the comparison between critical method (MSM method) and subcritical methods is still pending. The difficulties encountered with the calculations of correcting factors for these measurements are still to be addressed.

The GUINEVERE experiments were tailored considering MUSE feedback and conclusions. Core configurations, GENEPI-3C, materials and devices were designed to minimise all undesired effects and limitations observed during the previous programmes. The progress in the calculation domain and the combined use of Monte Carlo and deterministic codes should improve the understanding of the results and the uncertainty assessments.

The main challenges for GUINEVERE are: closing the comparison critical versus subcritical measurements and diminishing the discrepancies between the counters and the methods which are still around 10%. That is completely achievable thanks to the progress performed in the calculation of correcting factors during the YALINA and RACE experiments and the dedicated designs of the GUINEVERE core and the accelerator GENEPI-3C. All the progress registered during the 6th FP on the on-line monitoring of the system (beam, source and core) will afford more precise measurements of its behaviour for any future experiments at power [15,16].

Acknowledgements

The authors appreciate the efforts and support of all the scientists and institutions involved in EUROTRANS and the presented work, as well as the financial support of the European Commission through the contract FI6W-CT-2004-516520.

References

[1] Granget, G., *et al.*, *Final Report on the Second Feasibility Study Including Working Programme with Details on Milestones, Deliverables, Time Schedule, Financial Issues and Recommendations*, EUROTRANS Deliverable D2.1.

[2] Kiyavtskaya, A., *et al.*, *Report on the Core Definition and Characterization for YALINA*, EUROTRANS Deliverable D2.2.

[3] Rosa, R., *et al.*, *Report on the RACE-T Results*, EUROTRANS Deliverable D2.3.

[4] Agostini, P., *et al.*, *Report on the Solid Target Design*, EUROTRANS Deliverable D2.4.

[5] Carta, M., *et al.*, *Analysis Report of RACE-T Experiments*, EUROTRANS Deliverable D2.5.

[6] Jammes, Ch., *et al.*, *Report on the RACE-LP/IAC Results*, EUROTRANS Deliverable D2.6.

[7] Jammes, Ch., *et al.*, *Analysis Report of RACE-LP/IAC Results*, EUROTRANS Deliverable D2.7.

[8] Villamarin, D., *et al.*, *Report on the Current to Flux Monitoring and Interim Calibration Techniques in YALINA*, EUROTRANS Deliverable D2.8.

[9] Berglöf, C., *et al.*, *Report on Noise Techniques Applied in YALINA*, EUROTRANS Deliverable D2.9.

[10] Vittiglio, G., *et al.*, *Report on the Facility Design and Modifications*, EUROTRANS Deliverable D2.10.

[11] Billebaud, A., *et al.*, *Report on the GENEPI Design and Specifications*, EUROTRANS Deliverable D2.11.

[12] Mellier, F., *et al.*, *Report on GUINEVERE Core Specifications*, EUROTRANS Deliverable D2.12.

[13] Mercatali, L, *et al.*, *Report on GUINEVERE Safety Studies*, EUROTRANS Deliverable D2.13.

[14] Kochetkov, A., *et al.*, *Report on the GUINEVERE Experimental Programme Definition*, EUROTRANS Deliverable D2.14.

[15] Carretero, J.A., *et al.*, *Report on Licensing and Commissioning Aspects Gained with GUINEVERE to FASTEF*, EUROTRANS Deliverable D2.18.

[16] Burgazzi, L, *et al.*, *Transposition of RACE and MEGAPIE Experience to XT-ADS Design*, EUROTRANS Deliverable D2.19.

[17] Granget, G., *et al.*, "ECATS: An International Experimental Program on the Reactivity Monitoring of Accelerator Driven Systems – Status and Progress", *Advanced Nuclear Fuel Cycles and Systems* (*GLOBAL 2007*), Boise, Idaho, 9-13 September 2007.

[18] Struwe, D., J. Somers, "Overview of Activities Exploring Options for Transmutation", *7th European Commission Conference on the Management and Disposal of Radioactive Waste* (*EURADWASTE 2008*), Luxembourg, 20-22 October 2008.

[19] Baeten, P., *et al.*, "The GUINEVERE Project at the VENUS Facility", *Utilisation and Reliability of High Power Proton Accelerators (HPPA5)*, Mol, Belgium, May 2007, OECD/NEA, Paris (2008).

[20] Mellier, F., *et al.*, *The MUSE Experiments for Sub-critical Neutronics Validation*, Deliverables N°6 and 8 Contract N° FIKW-CT-2000-00063.

[21] Rimpault, G., *et al.*, "Core Instrumentation and Reactivity Control of the He Cooled Experimental ADS (XADS)", *Advanced Nuclear Fuel Cycles and Systems* (*GLOBAL 2007*), Boise, Idaho, 9-13 September 2007.

Minor actinide transmutation in the accelerator-driven system EFIT: Results from fuel developments in Domain AFTRA

Fabienne Delage[1], Renaud Belin[1], Xue-Nong Chen[2], Elio D'Agata[3], Frodo Klaassen[4], Werner Maschek[2], Jean Pierre Ottaviani[1], Sylvie Pillon[1], Andrei Rineiski[2], Vitaly Sobolev[6], Joseph Somers[5], Dragos Staicu[5], Roger Thetford[7], Janne Wallenius[8], Beat Wernli[9]

[1]Commissariat à l'énergie atomique (CEA), France; [2]Forschungszentrum Karlsruhe (FZK), Germany; [3]Joint Research Centre-Institute for Energy (JRC-IE), Netherlands; [4]Nuclear Research and Consultancy Group (NRG), Netherlands; [5]Joint Research Centre-Institute for Transuranium Elements (JRC-ITU), Germany; [6]Studiecentrum voor Kernenergie-Centre d'Étude de l'Énergie Nucléaire (SCK•CEN), Belgium; [7]Serco for United Kingdom National Nuclear Laboratory (UK-NNL), United Kingdom; [8]Royal Institute of Technology (KTH), Sweden; [9]Paul Scherrer Institut (PSI), Switzerland

Abstract

Studies on ADS fuel development within the framework of the EUROTRANS programme have provided a wide range of results.

Several cores loaded with primary fuel candidates, MgO-cercer and ^{92}Mo-cermet, have been designed and optima meeting the specification have been found. Preliminary thermo-mechanical calculations of hottest fuel pins have given evidence of good performances.

Based on current analyses and knowledge, these fuels do not pose safety limits. Nevertheless, safety margins for ^{92}Mo-cermet fuel are considerably higher than those for MgO-cercer fuel.

Irradiation tests FUTURIX-FTA and HELIOS, on Mo-cermet and MgO-cercer fuels have been completed. Helium behaviour in inert matrices during irradiation has been investigated within the BODEX irradiation test.

Thermal properties of a large range of fuels have been assessed.

Compatibility tests have been performed between actinide phases, inert matrix candidates, T91 cladding and Pb coolant.

Finally, great progress has been made in Pu-Am-O phase diagram investigation.

The current paper gives an overview of the results gained and some recommendations on the most promising fuel(s).

Introduction

One major part in the demonstration of the EFIT feasibility assessment deals with the fuel, which can be described as highly innovative in comparison with fuels used in a critical core. Indeed, ADS fuel is not fertile, i.e. there is no uranium to avoid any additional plutonium production. Moreover, it necessarily contains a high concentration (up to 50%) of minor actinides and plutonium whose isotopic vector typically consists of 80% to 90% of even isotopes ^{238}Pu, ^{240}Pu and ^{242}Pu, 10% to 20% of odd isotopes ^{239}Pu and ^{241}Pu. This unusual fuel composition results in high gamma, neutron emissions and heat in fabrication and handling stages as well as significant production of helium during irradiation.

Domain DM3 (AFTRA) has been responsible for fuel development within EUROTRANS [1]. In order to make recommendations on fuel design and performances for the most promising candidate(s) for effective and safe minor actinides transmutation in EFIT, AFTRA's objectives have been to:

- estimate neutronic, thermo-mechanical and transmutation performances of different TRU fuel candidates as well as optimise fuel designs at normal operation conditions in the reference EFIT machine designed by domain DM1;
- assess the safety behaviour of the primary fuel candidates in transient conditions, accidents and severe accidents;
- investigate the overall behaviour of ADS type fuels under irradiation in EFIT representative conditions as well as comprehensive mechanisms of helium build-up and release versus temperature and fuel microstructure;
- provide relevant and accurate experimental data on thermal and mechanical fuel properties, chemical compatibility within fuel components and between fuel core components (clad, coolant) as well as phase diagram of Pu-Am compounds of interest.

The current paper gives an overview of the results gained and some recommendations on the most promising fuel(s).

Fuel candidates

Emphasis has been placed on oxide fuels with coherence to the guidance of the European Technical Working Group on ADS [2] and:

- promising results according to performance, safety and fabricability criteria as well as first experimental feedback on $(Pu,Am)O_2$ fabrication and out-of-pile characterisations, gained within the FP5 FUTURE programme (2002-2006) [3];
- a strong synergy with R&D programmes on transmutation targets [4];
- a broad industrial experience on oxide fuel fabrication for critical reactors.

Nitride-based fuels have been considered as a possible back-up solution. Though their high attractiveness has been confirmed by the results of the FP5 CONFIRM programme (2001-2008) [5] and ongoing developments in Japan, knowledge and technical know-how in Europe remain limited. Thus, these fuels are considered to be at an early stage of development with longer-term R&D activities still required.

Two oxides were selected as primary candidates at the beginning of the project, from a ranking procedure based on criteria of fabrication, hydro-reprocessing, secondary waste stream, high-temperature stability as well as expected neutronic, transmutation and thermo-mechanical performances and safety margin to failure. The primary candidates are: MgO ceramic-ceramic and ^{enr}Mo ceramic-metallic fuels, consisting of $(Pu,MA)O_{2-x}$ particles dispersed respectively in a

magnesia matrix or a molybdenum matrix enriched in ^{92}Mo (to decrease Mo neutronic penalties as well as to prevent the production of the long-lived ^{99}Tc by neutron capture in ^{98}Mo). (ZrO_2 inert matrix fuels have been considered as a back-up option due to expected difficulties for hydro-reprocessing.)

TRU fuel pre-designs and performance assessment under normal operation conditions

EFIT is a 400 MW(th) machine aiming at high MA burning efficiency, low beam current requirement, flat power distribution, low reactivity swing during burn-up, low core pressure drop as well as safety requirements. Several design options for both MgO-cercer and ^{enr}Mo-cermet cores have been investigated throughout the project [6] to fit EFIT initial specification and updates given by DM1. The latest core design parameters are described in [7,8]: a proton beam of 800 MeV and 20 mA impinges on a 78.2 cm diameter windowless lead target (deposited thermal power of 11.2 MW(th) providing the neutron source for the subcritical system with the initial effective neutron multiplication coefficient (k_{eff}) of ~0.97. The inlet and outlet temperatures of the lead coolant in the ADS core are respectively 400 and 480°C. The structural material is ferritic-martensitic steel (FMS) T91. The isotopic vectors for the transuranic elements are given in Table 1.

Table 1: MA and Pu isotopic compositions [9]

MA	^{237}Np	^{241}Am	^{242m}Am	^{243}Am	^{243}Cm	^{244}Cm	^{245}Cm	^{246}Cm	^{247}Cm
at.%	3.384	75.510	0.254	16.054	0.066	3.001	1.139	0.089	0.002

Pu	^{238}Pu	^{239}Pu	^{240}Pu	^{241}Pu	^{242}Pu	^{244}Pu
at.%	3.737	46.446	34.121	3.845	11.850	0.001

The reference cercer core selected by DM1 [7,9], due to the fact that MgO-cercer properties have seemed better to match the objectives, and that cercer fuel manufacture is less expensive than the cermet due to the Mo enrichment requirement, consists of three zones loaded with fuel elements whose characteristics are summarised in Table 2. The transmutation rate for a residence time of three years is close to optimum: MA consumption of 42 kg/TWh(th) for a Pu balance close to 0 (see Table 3). The other parameters also match the specifications: k_{eff} fits the safety requirements; source efficiency and beam intensity remain rather constant over the cycle and the power density distribution is quite flat.

Table 2: Preliminary design data for fuel pin and subassembly

	MgO-cercer core [2]			^{92}Mo-cermet core [11]		
	Inner	Intermediate	Outer	Inner	Intermediate	Outer
Pu/MA (at%)	45.7/54.3			46/54		
Fuel/matrix	57/43	50/50		35/65	43/57	50/50
Fuel pellet diameter (mm)	7.10		8.00	8.00		
Clad inner diameter (mm)	7.42		8.32	8.32		
Clad width (μm)	600			600		
Fuel pin pitch (mm)	13.63		13.54	13.54		
Pin number/assembly	169			169		
Row number/assembly	7			7		
Assembly number/zone	42	66	72	42	90	84

Dealing with cermet fuel, from a first reference core design (see Table 2) which meets the main current specifications except the low reactivity swing criteria, improvements were performed to limit the reactivity variation while other characteristics remain quite similar [10,12,13]. These

advanced cores designed (see Table 3) by lowering Pu/MA ratio, increasing core fuel fraction with large fuel pellet diameters and reducing the pin number per SA to maintain thermo-hydraulics characteristics have shown that similar performances (see Table 3) are achievable for both MgO-cercer cores and ^{enr}Mo-cermet fuels.

Table 3: Transmutation performances of cercer and cermet designed cores

	Cercer [12]	Cermet [13]		
Nb pins per S/A	169	169	91	61
Pu/MA	46/54	46/54	40/60	35/65
Pin diameter	7.52-9.52	9.52	13.00	15.87
Fuel vol. (%)	23.33	26.73	29.79	31.24
K_{eff}:				
• initial	0.9655	0.9820	0.9724	0.9428
•after 1 098 EFPD	0.9654	0.9593	0.9625	0.9455
Initial mass (kg):				
• Pu	2 454	3 055	2 966	2 726
• MA	2 917	3 610	4 479	5 056
Δ(kg/TWh$_{th}$):	-42.00	-43.67	-43.92	-43.78
• Pu	-3.84	-5.71	+1.06	+7.95
• MA:	-38.16	-37.96	-44.98	-51.73
– U	+0.44	+0.48	+0.49	+0.50
– Am	-47.77	-46.80	-54.72	-63.40
– Cm	+10.54	+9.70	+10.70	+12.27
– Np	-1.37	-0.86	-0.96	-0.60

Regarding thermo-mechanic behaviour of the pins whose characteristics are described in Table 2, preliminary calculations have been performed with the codes TRAFIC (Serco) and MACROS (SCK•CEN) initially designed to model homogeneous fuels, which have been extended during the project to handle heterogeneous media [14]. As fission gas behaviour in ADS type fuels is poorly known, the parameters of the new TRAFIC model of gas behaviour in the inert matrix were tuned to fit available gas release results on MgO-cercer transmutation targets [15,16] before performing simulations of the ADS fuel behaviours under EFIT normal operation conditions. Results from TRAFIC for ADS fuels indicate that thermo-mechanical performances of cercer and cermet hottest pins are acceptable at least for peak linear powers around 200 W.cm^{-1} and a 1 098 EFPD operation time, with higher temperature margins to failure for cermet fuel. For cercer fuel at the start of life, the predicted centre temperature of 1 800 K, close to the temperature of MgO vaporisation beginnings (see Figure 2), falls quickly as the gap closes. At the end of life, the gap is closed and the peak temperature is about 1 400 K. Gas release ratio from pellets over a whole pin would be about 27% of the gas generated and the maximum clad stress (89 MPa) is still modest compared to T91 stress limit of 127 MPa. For cermet fuel, a centre peak temperature of 1 200 K at the beginning of life, due to the higher cermet thermal conductivity as compared to cercer, is quite constant up to the end of life as the gap remains open. Gas release ratio from pellets over a whole pin would be about 23% of the gas generated and the maximum clad stress is low (20 MPa). The MACROS results confirm in general the previous conclusions.

These promising first thermo-mechanical results remain nevertheless quite unreliable due to the lack of experimental knowledge on basic mechanisms of fuel behaviour under irradiation, and progress is still required.

Fuel safety assessment

Lack of sufficient negative feedback as well as deteriorated kinetics parameters, and high intrinsic core material reactivity worth are characteristics of an ADS type reactor loaded by U-free fuels, whose safety impact has to be assessed.

Fuel temperature limits for various accident conditions related to the different categories of the defence-in-depth concept have been specified [17] according to a very conservative approach owing to the limited amount of available data:

- The highest limit temperatures for design extension conditions (DEC) are lower for MgO-cercer than for Mo-cermet because of possible sizeable vaporisation of MgO above 2 130 K (see Figure 2) whereas the Mo-cermet stability limit temperature is about 2 450 K.
- The limit temperatures for design basis conditions (DBC) range according to the category of the event, from 1 750 to 1 950 K for cercer fuels and 2 300-2 400 K for cermet fuels.

Beside fuel temperature limits, clad characteristics are of major interest and creep failure temperature limits have been set up for T91 [18].

The safety behaviour of EFIT cores fuelled with cercer has been analysed within domains DM1 and DM3 for a broad set of scenarios: protected/unprotected transient over power (P/UTOP), unprotected transient over current (UTOC), beam trip (BT), unprotected loss of flow (ULOF) unprotected blockage accident (UBA). There are very few transients for which the core conditions could approach clad failure and/or release of radioactivity. The main one is the UBA, with the almost complete blockage of a subassembly without accelerator trip, whose detection in due time might be difficult, and which can lead to propagation and core damage [18]. Because the knowledge of the blockage scenario is very limited and materials properties under high temperatures are unsure, further investigations need to be performed both experimentally and theoretically concerning the material behaviours in a high-temperature range as well as the possible blockage phenomena. The analyses performed in DM3 show that except UBA, the EFIT cercer reference core can survive all the analysed transient conditions.

Regarding cermet cores, safety analysis has also been performed for the most important transients to identify key safety issues of cermet (and differences to cercer). ULOF simulations pointed out that both fuel and clad failure limits are respected [13]. Moreover, cermet fuel has very large safety margins to melting (>1 000°C) compared to cercer fuel (100-200°C). Simulations of UTOP have not shown any short time cermet fuel failures [11]. In the UBA, although the lead high boiling point prevents coolant boiling, local voiding can be caused by a helium blow-down from the gas plenum. A mitigating effect could be the sweep-out of fuel particles. Simulations have shown that pin failure would lead to a local voiding and reactivity addition but the fuel sweep-out effect would lead to a power reduction and would limit core degradation. The beam should finally be shut off to achieve stable post-accident heat removal conditions [11].

In conclusion, safety analyses have shown that for both cercer and cermet reference cores, safety limits for fuel are not violated with the exception of the UBA case for the cercer core. Moreover, safety margins are considerably higher for cermet than cercer fuels. Finally, the most limiting conditions would come from the T91 clad. Special effort is nevertheless still mandatory for understanding fuel behaviour under irradiation and the impact on operational conditions, transients and accidents.

Irradiation tests

Even if behaviour under irradiation of TRU fuel is quite unknown, results of post-irradiation examination (PIE) on irradiated targets with a few per cent of americium have already emphasised the major roles played by irradiation conditions (including temperature), helium production and material swelling due to the inert matrix amorphisation and helium accumulation. To go further with ADS-type fuels, the programme within AFTRA has investigated:

- irradiation effects on cercer and cermet fuels in EFIT representative conditions with FUTURIX-FTA test [19] in PHENIX reactor;
- helium behaviour vs. temperature and microstructure with HELIOS test in HFR reactor [20];

- helium build-up and release mechanisms versus temperature in ^{10}B (as Am surrogate) doped fuel matrices with BODEX test [21] in HFR reactor;
- PIE of nitride fuels ($Pu_{0.3}Zr_{0.7}N$) irradiated in the HFR reactor as a part of the 5th European Framework Programme CONFIRM project [22], as nitride fuels constitute a back-up solution for actinide burning. (These characterisations are ongoing at the present time.)

The composition of the pellets for FUTURIX-FTA and HELIOS experiments are given in Table 4. FUTURIX-FTA compositions specifically address ADS-type fuels. HELIOS compositions range from ADS-type fuels to transmutation targets, in order to link and thus to benefit from the experience gained within EFFTRA-T4 and -T4bis tests [23,24] for ADS fuel (and target) developments. The Am content ranges from 0.2 to 1.9 g.cm^{-3} in FUTURIX-FTA samples whereas it is about 0.7 g.cm^{-3} in all HELIOS samples.

Table 4: Fuel compositions for irradiation tests: FUTURIX-FTA and HELIOS

FUTURIX-FTA	HELIOS
$Pu_{0.80}Am_{0.20}O_{2-x}$ + 86 vol.% Mo	$Am_2Zr_2O_7$ + 80 vol.% MgO
$Pu_{0.23}Am_{0.24}Zr_{0.53}O_{2-x}$ + 60 vol.% Mo	$Zr_{0.80}Y_{0.13}Am_{0.07}O_{2-x}$ $Pu_{0.04}Am_{0.07}Zr_{0.76}Y_{0.13}O_{2-x}$
$Pu_{0.5}Am_{0.5}O_{1.88}$ + 80 vol.% MgO	$Am_{0.22}Zr_{0.67}Y_{0.11}O_{2-x}$ + 71 vol.% Mo
$Pu_{0.2}Am_{0.8}O_{1.73}$ +75 vol.% MgO	$Pu_{0.80}Am_{0.20}O_{2-x}$ + 84 vol.% Mo

These highly radioactive materials were fabricated at lab-scale in two steps [17]. The Am particles were firstly synthesised using two processes: an oxalic co-precipitation route for cercer compounds [25], and a combination of external gelation and infiltration methods for cermet and homogeneous compositions [26]. The following steps are based on conventional powder metallurgy and were similar for all compositions except HELIOS cercer fuel, whose porosity was tailored to remain open in order to allow helium to escape.

The FUTURIX-FTA irradiation test is currently complete with an irradiation time of 235 EFPD and cumulative neutron fluence of respectively ~1.0×10^{23} n.cm^{-2} and ~1.4×10^{23} n.cm^{-2} for cercer and cermet capsules. HELIOS irradiation occurred between 29 April 2009 and 19 February 2010.

Dealing with the BODEX experiment, which aims at investigating the He-induced swelling behaviour of inert matrices using ^{10}B as Am surrogate, ^{10}B- and ^{11}B-doped pellets as well as blank samples (without B) were fabricated in order to discriminate the effects related to helium production (^{10}B-doped samples) from irradiation (blank samples) and chemical (^{11}B-doped samples) ones. The boron compounds mixed with MgO, Mo and ZrO_2 are $Mg_3B_2O_6$, Mo_2B and ZrB_2, respectively. The boron content is about 1 wt.% in order to have a similar helium production (~0.3-0.4 mmol) after two HFR irradiation cycles (~56 EFPD) than in the HELIOS (or EFFTRA-T4) irradiation test. The irradiation test was performed at two temperatures: ~1 073 K and ~1 473 K. Moreover, the experiment included neutron fluence detectors in all the capsules and on-line pressure and temperature monitoring for two capsules.

First PIE: visual inspection (Table 5) and on-line pressure measurement analyses were performed on some MgO and Mo irradiated samples. They have shown that:

- Mo and MgO non-doped samples remain intact after irradiation.
- ^{10}B-doped Mo samples (whose initial density was very high with ~92%) developed cracks during irradiation whereas ^{10}B doped MgO samples (whose initial density was about 76%) did not.
- He release ratios calculated via on-line pressure monitoring during irradiation at high temperature for ^{10}B-doped samples indicated a lower He release out of Mo (dense) samples (7%) compared to MgO samples (30%), which is linked to the high porosity in MgO pellets.

Table 5: Visual inspection of Mo and MgO samples before and after irradiation

	Temperature	Samples without boron	^{10}B doped samples
Mo	Low	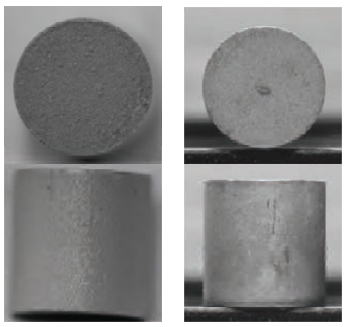	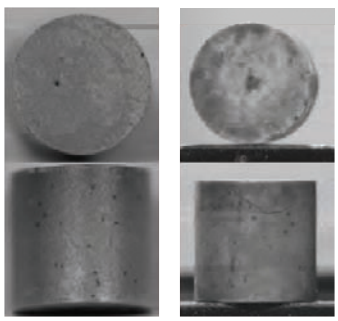
	High	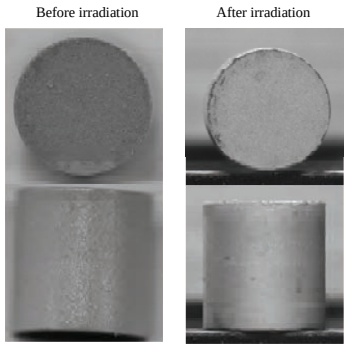	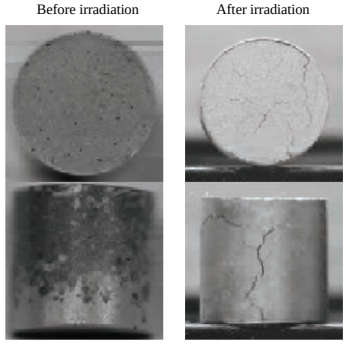
MgO	High	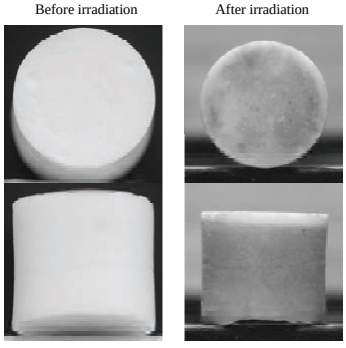	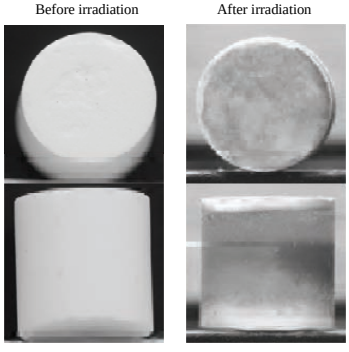

Out-of-pile measurements

Out-of pile measurements have aimed at increasing knowledge on the fuel thermal, mechanical and physical-chemical properties in order improve the databases with relevant and accurate data for the fuel design, fuel performance and safety modelling. Many results have been reported. Some specific points are highlighted hereafter.

Thermal conductivity of the FUTURIX-FTA (and HELIOS) samples was calculated from measurements of thermal diffusivity by the laser flash technique and heat capacity by differential scanning calorimetry. They highlight a significant drop at high temperatures ($T > 1\,500$ K) for cercer fuels, which was not predicted by calculations based on phase mixing models (Figure 1). The results obtained for FUTURIX-FTA cermet and HELIOS fuels [27] showed higher thermal conductivities for the cermet fuels ($\times 40$) compared to the conductivity of the inclusions. Theoretical curves for the thermal conductivity of cermet fuels calculated using an analytical

Figure 1: Thermal conductivity of FUTURIX-FTA and HELIOS fuels

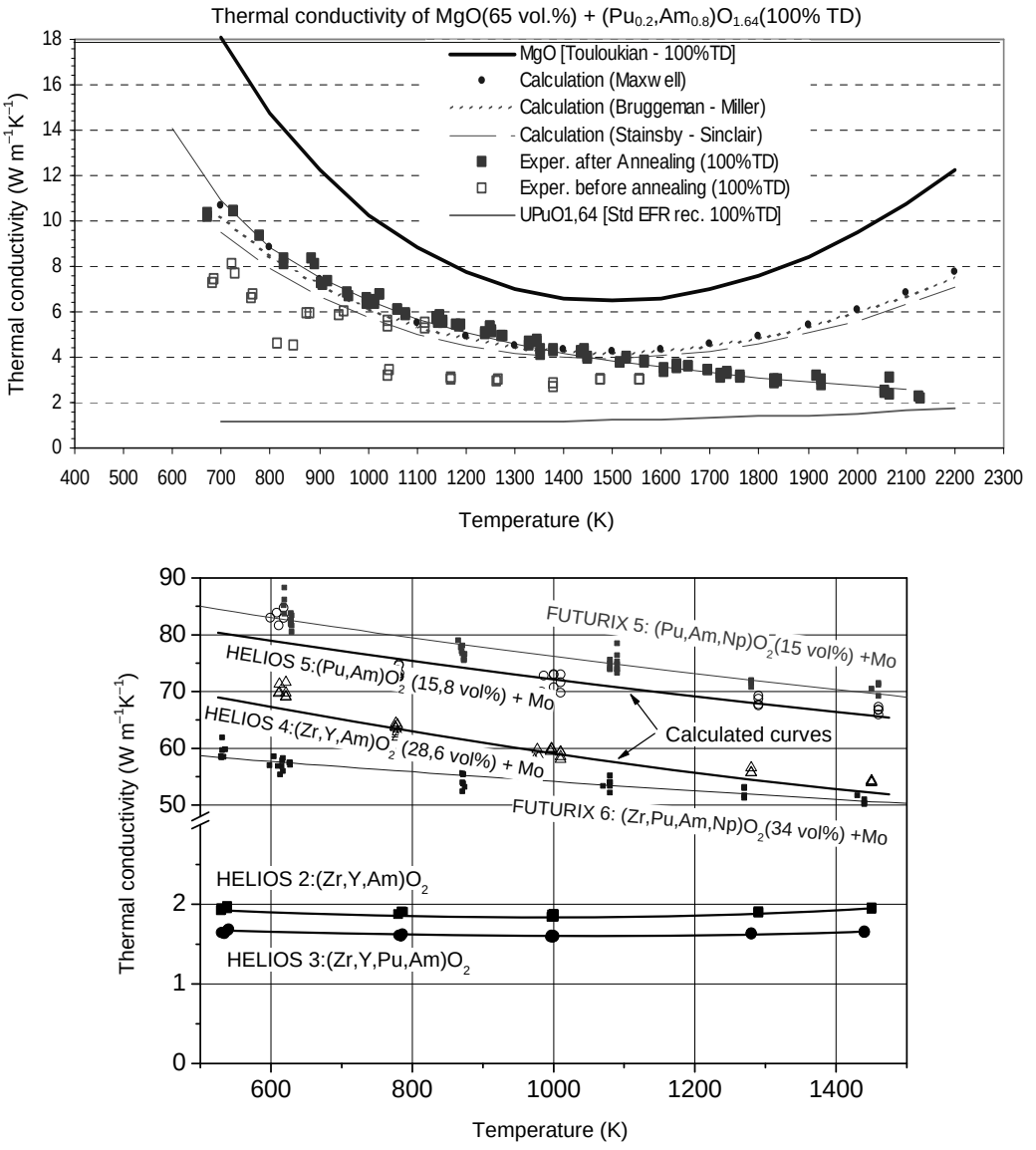

model taking into account the high volume fraction of inclusions and the large difference in thermal conductivity between the matrix and inclusions also showed a good agreement with the experimental measurements.

Vaporisation and melting temperature measurements made on cercer fuels have confirmed the MgO low thermal stability (T ~ 2 130 K) under vacuum and neutral atmosphere, for closed and open systems. Volatilisation species and temperature ranges have been made clear too (see Figure 2): MgO vaporisation according to the reaction: $MgO(s) = Mg(g) + 1/2O_2(g)$, begins at 1 750-1 800 K, becomes significant above ~2 130 K.

Chemical compatibility tests performed at 1 300 and 1 800 K under different atmospheres (air, Ar, Ar/H_2) have not shown any interaction between PuO_2, $Pu_{0.5}Am_{0.5}O_2$ and MgO, Mo under any atmosphere [28]. There is no interaction between Pb (EFIT coolant) and T91, Mo or MgO compounds too. Mo and MgO are compatible with the clad T91 beyond 550°C. Regarding the compatibility between fissile compounds and the clad T91, slight areas of interaction have been

Figure 2: High-temperature speciation of FUTURIX cercer fuel components $Pu_{0.5}Am_{0.5}O_{2-x}$ + 80 vol.% MgO

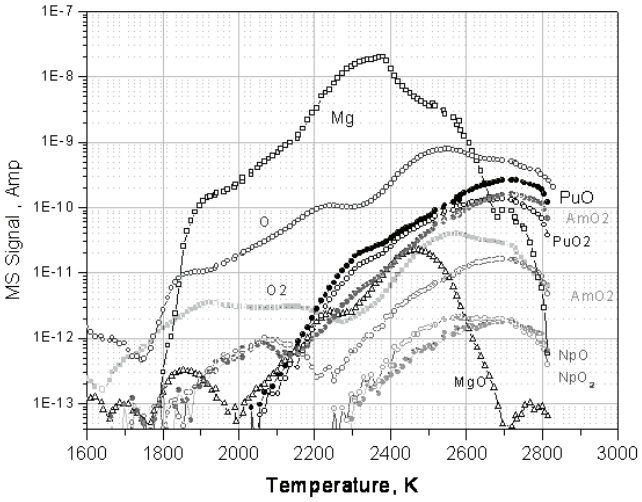

observed on the $Pu_xAm_{1-x}O_2$ edge opposite T91 for $x \geq 0.5$. This leads to the preliminary conclusion that the fissile particles have to be surrounded by the inert matrix to prevent interactions with the clad.

Finally experimental investigations on the Pu-Am-O phase diagram have provided relevant data to partially build the Pu_2O_3-Am_2O_3 phase diagram [29]. They have also pointed out that Am drives the reduction process in the oxygen sub-stoichiometric area.

Conclusion

Studies on fuel development within the EUROTRANS project, motivated by assessing the industrial practicability for actinide transmutation, have provided a wide range of results which reinforce the interest of both MgO-cercer and ^{enr}Mo-cermet for the 400 MWth EFIT machine with higher safety margins for the cermet fuel. The ranking between these two primary candidates seems nevertheless premature without the results of PIE of HELIOS and FUTURIX-FTA fuels, which are scheduled within the FP-7 FAIRFUELS programme.

Beyond the expected PIE of HELIOS and FUTURIX-FTA fuels, EFIT fuel qualification will require additional developments to demonstrate that the "fuel product fabricated in accordance with a specification behaves as assumed or described in the applicable licensing safety case, and with the reliability necessary for economic operation of the reactor" [30]. So, the next steps in ADS fuel R&D should include at least achievements on: predictive modelling of fuel behaviour under irradiation, fabrication techniques and processes for industrial scale transposition, experiments to improve the fuel behaviour understanding in off-normal operating conditions, fuel recycling including: reprocessability (hydro and pyro-reprocessing) and secondary waste management, properties measurements on irradiated fuels, irradiation tests on ADS fuel reference compositions and designs under nominal conditions of flux, temperature and doses.

Acknowledgements

The authors appreciate the support of all the scientists and institutions involved in IP EUROTRANS as well as financial support of the European Commission through the contract FI6W-CT-2004-516520.

References

[1] Knebel, J., "Opening and National ADS Programmes: The EUROTRANS Project – Partitioning and Transmutation Research in Europe", these proceedings.

[2] Rubia, C., *et al.*, *A European Roadmap for Developing Accelerator Driven Systems (ADS) for Nuclear Waste Incineration*, ISBN 88-8286-008-6 (2001).

[3] Pillon, S., *et al.*, "The European FUTURE Programme", *GLOBAL 2003*, New Orleans, LA, 16-20 November (2003).

[4] Pillon, S., *et al.*, "Contribution of PHENIX to the Development of Transmutation Fuels and Targets in Sodium Fast Breeder Reactors", *Nuc. Tech.*, 153, 264-273 (2006).

[5] Pillon, S., *et al.*, "Oxide and Nitride TRU-Fuels: Lessons Drawn from CONFIRM and FUTURE Projects of the 5th European Framework Programme", *Conference ATALANTE 2004*, Nîmes, France (2004).

[6] Sobolev, V., *et al.*, "Issues of Optimisation of the EFIT Fuel Design", these proceedings.

[7] De Bruyn, D., *et al.*, "Achievements and Lessons Learned Within the Domain 1 "Design" of the Integrated Project EUROTRANS", these proceedings.

[8] Mansani, L., *et al.*, "The Designs of an Experimental ADS Facility (XT-ADS) and of an European Industrial Transmutation Demonstrator (EFIT)", these proceedings.

[9] Artioli, C., *et al.*, "Optimization of the Minor Actinides Transmutation in ADS: The European Facility for Industrial Transmutation EFIT-Pb Concept", *Conference AccApp'07*, Pocatello, ID, 29 July-2 August (2007).

[10] Chen, X-N., *et al.*, "Design and Safety Studies of an EFIT Core with Cermet Fuel", these proceedings.

[11] Chen, X-N., *et al.*, "Design and Safety Studies on the EFIT with Cermet Fuel", *Conference PHYSOR'08*, Interlaken, Switzerland, 14-19 September (2008).

[12] Maschek, W., *et al.*, "Safety Concepts of the 400 MWth-class EFIT Accelerator Driven Transmuter and Consideration for Further Developments", *Conference ICENES'09*, Ericeira, Portugal, 9 June-3 July (2009).

[13] Maschek, W., *et al.*, "Design, Safety and Fuel Developments for the EFIT Accelerator-driven System with Cercer and Cermet Cores", *10th International Exchange Meeting on Actinide and Fission Product Partitioning and Transmutation (10-IEMPT)*, Mito, Japan, 6-10 October 2008, p. 387, OECD/NEA, Paris (2010).

[14] Lemehov, S., *et al.*, "Prognosis of Thermomechanical Behaviour of Cercer and Cermet Fuels in EFIT-400 Transmuter", these proceedings.

[15] Bonnerot, J.M., *et al.*, "Progress on Inert Matrix Fuels for Minor Actinide Transmutation in Fast Reactor", *Conference GLOBAL'07*, Boise, ID, 9-13 September (2007).

[16] Kryukov, N.F., *et al.*, "Results of Post-irradiation Examination of Inert Matrix Fuel Compositions Irradiated in the BOR-60 Reactor of 19 at% Under the Russian-French Experiment BORA-BORA, *Conference GLOBAL'09*, Paris, France, 6-11 September (2009).

[17] Maschek, W., *et al.*, "Accelerator Driven Systems for Transmutation: Fuel Development, Design and Safety", *Prog. Nuc. Energy*, 50, 333 (2008).

[18] Liu, P., *et al.*, "Analyses of Transients for 400 MWth-class EFIT Accelerator Driven Transmuter with the SIMMER-III Code", *Conference AccApp'09*, Vienna, Austria, 4-8 May (2009).

[19] Jaecki, P., *et al.*, "The FUTURIX-FTA Experiment in Phénix", *8th International Exchange Meeting on Actinide and Fission Product Partitioning and Transmutation (8-IEMPT)*, Las Vegas, NV, 9-11 November 2004, OECD/NEA, Paris (2005).

[20] D'Agata, E., *et al.*, "HELIOS: The New Design of the Irradiation of U-free Fuels for Americium Transmutation", *Conference GLOBAL'09*, Paris, France, 6-11 September (2009).

[21] Den Dexter, M.J., *et al.*, "Investigation of He-induced Swelling Behaviour of Inert Matrices by ^{10}B Doping: The BODEX Irradiation Experiment", *9th International Exchange Meeting on Actinide and Fission Product Partitioning and Transmutation (9-IEMPT)*, Nîmes, France, 25-29 September 2006, OECD/NEA, Paris (2007).

[22] Wallenius, J., *et al.*, "Collaboration on Nitride Fuel Irradiation and Modelling", *Conference AccApp'01*, Reno, NV, 11-15 November (2001).

[23] Konings, R.J.M., *et al.*, "The EFFTRA-T4 Experiment on Americium Transmutation", *Jour. Nuc. Mat.*, 282, 159 (2000).

[24] Klaassen, F., *et al.*, "Post Irradiation Examinations of an Americium Containing Transmutation Target (EFFTRA-T4 bis) at High Americium Burn-up", *Workshop IMF-11*, Park City, UT, 10-12 October (2006).

[25] Jankowiak, A., *et al.*, "Preparation and Characterization of $Pu_{0.5}Am_{0.5}O_{2-x}$-MgO Ceramic/ Ceramic Composites", *Nuc. Sci. Eng.*, 160, 378 (2008).

[26] Fernandez, A., *et al.*, "Advanced Fuel Fabrication Processes for Transmutation", *10th Int. Exchange Meeting on Actinide and Fission Product Partitioning and Transmutation (10-IEMPT)*, Mito, Japan, 6-10 October 2008, p. 155, OECD/NEA, Paris (2010).

[27] Staicu, D., *et al.*, "Thermal Properties of Cermet Fuels for P&T Concepts", *Conference of the American Nuclear Society*, Anaheim, CA, 8-12 June (2008).

[28] Gavilan, E., *et al.*, "Structural Investigation on Americium and Plutonium Mixed Oxides/ Inert Matrices", *Conference GLOBAL'09*, Paris, France, 6-11 September (2009).

[29] Delage, F., *et al.*, "Advanced Fuel Developments for an Industrial Accelerator Driven System Prototype", *Conference GLOBAL'09*, Paris, France, 6-11 September (2009).

[30] Crawford, D., *et al.*, "An Approach to Fuel Development and Qualification", *J. Nuc. Mat.*, 321, 232 (2007).

Development and assessment of structural materials and heavy liquid metal technologies for transmutation systems (DEMETRA): Highlights on major results

Concetta Fazio[1], Joris Van den Bosch[2], Francisco Javier Martin Muñoz[3], Jean Henry[4], Ferry Roelofs[5], Paolo Turroni[6], Luigi Mansani[7], Alfons Weisenburger[1], Dominique Gorse[8], Jordi Abella[9], Laurent Brissonneau[3], Yong Dai[10], Lida Magielsen[5], Jörg Neuhausen[10], Pavel Vladimirov[1], Andreas Class[1], Herve Jeanmart[11], Andrea Ciampichetti[6], Gunter Gerbeth[12], Thomas Wetzel[1], Aram Karbojian[13], Karsten Litfin[1], Mariano Tarantino[6], Luca Zanini[10]

[1]Karlsruher Institut für Technologie (KIT), Germany; [2]Studiecentrum voor Kernenergie-Centre d'Étude de l'Énergie Nucléaire (SCK•CEN), Belgium; [3]Centro de Investigaciones Energéticas, Medioambientales y Tecnológicas (CIEMAT), Spain; [4]Commissariat à l'énergie atomique (CEA), France; [5]Nuclear Research and Consultancy Group (NRG), Netherlands; [6]Agenzia naz. per le nuove tecnologie, l'energia e lo sviluppo economico sostenibile (ENEA), Italy; [7]Ansaldo Nucleare, Italy; [8]Centre national de la recherche scientifique (CNRS), France; [9]Institut Químic de Sarrià (IQS), Spain; [10]Paul Scherrer Institut (PSI), Switzerland; [11]Université Catholique de Louvain (UCL), Belgium; [12]Forschungszentrum Dresden-Rossendorf (FZD), Germany; [13]Royal Institute of Technology (KTH), Sweden

Abstract

The DEMETRA domain of the EUROTRANS project provides a wealth of experimental and theoretical results within key technological areas related to heavy liquid metal (HLM) technology. HLM as Pb and lead-bismuth eutectic (LBE) are the reference coolant and spallation materials choices for the ADS facilities studied within the EUROTRANS project.

For these coolants the key items that have been addressed within DEMETRA are:

- *coolant quality control in terms of oxygen and impurities control;*
- *materials compatibility in terms of corrosion, mechanical and irradiation resistance;*
- *thermal-hydraulics studies related to heat transfer in turbulent conditions through dedicated experiments on a single pin, a fuel bundle and integrated component tests;*
- *safety-related studies through experimental and simulation studies on HLM/water interaction;*
- *support to component design and testing, where in particular substantial support has been given to the development of the windowless neutron spallation target and the assessment of the window spallation target behaviour through the post-test analysis of MEGAPIE;*
- *measurement and operational techniques development;*

The technical work programme of DEMETRA is herein summarised and some major experimental results are discussed.

Introduction

Accelerator-driven systems are investigated in the EUROTRANS project for the transmutation of high-level nuclear waste [1]. These reactor systems have a subcritical core and the nuclear chain reaction is sustained by an external neutron source. The external neutrons are generated through the nuclear spallation reaction occurring between a proton beam and the target. In case of ADS the target material is the liquid Pb-Bi eutectic (LBE). Within the EUROTRANS project the designs and related safety analysis of two systems have been conducted, i.e. an experimental facility cooled with liquid LBE and an industrial facility where the selected coolant is liquid Pb. The objective of the experimental facility (XT-ADS) is to demonstrate the technical feasibility of an ADS and the transmutation feasibility at subassembly level.

On the other hand the objective of the European Facility for Industrial Transmutation (EFIT) is the demonstration of a core fully loaded with uranium-free minor actinide bearing fuel.

The DEMETRA domain has been established within the EUROTRANS project with the aim to address issues related to structural and clad materials performance in liquid metal and under irradiation, thermal-hydraulics of the core and the neutron spallation target, and development of coolant technologies and measurement techniques. All relevant DEMETRA results have been discussed and used to support specific design issues of both XT-ADS and EFIT components [2].

The issues addressed within DEMETRA have been:

- development and characterisation of technologies needed for the quality control of the coolant chemistry;
- materials procurement and materials characterisation in terms of corrosion and mechanical properties in the liquid metal, in irradiation fields and their combined effect;
- thermal-hydraulics studies for the measurement of heat transfer coefficient in single pin and in fuel bundle simulators;
- support to the design and experiments for the assessment of the free surface of the windowless spallation target and assessment of the window target through the post-test analysis of the MEGAPIE experiment;
- development and tests of components (heat exchanger, pumps, etc.) and measurement techniques (e.g. free surface measurement systems, flow and velocity meters, etc.).

The activities addressing the quality control of the coolant chemistry have included fundamental studies such as the measurement of diffusivity and solubility coefficient of metallic and non-metallic elements. Focus has been put on oxygen, since this element plays an important role in the definition of the corrosion mechanism and rate of the selected structural materials. Moreover, means to measure and adjust the oxygen potential in the liquid metal have been developed and tested. As for the other elements, here two classes have been investigated, steel elements such as Ni, Cr and Fe (to support corrosion studies and understanding of corrosion products behaviour) and spallation products such as Hg, Po, etc., which are data relevant for the operation of an ADS and for the safety analysis.

The materials investigated within DEMETRA have been the ferritic/martensitic steel T91 and the austenitic steel AISI 316L. Batches of both steels have been procured in order to assure a certain reproducibility of the experimental results. Moreover, in order to enhance the corrosion and/or oxidation resistance of the steels Fe, Al based coatings have been developed and tested as well. The selected materials have been tested in stagnant and flowing liquid metal and over a wide range of experimental conditions.

The thermal-hydraulics investigations have been focused on selected items related to the core and the neutron spallation target. The core studies were on heat transfer measurement of a

single pin and a fuel bundle simulator. Integral experiments to test the interaction of different components have also been designed.

In the following paragraphs the DEMETRA experimental programme and relevant design items of XT-ADS and EFIT will be presented. Furthermore, selected experimental results and possibly their impact on the designs will be discussed.

The DEMETRA experimental programme

The experimental programme conducted over a five-year period was formulated on the basis of a preliminary list of design needs defined within previous projects [3]. The activities defined within DEMETRA can be classified into four categories: coolant chemistry, materials, core thermal-hydraulics and neutron spallation target.

Coolant chemistry

The activities performed in this area were focused on aspects related to:

- Measurement of diffusivity and solubility coefficients of metallic and non-metallic elements in LBE. The focus has been on oxygen (relevant for corrosion behaviour and slag formation), steel elements and spallation products (relevant for operational aspects of the ADS system and for safety-related issues).
- Development and characterisation of systems to measure and adjust the oxygen potential in the liquid metal. For the oxygen potential measurement, the oxygen probe design was optimised and calibration procedures were defined. Moreover, measurement accuracy, precision and long-term stability were addressed. To adjust the oxygen potential in the liquid metal, gas/liquid and solid/liquid exchange systems were assessed.
- Characterisation of filters to remove slag from the liquid metal and aerosols from the gas phase above the liquid metal.

Materials

The chemical composition and the microstructure of the T91 and the AISI 316L steels (the selected materials for the DEMETRA experiments) are given in Table 1 and Figure 1 respectively [4].

In particular, due to the high strength, the good dimensional stability under irradiation and the apparently better corrosion resistance in the high-temperature range, the T91 steel has been indicated as candidate material for the core components and the neutron spallation target. The AISI 316L steel has been indicated as a candidate for the vessel and in-vessel components, since these components in principle are operated at lower temperatures and they experience lower irradiation doses. The experimental programme of the two steels (corrosion, mechanical and irradiation) has been defined in accordance with these considerations.

Table 1: Chemical composition of the austenitic steel AISI 316L and the ferritic/martensitic steel T91 [4]

Steel	**Austenitic steel AISI 316L**								
Element	C	Mn	P	S	Si	Ni	Cr	Mo	N
wt.%	0.019	1.81	0.003	0.0035	0.67	10.0	16.7	2.05	0.029
Steel	**Ferritic/martensitic steel T91**								
Element	C	Mn	P	V	Si	Ni	Cr	Mo	N
wt.%	0.1	0.4	0.02	0.21	0.23	0.1	9.0	0.9	0.044
Element	Cu	Nb							
wt.%	0.06	0.06							

Figure 1: Microstructure of the T91 (left) and the AISI 316L steels (right) [4]

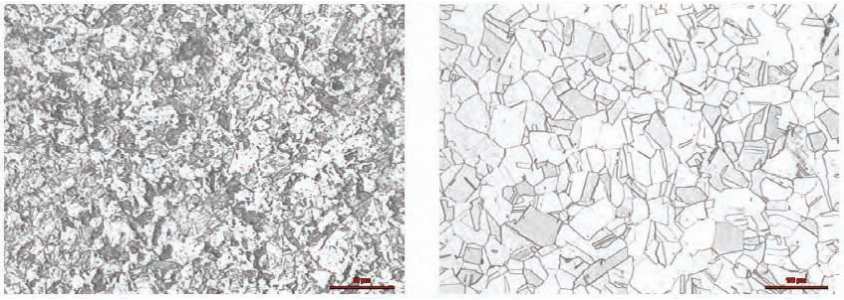

In Table 2 the list of loops and their operational conditions used in the DEMETRA domain for the corrosion studies is reported. As shown in this table tests in flowing HLM were performed in the temperature range 450-600°C, with prototypical flow velocities and oxygen concentrations ranging from oxidising to reducing conditions. All loops but CHEOPE III were operated with LBE. Additional tests in stagnant or semi-stagnant conditions were performed for different purposes, such as assessment of surface roughness on corrosion mechanism, determination of numerical models to describe corrosion mechanism and rate and evaluation of the effect of loss of oxygen and temperature transients on corrosion appearance.

Table 2: Test programme of the corrosion experiments performed in DEMETRA [2]

Loop	T (°C)	Max exposure time (h)	Flow rate (m/s)	Oxygen (wt.%)	Tested material
CORRIDA (KIT)	550	15 000	2	10^{-6}	T91, 316, FeCrAlY GESA
CU2 (IPPE/KIT)	480 550 600	6 587 6 587 8 500	1.3	10^{-6}	T91, FeCrAlY GESA
CU2 (IPPE/KIT)	550	2 000	1.0-3.0	10^{-6}	T91 FeCrAlY GESA
LINCE (CIEMAT)	450	10 000	1	10^{-8}	T91, 316L
LECOR (ENEA)	450	2 000	1	10^{-8}-10^{-10}	T91, 316L
CHEOPE III Pb (ENEA)	500	10 000	1	10^{-6}	T91, 316L

The development of a corrosion protection barrier has been based on the application of an Fe, Al coating on the steel surface. A technology has been developed to treat claddings, which consists in low pressure plasma spraying (LPPS) Fe-Al based powders and re-melting of these LPPS coatings with a pulsed electron beam (GESA). The coatings obtained in this way have been tested in the different facilities as shown in Table 2 and Figure 3.

A scheme of the mechanical tests performed on the two steels in contact with the HLM is given in Figure 2. This figure shows that a number of time dependent and time independent tests have been conducted over a wide temperature range. Almost all tests have been performed in HLM and *ad hoc* test section, measurement devices and measurement procedures have been developed.

The irradiation experimental programme initiated (see Figure 3) had the aim to support the materials characterisation of both the core components and the spallation target. In particular, irradiation experiments on T91 and coated T91 steel in Phénix, in HFR and BR2 have been launched. The samples irradiated in HFR and BR2 were encapsulated in LBE, in order to study LBE/n irradiation combined effect. However, it must be underlined that the time needed for the

design, start-up and completion of irradiation and execution of the post-irradiation examination (PIE) of such programmes normally take much longer than the duration of projects supported by the European Commission. For instance almost all PIE of the DEMETRA irradiation programmes are going to be performed in the FP7 Project GETMAT [5].

Figure 2: Scheme of mechanical tests performed in HLM on T91 and 316L [2]

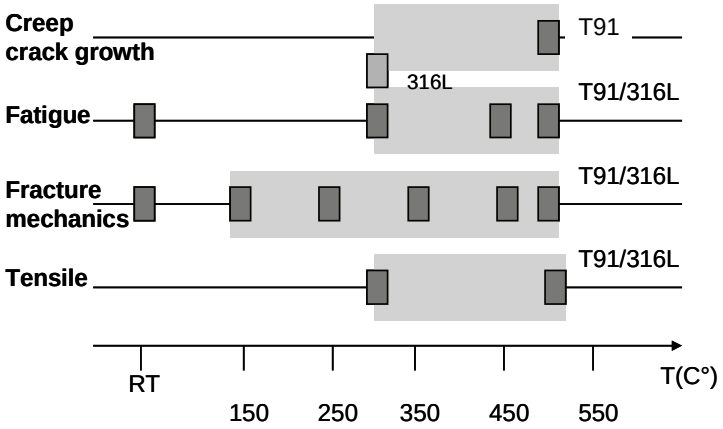

Figure 3: Scheme of the irradiation test programme started within DEMETRA [2]

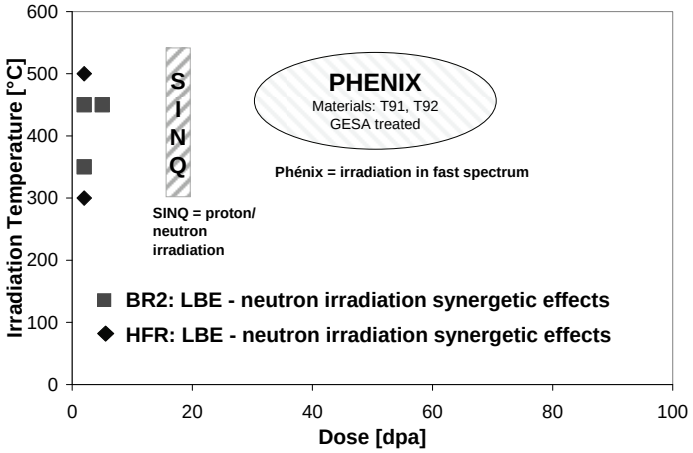

Core thermal-hydraulics and safety-related experiments

The core thermal-hydraulics studies had the objective to simulate the heat transfer characteristics in a single pin and a fuel bundle. Moreover integral experiments have been prepared to assess the interaction of components. Finally, safety-relevant experiments such as the LBE/water interaction have been conducted as well. All experiments have been supported in their preparation and evaluation of results with numerical simulations. Furthermore, many experiments served to validate new or existing numerical approaches. The objectives and scheduled experimental campaigns for these experiments are hereafter summarised.

Single-pin experiment in the TALL (KTH) [6]

To investigate thermal-hydraulics of an annular channel accommodating a single fuel rod simulator cooled by lead-bismuth eutectic (LBE), experiments were performed on the TALL test facility where the single rod test was conducted in a cylindrical geometrical configuration.

Figure 4 shows a schematic of the fuel pin simulator installed in the TALL facility. The experimental campaign foresaw the measurement of the heat transfer from the fuel pin simulator across a stainless steel cladding to the outer flowing channel of LBE coolant in turbulent conditions. Heat exchange correlations were defined and used in thermal-hydraulic computer code, and heat exchange coefficients across the cladding with a cylindrical subchannel geometry under different temperatures, flow rates and power rates at steady state and transient conditions were predicted. Several transients such as loss of heat sink, loss of external driving heat, start-up and shutdown, etc. were simulated.

Figure 4: Schematic view of the fuel pin simulator installed in the TALL facility

TC_S are multi-level thermocouples for temperature measurement in the heated part; TC are thermocouples for local temperature measurement at the inlet and outlet; ΔP is the differential pressure transducer for pressure measurement in the heater housing

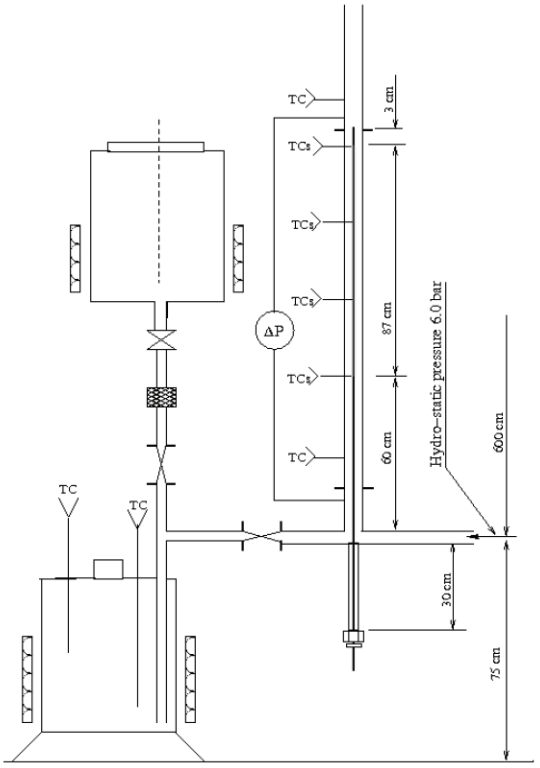

Fuel bundle experiment in KALLA (KIT) [6]

The objective of the fuel bundle experiment is to elaborate a data basis and numerical methods to estimate the performance of liquid LBE-cooled fuel assemblies and their behaviour at normal and abnormal operation conditions. Indeed, the experimental layout has not been selected to qualify a particular subassembly design; therefore it is clear that this experimental campaign is far beyond design qualification purposes. However, it has been attempted to construct the experimental set-up such that it is representative of the XT-ADS fuel assembly design, i.e. a hexagonal closed lattice is employed with a representative (small) rod diameter and pitch-to-diameter ratio. Hence, to establish qualified numerical tools which can predict the thermal-hydraulic operation characteristic of a fuel assembly in LBE, a coherent multi-step experimental programme has been conducted. The multiple steps are:

- *Single pin test* with the objective to perform detailed measurement of the temperature and velocity distribution along a vertical single pin in an annular cavity in forced convection, mixed convection and buoyant convection conditions. This experiment has

allowed the determination, for a thermally developing flow, the mean dimensionless temperatures at the fluid wall interface (which is the inverse of the Nusselt number) and the time dependent behaviour of the lateral and axial turbulent momentum and energy exchange. The latter is of crucial importance for the development of liquid metal adapted fluid dynamic codes. In the context of the experiment independent calculations using different commercial CFD codes have been performed [7,8].

- *Zero power isothermal fuel bundle test in water*, which is geometrically identical in all dimensions to the liquid metal experiment. The aim of the experiment performed in water is to optimise the flow conditioner and the assembly inlet upstream the fuel bundle in such a way that the flow rate through all fuel pins is (nearly) identical in order to ensure "clean" boundary conditions. Moreover, non-intrusive measurements of the lateral and axial velocity profiles as well as their fluctuations have been performed in order to qualify the numerical tools with respect to the simulation of the hydraulics as this will hardly be possible in the LBE experiment.
- *Fuel bundle experiment in liquid LBE at nominal power*, consisted of 19 identical rods with an active length of 870 mm, releasing a thermal power of 428 kW. Figure 5 shows the KALLA THEADES loop where the fuel bundle experiment in LBE is performed. Herein, the axial and lateral thermal energy transfer from the rods to the liquid metal is measured using traversable thermocouple arrays at different axial heights. Additionally, it is intended to measure the flow rate in subchannels using a Prandtl/Pitot tube. Pre-calculations of the fuel bundle experiment have been performed with subchannel code MATRA.

Figure 5: Three-dimensional sketch of the flow scheme and the main components of the THEADES loop in KALLA

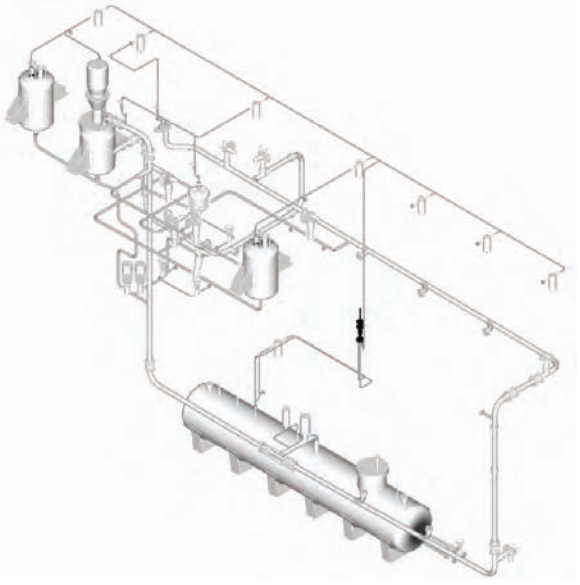

Integral experiment in CIRCE (ENEA) [6]

The aim of the Integral Experiment performed in the CIRCE facility (a scheme of CIRCE is presented in Figure 6) was the analysis of components and measurement systems such as the heat exchanger and chemistry quality control system, as well as the coupling of components (e.g. heat source and cold sink) in a pool configuration and under conditions as far as possible representative for the ADS systems designed within the project. Moreover, the planned study has foreseen the investigation of the behaviour of the integrated system under steady state

circulation and under transient conditions in the pool configuration. In particular, the characterisation of the natural circulation regime in the pool as well as the transition from forced to natural circulation has been planned.

Figure 6: Scheme of the CIRCE facility

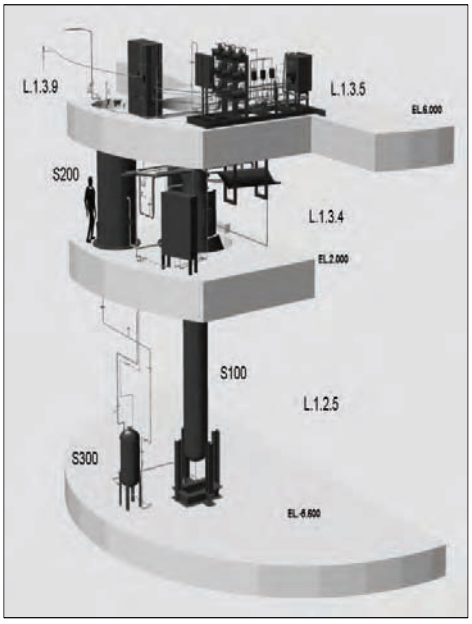

LBE/water interaction experiment in LIFUS-5 (ENEA) [9]

Both the XT-ADS and EFIT designs adopt steam generator modules placed into the liquid metal pool in order to extract the power from the main vessel. The objective of the LIFUS-5 experiment is to evaluate the consequences of water leakage in the pool due to steam generator tube ruptures. Even if chemical exothermic reactions of Pb and LBE with water are excluded, the interaction between hot pressurised water/steam and HLM can be a concern for this kind of reactor design. Indeed, the LBE/water interaction can lead to propagation of pressures waves which could damage the internal structures of the main vessel, causing an escalation of the accident. Moreover, the steam can flow through the core causing reactivity insertion due to the positive void reactivity coefficient. The LIFUS-5 experimental campaign has been aimed at the assessment of the physical effects and the possible consequences related to this kind of interaction and to provide data for the validation of the mathematical modelling [10].

Neutron spallation target and measurement techniques

As far as the design of the neutron spallation target was concerned, for the EUROTRANS project, mainly the windowless design has been investigated. However, the window option has not been completely rejected. Therefore, within DEMETRA both options were investigated by performing the post-test analysis of the window target MEGAPIE [11] and by supporting the development of the XT-ADS windowless target through design and experiments. Moreover, experimental techniques were developed for the free surface measurement of the target and for flow and velocity measurement of all thermal-hydraulic LBE experiments performed within DEMETRA [12].

Post-test analysis of the window target MEGAPIE

The MEGAPIE experiment has been very important since it was the first experiment to design, manufacture, commission and operate a liquid metal spallation target at the MW beam power

level [13]. The design phase of the project was supported by R&D work divided in several areas, and performed by specialists from the corresponding research fields, studying problems related to thermal-hydraulics, structural mechanics, materials issues, neutronic and nuclear assessment. After a test phase, the MEGAPIE target was irradiated in 2006 at the SINQ facility of the Paul Scherrer Institut [11]. The post-test analysis (PTA) of the MEGAPIE-SINQ Experiment (MSE) focused on three distinct areas: *i)* operational experience and components behaviour; *ii)* thermal-hydraulic behaviour; *iii)* neutronic and nuclear behaviour. The main objective of this task was the elaboration of lessons learnt by combining the pre-irradiation, irradiation and post-test analysis phases.

XT-ADS windowless target: Design and experiments

Within the XT-ADS core a limited space has been made available for the location of the neutron spallation target. This circumstance together with the high-power proton beam (3 mA and 600 MeV) envisaged for the XT-ADS led to high-power density deposition which might challenge the time-dependent performance of the structural material of a neutron spallation target beam window. Due to this consideration, a windowless target option has been investigated as the reference option for the XT-ADS. The thermal-hydraulics of the windowless target must ensure that the heat deposited into the HLM can be safely removed without jeopardising the vacuum of the proton beam line thus avoiding recirculation flow in the deposition zone [14]. The objectives of the activities were related to the definition of design rules for a stable free surface and the hydraulic validation of the selected design options with experiments performed in water and LBE [14]. These experiments should also serve as validation for numerical tools which should enable to analyse on top of the hydraulic behaviour also the heat transport, which cannot be done in an experiment.

XT-ADS and EFIT component design and R&D needs

The XT-ADS [15] and EFIT [15a] were designed during the five-year EUROTRANS project, while the DEMETRA experimental programme was defined at the beginning of the project. This combination was possible since previous projects, e.g. PDS-XADS [15b], TECLA [16], SPIRE [17] and MEGAPIE-TEST [11] have allowed a preliminary understanding of key technological issues in the HLM area. However, during the EUROTRANS project an intensive exchange of information between the DEMETRA domain and the designers occurred which allowed to support design choices for different components. In the following paragraphs some design highlights are given.

The XT-ADS system has been designed with a maximum core power of about 60 MWth and capability of the primary system corresponds to a power of 70 MWth. The coolant of XT-ADS is LBE and the core inlet and the mean outlet temperatures are 300°C and 400°C respectively. A scheme of the XT-ADS is shown in Figure 7, and Table 3 summarises the operational conditions of the XT-ADS key components.

The EFIT reactor has been designed with a maximum core power of 400 MWth. The EFIT coolant is pure lead and the core inlet and the mean outlet temperatures are 400°C and 480°C respectively. The EFIT is schematised in Figure 7 and Table 4 summarises the operational conditions of EFIT components.

A key issue to be addressed for the use of lead or lead-alloy as coolant in nuclear reactor systems is the selection and qualification of structure and clad materials. In the high-temperature operation range the molten lead and lead-alloy are corrosive towards structural materials and can induce/accelerate material failure under static loading, such as brittle fracture, and failure under time-dependent loading, such as fatigue and creep.

The main parameters impacting the corrosion rate of steels are the chemical and metallurgical features of the steel, the temperature, the liquid metal velocity and the dissolved oxygen concentration. For design purposes it is relevant to know the corrosion behaviour of the

Figure 7: Scheme of XT-ADS (top) and EFIT (bottom)

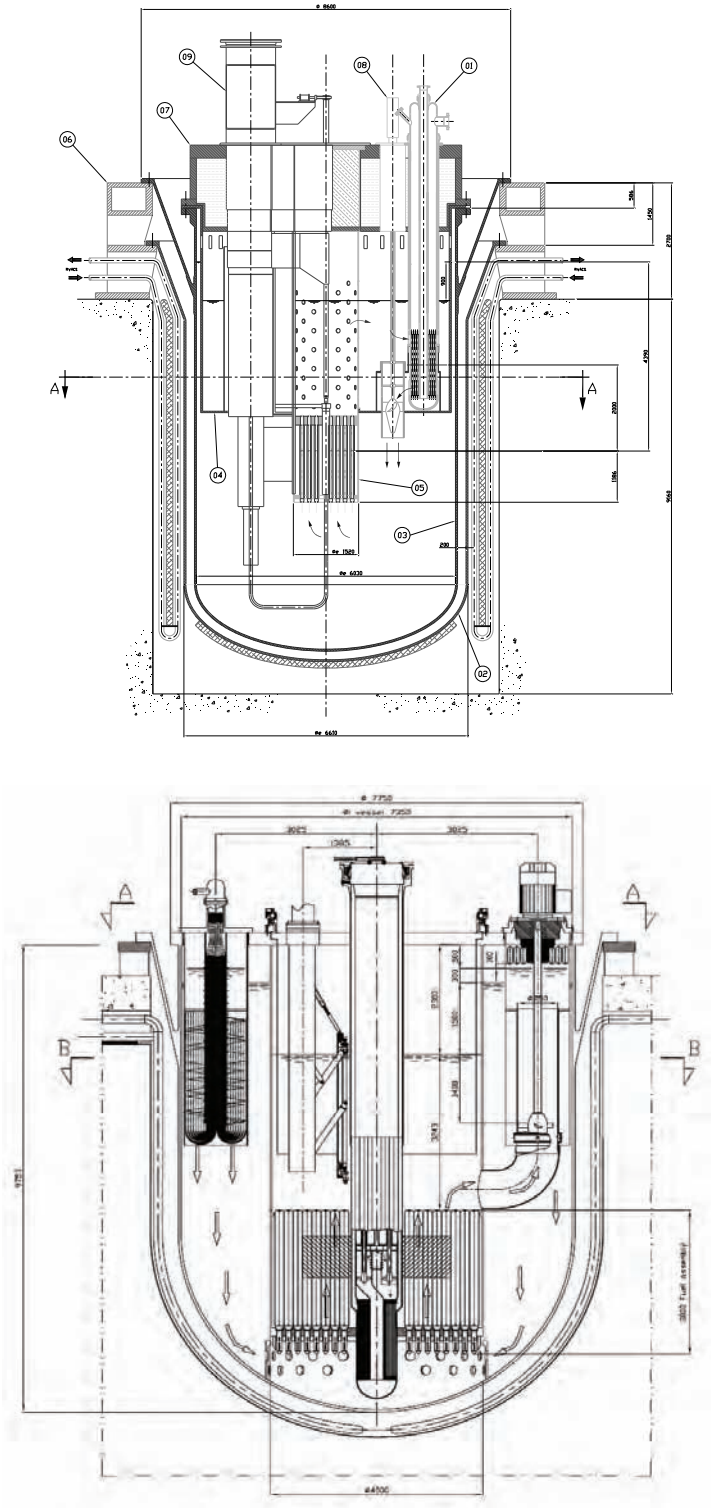

TECHNOLOGY AND COMPONENTS OF ACCELERATOR-DRIVEN SYSTEMS, ISBN 978-92-64-11727-3, © OECD 2011

Table 3: Summary of materials selection and operational conditions of XT-ADS

Component/subcomponent	Material	Replaceability Y = yes N = no	Operating temperature (°C)				Radiation damage (dpa/365 EFPD)	Local LBE velocity (m/s)	Mechanical stresses (MPa)
			Operation at max core power	Operation at max primary system power	DHR via safety system No. 1	DHR via safety system No. 2			
Fuel assemblies	T91	Y		NA					NA
• Lower region (up to lowermost fuel pin evaluation)			300		300	550		1.3	
• Hot fuel pin (clad)			430		370	550	29	1.6	
• Fuel pin grind region			430		370	550	29	2.3	
• Upper region (above fuel pin topmost elevation)			387		365	550	30	1.3	
Dummy assemblies	T91	Y	NA	NA	365	550		0.2	NA
Core barrel		Y		NA	365	550		–	110
• Lower region (below diagrid)	AISI316L		387				2.4		
• Diagrid	T91		387				1.4	0.3	
• Upper region (above diagrid)	AISI316L		356						
Steam generators	T91	Y							247
• Inlet (LBE side)			356	370	350	550	0.05	1.1	
• Outlet (LBE side)			300	300	270	550		1.1	
Circulation pumps	To be defined MAXTHAL (Ti_3SiC_2)	Y	300	300	270	550			NA
• Shaft (upstream the hub)								2	
• Impeller (around the hub)							0.1	9	
• Casing								3	
Reactor vessel	AISI316L	N							114
• Close to the coolant free surface			356	370	370	550	10^{-4}	0.01	
• Below inner vessel (lower plenum)			300	300	300	550		0.1	
Inner vessel	AISI316L	Y	356	370	370	550	1	0.1	234
Above core structures (IPS)			356	370	370	550	NA		NA
Refuelling equipment	AISI316L	Y	356	370	370	550	NA	–	NA
Target	T91	Y	Pertinent data reported in dedicated Table 4.1-2 of Ref. [4]						

Table 4: Summary of materials selection and operational conditions of EFIT

Component/subcomponent	Material	Replaceability Y = yes N = no	Operating temperature (°C)			Radiation damage		Local lead velocity (m/s)	Mechanical stresses (MPa)
			Operation at power (normal condition)	DHR via safety system No. 1	DHR via safety system No. 2	(dpa/years)	(dpa)		
Lower support structure	AISI316L	N	400	420	380	$< 10^{-5}$	$< 10^{-4}$	0.8	NA
Diagrid	AISI316L	Y/N	400	420	380	0.01	0.2	–	NA
Fuel assemblies Inner core zone peak pin, BOL-EOL • Lower region (up to lowermost fuel pin elevation) • Fuel pin region • Upper region (above fuel pin topmost elevation)	T91	Y	 400 519-555 480	 420 475 470	 380 425 420	NA	NA	 1.5 1.1 1	 13.7 12.2 12.2
Intermediate core zone peak pin, BOL-EOL • Lower region (up to lowermost fuel pin elevation) • Fuel pin region • Upper region (above fuel pin topmost elevation)	T91	Y	 400 511-538 480	 420 475 470	 380 425 420	NA	NA	 1.5 1.1 1	 13.7 12.2 12.2
Outer core zone peak pin, BOL-EOL • Lower region (up to lowermost fuel pin elevation) • Fuel pin region • Upper region (above fuel pin topmost elevation)	T91	Y	 400 526-541 480	 400 475 470	 380 425 420	NA	NA	 1.5 1.1 1	 13.7 12.2 12.2
Dummy assemblies	T91	Y	480	470	420	NA	NA	0.01	NA
Core restrain plate	AISI316L	Y/N	480	470	420	0.003	0.06	–	NA
Pump duct upstream the pump	AISI316L	Y/N	480	470	420	$< 10^{-3}$	0.01	3.0-1.6	NA
Circulation pumps • Shaft • Impeller • Casing	 MAXTHAL (Ti_3SiC_2) MAXTHAL (Ti_3SiC_2) MAXTHAL (Ti_3SiC_2)	Y	 480 480 480	 470 470 470	 420 420 420	$< 10^{-5}$	$< 10^{-4}$	 2 10 3	NA
Pump duct downstream the pump	AISI316L	Y	480	470	420	$< 10^{-5}$	$< 10^{-4}$	1.6	NA

steels in a relevant range of these parameters. Moreover, one of the provisions adopted in the design to impact the corrosion resistance of the selected candidate materials (T91 and AISI 316L steels) is to maintain a controlled amount of oxygen dissolved in the melt. Therefore oxygen control systems and strategy in a pool-type reactor need to be investigated and assessed.

In the high-temperature range, the corrosion resistance of structural materials can be enhanced by FeAl alloy coating. This is of great interest for the fuel cladding or in general for heat exchanger tubes for which protective oxide layer thickness shall be limited so that the heat transfer characteristics are not significantly affected.

The design approach for both LFR (ELSY) and ADS (XT-ADS; EFIT) has been to limit the mean core outlet temperature to less than 500°C, and to protect the T91 steel, as the construction material of the unavoidably thermally high loaded fuel cladding tubes, with Fe/Al alloy coating. However a qualification programme for the use of the coatings is mandatory in order to demonstrate their mechanical stability, adhesion to the substrate, etc., under relevant conditions.

Other provisions taken in the design to preserve structural material integrity against erosion phenomena have been to impose an upper limit of 2 m/s on the coolant flow velocity. An exception to this rule is for the mechanical pumps, where the maximum relative flow velocity is limited to 10 m/s. Alternative structural materials for the pump impeller, resistant to this high velocity, shall be identified and characterised. Promising candidates are silicon carbide and titanium based alloys.

The R&D programmes including corrosion tests in flowing liquid metal (with representative parameters of the fuel cladding and in-vessel components) to estimate corrosion kinetics and to assess the long-term stability of the protective layers, will confirm the design assumptions or will provide more suitable data.

In addition, the use of lead or lead alloy for both LFR and ADS concepts requires an assessment of their compatibility with structural materials under the fast neutron spectrum typical of fast reactors. The acquired experience with sodium-cooled fast reactors is not transferable to lead and lead alloys, owing to the significant differences in their physical and metallurgical properties. Therefore dedicated test plans should provide data, particularly in the higher-temperature range, on tensile, creep, creep-fatigue and fracture mechanics and fatigue crack growth of the selected steels in contact with lead.

Selected experimental results

Coolant chemistry

Particularly interesting for design purposes is the oxygen activity in the liquid metal since it is relevant for the corrosion behaviour of the selected steels. Indeed, it is recommended to keep the oxygen potential at an appropriate level to allow surface oxidation of the structural and clad materials (more details are given in the next sub-paragraph). However, this level must not exceed the potential of the lead oxide formation, since these oxides are normally solid and can create blockages of fuel bundle and/or heat exchanger channels with consequences that can be safety relevant. This oxygen potential range is schematised in Figure 8.

Therefore, an important parameter to be monitored in HLM system is the oxygen potential, which can be measured with electrochemical probes [19]. Figure 9 shows a scheme of such a probe.

All aspects related to the design and signal optimisation of the electrochemical probe have been investigated and described in several documents [19,20]. Hereafter only some aspects are summarised. The oxygen probe is made of a solid electrolyte (yttria-stabilised zirconia, YSZ) and studies have shown that the mechanical strength of the YSZ can be enhanced by addition of

Figure 8: Oxygen potential limits as function of temperature [18]

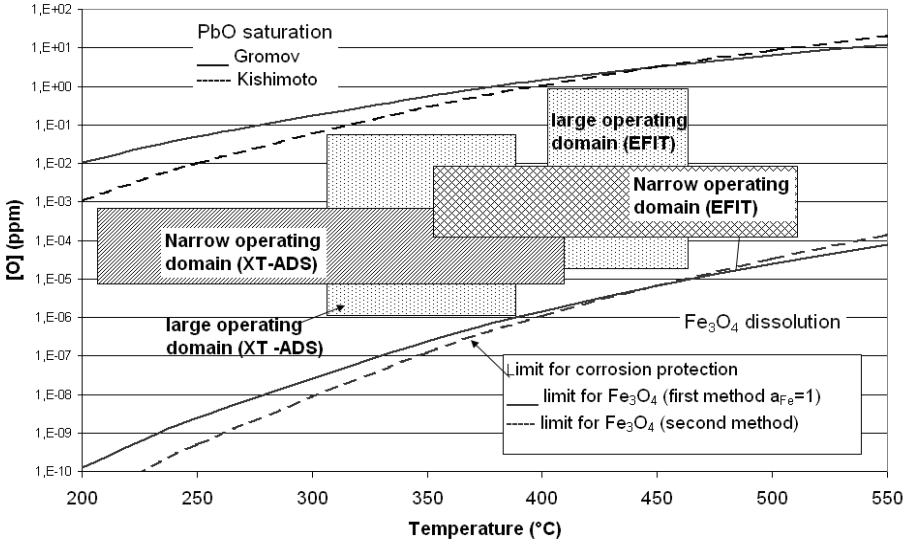

Figure 9: Scheme of the electrochemical oxygen probe [20]

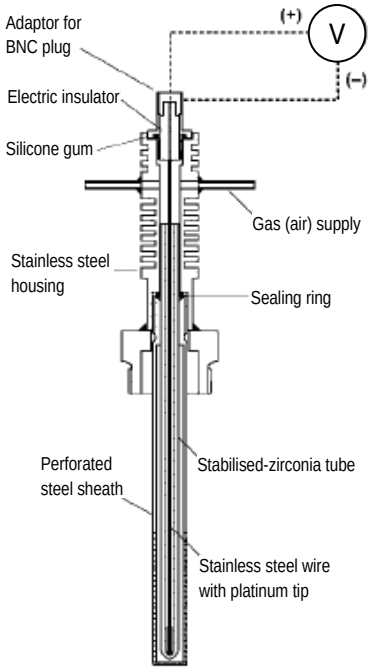

oxides as e.g. the Al_2O_3. Moreover, various reference electrodes have been tested and it has been shown that the Pt/air electrode reduces the requirements on the mechanical stability of the electrolyte, while for instance the Bi/Bi_2O_3 electrode increases the risk of electrolyte cracking. Finally, activities on the second (or working) electrodes have shown that application of a protecting sheath around the electrolyte gives rise to sensor fouling and should be avoided [19,20]. The optimised sensors have also been tested and several reports have been issued [19,20], some aspects on the sensor signal are herein summarised. The signal transmission is a key issue for application of these sensors in pool-type reactors. Moreover, if thermoelectric voltage corrections are performed, these sensors can reach an absolute accuracy corresponding to ±10% with respect

to oxygen concentration. In-plant testing has also allowed establishing methods to detect if the sensor is working or is flawed. Finally, long-term performance of the sensors has been confirmed in loop-type facilities. However, missing data are the performances of the sensors in pool-type systems and effect of, for instance, radiation fields on the signal.

Oxygen supply devices have been analysed as well, and in particular the amount of oxygen needed at start-up and during operation in the XT-ADS and EFIT device were determined. The oxygen supply rate and quantities are considerable and demonstration experiments of gas or solid phase supply systems are needed to assess their suitability for large-scale pool-type devices.

Oxygen supply at the beginning of the reactor might be lowered to more reasonable values by using passivated steels. For gas phase supply, it was shown that a gas mixture H_2O/H_2 which is currently used in small loop cannot lead to a proper regulation of oxygen content in large-scale facilities. In the CORRIDA loop [19,20], $Ar/O_2/H_2O$ mixtures, with 0.1-1 O_2%, were successfully used to obtain oxygen content around 10^{-6} wt.%. Most of the oxygen is brought in the liquid metal by O_2, and it was found that much more stable conditions are obtained with small water additions. Such mass exchangers could theoretically bring enough oxygen in large-scale facilities. However, further tests must be provided in order to prove that under such conditions no oxide formation is favoured at the gas/liquid interface. Another major drawback of a gas system is the risk of contamination by the volatile fission or activated products especially polonium, tritium and caesium. The studies performed on the solid phase supply exchanger [18] have shown that this technology requires carefully designed devices. Moreover, the validity of this technology for large-scale facilities (at least for EFIT) is questionable due to the frequent refilling needed associated with the possible contamination of the exchanger by activated products (mostly 54 Mn). Tests performed on these devices have demonstrated that a heterogeneous distribution of the oxygen content in the liquid metal could occur in small loops, especially when some pollution by oxides exists. It then stresses the necessity to install oxygen probes in each different part of the circuit (core and steam generators at least) to deliver proper oxygen content where needed.

Materials

The experimental results obtained from the T91 and the 316L steels can be summarised as shown in Figures 10 and 11, respectively.

The two figures indicate that for T91 steel selected as material for the core component the operational temperature window is between ~370 and ~480°C. As far as the neutron irradiation is concerned, in general for 9Cr martensitic steels, irradiation hardening and embrittlement are maximum in the temperature range 250-330°C. This is due to a high density of small dislocation loops formed by clustering of point defects. At higher irradiation temperatures, the loop density decreases. Experimentally it is found that hardening quickly drops with increasing irradiation temperature at above ~400°C [20a,20b]. At 450°C, 9Cr martensitic steels display no hardening. On the other hand the liquid metal can cause embrittlement if stresses and wetting exceed certain values. However, a ductility recovery is observed in the temperature range 400-480°C [20c-g]. In this range of temperature, data on liquid metal assisted cracking are not available. The high temperature range application of T91 steel is limited in principle by two factors. First of all, vigorous oxidation can occur with the occurrence of oxide damage and detachment. The damage of the oxide layer can allow a direct contact between the liquid metal and the base material and liquid metal assisted cracking can be initiated. Second, detached layers are solid impurities and can cause plugging in the core or heat exchanger regions with impact on the thermal-hydraulics and safety of the system. The second factor limiting the high-temperature application is inherently related with the T91 steel, which has a relatively low thermal creep resistance.

As far as the temperature range for application of the AISI 316L steel is concerned, in the low-temperature range irradiation hardening can occur. The upper temperature limit for the AISI 316L steel is dictated by the corrosion attack which occurs in a significant way even at

Figure 10: Summary of experimental results obtained on T91 steel

T	300-400°C	400-480°C	480-550°C
n irradiation	Hardening and embrittlement.	Slight or no hardening and embrittlement.	No hardening and no embrittlement.
Corrosion	No significant attack given that flow does not cause erosion.	No significant attack given that oxygen is controlled (thick scale to be avoided).	Even with oxygen control, too-high scale thickness (spall-off).
Mechanical in HLM	LME damage possible if wetting and stresses exceed a certain value.	No LME has been observed and ductility recovery has been postulated. Experiments on assess LM assisted degradation are needed.	LM assisted degradation (e.g. creep resistance reduction) if stresses exceed threshold conditions and oxide scale fails (wetting). **Alternative protection needed.**

Figure 11: Summary of experimental results obtained on AISI 316L steel

T	300-400°C	400-480°C	480-550°C
n irradiation	Hardening occurs.	No hardening and embrittlement (peak swelling).	No hardening and embrittlement (peak swelling).
Corrosion	No significant attack given that flow does not cause erosion.	Oxygen control is important (dissolution attack can start if no protection of the steel).	Even with oxygen control, dissolution can occur.
Mechanical in HLM	No significant impact.	No significant impact. Dissolution corrosion can cause wall thinning therefore reduce load bearing capability.	No significant impact. Dissolution corrosion can cause wall thinning therefore reduce load bearing capability. **Alternative protection needed.**

temperatures in the order of 450°C if the oxygen potential in the HLM is not properly adjusted. Even if a corrosion attack seems not to change the mechanical properties of the steel, the corrosion would reduce the load bearing capability due to wall thinning. In addition, it is well know that the austenitic steels show low stability in the high dpa range. Indeed, for 316L, under fission neutron irradiation and with a flux typical of fast reactors, maximum swelling occurs around 450-500°C leading at medium-high dpa to loss of dimensional stability and drastic decrease of impact and tensile properties, and toughness.

As far as oxidation rate is concerned, it has been confirmed that the rate is temperature and oxygen concentration dependant. The experimental matrix did not allow the definition of oxidation rate law which can be generally applied. However, some trends on T91 steel could be defined and are reported in Figure 12.

The assessment of the oxidation rate is of relevance for those components where heat exchange occurs, since oxides have a lower thermal conductivity compared to the steel. Indeed, oxide scale thickness on fuel pin claddings should not exceed a certain value in order to avoid that the cladding temperature increases above the maximum allowable. Similar considerations also need to be performed for the heat exchanger tubes.

For both steel candidates it has been suggested to use corrosion protection methods based on Fe, Al coatings in case of high temperature and/or long exposure times, where thick oxide scale can create issues related to protection effectiveness due to flawing of the scale or related to low thermal conductivity. The GESA coatings have been developed and tested within DEMETRA [23].

Figure 12: Trends of oxidation rate on T91 steel as function of temperature in Pb and LBE [21,22]

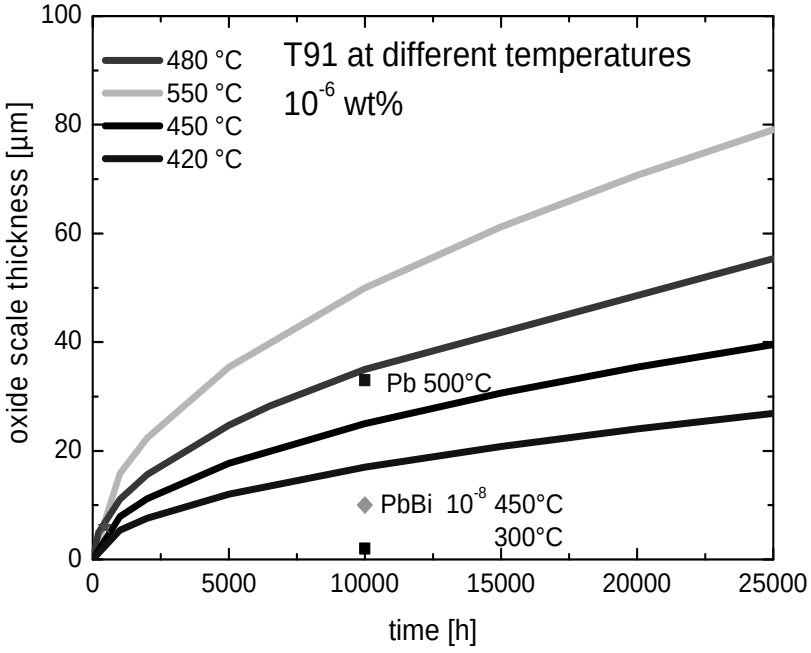

Long-term and high-temperature corrosion (up to 600°C) and erosion (up to 3 m/s HLM flow velocity) experiments have shown a high stability of the GESA coatings. However, it has been demonstrated that the Al content in the coating must be carefully set in order to get such satisfactory behaviour in a wide temperature and oxygen concentration range. Mechanical tests of the GESA-coated samples have been performed as well, showing that the mechanical performance of the steel is not affected by the coating, on the contrary the coating has a certain ability to protect the T91 steel against liquid metal mechanical properties degradation [24]. In summary, these coatings are very promising. However, further activities are needed in order to confirm the stability of the coatings under irradiation and in presence of the liquid metal and to define a quality assurance in the production of the coatings as far as chemical, physical and metallurgical homogeneity is concerned.

Core thermal-hydraulics and safety-related experiments

The experimental campaigns on the core thermal-hydraulics were conducted through the three large-scale experiments in the TALL, KALLA and CIRCE facilities. The TALL experiment on the single pin was the most conclusive one, while the experiments in KALLA and CIRCE have only produced preliminary results and further tests will be performed within the THINS project [25].

The objective of the single pin experiment performed at the TALL test facility was to investigate thermal-hydraulics of an annular channel accommodating a single fuel rod simulator cooled by LBE. Results of the thermal-hydraulic characteristics were obtained under steady-state transient and natural circulation conditions. The following findings are noteworthy [26]:

- The LBE temperature has a strong effect on its viscosity, which mainly contributes to the frictional resistance. A high resistance holds for a low-temperature flow.
- The effect of the heat source (heating) and the heat sink (cooling) on natural circulation flow rate can be reflected in the relation between the flow rate and temperature difference (as was shown previously).

- The most important from the safety performance point of view is the loss of heat sink, where the temperature increases first from the outlet of the heat exchanger rising downstream and draw the whole loop. The temperature keeps rising if no protective measures are taken to mitigate the transient.
- For the transient loss of external driving head, the temperature increases to a higher level and a significant natural circulation is obtained.

Moreover, simulations of the steady-state experiments have been performed with ANSYS CFX 11 where user expressions have been used to implement material properties of LBE. The results of the simulation show a reasonable agreement between the numerical data calculated with a standard turbulence model and the measurement data [26].

The fuel bundle experimental campaign performed at KALLA, as previously indicated, consisted of a three-step programme where a single pin in an isothermal bundle in water and a fuel bundle in LBE were tested. The results of the first experimental campaign are discussed in the following paragraphs [27].

As far as the single rod experiment is concerned, the large influence of buoyancy on the velocity profile even at relatively high Reynolds numbers was observed, while the temperature field is less influenced. This phenomenon yields to an enhanced heat removal and the currently used Nusselt correlations are rather conservative. The experiment allowed validation of numerical approaches to predict turbulent heat transport for a nuclear HLM core relevant rod geometry in a forced convection regime.

The water rod bundle experiment showed a very good agreement of measured pressure loss with numerical predictions in the fully turbulent flow regime whereas in the transitional regime secondary flow leads to a rising loss coefficient. Moreover, the measurements showed negligible flow induced vibrations onto the set-up, therefore the spacers as designed have also been retained for the LBE experiment.

The first LBE rod bundle experiment performed, which had a simplified configuration (i.e. only 3 out of the 19 fuel rod simulators were heated), showed that the pressure loss and temperature difference measurements agree with theoretical expectations. Moreover, a higher pressure loss in the first spacer of the set-up can most probably be ascribed to solids (e.g. oxides) present in the loop, causing a partial blockage of the channel.

For the integral experiment performed in CIRCE the effort was placed on the design of the test section, which has foreseen the coupling of a high-power heat source with a prototypical heat exchanger and implementing an oxygen control system. The first steady-state tests have been performed, and temperature profiles have been recorded and system analysis of these results will be performed. Moreover, additional tests are foreseen in the near future, simulating several operational and accidental transients to characterise the natural circulation flow regime. The objective will be the establishment of a reference experiment for the benchmark of commercial codes when employed in HLM pool systems [28].

The LBE/water experiments were performed in the LIFUS-5 facility [29]. During the experimental programme modifications of the LIFUS-5 facility were made in order to be more representative of the pool-type condition [29]. A scheme of the modified LIFUS-5 is given in Figure 13. The parameters that can be changed in this facility are the temperatures of water and LBE, the water injection pressure and flow rate and the quantity of LBE in the test section. Several combinations of experimental parameters have been used to run the experimental campaign. Moreover, the preparation of the experiments has been performed with the support of numerical calculations performed with the SIMMER code.

As example of one of the LIFUS-5 experiments performed with an LBE temperature of 350°C; a water injection pressure of 40 bar and a water temperature of 245°C, Figure 14 shows the trend of the pressure at the level of the water injection. As shown in this graph a pressure spike has

Figure 13: Scheme of the LIFUS-5 facility

The vessel S1 represents the test section, which is instrumented with thermocouples and pressure transducers at different heights. In S1 high temperature, high pressure water is injected from the bottom into the LBE.

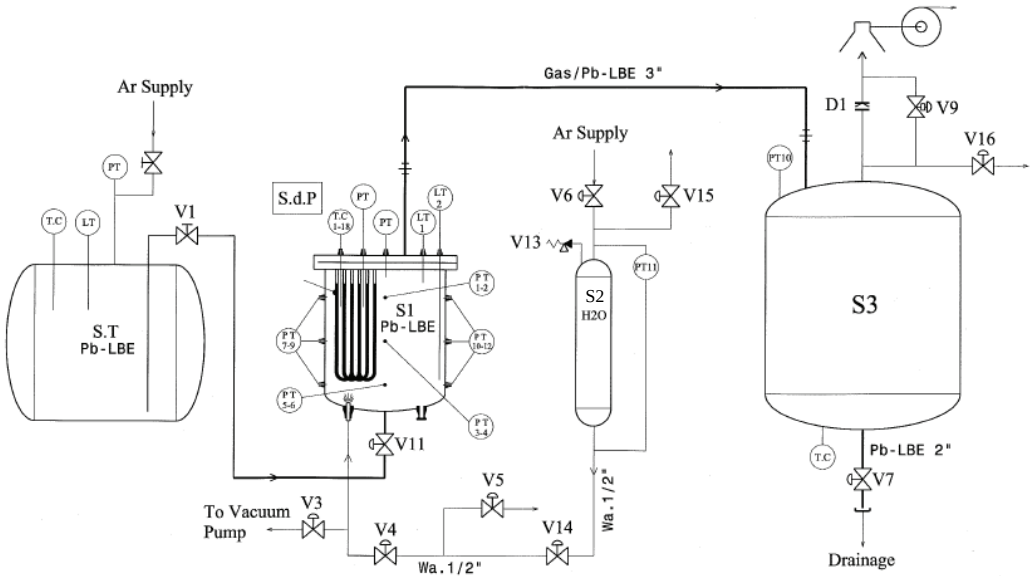

Figure 14: Pressure increase measure close to the water injector

At the beginning of the water injection a pressure spike has been measured [30]

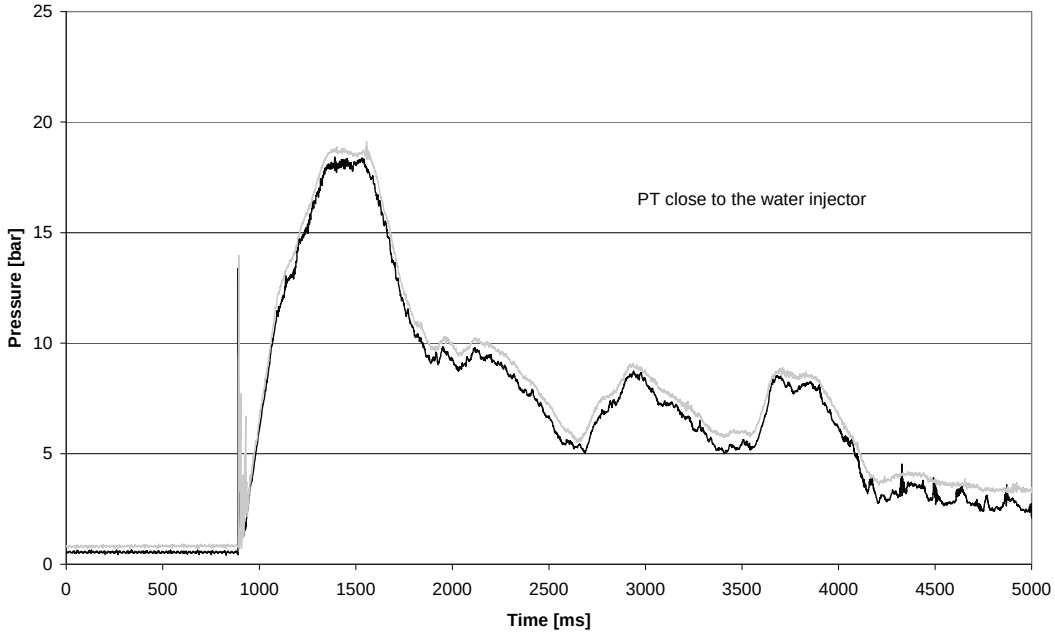

been observed at the beginning of the water injection. The occurrence of such spikes needs to be investigated more deeply in terms of thermo-mechanical impact on the tubes of the steam generator. These experimental results are useful for code validation. However, a direct application of the results to the real steam generator design of XT-ADS and EFIT is not possible since there is a large difference between the geometrical configuration of the experiment and the real steam generator.

Neutron spallation target

Within DEMETRA activities on the design of the windowless spallation target were performed. The objectives were the numerical support to design the water and LBE experiment and to find technical solutions that allow the stabilisation of the free surface [14]. In Figure 15 a scheme of the spallation target is shown.

Numerical tools and physical models were selected and evaluated in terms of capability and validated against the experimental results. As numerical methods the volume of fluid extended with mass transfer capabilities using existing models for cavitation prediction (VOF+) which are available in STAR-CD, STAR-CCM+ and CFX, Euler-Euler methods available in CFX, and Moving Mesh Algorithm were used and the pros and cons of the three methods were evaluated [31]. Various versions of the spallation target nozzle design were assessed numerically and together with the feedback from the first water experiments and design conditions of the XT-ADS, design rules in order to achieve stable free surface could be formulated as follows:

- the maximum allowable velocity in feeder nozzle is 2.5 m/s (due to corrosion);
- forced detachment by enlarging the guide tube is stabilising the free surface because it prevents stream downward disturbances propagating upwards;
- suppression of cavitation in feeder nozzle is achieved by radial fins which induce the necessary pressure loss or drag and by flow acceleration in the near nozzle region which is achieved by contracting nozzle geometry;
- minimising of recirculation zone is achieved by a small injection angle at feeder nozzle outflow.

The formulated design rules were applied in order to define the target nozzle to be tested in water. Figure 15 shows the target geometry and the nozzle design, where the radial fins on the nozzle are applied.

Figure 15: Scheme of the neutron spallation target (left) and "detached flow" target geometry (right) [32,33]

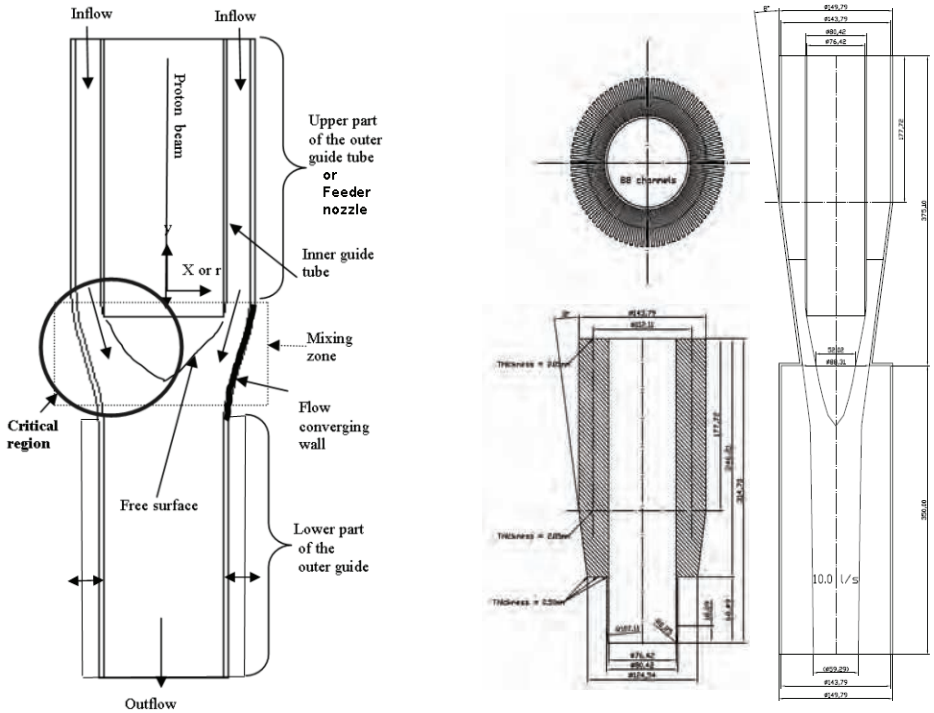

This design has been adopted to perform experiments in water. Experimental results and corresponding CFD calculations are shown in Figure 16 for nominal flow, 10 l/s. Moreover, in Table 5 the effect of the flow rate on the free surface position is shown. This table indicates that both experiments and physical simulation show the same trend, i.e. by increasing the flow velocity the position of the free surface moves to a higher position. The differences between experimental and numerical values are due to uncertainties in the measurement of the position from the experimental side and the exact definition of the boundary conditions from the numerical side.

Figure 16: Experimental results and corresponding CFD calculations for nominal flow, 10 l/s

Predicted water volume fraction (WVF) (dark grey is water, black is vapour) (left); observed free surface in the water loop experiments (middle); comparison of numerical and experimental results, the dark lines indicate the expected LBE flow profile, light grey lines highlight the experimentally observed free surface (right) [34]

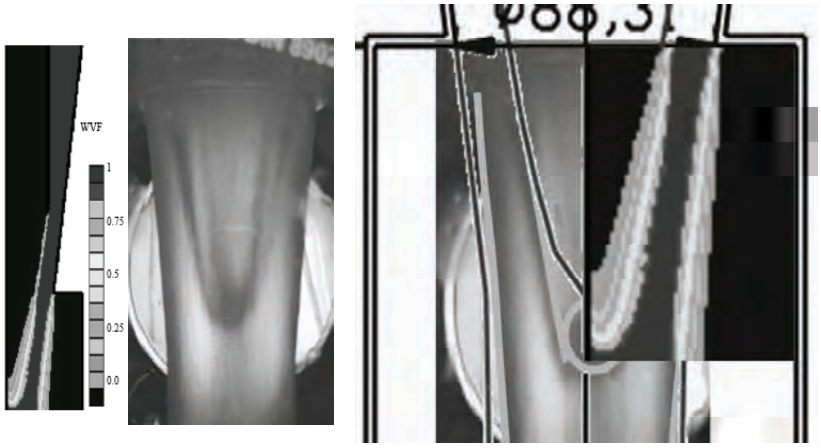

Table 5: Measured and calculated upper free surface position, experimental data based on maximum of light intensity RMS [33]

Flow rater (l/s)	Numerically calculated (mm)	Experimentally measured (mm)
9	102	86
10	90	74
11	83	62

It could be concluded that there is a good quantitative agreement between calculated and experimental data. Similar trends and results are predicted when operation conditions change [32]. This validated VOF+ simulation technique was used in a second phase for the simulation of the HLM target experiment. Three different investigations were performed. Firstly, the nominal flow has been investigated comparing different codes (STAR-CD and STAR-CCM+) in two different domains. One focuses on the flow upstream of the nozzle region in the space between fins installed in the feeder and considers only a 1.8° sector of the target. The second simulation excludes the feeder in order to study large scale asymmetry, and considers a 180° sector of the target. These simulations show near identical results, increasing confidence in the simulation method. After that, the effect of flow rate variation was studied. Reducing the flow rate leads to non-wetted fins and a free-falling LBE flow between fins (resulting in a sort of cavitation). The flow impinges on the slanted nozzle walls and eventually forms the conical free surface similar to the nominal case. The studied reduced flow rate may be considered a lower limit of target operation or one should consider implementing a larger number of fins. Finally, asymmetry is studied. For low asymmetry of the studied range (11%) virtually no changes of the free surface were observed [33].

Separate numerical simulations were performed to support the design of the flow further upstream of the nozzle region. Firstly, the target header was designed with the support of these simulations in order to direct a horizontal LBE pipe flow vertically downwards with a flow distribution as uniform as possible. Furthermore, options for upstream drag enhancement were assessed separately indicating that stacks of radial fins will be the preferred option and in-line arranged triangular tube banks may be an alternative.

Summary and conclusive remarks

The DEMETRA domain has produced important results on the basis of EFIT and XT-ADS needs. Moreover almost all of these results can be used as well for lead-alloy-cooled fast reactors. The experiments conducted and the analyses of the results have allowed the formulation of relevant recommendations in the following fields:

Coolant chemistry: Technologies to measure and adjust oxygen in HLM have been developed and tested also under long-term conditions. Recommendations on oxygen sensor design and calibration have been formulated. Filter systems for aerosol and slag removal have been assessed. For the implementation of all systems needed to maintain the quality control of the coolant chemistry important efforts are still needed for large-scale demonstration and possibly for characterisation of e.g. the oxygen probe in an irradiation field.

Materials: Application ranges of temperature, stresses and irradiation dose could be indicated for both T91 and AISI 316L steels. A deeper understanding of the mechanical and corrosion resistance performance of these two steels in HLM will occur as soon as the post-irradiation examination of the various irradiation programmes has been accomplished. Moreover, indications on corrosion protection systems have been given as well. The available results have shown that the operational window of the two steels is limited and for higher temperature and higher irradiation dose application an alternative material might be needed.

Thermal-hydraulics: Single rod, rod bundle and integral experiments have been set up and the first experimental results are available. More experiments will be conducted in the future with the objective to confirm numerical models defined for the simulation of turbulent heat transfer; validation of heat transfer correlation and simulation of transient conditions in order to measure the effect of transients on a fuel bundle and to assess the component interactions as e.g. the heat exchanger and the heat source in a pool-type system.

Components: Windowless spallation target design rules have been defined and initial experiments have allowed assessing the hydraulic performance. As for the window target, post-test analysis has been performed on MEGAPIE. In particular lessons learnt from the components, the thermal-hydraulics and the neutronics have been collected and evaluated.

Safety: LBE/water experiments have been performed with the objective to simulate a steam generator tube rupture and to validate the SIMMER code. Experimental results have confirmed that no exothermic reaction occurs between water and HLM. However, the injection of high-pressure water in an LBE pool generates a pressure spike at the level of the injector. The effects of such pressure spikes need a deeper investigation.

Fundamentals: Several activities, not mentioned in the previous paragraph, performed in DEMETRA have been of fundamental nature and were of support to the technological studies. In particular investigation of surface status on corrosion mechanism (e.g. it could be shown that roughness does not impact the oxidation mechanism [35]), corrosion modelling (thermodynamic and kinetic models have been defined and will be validated [36-38]), modelling of materials performance under irradiation (Fe and FeCr alloys have been simulated for a better understanding of basic properties [39]), chemical-physics behaviour of spallation products (the focus has been on Po, Hg and I). In particular Po behaviour under different temperature and cover gas conditions

has been assessed and methods to remove Po from LBE have been defined [40], and the solubility and diffusivity of oxygen [42,43] and metallic elements as e.g. Ni have been measured [41].

Finally, as far as the availability of the DEMETRA activities and results is concerned these have been presented and discussed at the HELIMNET/DEMETRA workshop and will be published as a proceedings in a special issue of *Journal of Nuclear Materials*. Moreover, the DEMETRA results will be included in the second version of the OECD/NEA Handbook on HLM technology which is in preparation.

Acknowledgements

The authors acknowledge gratefully the contributions of all colleagues involved in EUROTRANS and in particular in the DEMETRA domain. This work is supported by the FP6 EC Integrated Project EUROTRANS No. FI6W-CT-2004-516520.

References

[1] Knebel, J.U., *et al.*, "European Research Programme for the Transmutation of High Level Nuclear Waste in an Accelerator Driven System: Towards a Demonstration Device of Industrial Interest", *Proc. of FISA 2009 Conference*, Prague, Czech Republic, 22-24 June (2009).

[2] Fazio, C., *et al.*, "Assessment of Reference Structural Materials, Heavy Liquid Metal Technology and Thermal-hydraulics for European Waste Transmutation ADS", *Int. Conf. on Nuclear Energy Systems for Future Generation and Global Sustainability (GLOBAL 2005)*, Tsukuba, Japan, 9-13 October (2005).

[3] *Thematic Network on Advanced Options for Partitioning and Transmutation (ADOPT)*, Contract n° FIKW-CT-2001-20178, Dr. Hamid Aït Abderrahim (Ed., on behalf of ADOPT Members) SCK•CEN, Mol, Belgium, 13 October (2005).

[4] Van den Bosch, J., A. Almazouzi, *Procurement and Characterization of T91 and SS316L Plates*, Report EUROTRANS-DEMETRA, R-4197, Deliverable 4.1 (2005).

[5] Fazio, C., *et al.*, "European Cross-cutting Research on Structural Materials for Generation IV and Transmutation Systems", *J. Nucl. Mater.*, 392 (2), 316-323 (2009).

[6] Turroni, P., *et al.*, *Test Specifications of Single Pin/Pin Bundle/Integral Experiments*, Report EUROTRANS-DEMETRA, Deliverable D4.15, 29 April (2006).

[7] Chandra, L., *et al.*, "A Stepwise Development and Validation of a RANS Based CFD Modelling Approach for the Hydraulic and Thermal-hydraulic Analyses of Liquid Metal Flow in a Fuel Assembly", *Nucl. Eng. Des.*, 239 (10), 988-2003 (2009).

[8] Batta, A., J. Zeininger, R. Stieglitz, "Experimental and Numerical Investigation of Turbulent Liquid Metal Heat Transfer Along a Heated Rod in Annular Cavity", *Proceedings of ICAPP'09*, Tokyo, Japan, 10-14 May (2009), Paper 9439.

[9] Ciampichetti, A., Experimental Test Program and Test Set-up on the Basis of the Design Needs of the LBE/Water Interaction, EUROTRANS-DEMETRA Deliverable D4.14 and ENEA Report ET-S-R-001, 12 May (2006).

[10] Ciampichetti, A., *et al.*, "Experimental and Computational Investigation of LBE–water Interaction in LIFUS 5 Facility", *Nucl. Eng. Des.*, 239 (11), 2468-2478 (2009).

[11] Fazio, C., *et al.*, "The MEGAPIE-TEST Project: Supporting Research and Lessons Learned in First-of-a-kind Spallation Target Technology", *Nucl. Eng. Des.* 238 (6), 1471-1495 (2008).

[12] Gerbeth, G., *Status of the Measurement Techniques Development*, and R. Stieglitz *Electromagnetic Frequency Flowmeter*, EUROTRANS-DEMETRA Deliverables 13.a, 15 November (2006) and 13.b, 13 August (2008).

[13] Groeschel, F., *et al.*, "The MEGAPIE 1 MW Target in Support to ADS Development: Status of R&D and Design", *J. Nucl. Mater.*, 335 (2), 156-162 (2004).

[14] Roelofs, F., *DEMETRA Summary Report of WP4.4 Including Feedback to Designers*, EUROTRANS-DEMETRA Deliverable 4.67, 22 March (2010).

[15] De Bruyn, D., *et al.*, "From MYRRHA to XT-ADS: The Design Evolution of an Experimental ADS System", *8th International Topical Meeting on Nuclear Applications and Utilization of Accelerators (AccApp'07)*, Pocatello, Idaho, USA, 30 July-2 August (2007).

[15a] Barbensi, A., *et al.*, "EFIT: The European Facility for Industrial Transmutation of Minor Actinides", *8th International Topical Meeting on Nuclear Applications and Utilization of Accelerators (AccApp'07)*, Pocatello, Idaho, USA, 30 July-2 August (2007).

[15b] Cinotti, L., *et al.*, *XADS Pb-Bi Cooled Experimental Accelerator Driven System – Reference Configuration – Summary Report*, ANSALDO ADS1SIFX0500, Rev 0. ANSALDO, Technical Report, Technical Specification and Target Unit Interfaces (LDE and gas-cooled concepts, window and windowless options), 30.10.2001, ADS 43 TIIX 010, FIKW-CT-2001-00179.

[16] *Technologies for Lead Alloys*, TECLA Project within the 5th European Framework Programme, Ref. No. FIS5-1999-00308 (2000).

[17] "Irradiation Effects in Martensitic Steels Under Neutron and Proton Mixed Spectrum", *SPIRE 2000*, EC 5th FP FIKW-CT-2000-00058.

[18] Morier, O., F. Beauchamp, L. Brissonneau, *Final Report for the Purification Process Studies and Impurities Characterisation in the Gas and Liquid Phase*, EUROTRANS-DEMETRA Deliverable D4.57 and CEA Report DEN/CAD/DTN/STPA/LLTS/NT/2009/016, 12 May (2009).

[19] Colominas, S., J. Abellà, "Evaluation of Potentiometric Oxygen Sensors Based on Stabilized Zirconia for Molten 44.5% Lead–55.5% Bismuth Alloy", *Sensors and Actuators B: Chemical*, 145, 720-725 (2010).

[20] Schroer, C., *et al.*, "Design and Testing of Electrochemical Oxygen Sensors for Service in Liquid Lead Alloys", *Presented at the DEMETRA International Workshop*, Berlin, Germany, 2-4 March 2010, forthcoming in *Journal of Nuclear Materials*.

[20a] Alamo, A., *et al.*, "Mechanical Properties of 9Cr Martensitic Steels and ODS-FeCr Alloys After Neutron Irradiation at 325°C Up to 42 dpa", *Journal of Nuclear Materials*, Vols. 367-370, Part 1, pp. 54-59, 1 August (2007).

[20b] Klueh, R., D. Harries, *High-chromium Ferritic and Martensitic Steels for Nuclear Applications*, ASTM MONO3, American Society for Testing and Materials, West Conshohocken, PA (2001).

[20c] Legris, A., *et al.*, "Embrittlement of a Martensitic Steel by Liquid Lead", *Scripta Mater.*, 43, 997 (2000).

[20d] Long, B., *et al.*, "Liquid Pb-Bi Embrittlement Effects on the T91 Steel After Different Heat Treatments", *J. Nuclear Mat.*, 377, 219-224 (2008).

[20e] Long, B., Y. Dai, "Investigation of LBE Embrittlement Effects on the Fracture Properties of T91", *J. Nuclear Mat.*, 376, 341-345 (2008).

[20f] Serre, I., J-B. Vogt, "Heat Treatment Effect of T91 Martensitic Steel on Liquid Metal Embrittlement", *J. Nucl. Mater.*, 376, 330 (2008).

[20g] Auger, T., *et al.*, "Role of Oxidation on LME of T91 Steel Studied by Small Punch Test", *J. Nucl. Mater.*, 376, 336 (2008).

[21] Weisenburger, A., *et al.*, "Long-term Corrosion on T91 and AISI1316L Steel in Flowing Lead Alloy and Corrosion Protection Barrier: Experiments and Models", *Presented at the DEMETRA International Workshop*, Berlin, Germany, 2-4 March 2010, forthcoming in *Journal of Nuclear Materials*.

[22] Weisenburger, A., *et al.*, Final Report on Task 4.2.1: Long-term Corrosion on T91 and AISI1316L Steel in Flowing Lead Alloy and Corrosion Protection Barrier: Experiments and Models, Deliverable Corrosion 4.52, forthcoming.

[23] Weisenburger, A., *et al.*, "T91 Cladding Tubes with and Without Modified FeCrAlY Coatings Exposed in LBE at Different Flow, Stress and Temperature Conditions", *J. of Nucl. Mater.*, 376, 274-81 (2008).

[24] Weisenburger, A., *et al.*, "Low Cycle Fatigue Tests of Surface Modified T91 Steel in 10^{-6} wt.% Oxygen Containing Pb45Bi55 at 550°C", *J. Nucl. Mater.*, 377, 261-67 (2008).

[25] Thermal-Hydraulics of Innovative Nuclear Systems – THINS, EURATOM FP7 Project, Grant agreement No. 249337.

[26] Karbojian, A., T. Hollands, *Final Report on the Single Pin Experiment on TALL Facility*, EUROTRANS-DEMETRA Deliverable D4.103/D4.48, 10 September (2009).

[27] Litfin, K., *Final Report for the Fuel Bundle Experiment in KALLA*, EUROTRANS-DEMETRA Deliverable D4.68, 29 August (2009).

[28] Tarantino, M., *et al.*, "Integral System Experiment – Thermal-hydraulic Simulator of a Heavy Liquid Metal Reactor", *Presented at the DEMETRA International Workshop*, Berlin, Germany, 2-4 March 2010, forthcoming in *Journal of Nuclear Materials*.

[29] Ciampichetti, A., *et al.*, "LBE-water Interaction in Sub-critical Reactors: First Experimental and Modelling Results", *J. of Nucl. Mater.*, Vol. 376, Issue 3, pp. 418-423, 15 June (2008).

[30] Ciampichetti, A., *et al.*, "LBE-water Interaction in LIFUS V Facility Under Different Operating Conditions", *presented at the DEMETRA International Workshop*, Berlin, Germany, 2-4 March 2010, forthcoming in *Journal of Nuclear Materials*.

[31] Batta, A., *et al.*, *Report on the Development of Physical Models, the Interpretation of the Experiments and the Validation of CFD Models Based on Experiments, Containing a Database on Free Surface Models and Numerical Tools*, EUROTRANS-DEMETRA Deliverable D4.92, 26 February (2010).

[32] Batta, A., *et al.*, "Numerical Study of the Water Experiment for XT-ADS Windowless Spallation Target", *10th Information Exchange Meeting on Actinide and Fission Product Partitioning and Transmutation (10-IEMPT)*, Mito Japan, 6-10 October 2008, OECD/NEA, Paris (2010).

[33] Batta, A., A.G. Class, H. Jeanmart, "Comparative Experimental and Numerical Analysis of the Hydraulic Behaviour of Free-surface Flow in the Water Experiment of the XT-ADS Windowless Spallation Target", *Proc. of ICAPP'10*, San Diego, CA, USA, 13-17 June (2010), Paper 10342.

[34] Batta, A., A. Class, "Hydraulic Analysis of the Heavy Liquid Metal Free Surface in the Windowless XT-ADS Spallation Target", *Proceedings of the 13th International Topical Meeting on Nuclear Reactor Thermal Hydraulics (NURETH-13)*, N13P1151, Kanazawa City, Ishikawa Prefecture, Japan, 27 September-2 October (2009).

[35] Martin-Munoz, F.J., *Influence of Metallurgical Parameters on the Oxidation Behaviour of Reference Steels in Stagnant LBE. Surface Effect*, EUROTRANS-DEMETRA Deliverable D4.19a, 21 February (2008).

[36] Martinelli, L., *et al.*, "Oxidation Mechanism of a Fe–9Cr–1Mo Steel by Liquid Pb–Bi Eutectic Alloy (Part I)", *Corrosion Science*, 50 (9), 2523-2536 (2008).

[37] Martinelli, L., *et al.*, "Oxidation Mechanism of an Fe–9Cr–1Mo Steel by Liquid Pb–Bi Eutectic Alloy at 470°C (Part II)", *Corrosion Science*, 50 (9), 2537-2548 (2008).

[38] Martinelli, L., *et al.*, "Oxidation Mechanism of a Fe-9Cr-1Mo Steel by Liquid Pb–Bi Eutectic Alloy (Part III)", *Corrosion Science*, 50 (9), 2549-2559 (2008).

[39] Malerba, L., N. Sandberg, P. Vladimirov, *Report on the Complete Set of EAM Potentials for Fe-C and Cr-C, on the Validated Results of OKMC Simulations of Radiation Damage Evolution in Fe-Cr Alloys and on the Simulation of High-energy Atomic Displacement Cascades*, EUROTRANS-DEMETRA Deliverable D4.9, 2 October (2007).

[40] Neuhausen, J., *Final Report on Po, I and Hg Production and Deposition*, EUROTRANS-DEMETRA Deliverable D4.66, 1 February (2010).

[41] Martinelli, L., *et al.*, "Nickel Solubility Limit in Liquid Lead-bismuth Eutectic", *Journal of Nuclear Materials*, forthcoming.

[42] Abella, J., *Effect of Metallic Elements on Oxygen Concentration in LBE and on Determination of the Diffusion Coefficient of Oxygen in LBE*, EUROTRANS-DEMETRA Deliverable D4.22, 19 May (2009).

[43] Abella, J., *Diffusivity of Oxygen in LBE*, EUROTRANS-DEMETRA Deliverable D4.38, 20 May (2009).

NUDATRA/EUROTRANS nuclear data for nuclear waste transmutation*

E. González-Romero[1], **A. Koning**[2], **S. Leray**[3], **A. Plompen**[4], **J. Sanz**[5]
(on behalf of NUDATRA/IP-EUROTRANS)
[1]Centro de Investigaciones Energéticas, Medioambientales y Tecnológicas (CIEMAT), Spain; [2]Nuclear Research and Consultancy Group (NRG), Netherlands; [3]Commissariat à l'énergie atomique, (CEA), France; [4]Institute for Reference Materials-Joint Research Materials (IRMM-JRC), Belgium; [5]Universidad Nacional de Educación a Distancia (UNED), Spain

Abstract

NUDATRA, the fifth Domain of the EU Integrated Project EUROTRANS, is a project that, by joining new measurements, evaluations and development of the simulation codes, is contributing to improve and validate the nuclear data and simulation tools required for the development and optimisation of nuclear waste transmutation, ADS dedicated transmutation systems and the associated advanced fuel cycle.

The activities are essentially aimed at supplementing the evaluated nuclear data libraries and improving the reaction models for materials in transmutation fuels, coolants, spallation targets, internal structures, and reactor and accelerator shielding, relevant for the design and optimisation of the EFIT and XT-ADS. These activities are distributed over four main lines: sensitivity analysis and validation of nuclear data and simulation tools; low and intermediate energy nuclear data measurements; nuclear data libraries evaluation and low-intermediate energy models; and high-energy experiments and modelling.

The main accomplishments of NUDATRA had been:

- *New measurements of Pb-Bi cross-sections: inelastic, (n,xn), (n,nX), and isomer branching ratios (Po production) including the complete data cycle of analysis, evaluation, dissemination and validation with criticality benchmarks.*
- *New measurements and evaluations for minor actinides isotopes relevant for the advanced fuel cycles with transmutation, including several Am and Cm isotopes.*
- *New high-energy data and model improvements, based on previous and the new measurements, particularly for the prediction of the spallation wastes, damage and gas (H, He) production cross-sections.*
- *Development of new simulation systems and methodologies, for transmutation fuel cycles with multi-recycling, able to evaluate the sensitivity and uncertainty analysis, and the identification of the specific nuclear data needs with their target accuracies.*
- *Contribution to the training of young physicists (with many PhDs) and dissemination of results in a large number of conferences and journal papers.*

The article will provide an overview of the NUDATRA project and a summary of its main achievements.

* The full paper being unavailable at the time of publication, only the abstract is included.

Special Lecture

Subcritical thorium reactors*

Carlo Rubbia
European Organisation for Nuclear Research (CERN)
Geneva, Switzerland

Abstract

In the 1960s, "atoms for peace" promised cheap, abundant and universally available nuclear power, for which the few "nuclear" countries would ensure the necessary know-how to the many others which had renounced nuclear weaponry. Today, the situation is far from being acceptable: the link between peaceful and military applications has been shortened by inevitable developments and the corresponding widening of the know-how of nuclear technologies.

In order to ensure that nuclear energy becomes freely and abundantly available in all countries, some totally different nuclear technologies must be developed. Fuel availability, problems related to proliferation especially in the developing countries and the security of long-term waste disposal all demand radically new solutions.

Particularly interesting are fission reactions from ^{232}Th, progressively converted into a readily fissionable energy generating daughter element, where essentially the totality of the initial fuel can be burnt: the only waste are the much more short-lived fission fragments and the spent cladding materials.

Natural thorium on the earth's crust is nearly as abundant as lead, adequate for many tens of centuries at a level greater than today's primary fossil production. For instance, the continuous production of 1 000 MWatt of electric power requires 3.5 million t/y of coal, 200 t/y of natural uranium, but only 1 t/y of thorium. A thorium-driven reactor will be essentially proliferation free.

In the case of ^{232}Th two neutrons must be produced, one to maintain the chain reaction and the other to recreate the fertile material. Such very small neutron excess is essentially incompatible with the requirements of a critical reactor. An external neutron supply has to be added to ensure the balance. As it is well known, an ADS accelerator permits the production of the required complementary neutron flux with the help of the spallation in a heavy nucleus.

Several ADS driven thorium-based scenarios based on thermal, epithermal and fast neutrons will be described.

* The full paper being unavailable at the time of publication, only the abstract is included.

Session I

Current ADS Experiments and Test Facilities

Chairs: Th. Wetzel, S. Monti

Experiments on injection of spallation neutrons by 100 MeV protons in the Kyoto University Critical Assembly

Cheol Ho Pyeon, Jae Yong Lim, Tsuyoshi Misawa, Seiji Shiroya
Nuclear Engineering Science Division, Research Reactor Institute, Kyoto University
Osaka, Japan

Abstract

At the Kyoto University Research Reactor Institute, the world's first injection of spallation neutrons generated by the high-energy proton beams into a reactor core was successfully accomplished in 2009. By combining the fixed field alternating gradient (FFAG) accelerator with the A-core of the Kyoto University Critical Assembly (KUCA), a series of accelerator-driven system (ADS) experiments are carried out under the condition that the spallation neutrons are supplied to a subcritical core through an injection of 100 MeV protons onto a tungsten target, whose size is 80 mm diameter and 10 mm thickness. In these experiments, the proton beams from the FFAG accelerator are 30 Hz repetition rate and 10 pA current. The level of the neutron intensity generated at the tungsten target is around 1×10^6 *n/s.*

For the FFAG accelerator, a beam commissioning is still under way to realise the stable beam characteristics, including the beam intensity and the beam shaping. The present results could be expected to be useful for the further research and development of ADS at KUCA in the fields of both reactor physics experiments and nuclear design calculations, since the final objective is to carry out the ADS experiments with 150 MeV protons generated from the FFAG accelerator.

Introduction

At the Kyoto University Research Reactor Institute, the world's first injection [1] of spallation neutrons generated by the high-energy proton beams in a reactor core was successfully accomplished on 4 March 2009. By combining the fixed field alternating gradient (FFAG) accelerator [2,3] with the A-core (Figure 1; polyethylene-moderated and -reflected-core) of the Kyoto University Critical Assembly (KUCA), a series of the accelerator-driven system (ADS) experiments was carried out under the condition that the spallation neutrons were supplied to a subcritical core through the injection of 100 MeV protons onto a tungsten target, whose size was 80 mm diameter and 10 mm thickness. In these experiments, the proton beams from the FFAG accelerator were 30 Hz repetition rate and 10 pA current. A level of the neutron intensity generated at the tungsten target was around 1×10^6 *n*/s. The objective of these experiments was to conduct a feasibility study on ADS from a reactor physics viewpoint, in order to develop an innovative nuclear reactor for a high-performance transmutation system with a capability of power generation or for a new neutron source for scientific research.

Figure 1: Top view of configuration of A-core (E3 core) with neutron guide and beam duct carried out in the ADS experiments with 100 MeV protons

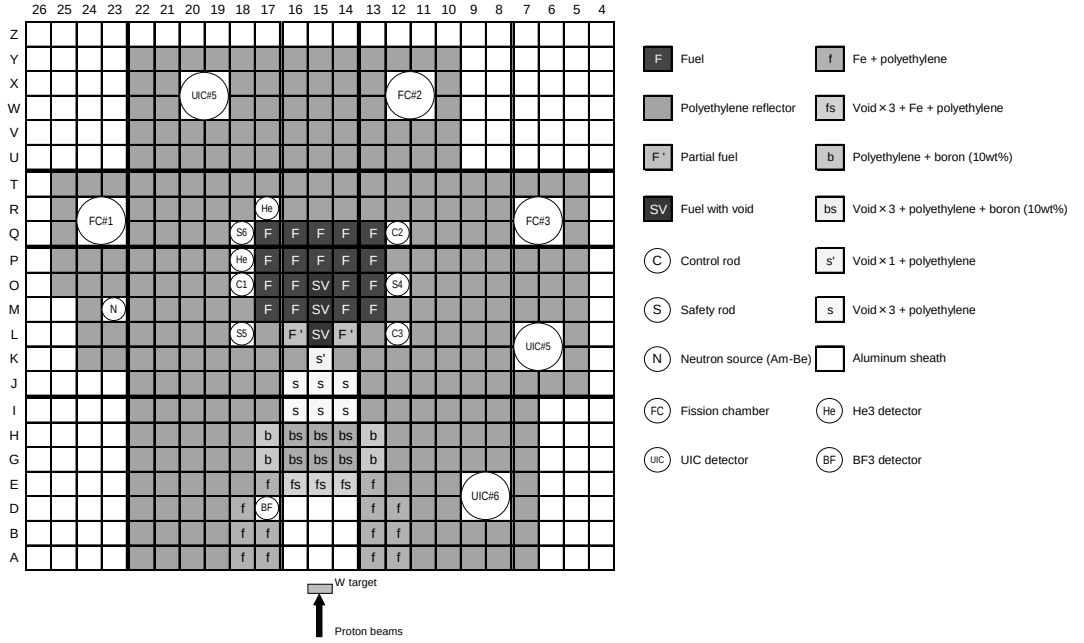

KUCA core configuration

The A-core employed in the ADS experiments was essentially a thermal neutron system composed of a highly-enriched uranium fuel and the polyethylene-moderator and -reflector. In the fuel region, a unit cell is composed of a 93% enriched uranium fuel plate 1/16″ thick and polyethylene plates 1/4″ and 1/8″ thick. In these ADS experiments, three types of fuel rods designated as the normal (F), partial (F′) and special fuel (SV) were employed (Figure 2). Due to KUKA safety regulations, the tungsten target was located not at the centre of the core but outside the critical assembly, and an outside location was almost the same as the previous experiments [4-9] using 14 MeV neutrons.

Figure 2: Fall sideways view of configuration of fuel rod of A3/8″P36EU(3) in the KUCA A-core

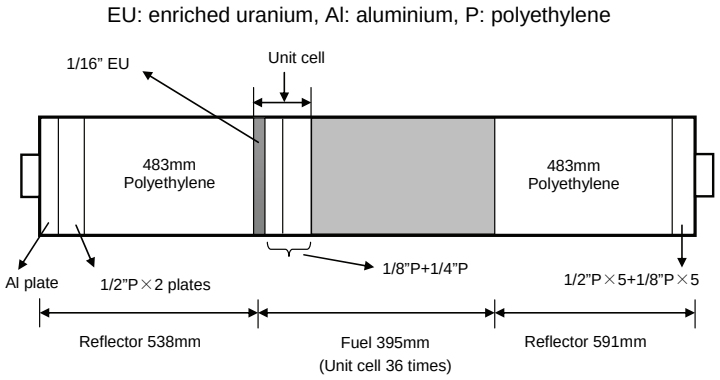

As in the previous ADS experiments with 14 MeV neutrons, an installation of a neutron guide and a beam duct is requisite to lead the high-energy neutrons generated from the tungsten target to the centre of the core as much as possible. The detailed composition of the normal, partial and special fuel rods, the polyethylene rod, and the neutron guide and the beam duct was described in Refs. [3-5].

ADS experiments with 100 MeV protons

The ADS experiments with 100 MeV protons were carried out varying the neutron spectrum: E3 (soft spectrum) and EE1 (hard spectrum) cores are shown in Figure 3. The E3 and EE1 were originally named in KUCA based on the difference between cell patters in the fuel rod.

Figure 3: Neutron spectra in E3 (soft spectrum) and EE1 (hard spectrum) cores

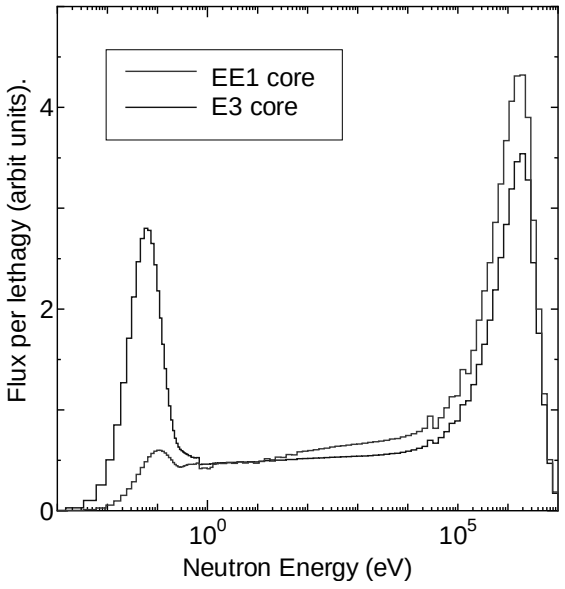

Neutron decay constant

To obtain the information on the detector position dependence of the prompt neutron decay measurement, the neutron detectors were set at three positions (shown in Figure 4): near the tungsten target [position of (17, D); 1/2″ϕ BF_3 detector]; around the core [positions of (18, M) and

(17, R); 1″ϕ ^{3}He detectors]. The prompt and delayed neutron behaviours were experimentally confirmed by observing the time evolution of neutron density in ADS: an exponential decay behaviour and a slowly decreasing one, respectively. These behaviours clearly indicated the fact that the neutron multiplication was caused by an external source: the sustainable nuclear chain reactions were induced in the subcritical core by the spallation neutrons through the interaction of the tungsten target and the proton beams from the FFAG accelerator. In these kinetic experiments, the subcriticality was deduced from the prompt neutron decay constant by the extrapolated area ratio method. The difference of measured results of 0.74% $\Delta k/k$ and 0.61% $\Delta k/k$ at the positions of (17, R) and (18, M) in Figure 4, respectively, from the experimental evaluation of 0.77% $\Delta k/k$, which was deduced from the combination of both the control rod worth by the rod drop method and its calibration curve by the positive period method, was within about 20%. Note that the subcritical state was attained by a full insertion of C1, C2 and C3 control rods into the core.

Figure 4: Measured prompt and delayed neutron behaviour obtained from BF_3 and ^{3}He detectors

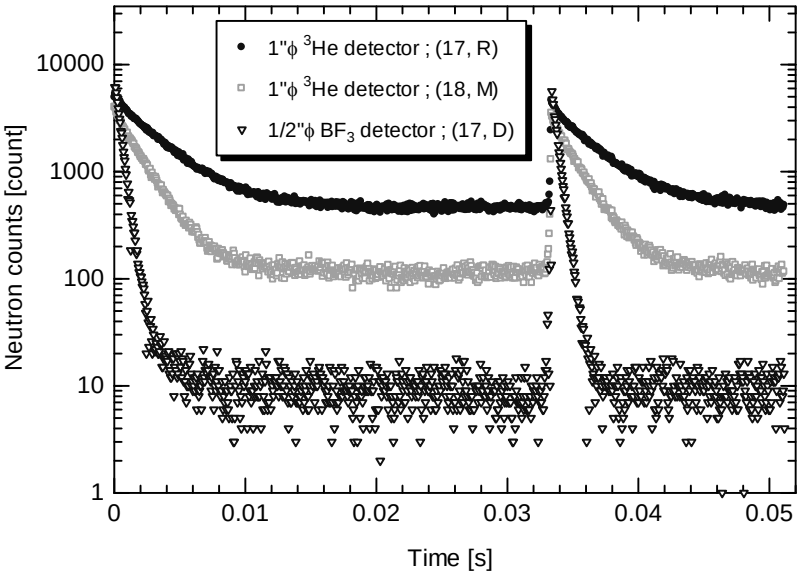

Reaction rate distribution

Thermal neutron flux distribution was estimated through the horizontal measurement of ^{115}In$(n,\gamma)^{116m}$In reaction rate distribution by the foil activation method using an indium (In) wire of 1.0 mm diameter. The wire was set in an aluminium guide tube, from the tungsten target to the centre of the fuel region [from the position of (13, 14-A) to that of (13, 14-P); Figure 5], at the middle height of the fuel assembly. The experimental and numerical results of the reaction rates were normalised using an In foil ($20 \times 20 \times 2$ mm^3) emitted by ^{115}In$(n,n')^{115m}$In at the target. In this static experiment, the subcritical state (0.77% $\Delta k/k$) was also attained by the full insertion of C1, C2 and C3 rods. The numerical calculation was executed by the Monte Carlo multi-particle transport code MCNPX [10] based on a nuclear data library ENDF/B-VII [11]. The generation of the spallation neutrons was included in the MCNPX calculation bombarding the tungsten target with 100 MeV proton beams. Since the reactivity effect of the In wire is considered to be not negligible, the In wire was taken into account in the simulated calculation: the reaction rates were deduced from tallies taken in the In wire setting region. The result of the source calculation was obtained after 2 000 active cycles of 100 000 histories, which led the statistical error in the reaction rates of less than 10%. The measured and the calculated reaction rate distributions were compared to validate the calculation method. The calculated reaction rate distribution (Figure 5) agreed

Figure 5: Comparison of measured and calculated reaction rate distribution from (13, 14-A) to (13, 14-P) in Figure 1

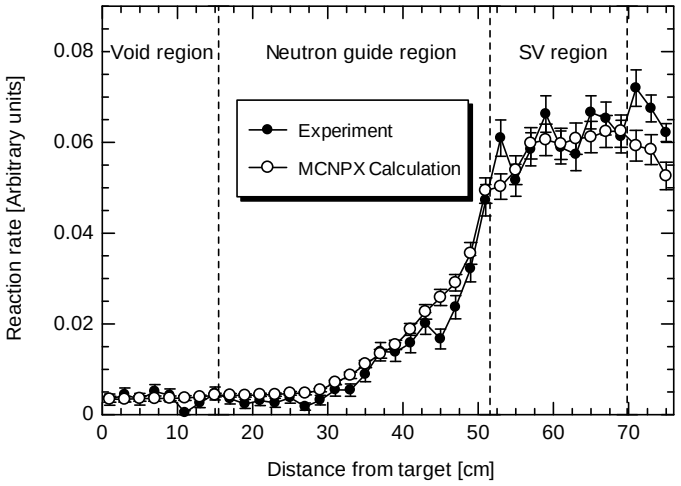

approximately with the experimental results within the statistical errors in the experiments, although these experimental errors were rather larger than those of the calculations. These larger errors in the experiments were attributed to the current status of the proton beams, including the weak beam intensity and the poor beam shaping at the target.

Proton beam trip and restart

The experiments of monitoring the reactor power change were carried out for the proton beam trip and restart. In the EE1 core (hard spectrum core), the neutron signals in time series obtained by two detectors were observed in a drastic change in an interval (one min) of beam trip and restart. The results of neutron signals revealed the tendency of a quick reduction and recovery of reactor power to the initial state during one minute. In this kinetic experiment, the subcritical state (0.69% $\Delta k/k$) was also attained by the full insertion of C1, C2 and C3 rods. And, as a result, the tendency of reactor power was confirmed to be almost same, even if the beam trip and restart incidents were repeated several times varying the time interval.

Figure 6: Power change for beam trip and restart in EE1core (subcriticality 0.69% $\Delta k/k$)

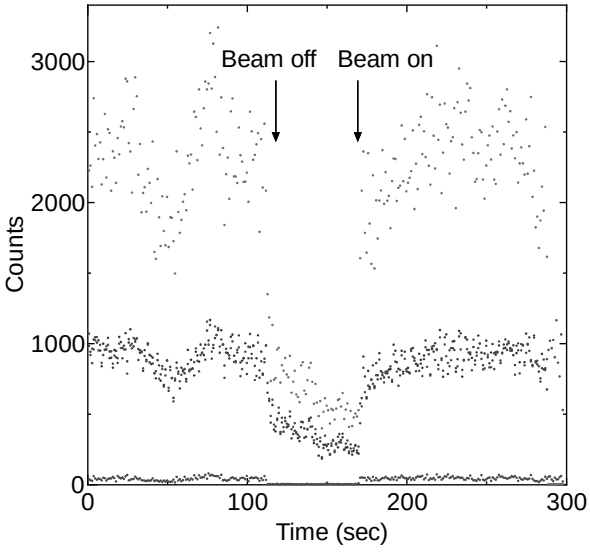

Summary

The first ADS experiments with 100 MeV protons generated from the FFAG accelerator were successfully carried out at the KUCA A-core (polyethylene-moderated and -reflected-core). For the FFAG accelerator, a beam commissioning is still under way to realise the stable beam characteristics, including the beam intensity and the beam shaping. When the stable proton beams are accomplished, the basic ADS experiments with 150 MeV protons could be conducted at KUCA on the basis of these accomplishment and experiences, as well as the ADS experiments with 14 MeV neutrons. The additional ADS experiments will be newly conducted using the thorium-loaded and beryllium- and/or graphite-moderated core. Further, it is expected to become open the results of these experimental and numerical analyses both in the actual and thorium ADS cores.

Finally, since the final objective is to carry out the ADS experiments with 150 MeV protons generated from the FFAG accelerator, the present results could be expected to be useful for the further research and development of ADS at KUCA in the fields of both reactor physics experiments and nuclear design calculations.

Acknowledgements

This work was partly supported by the "Energy Science in the Age of Global Warming" of Global Center of Excellence (G-COE) Programme (J-051) of the Ministry of Education, Culture, Sports, Science and Technology of Japan.

References

[1] Pyeon, C.H., T. Misawa, J.Y. Lim, *et al.*, "First Injection of Spallation Neutrons Generated by High-energy Protons into the Kyoto University Critical Assembly", *J. Nucl. Sci. Technol.*, 46, 1091 (2009).

[2] Mori, Y., "Development of FFAG Accelerators and Their Applications for Intense Secondary Particle Production", *Nucl. Instrum. Methods A*, 562, 591 (2006).

[3] Yonemura, Y., A. Takagi, M. Yoshii, *et al.*, "Development of RF Acceleration System for 150 MeV FFAG Accelerator", *Nucl. Instrum. Methods A*, 576, 294 (2007).

[4] Pyeon, C.H., Y. Hirano, T. Misawa, *et al.*, "Preliminary Experiments for Accelerator Driven Subcritical Reactor with Pulsed Neutron Generator in Kyoto University Critical Assembly", *J. Nucl. Sci. Technol.*, 44, 1368 (2007).

[5] Pyeon, C.H., M. Hervault, T. Misawa, *et al.*, "Static and Kinetic Experiments on Accelerator-driven System with 14 MeV Neutrons in Kyoto University Critical Assembly", *J. Nucl. Sci. Technol.*, 45, 1171 (2008).

[6] Pyeon, C.H., H. Shiga, T. Misawa, *et al.*, "Reaction Rate Analyses for on Accelerator-driven System with 14 MeV Neutrons in Kyoto University Critical Assembly", *J. Nucl. Sci. Technol.*, 46, 965 (2009).

[7] Pyeon, C.H., J.Y. Lim, T. Misawa, S. Shiroya, "Current Status of Accelerator-driven System with High-energy Protons in Kyoto University Critical Assembly", *Trans. Am. Nucl. Soc.*, 101, 25 (2009).

[8] Shahbunder, H., C.H. Pyeon, T. Misawa, S. Shiroya, "Experimental Analysis for Neutron Multiplication by Using Reaction Rate Distribution in Accelerator-driven System", *Ann. Nucl. Energy*, forthcoming.

[9] Taninaka, H., K. Hashimoto, C.H. Pyeon, *et al.*, "Determination of Lambda-mode Eigenvalue Separation of a Thermal Accelerator-driven System from Pulsed Neutron Experiment", *J. Nucl. Sci. Technol.*, forthcoming.

[10] Pelowitz, D.B., *MCNPX User's Manual Version 2.5.0*, LA-CP-05-0369, Los Alamos National Laboratory (2005).

[11] Chadwick, M.B., *et al.*, "ENDF/B-VII: Next Generation Evaluated Nuclear Data Library for Nuclear Science and Technology", *Nucl. Data Sheets*, 107, 2931 (2006).

Experimental validation of the industrial ADS reactivity monitoring using the YALINA-Booster subcritical assembly

M. Fernández-Ordóñez[1], V. Bécares[1], C. Berglöf[2], D. Villamarín[1], M. Becker[3], V. Bournos[4], Y. Fokov[4], P. Gajda[6], V. Glivici[5], E.M. González-Romero[1], J. Janczyszyn[6], S. Mazanik[4], B. Merk[5], J.L. Muñoz-Cobo[7], W. Pohorecki[6]

[1]Centro de Investigaciones Energéticas, Medioambientales y Tecnológicas (CIEMAT), Madrid, Spain; [2]Royal Institute of Technology (KTH), Stockholm, Sweden; [3]Forschungszentrum Karlsruhe (FZK), Karlsruhe, Germany; [4]Joint Institute of Power Engineering and Nuclear Research (JINPR), Sosny, Belarus; [5]Forschungszentrum Dresden-Rossendorf (FZD), Dresden, Germany; [6]University of Science and Technology (AGH), Krakow, Poland; [7]Universidad Politécnica de Valencia (UPV), Valencia, Spain

Abstract

An extensive experimental programme devoted to validation of reactivity monitoring techniques on ADS has been carried out at the subcritical facility YALINA-Booster in the framework of IP-EUROTRANS. Besides benchmarking of different reactivity determination methods, the main objective was to develop the validated methodology that can be used in a power ADS. YALINA-Booster is a D-T neutron generator coupled to a flexible zero-power subcritical assembly with a partially decoupled fast-thermal neutron spectrum. The high intensity of the accelerator and the possibility to work in continuous or pulsed mode allowed the performing of standard pulse neutron experiments, the current-to-flux relationship and beam trip experiments. In addition, it has provided the opportunity to test the electronic chains in current mode, which corresponds to the most probable condition in a power ADS.

Pulsed neutron source (PNS) experiments have been carried out to achieve the reference reactivity values for each configuration studied. The techniques applied were the Sjöstrand method and the prompt neutron slope fitting technique. The spatial dependences observed using both methods have been corrected by Monte Carlo simulations using different nuclear data libraries.

The reactivity of a subcritical system has also been determined, for the first time, by imposing short millisecond-scale interruptions to the continuous deuterium beam current. This technique provided the possibility to monitor the reactivity at each beam trip using source jerk methodology. The fast evolution of the neutron flux intensity within the reactor was monitored, for the first time, with fission chambers operating in current mode. This required the development of specific electronic chains specially designed for these experiments. In order to test the validity of these results, the reactivity values were also determined using pulsed-mode detectors.

Finally, the online monitoring of the reactivity was achieved using the current-to-flux technique. This method relies on continuously monitoring on one hand the ratio between the accelerator beam current and the neutron source intensity, and on the other hand the ratio between the neutron source intensity and the core power. With this methodology, it was possible to identify the origin of the observed changes in the system indicating possible reactivity transients.

Introduction

The transmutation of the radioactive waste is considered as a keystone for a sustainable nuclear energy and the accelerator-driven system (ADS) is one of the explored concepts for achieving the incineration of long-lived minor actinides. In the design of future ADS facilities, the reactivity monitoring system is of highest importance. An extensive experimental programme devoted to reactivity monitoring of ADS has been carried out in the framework of IP-EUROTRANS [1]. This experimental programme was performed at the YALINA-Booster subcritical facility located in the JIPNR-SOSNY institute in Belarus.

The main objectives of this project were the qualification of the reactivity monitoring techniques and developing the necessary electronic chains for operation in a full power ADS. The standard pulsed neutron source methods used in previous experimental campaigns such as MUSE-4 [2] for reactivity monitoring have been validated in the YALINA-Booster project. However, these techniques will not be suitable for a power ADS due to thermal stress and other effects. In addition, the electronic chains used in standard PNS techniques will not be useful in a full power subcritical core due to dead time effects. It is then a challenge to develop the necessary tools to measure the reactivity in a power subcritical reactor.

For this purpose, the YALINA-Booster facility couples a D-T neutron generator to a flexible zero-power subcritical assembly with a coupled fast-thermal neutron spectrum. The high intensity of the accelerator and the possibility to work in continuous or pulsed mode allowed the study of the current-to-flux relationship and beam-trip experiments. In addition, the experimental facility provided the opportunity to test electronic chains in current mode detection, which correspond to the most probable detector operation mode in a full power ADS.

Experimental set-up

The experimental set-up used in this work was made up by a subcritical fast-thermal reactor, a neutron generator feeding the nuclear core with the necessary neutrons and several detectors to determine the neutron flux intensity at several locations within the core. In what follows, each part of the experimental set-up will be briefly described.

Neutron generator

For the experiments presented here, we have used the NG-12-1 neutron generator [3], which accelerates a deuteron beam impinging on a Ti-T target to produce a quasi-isotropic neutron energy spectrum of 14 MeV fusion neutrons. With a diameter of 45 mm, the target is located in the centre of the core. The neutron generator can be operated in both continuous and pulse modes and gives thereby the possibility of performing both pulsed neutron source (PNS) measurements and continuous wave measurements. Moreover, the continuous wave can be promptly interrupted (~1 μs) followed by a fast beam restart. In this way, short repeated beam trips can be induced intentionally with interruption times in the millisecond scale. The maximum deuteron beam current in continuous mode is around 1.5 mA giving a maximum neutron yield of approximately 10^{11} neutrons per second.

YALINA-Booster core

The YALINA-Booster core [4], depicted in Figure 1, consists of a central lead zone (booster), a polyethylene zone, a radial graphite reflector and a front and back biological shielding of borated polyethylene. The booster zone has been loaded with two different arrangements, which will be described below. The fast-spectrum lead zone and the thermal-spectrum polyethylene zone are separated by a so-called thermal neutron filter, or valve zone, consisting of one layer of 10^8 pins with metallic natural uranium and one layer of 116 pins with boron carbide (B_4C), which are

Figure 1: Schematic cross-sectional view of the YALINA-Booster reactor core

The experimental channels are also shown in this figure

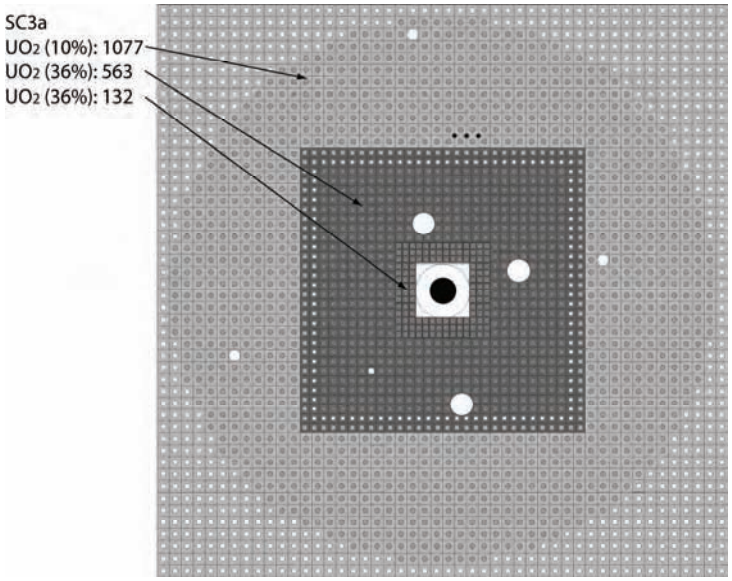

located in the outermost two rows of the fast zone. Hence, thermal neutrons diffusing from the thermal zone to the fast zone will either be absorbed by the boron or by the natural uranium. In this way, a coupling of mainly fast neutrons between the two zones is maintained. The three B_4C-control rods that can be inserted in the thermal zone have allowed us to slightly change (~400 pcm) the reactivity of the system. Hence, the sensitivity of the different reactivity monitoring techniques can be tested. In addition, the fuel configuration of the core can be customised, allowing the study of its influence in the core kinetical properties. Although the experimental results concerning different geometrical configurations will not be discussed in this work, they have been submitted for publication [5].

For measurement purposes, there are seven axial experimental channels (EC1B-EC4B and EC5T-EC7T) in the core, two axial (EC8R and EC9R) and two radial experimental channels (EC10R and EC11R) in the reflector. In addition, there is one neutron flux monitoring channel in each corner of the core (MC1-4).

Neutron source monitor

The determination of the neutron source intensity relies in measuring neutrons emitted in the D-T fusion reactions (14 MeV), which have energies larger than the fission neutrons created within the reactor. In this work we have used a BC501A [6] liquid organic scintillator acting as a veto detector to measure high-energy neutrons coming from the D-T source. The BC501A scintillation detector consists of a stainless steel cell filled with the organic liquid scintillator NE213, especially suitable for pulse shape discrimination. An extensive discussion on the neutron-gamma discrimination techniques using a BC501A liquid scintillator and deuterium-tritium neutron sources is performed in [7] and [8]. In order to increase the efficiency of the measurements and save data storage, the signals measured with the BC501A have been filtered with a constant fraction discriminator (CFD). In this sense we were able to eliminate the low energy counts and select a measurement window better suited for high energy neutrons. The threshold detection energy was fixed by using a typical neutron fission spectrum from a ^{252}Cf source. With this method we were able to neglect any neutron with energy below 7 MeV, avoiding the detection of fission neutrons coming from the YALINA-Booster fuel.

Data acquisition system

The data acquisition system used for the YALINA-Booster experiments is composed of three parts:

- pulsed mode electronic chain;
- current mode electronic chain;
- specific electronic chain for the neutron source monitor.

Two types of detectors were placed in the experimental channels to monitor the neutron flux, ^{235}U fission chambers and ^{3}He detectors. Both have been used for pulsed mode electronic chains, while only ^{235}U fission chambers have been used in current mode. In addition, there was a specific liquid scintillator with gamma-neutron discrimination capabilities to monitor the 14 MeV neutron source.

Pulsed mode electronics was similar to MUSE-4 experiments. It consisted of fast amplifiers/discriminators recorded with 80 MHz counter/timer National Instruments cards, which stored the absolute time of arrival of any signal coming from the detectors. The liquid scintillator was also recorded with the National Instruments cards after discriminating the particle deposited energy with a CFD.

Current mode electronics was specifically design at CIEMAT to measure the current generated in large fission detectors during the beam trip experiments. The set-up involved the HV to be applied in the outer carcass while the inner wire remained at ground level to make use of commercial current amplifiers. However, due to this arrangement, the chambers were no longer shielded and the level of the pick-up noise was not negligible. It is important to stress that due to the relatively low intensity of the source, the current in the 500 mg ^{235}U fission chamber was 1 μA at maximum, what obliged us to use amplification factors of 10^5-10^6 V/A in the current amplifier.

To record the fast variations in the neutron population after a beam trip, the current in the fission chambers was sampled with ADC in the MHz range, which has been the main reason for not using the standard electronic chain used in power reactors. Even more, to obtain a good uncertainty in the measurements, it was necessary to use 14-bit resolution. The acquisition system used in the YALINA experiments has been based on fast ADC modules. We have used 14-bit digitisers with 125 MHz sampling rate. However, detector signals were measured at 10 MHz sampling rate and filtered afterwards with a 100 kHz low-pass filter to reduce electronic noise introduced in the signal due to the large amplification. This situation is unlikely to happen at high power, when the current in the detector is usually three orders of magnitude larger and the amplification of pick-up noise should become negligible.

Reactivity determination

Pulsed neutron source technique

In the Pulsed Neutron Source (PNS) techniques the kinetic evolution of the system is measured after the repetitive injection of neutron pulses in the reactor. These reactivity determination techniques had been already validated in previous experimental programmes such as MUSE-4, TRADE or RACE [9-12] and the measurements have been repeated in the YALINA-Booster experimental campaign. Using PNS techniques the reactivity of the system can be calculated, according to the point kinetics model, by means of two different methods: the area ratio by Sjostrand [13] and the prompt-decay constant by Simmons and King [14].

In the first technique, the reactivity expressed in dollar units can be directly obtained from the prompt and delayed neutron populations in the following way (see left panel of Figure 2):

$$\frac{\rho}{\beta_{eff}} = -\frac{A_p}{A_d}$$

Figure 2: Schematic evolution of the neutron counting after the injection of an external neutron pulse in the reactor

Left – prompt and delayed neutron counting rates for the area method. Right – fit to the prompt neutron decay constant.

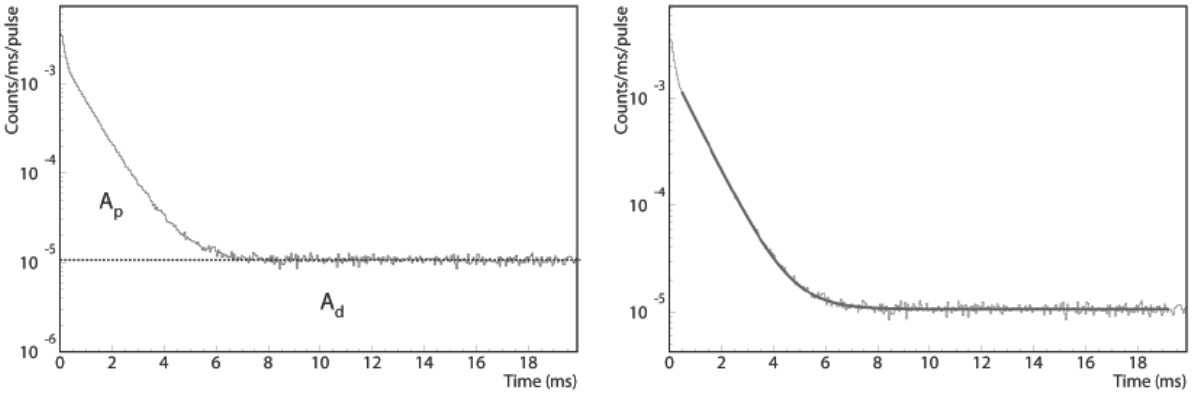

The second technique relies on the evolution of the prompt neutrons. As can be observed in the right panel of Figure 2, after the injection of an external neutron pulse, the prompt neutron population decays exponentially with a decaying constant related to the reactivity (following the point kinetics):

$$\frac{\rho}{\beta_{eff}} = \frac{\alpha}{\frac{\beta_{eff}}{\Lambda}} - 1$$

The β_{eff}/Λ ratio was determined by means of Monte Carlo simulations using the MCNPX code [15]. In Figure 3 we present the kinetic evolution of the neutron population measured at several locations within the reactor. As can be observed, the evolution of the system (especially at short times) is very different depending on the spatial location. However, after ~2 milliseconds, the evolution of the prompt neutron flux is very similar in all the experimental channels, indicating that the neutron population is driven by the fundamental mode of the reactor.

Figure 3: Evolution of the neutron counting rate at different detector locations within the YALINA subcritical core

The histogram accumulates ~10^5 pulses with a repetition rate of 57 Hz, a pulse duration of 5 μs and a pulse intensity of 6 mA. For visualisation, the counting rates in the 1 mg fission chamber have been scaled by a factor 500.

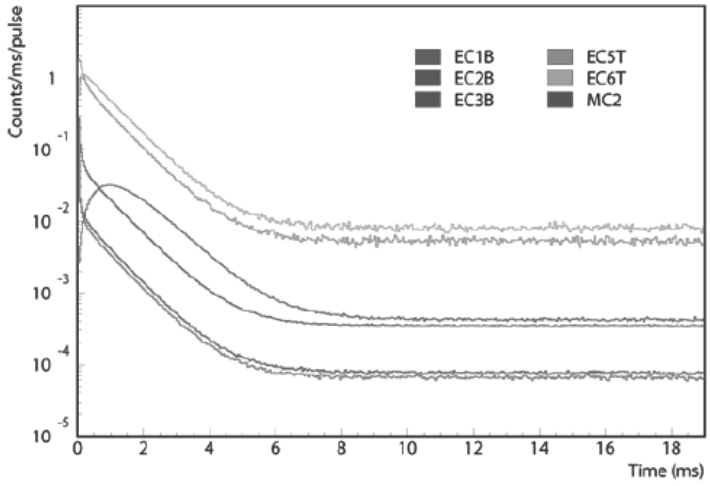

The complete set of experimental reactivity values for different fuel/libraries/geometric configurations can be found in [16]. As an example, some of the experimental results obtained in this work are presented in Table 1.

Table 1: Experimental values of the reactivity obtained with the prompt-decay constant and area methods

The reactivity values have been measured at different locations inside the subcritical core. The value of the decay constant is also shown in the table.

Channel	α	ρ_{decay} ($)	ρ_{area} ($)
EC1B	-1 102 ± 4	-9.14 ± 0.29	-9.21 ± 0.01
EC2B	-1 098 ± 10	-9.11 ± 0.31	-9.45 ± 0.01
EC3B	-1 092 ± 5	-9.07 ± 0.29	-9.60 ± 0.01
EC5T	-1 102 ± 7	-9.13 ± 0.30	-9.67 ± 0.01
EC6T	-1 086 ± 10	-9.03 ± 0.30	-9.17 ± 0.01
MC2	–	–	-9.28 ± 0.01
MC3	–	–	-9.73 ± 0.03
Average	–	-9.10 ± 0.13	-9.44 ± 0.23

Beam trips technique

Unfortunately, the PNS techniques described above cannot be used in a power ADS due to thermal stress. In addition, the neutron flux in a power ADS will be too high for using fission chamber operating in the standard pulsed mode due to dead-time effects. During the YALINA-Booster experimental campaign we reached counting rates close to 10^6 neutrons per second, leading to dead-time correction factors about 25%. For higher neutron fluxes the dead time would spoil the measurements. A double challenge, thus, has been faced: developing a new method avoiding the pulsed source techniques and developing the necessary electronic chains to avoid the operation of fission chambers in pulse mode. For the first challenge we have proposed to use short interruption of the external neutron source (beam-trips) and, concerning the electronics, we have proposed to invert the polarity of the fission chambers and measure, directly, the current created by the fission fragments in the inner wire of the chamber.

Due to the characteristics of the YALINA neutron generator, it was possible to promptly interrupt the deuteron beam current (~1 μs) and to recover the beam after 30-40 milliseconds. The time evolution of the deuteron beam current during a typical beam trip is shown in the black line of Figure 4. The beam current presents large fluctuations due to pick-up noise. The blue line in the figure represents the evolution of the neutron flux within the reactor core when a beam trip is forced. As can be observed in the figure, when the external source drops, the neutron population decays exponentially, reaching a level given by the delayed neutron population. In the figure we can observe an oscillation with 50 Hz frequency. This oscillation was observed in all the detectors and seems to be related with the deuteron beam intensity on the tritium target. Although the origin of this effect was not completely clarified, it was (with high confidence) stated that there was a 50 Hz oscillation in the horizontal impact position of the deuteron beam on the tritium target. In this sense, during the oscillation part of the deuterons were not hitting the tritium target and, hence, the intensity of the neutrons created in the source should also be oscillating. It is worth saying that this oscillation is not affecting the results if the neutron level is calculated within an integer number of oscillations.

Using this beam trip technique, two different methods can be used to determine the reactivity value of the system: the prompt-decay constant fit and the source-jerk methods. The first is analogous to the PNS case given in expression 2. The source-jerk method can be considered analogous to the Sjostrand method of PNS techniques. In the right panel of Figure 4

Figure 4: Left – evolution of the deuteron beam current and the neutron flux inside the reactor measured during a beam trip. Right – schematic view of the source-jerk technique.

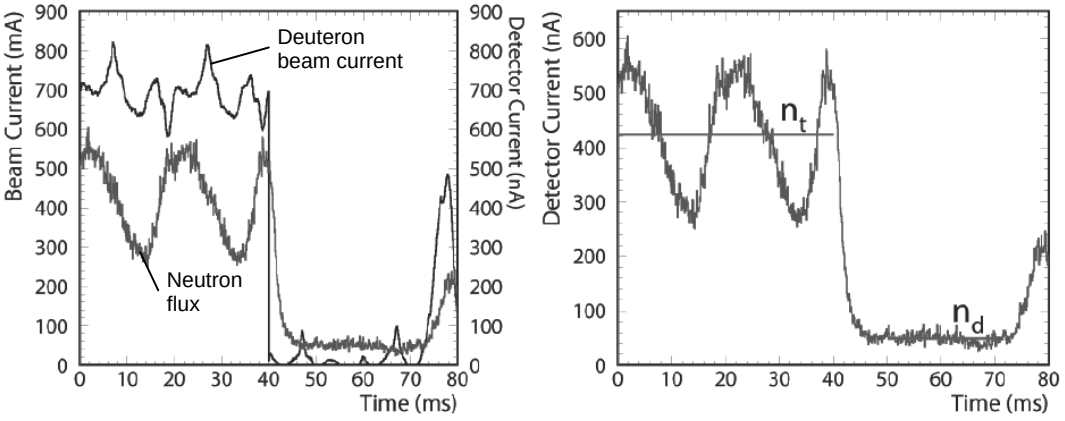

we present the schematic view of the neutron population before and after the beam interruption measured with a fission chamber operating in current mode. Applying the point kinetics model, the reactivity of the system can be described as:

$$\frac{\rho}{\beta_{eff}} = -\frac{n_{prompt}}{n_{delayed}} = -\frac{n_{total} - n_{delayed}}{n_{delayed}}$$

Thus, operating the fission chambers in current mode, we can use two methods analogous to those used in standard PNS reactivity determination. The prompt-decay fit method presents larger uncertainties than the source-jerk method due to the short time range for the fit. The good performance of the deuteron accelerator allowed forcing beam trips at 1 Hz repetition rate. In this sense, we were able to determine the absolute value of the system reactivity on each second. In Figure 5 we present the reactivity values obtained in 1 000 consecutive seconds using the source-jerk technique with a fission chamber operating in current mode and located in the booster region of the YALINA core.

Figure 5: Time evolution during 1 000 seconds of the reactivity values (in dollars) measured with a fission chamber operating in current mode located in the reflector region of YALINA-Booster

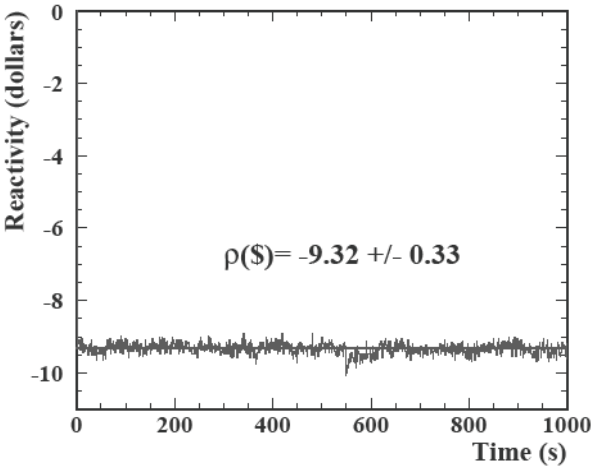

These measurements present a dispersion of ~0.3$ around a mean value of 9.32$. These results are compatible with those obtained with standard PNS techniques: $9.10 \pm 0.13$$ in the case of prompt-decay constant method and $9.44 \pm 0.23$$ in the case of the area method. These results provide the first experimental confirmation that the beam trips are a useful technique to calculate reactivity values in a subcritical core and, in addition, together with fission chambers operating in current mode can be used to determine the reactivity values of a power ADS.

On-line reactivity monitoring: Current-to-flux

A key point of the future ADS facilities will consist of a robust on-line and continuous monitoring of the subcritical assembly reactivity. This monitoring system must yield valuable information concerning the rapid relative change of the reactivity, which in a subcritical assembly is given by:

$$\rho = q\Phi\frac{S}{P}$$

where q is the energy released by fission, Φ is the source importance, P is the core power (neutron flux) and S is the external neutron source intensity. It is generally assumed that the source strength is proportional to the beam current and, hence, any change in the reactivity is accessible through the beam current ($S = \kappa I$) and the neutron flux (P). The on-line determination

Figure 6: Time evolution of the deuteron beam current (top), the 14 MeV neutron source (middle) and the core power measured in the EC2b experimental channel (bottom)

These data correspond to a typical beam trip in the SC3b configuration

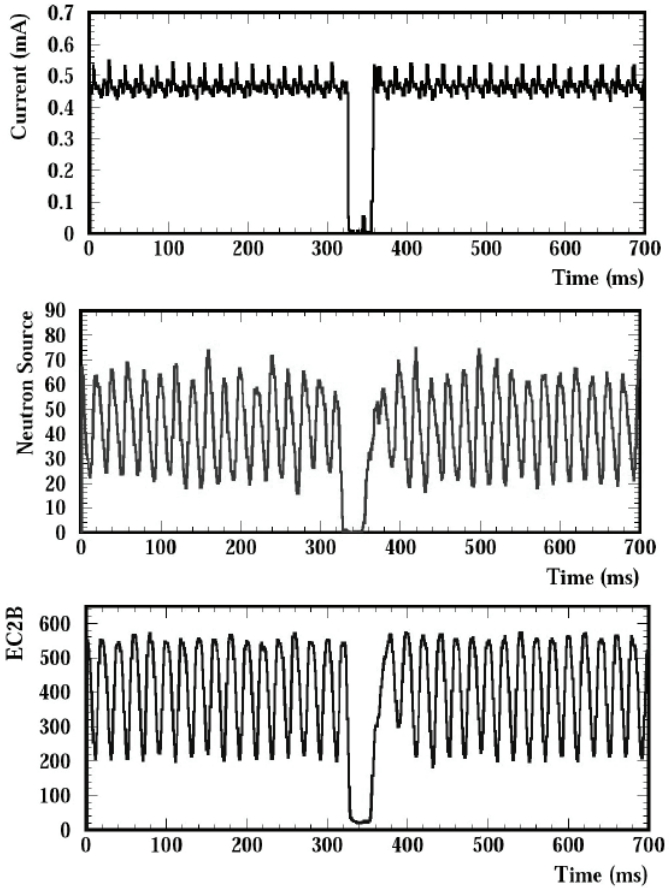

of the reactivity, then, requires the monitoring of three quantities, the accelerator intensity (*I*), the neutron source intensity (*S*) and the core power (neutron flux) *P*. Actually two ratios must be determined, *S/I* and *P/S*. However, several factors exist which can affect this proportionality such as the impinging position of the beam at the tritium target, the beam emittance, the beam oscillations or even the target consumption.

Due to the precision of the data acquisition developed for this experimental campaign, we were able to monitor the deuteron beam intensity, the neutron flux within the reactor and the neutron source intensity in the milliseconds time scale, as shown in Figure 6. From the figure, when the deuteron beam current is suddenly removed, the current in the Faraday cup drops to zero (top panel). The counting rate in the 14 MeV neutron source monitor, consequently, also drops to zero because no 14 MeV are created in the tritium source (middle panel). However, the counting rate at any detector located in the reactor core will drastically drop, but it will not reach zero because there still exist a neutron population due to the fission products (bottom panel). This effect can be clearly seen in the bottom panel of the figure, where the data from the EC2B detector for the SC3b configuration are shown.

As a consequence of monitoring the relevant quantities involved in the evolution of the reactor in a millisecond scale, several effects (hidden at larger time intervals) appeared. For instance, a loss of proportionality between the core power and the deuteron beam current was observed. This effect is related to the beam current monitoring. The deuteron current is measured with a Faraday cup located before the tritium target. In this sense, the detector does not monitor the real deuteron current on the tritium target. If, for instance, the beam position is oscillating this effect would not be reflected in the deuteron current monitoring, but it will definitely affect the intensity of 14 MeV neutron source. In addition, as the experiments took

Figure 7: Neutron source of 14 MeV counting rate versus the core power (neutron flux) measured in the MC4 experimental channel with a fission chamber operating in current mode (top) and measured in the EC1B experimental channel with a fission chamber operating in pulse mode (bottom)

The data from MC4 correspond to the SC3b configuration while the data from EC1B correspond to the SC3a configuration. These experimental data correspond to the complete measured range of the deuteron beam intensity, from 0.03 mA to 1.5 mA.

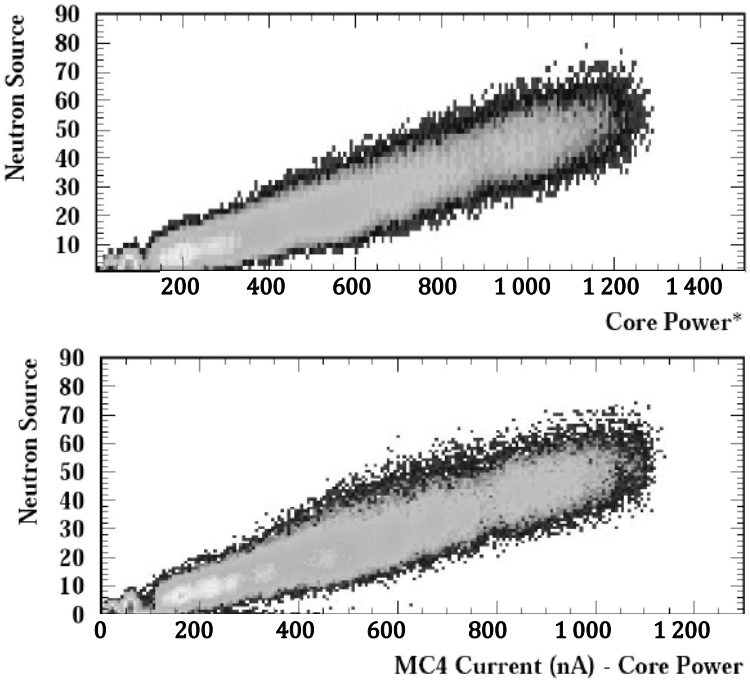

place in a highly noisy environment, the Faraday cup picks up electrical signals that also affect the measurements. In future ADS projects it would be crucial to implement accurate methods to determine the beam current intensity and to develop techniques to accurately determine the impact position of the beam onto the production target. It is worth saying that these effects are hidden at larger time intervals. When looking at the time scale of seconds, the time averaging hides the 50 Hz oscillation in the neutron source and the core power and also hides the structure of the beam current signal (pick-up noise).

We have found, however, a clear proportionality between the 14 MeV neutron source intensity and the core power (neutron flux). In Figure 7 we present the experimental data measured with two different fission chambers: one operating in pulsed mode (top panel) and the other operating in current mode (bottom panel). As can be observed, both fission chambers provide similar results, stating that the electronic chains developed to operate the fission chambers in current mode are suitable for measuring in future power ADS. The proportionality between the neutron source intensity and the core power has been validated over a wide range of deuteron current intensity, almost two orders of magnitude.

Conclusions

We have presented some of the experimental results obtained during the EUROTRANS experiments at the YALINA-Booster facility. The main objective has been the qualification of reactivity monitoring techniques to be used in future power ADS systems.

The possibility of continuous on-line reactivity monitoring was demonstrated by a continuous evaluation of the deuteron accelerator current, the 14 MeV neutron source intensity and the reactor power. These quantities were monitored at intervals as short as 1 millisecond, allowing the observation of effects hidden at large time intervals. Using this current-to-flux technique it was possible to isolate and identify the origin of events where the proportionality between, for instance, the deuteron current and the core power is lost.

The current-to-flux technique, however, provides relative changes in the system reactivity. In order to determine the absolute value of the reactivity, additional techniques must be used. The standard Pulsed Neutron Sources methods tested in previous experimental projects were also validated in this work but, unfortunately, these methods cannot be used in power ADS for two reasons: it is not possible to pulse a power reactor and the pulsed electronic cannot be used at high neutron fluxes due to dead time effects.

A new electronic approach based on fission chambers operating in current mode was proposed in this work. The results obtained with these fission chambers were compatible with those obtained with fission chambers operating in standard pulsed mode, stating the validity of this technique to be used in power ADS.

In addition, forcing short interruptions of the neutron source (beam trips) we were able to apply two different methods to determine the absolute reactivity of the system. We have applied both methods with fission chambers operating in current mode and the experimental results obtained are compatible with those obtained by standard PNS techniques. These results stated the validity of the beam trip technique, which can also be used in future power ADS. To our knowledge, it is the first time that detectors in current mode are used to determine the reactivity values in a subcritical assembly and it is the first time that the beam trip technique is used in a subcritical assembly.

For future projects, reducing the pick-up noise in the fission chambers would largely improve the uncertainty in the reactivity values. Double shielding of the fission chambers must be explored. Stable beam conditions and a system to monitor the impact position of the deuteron beam onto the tritium target must also be developed. In a higher power ADS the reactivity values could be determined with uncertainties close to 1% or below.

Acknowledgements

This work was partially supported by IP-EUROTRANS contract No. FI6W-CT2005-516520, by the ENRESA-CIEMAT agreement for the Transmutación Aplicada a los Residuos Radiactivos de Alta Actividad and by the Swedish Institute.

References

[1] Knebel, J., *et al.*, "European Research Programme for the Transmutation of High Level Nuclear Waste in an Accelerator Driven System", *Conference on EU Research and Training in Reactor Systems (FISA 2006)*, Luxembourg, 13-16 March (2006).

[2] Soule, R., *et al.*, "Neutronic Studies in Support to ADS: The Muse Experiments in the MASURCA Facility", *Nucl. Sci. and Engin.*, 148, pp. 124-152 (2004).

[3] Chigrinov, S.E., *et al.*, *Booster Subcritical Assembly Driven by a Neutron Generator*, Preprint JIPNR-Sosny, Minsk, p. 31 (2004).

[4] Kiyavitskaya, H., *YALINA-Booster Benchmark Specifications for the IAEA Coordinated Research Projects on Analytical and Experimental Benchmark Analysis on Accelerator Driven Systems and Low Enriched Uranium Fuel Utilization in Accelerator Driven Sub-Critical Assembly Systems*, IAEA (2007).

[5] Berglöf, C., *et al.*, "Spatial and Source Multiplication Effects on the Area Ratio Reactivity Determination Method in a Strongly Heterogeneous Subcritical System", submitted to *Nucl. Sci. and Eng.* (November 2009).

[6] BICRON Corporation, *BC501a Liquid Scintillation Data Sheets*.

[7] Guerrero, C., *et al.*, "Analysis of the BC501A Neutron Detector Signals Using the True Pulse Shape", *Nucl. Instr. Meth. A*, 597, pp. 212-218 (2008).

[8] Fernández-Ordóñez, M., *et al.*, "Characterization of a BC501A Detector for Monitoring 14 MeV Neutrons from a Deuterium-tritium Source", *Proc. of the Int. Conference AccApp'07*, Pocatello, Idaho, USA, 30 July-2 August (2007).

[9] Lebtrat, J.F., *et al.*, "Global Results from Deterministic and Stochastic Analysis of the MUSE-4 Experiments on the Neutronics of Accelerator-driven Systems", *Nucl. Sci. and Eng.*, 158, pp. 49-67 (2008).

[10] Rubbia, C., *et al.*, "TRADE: A Full Experimental Validation of the ADS Concept in a European Perspective", *Proc. of the Int. Conference AccApp'03*, San Diego, USA, 1-5 June (2003).

[11] Beller, D., *et al.*, "Overview of the US Reactor-accelerator Coupling Experiments (RACE) Project", *Proc. of the Int. Conference AccApp'07*, Pocatello, Idaho, USA, 30 July-2 August (2007).

[12] Persson, C-M., *et al.*, "Analysis of the Reactivity Determination Methods in the Subcritical Experiment Yalina", *Nucl. Instr. Meth. A*, 554, pp. 374-383 (2005).

[13] Sjostrand, M.G., "Measurements on a Subcritical Reactor Using a Pulsed Neutron Source", *Ark. Fys.*, 11, pp. 233-246 (1956).

[14] Simmons, B.E., "A Pulsed Neutron Technique for Reactivity Determination", *Nucl. Sci. and Eng.*, 3, pp. 595-608 (1958).

[15] Pelowitz, D.B. (Ed.), *MCNPXTM User's Manual. Version 2.5.0*, LA-CP-05-0369 (2005).

[16] Bécares, V., *et al.*, "Correction Methods for Reactivity Monitoring Techniques in Pulsed Neutron Source (PNS) Measurements", *Proc. of PHYSOR 2010*, Pittsburgh, USA, 9-14 May (2010).

Integral Circulation Experiment: Thermal-hydraulic simulator of the ETD primary system

M. Tarantino, G. Benamati, P. Gaggini, V. Labanti
ENEA UTIS, C.R. Brasimone
Camugnano, Bologna, Italy

Abstract

In the framework of the IP-EUROTRANS (6th Framework Programme EU), domain DEMETRA, ENEA C.R. Brasimone is strongly involved in the Work Package 4.5 "Large Scale Integral Test". This WP foresees large-scale tests to characterise a relevant portion of a subcritical ADS reactor block (core, internals, heat exchanger, cladding for fuel elements) in steady-state, transient and accidental conditions. ENEA, as leader of the Task 4.5.3, assumed the commitment to perform an integral experiment with the aim to reproduce the primary flow path of the "European Transmutation Demonstrator" ETD pool nuclear reactor, cooled by lead-bismuth eutectics (LBE).

This new experimental activity, named "Integral Circulation Experiment" (ICE) will be performed by the ENEA C.R. Brasimone, where an appropriate test section has been designed to be installed in the CIRCE facility.

The paper reports a description of the experiment, the designed test section and an overview of its main components (heat source, heat exchanger) as well as the experimental activities carried out in support to the design of the ICE by the NACIE loop facility.

Introduction

Presently the European Union relies for 35% of its electricity on nuclear fission energy leading to the annual production of 2 500 t/y of used fuel, containing 25 t of plutonium, 3.5 t of minor actinides (MA, namely Np, Am, Cm) and 3 t of long-lived fission products (LLFP). These MA and LLFP stocks need to be managed in appropriate way. The used fuel reprocessing followed by the geological disposal or the direct geological disposal are today the envisaged solutions depending on national fuel cycle options and waste management policies.

The required time scale for the geological disposal exceeds our accumulated technological knowledge and this poses problems of public acceptance. Partitioning and transmutation (P&T) has been pointed out in numerous studies as the strategy that can relax the constraints on geological disposal and reduce its monitoring period to technological and manageable time scales. Therefore a special effort has been initiated at the European level thanks to the effort of the European Commission and some major European research institutions and industries to integrate P&T and advanced fuel cycles based on critical and/or subcritical fast spectrum transmuters, in order to assess the technical and economical feasibility of this waste management option, which could ease the development of a deep geological storage.

The ongoing research shows the potential benefits of P&T including the large reduction of long-term radioactivity, radiotoxicity and fissile materials inventories that can contribute to improving public acceptance of the unavoidable geological repositories, and the minimisation of short- and medium-term heat sources that can allow a reduction in the volume required by the high-level wastes in repositories, increasing their effective capacity and reducing their number.

With this background, in the Euratom 6th Framework Programme (FP6), the Integrated Project (IP) EUROTRANS (European Research Programme for the Transmutation of High-level Nuclear Waste in an Accelerator-driven System) has been launched.

The strategic objective of IP-EUROTRANS is to work towards a European Transmutation Demonstration (ETD), carrying out a first advanced design of an approximately 50 to 100 MWth Experimental facility (short-term development) demonstrating the technical feasibility of Transmutation in an Accelerator-driven System (XT-ADS), as well as to accomplish a generic conceptual design (several 100 MWth) of a modular European Facility for Industrial Transmutation (EFIT) (long-term development).The work of the project has been structured into technical domains, and in particular the domain DEMETRA (Develop and Assessment of Structural Materials and Heavy Liquid Metal Technologies for Transmutation Systems) is focused on the improvement and assessment of the Heavy Liquid Metal (HLM) technologies, thermal-hydraulics, and materials to support the XT-ADS and EFIT development.

In the framework of the DEMETRA domain, ENEA assumed the commitment to perform an integral experiment with the aim to reproduce the primary flow path of the ETD pool nuclear reactor, cooled by lead-bismuth eutectics (LBE). The designed experimental activity, named ICE (Integral Circulation Experiment), will be performed by the ENEA C.R. Brasimone, where an appropriate test section has been designed and installed in the large-scale multi-purpose facility CIRCE [1]. The design and implementation of the ICE activity required the development of a support facility, NACIE (Natural Circulation Experiment) [2] built to carry out experimental tests needed to address the phenomena related to the natural and gas enhanced circulation flow regimes, and to test and qualify components for heavy liquid metal cooled systems.

The Integral Circulation Experiment

Aim of the experiment

In the framework of the DEMETRA domain, large-scale tests to characterise a relevant portion of a subcritical ADS reactor block (core, internals, heat exchanger, cladding for fuel elements) in

steady-state, transient and accidental conditions were scheduled. The foreseen activities were focused on the single pin, fuel rod bundle and pool reactor primary loop.

To this aim, ENEA designed and implemented the ICE activity, with the objective to obtain information about different topics such as:

- the thermal-hydraulics behaviour of a HLM pool system by the analysis of the coupling between an appropriate heat source and a cold sink placed inside;
- characterisation of representative components (i.e. prototypal heat exchangers) for the ETD concepts;
- operational and accidental transients;
- transition from the forced to the natural circulation flow regime;
- qualification of a chemistry control system for HLM pool.

Moreover the ICE activity will allow establishing a reference experiment for the benchmark of commercial codes when employed in HLM pool systems.

CIRCE facility

The ICE activity has been designed to be implemented on the CIRCE facility. CIRCE basically consists of a main cylindrical vessel (S100) with an outer diameter of 1 200 mm and a height of 8 500 mm. The main vessel can be filled with about 70 tonnes of molten lead-bismuth eutectic (LBE), and it has been designed to host different test sections welded to and hung from bolted vessel heads for the study of the thermal-hydraulic issues related to the HLM pool systems. The main vessel is moreover equipped with auxiliary systems for eutectic circulation, with argon cover gas and recirculation system, LBE heating and cooling systems.

The facility is complete of a LBE storage tank (S200), of a small LBE transfer tank (S300) and of the data acquisition system. In Figure 1, an isometric view of the facility is shown. The main parameters relevant to the test vessel are listed in Figure 1.

Figure 1: CIRCE isometric view and main vessel parameter

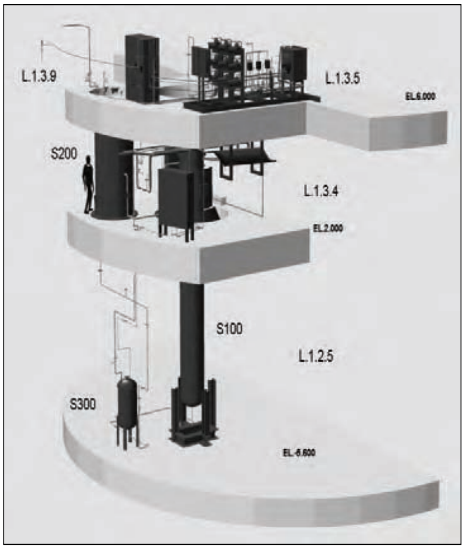

Parameters	Value
Outside diameter	1 200 mm
Wall thickness	15 mm
Material	AISI 316L
Max LBE inventory	90 000 kg
Electrical heating	47 kW
Cooling air flow rate	3 Nm3/s
Temperature range	200 to 500°C
Operating pressure	15 kPa (gauge)
Design pressure	450 kPa (gauge)
Argon flow rate	15 Nl/s
Argon injection pressure	600 kPa (gauge)

ICE test section

The ICE test section was designed to reproduce, as closely as possible, the thermal-hydraulic behaviour of the XT-ADS and EFIT primary systems [3-7] .The main experimental parameters characterising the ICE experiments are reported in Table 1, where they are compared to the values characterising XT-ADS and EFIT.

Table 1: Overview of the experimental parameters adopted for the ICE activity

	XT-ADS	EFIT	ICE
Coolant	LBE	Pure lead	LBE
Primary loop circulation	Mechanical pump	Mechanical pump	Gas lift technique
Fuel assembly lattice	Hexagonal	Hexagonal	Hexagonal
Fuel assembly type	Wrapper	Wrapper	Wrapper
Fuel assembly spacer	Grid	Grid	Grid
Fuel pin diameter (D) [mm]	6.55	8.72	8.2
Pitch to diameter ratio (P/D)	1.41	1.56	1.8
Fuel heat flux q″ [W/cm^2]	85-115	100-140	100
Fuel power density q″ [W/cm^3]	500-700	450-650	488
Average velocity fuel pin region [m/s]	1	1	1
Fuel pin active length [mm]	600	900	1 000
T_{in}/T_{out} core [°C]*	300/400	400/480	300/400
T_{HS}/L_{act} [°C/m]	167	88	100
Fuel pin cladding material	T91	T91	AISI 316L
Secondary coolant	Low pressure boiling water	Water with superheated steam	Low pressure boiling water

* This value refers to the thermal difference between the inlet and outlet section of the ICE heat section (made by a single bundle); for EFIT and XT-ADS it refers to the thermal difference between the upper plenum and lower plenum of the core.

As can be noted, the main ICE experimental parameters are roughly in the range expected for the XT-ADS and EFIT concepts. The main difference between ICE and XT-ADS/EFIT concepts is the P/D ratio value. In fact, for the ICE test section a P/D ratio value of 1.8 is adopted to reduce the overall pressure drop along the primary flow path, still preserving the main characteristics of the heat source and allowing performing the tests with the available pumping system (gas-lift technique).

The ICE test section, to be placed inside the CIRCE main vessel (S100), consists of the following main components, as depicted in Figure 2:

- *Downcomer*: It is the volume between the test section and the main vessel which allows the hydrodynamic connection between the outlet section of the HX and the inlet section of fuel pin simulator.
- *Flow meter*: It is a Venturi-Nozzle flow meter; bubble tubes [8] are adopted to measuring the pressure gradient along the throat of the Venturi pipe. The flow meter is directly connected to the heat source, without bypass, allowing measuring directly the primary flow rate through the pin bundle.
- *Fuel pin simulator* (FPS): It is a mechanical structure needed to take on the heat source (HS). It is connected in the lower section to the flow meter, and in the upper section to the insulation volume.
- *Fitting volume*: It is placed in middle part of the test section, allowing the hydraulic connection between the HS and the riser.
- *Riser*: It is a pipe which connects the fitting volume with the separator. In the lower section a nozzle is installed to allow the argon injection and to promote the circulation.

- *Separator*: It is a volume needed to connect the riser with the HX. It allows the separation between the LBE, which flows downward into the HX, and the argon flowing in the test section cover gas through the free level. Moreover, the separator assures that the overall LBE flow rate flows directly into HX (shell-side) before falling down in the downcomer.
- *Heat exchanger*: It is a prototypical component and it constitutes the heat sink of the system.
- *Dead volume*: It is a component made of two concentric pipes. The inner pipe is connected to the fuel pin simulator and to the cover head. The volume inside the inner pipe is called insulation volume. The annulus between the inner and outer pipe, is kept melt-free by design, and it is linked to the cover gas.
- *Insulation volume*: It encloses the power supply rods feeding the HS. Due to the self-heating by Joule effect of the power supply rods, an insulation volume cooling system (IVCS) has been foreseen, with a thermal duty of 40 kW.

Heat source

The heat source is coupled with the test section by an appropriate mechanical structure. The HS and the mechanical structure which surrounds it make up the so-called fuel pin simulator (FPS).

The ICE heat source consists of a pin bundle made by electrical heaters with a nominal thermal power of 800 kW (total power of 925 kW); it has been designed to achieve a difference temperature through the HS of 100°C, a fuel power density of 500 W/cm^3 and an average liquid metal velocity of 1 m/s, in accordance with the reference values adopted for the ETD concepts.

The ICE heat source consists of 37 pins placed in a wrapped hexagonal lattice with a pitch to diameter ratio of 1.8 (see Figure 3). Each pin has an outer diameter of 8.2 mm, a power of about 25 kW and a wall heat flux of 1 MW/m^2; the selected active length is 1 000 mm and the adopted cladding material is AISI 316L. To get an average LBE velocity of 1 m/s, a flow rate of 55.2 kg/s is needed through the HS.

Along the HS, three spacer grids (see Figure 3) are placed aiming to assure the relative position of the pins inside the bundle, improve the mixing of the coolant and guarantee a uniform and constant sub-channel cross-section during the tests.

As already mentioned, the main difference between the ICE heat source and ETD fuel assembly concepts is the P/D ratio value. In fact, such a high P/D value has been adopted to reduce the overall pressure drop along the primary flow path, preserving the high thermal performance of the heat source. Due to the available pumping system in the CIRCE facility, namely the gas lift pumping system, in order to carry on the ICE activity it was necessary to decrease as much as possible the pressure drop along the heat source, which amount to about the 70-80% of the overall pressure drop. The gas lift technique [9] was successfully tested and qualified during the previous experimental campaigns performed in CIRCE [10,11] and a pressure head of 40 kPa is available to promote the LBE circulation along the flow path.

The reference reactor fuel rods will be simulated by prototypical electrical pins constituting the heat source. Before ICE activities can be run the prototypical pins needed to be tested and qualified by a dedicated experimental campaign. The qualification tests were performed on the NACIE loop.

Heat exchanger

For the ICE activity the cold sink consists of a cooling water circuit, a LBE-low pressure boiling water shell heat exchanger, interconnecting piping, and steam vent piping to discharge steam into the atmosphere.

Figure 2: ICE test section overview

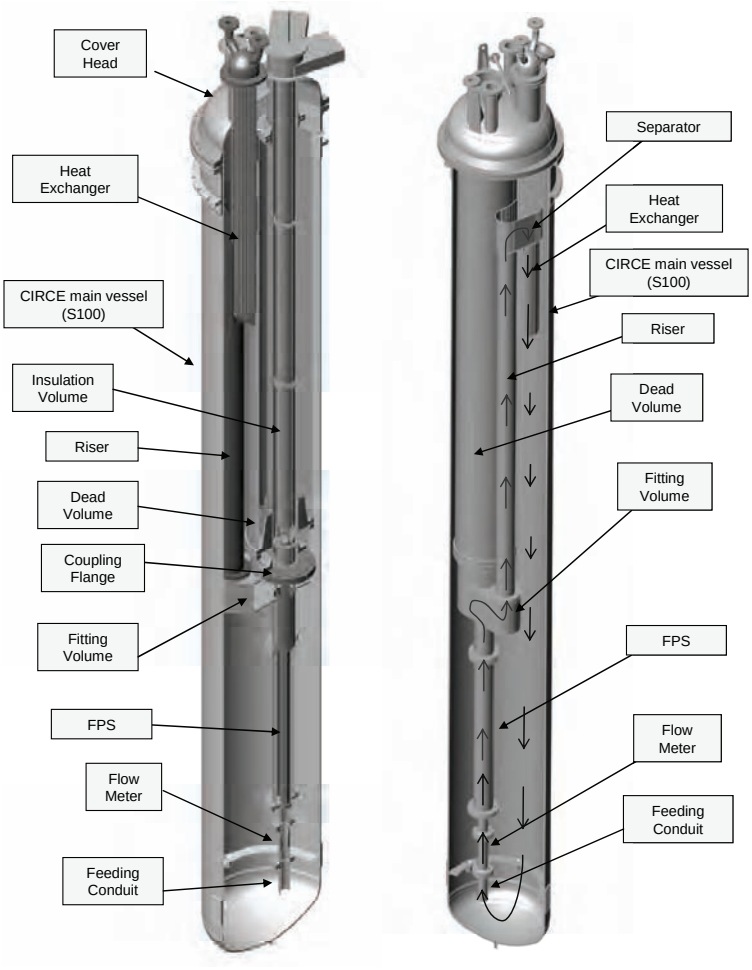

Figure 3 .Cross-section of the ICE heat source, and view of the spacer grid

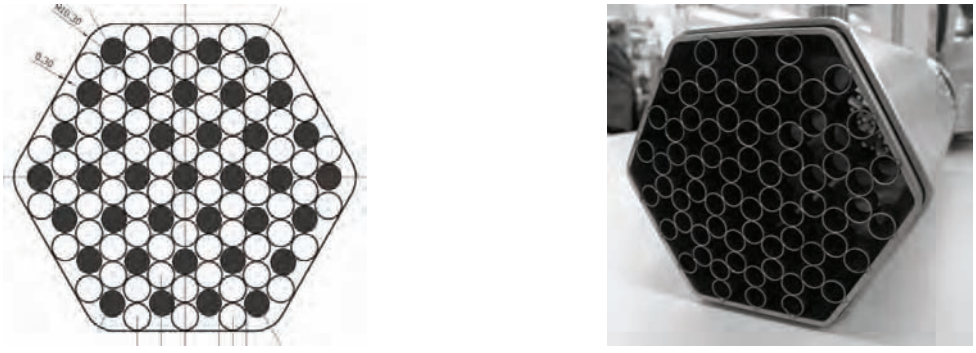

In particular, the HX is made of bayonet tubes. The bayonet consists of three concentric tubes (see Figure 4), the outer two of which have the bottom end sealed. The water flows downward in the inner pipes, and then upward in the annulus between the inner and intermediate pipes. In the annulus vaporisation takes place. The annulus between the middle and outer pipes is filled by pressurised helium (4.5 bar). All annuli are interconnected to form a common gas plenum, the pressure of which is continuously monitored. A leakage from either wall of any of the outer

Figure 4: Layout of the bayonet tube and view of the HX in the test section

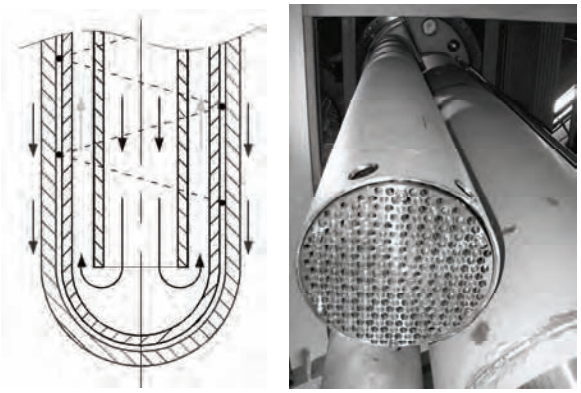

tubes is promptly detected because of depressurisation of the common helium gas plenum. The two outer tubes are mechanically and thermically decoupled. This configuration allows localising the most part of the thermal gradient, between lead and boiling water across the gas layer, avoiding both risk of lead freezing and excessive thermal stresses across the tube walls during steady-state operation and transients.

Experimental support for heat section design

NACIE loop

In the framework of the R&D activities ongoing by ENEA for the LFR/ADS development, by the Brasimone research centre a LBE loop was built in 2008, named NACIE [2,12]. The aim of the NACIE loop (Figure 5) is to set up a support facility able to qualify and characterise components, systems and procedures relevant for HLM nuclear technologies. Moreover, with this facility it will be possible to perform several experimental campaigns in the field of thermal-hydraulics, fluid-dynamics, chemistry control, corrosion protection and heat transfer, allowing to obtain correlations essential for the design of the nuclear power plant cooled by heavy liquid metal. Finally, the possibility to test prototypical pin simulators as well as all their ancillary systems and mechanical connections it has been mandatory in order to confirm the design of the ICE test section. For this reason the NACIE loop was prepared to house a bundle made with prototypical pin simulators in full scale to the ones which will be manufactured for the ICE test section.

NACIE is a HLM rectangular loop which basically consists of two vertical pipes (O.D. 2.5″) working as riser and downcomer, connected by means of two horizontal branches (O.D. 2.5″).The adopted material is stainless steel (AISI 304) and the total inventory of LBE is about 1 000 kg; the design temperature and pressure are 550°C and 10 bar respectively. In the bottom part of the riser a heat source is installed through an appropriate flange, while the upper part of the downcomer is connected to an heat exchanger. The difference in level between the thermal centre of the heat source and the one of the heat sink was fixed to reproduce the same height that characterises the ICE test section (H = 4.5 m). The loop is completed by an expansion vessel, installed on the top part of the loop, coaxially to the riser.

Performed test

The experimental activity performed on the NACIE facility to support the design of the ICE heat source included several tests concerning natural and gas enhanced circulation. In particular, each test was performed with only one pin activated inside the heating section, with a power of 22.5 kW.

Figure 5: NACIE loop layout and a view of the facility

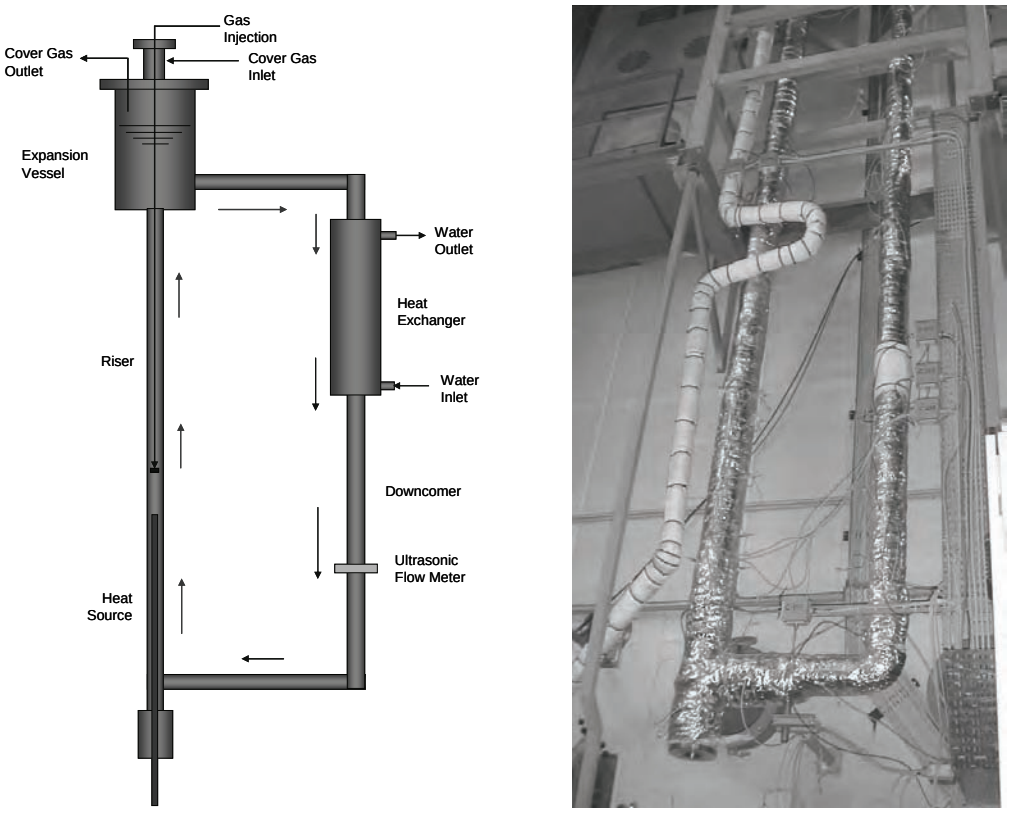

The NACIE bundle consists of two high thermal performance electrical pins and two dummy pins to support the bundle itself. In the middle section of the active length an appropriate spacer grid is installed, designed to be similar as close as possible to the one adopted for the ICE bundle. Along each pin seven thermocouples have been installed, in order to monitor the trend of the cladding temperature during the test in different position. Appropriate thermocouples have also been installed in order to make a rough evaluation of the hot spot factor on the pin due to the spacer grid installation.

Natural circulation test

In Figure 6 the trend of the HLM flow rate carried out for a natural circulation test is reported. The tests were performed by supplying electrical power to the heater under qualification and circulating coolant in the secondary side of the heat exchanger. During the tests, no gas is injected in the riser, so the only driving force for fluid circulation in the loop results from thermal buoyancy. After about 2 000 seconds a steady-state condition is obtained with an estimated flow rate of about 5.5 kg/s.

In Figure 7 the trend of the inlet and outlet temperature through the heating section is reported, depicting the transients during the natural circulation tests. For the same test, Figure 8 reports the value of the Reynolds number and average lead-bismuth velocity through the HS. The cladding temperature trend of the active pin on the matching surface between pin and spacer grid is depicted in Figure 9. Nevertheless the performed test is really severe, with the temperature being close to 500°C. The hot spot factor clearly appears in this figure, being the temperature below the spacer grid higher of about 25°C than the upstream temperature.

Figure 6: Heavy liquid metal flow rate (NC)

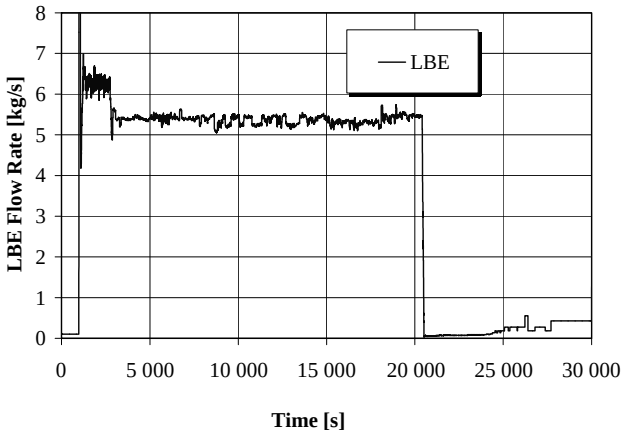

Figure 7: Inlet and outlet temperature through the HS (NC)

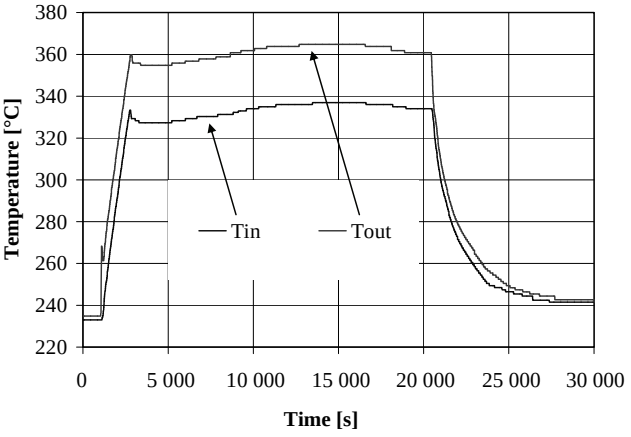

Figure 8: LBE velocity and Reynolds number through the HS (NC)

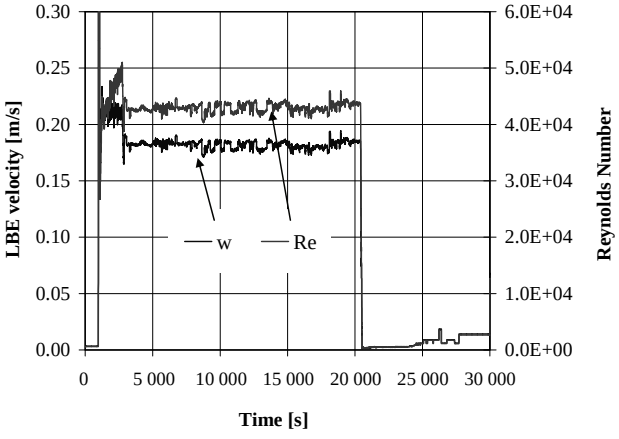

Figure 9: Cladding temperature trend upstream and downstream the spacer grid (NC)

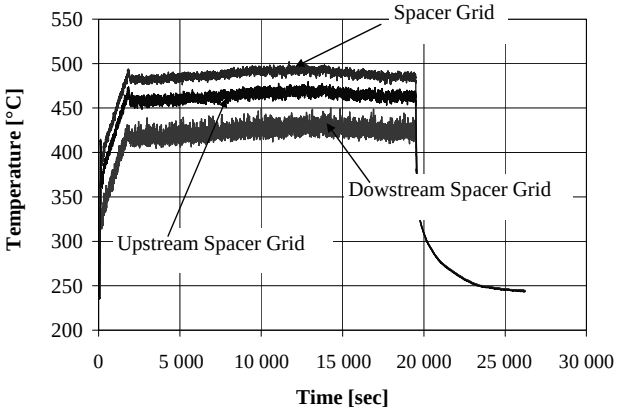

Gas-enhanced circulation test

As concerns the gas-enhanced circulation tests, Figure 10 reports the HLM flow rate trend compared with the gas injection flow rate, which promotes the LBE circulation along the loop. Gas-enhanced circulation tests were performed by supplying electrical power to the heater starting the argon injection and circulating coolant in the secondary side of the heat exchanger. During the tests, because argon is injected in the riser, the driving force for fluid circulation in the loop results from void buoyancy in the riser.

As reported in Figure 10, for the gas-enhanced circulation tests the LBE flow rate obtained is higher than the one obtained under natural circulation. With a gas injection of about 5 Nl/min, the liquid metal flow rate falls around 13 kg/s. In Figure 11 the trend of the inlet and outlet temperature through the heating section is reported, depicting the transients during the gas-enhanced circulation tests, and highlighting that also in this case a steady-state condition is obtained after about 2 000 seconds.

For the same test, Figure 12 reports the value of the Reynolds number and average liquid metal velocity through the HS; as can be noted the LBE velocity reaches a value of 0.45 m/s, against the 0.18 m/s obtained during the natural circulation tests, and a Reynolds number of about 100 000, underlining the higher turbulent behaviour of the main stream line in the case of void buoyancy promoted flow.

Figure 10: HLM flow rate and gas injection flow rate (GEC)

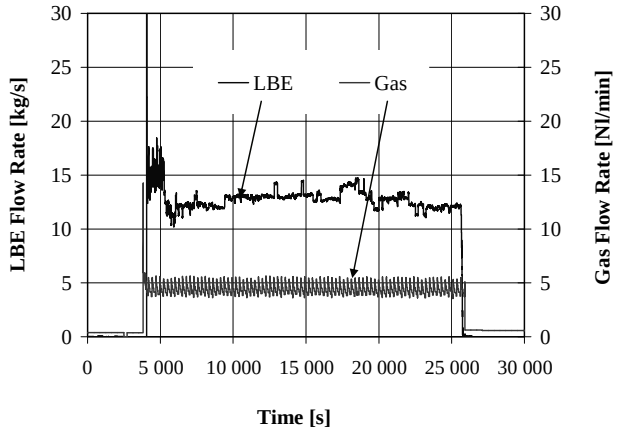

TECHNOLOGY AND COMPONENTS OF ACCELERATOR-DRIVEN SYSTEMS, ISBN 978-92-64-11727-3, © OECD 2011

Figure 11: Inlet and outlet temperature through the HS (GEC)

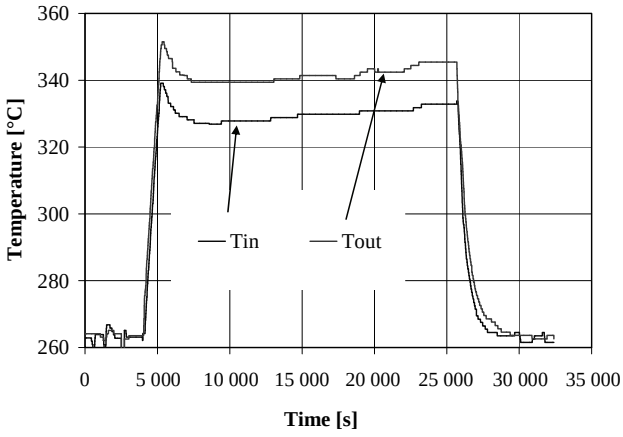

Figure 12: LBE velocity and Reynolds number through the HS (GEC)

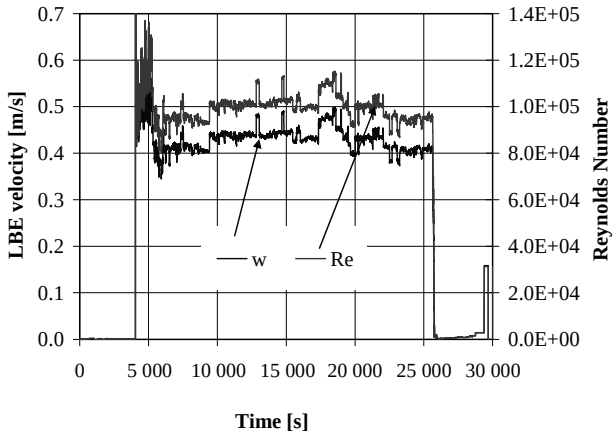

Figure 13: Cladding temperature trend upstream and downstream the spacer grid (GEC)

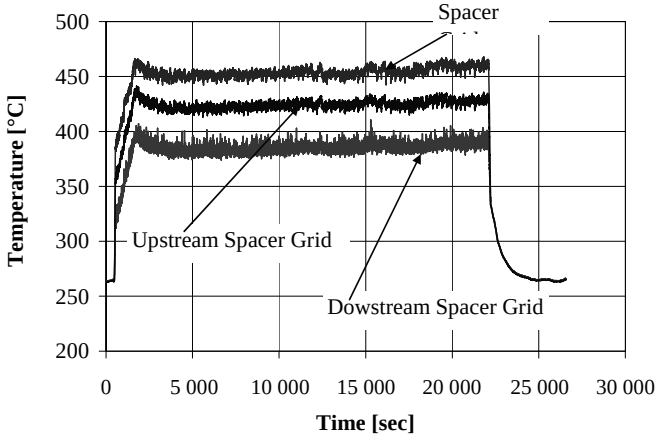

For the gas lift tests, the maximum temperature on the pin is close to 450°C, highlighting that the heat transfer coefficient between the liquid metal and the pin is really increased if compared with the natural circulation tests.

Figure 13 depicts the cladding temperature trend upstream and downstream the spacer grid, compared with the trend obtained on the matching surface. Also for this test the hot spot factor clearly appears, and also in this case the temperature below the spacer grid is higher by about 25°C than the upstream temperature. So, for the experimental test carried out on the NACIE loop, the magnitude of the hot spot factor seems quite independent from the turbulence and liquid metal velocity, at least in the investigated range.

Conclusions

The Integral Circulation Experiment (ICE) will be carried out to reproduce the thermal-hydraulic behaviour of an ETD pool nuclear reactor, adopting LBE as working fluid. In order to achieve the above-mentioned goal, the ICE test section has been designed to be similar to a HLM primary system. In this aim, the ICE test section, to be placed inside the CIRCE multi-purpose facility, couples an appropriate heat source with a heat exchanger.

The heat source was designed to have high thermal performance, similar to that expected for an ADS systems. In particular, the envisaged thermal power is 800 kW, the fuel power density is 500 W/cm^3 and the pin heat flux is 1 MW/m^2; all these values are typical of HLM fast reactors.

The reference heat sink designed for the ICE test section is a prototypical LBE low pressure boiling water heat exchanger made of two walls of bayonet tubes.

Thanks to the above-mentioned features, the experiment will allow for an in-depth investigation of the thermal-hydraulic behaviour of an HLM pool system. By the data to be collected by the ICE activity it will possible to obtain the knowledge necessary to understand the thermal-hydraulics behaviour of an HLM pool system. The ICE activity will contribute to the demonstration of the HLM pool-type nuclear reactor feasibility.

The NACIE loop was also designed and built to support the ICE test section design. In fact, due to the high thermal performance required for the ICE heat source, prototypical pin elements have been realised. The aim of the NACIE loop is to house a high flux bundle, made by prototypical pins and to test and qualify the elements before the installation in the ICE bundle.

The tests were successfully run, both under natural then gas-enhanced circulation, showing that the prototypical pins adopted for the ICE bundle match the needs required for the ICE activity.

References

[1] Turroni, P., *et al.*, "The CIRCE Facility", *Nuclear Application in the New Millennium (AccApp'01 and ADTTA'01)*, Reno, Nevada, USA, 11-15 November (2001).

[2] Benamati, G., *et al.*, "Natural Circulation in a Liquid Metal One-dimensional Loop", *Journal of Nuclear Materials*, 376, 409-414 (2008).

[3] Barbensi, A., G. Corsini, *Specification for the EFIT Primary System*, Deliverable D.1.4, DM1 DESIGN, IP-EUROTRANS (2006).

[4] Giraud, B., *Review and Justification of the Main Design Options of XT-ADS*, Deliverable D.1.5, DM1 DESIGN, IP-EUROTRANS (2006).

[5] Artioli, C., *Specification for the EFIT Core and Fuel Element Design*, Deliverable D.1.6, DM1 DESIGN, IP-EUROTRANS (2006).

[6] Van den Eynde, G., *Specification for the XT-ADS Core and Fuel Element Design*, Deliverable D.1.7, DM1 DESIGN, IP-EUROTRANS (2007).

[7] Mansani, L., *Candidate Materials for XT-ADS and EFIT, Operating Conditions and Testing Requirements*, Deliverable D.4.1, DM4 DEMETRA, IP-EUROTRANS (2005).

[8] Benamati, G., *et al.*, "Experimental Study on Gas-injection Enhanced Circulation Performed with the CIRCE Facility", *Nuclear Engineering and Design*, Vol. 237, pp. 768-777, Issue 7 (2007).

[9] Ambrosini, W., *et al.*, "Experimental Study on Combined Natural and Gas-injection Enhanced Circulation", *Nuclear Engineering and Design*, Vol. 235, pp. 1179-1188, Issue 10-12 (2005).

[10] Benamati, G., *et al.*, "Experimental Study on Gas-injection Enhanced Circulation Performed with the CIRCE Facility", *Nuclear Engineering and Design*, Vol. 237, pp. 768-777, Issue 7 (2007).

[11] Tarantino, M., *Gas Enhanced Circulation Experiments on Heavy Liquid Metal System*, Report ENEA HS-F-R-001 (2007).

[12] Tarantino, M., *et al.*, "Heavy Liquid Metal Natural Circulation in a One-dimensional Loop", *17th Int. Conf. on Nuclear Engineering (ICONE 17)*, Brussels, Belgium, 12-16 July (2009).

The GUINEVERE experiments at the VENUS facility: Status and perspectives

Luigi Mercatali[1], **Peter Baeten**[2], **Anatoly Kochetkov**[2], **Wim Uyttenhove**[2], **Guido Vittiglio**[2]
[1]Karlsruhe Institute of Technology (KIT), Karlsruhe, Germany; [2]Studiecentrum voor Kernenergie•Centre d'Étude de l'Énergie Nucléaire (SCK•CEN), Mol, Belgium

Abstract

Within the framework of the ECATS (Experimental Activities on the Coupling of an Accelerator, a Spallation Target and a Subcritical Blanket) research domain of the IP-EUROTRANS programme, the GUINEVERE (Generation of Uninterrupted Intense Neutron Pulses at the Lead Venus Reactor) project was launched in 2006 with the purpose to perform a series of experiments in order to implement together the individual techniques for the subcriticality monitoring already tested during the MUSE programme and to provide an answer to the main R&D issues related to on-line reactivity monitoring, subcriticality determination and operational procedure of an accelerator-driven subcritical system (ADS). This mission will be accomplished by coupling a fast lead "simulated-cooled" reactor operated in subcritical conditions with a TiT target and the GENEPI-3C neutron generator, this being an updated version of the GENEPI-2 generator previously used for the MUSE programme. The new facility hosting the GUINEVERE experiments, designated as VENUS-F, is located at the VENUS light water moderated critical facility at the SCK•CEN site of Mol (Belgium) and an overview of its features is given in the paper. The VENUS-F core has been designed starting from a critical reference configuration which will be turned into a subcritical core by replacing the four central fuel assemblies with a lead buffer, a channel for the beam line and a target. The definition of the core has been strongly influenced by a number of constraints that were needed to be taken into account in order to properly conjugate the technical feasibility of the facility with the necessity to comply with the envisioned experimental programme and its associated scientific outcome. A summary of the design study for the VENUS-F core is given in the paper and the critical core configuration to be used as reference for absolute reactivity measurements is presented along with its associated reactor physics parameters. The GUINEVERE facility must satisfy the nuclear safety criteria required by the Belgian safety authorities to be licensed, and in the paper an overview of the safety analysis performed with regard to the core physics, thermal assessment and shielding issues is also provided. Finally a summary of the envisioned experimental activities to be performed in the GUINEVERE facility is also given.

Introduction

Within the framework of the IP-EUROTRANS programme [1], the GUINEVERE (Generation of Uninterrupted Intense Neutrons Pulses at the Lead Venus Reactor) project [2] was launched in 2006 with the main objective to perform source driven subcritical experiments, implementing together the individual techniques for the subcriticality monitoring already tested during the MUSE programme [3]. This mission will be accomplished by coupling a fast lead "simulated-cooled" subcritical reactor with the GENEPI-3C neutron generator. The new GENEPI-3C neutron source [4], developed at the CNRS site of Grenoble (France), is the third of a series of machines designed for reactor physics purposes. It consists of a 250 KeV deuteron accelerator producing neutrons by the $D(d,n)^3He$ or $D(t,d)^4He$ nuclear fusion reactions in a target. The accelerator will be able to operate both in the continuous and pulsed mode, as needed to fully validate the different techniques for reactivity monitoring. The specifications of the two operational modes are summarised in Table 1. The new facility hosting the GUINEVERE experiments, henceforth referred to as VENUS-F, will be located at the VENUS light water moderated research reactor at the SCK•CEN site of Mol (Belgium), which needed to be modified in order to accommodate a completely different and new type of core.

Table 1: The GENEPI-3C specifications

Parameter	Pulsed mode	Continuous mode
Energy	140-240 keV	140-240 keV
Mean current	40 mA	160 μA-1 mA
Beam trip rate	10-4 700 Hz	0.1-100 Hz
Beam trip duration	–	20 μs-10 ms
Pulse FWHM	700 ns	–
Transition time (on/off)	–	1 μs
Pulse (current) stability	1%	1%
Beam spot size	20 mm	20-40 mm
Source intensity	8×10^9 n/s	5×10^{10} n/s

The VENUS reactor

The VENUS reactor, built in 1963, is a water-moderated zero-power critical facility. The criticality is reached by increasing the water level in the core and the reactor is shutdown by a fast water dump system. In case of an emergency stop (scram) the water can be evacuated in a very short time by opening the safety valves to the so-called dump tanks. The execution of the GUINEVERE project implies two major types of modifications in the existing VENUS reactor. First of all, the ones connected to the installation of the new GENEPI-3C accelerator and its coupling to the core. Secondly, the modifications linked with the adaptation of the VENUS critical facility to host a fast lead core. The vertical penetration of the beam line is preferred because it enables a perfect radial symmetry and simplifies the fuel loading procedures. As a consequence, a new accelerator room on the top of the core needs to be designed. A schematic view of the modified VENUS facility is shown in Figure 1. Two main modifications are needed to convert the water-moderated thermal reactor into a fast lead reactor:

- the installation of a shutdown system based on shutdown rods suspended by electromagnets;
- the construction of specific fuel assemblies (FA) with lead blocks and uranium fuel for the core and large lead blocks for the reflector.

Figure 1: Cross-section of the modified VENUS facility

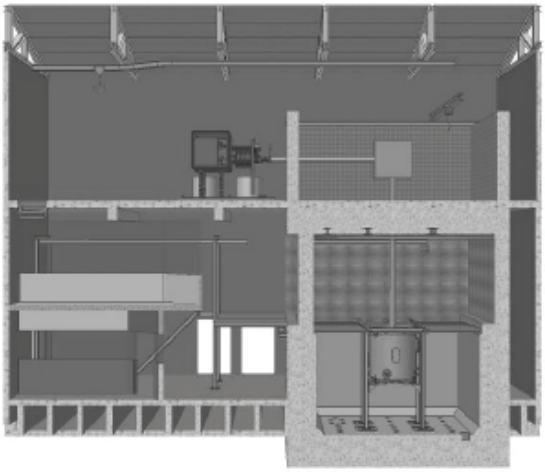

The VENUS-F core design

In order to properly accomplish the validation of the various methodologies for the subcriticality measurements during the GUINEVERE programme, the strategy is to start with a reference experimental phase with a critical core configuration, referred to as CR0. The measurements performed in such a configuration are of major interest since they will give the reactivity scale for all the reactivity measurements performed in subcritical conditions. Therefore, the design of the VENUS-F critical configuration has been the priority task of the design phase. Starting from CR0, the subsequent subcritical states will be obtained by the removal of a number of FA. From the very beginning the design of the VENUS-F core was influenced by several required specifications and technical constraints, as follows:

- The core is a fast lead one with a fuel zone surrounded by a lead radial reflector arranged within the VENUS vessel (160 cm in diameter).
- The fuel subassemblies (FA) are composed of a fuel part surrounded by two lead axial reflectors.
- The fissile material (provided by CEA) is metallic uranium 30% enriched. Bars of cylindrical shape are ½ inch in diameter and 8 inches in length and are covered with a nickel deposit of about 70 μm in thickness.
- The amount of fuel is limited (~1 200 kg.)

An additional feature to be taken into account in the core design was the necessity to arrange fuel and lead rods in a symmetric pattern in order to avoid loading errors and any orientation constraint. Also, the reactivity worth of the peripheral FA should be limited to less than 0.5$. Based on these initial specifications, several basic fuel lattices were analysed with the global objective to obtain a core as large as possible. These parametric studies converged into the so called "5 × 5 with lead plates" pattern with 9 fuel stacks and 16 lead stacks. The VENUS-F standard FA is shown in Figure 2. It consists of the fuel part, an upper stainless steel block and a lead top reflector. Each element has a height of 60.96 cm and a square section width of 1.27 cm. The 5 × 5 sub-lattice structure is cladded by four AISI 304 stainless steel slabs and then surrounded by four lead slabs 0.525 cm thick. Each fuel stack comprises three cylindrical fuel rodlets of 1.27 cm diameter and 20.32 cm height. Each lead stack comprises six cylindrical lead rodlets of 1.27 cm diameter and 10.16 cm height.

Figure 2: VENUS-F fuel assembly

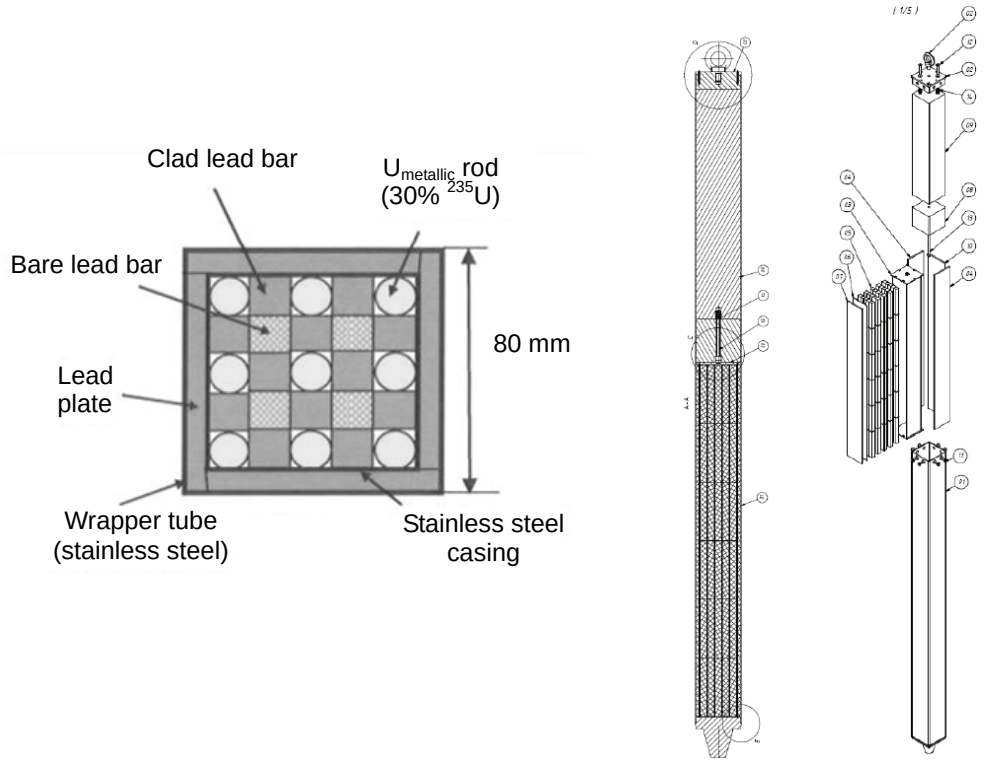

During the first phase of the CR0 design the possibility was studied to insert a lead buffer surrounding the target region in order to soften the 14 MeV source neutrons. Although the study demonstrated that a thickness of more than 25 cm was necessary to slow down 95% of the neutrons provided by the generator, the principle to set up such a device was nevertheless kept in order to let some space free for the crossing of the neutron generator thimble. Two solutions were envisaged: *i)* a large buffer zone corresponding to the volume of nine central FA, *ii)* a smaller buffer zone obtained by removing only four FA. In both the cases calculations showed that it would be difficult to reach the criticality taking into account the limited amount of fuel available. It was demonstrated to be feasible only when using, as a complement, FA with higher fuel content (13 fuel stacks and 12 lead stacks). This solution was also considered unsatisfactory, however. As a result it was decided to design at first a "clean" critical core for the assessment of the reactivity scale and to remove in a second step the four central FA to set up the buffer and the beam tube. This arrangement will correspond to the so-called SC1 configuration (k_{eff} ~ 0.97).

As far as the neutronic control of the core, at first the absorber rods were supposed to be made of a natural boron carbide block (B_4C), 7 cm in diameter and 60.96 cm long. Furthermore, a maximum of eight absorber rods were considered, corresponding to the number of control rod mechanisms actually available at the VENUS facility. Preliminary calculations showed that the critical configuration minimised the efficiency of the absorber rods compared to the configurations with the central channel. Because of this reason the study was then conservatively performed on the critical configuration. Since the aim was to design the core as "clean" as possible, several possibilities were envisaged to locate the absorber rods in the radial reflector at the periphery of the fuel zone. The results showed that the total reactivity worth of the absorber rods placed in such a region ranged from 4.9$ to 6.9$. These values were considered too small. Consequently the possibility to use enriched boron carbide as an absorbing material was investigated. Even if this solution were found to widely improve the results, two major stumbling blocks were pointed out: the core reactivity with all rods up was reduced and the manufacturing costs of such

absorber rods would increase. The remaining way to increase the absorbing efficiency was then to place them inside the fissile zone. In this case the negative effect produced by the removal of the fuel part from the core and the insertion of the B_4C into the core was found to vary from 8.5$ up to around 19$, depending on the locations of the rods. In the final design of the VENUS-F core a total of height absorber rods for the safety of the reactor are envisioned: two control rods (CR) and six safety rods (SR). The CR are void followed and consist of an absorber part sliding inside a wrapper tube. They are normally placed in the reflector part of the core at the periphery of the fuel zone. The SR consist of a lower part with fuel and an upper part with B_4C neutron absorber, separated by a stainless steel (AISI 304) block. During normal operation, the fuel part of the rod is inserted inside the core lattice. When the upper part drives into the core, the fuel part is rejected towards holes in the lower reflector. As a consequence, the insertion of the SR induces a double anti-reactivity effect. While the CR can be moved through the lattice, the position of the six SR is frozen. Every FA rests on a square section stainless steel grid able to host 12×12 FA and lead reflector assemblies, which are built following the same principles as the FA. According to MCNP calculations [5] the critical state will be reached with 88 FA (82 FA + 6 SR). The main neutronic parameters of the VENUS-F critical core are summarised in Table 2. The horizontal cross-section of the VENUS-F CR0 configuration is shown in Figure 3.

Table 2: Main neutronic parameters of the VENUS-F CR0 configuration

Fuel volumic content	17%
Critical mass	88 FA
Spectrum hardness index	0.64
Peripheral FA reactivity worth	240 pcm
β_{eff}	740 pcm
Λ (prompt neutron generation time)	3.8×10^{-7} s
Safety rod reactivity worth	14$
Control rod reactivity worth	1.2$
Flux peaking factor [n/(cm².s)/W]	3.623×10^{7}
Power peaking factor	1.349

Figure 3: Horizontal cross-section of the VENUS-F core

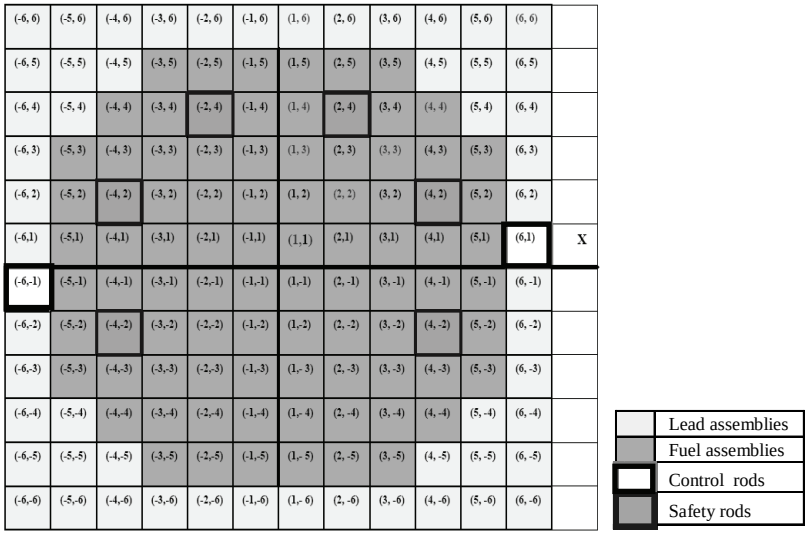

The GUINEVERE safety analysis

The VENUS-F facility must satisfy the nuclear safety criteria required by Belgian safety authorities to be licensed [5]. As a part of the safety-related studies and in order to have a better knowledge of the VENUS-F core neutronics, reactivity coefficients relative to an envelope of core configurations have been calculated and a conservative scenario of reactivity insertions has been assumed. The final goal is to prove the safe neutronics behaviour of the reactor. The results produced by means of MCNP calculations and relative to the CR0 configuration are summarised in Table 3. They show that only the complete flooding of the core without integrity of the FA cannot be compensated by the reactivity worth of the SR. However, measures have been taken in the design of the FA that should exclude water ingress and the tests performed have confirmed the effectiveness of such a design.

Table 3: Reactivity effects in the CR0 configuration

Safety rods worth [pcm]:	*10 270 ± 40*
Control rods worth [pcm]:	*794 ± 40*
REACTIVITY EVENT	$\Delta\rho = \rho - \rho_{ref}$ [pcm]
Void coefficient:	
without fuel fusion	-12 214 ± 39
with fuel fusion	-11 045 ± 39
Partial voiding	-63 ± 41
Fuel fusion coefficient without voiding	1 635 ± 41
Coolant insertion in the central hole	-1 268 ± 39
Presence of persons:	278 ± 42
Flooding of the reactor:	
with assembly integrity	4 220 ± 42
without assembly integrity	11 197 ± 42
Loading errors	1 653 ± 42

The Doppler coefficient (both fuel and total) has also been evaluated and was found to be negative as shown in Figure 4.

Figure 4: Total Doppler coefficient

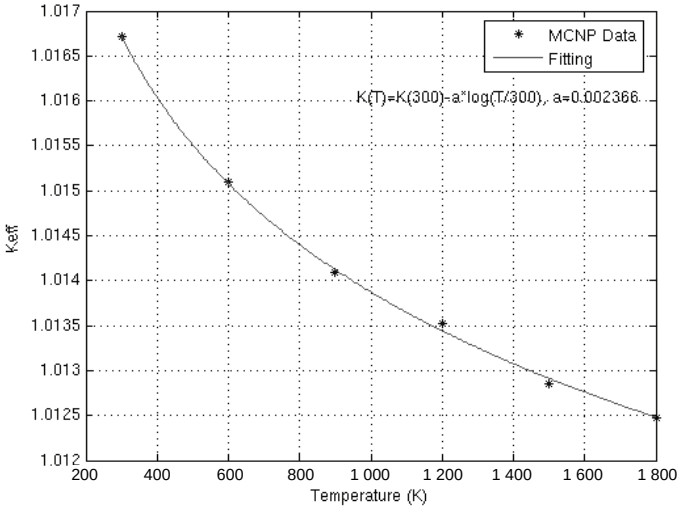

One of the main safety-related issues for the licensing of the VENUS-F facility was the assessment of the radiological impact of the modification of the VENUS facility into VENUS-F. For this purpose shielding studies have been performed with the final goal to provide the complete neutron and photon dose mapping of the entire GUINEVERE building [6]. The MCNP model of this building is shown in Figure 5.

Figure 5: MCNP model of the GUINEVERE building

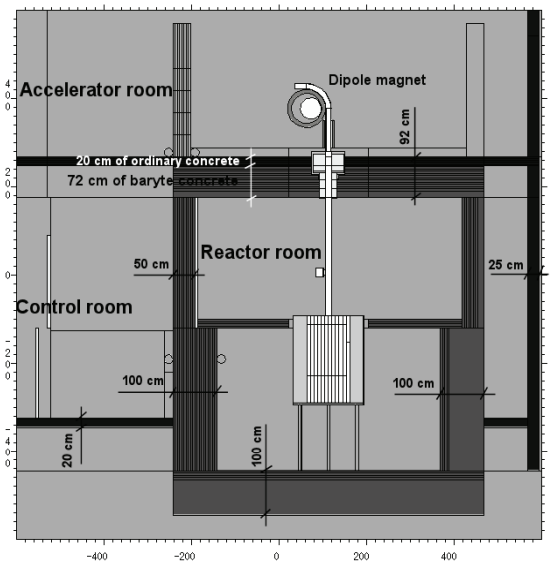

The core is shielded by means of different thicknesses of ordinary and barite concrete. The main difference with respect to the VENUS-thermal is the substitution of the upper protection of the casemate (12 cm of barite concrete followed by 24 cm of paraffin) with 72 cm of barite concrete followed by 20 cm of ordinary concrete. The beam line is modelled as a cylinder (14.9 cm in diameter). At the level of the control room the neutron dose rate in VENUS-F was found to be about half of that estimated for VENUS-thermal. This can be explained by the absence of the axial reflector under the fuel in the VENUS-thermal configuration which implies a neutron flux axially leaking with a hard spectrum. Moreover in the case of VENUS-F the radial and axial lead reflectors contribute significantly to the degradation of the spectrum. As far as the gamma dose, while in the case of VENUS-F it is of the same order of magnitude of the neutron dose, in the VENUS-thermal it is only ~25% of the neutron dose. In conclusion, VENUS-thermal and VENUS-F are equivalent from the point of view of the total dose in the control room at the same power level. As far as the accelerator room, results show that the beam line increases the diffusion of the particles and the dose rate is maximum around the penetration of the beam with a peak value of 3.25 mSv/h at a power level of 500 W. Moving away from this point the dose rate rapidly decreases to 152 μSv/h. In any case, the doses in the accelerator room remain within acceptable values in the case of intrusion inside the room with the reactor in operation. The contribution to the total dose coming from the D-T and D-D reactions has also been evaluated. This was found to be negligible (several orders of magnitude lower) with respect to the contribution coming from the fission source. Thus, the shielding analysis has demonstrated that the modification of the VENUS-thermal into VENUS-F does not result in higher doses. As general criteria, one can consider the limit for the personal dose to be ~1 mSv/month.

A thermal analysis has also been performed, with the main objective to assess the temperature profiles in the reflector and in the core both in steady-state and transient conditions under the assumptions that the cooling is provided by the natural convection of the surrounding air. Results show that the maximum lead temperature never exceeds the lead

melting temperature (325.5°C) during all standard operating conditions. For a realistic weekly operational regime and a maximum subcritical (k_{eff} = 0.99) power of 64 W, the maximum lead temperature is about 35°C. For the maximum core power of 500 W (critical state) the lead temperature never exceeds 96°C. Even for 1 000 W the lead temperature rises to only 154°C. In steady-state conditions (i.e. continuous operation, 24 hours/day, sustained for a long period of time) the lead temperature would saturate at 55°C and 210°C at 64 W and 210 W respectively. However, such a regime will never be applied during the GUINEVERE experiments.

For licensing purposes, a study [7] was also conducted aiming to investigate the maximum reactivity that can be inserted in the reactor without causing any damage to the FA. As an accidental scenario of reactivity insertion it was considered a two-step event. The first step is a reactivity ramp consequent from a CR withdrawal. The power excursion resulting from this reactivity insertion is detected and when the reactor power reaches a threshold value of 1 000 W a signal is sent to the scram system to shut down the reactor and the effective SR insertion occurs with a delay of 125 milliseconds. During this delay the reactivity ramp is going on. The SR fall down by gravity and the inserted anti-reactivity evolves according to a law involving the SR position. The faster the reactivity is inserted, the sooner the power threshold for the scram signal is reached. Moreover, when the SR anti-reactivity is introduced, and power suddenly drops, temperatures will still rise until all the accumulated energy begins to be released (which will happen around the characteristic thermal time). Also the initial value of the core power (P_0) is a free parameter which heavily influences the results. Reactivity feedbacks have also been considered because of their role in the control of the system once prompt-criticality is reached. Figure 6 shows the iso-curves of fuel temperature as a function of the initial power and the reactivity insertion velocity. The red solid line is the temperature limit iso-curve corresponding to the lead melting point. Above it all the possible configuration states fulfil the melting point safety criteria during all the accidental situations.

Figure 6: Iso-curves for different reactivity insertion velocity limits in the VENUS-F facility

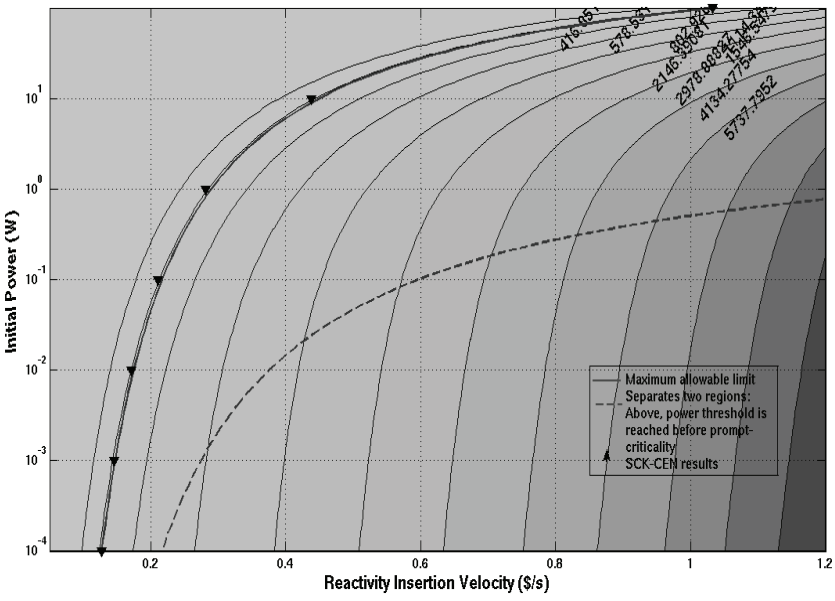

The calculations of the activity level for the materials involved in the GUINEVERE experiments at the end of an assumed realistic irradiation scenario have demonstrated that only the steel of the core vessel and its supporting structures will have to be managed as nuclear waste while all other materials can be treated as ordinary waste (i.e. can be released after a temporary storage). The fuel, provided by CEA, will be returned after completion of the project.

Summary and overview of the GUINEVERE experimental programme

Within the framework of the GUINEVERE project, the VENUS facility at the SCK•CEN site of Mol (Belgium) has been modified in order to be coupled with the GENEPI-3C deuteron accelerator and a TiT target. The VENUS-F reactor core has been designed starting from a critical reference configuration loaded with FA with lead and uranium rodlets, which will be turned into a subcritical core by replacing the four central FA with a lead buffer, a channel for the beam line and a target.

The GUINEVERE experimental programme will start in May 2010 and is expected to provide an answer to the main R&D issues related to the on-line reactivity monitoring, subcriticality determination and operational procedures of an ADS. Within the IP-EUROTRANS programme two different experimental core configurations will be analysed, namely CR0 (reference critical) and SC1 (k_{eff} ~ 0.97). A number of experiments are planned, as follows:

- CR0:
  - calibration of control rod worth by means of the stable period measurements;
  - axial traverses by ^{235}U, ^{237}Np and ^{238}U fission chambers in special channel of the experimental assembly;
  - radial traverses by ^{235}U and ^{238}U foils;
  - spectral indices F238/F235, C238/F235, F239/F235 by foil activation and fission chambers simultaneously;
  - rod-drop measurements to determine the subcritical reactivity scale for MSM method;
  - β_{eff} measurements by Rossi-α technique.
- SC:
  - reactivity calibration by PNS area method;
  - on-line reactivity monitoring by current-to-flux measurement:
    - static measurements (current variation, reactivity variation, combination of both);
    - kinetic measurements (current variation, reactivity variation, combination of both);
  - interim cross-checking techniques at beam interruptions (PNS fitting techniques of the prompt decay part and source jerk technique).

In the near future, other configurations with different levels of subcriticality representative of ADS operational conditions (k_{eff} ~ 0.95, k_{eff} ~ 0.99, k_{eff} ~ 0.85) will also be considered. Moreover, in the coming years, VENUS-F will serve as a unique facility in support to R&D activities related to lead-cooled Gen-IV fast reactors.

Acknowledgements

This work was partially supported by the 6th Framework Programme of the European Commission through the EUROTRANS Integrated Project under contract No. F16W-CT-2005-516520.

References

[1] Integrated Project on European Research Program for the Transmutation of High Level Nuclear Waste in an Accelerator Driven Systems (IP-EUROTRANS), Contract No. F16W-CT-2005-516520, *http://nuklear-server.ka.fzk.de/Eurotrans/Start.html*.

[2] Aït Abderrahim, H., *et al.*, "The GUINEVERE Project at the VENUS Facility", *Proceedings of the 5th International Workshop on the Utilisation and Reliability of High Power Proton Accelerators*, Mol, Belgium, May 2007, OECD/NEA, Paris (2008).

[3] Soule, R. *et al.*, "Neutronic Studies in Support of Accelerator-driven Systems: The MUSE Experiments in the MASURCA Facility", *Nucl. Sci. Eng.*, 148, 124-152 (2004).

[4] Baylac, M., *et al*, "The GENEPI-3C Accelerator for the GUINEVERE Project", *Proc. of the 8th Int. Topical Meeting on Nuclear Applications and Utilization of Accelerators/5th Annual Workshop on Accelerator-driven Subcritical Systems Experiments*, Pocatello, Idaho, USA, 30 July-2 August (2007).

[5] Mercatali, L., *et al.*, *Report on the GUINEVERE Safety Studies*, European Commission Report, IP-EUROTRANS Deliverable 2.13, May (2009).

[6] Serikov, A., *et al.*, "Radiation Shielding Analyses for the GUINEVERE Project", *Proceedings of the 11th International Conference on Radiation Shielding (ICRS-11)*, Callaway Gardens, Georgia, USA, April (2008).

[7] Lafuente, A., *et al.*, "Reactivity Accidents in the GUINEVERE Facility", *Proc. of the 10th Information Exchange Meeting on Fission Product P&T*, Mito, Japan, October (2008).

Experimental investigation of turbulent flow distribution in a hexagonal rod bundle for ADS prototype application

Th. Wetzel, K. Litfin, R. Stieglitz, A.G. Class, M. Daubner, F. Fellmoser, A. Batta
Karlsruhe Institute of Technology
Institute for Nuclear and Energy Technologies
Karlsruhe, Germany

Abstract

In the framework of accelerator-driven subcritical reactor systems (ADS), heavy liquid metals (HLM) like lead or lead-bismuth eutectic (LBE) are considered as coolant for the reactor core and the spallation target due to their efficient heat removal properties and high production rate of neutrons. The excellent heat conductivity of LBE flows expressed by a low molecular Prandtl number of the order 10^{-2} however leads to modelling problems of the turbulent heat transfer, because the scale of the thermal and viscous boundary layers separates both in the time and spatial domain. This effect cannot be treated adequately by commercially available fluid dynamic code systems. Therefore, a series of experiments has been launched at the KArlsruhe Liquid metal LAboratory (KALLA) aimed to quantify and separate the individual phenomena with the final goal to describe the momentum and the energy transfer in a liquid metal operated fuel assembly in a physical model.

Introduction

Liquid metals are often considered as coolant for an efficient heat removal of thermally high loaded surfaces. Due to their high thermal conductivity heavy liquid metals allow rather simple geometries of the heat transfer unit employed. However, the high conductivity leads to a violation of the analogy of turbulent heat and momentum transfer. The spatial extension of viscous and thermal boundary layer is different and the concept of a constant turbulent Prandtl number employed in most engineering turbulence models does not apply. While for momentum transport the turbulent contribution is dominant, the molecular contribution is of equal or even stronger importance for heat transfer. The common turbulence models in commercially available code packages (like k-ε model, Reynolds stress model, k-ω model) lead to considerable errors compared to the experimentally obtained temperatures.

Only detailed knowledge of the convective-diffusive heat transport phenomena in laminar and turbulent liquid metal flows enables an adequate design of heat transfer units near highly heat loaded surfaces such as nuclear fuel bundles. This problem is particularly prominent in the weakly turbulent Reynolds number regime, where buoyancy plays a non-negligible role. Moreover, in most technical applications the flows are thermally developing so that the heat exchange trough the boundary layer plays a significant role. Only the detailed knowledge of the momentum and energy transfer in the thermal boundary region allows the understanding of the discrepancies between computational results and the experimental observation. Therefore, a series of experiments has been initiated at the Karlsruhe Liquid Metal Laboratory (KALLA) of the Karlsruhe Institute of Technology (KIT). In order to quantify and separate the individual phenomena occurring in the momentum and the energy transfer domain of a fuel assembly the experimental programme is composed of three major experiments.

In a first step the convective turbulent heat transfer of a turbulent lead bismuth flow along a vertically arranged, uniformly heated rod placed concentrically in an annular cavity is investigated at high power densities. This essentially thermally developing flow is studied experimentally by means of thermocouples, a traversable combined velocity-temperature sensor based on a pitot tube as well as thermocouple (TC) rakes consisting of 60 TC. The attainable heat flux is 100 W/cm^2 in a Reynolds number range from $6{\cdot}10^4$ up to $6{\cdot}10^5$. The experimental data exhibit that commercial CFD codes describe the temperature distribution adequately if the flow is mainly driven by forced convection and a fine mesh resolution is chosen. If, however, significant density gradients occur, mixed convection sets in even at high Reynolds numbers and significantly larger Nusselt numbers than numerically predicted appear. This is accompanied by an altered turbulence structure in the thermal boundary layer.

In the second experiment an isothermal 19-pin hexagonal rod bundle assembly has been investigated in a turbulent water flow in a Reynolds number range from $5{\cdot}10^3$ up to $9{\cdot}10^4$ covering both the transitional and the fully turbulent flow regime. Both pin to pitch ratio of 1.4 as well as the axial dimensions correspond 1:1 to the dimensions of the XT-ADS accelerator-driven subcritical reactor system considered in the IP-EUROTRANS research programme. Because of the opaqueness of the liquid metal flow the rod bundle water experiment is inevitable to gain information about the flow distribution in the sub-channels by means of Laser Doppler Anemometry (LDA) and Ultrasonic Doppler Velocimetry (UDV) technique. Due to the flow interaction with walls and tubes a non-isotropic momentum field is present in the assembly, which yields an uneven flow rate in the individual ducts. The measurements of the static pressure loss of a single spacer and the complete test section show very good agreement of the loss coefficient with numerical predictions made by the sub-channel analysis code MATRA for the fully turbulent flow regime, whereas in the transitional flow regime with Reynolds numbers $< 3{\cdot}10^4$ the secondary flow leads to a rising loss coefficient.

The third experiment in KALLA corresponds geometrically 1:1 to the water experiment and is conducted in LBE using electrically heated pins. The heated length of this 19-pin hexagonal

rod bundle is 870 mm with a heat flux of 100 W/cm^2 producing a total heating power of up to 430 kW. The measurements cover a temperature range from 200-400°C and Reynolds numbers up to 10^5.

Single rod experiment

The single rod experiment is set up in the THESYS2 loop of KALLA as shown in Figure 1. It consists of an electrically heated cylindrical rod with a sharp tip placed vertically in a circular tube. It is moveable over a length of 870 mm, the heated section has a length of 860 mm.

The axial location of the rod is fixed by three spacers placed in equidistant positions of 370 mm. The lower two spacers contain three wings, the upper spacer is built of four wings that are equipped with about 60 calibrated thermocouples forming rakes that allow measuring the temperature distribution in the thermal boundary layer. The thermocouples have an outer diameter of 0.25 mm and are located 2 mm upstream the wing tip to minimise the heat transport through the wing distorting the temperature measurements. The wing tip thickness is 1 mm in flow facing direction and spreads up to 2 mm to house all the thermocouple wiring. It is polished to provide a hydraulically smooth surface. In the centre of the wing a tube ring is mounted 5 mm downstream to fix the rod position. At operating conditions of 300°C the mean gap between the rod and the tube ring is 0.15 mm. A flow straightener is installed upstream the test section containing wings to break secondary flows induced by the 90° bend. Subsequently a venturi tube is embedded to obtain a local velocity rise followed by a grid array of single tubes with a length of 100 mm and a diameter of 10 mm that are placed in the stream to ensure a homogenisation of the mean flow distribution at the test section inlet. The developing length of the tube flow is about 30 hydraulic diameters to obtain a hydrodynamically developed flow.

Figure 1: THESYS2 LBE loop (left) and detailed view of the test section set-up (right)

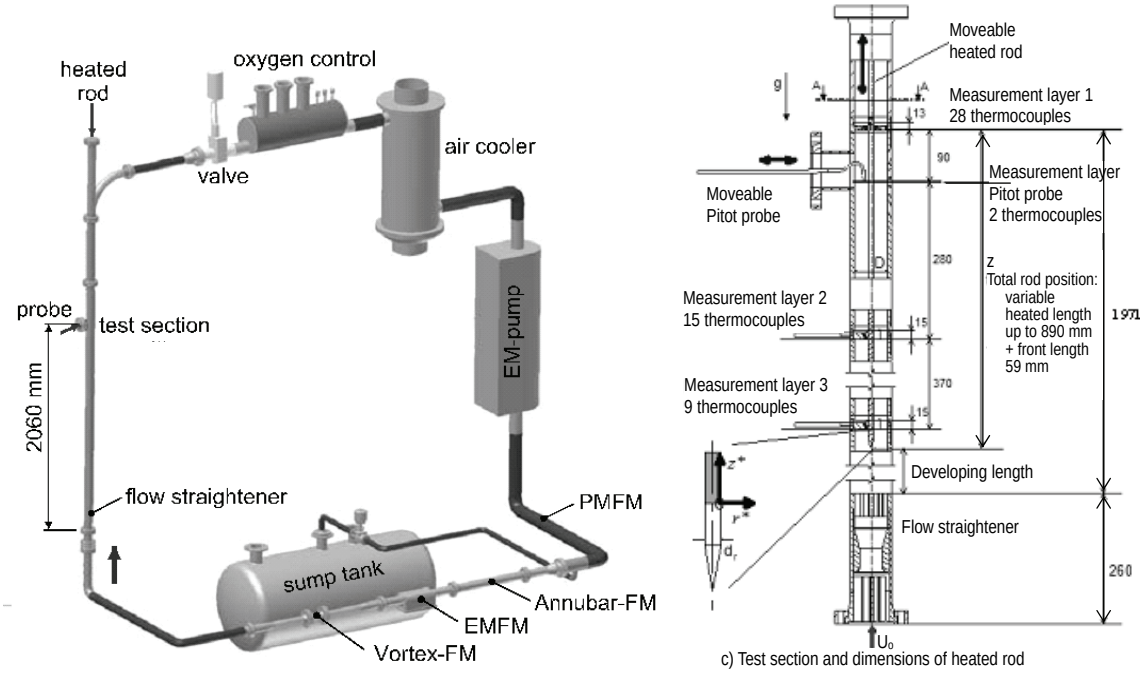

The figure also shows a moveable pitot tube with an orifice of 0.5 mm that is located between the second and third spacer. It is equipped with two thermocouples arranged 0.5 mm upstream the orifice to enable a simultaneous measurement of temperature and pressure. A thermal

isolation is wrapped around the test section set-up to minimise heat losses. The flow rate is measured by four physically different flow meters of the THESYS2 loop, an electro-magnetic frequency flow meter, a vortex flow meter, a pressure difference and a permanent magnet based velocity measurement. The accuracy of the flow rate meters is ±0.3% determined by additional heat balance calculations. The flow rate oscillation is of the same order of magnitude. The long-term loop temperature stability is better than ±0.1 K.

Numerical and experimental studies

The experiment is accompanied by several numerical studies. They all assume that the flow upstream of the heater is symmetrical. In some of the studies the spacer effect on the flow is neglected whereas in others the spacer effect is retained [1-4]. The different studies indicate that the flow in the measuring plain is only slightly affected by the spacer. For detailed results the reader might refer to the mentioned papers and the DEMETRA final report published by the European Union. Here only some exemplary results are given.

One quantitative comparison is given in Figure 2. It shows measured and computed temperature data in the measurement plane of the pitot tube as a function of the radius r^*. Two thermocouples are mounted on the pitot tube. $r^* = 0$ represents the pin wall. The presented experimental results at $r^* = 0$ are extrapolated from the measured values by a logarithmic fitting procedure assuming pure molecular heat conduction from the wall nearest thermocouple position towards the wall (conservative approach).

Figure 2: Measured and calculated temperature rise as a function of r* for similar heated distance preceding measuring position, z = 0.645 m, z* = 78.66

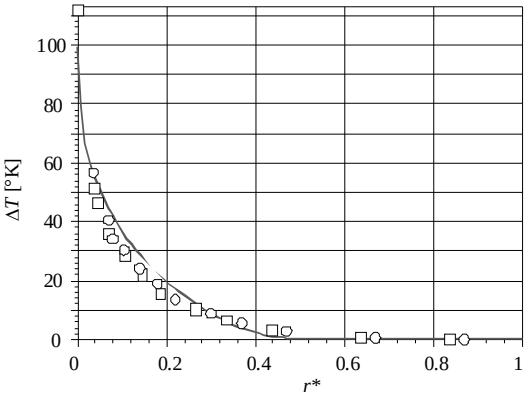

Figure 3: Measured and calculated temperature for different lateral angles

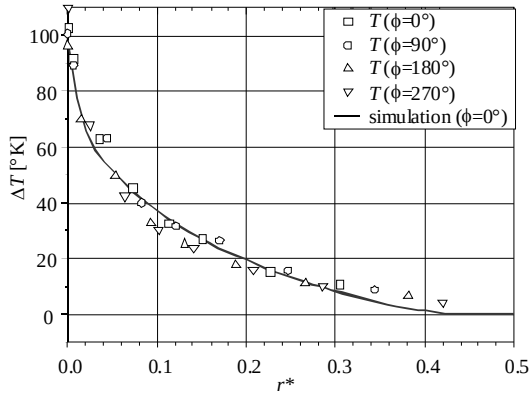

The comparison of the data in Figures 2 and 3 shows at a first glance a reasonably good coincidence between measurement and experiment. However, a closer view exhibits that the simulation slightly underpredicts the spanwise extension of the thermal boundary layer. This may be attributed to a weak buoyant effect at the measurement position. An analytical estimate of the buoyant velocity u_b based on the temperature rise near the wall compared to the mean velocity w_0 exhibits a ratio of approximately 0.04, which may partly explain the deviations. A more detailed physical evaluation of the vast experimental data obtained will be given in a subsequent paper. In Figure 3 the measured and simulated temperature data at the final downstream rake are shown as a function of r^* for different lateral angles (four wings, all equipped with thermocouples). Due to ideally symmetric assumed geometric set-up and the assumption of a uniform flow, similar temperature values are expected on the lines $\theta = 90°$ and 270°. However, different temperature readings are acquired, which can differ by 5-8 K. This may be attributed to a non-uniform spatial flow distribution at the inlet of the rod section, due to a remaining asymmetry of the elbow flow further upstream. We will discuss this in detail in the mentioned subsequent paper.

Water rod bundle experiment

The set-up of the water rod bundle is of hexagonal shape and contains 19 non-heated fuel pin simulators. It represents part of the fuel assembly proposed for the PDS-XADS (Preliminary Design Studies of an Experimental Accelerator-driven System) that contains 91 pins. The design parameters of the proposed PDS-XADS geometry together with the experimental set-up for both water and LBE rod bundle experiments are listed in Table 1. The design of the rod bundle test section is shown in Figure 4.

The entire fuel bundle simulator is composed of four modules flanged to each other and is fabricated from stainless steel. For the LDA measurements in the water experiment some parts of the test section are replaced by windows made of polymethylmethacrylate (PMMA). The sensor instrumentation for pressure and fluid velocity measurements of the water rod bundle experiment is also depicted in Figure 4. To ensure the comparability of both water and LBE rod bundle measurements, the geometrical design and material used are identical except for the windows made of polymethylmethacrylate (PMMA) that are required in the water experiment for the Laser Doppler Anemometry (LDA) measurements determining the velocity distribution. The water experiment is run isothermally and concentrates on the determination of local flow velocities, which are much more difficult to obtain in LBE, and pressure data. The Re-number is chosen similar to that of the later LBE-experiment by increasing the mass flow rate.

Table 1: Rod bundle and PDS-XADS design parameters

	PDS-XADS	Exp. H_2O	Exp. LBE
Geometry	Hexagonal	Hexagonal	Hexagonal
Total power	0.775 MW	–	0.43 MW
Fuel pins	90	19	19
Pin diameter	8.5 mm	8.2 mm	8.2 mm
Pitch	13.41 mm	11.48 mm	11.48 mm
Pin length	1 272 mm	1 272 mm	1 272 mm
Active height	870 mm	870 mm	870 mm
Grid spacer	3	3	3
Mean velocity	0.42 m/s	10 m/s	2 m/s
Mass flow	~41 kg/s	~13 kg/s	~26 kg/s
Sub-channel area	9 330 mm^2	1 260 mm^2	1 260 mm^2
Max. heat flux	150 W/cm^2	–	100 W/cm^2
Inlet temperature	~300°C	~25°C	~300°C
Outlet temperature	~400°C	~25°C	~415°C

Figure 4: Instrumentation of the water rod bundle test section

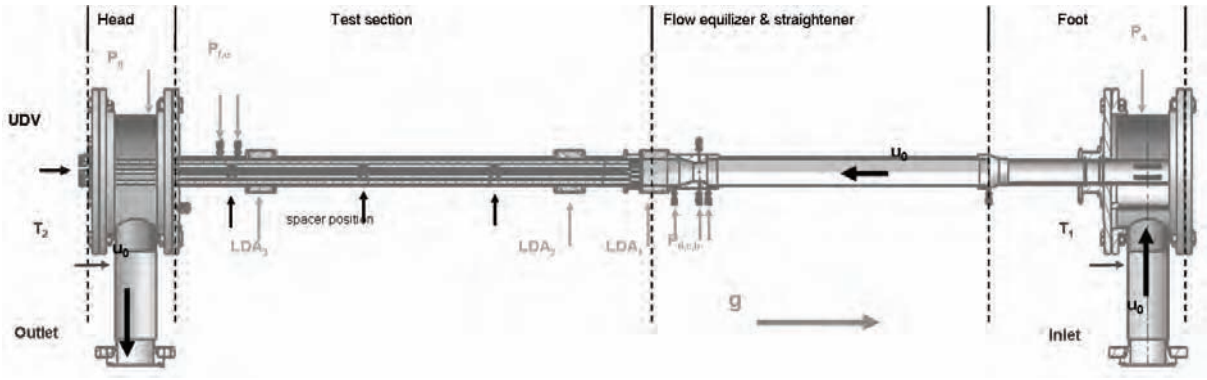

Measurements and comparison with numerical data

A crucial element of the rod bundle is the spacer which ensures at all operational conditions a constant P/D ratio and thus guarantees a defined neutronic and thermal-hydraulic performance of the reactor system. The spacer design is kept as close as possible to that originally developed in the context of the PDS-XADS and is shown in Figure 5.

Figure 5: Spacer used for the rod bundle experiments (left: picture, right: CFD mesh)

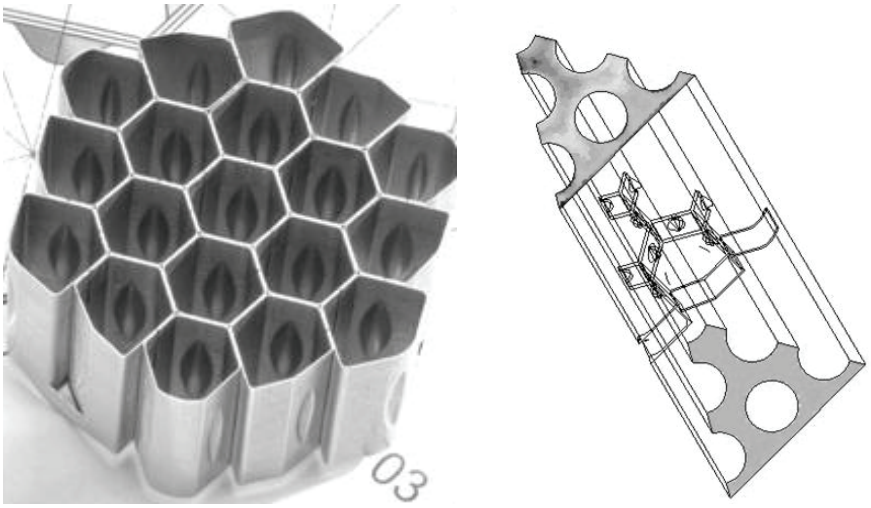

It is composed of a honeycomb structure requiring four different sub-channel types to fit into the hexagonal shape of the rod bundle cross-section. The rods are fixed by point contacts embossed in the honeycombs to compensate for the lateral and axial expansion of the rods. Moreover, the point contact reduces the extent of the hot spot. Optimisations regarding enhanced flow conditioning have not been evaluated as these are not regarded to be necessary for liquid metal flows. In contrast to the original design which suggests bending and welding of steel plates, the spacer fabrication employs selective laser melting. An additional surface treatment reduces surface roughness from 30 μm to 15 μm after polishing. This is of the same order as the laminar viscous sub-layer thickness in the liquid metal sub-channel flow. The material thickness is 0.5 mm in the inner structure and 0.25 mm at the outer sub-channels respectively. This leads to an average blockage ratio of 0.30 if the whole cross-section of the spacer including point contact structures is taken into account. The resulting loss coefficient can be determined with the Rehme-correlation [4] to $C_D = 0.65$, the pressure drop at maximum velocity of 10 m/s calculates to

0.38 bar using the sub-channel analysis code MATRA [5]. Further numerical calculations have been performed by using the commercial CFD code StarCD with a fully meshed spacer geometry using $1.2 \cdot 10^6$ cells and k-ε model calculating a pressure loss of 0.40 bar.

Pressure loss measurements in the water rod bundle experiment have been carried out at temperatures of 25°C and fluid flow rates from 0 m³/h up to 45 m³/h resulting in fluid velocities up to 5 m/s in the flow conditioning section and velocities up to 10 m/s in the rod bundle test section area. Differential pressure sensors have been used at positions P_a to P_g as described above. The loss coefficient was calculated for the rod bundle test section and the uppermost spacer using a hydraulic diameter for the rod bundle test section of $d_h = 7.58$ mm. This leads to Reynolds numbers up to 10^5 in the measured area. The results of the measured loss coefficients together with numerical calculations performed by MATRA for the spacer and the complete test section are shown in Figure 6.

Figure 6: Spacer pressure loss coefficient (left) and test section pressure loss coefficient (right)

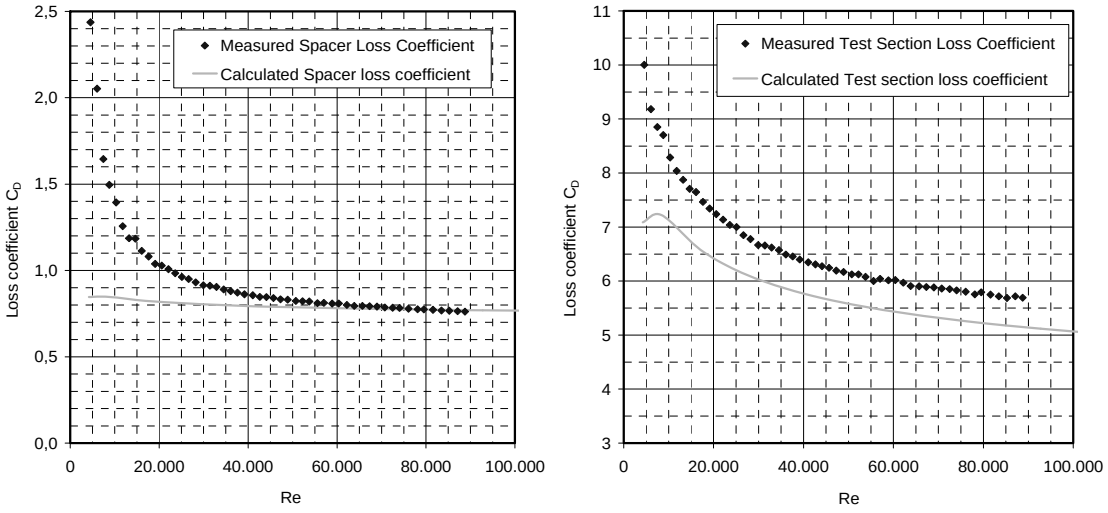

The measurement results show that the estimated pressure loss and thus the loss coefficient of the spacer for the calculated blockage ratio agrees almost perfectly with the measurements in the region with Reynolds numbers higher than $4 \cdot 10^4$ where the flow is fully turbulent. In the transitional flow regime with Reynolds numbers between $5 \cdot 10^3$ and $3.5 \cdot 10^4$ the influence of the secondary flow is relatively high and leads to a rising loss coefficient, not predicted by the MATRA code. The measured overall pressure loss at the velocity of 10 m/s is 0.37 bar and agrees very well with the pre-calculations shown before. For the complete rod bundle test section the numerically predicted pressure loss underestimates the measurements by approximately 10% leading to a slightly lower loss coefficient. In contrast to the spacer pre-calculations the variation also stays constant in the transitional flow regime for lower Reynolds numbers giving reasonable agreements down to Re = 10.000. One possible reason for the difference between measurement and calculation is the entrance guide at the beginning of the test section that has to be taken into account as an additional blockage for the sub-channel analysis. Another reason can be found in the flow separation at the upper vessel leading to additional momentum losses.

LBE rod bundle experiment

The LBE rod bundle experiment is set up in the THEADES (thermal-hydraulics and ADS design) loop of KALLA as shown in Figure 7. In these experiments the maximum flow rate of the loop is 47 m³/h with a pressure head of 5.9 bar. The total loop inventory is about 4 000 l. The loop is

Figure 7: THEADES LBE loop (left) and instrumentation of the LBE test section (right)

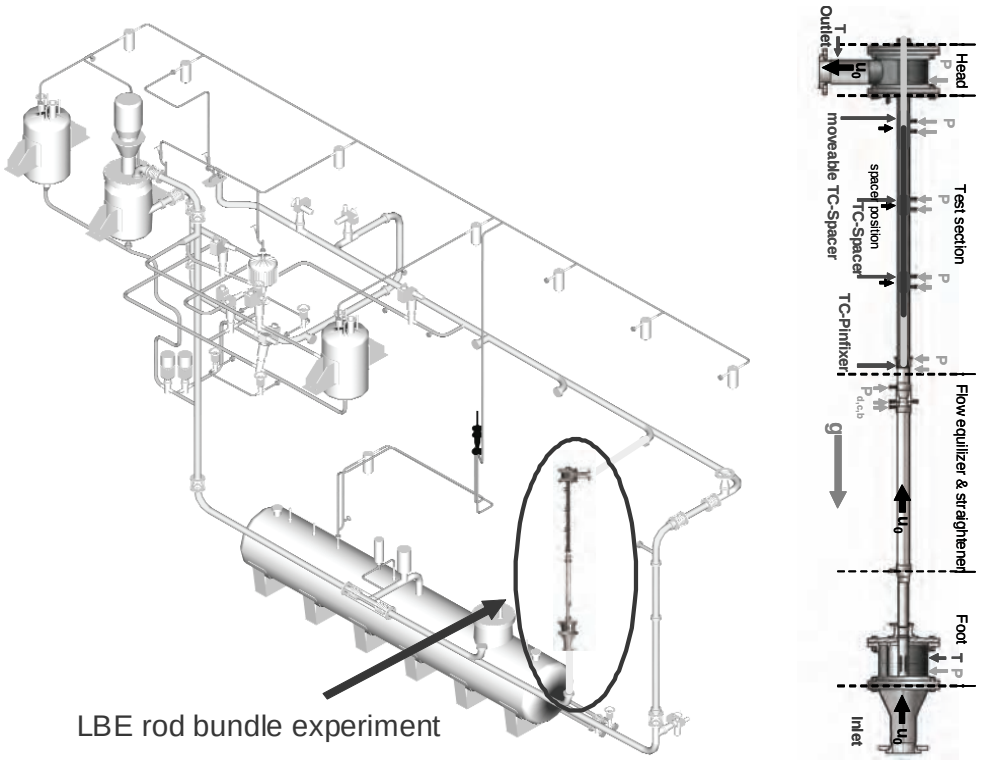

equipped with a heat exchanger to keep a constant fluid temperature and an oxygen control system. The flow rate is measured by two different commercial flow meters, a vortex flow meter and an annubar differential pressure flow meter. The hexagonal bundle contains 19 heated fuel pin simulators with a total heating power of 0.43 MW. The heating power is provided by a controlled DC power supply.

The design of the LBE rod bundle with the instrumentation is also shown in Figure 7. The entire fuel bundle simulator is composed of four modules welded and flanged to each other and is fabricated from stainless steel. The design is identical with the water rod bundle experiment with some exceptions. The inlet into the foot vessel is mounted at the bottom in order to mount the rod bundle experiment into the THEADES loop. As the fluid velocity in the foot vessel is very low the flow conditioning by the riser tube is not affected. There are no windows in the test section area, the used spacers are equipped with thermocouples with a moveable uppermost spacer to determine the axial temperature distribution at the end of the heated section of the rod bundle. Additional pressure sensor positions allow determining the pressure loss of each spacer individually.

Pressure loss measurements

Pressure loss measurements have been carried out at temperatures from 200°C to 350°C and fluid flow rates from 0 m³/h up to 12 m³/h resulting in fluid velocities up to 1.5 m/s in the flow conditioning section and velocities up to 2.6 m/s in the rod bundle test section area. Differential pressure sensors have been used for the measurement of the pressure loss of each spacer and the complete test section. The pressure losses vs. flow rate are shown in Figure 8.

At the nominal velocity of 2.0 m/s that corresponds to a flow rate of 9.1 m³/h and a temperature of 200°C the pressure loss for Spacers 2 and 3 is about 400 mbar. The sub-channel analysis code MATRA calculates a pressure loss of 370 mbar for the loss coefficient $C_D = 1.47$.

Figure 8: Measured pressure loss of the LBE rod bundle test section (left) and all three spacers (right) as a function of flow rate at temperatures of 200°C and 350°C

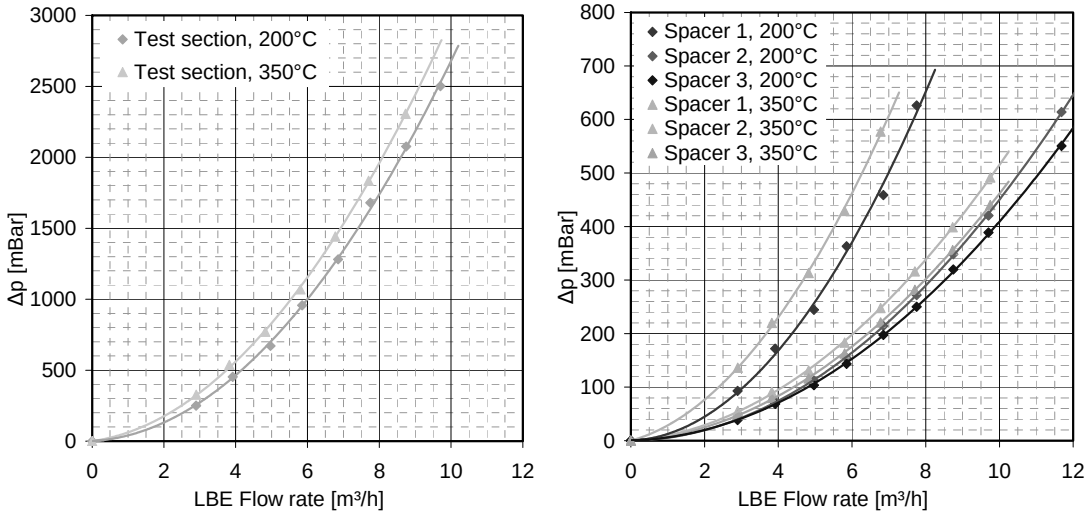

This is a very good agreement with the measurement. In contrast, the pressure loss of the first spacer is much higher than expected. This could be caused by oxide particles in the loop that cause an additional blockage on the first spacer. The loop will therefore be equipped with a filter for a next series of measurements. Besides, the expected pressure loss of the complete test section is significantly lower than expected from the results for a spacer loss coefficient of $C_D = 1.47$. These points have to be further investigated in future work.

Integral temperature measurements

Rod bundle temperature measurements have been carried out at temperatures of 200°C and 350°C and fluid flow rates from 0 m³/h up to 9.5 m³/h resulting in fluid velocities up to 2.1 m/s in the rod bundle test section area. This corresponds to Reynolds numbers up to $6.9 \cdot 10^4$ for 200°C and $9.7 \cdot 10^4$ for 350°C. In a first step only three rods were heated. The maximum heating power applied in this measurement was 30 kW resulting in a heat flux of 45 W/cm² on the surface of the heated rods. The temperature difference was measured by calibrated thermocouples at the foot and the outlet of the rod bundle and is depicted together with the expected temperature rise in Figure 9 as a function of the Reynolds number.

The measured temperature increase is in good agreement with the calculated temperatures using the LBE heat capacity of the OECD-NEA LBE Handbook [5]. The maximum deviation is less than 3.5% and can be explained by uncertainties in the flow rate measurement in the range of 3.5% on one hand and uncertainties in the temperature measurement of 0.1 K, i.e. 0.5% to 2.5% of the measured values on the other. The uncertainty in the electric power measurement is expected to be negligible compared to the uncertainties in flow rate and temperature measurements. This allows inferring that the temperature, flow rate and electric power measurement equipment have been set up with good precision. Further, repeated measurements show the reproducibility to be in the same range. The chosen measurement techniques allow precise determination of thermal-hydraulic characteristics of the rod bundle liquid metal heat transfer. The real deviations in the various quantities are obviously lower than the expected uncertainties. Compensation effects should not be dominant, as the temperature und flow rate deviations are not correlated. This proves that the used calibration methods for ΔT and flow rate are suitable. Detailed results of the local T measurements along with physical interpretation and heat transfer modelling will be presented in a series of subsequent papers.

Figure 9: Measured (points) and calculated (lines) temperature increase in the rod bundle experiment at 200°C and 350°C as a function of Re

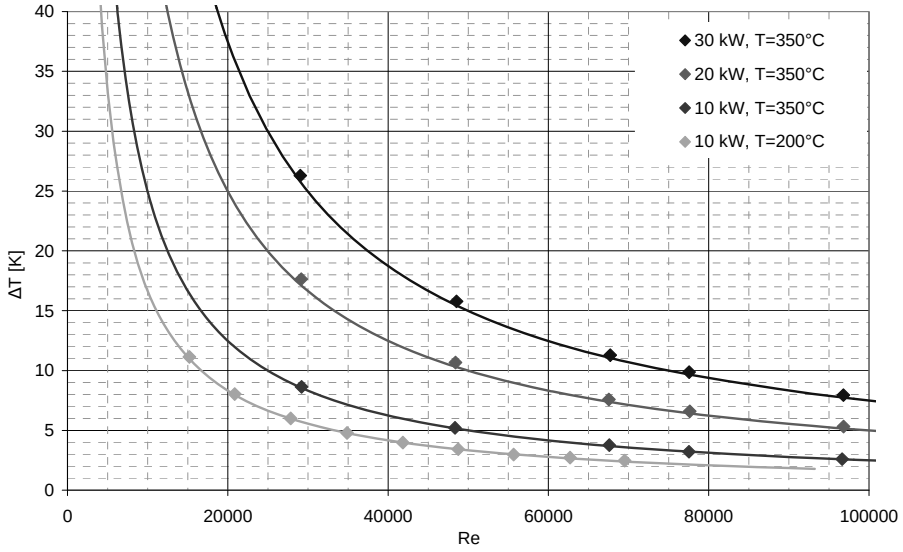

Conclusions

A series of three different experiments to examine the flow distribution and the turbulent heat transfer in a hexagonal rod bundle has been set up in the context of IP-EUROTRANS. In the single rod experiment a large influence of buoyancy on the velocity profile even at relatively high Reynolds numbers was found while the temperature field is less influenced. This yields an enhanced heat removal and suggests that currently used Nusselt correlations are rather conservative. The water rod bundle experiments show a very good agreement of the measured pressure loss with numerical prediction in the fully turbulent flow regime whereas in the transitional regime secondary flow seems to lead to a rising loss coefficient. The LBE rod bundle experiment is set up and first conducted experiments on pressure loss and integral heat transfer at flow velocities up to 2 m/s, inlet temperatures from 200°C up to 350°C and heating powers up to 30 kW have been performed.

Acknowledgements

The work is supported in the framework of the IP-EUROTRANS project; contract No. FI6W-CT-2004-516520.

References

[1] Batta, A., *et al.*, "Turbulent Liquid Metal Heat Transfer Along a Heated Rod in an Annular Cavity", *Proc. Jahrestagung Kerntechnik 2007*, Karlsruhe, Germany, 22-24 May (2007).

[2] Batta, A., *et al.*, "Numerical Study of Turbulent Heat Transfer Along a Heated Rod in an Annular Cavity", *Proc. Jahrestagung Kerntechnik 2008*, Hamburg, Germany, 27-29 May (2008).

[3] Batta, A., *et al.*, Numerical and Experimental Investigation on Turbulent Forced Convection Liquid Metal Heat Transfer Along a Heated Rod in Annular Cavity", *Proc. HeLiMeRT-2009 Part I*, Mol, Belgium, 20-22 April (2009).

[4] Batta, A., J. Zeininger, R. Stieglitz, Experimental and Numerical Investigation on Turbulent Liquid Metal Heat Transfer Along a Heated Rod in Annular Cavity", *Proc. ICAPP 2009*, Tokyo, Japan, 10-14 May (2009).

[5] Nuclear Energy Agency, *Handbook on Lead-bismuth Eutectic Alloy and Lead, Properties, Materials, Compatibility, Thermal-hydraulics and Technologies*, Chapter 2, OECD/NEA, Paris (2007).

A review of lead-bismuth alloy purification systems with regard to the latest results achieved on STELLA loop

François Beauchamp[1], **Olivier Morier**[2], **Laurent Brissonneau**[3], **Jean-Louis Courouau**[4], **Cyril Chabert**[3], **Françoise Reyne**[3]
[1]Commissariat à l'énergie atomique (CEA), DEN, DTN, STPA, Laboratoire de Traitement et d'Études des Risques Sodium, Saint-Paul-lez-Durance, France; [2]CEA, DEN, DTN, STPA, Laboratoire d'Instrumentation et d'Essais Technologiques, Saint-Paul-lez-Durance, France; [3]CEA, DEN, DTN, STPA, Laboratoire d'Études des Interactions et Procédés sur les Caloporteurs; Saint-Paul-lez-Durance, France; [4]CEA, DEN, DPC, SCCME, Laboratoire d'Étude de la Corrosion Aqueuse, Gif-sur-Yvette, France

Abstract

This paper presents the last STELLA loop operations and experiments related to the lead-bismuth eutectic (LBE) control of chemical conditions. Operating a system using LBE requires a control of the dissolved oxygen concentration to avoid plugging and corrosion of structural materials. Reliable devices are therefore needed to measure and adjust the oxygen concentration and to remove impurities during operation. One of the issues is the management of impurities (lead oxides and corrosion products) the presence of which in the liquid phase or in the aerosols is likely to impair the facility, instrumentation and mechanical devices. To avoid the long-term build-up of impurities, purification of LBE is required to keep the impurity inventories low by trapping oxide and metallic impurities in specific filter units. On the basis of impurities characterisation and experimental results gained through filtration tests in STELLA loop, this paper gives a description of the state-of-art knowledge of LBE purification with different filter media. It is now understood that the nature and behaviour of impurities formed in LBE will change according to the operating modes (initial start-up and filling, re-start or transient states, off-normal operating conditions, normal operations) as well as the method proposed for impurity removal. This review of knowledge gained from STELLA filtering test can serve to validate the basic filtration process, define the operating procedures and assess the perspectives for the design of purification units for long-term application in lead-alloy liquid metal coolant systems.

Introduction

The development of the heavy liquid metal chemistry control and monitoring is one of the issues that is critical for nuclear systems using lead alloys either as a spallation target or as a coolant [1]. ADS (EFIT and XT-ADS demonstrator project) and some of the future Gen-IV concepts (LFR or SFR) are foreseen to be cooled by lead or lead alloys. Indeed, the chemistry interacts with operating specifications of a nuclear system; the contamination control is necessary to ensure stable hydrodynamics and heat transfer during service life time. The aim is to avoid lead oxide clogging or even corrosion product plugging due to mass transfer in a non-isothermal system and then fouling from deposits that eventually reduce the heat transfer capacity, etc. These points were included in the framework of the DEMETRA studies (Development and Assessment of Structural Materials and Heavy Liquid Metal Technologies for Transmutation systems) of the EUROTRANS (European Research Programme for the Transmutation of High-level Nuclear Waste in Accelerator-driven Systems).

One of principal scopes of development or validation is the management of impurities (lead oxides and corrosion products), the presence of which in the liquid phase or in the aerosols is likely to impair the facility, instrumentation and mechanical devices. The main contamination sources (apart oxygen) are identified as the corrosion products (Fe mainly, Ni, Cr, etc.) expected to be generated continuously at a rate depending on the operating temperature, liquid metal flow rate, materials, etc. Contamination by impurities will occur mainly during start-up operation (first filling) or after maintenance or repair phases, and under normal operation of the system at a continuous but very low rate. However, some impurities such as iron potentially present long-term and cumulative effects. Pipe clogging due to corrosion products was experienced in several loops: hot or cold stop may lead to a rapid redistribution of the deposited impurities, within a few hours, eventually clogging the cold pipes.

One of the processes considered for purifying lead-bismuth eutectic (LBE) relies on filtration: surface filtration (cake on a support) or deep bed filtration (in the mass of the filter medium), to trap impurities [2]. The present study focuses on the results of impurities filtration tests and characterisations in liquid phase.

Impurities observed in LBE (during STELLA loop operation)

Some tests carried out in STELLA loop have contributed to characterise impurities in LBE, mainly their nature, composition and size. Depending on the level of the dissolved oxygen content in the liquid metal, impurities should be present either in the oxide or dissolved form. Moreover, insoluble metallic particles could be found [3]. Some impurities, such as iron, potentially present long-term and cumulative effects. Oxide particles in the LBE are of several types, detailed hereafter [2,4,5].

Particles of lead oxide could be formed when the oxygen concentration is higher than the oxygen solubility limit in the LBE. This phenomenon occurs during spurious air ingresses into the loop and during start-up after the loop has been opened for maintenance (oxygen residue on the filter, desorption of the metal walls). These lead oxides can also form in non-isothermal operating conditions upon contact with the cold spot in the loop where the oxygen saturation level in the LBE is reached. An excess of oxygen gives rise to precipitation of lead oxide on nucleation sites. These sites could be either localised on cold surfaces of the circuit, or on solid particles present in solution (heterogeneous crystallisation). Then, the particles of PbO increase their size by crystal growth (micrometer size), the mechanism of which could be counteracted by the presence of impure products in the liquid solution (mainly iron, giving rise to the formation of iron oxide on the surface of these particles).

Other impurities are assumed to be composed of fine dispersed particles of iron and chromium oxides which are coming from metallic impurities dissolved in the coolant by diffusion through the oxide coating of structural materials. These particles are colloids with nanometre size. Their mechanism of formation is based on nucleation and crystal growth: heterogeneous nucleation on cold section of the circuit which can later be driven to the liquid metal by erosion or homogeneous nucleation in the liquid metal bulk. Particles grains can grow up to 0.01-0.1 μm size. These aggregates structures, referred to as "slags" are present in the liquid metal volume, on the walls and in the aerosols. These slags are formed during normal operating conditions, mainly in stagnant areas by sedimentation-coagulation processes, or in systems favouring the adhesion of particles [6].

These different categories represent the main source of impurities in the loop, although there are no quantitative and on-line measurements of particle mass concentration and distribution. Such deposits have been found on metallic filters, in the test line and at the free surface of the STELLA testing tank. The chemical analyses of the so-called black powder showed that it was made up of a heterogeneous mixture of lead oxide, bismuth and corrosion products (oxides of the metal elements composing stainless steel: iron, chrome, nickel).

Description of STELLA facility and filter unit

STELLA loop (Figure 1) was used to assess the performance capacity of some media filters. Chemical analyses and characterisations of samples coming from filters or deposits were carried out at the metallographic laboratory [2]. STELLA is a dynamic test loop which contains about 330 kg of LBE. The maximum operating temperature can reach 550°C. The loop is fed by a blanket gas of argon mixture at a pressure below 100 mbar. The main loop equipment includes a storage tank containing a submerged rotor mechanical pump to fill and feed the testing tank and the test lines. Two test lines are positioned in parallel, each made up of three removable modules. The first test line was equipped with electrochemical oxygen sensors (removable) to measure the oxygen in the liquid metal. Filters to be tested were placed in the second test line with dedicated instrumentation to monitor the filtration tests. A differential pressure transmitter (MP1) monitored the change in the pressure loss over time, giving an indication of increasing

Figure 1: Flow sheet of STELLA loop

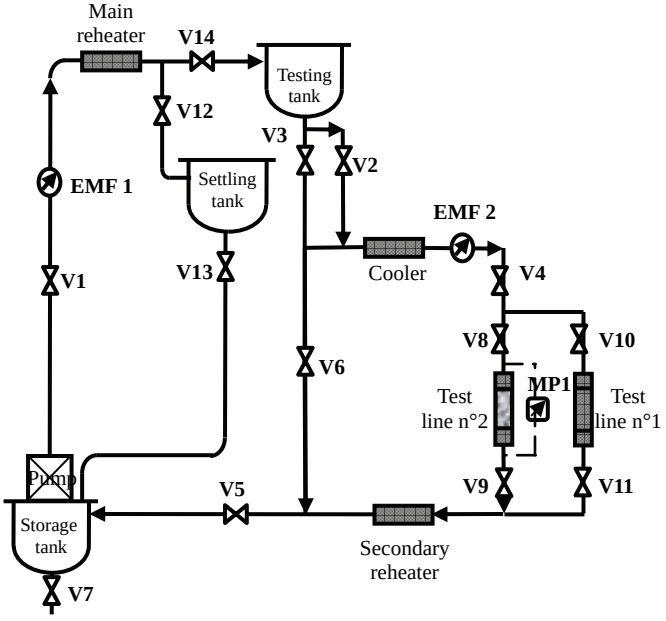

resistance related to the retention of particles in the filter. In order to measure the oxygen content dissolved in the lead-bismuth during a filtration cycle, an oxygen sensor (yttria-stabilised zirconia ceramic with internal Bi/Bi_2O_3 reference) was installed in the "downstream" module at the filtration outlet. Temperature measurements of the test line were ensured by thermocouples upon contact with the piping.

Design parameters and operating conditions (for the choice of media filters)

In principle, only the solid impurities, non-dissolved elements or oxide particles should be gathered in a line containing filtration capabilities. The filtration operation is typically a chemical engineering operation, difficult and complex to investigate in liquid metal. Its efficiency depends on numerous parameters, constants or variables during the operations [5].

Knowledge of impurities (nature, form and size, concentration and properties) in a LBE system is required for the design of a filtration process. Indeed, their behaviour influences the choice of the filtration method to trap impurities (surface filtration or deep bed filtration), the type of filter medium, the filter removal rate and the required level of filtering as well. The review of the literature for other liquid metals (Na, Pb-Li, Fe, Al), the achievement of preliminary experiments on the STELLA loop in 2005 and 2006 [7], as well as Russian feedback indicated that the filtering media used in deep bed filtration with a texture promoting coagulation-sedimentation and adhesion mechanisms were more promising to retain fine dispersed particles (size ≤ 1 μm) [6,8].

Liquid metal properties (viscosity, density, corrosion properties) and operating parameters (flow conditions, flow rate control range and temperature ranges, pressure, filter pressure drop monitoring) can affect the choice of the filter medium and the design of the filter unit. The flow rate through a filter medium affects the retention of colloidal particles and aggregates. Some manufacturers recommend not exceeding a filtration rate of around 2 cm/s for liquid metals. Otherwise, the filter housing must be properly implemented in the loop to avoid turbulence at the inlet of the filters created by elbows or valves. In STELLA loop, a horizontal portion of the circuit was selected for the filter housing location to avoid the return of impurities trapped by the filter to the liquid metal flow by hydrodynamic separation. Moreover, the implementation of the filter unit in the cold parts of the circuit must be preferred compared to hot zones to prevent dissolution of metal from structural wall and mass transfer to other cold surfaces of the system. The mode of operation (continuous or batch), the duration of the process and the regeneration process are other parameters to consider for the design of the filtration system. Analysis of these design parameters in the comparison of the possible filtering media depends mainly on technical characteristics data given by manufacturers (removal rate, holding capacity or the filter surface area, thermal and mechanical strength, maximum admissible pressure loss, initial clean pressure loss, filtering rate threshold regeneration ability, geometry) and filtration feedback in similar applications [4,5].

Russian LBE filtration processes studies [6] highlighted the use of materials based on deep bed trapping. Tests had been carried out on filter prototypes made of multi-layer silica grain-oriented glass fabric, needle-punched fabric of metal fibre filters and Al_2O_3 aluminium oxide bead filters. The most promising results were obtained with the glass fibre filters and the metal fibre filters with similar filtration efficiency twice as high as that with the aluminium oxide beads. However, the thermal resistance of glass fibre limits its use to temperatures under 400°C. The use of metal fibre filter prototypes for maximum temperatures of 550-600°C was recommended in the Russian studies. Experiments conducted by ENEA with multi-layer glass fibre tissues confirmed the selectivity towards PbO particles of this type of filter. In comparison with sintered metal filters, glass fibre filters seem to be more suitable for normal, continuous and long-term operations and large capacities [9].

The aim of the STELLA filtration test programme was to assess the suitability of applying commercialised filters to LBE purification. According to design parameters, three kinds of filters (Poral, PALL Dynalloy and PALL PMM filters) were selected by privileging media with appropriate removal ratings and specifications like high holding capacity or high filter area, low clean pressure drop, good mechanical strength for high operating pressures and temperatures.

Figure 2: Poral filter (left), Dynalloy filter (middle), PMM cartridge (right)

Poral filters (Figure 2) are made of a sintered stainless steel (316L) matrix and are generally more appropriate for cake filtration. These filters are known to have very good resistance to high temperatures and high flow rates. PALL Dynalloy mesh media filters (Figure 2) are specifically used for deep bed filtration. They are made of a uniform layer of woven stainless steel (316L) fibres. This layer is compacted and sintered to ensure good resistance and integrity. The porosity of this medium is high (~60%) which improves its hydraulic resistance and its retention capacity. These Dynalloy mesh medium filters have good mechanical resistance at high temperature – up to 477°C according to manufacturer data. A particular welding technique (steel/mesh sandwich weld method) has been developed to improve the thermal and hydraulic resistant of Dynalloy media filter prototypes. For PALL Standard PMM cartridges (Figure 2), the medium is a thin matrix of stainless steel (316L) powder within the pore of SS wire mesh. This produces a very strong porous material (no wire mesh shift, pore size integrity maintained). The maximum admissible temperature for use is 677°C.

Filtration tests results and metallographic analyses

The main results and operating conditions of STELLA filtration tests are summarised in Table 1 [4].

Table 1: Synthesis of results and operating conditions of LBE filtration tests

Type		Poral filter CL20	Poral filter CL10	Dynalloy filter 15CO	PMM 150 filter
Filter characteristics	Removal rates	35 μm	20 μm	10 μm	9 μm
Operating conditions	Temperature	400°C	400°C	400°C	400°C
	Flow rate range (m^3/h)	0.25/0.36	0.44/0.3	0.2/0.5	0.08
	Oxygen concentration	3.10^{-7} wt.%	–	–	$1.9.10^{-5}$ wt.% $1.9.10^{-7}$ wt.%
Filtration tests parameters	Average pressure drop rise	1.8/3.2 mbar/h	30 mbar/h	–	2.5 mbar/h
	Duration of the test	156 h	24 h	98 h	306 h
Impurities characterisation		Pb_7Bi_3-Bi with PbO-Bi micron-size agglomerated particles forming filaments containing iron, chromium oxides + In, Sn, Pb, Si			
Trapping method		Surface (inner layers into filters)			

Monitoring of the pressure drop values (Figure 3) showed a steady increase over time for the four filters tested. It suggests that impurities were gradually trapped. It could be assumed that the pressure drop continued to increase beyond the maximum value of the pressure transmitter measurement range (max. 1 040 mbar) and would have been rising up to a plateau. Only the

Figure 3: Filter tests, pressure drop versus time

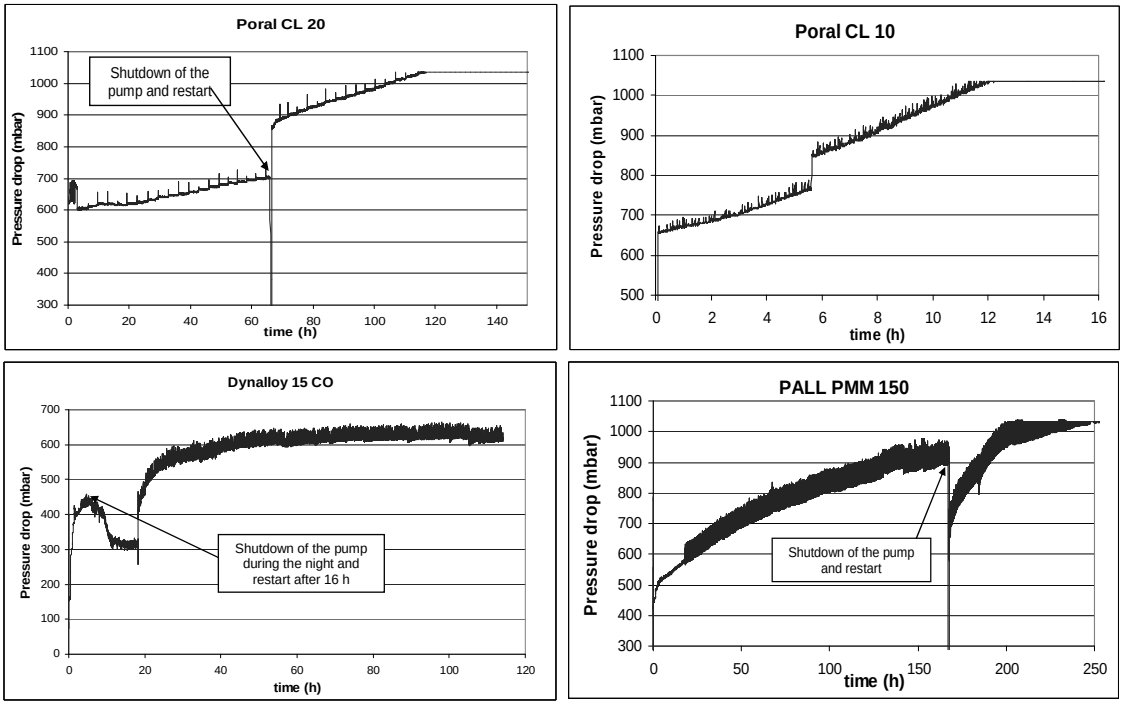

Dynalloy filter pressure drop monitoring reached this plateau (about 620 mbar) whereas other tests were stopped before reaching it. Many assumptions are possible to explain this plateau: hydraulic limit of the line, no more impurities in LBE to be trapped by the filter or as meshes structure of the filter had been locally distended, some particles trapped might have been released from the medium filter.

Visual observations of the two Poral filters (Figure 4) after tests did not show any visual structural or welding defects nor any distortion of the structural matrix nor heterogeneity of pores sizes of the filters. The two filters had grey deposits (optical microscopy) on their inner surface but almost nothing on outside surfaces. Thicknesses of the inner layers were not uniform: varying from 90 to 200 μm on the downstream part and from 200 to 0 μm on the upstream part of the CL10 filter, and up to 650 μm for CL20 filter, with a compact layer on the inner side (near the filter pores) of maximum 400 μm and a porous layer in the outer side (toward the centre of the filter) of 250 μm. Heterogeneous porosities were observed: generally very small in the vicinity of the media filter and much higher in the last 100 microns of deposits. Deposits were mainly composed of a biphasic mixture of Pb_7Bi_3-Bi with sometimes locally PbO-Bi. In general, PbO was easier to evidence by X-ray diffraction (XRD) than by Scanning Electron Microscopy (SEM). The

Figure 4: SEM observation of deposits on the inner surface of CL10 Poral filter

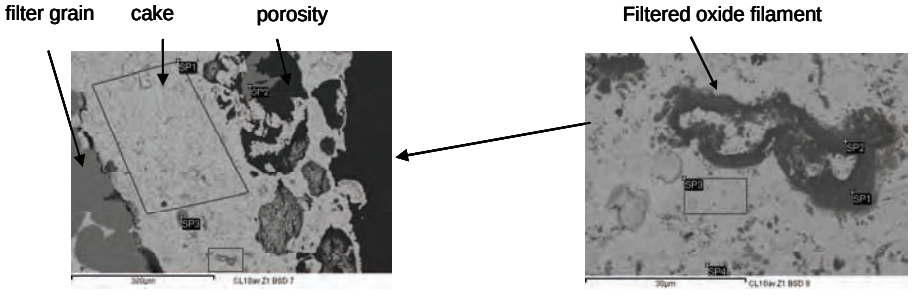

TECHNOLOGY AND COMPONENTS OF ACCELERATOR-DRIVEN SYSTEMS, ISBN 978-92-64-11727-3, © OECD 2011

deposits contain micron-size aggregated particles forming filaments (from 0.1 μm thick and 5 μm long up to 4 μm thick and to hundred microns long) or larger particles of 0.1 to 20 μm size. The filaments and particles are iron oxides or iron-chromium oxides in majority. The particles are mainly composed of iron oxide with a mixture of other elements such as lead, tin, nickel, aluminium, silica and indium. Particles of Pb, In and Sn oxides, or silica can be also found individually. The atomic ratios of metallic species from grey deposits were Cr: 1; Fe: 2-2.5; Pb: 7-8; Bi: 9-10.

For the two Poral filter grades, it was observed that the matrix of the medium filters was 80-90% full of LBE. It had been supposed that LBE (with higher ratio Pb/Bi) remained trapped in the medium filter after filtration operating and draining. Deposits observed at the inner surface did not seem to have entered into the medium filter. Globally, impurities were trapped by surface filtration, not by in-depth retention.

For Dynalloy 15CO (Figure 5) no visible defects of the medium filter or weld failures were found. Macrographic analyses showed that the meshes were little stretched and some wires seemed to be detached from the surface of the filter. The filter had a thin grey deposit on the inner surface but nothing at the outside surface. Deposits were composed of a biphasic mixture of Pb_7Bi_3-Bi, micron-size particles of lead oxide (PbO) and agglomerated particles of about 1 μm size forming filament like structure (up to 100 μm long) or small aggregates composed of iron and iron-chromium oxides. Other impurities were found in some oxides such as silicon, lead, nickel, tin and indium. The oxide composition was complex and varied quite a bit from one particle to another. The atomic ratios of metallic species from deposits were Cr: 1; Fe: 2; Pb: 5-6; Bi: 8-9. The thickness of the inner layer varied from 100 μm in the upstream part of the filter to 300 μm in the downstream part. Globally, the mesh of the media filter was empty of LBE, particularly in the upper part. There was no in-depth retention. Impurities were trapped by surface filtration.

Figure 5: SEM observation of deposits on the inner surface of 15 CO Dynalloy filter

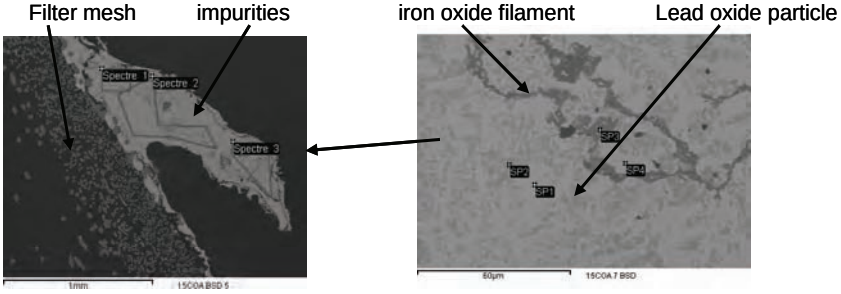

For PALL PMM 150 cartridge (Figure 6), observation and macrographic analyses did not show either visual tears or stretch of the wires, or structural or welding defects. Very few deposits were observed on this filter. Some deposits (forming partially layers with 200 μm thickness) were found on the surface of the perforated internal wall of the filter. Other deposits were within the meshes but the wire meshes were rather empty compared to those of previous filters (Poral and Dynalloy filters). These deposits were composed of a biphasic mixture Pb_7Bi_3-Bi, lead oxide (PbO) and micron-size agglomerated particles forming filaments composed of iron and chromium oxides (in the downstream part of the filter). Some particles (up to 10 μm) rich in iron and chromium oxides might contain lead, indium and some filaments indium, tin and silicon. To be noted that a bismuth iron mixed-oxide was found by XRD examination in upstream part of the deposit. Fewer filaments were retained than in the other media filters: a few on the surface of the mesh and nothing on the surface of the perforated internal wall. This could explain the very few iron and chromium oxides found in the global analyses of deposits. Other impurities in minority were found such as constituent elements of steel, tin and indium.

Figure 6: SEM observation of deposits on the inner surface of PALL PMM filter

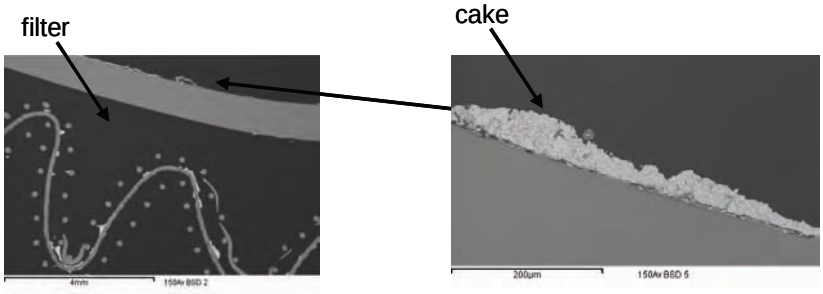

Discussion

Results of metallographic analyses showed that impurities were trapped mainly by surface (cake) filtration for these conventional type filters. Analyses detected lead oxide (PbO) in deposits but not in large amounts and also the presence of iron and chromium oxides. These oxides may come from peeling of the oxide coatings of structural materials. The initial impurities of lead bismuth (tin, indium) also tend to be trapped. Deposits formed uniform layers on the inner surface of filters: sometimes thicker in the downstream part of the filters with variable thickness, according to the radial height in the filter. Trapped particles varied in size and shape. They ranged from micron-size aggregated particles of lead oxide to long micron-size filaments of iron and chromium oxides contained in a heterogeneous mixture composed of Pb_7Bi_3-Bi (and to some extent PbO). These differences in size, structure and shape involve different mechanisms and rates of trapping according to the medium design parameters (removal rate and the holding capacity), but also depending on operating conditions. The deposits' composition obtained by EDS analyses showed no differences in the downstream and upstream parts (same Cr, Fe, Pb, Bi ratios and same phases Bi, Pb_7Bi_3, Fe and Cr oxides): However, in XRD analyses, PbO, Bi and magnetite were found inside the filter, whereas Pb_7Bi_3, Bi and magnetite were found in the sampling at the inlet part of the filter. These differences were attributed to the following reasons: the PbO particles are too small to be detected by SEM and/or the samplings at the inlet part of the filters contain more LBE due to liquid retention on the flange.

It must be considered that the amount of impurities present in LBE was probably not the same at the beginning of each test. Operating conditions were different for any tests: solid impurities concentration and oxygen content in LBE. The first test with Poral CL20 filter was performed after a period of maintenance when the amount of impurities was assumed as not negligible. However the level of impurities in the loop was never known, nor was the rate of their formation. It was therefore difficult to compare filter tests, and impossible to provide a quantitative analysis of filter efficiency. The only way to evaluate filter real-time performance was by following the variations in the pressure drop over time due to the filter module, thus giving an indication of the increase in resistance linked to particle retention in the filter.

In order to provide efficient removal of impurities from the liquid and gas systems by filtration devices, impurities have to circulate through this one for being trapped. The impurities that remain stagnant or stuck to walls cannot be trapped and could contribute to mass transfer. Moreover, it is known that impurities are not uniformly present in all cold and hot parts of a circuit. Whatever the choice of the filter medium, these points must be solved when designing the circuits and the purification unit, as should the issue of the filter replacement after lifetime expiration.

Finally, these filter media are promising. The real trapping of impurities for all filters tested (Poral, Dynalloy and PMM cartridge filters) was confirmed by the pressure drop monitoring as well as the metallographic post-analyses. Tests of about hundreds of hours of operation had

shown a good mechanical resistance at 400°C: no welds defects, no stretch of the wires (only little distended for Dynalloy) and pore size integrity maintained. Qualification by more long-term tests (2 000 hrs) using other removal rates and under various operational conditions (high or low air pollution level) with monitoring of the impurities contents by regular sampling would better assess their performance in terms of mechanic and thermal resistance, trapping efficiency,… Moreover, a more optimised design of the filter units is necessary, and should take into account the coagulation and adhesion mechanisms which depend mainly on the filtration medium holding capacity and characteristics (tortuousity, porosity, specific surface area,…). For instance, the combination of multiple layers of Dynalloy medium should improve the deep bed filtration.

Recommendations for basic processes definition

Nature and behaviour of impurities formed in LBE change according to the operating mode (initial start-up and filling, re-start or transient states, off-normal operating conditions, normal operations and steady states) as well as the method to propose for impurities removal.

Impurities (lead oxides) are formed under off-normal operating conditions or initial start-up or restart after maintenance or repair. The subsequent destruction of these oxide particles is then only possible by using micrometric hydrogen gas bubbles for a combined action: first the breaking of the crystallite or agglomerate structure, and then the lead oxide reduction with hydrogen through the lead oxide surface newly generated by the cracking of the particles. The iron oxide reduction is kinetically very slow so that these particles or aggregates containing iron oxides remain stable in solution and should be trapped in a special filtration unit. The bubbling allows for the removal of the sticking deposits on the structures, drives them to the purification unit [6,8].

For normal operating conditions, under air ingress control, finely dispersed particles of iron and chromium oxides originate from metallic impurities dissolved in the coolant by diffusion through the oxide coating of structural materials. Then, formed slags are purified in the filtration medium not only by filtration, but by combined mechanisms of coagulation/concentration and filtration. The trapping in filters is done by adhesion strength between particles aggregates and the surface of the filter material. The use of a reducing gas in the filter unit should make it possible to reduce the quantity of impurities, the main impurities being the lead oxide that is reduced back to liquid lead. Under these operating conditions, mainly non-reducible iron and chromium oxides (Fe_3O_4, Fe_2O_3, Cr_2O_3) should be trapped by the filtration process.

Two filtration methods and systems could be proposed. Conventional filters (Poral, Dynalloy and PMM cartridge filters) are suitable to remove impurities formed consequently to an excess of oxygen (after a large air ingress and during filling, start-up and re-start operations) in order to prevent a large oxidation of the structure and the formation of lead monoxide. These filters could be located in filtration units especially designed for batch operation. For the whole service time and normal operating modes, active oxygen control for corrosion protection, and impurities reduction and elimination processes are required. Special prototype filters have to be designed promoting deep bed trapping with coagulation and adhesion mechanisms. Filter unit systems could be proposed for semi-continuous operations in auxiliary circuits or bypass lines of the facility. Moreover, filtration processes need to be coupled with other systems of management of impurities: H_2 gas bubbling (in a vessel or in the filter housing) could be used for the reduction of lead oxides and the cracking of oxide particles.

After an oxygen contamination of the circuit, and its purification in the filtration units, the issue of regeneration of the filtration media is raised, in order to increase the service lifetime of these units, and reduce the need for removal/replacement, especially for the coolant circuit, which is highly activated (^{54}Mn, ^{60}Co…).

Conclusions

There is a significant knowledge data basis on the nature of impurities present in liquid (and in gas) of a LBE system. It is now understood that the nature and behaviour of impurities formed in LBE will change according to the operating modes (initial start-up and filling, re-start or transient states, off-normal operating conditions, normal operations) as well as the method proposed for impurity removal.

The present study gives a review of knowledge gained from STELLA filtering tests. It can serve to validate the basic filtration processes, define the operating procedures and evaluate perspectives for the design of purification units for long-term application in lead-alloy liquid metal coolant systems.

Nevertheless, the kinetics of impurity formation remain unknown, especially under the non-isothermal conditions of dynamic loop and transient states. This is coupled with the issue of on-line and quantitative measurements of impurities contents in liquid or gas. Thus, most of the filtration experimental programme does not lead to a parametric and qualitative definition of the process. This point should be improved in the future for the next steps of performance assessment, engineering study and design, and finally the demonstration of an industrial system.

Acknowledgements

This work was partly supported by the European Union under contract FI6W-CT-2004-516520 (IP-EUROTRANS). Special thanks to Mr. Honnorat, from PALL France Company, for filter media.

References

[1] Nuclear Energy Agency (NEA), "Chemistry Control and Monitoring Systems", Chapter 4 of the *Handbook on Lead-bismuth Eutectic Alloy and Lead Properties, Materials Compatibility, Thermal-hydraulics and Technologies*, OECD/NEA, Paris (2007).

[2] Beauchamp, F., *Purification Test Programme – Filtration of Lead-bismuth in the STELLA Loop*, DEMETRA WP 4.2.4 Deliverable D4-25.

[3] NEA, "Thermodynamic Relationships and Heavy Liquid Metal Interaction with Other Coolants", Chapter 3 of the *Handbook on Lead-bismuth Eutectic Alloy and Lead Properties, Materials Compatibility, Thermal-hydraulics and Technologies*, OECD/NEA, Paris (2007).

[4] Morier, O., F. Beauchamp, L. Brissonneau, *Final Report for the Purification Process Studies and Impurities Characterisations in the Gas and Liquid Phase*, DEMETRA WP 4.2.4 Deliverable D4-57.

[5] Morier, O., F. Beauchamp, *Status of the Required Technologies for Purification Systems*, VELLA Deliverable D44.

[6] Melnikov, V.P., V. Alexeev (SSC RF – IPPE); Personal communication.

[7] Courouau, J-L. (CEA, DEN, DPC, SCCME, LECNA); Personal communication.

[8] Papovyants, A.K., *et al.*, "Purifying Lead-bismuth Coolant from Solid Impurities by Filtration", *Proceedings of the Conference of the Heavy Liquid Metal Coolants in Nuclear Technology*, Obninsk, Russian Federation, 5-9 October 1998, pp. 675-682 (in Russian).

[9] Gessi, A., *Experimental Results for the Purification Process Studies, Including Design and Impurities Characterisation in the Gas and the Liquid Phase*, DEMETRA WP 4.2.4 Deliverable D4-25.

Reliability in liquid lead-bismuth of the 316L and T91 steels: Coupling effects between corrosion and fatigue

Jean-Bernard Vogt[1], **Ingrid Proriol-Serre**[1], **Laure Martinelli**[2], **Kevin Ginestar**[2]
[1]Centre national de la recherche scientifique (CNRS), Lille University, France; [2]Commissariat à l'énergie atomique (CEA), Saclay, France

Abstract

The paper analyses the impact of long-term immersion in LBE of T91 and 316L steels on their further fatigue behaviour in LBE. At first, corrosion processes in the regime of dissolution are studied by immersion of the 316L steel and the T91 steel in an LBE bath respectively at 500°C and 600°C and with oxygen content less than 10^{-11} wt.% and less than 10^{-10} wt.%. For both alloys, the dissolution is inhomogeneous but the elements dissolve at the same rate in the T91 steels and at different rates in the 316L steel. In addition, in the 316L, a preferential dissolution of nickel in LBE leads to formation of a ferritic layer at the steel surface.

The low cycle fatigue behaviour is studied on non-corroded (as-received) and pre-corroded specimens (after immersion) at 300°C in air and in oxygen saturated LBE. For as-received materials, the fatigue life is reduced in LBE as compared in air. The decrease in crack density after tests in LBE suggests that LBE allows short cracks overcoming microstructural barriers. Pre-corrosion has a negative effect on the fatigue resistance of the T91 steel, while it seems that 316L was not affected by pre-corrosion. However, in both alloys, pre-immersion in LBE results in corrosion defects at the surface of fatigue specimens. The corrosion microcracks appear latent because the pre-immersion had also produced a softening of the 316L steel. Otherwise, LBE can be considered as a source of "microcracks" when dissolution process occurs and a promoter of short crack growth.

Introduction

Besides irradiation degradation, the main sources of damage of nuclear reactors, e.g. ADS, LFR, PWR,… include corrosion, thermo-mechanical loading and corrosion-deformation interaction. Low cycle fatigue and creep are the two principal causes of likely fracture, and this can be accelerated by the environment. While thermo-mechanical damage may be approached with a similar view for all the different types of reactors, environmental effects – namely corrosion and environment-assisted mechanical damage – must be considered separately according to the nature of the coolant. Water-cooled reactor materials are basically subjected to corrosion, stress corrosion cracking and corrosion fatigue. This implies considering anodic and cathodic reactions where dissolution, passive film breakdown or hydrogen production… are key events in the damage processes. In liquid metal reactors, corrosion processes do not involve oxidation-reduction reactions in case of steel dissolution. However, in both, the chemistry of the liquid is very important. In liquid Pb-Bi eutectic (LBE) alloys, oxygen content has been found to be one of the most striking parameters that govern the mechanism of corrosion which afterwards is expected to affect mechanical properties. The chemistry control of the liquid during mechanical testing as done in aqueous environments (e.g. Cl^-, B… contents) appears to be more difficult to be experimentally performed for liquid LBE alloys. Indeed, at first, the oxygen purification of liquid Pb-Bi is a tough task and requires a good technical mastery of oxygen sensors. Secondly, the corrosion kinetics are very low, which requires long-term immersions for metals in the liquid metal pool. In recent years, CEA Saclay and CNRS-University of Lille have been studying in their respective laboratories the corrosion resistance and low cycle fatigue resistance of structural steels. Based on their extensive acquired experience in this field, CEA Saclay and CNRS-University of Lille have found it relevant to couple liquid metal corrosion investigation with fatigue experiments.

The objective of the paper is to investigate the role of a pre-corrosion that leads to a more or less homogeneous dissolution of the fatigue resistance. Indeed, fatigue resistance is very sensitive to surface roughness or surface alteration, here resulting from the pre-corrosion. Therefore, the work includes two successive stages: the first is the corrosion study carried out at CEA, followed by the second stage concerning mechanical resistance at CNRS-Lille University.

Experimental

Materials

Two structural steels have been investigated: T91 steel and 316L steel. Their chemical compositions are displayed in Tables 1 and 2, respectively, and their heat treatment is described.

Table 1: Chemical composition of the T91 steel (wt.%)

Cr	Mo	Ni	Mn	Si	V	C	Nb	Fe
8.50	0.95	0.12	0.47	0.22	0.21	0.10	0.06	Bal

Samples and fatigue specimens of T91 steel were subjected to the standard heat treatment: austenisation at 1 050°C and air quenching followed by a tempering at 750°C for 1 h to obtain a fully martensitic microstructure characterised here by an average grain size of 20 μm.

Table 2: Chemical composition of the 316L steel (wt.%)

Cr	Ni	Mo	Mn	V	Si	C	N	Fe
16.73	9.97	2.05	1.810	0.07	0.67	0.02	0.029	Bal

The 316L steel was solid solution annealed at 1 050:1 100°C and then water quenched. The heat treatment was performed by the supplier on 14 mm thick plates. The material is austenitic with an average grain size of 25 μm and contains about 5% of δ-ferrite.

The two steels differ not only by their quantity of chemical elements (Cr, Ni), all being in solid solution for the 316L while carbides are present in the T91 steel, but also by homogeneous grains for the former alloy instead of structured grains (former austenitic grain boundaries, martensite laths, dislocation subgrains, carbides) for the latter.

Corrosion experiments

The corrosion experiments were performed in the static facility called COLIMESTA [1]. In this facility, corrosion plate specimens as well as all kinds of mechanical testing specimens can be immersed together in an about 7 L of static LBE. Oxygen removal necessary to obtain dissolution of the samples is achieved by sweeping the LBE bath with a gas mixture of Ar-4.5 or 5% H_2. The oxygen concentration was continuously measured via an oxygen sensor [2].

The corrosion specimens were plates the dimensions of which vary from $12 \times 10 \times 2$ mm^3 to $15 \times 10 \times 2$ mm^3.

316L samples were corroded at 500°C in a LBE bath where the oxygen concentration was 10^{-11} wt.%. For T91 samples, the corrosion tests were performed at 600°C with an oxygen concentration in the LBE bath ranging from 10^{-10} to 5×10^{-10} wt.%.

Low cycle fatigue experiments

At first, low cycle fatigue (LCF) tests were performed at 300°C in air and in liquid LBE on as-received specimens (without pre-corrosion) before testing the pre-corroded fatigue specimens. All tests are performed without any control of oxygen using a servo-hydraulic MTS machine with a load capacity of 100 kN. No particular care was taken to control or measure oxygen activity.

The fatigue tests were carried out in a fully push pull mode ($R_\varepsilon = -1$) at different imposed total strain variations ranging from $\Delta\varepsilon_t = 0.4\%$ to 2.5%. A strain gauge extensometer for the strain control, a triangular wave and a constant strain rate of 4.10^{-3} s^{-1} were used. During cycling, hysteresis loops were periodically recorded allowing the measurement of the stress variation $\Delta\sigma$ for each cycle. The fatigue life is defined as the number of cycles from which a 25% drop in the quasi-stabilised tensile stress occurs.

The fatigue specimens were smooth and cylindrical with a gauge length of 13 mm and a gauge diameter of 10 mm for the T91 steel and 6 mm for the 316L steel. For the study of the LCF behaviour without effect of pre-immersion, their surface was carefully electro-polished before cycling. In the case of a pre-immersion in LBE, the surface was electro-polished before introduction in the LBE loop but no further preparation of the surface was carried out before cycling. The T91 steel was pre exposed at 600°C for 620 h in LBE where the oxygen concentration was between 10^{-10} and 5.10^{-10} wt.%. The 316L steel was pre-exposed at 500°C for 1 000 h in LBE where the oxygen concentration was 10^{-11} wt.%.

Results

Corrosion kinetics

The corrosion kinetics of these tests are presented in Figure 1.

The 316L weight loss by surface unit is linear as a function of time. The line intersects the abscissa line at 185 h for experiment performed at 500°C. This leads to consider that a latent time is necessary to dissolve the former oxide scale before wetting the specimen and to corrode. The corrosion rate is then equal to 0.05 g m^{-2} h^{-1}.

Figure 1: Corrosion kinetics of 316L at 500°C and T91 at 600°C in LBE with low oxygen concentration

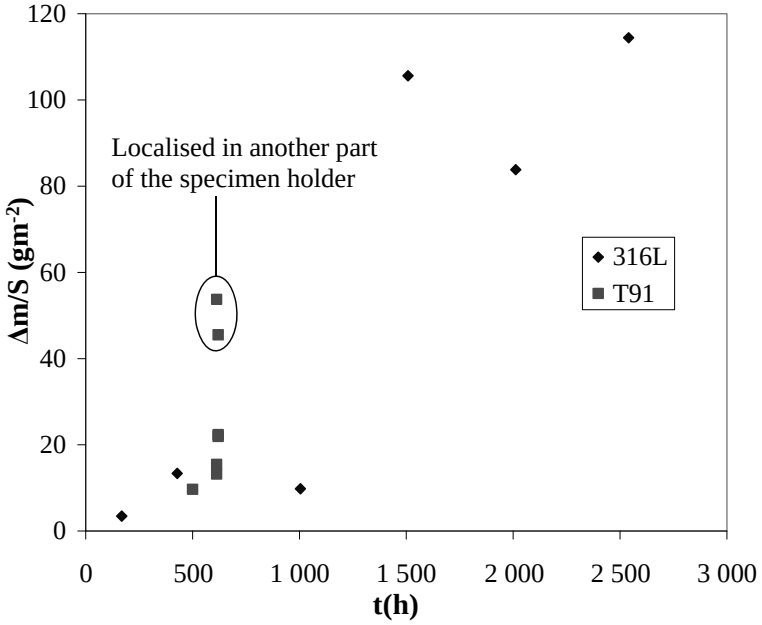

Figure 2 presents two SEM pictures of a 316L cross-section. One can observe that the corrosion is not homogeneous:

- The corroded layer does not cover the whole specimen surface [Figure 2(b)], the native oxide layer is then not totally dissolved and the whole specimen is not wetted.
- Moreover, in some parts of the specimen, the corroded layer thickness is not constant [Figure 2(a)].
- EDS/SEM analysis shows that the corroded layer is completely nickel depleted and partially chromium depleted (Figure 3).

Consequently, all the elements do not dissolve at the same rate. As the corrosion is not homogeneous, the corrosion rate deduced from the corrosion kinetics (Figure 1) corresponds to an average value.

Figure 2: SEM pictures of cross-section of 316L corroded at 500°C during 2 012 h

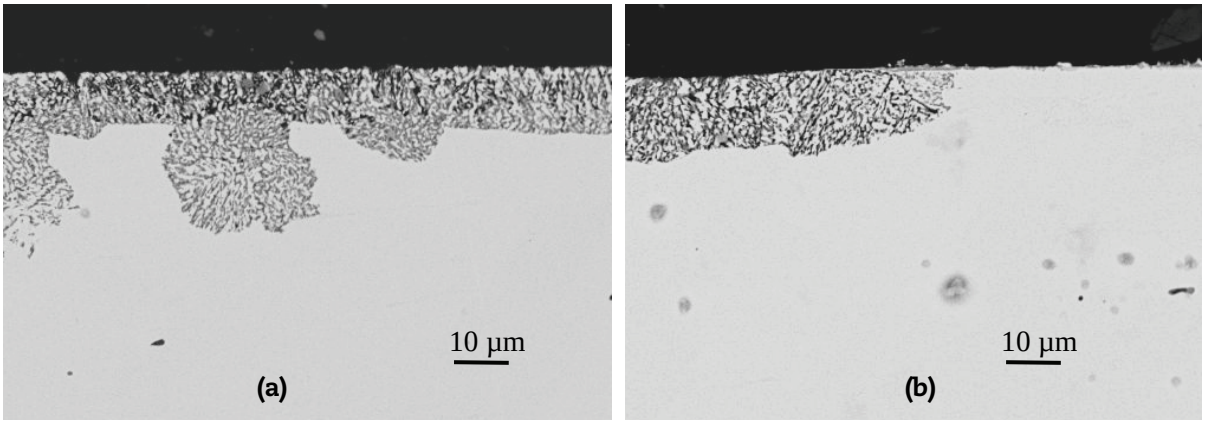

Figure 3: SEM/EDX profile of cross-section of 316L corroded at 500°C during 2 012 h

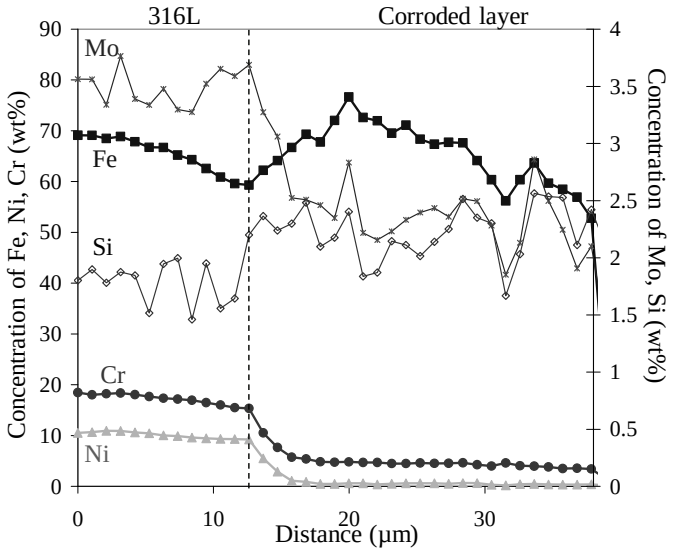

For the T91 specimens, at 600°C, only three durations are performed: 500, 613 and 620 h. An important weight loss discrepancy is observed for two experimental points at 613 h and 620 h. This discrepancy could be explained by a downstream effect as the most corroded samples were not situated at the same position as the others. Even without considering these two points, it is difficult to determine if the weight loss is linear as a function of time. However, considering a linear weight loss as a function of time, the latent time needed to corrode is 380 h, the average corrosion rate is then 0.078 g m^{-2} h^{-1}. Figure 4 shows two optical microscope micrographs of cross-section of T91 immersed 620 h (a) and 613 h (b) in LBE at 600°C. Figure 4(a) shows that T91 corrosion is not homogeneous: some parts of the specimen are corroded while other parts are not. However, there is no corroded layer; all the elements are dissolved with the same rate [see Figure 4(b)]. Figure 4(b) shows that the dissolution seems to occur preferentially in the grain boundary leading to an important roughness in the corroded part.

Figure 4: Optical microscope micrographs of cross-section of T91 corroded at 600°C during 620 h (a) and 613 h (b). The picture (b) is done after treatment with oxalic acid.

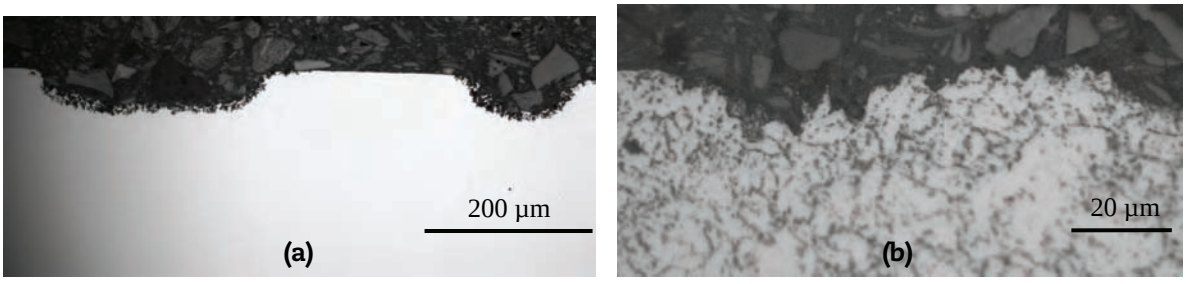

Stress response to strain cycling

The stress response to strain cycling of the T91 and 316L was similar for tests in air and tests in LBE. For the T91 steel, it consists of a cyclic softening period, very pronounced at the beginning of the test and then more moderate. Then, a marked decrease of the stress amplitude occurred, which is related to the propagation of a macroscopic crack into the bulk before final failure. This cyclic softening is a typical response to strain cycling of the microstructure evolution of high

dislocation density containing materials such as martensitic steels or cold worked materials [3]. For the 316 L steel, the response is a bit complex since hardening precedes the softening period before the stress tends to stabilise, as indicated in the literature [4]. As occurs for corrosion fatigue tests in aqueous solution, the LBE environment did not affect bulk properties as depicted by the macroscopic stress but can modify the surface properties

Pre-immersion of the fatigue specimens in LBE had no major impact on their further cyclic response. As compared to as-received materials, for a same strain variation applied, the evolution of the stress amplitude during cycling was similar for pre-exposed specimens. The values of the stress were a little lower, especially for the T91 steel, but the difference was of the order of scattering. For the 316L steel, a softening effect induced by LBE immersion was observed (Figure 5). This surprising effect may be due to the fact that 316L steel was treated as a form of massive plate by the supplier. Thus, specimens for tests in air or LBE in the as-received condition may be not as much annealed as those after 1 000 h immersion at 500°C.

Figure 5: Cyclic stress strain curves of the 316L and T91 steel for fatigue tests at 300°C in air and LBE on as-received and pre-immersed specimens

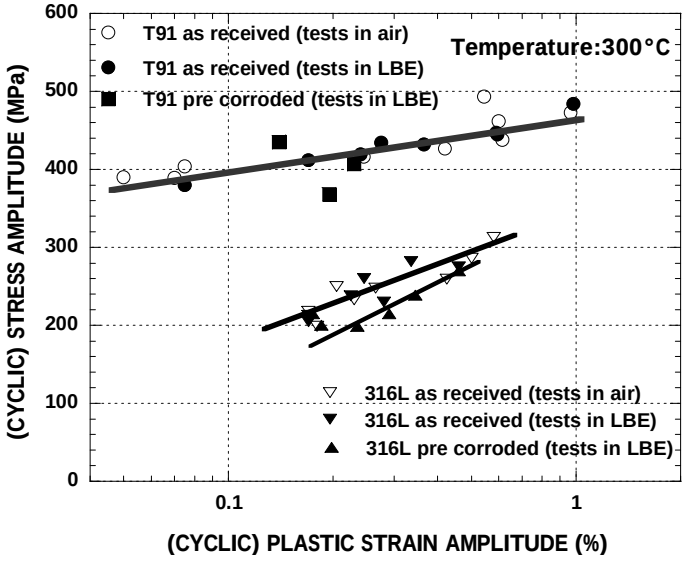

Effect of pre-immersion in LBE on fatigue resistance

First, let us point out that the fatigue resistance of both alloys is decreased when the materials are tested in LBE, especially at high strain range. At low strain range, fatigue lives in air and LBE are nearly the same whatever the environment (Figures 6 and 7). Such detrimental effects of LBE on fatigue resistance have been also reported for a 10.5Cr steel Manet-II at 260°C [5]. This suggests that the liquid metal accelerated damage (LMAD) observed requires a given amount of cyclic plastic deformation. As well, LBE should play an effect on initiation of short cracks and their further transformation into long cracks.

For the T91 steel, the fatigue resistance was considerably dependant on the pre-exposition condition (Figure 6). A pre-exposition in low oxygen concentration LBE bath for 500 h followed by further cyclic deformation in LBE at 300°C resulted in shorter fatigue lives as compared with as-received specimens (except for one test). To our knowledge, no literature on fatigue properties after exposure in heavy liquid alloy is available. The only investigation on this topic concerns monotonic tensile properties [6] where a decrease in ductility was observed in the T91 after exposure at 400°C in LBE (low oxygen content) for 4 500 h.

Figure 6: Fatigue resistance curves of the T91 steel for fatigue tests at 300°C in air and LBE on as-received and pre-immersed specimens

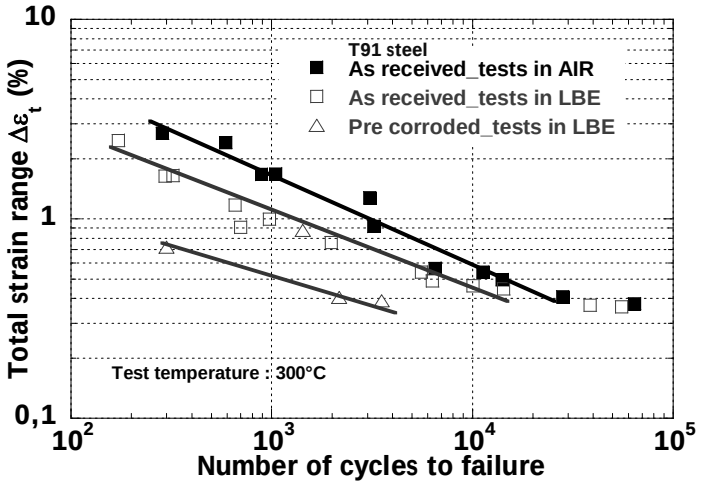

For the 316L steel, in the as-received condition, the fatigue resistance was dependent on whether tests were carried out in air or LBE. Again, LBE reduces the fatigue lives (Figure 7). However, the pre-corroded specimens (500°C for 1 000 h) have the same fatigue resistance as the as-received ones.

Figure 7: Fatigue resistance curves of the 316L steel for fatigue tests at 300°C in air and LBE on as-received and pre-immersed specimens

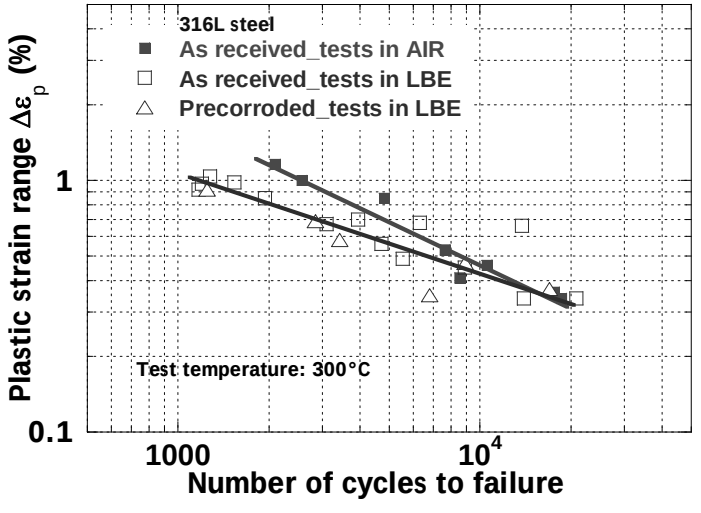

Role of pre-immersion in LBE on fatigue crack initiation

After fatigue, the specimens, both the as-received and the pre-corroded ones, were longitudinally cut for SEM observations. The analyses of the transverse cross-sections provide information on the depth of the short cracks formed at the specimen surface and their density.

In both as-received materials, cycling in air results in crack nucleation in slip bands, formation of grain-sized length microcracks and their growth. Grain boundaries behave as barriers for crack extension which results in a high density of short cracks and crack propagation into the bulk is essentially transgranular. The same materials tested in LBE exhibited a very much

smaller crack density, especially in the T91 steel specimen where major crack propagates into the bulk and very few secondary short cracks were observed. It turns out that the effect of LBE is to overcome structural barriers, thus encouraging the formation of a long crack. Therefore less fatigue cycles are necessary to fail the specimen in agreement with the fatigue resistance curves.

In pre-corroded specimens, the external surface is not as smooth as for as-received specimens as a result of corrosion surface degradation. Therefore the surface defects can act as preferential fatigue crack initiation. At surface defects induced by corrosion, fatigue cracks were indeed observed (Figure 8).

In the zone of selective dissolution of the 316L, microcracks could also initiate at spots where sharp defects were not observed (Figure 9).

Figure 8: Crack initiation at pre-immersion induced defects in the T91 steel (a) and 316L (b) specimens after fatigue tests at 300°C in LBE

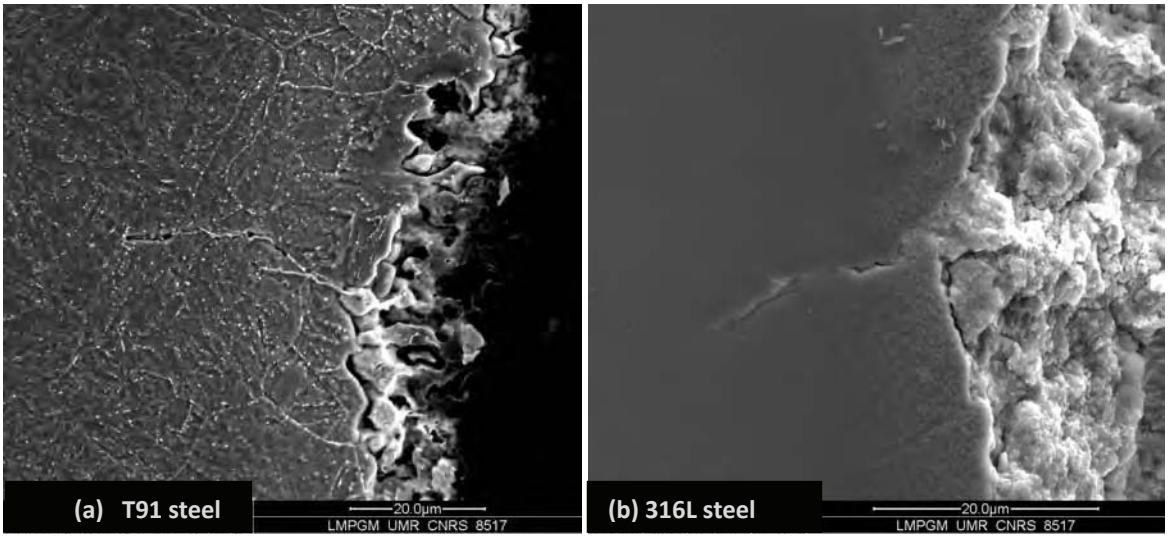

Figure 9: Crack initiation in selective dissolution zones resulting from immersion in low oxygen LBE of the 316L and then fatigued at 300°C in LBE

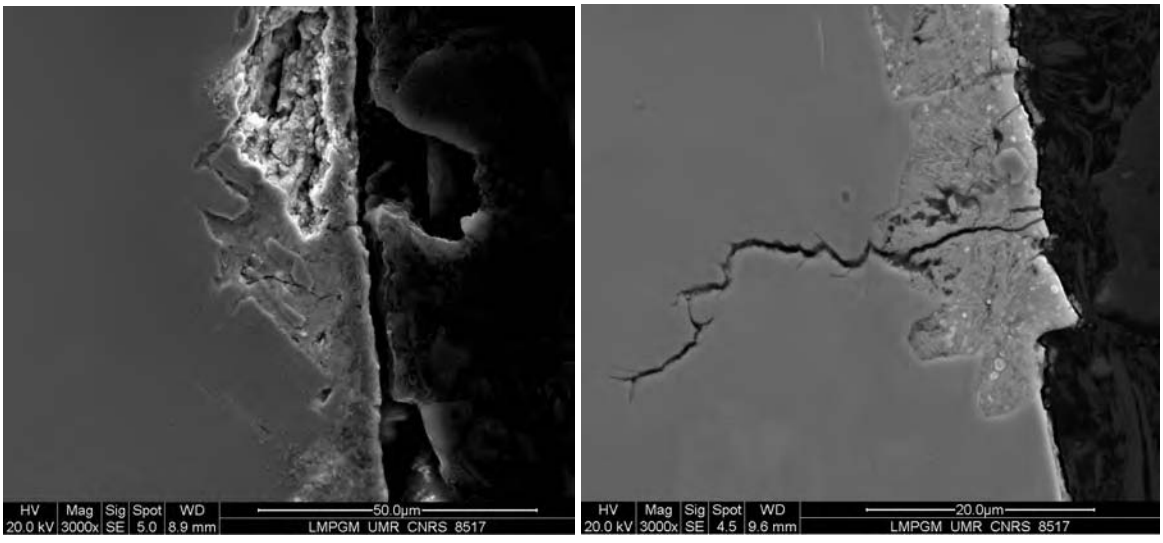

Discussion

The present study devoted to examining the coupling effect between corrosion and fatigue of two structural steels consisted first in damaging the material surface by corrosion before subjecting the specimen to cyclic loading. Oxygen concentration as low as 10^{-10} wt.% in a liquid lead-bismuth eutectic (LBE) allows corrosion through a dissolution process. For T91 and 316L, corrosion is not homogeneous at the surface of specimen, with some spots highly dissolved and others unaffected. The most striking difference is that in the T91 steel all the chemical elements dissolve at a same rate, which is not the case of those of the 316L stainless steel. It turns out that the modifications in the surface of each steel are different in nature. In the T91 steel, the modification of the surface can be essentially comparable to a pure "topographic" roughness. On the other hand, in the 316L steel, selective dissolution leads to ferrite formation in addition to roughness. From these conclusions, one would suspect a more detrimental effect of pre-corrosion in the 316L steel than in that of T91. However, the fatigue resistance curves do not support this assumption; on the contrary the 316L seems to be unaffected by the pre-corrosion stage. It is clear that pre-corrosion provides in both alloys sharp defects which can play the role of stress concentrator. Their propagation occurs if the local cyclic critical stress factor exceeds a threshold in a similar way as short cracks formed in intrusions do. The micro plastic zone ahead of the microcrack acts as a shield the strength of which depends on material properties. In the as-received 316L steel as well as in the T91 steel (as-received or pre-corroded) tested in liquid metal, the shield is weak, does not oppose crack growth and appears easy to overcome. For the latter material, a lot of conditions favourable to crack growth are easily encountered: reduced plastic zone due to higher cyclic stress (Figure 3), likely decrease of threshold stress intensity factor due to liquid embrittlement (as suggested by the sensitivity of liquid embrittlement), substructured martensitic grain. This is also true for the as-received 316 steel tested in LBE even if the soft and tough properties of the material should lessen the efficiency of the shield. Nevertheless, these properties are not sufficiently marked to affect the behaviour of short cracks in the as-received 316L steel and therefore to immune the material against LMAD (as shown by the fatigue resistance curves). However, the long-term immersion in the pre-corrosion liquid metal bath which gives rise to defect nucleation also produces a softening effect of the material. This allows strengthening the shielding effect at corrosion defect tip and renders it more stable. Therefore, it cannot be said unambiguously that pre-corrosion has no effect on further fatigue resistance but, in the present case, provides a couple of changes in the material that annihilate a detrimental effect.

Conclusions

The study aimed at understanding the coupling effect between corrosion degradation and low cycle fatigue damage in T91 and 316L steels has been conducted in two successive stages. The main conclusions are:

- Corrosion of the 316L steel and the T91 steel in a LBE bath respectively at 500°C and 600°C and with oxygen content less than 10^{-11} wt.% and less than 10^{-10} wt.% occurs by dissolution.
- For both alloys, the dissolution is inhomogeneous but the elements dissolve at the same rate in the T91 steels and at different rates in the 316L steel.
- In the 316L, a preferential dissolution of nickel in LBE leads to formation of a ferritic layer at the steel surface.
- On non-corroded specimens, cycling in LBE instead of air results in a decrease of fatigue resistance.
- Pre-corrosion has a negative effect on the fatigue resistance of the T91 but not in 316L.

- The corrosion microcracks appear latent in 316L because of the softening induced by the pre-immersion which acts as stress relief thermal treatment for the steel.
- LBE can be considered a source of "microcracks" when the dissolution process occurs and a promoter of short crack growth.

Acknowledgements

The authors would like to acknowledge the financial support of the FP6 European programme IP-EUROTRANS (contract No. FI6 W-CT-2004-516520).

References

[1] Deloffre, P., A. Terlain, F. Barbier, *Journal of Nuclear Materials*, 301, 35-39 (2002).

[2] Courouau, J-L., *et al.*, *Journal of Nuclear Materials*, 301, 53-59 (2002).

[3] Nagesha, A., *et al.*, *International Journal of Fatigue*, 24, 1285-1293 (2002).

[4] Vogt, J-B., *Journal of Materials Processing Technology*, 117, 364-369 (2001).

[5] Kalkhof, D., M. Grosse, *Journal of Nuclear Materials*, 318, 143-150 (2003).

[6] Aiello, A., *et al.*, *Journal of Nuclear Materials*, 335, 217-221 (2004).

Compatibility of different steels and alloys with lead up to 750°C*

Alfons Weisenburger, Mattia del Giacco, Adrian Jianu, Georg Müller
Institut für Hochleistungsimpuls und Mikrowellentechnik, Forschungszentrum Karlsruhe
Germany

Abstract

Under transient and abnormal conditions the lead foreseen as on possible coolant in subcritical systems can reach temperatures above 750°C. To address high temperature compatibility with lead a loop will be installed at Forschungszentrum Karlsruhe. During the design phase different potential alloys were tested in liquid lead for 1 000 hours at three different temperatures (500, 600 and 750°C) and two oxygen contents (10^{-6} and 10^{-8} wt.% oxygen). One group was Al containing FeCrAl alloys (from Kanthal) with different Al and Cr content. One high-temperature Ni-based Alloy 800, the 1.4571 steel and several steels used as material for pumps in industry were tested too. The latter were not exposed to 750°C but up to 4 000 hours. In lead with 10^{-6} wt.% oxygen the Al containing materials form protective layers. However at lower temperatures some of the FeCrAl alloys showed duplex oxide layer formation. The 1.4571 showed clear signs of dissolution at 600°C, while the Ni-based Alloy 800 showed already at 500°C the first signs of dissolution attack. This confirms the known negative influence of Ni on the corrosion resistance. The influence of the alloying elements on the corrosion resistance will be addressed in the paper.

* The full paper being unavailable at the time of publication, only the abstract is included.

Session II

Accelerators

Chair: H. Klein

Accelerator reference design for the European ADS demonstrator

Jean-Luc Biarrotte, Alex C. Müller
CNRS/IN2P3, IPN Orsay, France
On behalf of the EUROTRANS WP1.3 collaboration

Abstract

An accelerator-driven system (ADS) for transmutation of nuclear waste typically requires a 600 MeV-1 GeV accelerator delivering a proton flux of a few mA for demonstrators, and of a few tens of mA for large industrial systems. Such a machine belongs to the category of high-power proton accelerators, with an additional requirement for exceptional reliability: because of the induce thermal stress to the subcritical core and for availability reasons, the number of unwanted beam trips should not exceed a few per year, a specification that is far above usual performance. This paper describes the reference solution adopted for such a machine, based on a so-called "fault tolerant" linear superconducting accelerator, and briefly presents the status of the associated R&D. This work has been performed within the EC FP6 EUROTRANS project.

The European ADS demonstrator

The basic purpose of accelerator-driven systems (ADS) is to reduce – by orders of magnitude – the radiotoxicity, volume and heat load of nuclear waste before their underground storage in deep geological depositories [1]. In this context, the European Research Programme for the Transmutation of High-level Nuclear Waste in Accelerator-driven Systems (EUROTRANS) is funded by the European Commission within the 6th Framework Programme, and involves more than 40 partners (research agencies, universities and nuclear industries). It is a five-year programme (2005-2010), extending previous R&D (e.g. the EC FP5 PDS-XADS project), for which activities are split into several main domains, devoted to: the advanced design of a transmuter demonstrator (XT-ADS) including all its subcomponents, the generic conceptual design of an industrial transmutation facility (EFIT), experimental work dealing with the coupling of an accelerator, a spallation target and a subcritical core, like the very low power (about 100 W thermal) GUINEVERE experiment [2], and finally, studies on advanced fuels for transmuters, investigations on suited structural materials and collection of nuclear data for transmutation. The specifications for demonstrator and industrial transmuters are shown in Table 1.

Table 1: European transmuters' general specifications

Transmuter demonstrator (XT-ADS/MYRRHA project)	Industrial transmuter (EFIT)
50-100 MWth power	Several 100 MWth power
k_{eff} value ~ 0.95	k_{eff} value ~ 0.97
Highly-enriched MOX fuel	Minor actinide fuel
Pb-Bi eutectic coolant and target	Pb coolant and target
600 MeV-4 mA CW proton beam	800 MeV-20 mA CW proton beam

The main objective of the EUROTRANS programme is actually to pave the road towards the construction of an experimental facility (MYRRHA) willing to demonstrate the technical feasibility of transmutation in an accelerator-driven system: this is the XT-ADS concept. SCK•CEN (Mol, Belgium) initiated the MYRRHA project in 1998 [3]. Its purpose is to design and later build a flexible irradiation facility as a suitable replacement for the existing Material Testing Reactor BR2 that has been operating since 1962. The new facility would serve both as a test-bed for transmutation and as a fast spectrum facility for material and fuel developments. It would operate first as a subcritical (accelerator-driven) system and later as a critical reactor. A Central Design Team (CDT) is presently being settled to further develop the engineering design of such a facility, which should be fully operational within 10 to 15 years. The CDT project is supported by the EC FP7.

The reference ADS accelerator

Both European ADS machine concepts require a high-power proton accelerator operating in CW mode, ranging from 2.4 MW (XT-ADS operation) up to 16 MW for the industrial EFIT. The accelerator delivers a proton beam on a spallation target to provide an external neutron flux source to feed the subcritical core. In principle, both cyclotrons and linear accelerators are relevant candidates for providing such beams, at least in the XT-ADS case. Because of several conditions such as the reliability and availability target values and the required beam stability, but also to keep the same concept for both demonstrator and industrial machines, the decision to use a linear accelerator type is to be preferred, as already pointed out within the PDS-XADS project [4].

The main beam specifications as established at the beginning of the EUROTRANS project are given in Table 2. At first glance, the extremely high reliability requirement (beam trip number) can immediately be identified as the main technological challenge to achieve. As a matter of fact,

Table 2: Proton beam general initial specifications within EUROTRANS

	Transmuter demonstrator (XT-ADS/MYRRHA project)	Industrial transmuter (EFIT)
Proton beam current	2.5 mA (and up to 4 mA for burn-up compensation)	~ 20 mA
Proton energy	600 MeV	800 MeV
Allowed beam trips nb (> 1 s)	~ < 5 per three-month operation cycle	~ < three per year
Beam entry into the reactor	Vertically from above	
Beam stability on target	Energy: ±1% – Current: ±2% – Position and size: ±10%	
Beam time structure	CW (w/ low frequency 200 μs beam "holes" for subcriticality monitoring)	

the ADS core is designed to accept a limited number of emergency stops due to beam trips (about five per year). This number, as well as the requirement of a 1 second limit for the beam trips, has been reconsidered during the project (see the dedicated section on the reliability issue hereafter). Presently, the maximum beam trip duration has been lengthened up to 3 seconds, because both the XT-ADS and the EFIT cores exhibit large thermal inertia due to the large LBE or Pb pool they offer, and to the margins that seem to exist with the fuel and cladding behaviour during these transients. The number of allowable beam trips has been also increased to 10 beam trips per cycle in the XT-ADS case, but kept to the three per year value for the industrial application where availability is of prime importance.

The conceptual design of the accelerator has been developed during the PDS-XADS project. It is a superconducting linac-based solution (see Figure 1), leading to a very modular and upgradeable machine: the same concept remains valid both for the XT-ADS demonstrator and for the industrial scale facility EFIT. Thus, in order to upgrade the XT-ADS accelerator into the EFIT one, additional accelerating modules have to be "simply" added at the high-energy end of the beam line to match with the final energy increase, while more powerful RF power stations have to be installed to take into account the higher beam intensity; all other elements remain similar at first order.

Figure 1: European ADS accelerator conceptual scheme [4]

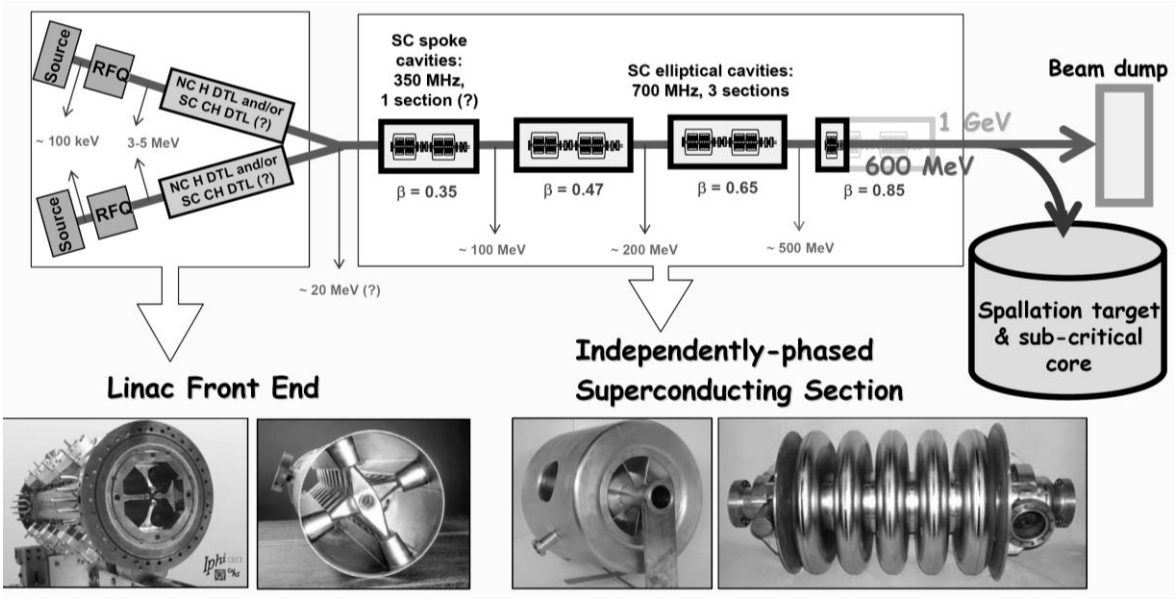

Such a solution also leads to a high RF-to-beam efficiency thanks to superconductivity (optimised operation cost) and an excellent potential for reliability, both in the main linac, which is designed to be intrinsically "fault tolerant", and in the front-end section where a hot stand-by redundant injector, with fast switching capability, can be installed if needed. An advanced reference design of this accelerator has been settled during the EUROTRANS project, mainly focusing on the XT-ADS case in the MYRRHA context. The characteristics of this reference accelerator are detailed hereafter; more details are available in [5]. It is mainly composed of a 17 MeV injector followed by a 17-600 MeV fully superconducting linac with independently-phased cavities. The investment cost for such an XT-ADS machine has been assessed around EUR 240 M (manpower and contingencies included, buildings and general utilities excluded).

The linac injector

The linac injector is composed of a 50 kV ECR proton source, a short magnetic low energy beam transport line and a 3 MeV four-vane copper RFQ operating at 352 MHz. This RFQ, designed to handle up to 30 mA CW beams with close to 100% transmission for all currents, is about 4.5 metres long, operates with moderated Kilpatrick factors (~1.7). This "classical" injection section is then followed by a more "exotic" but promising energy booster [6], that is a combination of two normal conducting and four superconducting Crossbar H-mode (CH) DTL structures as shown in Figure 2, bringing the beam up to 17 MeV. Focusing is ensured by quadrupole triplets and superconducting solenoids inside the cryomodule containing the superconducting CH cavities, and a couple of re-bunchers is used to perform the longitudinal beam adaptation. The design of the DTL structures is based on the KONUS beam dynamics concept [7], which allows exhibiting excellent accelerating efficiency at these low energies with a net energy gain of 14 MeV in less than 10 metres, while having very low power consumption in CW operation.

Figure 2: The reference ADS linac 17 MeV injector

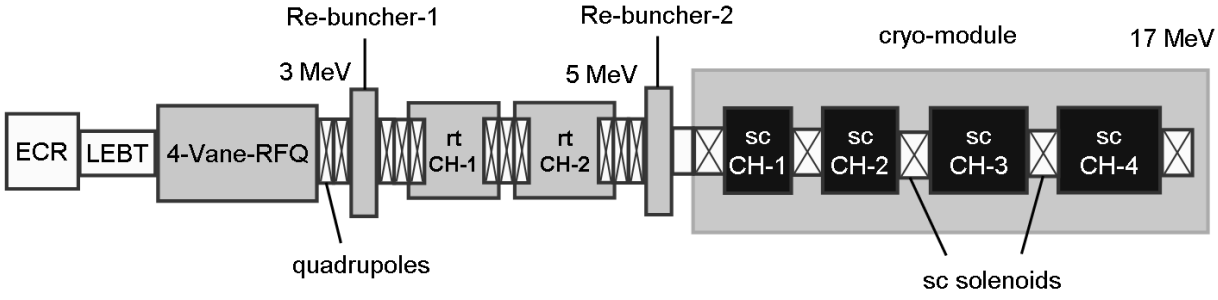

Multi-particle beam-dynamics simulations of the whole front end show very good beam behaviour and low sensitivity to errors. Moreover, the proposed solution can cope with various beam currents, with very reasonable emittance growth of about 10% at 5 mA, and 30% at 30 mA. This means that the same machine design can be used for a low current machine (XT-ADS) and for a high current machine (EFIT). Only the RF power and the setting of the re-bunchers have to be adjusted.

Of course, in this front end line, the beam beta profile is frozen by design, so that any accelerating section failure will inevitably lead to a beam interruption. For this reason and in order to enhance the machine reliability, it is proposed, if needed, to duplicate the injector (at least the ion source, at most the whole 17 MeV front end) to provide a hot stand-by injection line able to relieve the main one in case of failure. The detailed design of the corresponding connecting line remains to be worked out.

The independently-phased superconducting main linac

From 17 MeV, a fully modular superconducting linear accelerator accelerates the proton beam up to the final energy. This corresponds in the XT-ADS case (600 MeV) to a length of about 240 metres from the ion source. The linac is composed of an array of independently-powered spoke and elliptical cavities with high energy acceptance and moderate energy gain per cavity – low number of cells and conservative accelerating gradients (around 50 mT and 25 MV/m peak fields nominal operation point) – in order to increase as much as possible the tuning flexibility and provide sufficient margins (about 30%) to allow the implementation of fault-recovery scenarios (see dedicated section hereafter). It has been shown that such a reliability-oriented design choice leads to an about +20% extra length [5], which can be considered as "the price to pay" for reliability.

The 600 MeV XT-ADS baseline linac architecture is summarised in Table 3. This linac design has been optimised in terms of total length using the CEA Saclay code package [8]. It is based on the use of regular focusing lattices, with not-too-long cryostats and room temperature quadrupole doublets in between. Such a scheme provides several advantages: easy maintenance and fast replacement if required, easier magnet alignment at room temperature and no fringe field issues, possibility to provide easily reachable diagnostic ports at each lattice location, and last but not least, nearly perfect optical lattice regularity (no specific beam matching required from cryostat to cryostat). The beam tuning has been performed with great care: phase advances are limited below 90° per lattice and parametric resonances are avoided, phase advances per metre are tuned as continuously as possible so as to ease the beam matching, and a very safe and constant longitudinal acceptance is maintained all along the accelerator, especially at the 350-700 MHz frequency jump transition, as recommended in [9].

Table 3: The 17-600 MeV XT-ADS reference design

Section number	1	2	3
Input energy (MeV)	17.0	86.4	186.2
Output energy (MeV)	86.4	186.2	605.3
Cavity technology	Spoke 352.2 MHz	Elliptical 704.4 MHz	
Cavity geometrical β	0.35	0.47	0.66
Cavity optimal β	0.37	0.51	0.70
No. of cells/cavity	2	5	5
Focusing type	NC quadrupole doublets		
No. of cavities/cryomodule	3	2	4
Total No. of cavities	63	30	64
Acc. field (MV/m @ opt. β)	5.3	8.5	10.3
Synchronous phase (deg)	-40 to -18	-36 to -15	
5 mA beam loading/cav (kW)	1 to 8	3 to 22	17 to 38
Section length (m)	63.2	52.5	100.8

This "conservative" optical design leads to very safe beam behaviours, with low sensitivity to mismatched conditions or current fluctuations, and producing very low emittance growths (about 5%). No beam loss is observed in the multi-particle simulations that have been performed using a 100 000 particle input distribution, coming from the simulation of the 17 MeV full injector, transported and matched through a typical MEBT – not yet optimised – composed of a quadrupole triplet, a quadrupole doublet and two re-bunching cavities. The obtained beam envelopes are shown in Figure 3 (left).

One has to note that in the 800 MeV EFIT linac case, the very same modular scheme applies, but a fourth family section is added to cover the 600-800 MeV energy range, using 704.4 MHz superconducting elliptical cavities with a geometrical beta of 0.85. This EFIT accelerator is therefore longer by about 75 metres, reaching about 320 metres overall. Due to the higher beam current, more powerful RF amplifiers (4 to 5 times more) are also required for all cavities, leading

to beam loading figures up to around 250 kW for the more demanding high-energy cavities (instead of about 40 kW in the XT-ADS case). Another slight change will be of course the total capacity of the cryogenic refrigerator, to be increased from 3.5 kW (XT-ADS case) up to about 6 kW @ 2 K.

The final beam transport line

The objective of the final transport line is to safely inject the proton beam with the specified footprint – donut-shaped – onto the spallation target located inside the reactor (~25 metres deep). The line is composed of two non-dispersive $2 \times 45°$ achromats, so that the beam spot position and size at the target is independent from energy jitter and spread. In the dispersive region of the last achromat, position and size monitors will be able to provide information on proton energy variations, and to trigger a feedback system. Natural defocusing is used in the last straight line to get the desired beam spot size, and the footprint is then obtained by raster scanning, using a redundant set of fast steering magnets operated at frequencies of 50 to a few hundred Hz, and acting in the two transverse directions. The obtained beam footprint on target, obtained via multi-particle simulation, is represented on Figure 3 (right).

Figures 3: 17-600 MeV linac 95% beam envelopes (left); beam footprint on target (right)

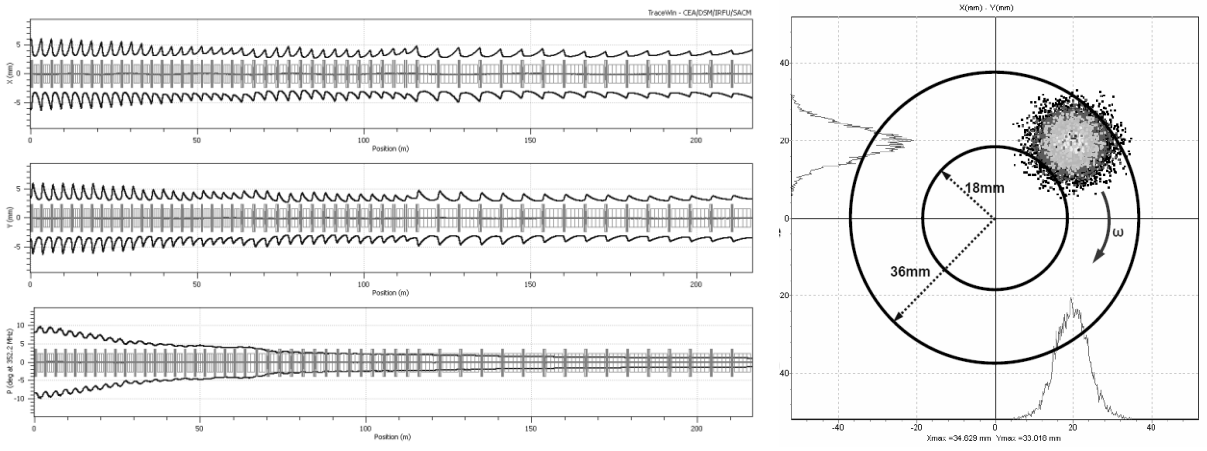

The accelerator reliability issue

As already underlined, the ADS accelerator is expected – especially in the industrial scenario – to have a very limited number of unforeseen beam interruptions per year. This requirement is motivated by the fact that frequently repeated beam interruptions can induce high thermal stresses and fatigue on the reactor structures, the target or the fuel elements, with possible significant damages especially on the fuel claddings; moreover these beam interruptions dramatically decrease the plant availability, possibly implying plant shutdowns of tens of hours in most of the cases. The initial recommendations concerning these beam trips (for XT-ADS: less than five beam trips longer than 1 second per three-month cycle) have been revisited during the course of the project [10], taking advantage of the PHENIX plant operation analysis, and of the results of new studies demonstrating the possibility of maintaining the reactor structure but also the fuel cladding integrity under repeated beam trips, even if some complementary R&D is still pending, especially at FZK on the study of the integrity of the oxide layer over the clad under equivalent load conditions. A new tentative limit to the allowable beam trips is now proposed for the XT-ADS case: 10 transients longer than 3 seconds per three-month operation cycle.

In any case, in order to reach such extremely ambitious reliability goals, it is clear that reliability-oriented design practices needed to be followed from the early design stage of the ADS accelerator. In particular, "strong design" is required: every linac main component has to be de-rated with respect to its technological limitation ("over-design"). A high degree of redundancy also needs to be planned in critical areas; this is especially true for the identified "poor-reliability" components like the linac injector area, which may be duplicated, or the RF power systems, where solid-state amplifiers should be used as much as possible. And finally, the accelerator should be able, to the maximum extent, to pursue operation despite some major faults in basic components ("fault tolerance" capability); it has been shown in [11] that a solution based on a modular independently-phased SC linac is indeed able to easily adapt its nominal tuning in the case of a loss of any RF cavity or power loop unit (see hereafter), and even of a quadrupole doublet, while keeping beam dynamics and beam properties on target into specifications.

Tolerance to RF faults in the superconducting main linac

Because we deal with a non-relativistic proton beam, any RF cavity fault implying beam energy loss will also lead to a phase slip along the linac. It will increase with distance, and thus push the beam out of the stability region: the beam will be completely lost. To recover such RF fault conditions, the philosophy is to re-adjust the accelerating fields and phases of some non-faulty RF cavities to recover the nominal beam characteristics at the end of the linac, and in particular its transmission, phase and energy. A simple way to perform is to react on the accelerating cavities neighbouring the failing one. This so-called "local compensation method" has the advantage of involving a small number of elements, and therefore of being able to compensate multiple RF faults in different sections of the machine at the same time.

Beam dynamics simulations show that nominal beam parameters at the target can always be restored using such a retuning method, given the condition that a 20-30% rise in accelerating field and RF power can be sustained in the few (4-8) retuned elements [11]. This method is of course rather demanding in terms of linac length – about +20%, as mentioned previously – and installed RF power budget, but is on the other hand totally in line with the ADS over-design criterion, and in any case required to try to reach the necessary reliability level.

Transient beam dynamics have been performed to better analyse what happens to the beam during such retuning procedures, keeping in mind that they have to be performed in less than one (or a few) second. A new simulation tool has been developed, based on the TraceWin code [8], allowing analysing the effect of time-dependent perturbations on the beam through RF control loop modelling. From this work [12], a reference "fast failure recovery scenario" has been defined, that consists in stopping the beam for 1 second maximum while achieving the retuning using the following sequence:

1. The RF fault is detected (or anticipated) via suited dedicated diagnostics and interlocks, and a fast beam shutdown is triggered.
2. The new correcting field and phase set-points (previously stored in the low-level RF cards' memory during the commissioning phase) are updated.
3. The failed cavity is quickly detuned (using piezoactuators) to avoid the beam loading effect, and the associated failed RF loop is cut off.
4. Once steady state is reached, beam re-injection is triggered.

In this context, a conceptual design of a suitable low level RF (LLRF) system has been performed [13], based on the use of an integrated digital board containing a FPGA chip able to process the feedback control algorithms, several ADC and DAC to convert the received and produced signals, a RAM memory used to store set points or save operating parameters, a serial bus to communicate with the general control/command system, and a fast serial bus to communicate with boards of adjacent cavities.

Reliability analysis and discussion

Two independent integrated reliability analyses have been performed so far to try to estimate the number of malfunctions of the XT-ADS accelerator that could cause beam/plant shutdowns per three-month operation cycle, and to analyse the influence of the mean time between failures (MTBF), mean time to repair (MTTR), and of the whole system architecture on the results. These studies have been respectively performed by means of a reliability block diagram analysis using the Relex© software [14] and by homemade Monte Carlo simulations [15] with slight differences in the hypotheses. In both cases, the results show that such linacs have a high potential for reliability improvement if the system is properly designed with this particular objective: from about 100 unexpected beam shutdowns per three-month operation period for a classical "all-in-series" linac, this figure falls around three to five beam interruptions in the case where a second redundant injector stage with fast switching capabilities is used, and mostly when fault-tolerance is included in the independently-phased linac via fast fault-recovery scenarios. Nevertheless, the obtained absolute figures remain highly questionable, because of the somewhat crude modelling used for such a complex system, and because of the lack of a well-established component reliability figures database.

Having a look at present high-power hadron facilities – like the SNS, not specifically designed for reaching a high reliability – it appears that the experienced number of beam trips longer than 1 second is much higher, by at least one order of magnitude [16], showing that there is still a long way to go on this topic. But on the other hand, facilities like ESRF, which is very much concerned by the reliability issue, prove that overall MTBF of several days can already be obtained routinely [17], leading to an equivalent of less than 20 beam interruptions per three-month operation, this figure being improved year after year.

As a conclusion, it seems at least not completely unrealistic to approach and ultimately reach the ADS accelerator reliability goal. It will imply, as underlined before, to include in the linac design de-rating, redundancy and fault tolerance, to focus the work on more detailed and relevant reliability studies (such activities are planned within FP7), and after the machine construction, to have a few years of commissioning and training to identify and fix the weak elements. Approaching the goal "from the other side", i.e. relaxed specifications on beam trip numbers and their durations by appropriate design measures in the target/reactor system, would also help. Some first steps have been already taken in this direction, as mentioned earlier.

Related R&D activities and perspectives

A huge R&D effort has been performed during the EUROTRANS project, including activities on the injector side and the superconducting linac side. A brief summary of the main achievements and conclusions is proposed here after.

In past years, the CEA Saclay SILHI source has been successfully used for several week-long reliability tests at currents of 30 mA, showing no beam stops and occasional sparks in the extraction region, causing no beam interruptions [18]. In the EUROTRANS context, these tests are planned to be extended using the 3 MeV IPHI four-vane 352 MHz RFQ [19] for a two-month long-run reliability beam test. The IPHI RFQ is still presently under final construction, mainly due to delays encountered relating to technological difficulties, particularly with regard to brazing procedures. Waiting for the final results of the reliability test, a preliminary conclusion on this topic is that such high frequency four-vane RFQ are very difficult to build, and that the alternative of a 176 MHz injector based on a less demanding four-rod RFQ should be explored. Within the injector context, a 19-gap superconducting 352 MHz low-energy CH prototype, first of its kind, has also been successfully built and tested at IAP Frankfurt in vertical cryostat, with excellent measured gradients of 7 MV/m. The cavity has been then tested in a horizontal cryostat with its associated

tuners. Activities will be pursued in the following years, with the construction of a new optimised prototype cavity, its test under realistic conditions (horizontal cryostat, high RF power), and ultimately with beam at GSI. More information can be found in [20] and [21].

Many R&D activities have also been performed in the main superconducting linac area, both by CNRS IPN Orsay and INFN Milano. A 352 MHz spoke cavity has been successfully tested at 4 K and 2 K in an "accelerator-like" horizontal cryostat configuration, fully equipped with its tuning system, magnetic shield, RF power coupler, and fed by a 10 kW 350 MHz solid-state amplifier and its associated digital LLRF loop. RF couplers have been successfully conditioned up to 10 kW in TW mode, with only a few easily processed multi-pacting barriers above 7.5 kW [22]. The tuning system, equipped with two piezo-actuators, has been validated together with the digital low level RF control system, reaching a field and phase stability respectively better than 1% and 0.5° at 2σ. In the fault-recovery scenario context, preliminary experiments have also been performed to test the fast cavity detuning procedure, with very good results (~1 kHz detuning in less than 5 ms). These activities will be pursued within FP7, focusing on the detailed design of a MYRRHA-like spoke cryomodule, and on the choice of the optimal operation temperature of such cavities (2 or 4 K). Finally, one can note that multi-spoke cavities have also been identified as serious alternative candidates for the high-energy section of the linac, even if the technology is not yet mature enough. Concerning this high-energy section, a prototypical 700 MHz cryomodule [23], funded by the EUROTRANS project, has been designed from scratch, built and installed in a former cyclotron pit at IPN Orsay. It contains a five-cell β 0.5 elliptical superconducting, equipped with its blade tuner system, and fed by a 80 kW Thales Electron Devices® IOT by means of a 150 kW power coupler and its associated door-knob transition. Part of the system has been successfully tested, and activities will be pursued in the following months to better evaluate the efficiency, but above all the reliability, of such an accelerating device. In particular, the capability of the piezo-based tuning system coupled with the digital LLRF I/Q feedback loop and the microphonics influence on the cavity resonance frequency will be estimated. Experimental results will be compared to MATLAB Simulink® simulations of the cavity's behaviour. Last but not least, this experiment set-up will also be able to provide a testing bench for specific sequences of the XT-ADS fast fault-recovery reference scenario, which will be the focus of FP7 activities in this area. More information on both spoke and elliptical activities can be found in [24].

Conclusion

A reliability-oriented superconducting linac has been identified as the reference solution for the European ADS concept, and an advanced design of the machine is proposed for the MYRRHA/XT-ADS project, composed by a 17 MeV injector, possibly doubled, followed by independently phased modular superconducting cavities with fault tolerance capability. Numerous R&D efforts have been performed during the EUROTRANS project, with very successful results and conclusions. These activities will be pursued within FP7, focusing on several main aspects: design consolidation, investigations on a 176 MHz injector alternative, experiments on fault recovery scenarios and several activities on system optimisation (operating cryogenic temperature, RF system optimisation with special focus on 700 MHz solid-state amplifiers, more detailed and relevant reliability analyses…). The goal is be to be ready for the actual construction of MYRRHA, foreseen to start in 2015.

References

[1] European Technical Working Group, *The European Roadmap for Developing ADS for Nuclear Waste Incineration*, ISBN 88-8286-008-6, ENEA (2001).

[2] Billebaud, A., *et al.*, "The GUINEVERE Project for ADS Physics", *Proc. of GLOBAL 2009*, Paris, France.

[3] Aït Abderrahim, H., *et al.*, "MYRRHA: A Multipurpose Accelerator Driven System for Research and Development", *Nucl. Instr. and Meth. in Phys. Res.* A, 463, pp. 487-494 (2001).

[4] Biarrotte, J-L., A.C. Mueller, *et al.*, "A Reference Accelerator Scheme for ADS Applications", *Nucl. Instr. and Meth. in Phys. Res.* A, 562, pp. 565-661 (2006).

[5] Biarrotte, J-L., *et al.*, EUROTRANS WP1.3 Final Deliverable, DEL n°1.74, 2010 (forthcoming).

[6] Zhang, C., *et al.*, "Conceptual Studies of the EUROTRANS Front End", *Proc. PAC 2007*, Albuquerque, USA.

[7] Ratzinger, U., R. Tiede, "Status of the HIIF RF Linac Study Based on H-mode Cavities", *Nucl. Instr and Meth. in Phys. Res.* A, 415, pp. 229-235 (1998).

[8] See *http://irfu.cea.fr/Sacm/logiciels/index.php*.

[9] Duperrier, R., *et al.*, "Frequency Jump in an Ion Linac", *Phys. Rev. ST Accel. Beams*, 10, 084201 (2007).

[10] Rimpault, G., *et al.*, EUROTRANS DM1 Final Deliverable, DEL n°1.70, 2010 (forthcoming).

[11] Biarrotte, J-L., *et al.*, "Beam Dynamics Studies for the Fault Tolerance Assessment of the PDS-XADS Linac Design", *Proc. HPPA 2004*, Daejeon, Korea.

[12] Biarrotte, J-L., D. Uriot, "Dynamic Compensation of an RF Cavity Failure in a Superconducting Linac", *Phys. Rev. ST – Accel. & Beams*, Vol. 11, 072803 (2008).

[13] Piquet, O., *et al.*, EUROTRANS Task 1.3.4 Final Deliverable, DEL n°1.66 (2008).

[14] Burgazzi, L., P. Pierini, "Reliability Studies of a High-power Proton Accelerator for Accelerator-driven System Applications for Nuclear Waste Transmutation", *Reliability Eng. & Systems Safety*, Vol. 92, n° 4, pp. 449-463 (2007).

[15] Brucker, R., "Integrated Reliability Analysis of the EUROTRANS Accelerator", these proceedings.

[16] Galambos, J., *et al.*, "Commissioning Strategies, Operations and Performance, Beam Loss Management, Activation, Machine Protection", *Proc. ICFA HB 2008*, Nashville, USA.

[17] Hardy, L., *et al.*, "Operation and Recent Developments at the ESRF", *Proc. EPAC 2008*, Genoa, Italy.

[18] Gobin, R., *et al.*, "Saclay High Intensity Light Ion Source Status", *Proc. EPAC 2001*, Paris, France.

[19] Beauvais, P-Y., "Recent Evolutions in the Design of the French High Intensity Proton Injector (IPHI)", *Proc. EPAC 2004*, Lucerne, Switzerland.

[20] Podlech, H., *et al.*, "Recent Developments on Superconducting CH-structures and Future Perspectives", *Proc. LINAC 2008*, Victoria, Canada.

[21] Podlech, H., *et al.*, "The 17 MeV Injector for the EUROTRANS Proton Driver", these proceedings.

[22] Rampnoux, E., *et al.*, "RF Power Coupler Development for Superconducting Spoke Cavities at IPN Orsay", *Proc. PAC 2009*, Vancouver, Canada.

[23] Barbanotti, S., *et al.*, "Design of the Prototypical Cryomodule for the EUROTRANS Superconducting Linac for Nuclear Waste Transmutation", *Proc. EPAC 2008*, Genoa, Italy.

[24] Bouly, F., S. Bousson, *et al.*, "Developments of 350 MHz and 700 MHz Prototypical Cryomodules for the EUROTRANS ADS Proton Linear Accelerator", these proceedings.

The 17 MeV injector for the EUROTRANS proton driver

H. Podlech, M. Busch, F. Dziuba, U. Ratzinger, H. Klein, R. Tiede, C. Zhang
Institute for Applied Physics (IAP), Goethe University
Frankfurt, Germany

Abstract

Accelerator-driven systems (ADS) for nuclear waste transmutation require proton drivers with energies between 600 and 800 MeV and beam currents of several mA for demonstrators and up to 25 mA for large industrial systems. Within the EUROTRANS project a 600 MeV linac has been designed to meet the stringent requirements regarding reliability, availability and extreme low beam losses. The first accelerating section accelerates the beam to 17 MeV at the injection point into the main linac. This EUROTRANS front end consists of a 3 MeV four-vane RFQ, two short room temperature (RT) CH-cavities and four superconducting CH-cavities. CH-cavities are multi-cell structures providing high real estate gradients with moderate peak fields. The use of multi-cell cavities reduces the number of cavities and their sub-systems like amplifiers, tuner and coupler significantly. The status of the injector design including prototype measurements is presented.

Introduction

In the European Union there are presently about 145 nuclear power plants in operation. The annual amount of electric energy is about 850 TWh which corresponds to 35% of the total electric energy. This results in the production of 2 500 tonnes of spent fuel per year [1]. A small fraction of this nuclear waste, i.e. long-lived fission fragments (~3 t) and minor actinides (~3.5 t) are considered to be extremely problematic because of the long decay times and their high radiotoxicity. It is well known that the quest of minimising the long-term environmental impact of this nuclear waste inventory is one of the most challenging scientific subjects in nuclear energy research. In principle, there are two different options to deal with it, long-term storage in geologically stable caves or reducing the amount of waste by using appropriate partitioning and transmutation technologies. Transmutation of nuclear waste based on accelerator-driven systems (ADS) is one of the most promising concepts to reduce radiotoxicity and life time [2].

The driver accelerator for an accelerator-driven system like EUROTRANS has to deliver a continuous wave proton beam with a beam power ranging from about 1.5 to 16 MW depending on the specific project. Obviously this accelerator belongs to the class of high-power proton accelerators (HPPA). The main challenge of this proton driver is the extreme reliability to avoid unwanted beam trips which can lead to thermal stress in the target and the cladding of the reactor core. The required CW operation is another challenge. Although there are powerful CW proton cyclotrons in operation like at PSI [3] it has been decided to use a proton linac. The main advantages of the linac solution are given in the following list:

- more flexibility in final energy;
- possibility for energy upgrades;
- higher reliability with independently phased cavities;
- lower beam losses;
- less activation.

The required CW operation is another challenge especially for the low energy part using room temperature RF structures. The main acceleration will be provided using superconducting RF cavities. These cavities will decrease the operational costs significantly compared to a fully on room temperature structures based linac. Additionally the beam aperture can be chosen much larger in superconducting cavities which lead to lower beam losses and less activation.

The conceptual design for the driver has been developed during the PDS-XADS-project [4]. It is a very modular and upgradeable machine which can be used for an experimental as well as for an industrial system. It shows excellent potential for high reliability and high efficiency because of the superconducting operation. The linac consists of two 17 MeV injectors, an intermediate and a high energy section consisting of independently phased superconducting spoke type and elliptical cavities. Figure 1 shows the conceptual design of the EUROTRANS reference design.

General injector layout

The injector of the EUROTRANS proton driver linac consists of an Electron Cyclotron Resonance Ion Source (ECRIS), an Radio Frequency Quadrupole (RFQ) accelerator, two short RT Crossbar H-mode (CH) cavities and four SC CH cavities providing 17 MeV total energy gain [5]. Figure 2 shows the schematic layout of this injector.

Presently an ECR source with an extraction voltage of 50 kV is foreseen. At CEA Saclay the SILHI source showed reliable operation with beam currents exceeding 100 mA [6]. In principle it is also possible to use volume sources which provide typically beams with smaller emittance.

Figure 1: Scheme of the proposed 600 MeV EUROTRANS proton driver

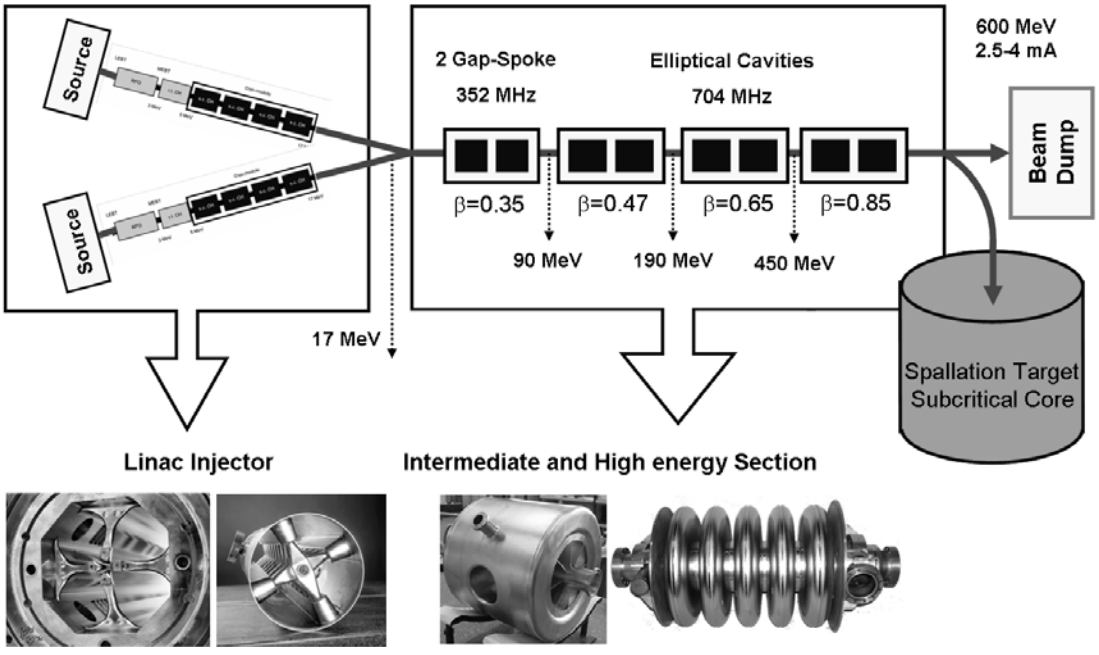

Figure 2: Layout of the 17 MeV injector for the EUROTRANS proton driver

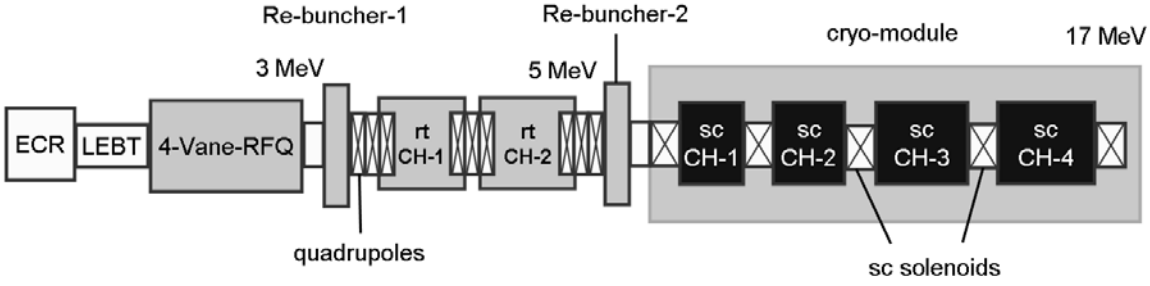

As RFQ RF-structure a four-vane RFQ has been chosen because this structure seems to best suited for CW operation at the frequency of 352 MHz. Presently a 3 MeV, 100 mA prototype RFQ is under construction.

The beam is then injected into two short RT CH cavities to increase the beam energy to 5 MeV for the injection into the superconducting part which consists of four CH cavities. The advantage of using multi-cell cavities like the CH cavity is the much higher real estate gradient and the reduction of the number of cavities and their related sub-systems like tuners and amplifiers to increase the reliability of the whole system. Because of the low energy and the large energy gain per cavity (2.5-3.5 MeV) each CH-cavity has an increasing cell length (graded β-structure).

3 MeV RFQ

The first RF accelerating structure is an RFQ accelerator which can focus, bunch and accelerate the beam. The input energy has been set to 50 keV. This value is high enough to avoid space charge effects in the low energy beam transport (LEBT). On the other hand it is low enough for safe and reliable operation. The electrode voltage of the RFQ is 65 kV which results in low peak

fields with a Kilpatrick value of 1.7. The emphasis of the design was on the minimisation of particle losses, emittance growth and on maximum expected reliability. The length of the RF structure is 4.3 m. The modulated electrodes have 348 cells. Figure 3 shows the electrode parameters along the vanes and Table 1 summarises the main RFQ parameters.

Figure 3: Vane parameters of the 3 MeV RFQ

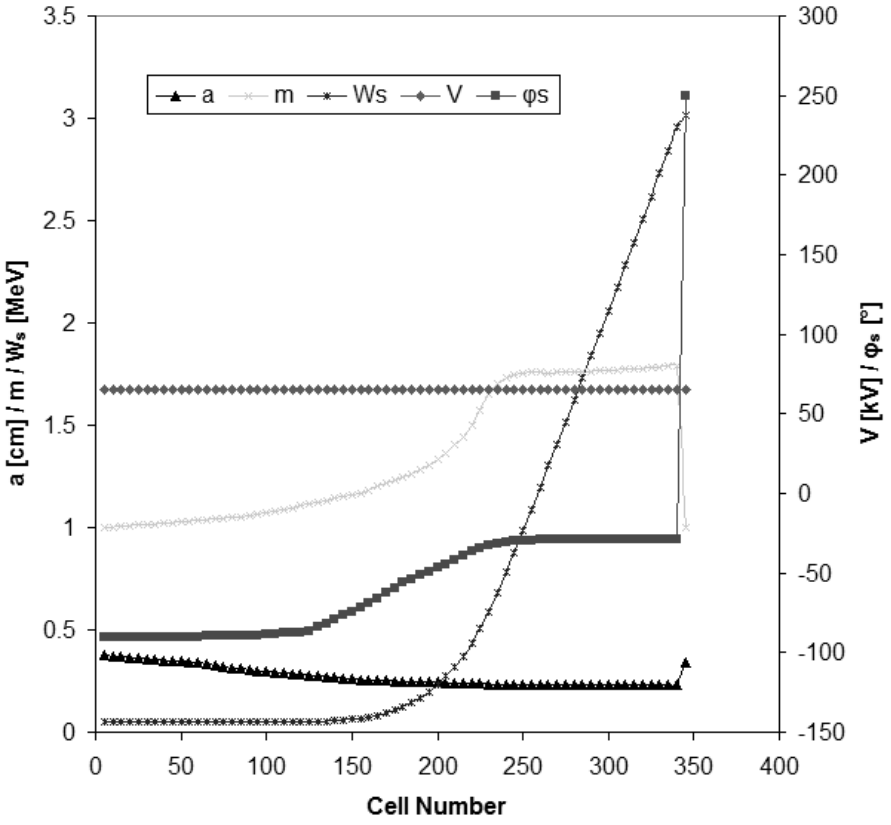

Table 1: Main parameters of the 3 MeV RFQ

RFQ type	Four-vane
Frequency (MHz)	352
Input energy (keV)	50
Output energy (MeV)	3
Design current (mA)	5
Length (m)	4.3
Vane voltage (kV)	65
Trans. input emittance (π mm mrad)	0.2
Output emittance X/Y (π mm mrad)	0.20/0.21
Max. modulation	1.8
Transmission (%)	≈100

CH drift tube linac

The CH structure is a multi-cell cavity and belongs to the family of H mode cavities which are operated in an H_{n1}-mode. This new structure has been named CH structure because of its cross-bar geometry and the H_{21}-mode. The CH structure can be used between 150 MHz and 700 MHz. The

typical energy range of the CH structure is between 3 and 100 AMeV. One main feature of H-mode drift tube cavities which boosts the efficiency and make long lens free multi-cell cavities possible is the Kombinierte Null-Grad-Struktur (KONUS) beam dynamics [7]. The KONUS concept reduces the transverse RF defocusing by using 0° main accelerating sections. A KONUS-period consists of three sections with separate functions. The first section consists of a few gaps with a negative synchronous phase of typically -35° and acts as a rebuncher. The beam is then injected into the 0° section with a surplus in energy as compared with a "synchronous" particle. This multi-gap main accelerating section is then followed by transverse focusing elements which are magnetic quadrupole triplets or superconducting solenoids. In case of the EUROTRANS the cavities house only the rebuncher and the main acceleration section. The transverse focusing elements will be located in the inter-tank sections which simplifies the cavity production.

The first part of the drift tube linac consists of two 352 MHz RT CH cavities providing a voltage of 1 MV each. The gradient has been limited to about 2 MV/m to reduce the thermal load of the cavities below 70 kW/m which increases operation safety and reliability. Figure 4 shows the geometry of the RT CH cavities and the distribution of RF losses, Table 2 summarises the main parameters.

Figure 4: Geometry of the first and second RT CH cavity (left) and the power loss distribution (right)

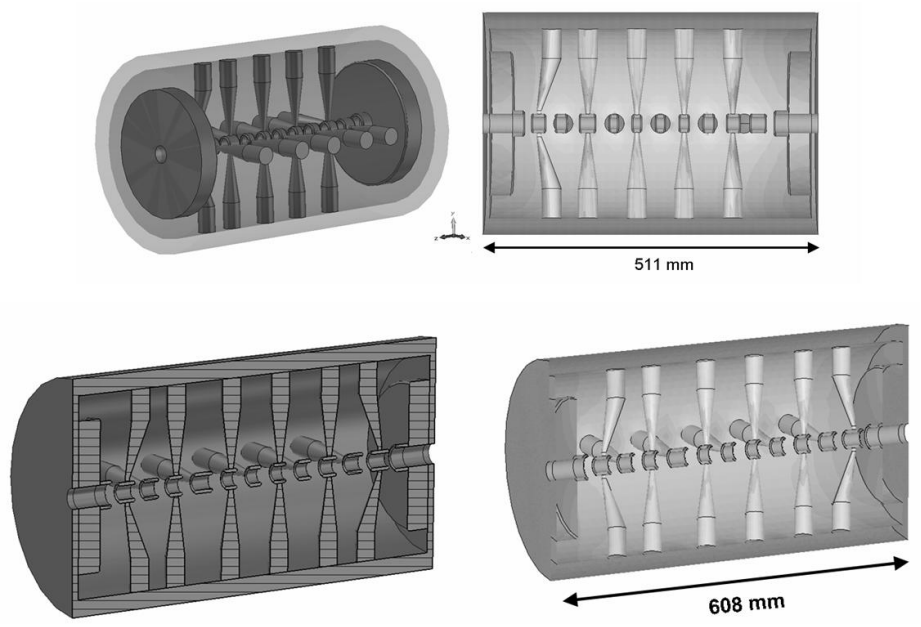

Table 2: Main parameters of the two RT CH cavities

Cavity type	CH	CH
Frequency (MHz)	352	352
Length (mm)	511.5	608.5
Inner diameter (mm)	289	292
Lens diameter (mm)	220	220
Z_{eff} (MΩ/m)	95	112
RF power (only losses) (kW)	35	38
Power density max. (W/cm²)	16	13.5
Effective voltage (MV)	1.16	1.30
Accelerating cells	11	12

The main accelerating section of the injector linac (5-17 MeV) consists of four superconducting CH cavities with superconducting solenoids as focusing elements in between. The superconducting CH cavity is the first multi-cell cavity for the low and intermediate energy range. Compared with more conventional half-wave resonators the number of drift sections between the cavities is significantly reduced resulting in a much higher real estate gradient. Additionally the number of cavities and related sub-systems is reduced by a factor of 5-10.

A prototype cavity has been developed and tested successfully at IAP during the last years [8]. Effective accelerating gradients of 7 MV/m have been achieved. Figure 5 shows the CH cavity and the measured performance. The measured Q-value and the gradient are almost a factor of two higher than is required for EUROTRANS [9].

Figure 5: Superconducting CH prototype cavity (left), measured performance of the cavity (right)

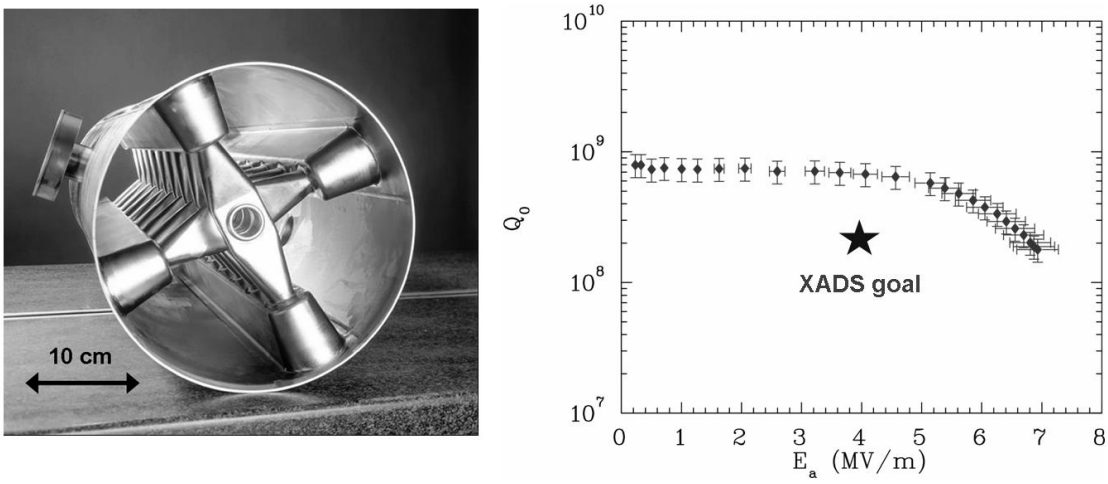

Based on the experience with the prototype cavity the geometry has been further optimised. The stem geometry of the CH cavities has been changed to accommodate larger power couplers up to several 10 kW CW between the stems. Via integration of inclined stems the end cell length and unwanted drift sections could be reduced significantly while reaching a high beam quality. The minimisation of unnecessary drift sections reduces the total cavity length by about 20% without changing the voltage and peak fields.

The cavity tuning will be done by capacitive tuners through the girders. Two different types of tuner are currently foreseen. For coarse voltage and frequency adjustment during fabrication cylindrical fixed tuners will be used. Additionally, bellow tuners are foreseen with a tuning range of several hundred kHz. For example, the first superconducting EUROTRANS CH cavity includes seven fixed cylindrical tuners, one fast membrane tuner to control fast frequency changes due to microphonics and two slow bellow tuners to readjust the frequency at 4.2 K. The advantage of these membrane tuners is the minimisation of the required longitudinal space which would be essential by using a tuner system pushing on the end cells.

Presently a 325 MHz seven-cell superconducting CH cavity is under fabrication. This cavity will be fully equipped with helium vessel, tuning system and high power coupler. It is planned to test the cavity with a high current beam under realistic conditions at GSI/Darmstadt. The frequency of 325 MHz has been chosen because it is the higher harmonic of the operation frequency of the UNILAC heavy ion linac (108.4 MHz). Figure 6 shows the geometry of this new cavity.

The geometry of the EUROTRANS CH cavities is very close to the geometry of the 325 MHz cavity. Only the diameter, the number of cells and the individual cell length has to be adjusted.

Figure 6: 325 MHz superconducting CH cavity which is presently under fabrication

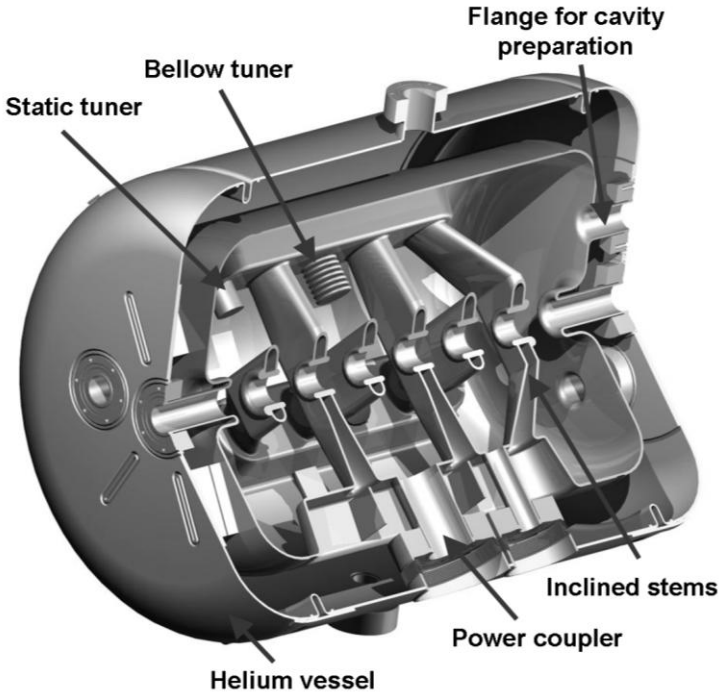

Acknowledgements

This work has been supported by Gesellschaft für Schwerionenforschung (GSI), BMBF contract No. 06F134I and EU contract No. 516520-FI6W.

References

[1] *The European Roadmap for Developing ADS for Nuclear Incineration and Energy Production*, Technical Report, ISBN 88-8286-008-6, ENEA (2001).

[2] Rubbia, C., "A High Gain Energy Amplifier Operated with Fast Neutrons", *Proc. of the International Conference on Accelerator Driven Transmutation Technologies and Applications*, AIP Conf. Proc. 346 (1994).

[3] Schmelzbach, P.A., "Upgrade of the PSI Proton Accelerator Facility", *Proc. of the International Workshop on Utilisation and Reliability of High Power Proton Accelerators*, Mol, Belgium, 6-9 May 2007, OECD/NEA, Paris (2008), pp. 125-133.

[4] Biarrotte, J-L., *et al.*, "A Reference Accelerator Scheme for ADS Applications", *Nucl. Instr. and Meth. in Phys. Res. A*, 463, pp. 487-494 (2006).

[5] Zhang, C., *et al.*, "Conceptual Studies of the EUROTRANS Front-end", *Proc. of the International Particle Accelerator Conference*, Albuquerque, NM, USA, pp. 3274-3276 (2007).

[6] Hollinger, R., *et al.*, "High-current Proton Beam Investigations at the SILHI-LEBT at CEA/Saclay", *Proc. of the Linear Accelerator Conference 2006*, 232-236 (2006).

[7] Ratzinger, U., *Proc. 1991 Particle Accelerator Conference*, pp. 567-571 (1991).

[8] Podlech, H., *et al.*, "Superconducting CH-Structure", *Phys. Rev. ST Accel. Beams,* 10, 080101 (2007).

[9] Podlech, H., *et al.*, "New Cavity Shape Developments for Low Beta Applications", *Proc. of International Conference on Superconducting RF*, Berlin, Germany, pp. 473-476 (2009).

Developments of 350 MHz and 700 MHz prototypical cryomodules for the EUROTRANS ADS proton linear accelerator

F. Bouly, S. Bousson, J-L. Biarrotte, P. Blache, F. Chatelet, C. Commeaux, P. Duthil, C. Joly, J. Lesrel, G. Olry, E. Rampnoux, H. Saugnac
IPNO, Orsay, France

S. Barbanotti*, A. Bosotti, R. Paparella, P. Pierini
INFN/LASA, Milano, Italy
Present address: FNAL, Batavia, IL, United States

Abstract

Accelerator-driven systems (ADS) are being considered for their potential use in the transmutation of nuclear waste. Such a device typically requires a 600 MeV to 1 GeV accelerator delivering a beam intensity of a few mA. Because of the induced thermal stress to the subcritical core, the high-power proton linac will have to fulfil stringent reliability requirements. Working packages of the EUROTRANS project are dedicated to the design, realisation and tests of prototypical cryomodules for the "intermediate" and high-energy sections of the linac.

Spoke resonators are capable of efficiently accelerating protons intense beams in the "intermediate" energy section of such accelerators. IPN Orsay has been studying such cavities as well as their associated sub-systems for several years. In this paper, we report on the latest developments on spoke cavities as well as final complete test in a horizontal cryostat dedicated to spoke cavities.

The high-energy section will be composed of five cells elliptical cavities. A prototypical cryomodule, equipped with a $\beta = 0.47$ superconducting cavity and its tuning system, developed by INFN Milano will be tested mid-2010 at IPN Orsay. Experiment aims to evaluate the cavity performances but above all the cryomodule reliability to fulfil ADS needs. We report here the RF and cryogenics developments of this module as well as preliminary considerations regarding feedback controlling aspects for "fast fault recovery" scenarios.

Introduction

The design of the MYRRHA proton accelerator for the European ADS Demonstrator, exposed in [1] leads to a superconducting linac in CW mode. To minimise the thermal stress inside the transmutation reactor, the number of unwanted beam trips longer than 1 second should not exceed five per three-month operating cycle [2]. This extremely high reliability requirement can immediately be identified as the main technological challenge to achieve.

The intermediate energy section of the linac (from 20-100 MeV) will be composed of 352 MHz spoke resonators. These accelerating structures have been under development in several laboratories for the past 15 years, but only a few prototypes have been fabricated and tested. The promising results on the achievable accelerating gradients in FermiLab [3] and Orsay [4] lead us to push the investigations on spoke resonators one step further with the construction and test of a spoke prototype cryomodule, in view of accelerator-like configuration tests. This development was possible due to the existing synergy between several high-power proton accelerator developments, such as EURISOL and EUROTRANS. The cryomodule integrates a β 0.15 single spoke cavity equipped with all its ancillaries: helium tank, power coupler and cold tuning system. The results of this integrated test are described in the first part of this paper.

The linac high-energy part (from 100-600 MeV) will be composed of five-cell superconducting cavities ($\beta = 0.47$ and $\beta = 0.65$) operating in CW at 704.4 MHz. A prototypical cryomodule is presently being built in view of a full scale cavity test in an accelerator coupling configuration. The status of R&D activities concerning the cryomodule as well as the power couplers design will be recounted in the following lines. Experimental perspectives and a preliminary discussion in terms of reliability evaluation of the whole device, with its digital low-level RF (LLRF) feedback loop system, will conclude this paper.

352 MHz superconducting accelerating module

Spoke cavities are superconducting accelerating structures which are very promising for accelerating hadron beams up to 150 MeV/u (and more). Their main advantages are the capability to deliver high accelerating gradients, the possibility to have multi-cell structures, leading to a high real-estate gradient, and their natural stiffness (important parameter in the case of a pulsed operation to lower the effect of Lorentz forces detuning). As a matter of fact, such cold and modular cavities can produce, especially in the case of high duty cycle machines, very good accelerating performance, together with very high acceleration flexibility and reduced operation cost. For these reasons, spoke-type cavities can be found nowadays in several reference designs of high-power linear accelerators, like EURISOL [5], HINS [6], Project X [7] or ESS [8,9]. Up to now, none of them have been used in an accelerator, but the very promising results of the spoke prototypes have been obtained in several laboratories. Two single-gap spoke prototypes (β 0.15 and β 0.35) have been developed, fabricated and tested in IPN Orsay. The cavities' geometry and RF parameters are detailed in [10]. The maximum achievable field for the low β cavity (Figure 1) when tested in vertical cryostat was 4.8 MV/m, a performance lower than the β 0.35 prototype, leading us to suspect the presence of a rather important defect on the RF surface. For the integrated test in the cryomodule, we took the low β cavity, the only one to be equipped with its helium tank.

The spoke cold tuning system (CTS)

The spoke CTS is an adaptation of the CTS we developed for the elliptical 700 MHz five-cell cavities. It consists in a mechanical system (Figure 2) driven by a cold stepping gear-motor operating under vacuum. The motor drives a ball screw, linked to a double lever arm mechanism which can act on four rods attached to the cavity. The design was optimised to obtain high rigidity,

Figure 1: The IPN Orsay β 0.15 spoke prototype: 3-D modelling and picture

Figure 2: Cold tuning system for spoke resonators: schematics and picture

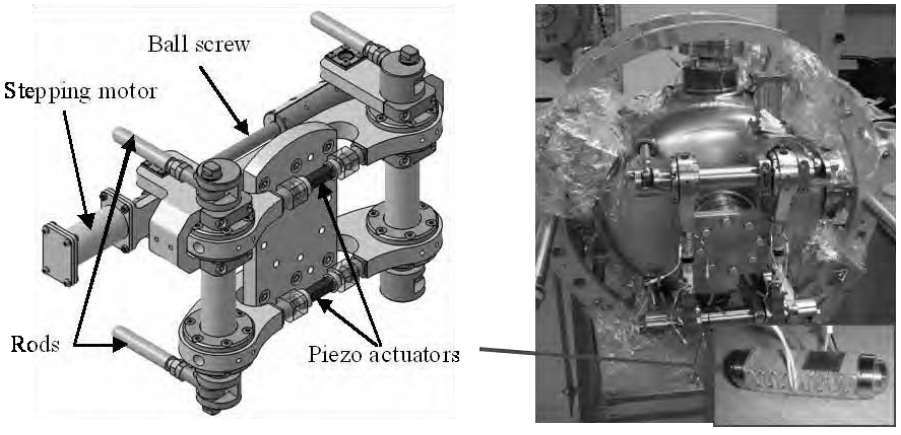

lowest possible weight and cost. The system also includes the possibility to use piezoelectric actuators for the fast compensation of frequency shifts. The theoretical resolution of the system is 1 nm per micro-step, giving a frequency resolution of 1 Hz. Another important requirement is the CTS mechanical rigidity, which should be much higher than the cavity rigidity in order to keep all the longitudinal displacement available for the cavity deformation. The β 0.15 spoke cavity axial rigidity was estimated at 6 kN/mm. Calculations performed with CATIA give a CTS rigidity estimation of 162 kN/mm. This high value allows 96% of the CTS longitudinal displacement to be effectively seen by the cavity. The cold tuning system was first tested at room temperature and then at 4.2 K in the spoke cryomodule. This first frequency regulation in cold conditions was achieved successfully, with a regulation better than ±10 Hz over several hours. No mechanical problem was observed, except a minor hysteresis.

The piezoelectric actuator operation was also tested successfully under cold conditions, with a very good reproducibility and no hysteresis. The measured sensitivity was about 100 Hz/μm, as shown in Figure 3. Moreover, some preliminary fast detuning tests were performed at room temperature, in the view of the fault recovery scenarios. A fast 1.5 kHz cavity detuning was performed in less than 10 ms using the piezo actuators at 50 V, with no significant instabilities during the transient. Given the piezo degraded efficiency at cryogenic temperature (about 10%), a fast 500 Hz cavity detuning can be expected at 4 K with the nominal 150 V excitation. This is enough to immediately put the spoke cavity off resonance by three times the bandwidth.

Digital low level RF (DLLRF) developments

A DLLRF control system has been developed (Figure 4). It is mainly composed of a down converter system, which allows to translate the amplitude and phase information from 352.2 MHz down to

Figure 3: CTS operation using piezo actuators at 4.2 K

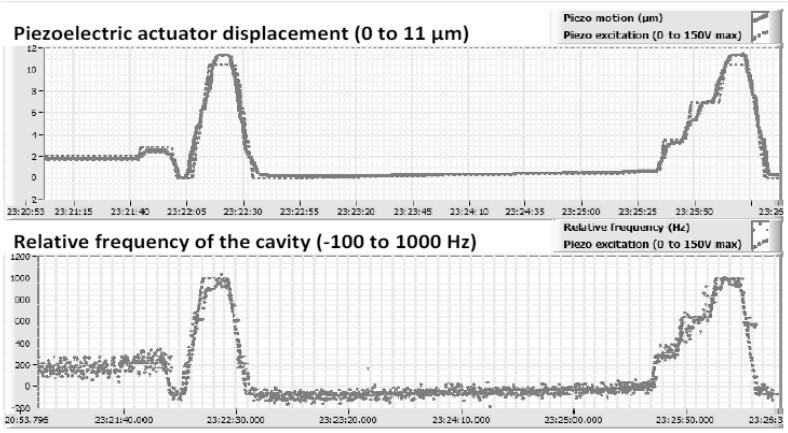

Figure 4: Scheme of the digital feedback system

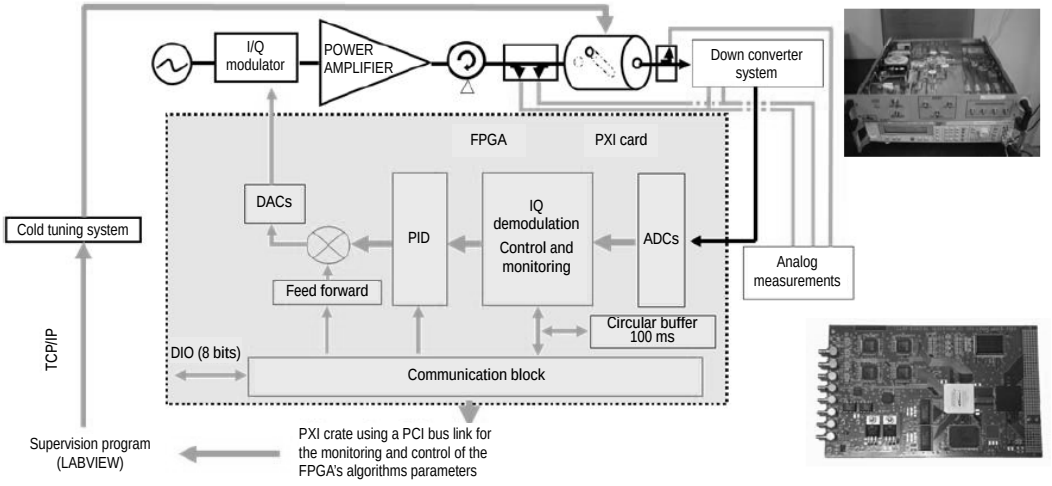

10 MHz for digitalisation, associated to a PXI board containing two FPGA ships, one for the communication with the PCI bus and another for digital IQ demodulation, plus a circular buffer to record events during 100 ms. Two prototypes of such digital boards have been developed by IPN Orsay, in collaboration with LPNHE. This digital LLRF system has been first tuned and tested successfully at room temperature with a copper model of the spoke cavity. It was then tested at 4.2 K on the β 0.15 spoke cavity equipped with its cold tuning system inside the spoke cryomodule. These first low power measurements have shown that for a short time, the achieved regulation precision is very good, with about ±0.1° rms in phase, and ±0.2% rms in amplitude.

The spoke power couplers

A 352 MHz capacitive power coupler has been developed for the two-gap spoke cavities to be mounted on the 56 mm diameter port. The coupler geometry is coaxial, at 50 Ω using a warm disk ceramic window. The coupler is designed to be able to transfer 20 kW of RF power to the cavity. Two pipes located on the window outer diameter give the possibility to water-cool the ceramic. Several window geometries were studied: cylindrical, disk (with and without chokes), travelling wave. For each geometry, the HFSS® software was used to calculate the RF parameters, the surface field on the ceramics, the bandwidth and the RF losses. Finally, the design based on a

disk ceramic without choke was chosen because it was the best compromise between good RF performances and simplicity, leading to a reliable and cost-effective design. The computed S11 parameter is shown in Figure 5: a value of -57 dB is obtained at the nominal frequency. The coupler exhibits a very large bandwidth, allowing having standard fabrication tolerances.

Figure 5: Overall drawing of the 352 MHz power coupler (left) and computed S_{11} parameter (right)

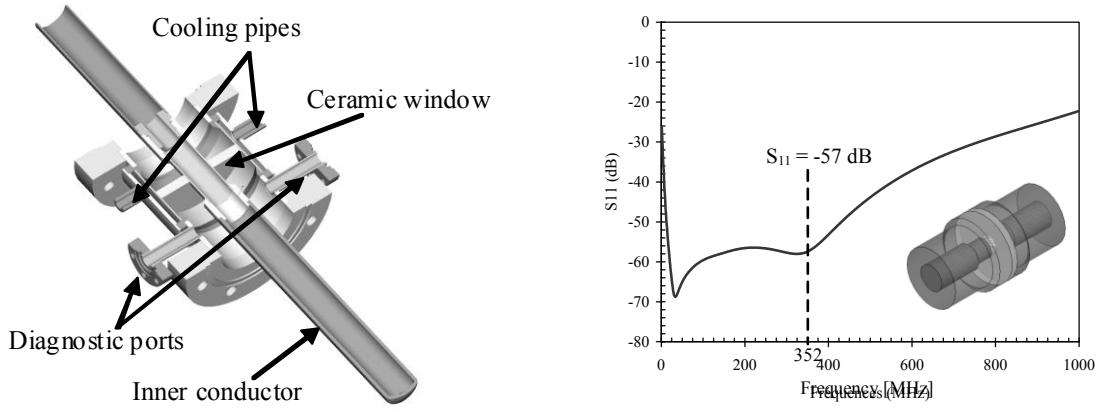

Two ceramic windows prototypes have been ordered from the SCT company. They have been characterised at low power (measurement of RF parameters) before the antenna welding. After reception of the two complete power coupler prototypes, the assembly of the conditioning test bench has been achieved after careful cleaning and final assembly of the important parts (RF ceramic windows, coaxial part between the cavity and window, conditioning cavity) in the IPN Orsay clean room.

The conditioning of the power coupler started with the warm test bench (Figure 6). This important stage consists in feeding the two power couplers mounted in series with a gradually increasing RF power, from 0 to 10 kW, step by step. The aim is to condition the RF surface to get rid of any electron emission or multi-pacting in the coupler, which strongly degrades the vacuum. At each power level preset the LabView® program switches ON the RF for 2 min 30 s and after

Figure 6: Power coupler conditioning bench and parameter monitoring

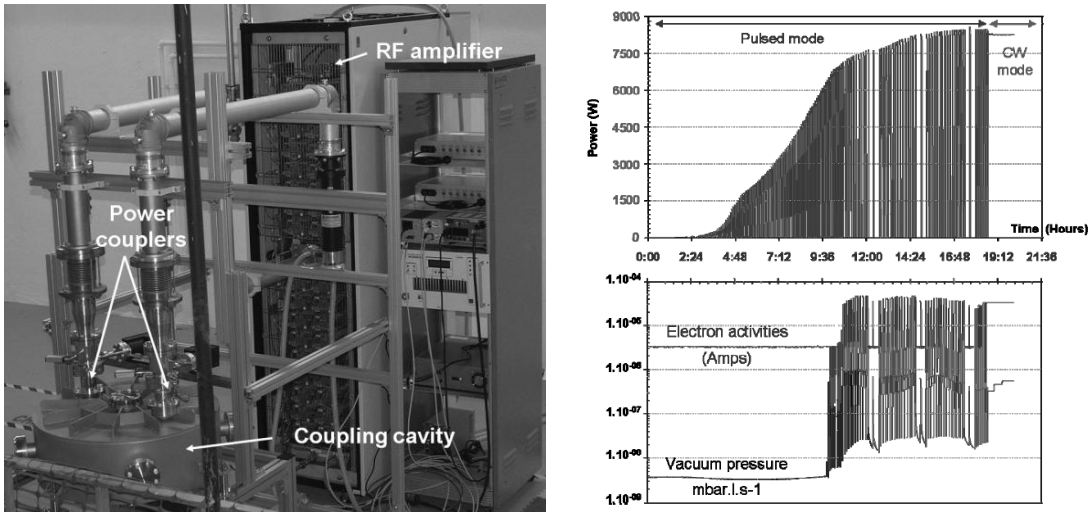

switches off the RF power during 2 min 30 s so that the vacuum goes down again; and if all parameters are right, the program passes to the higher RF power level. With this procedure, it took roughly 20 hours to condition our two power couplers (Figure 6). In certain cases of high activity the program procedure was to cut the RF power for 10 minutes, or even to go back to the previous power step, to enable the vacuum pressure to decrease. The intense electron activity was noticed from 7 kW until 8.8 kW, the maximum amount of RF power available [11].

The spoke cryomodule

To assess that spoke cavities are capable of efficiently accelerate particles with the designed performances, one key test consists in a cold test of a superconducting spoke cavity fully equipped with all its ancillary systems: helium tank, power coupler, cold tuning system. Such a test allows addressing almost all potential difficulties in the operation of a superconducting cavity in a real accelerator. The mechanical, thermal and RF behaviour of the full system is tested in a cavity configuration close to the final one in the accelerator.

The spoke cryomodule is composed of two main components (Figure 7): the vacuum tank, which is hosting the cavity and its ancillaries, a helium Dewar flask, the cryogenic piping and instrumentations and the "cold box", external to the cryomodule, which provides the module with the cryogenic fluids (liquid, gas).

Figure 7: Pictures of the spoke test cryomodule and its associated ancillaries ready for 4.2 K tests

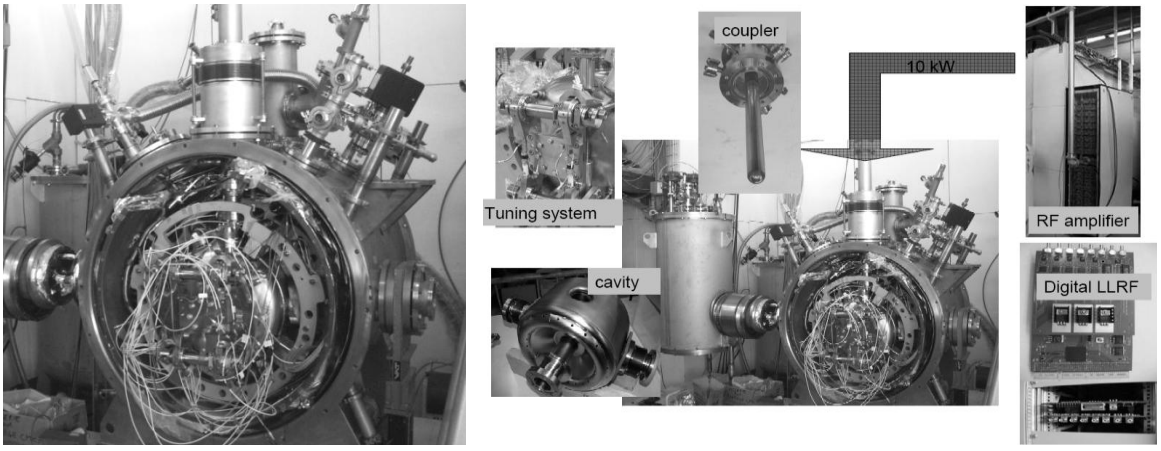

The module was designed to be a laboratory test stand to test several spoke cavity types under several configurations. It was conceived to have dimensions long and wide enough to host a fully equipped spoke cavity, low or medium β. The temperature operation point is 4.2 K but both module and cold box have the possibility to operate using a depressed helium bath to perform cavity tests at lower temperature (typically 2 K). On this prototype, the power coupler could be mounted with two different configurations: a vertical position (better for mechanical reasons), or with a 45° inclination with respect to the vertical position (potentially better for the spoke bar cooling by liquid helium).

The integrated test at high power

At IPN Orsay, the last preparation steps of this final test were done in the SUPRATech infrastructures. In the Class 10 clean room, the β 0.15 spoke cavity was prepared before its assembly. The cavity was removed from the cryomodule, underwent high pressure water rinsing at 100 bars with ultra-pure water (resistivity of 18.2 $M\Omega.cm^{-1}$). The power coupler, dismounted under the clean room laminar flow from the conditioning cavity has been mounted on the spoke

cavity. The cavity/coupler assembly was pumped out and a final leak check was performed, in order to assess the vacuum tightness of the assembly. The module final assembly was then performed: the cavity/coupler assembly was inserted into the module vacuum tank. The coupler external coaxial conductor and the below was mounted. The cavity tuner and all the instrumentations were then installed (Figure 7).

The complete assembly was then installed into the cryogenic test stand. The INFN/LNL 10 kW power amplifier was connected to the module by means of a coaxial standard rigid RF line, the cold box connected to the module cryo-fluids inputs and outputs. The 352 MHz low-level digital RF controller developed by IPN Orsay and LPNHE laboratories was used to control the RF excitation of the cavity. For this experiment, we have set the different parameters to simulate a coupler and cavity operation such as the cavity was set to accelerate a beam (i.e. operation with beam loading). The coupling factor of the antenna to the cavity was set to 1.10^6. In this configuration, but without beam, most of the incident RF power is reflected into the RF line, and the maximum achievable field in the cavity is about 1 MV/m. The main objective is to test all the RF line and the coupler up to the cavity flange at the nominal RF power.

The main results of this final experiment are the following:

- The cryogenic operation of the cryomodule was successful: modifications performed after a first cryogenic test enable to efficiently cool the entire system, including the CTS, without important temperature differences between this ancillary system and the cavity.
- The power coupler was conditioned in the configuration where the power was all reflected. Consequently, the maximum of incidental RF power was limited to 4 kW. During conditioning, the level of RF power was increased gradually up to 4 kW. Each level of RF power lasted 2 min 30 s, and if no event occurred like a break of vacuum or a too-strong electronic activity on the ceramic disc, the program passed to a following state by increasing the level of RF power. The power coupler conditioning lasted only 2 hours. During all this time, conditioning proceeded very well without being stopped by a possible vacuum defect or a too-strong phenomenon of multi-pacting. Indeed, the electronic activity remained in the neighbourhood of 1.10E-06 Amps and the level of vacuum was stabilised around 5.10E-09 mbar.l.s-1.
- The estimated Q_0 (a precise measurement is impossible with a high RF coupling) showed that the magnetic shielding was efficient and that the power coupler has no influence on the cavity dissipation at low accelerating fields.
- The cold tuning system and the digital LLRF regulation loop could operate successfully. Nevertheless, fine tuning of the whole regulation process (CTS + LLRF at high power) is still required before closing this high-power test campaign, especially at 4 K where He pressure variations in our cryostat are much larger and difficult to handle than at 2 K. This remaining work will be achieved in 2010.
- A cryogenic test at 2 K was also successfully performed, just to check the overall capability of the whole system to operate with a depressed helium bath. This configuration might be a very interesting alternative to a 4 K operation because of increased performances in terms of accelerating field and Q_0, but also in terms of regulation stability (much less He pressure variations).

700 MHz superconducting accelerating module

The development of an accelerating superconducting cavity requires the prototyping of all the auxiliary systems needed for its operation in a real environment. In this context, R&D activities involve INFN and CNRS resulting in the design and fabrication of a cryogenic real scale module dedicated to be tested in new experimental area. INFN contributed to the development of the

cryomodule and made available its β 0.47 TRASCO cavity equipped with a cold tuning system. IPN Orsay (CNRS/IN2P3) participated in the development of the cryogenic valve box, one of the power couplers and makes available its new facility SUPRATech dedicated to the preparation (chemistry, clean room) and cavity tests (experimental area set-up in progress) with an 80 kW RF power supply.

The cryomodule

The cryomodule design (see Figure 8) was performed by considering reliable aspects for the assembly, and the cavity handling, derived from the experience accumulated by the TESLA Test Facility (TTF) and the Spallation Neutron Source (SNS).

Figure 8: Scheme of the prototypical EUROTRANS 700 MHz cryomodule, with its dressed cavity inside (left); the module during vacuum leak tests at SIMIC company (right)

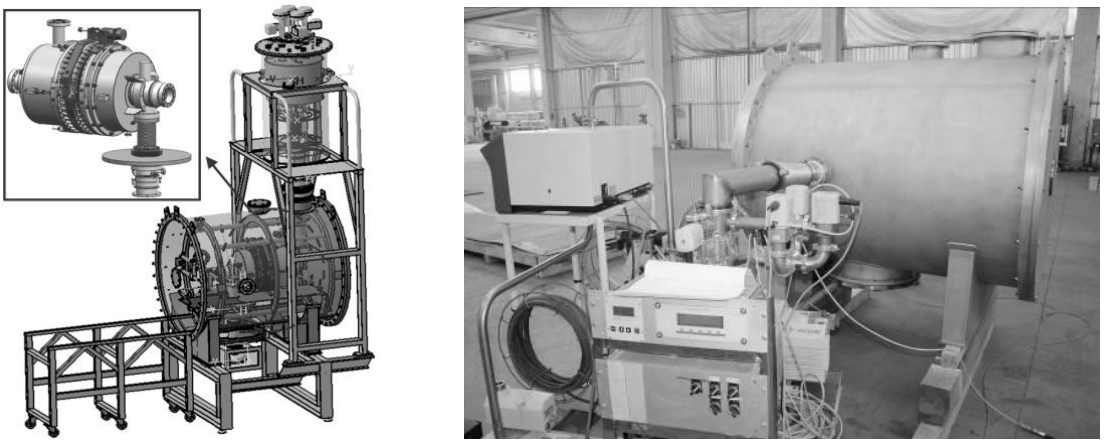

The module is 1.5 m long, for a diameter of about 1.4 m with the cold box assembled on top of it. The module was designed to operate at 2 K for a nominal accelerating gradient of 8.5 MV/m and an assumed conservative quality factor value of $Q_0 = 5.10^9$ for computations. At 2 K, the dynamic heat load had been estimated at 25 W for 4 W in static conditions. More details concerning the thermal design are given in Ref. [12]. Static losses are kept in the module by minimising the heat flow toward the 2 K helium bath. Therefore, the thermal radiation, flowing from surfaces at room temperature, is intercepted by a thermal shield at intermediate temperature (nitrogen at 77 K) and minimised by using a multi-layer insulating blanket (doubly aluminised Mylar® sheets separated by a low thermal conducting material). The cryogenic cold valve box, derived from the IPN Orsay EURISOL design, has a nominal cooling capacity of 50 W at 2 K. A 20 litre helium buffer is placed inside the box to prevent pressure perturbations in the cavity tank. The cold box thermal shield, made of copper and covered with multi-layer insulation, is able to evacuate 60 W at around 80 K.

The power coupler

Fundamental power coupler (FPC) development has been carried out at IPN Orsay. Based on the SNS power coupler design [13] it was adapted and optimised to transmit to the cavity up to 150 kW RF power at 704.4 MHz with a capacitive coupling of $Q_{ext} = 1.10^7$, adapted to the experimental needs (i.e. without the beam).

Figure 9 shows a section of the final coupler design. To ensure the waveguide geometrical transition between rectangular waveguide (WR1150) and the coaxial power coupler a "doorknob" type impedance matching structure was designed. The transition alone must have good impedance matching to enable good performances when integrated with the RF ceramic window.

Figure 9: Section view of the power coupler and its fabricated elements: heat exchanger, RF window + antenna, doorknob transition

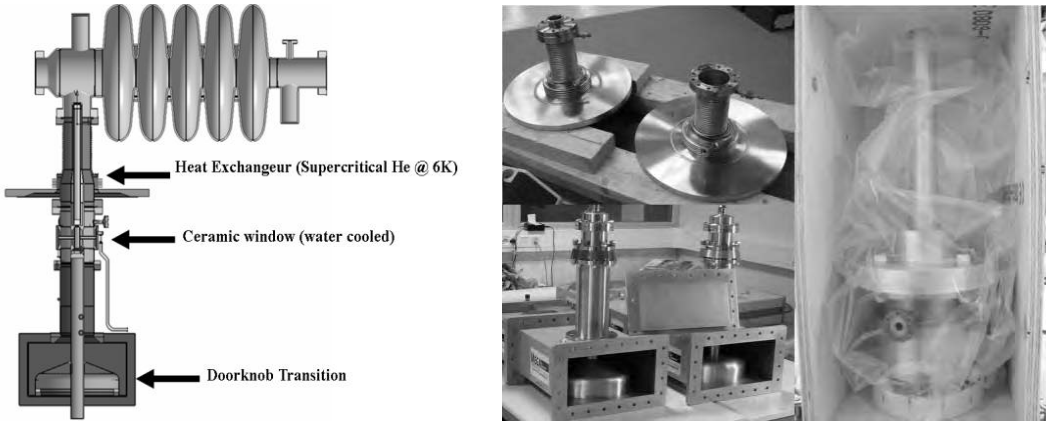

The ceramic window is the critical element in the power coupler. It has to ensure the tightness between air environment and vacuum environment but also the good transmission of the RF power through the coaxial waveguide. This vacuum tightness is achieved thanks to a ceramic disc, which is made of 97% of alumina and dug in its centre. Brazed at both time on the external and internal conductors, the ceramic part ensures the vacuum tightness. But it also ensures the internal conductor's mechanical position (antenna), centred with regard to the external conductor, and consequently forming the RF window.

In order to minimise thermal losses (Joule and dielectric losses), the inner conductor and the ceramic window are water-cooled [14]. The FPC outer conductor RF and static losses are removed by a supercritical helium heat exchanger (P = 3 bar, T = 6 K) in order to minimise heat loads to the cold extremity of the cavity maintained at 2 K and to ensure the transition between 300 K and 6 K. A dedicated test facility named SUPERCRYLOOP was developed and successfully operated at IPN Orsay for measuring the performance of the cold heat exchanger and the first experimental results have confirmed its excellent performances [15].

The "dressed" cavity and its tuning system

The cryogenic module will be equipped with one of the two TRASCO cavities (geometrical $\beta = 0.47$) fully "dressed" (see Figure 10). A magnetic shield made of 1 mm Cryoperm10® sheets encloses the cavity and is located inside the helium tank [16]. Magnetic shield measurements showed that the contribution to the surface resistance by trapped magnetic field is estimated to be below 10 nΩ, which guarantees a quality factor higher than 5.10^9.

Figure 10: The Z501 TRASCO cavity fully dressed with the stepper motors and the piezoelectric actuators

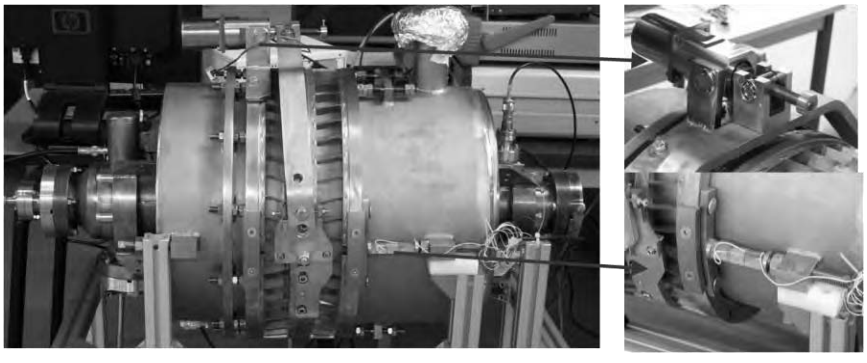

The cavity and its shield are placed in a titanium helium tank which provides the low pressure helium bath for 2 K operations.

A coaxial blade tuner derived from the one successfully tested at TTF [17] has been developed and fabricated. This device, mounted on the tank, will allow slow and fast tuning compensation. A rotation torque, provided by a stepper motor, is transferred into longitudinal strength by means of bending blades and enables static compensation of Lorentz forces detuning. This coaxial device is also assisted by piezoelectric actuators which enable dynamic cavity frequency adjustments.

The piezos system is made for quickly compensating for the perturbations that could detune the cavity, as for example microphonics or Lorentz force due to a fast increase of the electric field. It is therefore interesting to identify the transfer function (TF) of this tuning system.

To this purpose, the experiment, described by Figure 11, was set up for a first study at room temperature. A low-power RF signal at the resonating frequency (π-mode) of the cavity is introduced. In this way, the detuning is deduced by measuring the phase between the input and the output signal. At the same time, this phase oscillation is compared to the piezos driving signal by using a lock-in amplifier which provides an excellent noise rejection [18]. The Bode diagram of the tuning system (gain in Hz/V and phase) can therefore be deduced from the harmonic response of the discrete frequency sweep.

The piezos driving signal was swept on a frequency range from 0 to 1 kHz with steps of 0.5 Hz. Several microphonic disturbances were identified. The plot in Figure 11 shows the gain (Hz/V), deduced from those measurements, for low frequency excitations. The dashed curve is the result of a sum of first order and second order transfer functions. The first order transfer function enables to adjust the gain at low frequency whereas the second orders imitate the mechanical resonances [19].

Figure 11: Experimental set-up for tuning system FT measurements (left); the measured and modelled gain of the FT at room temperature (right)

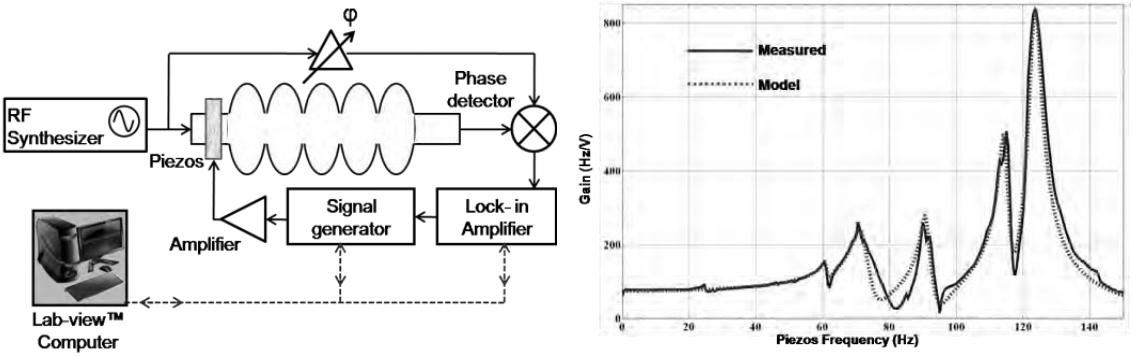

The model can be extrapolated by adjusting the half bandwidth of the mechanical resonances and their microphonic pulsations as well the peak amplitudes. Knowledge and understanding of this transfer function will enable to establish the best solution for feedback control of the tuning system. Such a model will also be used to complete a preliminary theoretical study of the cavity behaviour with its entire LLRF control feedback loop system. Therefore, the same measurement will be carried out in cryogenic conditions to characterise the TF in real accelerating conditions.

Experiment

During the power coupler conditioning, it is foreseen to proceed to the first low power tests of the cavity inside the cryomodule. Those tests will help in evaluating the cavity quality factor

with its new "clothing". It is also planned to evaluate the Lorentz factor and to identify all the microphonic disturbances. This first test will also be useful to check the good functioning of the whole cryogenic device.

The first results will help to define a procedure for the ramping up of the field in the cavity during high-power testing and the controlling of the tuning system. For all the experiments the cryomodule will be set up in the former IPNO cyclotron pit. The cavity will be RF fed thanks to a Thales Electron Devices® Induced Output Tube (IOT) able to provide an 80 kW continuous wave signal at 704 MHz. This IOT requires a 36 kV cathode voltage and the electron beam intensity in the tube can reach 3.3 A. Therefore, it is DC power supplied thanks to a 160 kW (40 kV-4 A) alimentation provided by Brucker®. The RF low power signal injected in the IOT is piloted by a synthesiser signal which is amplified beforehand by a 1 kW Brucker® amplifier (gain of 60 dB).

The entire power supply chain has been installed, tested and is now fully operational. The Thales® IOT was successfully tuned, and an expected average gain of 21 dB was measured (the gain is slightly changing as function of the output power, maximum: 21.5 dB for 60k W).

The high power tests will be a second evaluation of the module cryogenic efficiency. But, above all it is the capability of the piezo-based tuning system coupled with the prototypical digital LLRF I/Q feedback loop which will be evaluated. The reliability of the entire installation and its response time for fast set points update of the entire installation will be tested.

Reliability considerations

EUROTRANS linac reliability analysis estimates the number of malfunctions that could cause beam/plant shutdowns per three-month operation cycle. Results show that such linacs have a high potential for reliability improvement. For the XT-ADS, the objective is to admit only a maximum of five beam trips (longer than 1 s) per cycle.

To reach this goal a fast fault recovery scenario has been established [2]. When a cavity or its power supply fails, the philosophy is to re-adjust the accelerating fields and phases of some non-faulty RF cavities, for a short beam interruption of about 100 ms, to recover the nominal beam characteristics.

To forecast future reliability tests of the 704 MHz cryomodule and evaluate the technical feasibility of such retuning, we computed a model of the cavity with the main characteristics of its LLRF system in the MATLAB Simulink® environment.

We established our calculations on a simple model (see Figure 12) in the frequency analysis to estimate the gain and the integration time of the corrector (PI), taking into account the sampling operation in a digital system. A delay and sampling time (zero order hold function, ZOH) were introduced [20]. The IOT gain variation as function of the power delivered and non-linearity are also taken into account. The cavity voltage is deduced by modelling the cavity as an RLC resonant circuit [21]. The detuning induced by the Lorentz forces and microphonic perturbations were also implemented. For the preliminary analysis, the fast cold tuning system behaviour is simplified compared to the TF presented previously. It is considered as a simple first order filter, consequently its feedback control loop, for those simulations, is also simplified. The main calculation parameter values are detailed in [22].

Figure 12: Simple model base for the sample feedback analysis

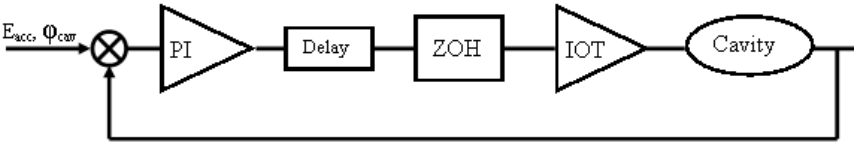

Figure 13 presents the simulation results during a fast fault recovery procedure where the cavity field has to be increased by 15% and its phase changed by 3°. The process for this scenario is described by the following steps:

1. The cavity accelerating field and phase was set to the nominal working points (8.5 MV/m, -30°); the beam is switched on.
2. A failure on another accelerating device is detected the beam is switched off.
3. The accelerating field is quickly ramped up (10 MV/m).
4. The phase set points is updated (33°).
5. The cavity field is stable, the beam can be injected again.

Figure 13: Simulation results for the update of the accelerating field and cavity phase during a fast-fault recovery scenario

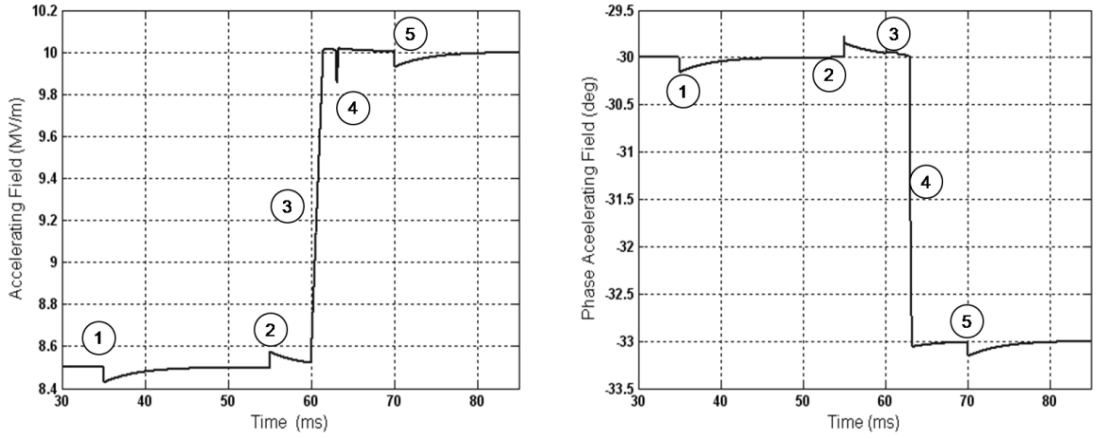

Results from this preliminary simulation study shows that during a short beam trip, the phase and the field amplitude in the cavity could be updated in less than 30 ms, with a good control of the feedback loop. For those simulations, the proposed solution for the PI corrector was to use an "aggressive" integration time. So, for this solution, the electric field overtaking risks are significant. As a consequence the field ramping settings have to be carefully controlled. But in this case the regulated system seems to be quite fast and very accurate. Indeed, when the phase set point is changed, deviation of 0.1 MV/m is observed but is quickly compensated. The real transient effect, due to beam loading, is observed when the beam is switched on (or switched off), but one can see that it is also under control and corrected in 10 ms.

The study still needs deeper investigations and this computed program still needs to be improved, especially regarding the tuning system behaviour. Nevertheless, a possible procedure for a "fast fault recovery" scenario had been pointed out and a technical solution envisaged. The future full scale experiment will be crucial in the orientation of the improvements of the prototype digital feedback control system already developed.

Conclusion

Important prototyping work was performed on spoke resonators in order to assess their capability to efficiently accelerate intense hadrons beams. The obtained performances on these accelerating structures and their ancillary systems proved that this technology is now in an advanced stage and can be considered as a reliable reference solution for the EUROTRANS accelerators.

The experimental campaign on the EUROTRANS 700 MHz full scale cryomodule will start in 2010. In the long run, the experiment will be able to provide a testing bench for specific sequences of the XT-ADS fast fault-recovery reference scenario. The aims of reliability tests will be to recover similar results than computations for the set points updating and validate an efficient and safe procedure.

Acknowledgements

Work supported by EU FP6 through the EUROTRANS programme (contract No. FI6W-516520).

References

[1] Biarrotte, J-L., A.C. Mueller, "Accelerator Reference Design for the EADS Demonstrator", these proceedings.

[2] Biarrotte, J-L., *et al.*, "Accelerator R&D for the European ADS Demonstrator", *Proc. PAC 2009*, Vancouver, Canada (2009).

[3] Webber, R.C., "Overview and Status Update of the Fermilab HINS Linac R&D Program", *Proc. PAC 2009*, Vancouver, Canada (2009).

[4] Bousson, S., *et al.*, "Spoke Cavity Developments for the Eurisol Driver", *Proc. LINAC 2006*, Knoxville, USA (2006).

[5] Facco, A., *et al.*, "Beam Dynamics Studies on the EURISOL Driver Accelerator", *Proc. LINAC 2008*, Victoria, Canada (2008).

[6] Webber, R.C., "Overview and Status Update of the Fermilab HINS Linac R&D Program", *Proc. PAC 2009*, Vancouver, Canada (2009).

[7] Holmes, S.D., "Project X at Fermilab", *Proc. PAC 2009*, Vancouver, Canada (2009).

[8] Bermejo, B.J., *et al.*, "Baseline Design for the ESS-Bilbao SPA", *Proc. PAC 2009*, Vancouver, Canada (2009).

[9] Peggs, S., M. Lindroos, "Conceptual Design of the ESS-Scandinavia Accelerator and Target", *Proc. PAC 2009*, Vancouver, Canada (2009).

[10] Olry, G., "SRF Developments for Ion Acceleration", *Proc. LINAC 2008*, Victoria, Canada (2008).

[11] Rampnoux, E., "RF Power Coupler Development for Superconducting Spoke Cavities", *Proc. LINAC 2008*, Victoria, Canada (2008).

[12] Barbanotti, S., *et al.*, "Design of the Prototypical Cryomodule for the EUROTRANS Superconducting Linac for Nuclear Waste Transmutation", *Proc. EPAC 2008*, Genoa, Italy (2008).

[13] Kang, Y., *et al.*, "Electromagnetic Simulations and Properties of the Fundamental Power", *Proc. PAC 2001*, Chicago, USA (2001).

[14] Souli, M., *et al.*, "Study of Thermal Interaction Between a 150 kw CW Power Coupler and a Superconducting 704 MHz Elliptical Cavity", *12th International Workshop on RF Superconductivity*, Ithaca, NY, USA (2005).

[15] Souli, M., *Étude et développement d'un coupleur de puissance pour les cavités supraconductrices destinées aux accélérateurs de protons de haute intensité*, PhD Thesis IPNO-T-00-07, Orsay, France, 13 July (2007).

[16] Pierini, P., *et al.*, "Design of the Magnetic Shield for TRASCO Low Beta Elliptical Cavities", *Proc. SRF 2007*, Genoa, Italy (2007).

[17] Pierini, P., *et al.*, *Report on Tuner Design*, CARE Note-2006-003-HIPPI (2006).

[18] Luong, M., *et al.*, "Analysis of Microphonics Disturbances and Simulation for Feedback Compensation", *Proc. EPAC 2006*, Edinburgh, Scotland (2006).

[19] Devanz, G., *et al.*, "Numerical Simulations of Dynamics Lorentz Detuning of SC Cavities", *Proc. EPAC 2002*, Paris, France (2002).

[20] Luong, M., O. Piquet, *RF Control System Modeling*, Internal EUROTRANS Deliverable n°1.40 (2007).

[21] Schilcher, T., "Vector Sum Control of Pulsed Power Accelerating Field", Universität Hamburg, Hamburg, Germany (2008).

[22] Bouly, F., *et al.*, "Construction of a 700 MHz Prototypical Cryomodule for the EUROTRANS ADS Proton Linear Accelerator", *Proc. SRF Workshop 2009*, Berlin, Germany (2009).

Estimation of acceptable beam trip frequencies of accelerators for ADS and comparison with performances of existing accelerators

Hayanori Takei, Kenji Nishihara, Kazufumi Tsujimoto, Hiroyuki Oigawa
Japan Atomic Energy Agency (JAEA), Japan

Abstract

Frequent beam trips as experienced in existing high-power proton accelerators may cause thermal fatigue problems in ADS components which may lead to degradation of their structural integrity and reduction of their lifetime. Thermal transient analyses were performed to investigate the effects of beam trips on the reactor components, with the objective of formulating an ADS design that had higher engineering possibilities and determining the requirements for accelerator reliability. These analyses were made on the thermal responses of four parts of the reactor components; the beam window, the cladding tube, the inner barrel and the reactor vessel. Our results indicated that the acceptable frequency of beam trips ranged from 50 to 2×10^4 times per year depending on the beam trip duration. The former was corresponding to the beam trip duration exceeding five minutes. On the other hand, the latter was corresponding to the beam trip duration of 10 seconds or less. And the plant availability was estimated to be 70% or greater in cases where the beam trip frequency decreased to the acceptable frequency of beam trips.

In order to consider measures to reduce the frequency of beam trips on the high-power accelerator for ADS, we compared the acceptable frequency of beam trips with the operation data of existing accelerators. The result of this comparison showed that for typical conditions the beam trip frequency for durations of 10 seconds or less was within the acceptable level, while those exceeding five minutes should be reduced to about 1/30 to satisfy the acceptable level.

Introduction

To realise effective transmutation of minor actinides (MA) by an accelerator-driven subcritical system (ADS), a high-power spallation target should be installed at the centre of the core. In the case of JAEA's reference ADS [1], proton beam power of ~30 MW is necessary to keep the thermal power at the subcritical core at 800 MW. Frequent beam trips, as experienced in existing high-power proton accelerators, may cause thermal fatigue problems in ADS components which may lead to degradation of their structural integrity and reduction of their lifetime.

In general, beam trips are caused by two reasons: one is the failure of the accelerator components, and the other is the interruption by a Machine Protection System (MPS) to protect the accelerators against failures. For reference, the beam trip frequency caused by the "dead component" is assessed on the basis of techniques such as Failure Mode and Effect Analysis (FMEA) [2]. For these assessments, the reliability parameters of accelerator components, such as a failure rate, are usually used. However, the influence for the thermal shock damage on the ADS reactor system caused by beam trips has not been evaluated sufficiently. Conversely, it is not yet clear what times in the ADS reactor system are acceptable for the beam trips. The purpose of the present study is to know the present level of accelerator technology by comparing beam trip frequencies estimated from operation data of existing accelerators and the requirement from transient analyses of the ADS reactor system.

In this article, the following items were revised from the article presented at the 5th HPPA workshop in Mol [3]:

- The cladding tube was also picked to discuss the influence of thermal shock.
- The acceptable number of beam trips for the inner barrel and the reactor vessel was re-evaluated.

Design study of future ADS

General scheme

JAEA's reference design of ADS is a tank-type subcritical reactor, where lead-bismuth eutectic (LBE) is used as both the primary coolant and the spallation target, as shown in Figure 1. The proton accelerator for the ADS must have high power intensity, more than 20 MW, with good economic efficiency and reliability. To realise such an accelerator, energy efficiency must be enhanced to assure the self-sustainability for electricity of the whole system. Taking these requirements into account, the superconducting linac (SC-Linac) is regarded as the most promising choice. Considering the production efficiency of the spallation neutrons in LBE, the accelerated energy of the SC-Linac was set at 1.5 GeV. In order to maintain the thermal power at 800 MW, the beam current was adjusted from 8 to 18 mA (i.e. 12 to 27 MW) depending on the effective multiplication factor (k_{eff}). Taking into account these requirements, the maximum beam current of the SC-Linac was set at 20 mA.

Basic parameters of the SC-Linac, such as the number of cryomodules, the output power of the klystron and the total length of the SC-Linac, were optimised for accelerated energies from 100 MeV to 1.5 GeV [4]. The SC-Linac consists of a series of 89 cryomodules, which were designed for a 972 MHz RF wave. One klystron was provided for each cryomodule giving a total of 89 klystrons. These klystrons were classified into three categories, according to rated output power: 197, 425 and 750 kW.

Cooling system

The ADS plant was assumed to have a primary LBE cooling system and a water/steam system for power conversion through a saturated steam cycle. As shown in Figure 1, all other components

Figure 1: Concept of 800 MW_{th}, LBE-cooled, tank-type ADS

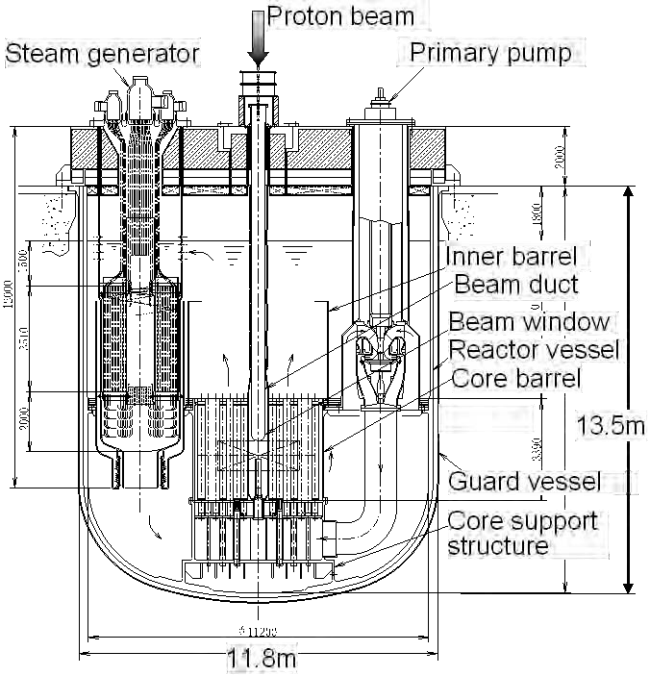

of the primary system, including four steam generators, two primary pumps and auxiliary heat exchangers, are accommodated within the reactor vessel. The heat generated in the target and the subcritical core is removed by forced convection of the primary LBE, and transferred through the steam generators to water/steam for power conversion.

Figure 2 is a simplified flow diagram of the ADS. Primary LBE coolant flows upward through the subcritical core and exits into an upper plenum. Then, the coolant flow divides equally among four steam generators. The flow passes through heat transfer sections in the steam generators and enters a lower plenum. The LBE coolant is then returned back into the subcritical core by primary pumps. The water/steam system has four steam drums, four recirculation water pumps, a turbine generator unit and a feedwater pump. Steam generated in the steam generators is directed to the steam drums. The steam from all four steam drums is combined and drives the turbine generator unit. The steam is cooled down into water in a condenser at the turbine exit, and the feedwater pump returns the water back to the steam drums through a feedwater heater that is not shown in the figure. The recirculation water pump delivers the water from the steam drum to the steam generator.

Preliminary analysis was performed for transients in the ADS plant caused by the beam trip [5]. The primary LBE cooling system and the water/steam power conversion system were modelled with a simple one-dimensional flow network. As a result, about 400 seconds of turbine operation may be possible without the beam. When the duration of the beam trip exceeds this limit, the pressure of the steam drum and the LBE temperature become too low to prevent its freezing.

Estimation of acceptable beam trip frequency

Restriction from the subcritical reactor

As shown in Figure 3, four parts of the reactor component, i.e. the beam window, the cladding tube, the inner barrel and the reactor vessel, were picked as representatives to discuss the influence of thermal shock. In the following discussion, the expected life time of the subcritical

Figure 2: Simplified flow diagram of ADS plant

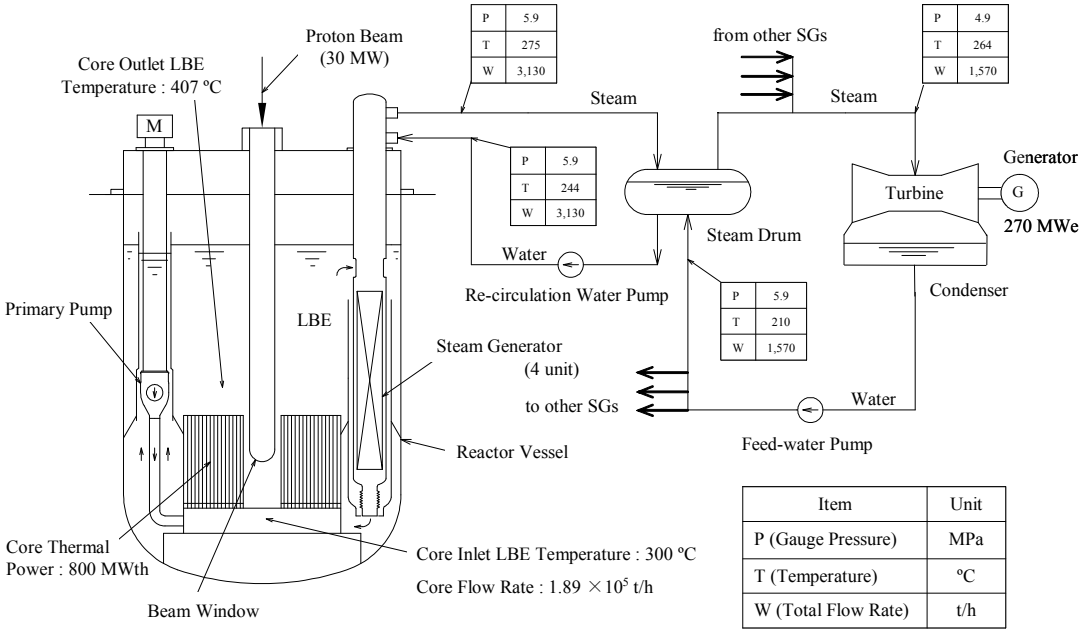

Figure 3: Influence of beam trip transient on reactor structure

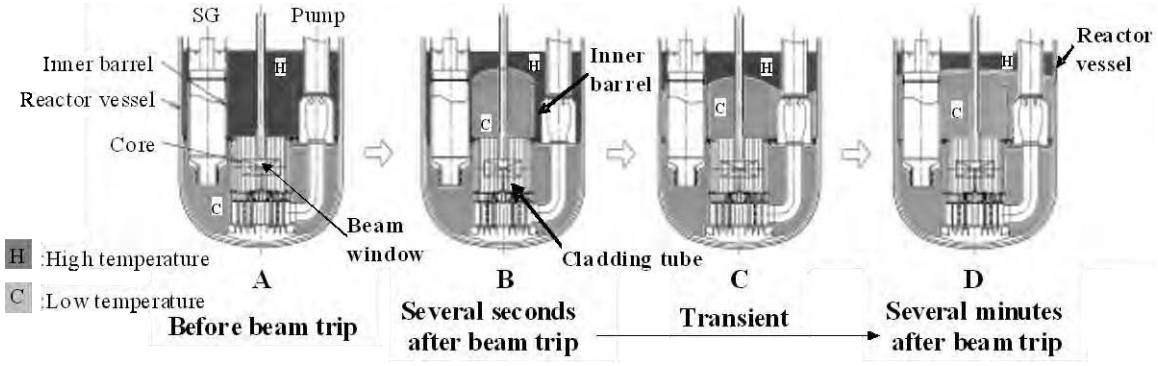

reactor is defined as 40 years and no replacement of the inner barrel and the reactor vessel is assumed during this period. On the other hand, the replacement of the beam window and the cladding tube is assumed once every two years. And the harshest conditions for the thermal load were applied.

As for the beam window, a beam trip causes a rapid temperature drop, which in turn causes thermal stress because of the temperature difference between the inner and the outer surfaces of the beam window. The temperature response of the beam window (inner diameter: 450 mm, thickness: 2 mm, material: 9Cr-1Mo steel, beam power: 30 MW) was evaluated using the finite element method FINAS code [6]. In the evaluation, the beam is assumed to be restarted five seconds after the beam trip. Figure 4(a) shows the temperature change for the apical region of the beam window. On the beam trip at t = 0, the surface temperature starts to drop rapidly and asymptotically approaches the coolant temperature within about three seconds. The maximum thermal stress of 179 MPa is expected at a time 0.5 seconds after the beam trip. This thermal stress is much lower than what would cause buckling failure. The total strain range caused by the beam trip and restart becomes the maximum of 9.3×10^{-4}. From the relationship between total strain range and number of cycles to failure for 9Cr-1Mo steel, shown in Figure 5, the

Figure 4: Change of the surface temperature after the beam trip for (a) the beam window and (b) the cladding tube

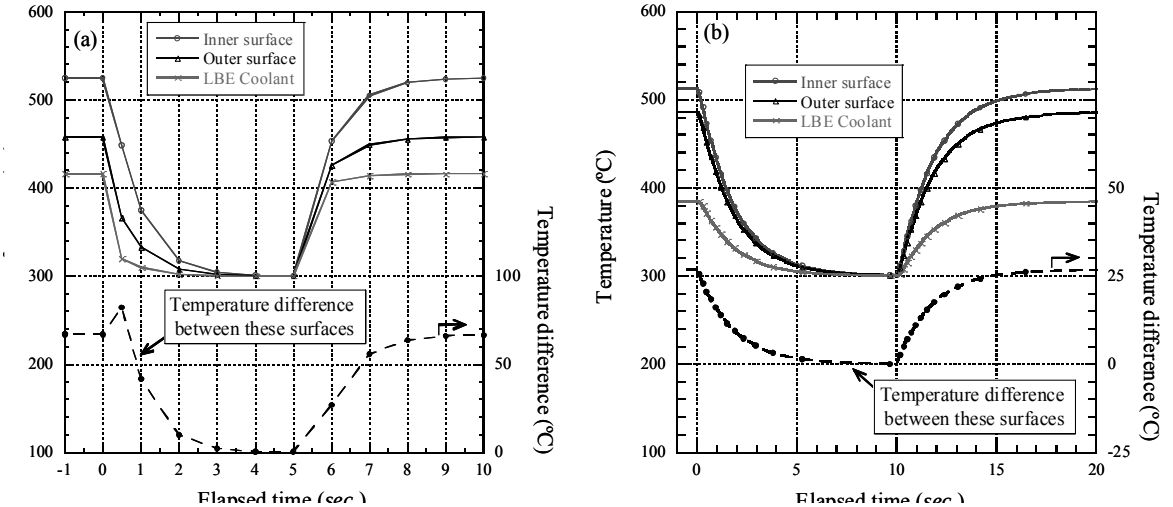

Figure 5: Relationship between total strain range and number of cycles to failure for 9Cr-1Mo steel

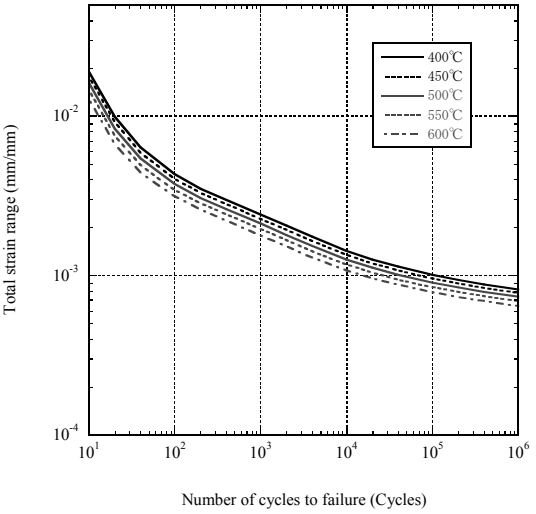

acceptable number of these thermal shocks is estimated to 4×10^4, which means that several beam trips per one hour may be acceptable for two years of the expected lifetime of the beam window (about 15 000 hours). It should be noted that this estimate is based on the material data without radiation damage, and therefore experimental verification for the effect of the proton and neutron irradiation is indispensable.

As for the cladding tube, a beam trip causes a rapid temperature drop similar to that for the beam window. The temperature response of the cladding tube was evaluated using the finite element method ABAQUS code [7]. Design parameters used for the evaluation are listed in Table 1. The distance from the centre of the active core to the cladding tube was 27.9 cm. In the evaluation, the beam is assumed to be restarted 10 seconds after the beam trip, and the corrosion depth of the outer surface is estimated as 125 μm. Figure 4(b) shows the change of the surface temperature in such a position that the total strain range caused by the beam trip and restart becomes the maximum of 6.2×10^{-4}. This position is located on the outer surface at 50.4 cm

Table 1: Parameters used for the evaluation of the cladding tube

Fuel composition	(Pu+MA)N +ZrN*
Bond	He
Cladding	9Cr-1Mo steel
Pin outer diameter	7.65 mm
Thickness of cladding tube	0.5 mm
Pellet smear density	95%
Pin pitch	11.48 mm
Pin length	3 050 mm
Active height	1 000 mm
Gas plenum height	1 050 mm
Production rate of fission product (FP) gas	27%
Release rate of FP gas	100%
Linear power rating	343 W/m (average)
Coolant velocity	2.0 m/s
Inlet temperature	300°C

* Fuel is composed of 50.3% (MA+Pu)N, which is a mixture of MA nitride (MAN) and Pu nitride (PuN), and 49.7% zirconium nitride (ZrN) in weight basis.

below from the top of the active core. After the beam trip, the temperature difference between the inner and outer surface starts to drop rapidly and asymptotically approaches zero within about five seconds. Considering the magnitude of the strain range, the acceptable number of beam trips for the cladding tube is estimated to exceed 10^6 times.

The inner barrel is a cylindrical structure made of 3 cm thick 9Cr-1Mo steel and installed to straighten the LBE flow above the subcritical core. During normal operation, it is kept at the average outlet temperature 407°C. In the case of the beam trip, the inner surface of the cylinder is immediately cooled by the cold LBE (about 300°C), causing a temperature difference between the inner and outer surfaces. The temperature for 120 seconds after the beam trip was calculated by means of the ABAQUS code. In the calculation, the temperature for the outer surface is taken to be the steady value, 407°C, because it is difficult for the cold LBE to reach the outer surface in a short period of time. And the beam is assumed to be restarted 30 seconds after the beam trip. According to the results, shown in Figure 6(a), a temperature difference of 54°C will be observed

Figure 6: Change of the surface temperature after the beam trip for (a) the inner barrel, and (b) the reactor vessel

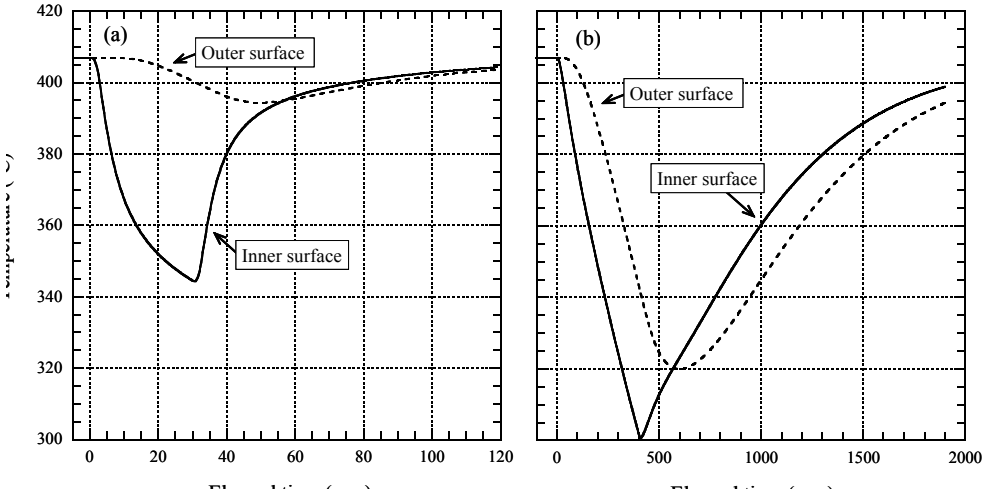

at 24 seconds after the beam trip, which will cause maximum stress of 144 MPa. At the restart of the beam, the stress in the inverse direction will be added to the inner barrel. The stress range for fatigue evaluation, therefore, is 159 MPa. Considering this magnitude of stress, the acceptable number of beam trips for the inner barrel is estimated at about 10^5 times. If the duration of the beam trip is less than 24 seconds, the stress to the inner surface becomes smaller than the maximum. In this example, the stress at the inner surface at five and ten seconds after the beam trip is 74 and 121 MPa, which is roughly equivalent to exceed 10^6 and 10^6 beam trips, respectively. Therefore, the influence of the thermal shock to the inner barrel could be reduced, provided that the beam was reinjected into the subcritical core within about ten seconds after the beam trip.

As for the reactor vessel, the beam trip causes a temperature change between the inner and outer surfaces similar to that for the inner barrel, and the formation of temperature stratification and the lowering the LBE level because of thermal shrinkage both cause thermal stress. The stress range for the fatigue evaluation was estimated for the reactor vessel made of 5 cm thick 9Cr-1Mo steel under the assumption that the beam is restarted 120, 300 and 400 seconds after the end of the beam trip. The result for the beam trip duration with 400 seconds is shown in Figure 6(b). We observed that the peak value of the temperature difference between the surfaces occurred at 293 seconds after the beam trip. The maximum stress range calculated from the axial and circumferential stress was about 187 MPa. Considering this magnitude of stress, the acceptable number of beam trips for the reactor vessel is estimated at about 2×10^4 times. The results for 120 and 300 seconds are given in Table 2.

Table 2: Acceptable number of the beam trip for each component

Component	Expected lifetime (year)	T_{max}* (sec.)	Total strain range**	Acceptable number (times)	Acceptable frequency (times/year)
Beam window	2	0.5	9.3×10^{-4}	4×10^4	2×10^4
Cladding tube	2	0	6.2×10^{-4}	$> 1 \times 10^6$	$> 5 \times 10^5$
Inner barrel	40	24.4	4.9×10^{-4} (5 sec.)	$> 1 \times 10^6$	$> 2.5 \times 10^4$
			8.1×10^{-4} (10 sec.)	1×10^6	2.5×10^4
			1.0×10^{-3} (30 sec.)	1×10^5	2.5×10^3
Reactor vessel	40	293	8.5×10^{-4} (120 sec.)	4×10^5	1×10^4
			1.1×10^{-3} (300 sec.)	4×10^4	1×10^3
			1.2×10^{-3} (400 sec.)	2×10^4	500

* The value represents the elapsed time after the beam trip when the stress range or the strain range is maximised.

** The value in parentheses represents the beam trip duration.

Acceptable number of beam trips per year

Taking the above discussions into account, the acceptable number of beam trips for each component is summarised in Table 2. In this table, the elapsed time (T_{max}) after the beam trip when the stress range or the strain range is maximised and the expected lifetime for each component are also listed. The acceptable frequency of beam trips, obtained by dividing the acceptable number of beam trips by the expected lifetime for each component, ranges from 500 to 2×10^4 times per year depending on the beam trip duration.

Therefore, the acceptable frequency of beam trips was classified by three criteria, according to the beam trip duration, as shown in Table 3. The acceptable frequency of beam trips for the beam window was adopted for the criteria for a beam trip of 10 seconds or less, because the acceptable frequency of beam trips for the beam window was lower than that for the cladding tube and the inner barrel. For the criteria where the beam trip duration ranged from 10 seconds to five minutes, the acceptable frequency of beam trips for the reactor vessel was adopted. The requirement for thermal transient analyses is that the acceptable frequency of beam trips with

Table 3: Acceptable frequency of beam trips according to the beam trip duration

Criteria	Acceptable value (times/year)	Component that imposed limits
0 sec. $\leq T \leq$ 10 sec.	2×10^4	Beam window
10 sec. $< T \leq$ 5 min.	1×10^3	Reactor vessel
$T >$ 5 min.	50	Plant availability

duration over five minutes be limited to 500 times per year. The influence of the beam trip on the power generation system is also important from the viewpoint of the plant availability because the restart procedure of the system usually takes a long period of time, typically several hours, once the power generation turbine stops. If the acceptable frequency of beam trips with duration over five minutes is assumed to be once a week, the plant availability is estimated to be 70% [8]. To maintain plant availability at 70%, therefore, the acceptable frequency for this long beam trip is assumed to be once a week.

This acceptable frequency of beam trips is compared with the current experimental data presented in the next section.

Estimation of the beam trip frequency based on the current experimental data

Estimated number of beam trips per year

LANSCE is a spallation neutron source based on a linac [9]. The accelerator facility is one of the most powerful linear proton accelerators in the world. The proton linac delivers two proton beams at 800 MeV: the H^+ and the H^- beam. The H^+ beam can deliver 1.25 mA and the H^- beam can deliver 70 μA. Each injector system includes a 750 keV Cockcroft-Walton type generator. The heart of the RF system is the klystron system which provides RF power at 805 MHz to the side coupled linac.

A thorough failure analysis has been conducted for years at LANSCE. The average value of beam trips for H^+ was 1.62 trips/h whilst this value was 0.78 for the H^- beam. Detailed statistics give no room for doubt; the H^+ injector was responsible for 86% of beam trips. Next to the injector is the RF system, responsible for 8% of all beam trips linked to the H^+ beam. Detailed information can be found in Ref. [10].

An electron/positron injector linac at KEK [11], capable of providing electrons at energies up to 8 GeV and positrons up to 3.5 GeV, is used as a multi-purpose injector not only for the KEK B Factory (KEKB), but also for the Photon Factory (PF). At present, it delivers full-energy beams of 8 GeV electrons to the KEKB High-energy Ring and 3.5 GeV positrons to the KEKB Low-energy Ring. The whole linac consists of 60 S-band (2 856 MHz) main accelerator modules. 50 MW pulse klystrons with a time duty factor of 0.02% were developed.

Statistics on interruptions and the down time distribution of KEK klystrons were obtained from the operation data in FY2005. The scheduled beam time and down time for the whole system were 6 815 h and 52.5 h, respectively. The total number of interruptions was 16 421, including 13 453 accidental interruptions and 2 968 censored events. Accidental interruptions were caused by the failure of the RF system. Censored events were the manual terminations for regular maintenance every two weeks.

Because 85% of all beam trips were caused by the injector and the RF system of LANSCE, the beam trip frequency of the JAEA's SC-Linac for ADS, N_{ads}, was roughly estimated as:

$$N_{ads} \sim N_{inj} + N_{rf} \tag{1}$$

where the N_{inj} and N_{rf} are the beam trip frequency caused by the injector and the RF system of the JAEA's SC-Linac for ADS, respectively. And the N_{inj} and N_{rf} are estimated as:

$$N_{inj} = \frac{T_s}{\bar{t}_i + \bar{\tau}_i}, \quad N_{rf} = N_{kly} \frac{T_s}{\bar{t}_r + \bar{\tau}_r} \tag{2}$$

where T_s is the total scheduled beam time per year for the ADS plant (7 200 h/year), $\bar{t}_i$ and $\bar{\tau}_i$ are the mean time between beam trips and mean time to repair (MTTR) obtained from the data of the LANSCE H^+ injector: 0.77 h and 3.4×10^{-2} h, respectively [10]. N_{kly} is the number of klystrons of the JAEA's SC-Linac for ADS, that is, 89. And $\bar{t}_r$ and $\bar{\tau}_r$ are the mean time between beam trips and MTTR obtained from the data of the RF system of the electron/positron injector linac at KEK: 54.6 h and 7.3×10^{-2} h, respectively [8]. Finally, we obtained a value for N_{ads} of 21 000 times/year.

Comparison and discussion

From the above analysis, using the distribution of beam trip durations obtained from the data of the LANSCE and the KEK [8], the down time distribution of the JAEA's SC-linac is a straight line as shown in Figure 7. Further, the acceptable frequency of beam trips is shown in this figure as a histogram. Comparing the two shows that even at the present technological level of accelerators, the beam trip frequency for durations of 10 seconds or less is within the acceptable level. On the other hand, for the beam trip frequency with duration exceeding five minutes, it is necessary to improve the technology level to about 30 times of present accelerator technology.

Figure 7: Comparison of the acceptable frequency of beam trips and the estimated frequency of the JAEA's SC-linac for ADS

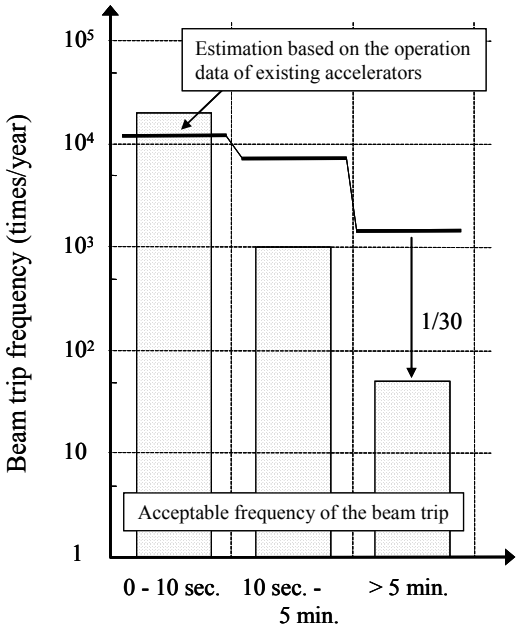

Conclusion

Frequent beam trips as experienced in existing high-power proton accelerators may cause thermal fatigue problems in ADS components which may lead to degradation of their structural integrity and reduction of their lifetime. Thermal transient analyses were performed to investigate the

effects of beam trips on the reactor components, with the objective of formulating ADS design that had higher engineering possibilities and determining the requirements for accelerator reliability. These analyses were made on the thermal responses of four parts of the reactor components; the beam window, the cladding tube, the inner barrel and the reactor vessel. Our results indicated that the acceptable frequency of beam trips ranged from 50 to 2×10^4 times per year depending on the beam trip duration. The former was corresponding to the beam trip duration exceeding five minutes. On the other hand, the latter was corresponding to the beam trip duration of 10 seconds or less. And the plant availability was estimated to be 70% or greater in cases where the beam trip frequency decreased to the acceptable frequency of beam trips.

In order to consider measures to reduce the frequency of beam trips on the high-power accelerator for ADS, we compared the acceptable frequency of beam trips with the operation data of existing accelerators. The result of this comparison showed that the beam trip frequency for durations of 10 seconds or less was within the acceptable level, while that exceeding five minutes should be reduced to about 1/30 to satisfy plant availability conditions.

As the acceptable frequency of beam trips is different for each ADS reactor system design, this solution for the beam trip problem is not valid for all ADS accelerators. However, we believe that this evaluation technique of the beam trip is of potential utility in ADS system planning.

References

[1] Tsujimoto, K., *et al.*, "Research and Development Program on Accelerator Driven Subcritical System in JAEA", *Journal of Nuclear Science and Technology*, 44, 483 (2007).

[2] Burgazzi, L., P. Pierini, "Reliability Studies of a High-power Proton Accelerator for Accelerator-driven System Applications for Nuclear Waste Transmutation", *Reliability Engineering and System Safety*, 92, 449 (2007).

[3] Takei, H., *et al.*, "Comparison of Beam Trip Frequencies Between Estimation from Current Experimental Data of Accelerators and Requirement from ADS Transient Analyses", *Proc. of 5th Workshop on Utilisation and Reliability of High-power Proton Accelerators*, 181, OECD/NEA, Paris (2008).

[4] Ouchi, N., *et al.*, "Development of a Superconducting Proton Linac for ADS", *Proc. of 4th Workshop on Utilisation and Reliability of High-power Proton Accelerators*, 175, OECD/NEA, Paris (2004).

[5] Tsujimoto, K., *et al.*, "Feasibility of Lead-bismuth-cooled Accelerator-driven System for Minor-actinide Transmutation", *Nucl. Technol.*, 161, 315 (2008).

[6] *FINAS, FInite element Nonlinear structural Analysis System*, ITOCHU Techno-Solutions Co., 2-5, Kasumigaseki 3-chome, Chiyoda-ku, Tokyo 100-6080, Japan.

[7] *ABAQUS, Unified Finite Element Analysis*, Dassault Systemes Simulia Corp., Rising Sun Mills, 166, Valley Street, Providence, RI 02909-2499, USA.

[8] Takei, H., *et al.*, *Estimation of Acceptable Beam Trip Frequencies of Accelerators for ADS and Comparison with Performances of Existing Accelerators*, JAEA-Research 2009-023, Japan Atomic Energy Agency, (2009) (in Japanese).

[9] LANSCE, Los Alamos Neutron Science Center, (online) available from *http://lansce.lanl.gov/* (accessed 27/10/2008).

[10] Eriksson, M., "Reliability Assessment of the LANSCE Accelerator System", M.Sc. thesis at the Royal Institute of Technology, Stockholm, Sweden (1998).

[11] Abe, I., *et al.*, "The KEKB Injector Linac", *Nucl. Instrum. Methods Phys. Res.*, A499, 167 (2003).

High-power operational experience at the Spallation Neutron Source (SNS)

Sang-Ho Kim, J. Galambos
Spallation Neutron Source, Oak Ridge National Laboratory, United States

Abstract

The SNS is a short pulse spallation neutron source with full energy acceleration provided by a linac, and pulse compression with an accumulator ring. Operational beam power has reached 1 MW. The operational power was ramped to 1 MW in a period of about three years. At least as important as beam power is the machine availability for neutron scattering users. Providing reliable operation has proved to be as strong a driver as controlling beam loss in the power ramp up. The SNS experience regarding beam loss, machine activation, equipment reliability and overall availability will be reviewed, with emphasis on the Superconducting RF Linac.

Introduction

The SNS is the highest power pulsed Spallation Neutron Source [1]. Operations began in October 2006 at a few kW, with a steady increase in beam power, reaching 1 MW operation in September 2009. Previous short pulsed spallation neutron sources operated in the 100-200 kW range. As a neutron scattering facility, both beam power (which is proportional to the neutron intensity) and availability are important to the users. Many users are only given a few days allotted beam time per year, so down time of a day can have a large impact on their progress. As SNS accommodates more users availability becomes ever more critical, and has been a driver in the power ramp-up progress. The original power ramp-up plan was more aggressive than presently achieved, and has been scaled back to allow equipment improvements aimed at improving reliability to be implemented.

Another key concern in the operation of a high-power accelerator is the machine activation. At the 1 MW level beam loss must be kept below one part per million per meter to keep activation acceptable for hands-on maintenance. We have observed beam loss higher than predicted, but still below limits for hands-on activation. Beam loss has not restricted the power ramp-up.

In this paper we discuss the progress in the power ramp-up from both the beam loss and equipment availability perspectives.

Power ramp-up

Figure 1 shows the operational beam power over the first three years of operation. The beam power exceeded the previous pulsed power record of 160 kW in the summer of 2007 and reached 1 MW in September 2010. The design power is 1.4 MW, so further power increases are expected, albeit at a slower pace. The power ramp-up was aggressive, and occurred faster than most new large-scale facilities. While difficult, the rapid pace of the power ramp-up had some advantages. Equipment issues were identified earlier this way, enabling modifications to start sooner. Also, fewer neutron users were using the beam initially (see Figure 2), so taking the inevitable risks associated with the power increase was more tolerable early on.

Figure 1: Beam power on target (dots) vs. time after the start of SNS operations

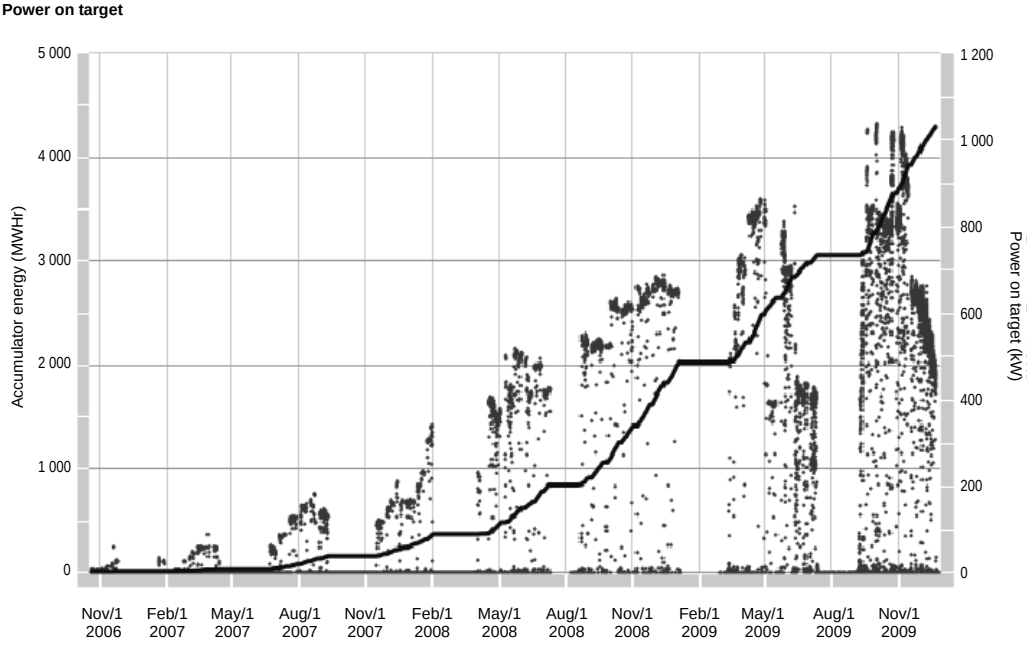

Figure 2: Increase in neutron users at the SNS since the start of operations in FY 2007

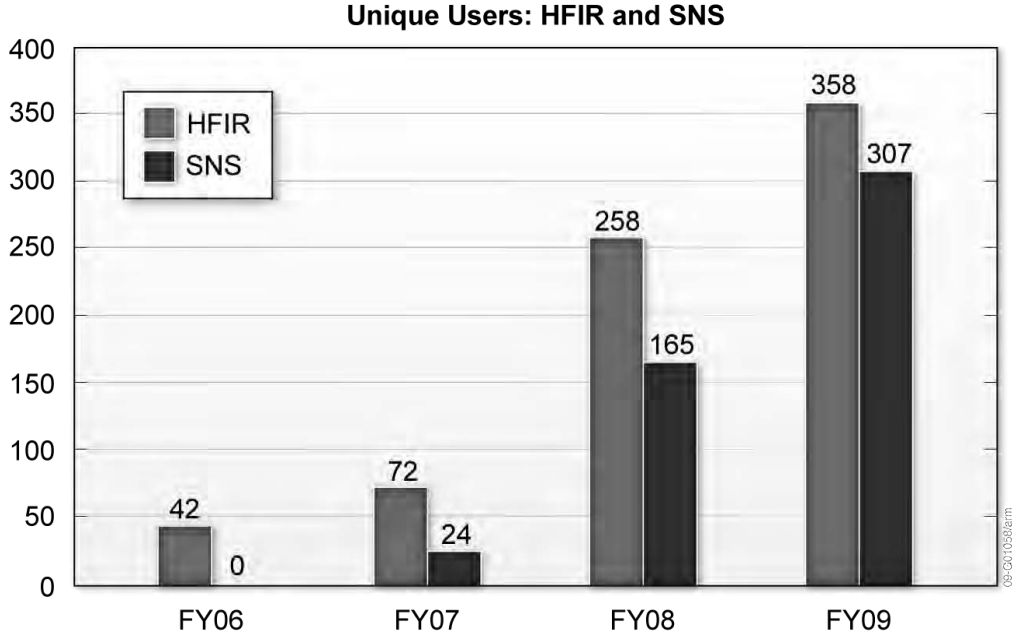

Machine availability

As the design beam power is almost an order of magnitude higher compared to existing neutron facilities, all subsystems of the SNS were designed and developed for substantial improvements compared to existing accelerators and some subsystems are first of a kind. Many performance and reliability aspects were unknown and unpredictable; it takes time to understand the systems as a whole and/or identify areas where additional performance improvements are necessary.

We define the machine availability as (time the beam was on)/(time the beam was promised to users to be on). The machine availability for SNS since initial operations is shown in Figure 3. There is a steady increase in machine availability, as one would expect, with availability approaching 85% for the run ending in December 2009. The decrease in the availability goal in FY2009 was a reflection of the realisation of the difficulty in attaining high availability. Concurrent with the increase in availability was an increase in operational hours from 3 779 hours in FY2007 to 4 916 hours in 2009 (ultimate goal is 5 500 hours). The rapid rise in availability over the first few years was accomplished by addressing the most serious issues, and attacking the easiest problems. Further reductions in down time become harder to address. We expect to approach something like 90% availability. We are developing a plan to achieve 95% availability, but this is expected to be achievable only at some fairly large cost, likely beyond the scope of the normal operating budget.

Typically during a year SNS operates for two major run periods of about four months each. Between these run periods is a long maintenance period of about seven weeks, At the beginning of each long run period a beam start-up and study time is allotted for about one week. Additional beam study periods are allotted about four days once per month, including one day for equipment maintenance. These long maintenance periods are critical to implementing equipment upgrades needed for power ramp-up and addressing availability issues, as well as addressing routine maintenance. Having planned outages of over three months per year as well as other day-long maintenance outages is typical for large accelerators.

Figure 3: SNS availability goals and performance by FY

Note FY10 performance is year-to-date through January 2010

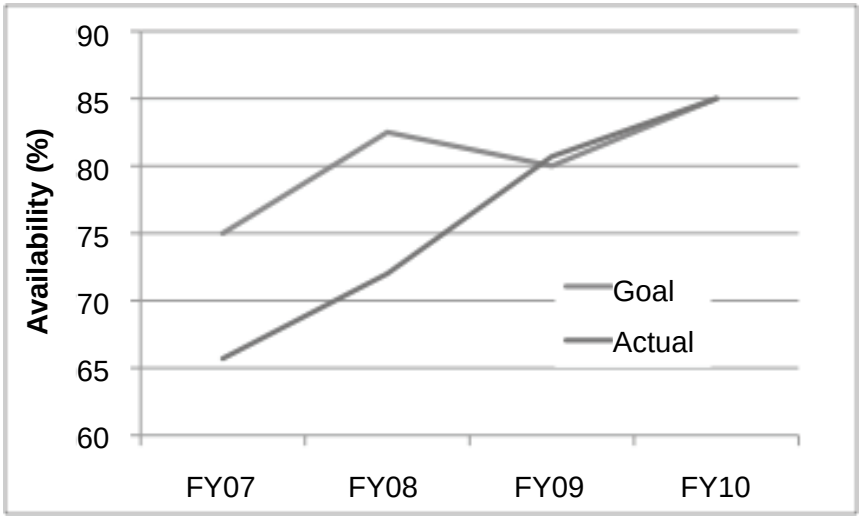

Figure 4 shows the down time broken down by equipment type and year. The largest down time components are the high voltage convertor modulators which are the high voltage power supply and pulse forming network for the RF klystrons. These components use a new solid-state IGBT technology, and have had a number of issues.

Figure 4: Downtime vs. equipment type and year

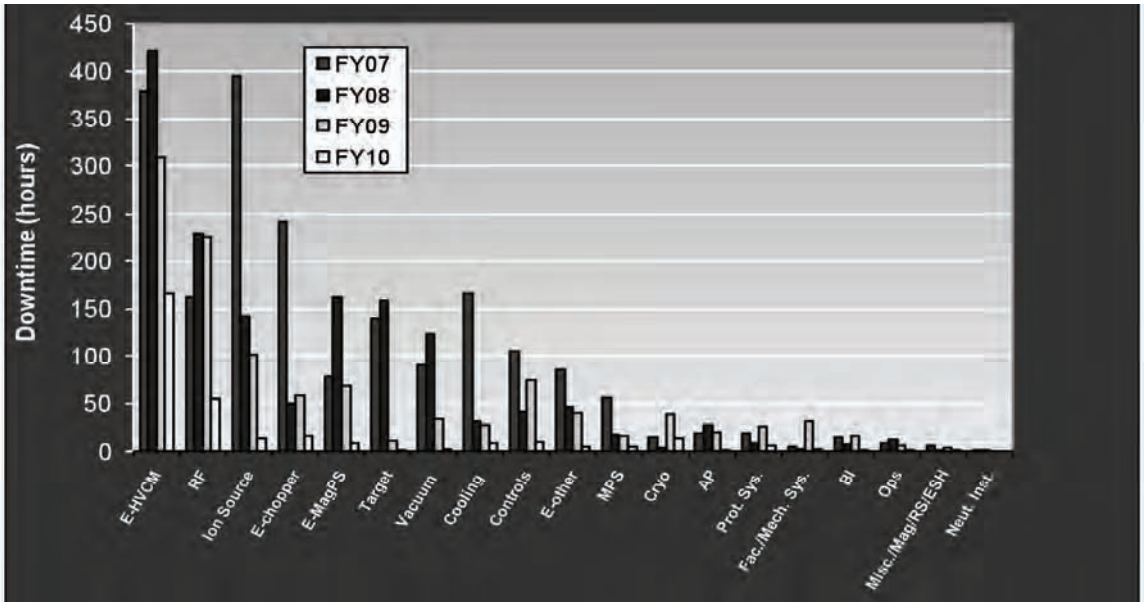

As the duty factor was increased component shortcomings became evident and are being addressed. The RF down time category was largely from rebuncher cavities in the front end of the accelerator; this is no longer an issue. The large collections of high power RF systems (klystrons and transmitters) and low-level RF systems for the superconducting linac have been quite reliable compared to other components. Other major down time contributors are the ion source and other power supplies. The power supply failures are generally pulsed systems associated with our ring.

Another important down time consideration for ADS systems is the trip frequency vs. outage length. Figure 5 shows a comparison of the down time frequency for several high-power proton machines, with data collected in 2008 [2]. There is general consistency in trip rates between the different facilities, with several tens of trips/day of > 1 second on average. It should be noted that none of these facilities were designed for minimal trips. Having 10-20 trips/day of a few seconds or a minute is a small impact on availability as defined here.

Figure 5: (a) Trip frequency vs. outage length from different facilities [2] and (b) SNS trip frequency by year

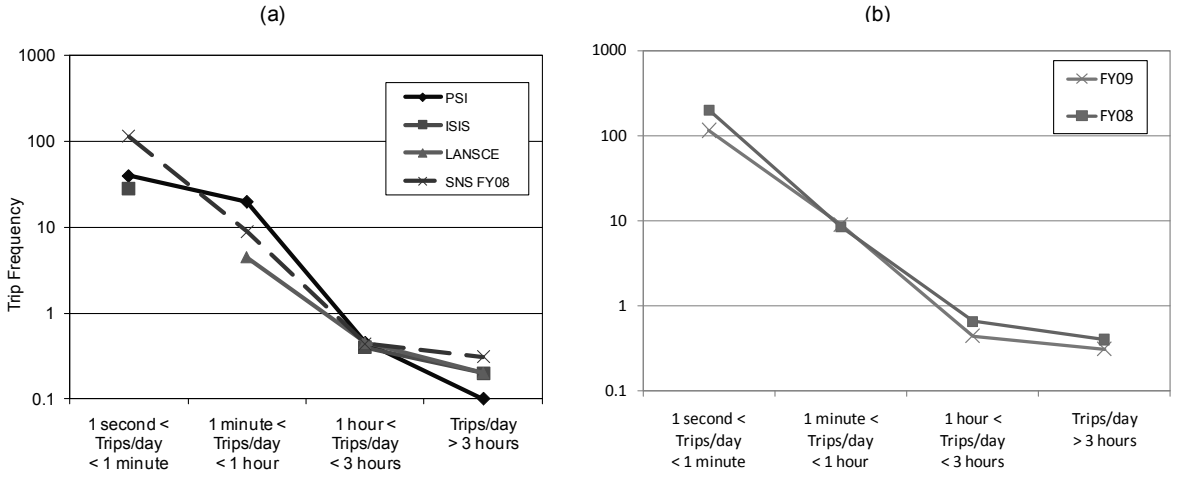

Beam loss/machine activation

Beam loss is a major consideration for high-power accelerator operation. At SNS the beam loss and resultant machine activation has been well controlled, and has not been a limitation to the power ramp-up. Nominally a 1 W/m uncontrolled beam loss is considered the maximum loss rate for hands-on maintenance [3]. Beam tracking studies during the design stage, with expected errors, indicated no beam loss in the SCL [4], but in actual operation we do observe a small level of beam loss. During the ramp-up beam loss was monitored during operation, and the resultant residual activation measured after shutdown. The correlation between loss level, run length and residual activation was tracked as the power was ramped up, and adjustments made to loss monitor locations when more beam loss measurement sensitivity was needed. Figure 6 shows the measured beam loss through the SC-Linac normalised to the charge delivered for a one-month run period. While the actual loss is reported in rads, the loss monitor response is highly sensitive to beam energy and to the geometry between the loss distribution and the loss monitor. For the first few years minimal progress was made in reducing the normalised beam loss. Recently we found that reducing the quadrupole focusing strength has lowered beam loss in the SCL.

Figure 7 shows the history of the residual activation in the SC-Linac, as the power has been ramped up. Activation reported in Figure 7 is the average hot spot level in the warm sections between the cryomodules in the SC-Linac, taken at 30 cm, approximately 1-2 days after the end of neutron production. The activation near the cryomodules themselves is much lower. Over the past year the activation level has remained fairly constant even though the power level has been increased. Figure 8 shows the collective worker dose by year since the start of operations (note: this also includes work done in the ring, transport lines and target areas). The collective dose rate is lower than that at other high-power hadron facilities [3], and is not increasing as SNS increases the beam power over the past year.

Figure 6: Beam loss throughout the SC-Linac

December 2008 represents the historical level prior to quadrupole strength reductions

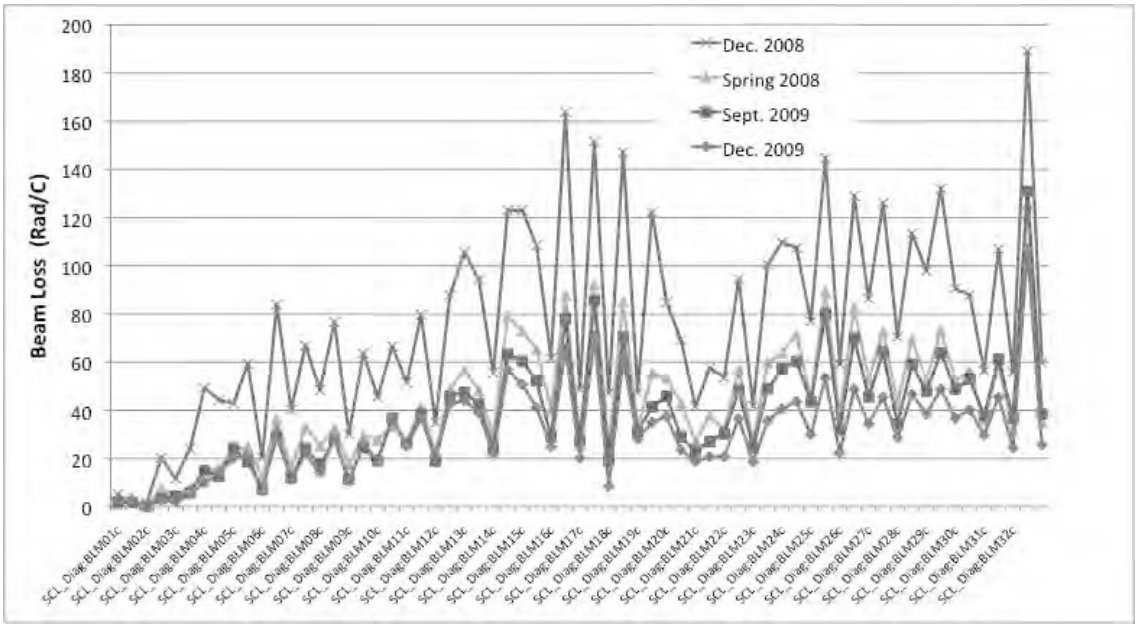

Figure 7: Residual activation along the SC-Linac over the power ramp-up

Squares are the average hot spot activation level for the SC-Linac warm sections, and circles are the charge sent through the linac prior to the activation measurements

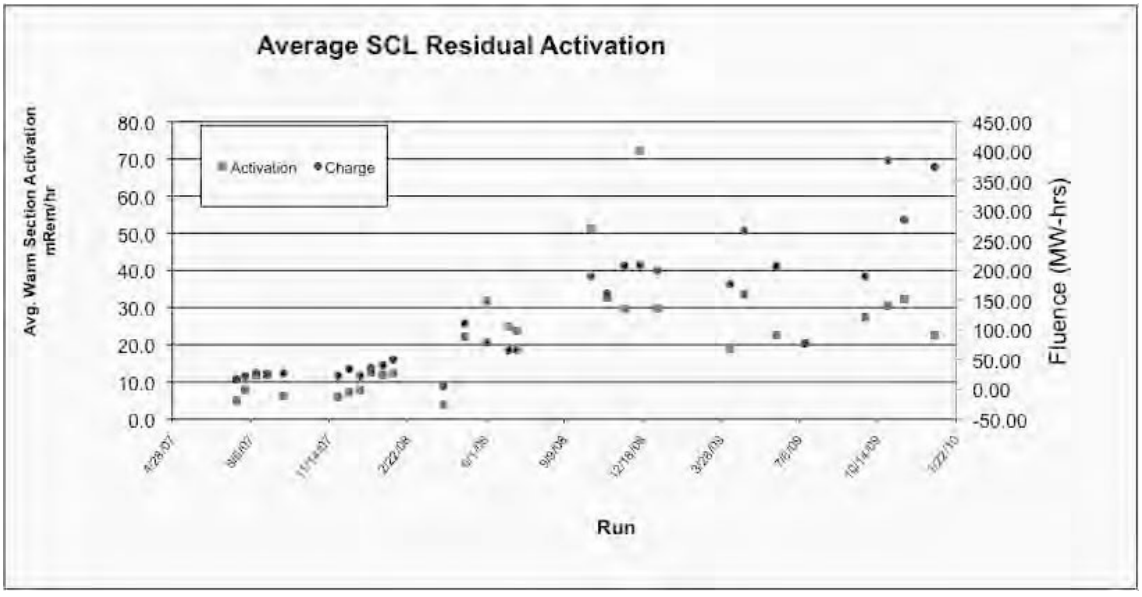

Figure 8: Collective worker dose as measured each six months

Also shown are the average dose rate while working in radiation-controlled areas and the amount of beam charge delivered to the target over the same periods

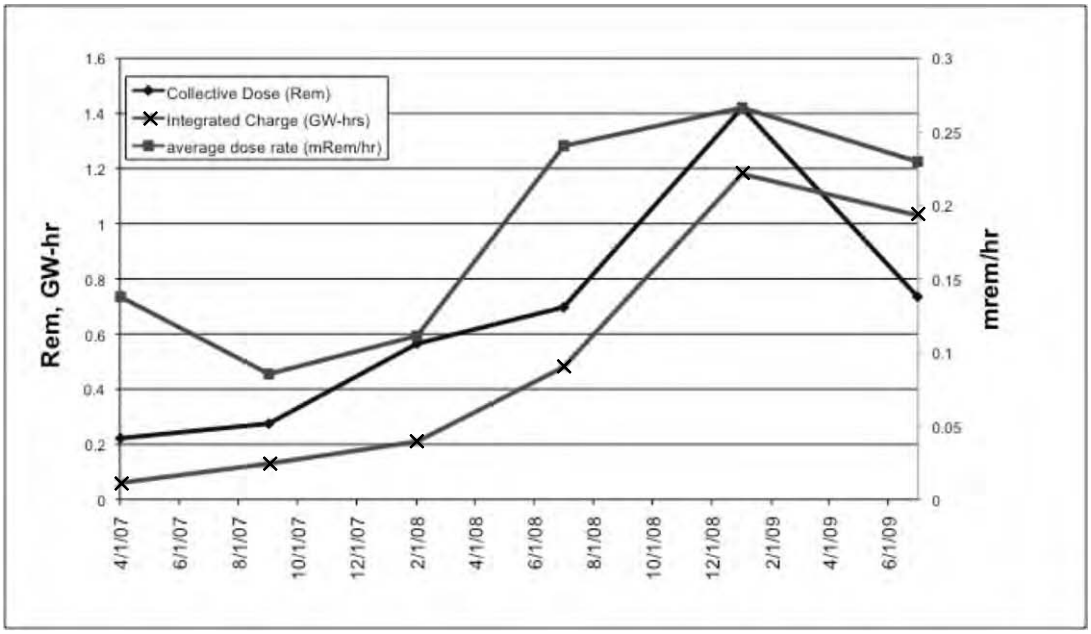

Discussion

The SNS has finished the initial period of power ramp-up, and is approaching its initial design goal. The ADS community can use many of the lessons learnt from SNS. One lesson is that it does take a period of years to bring a MW class machine to full power. New technologies will not always perform as expected initially, and higher down time, trip rates, etc. should be expected early on. So even if extremely high equipment availability is planned for, one should carefully consider planning ramping up to this goal, with consideration for increased trip rates during early operation as the power level is being increased. Namely, even if an end goal of operation at multi-MW levels with only a few trips/year is envisioned, one should plan how to get there. Inevitably new systems will have higher trip rates initially as they are shaken out. Also, a slow power ramp-up is needed to understand the beam loss and equipment activation issues. Predicting actual residual activation levels from the prompt beam loss measurements is imprecise. Rather comparisons of measured residual activation levels after sustained operation at different loss levels is needed to understand the tolerable prompt beam losses.

References

[1] Holtkamp, N., "Status of the SNS Project", *Proceedings of the 2003 Particle Accelerator Conference*, *http://accelconf.web.cern.ch/AccelConf/p03/PAPERS/MOAL003.PDF*.

[2] Galambos, J., et al., "Commissioning Strategies, Operations and Performance, Beam Loss Management, Activation, Machine Protection", *Proceedings of Hadron Beam 2008*, Nashville, Tennessee, USA, *http://accelconf.web.cern.ch/AccelConf/HB2008/papers/cpl04.pdf*.

[3] Alonso, J., *et al.*, "Beam Loss Working Group Summary", *7th ICFA Mini-workshop on High Intensity High Brightness Hadron Beams*, Lake Como, Wisconsin (1999).

[4] Catalan-Lasheras, N., *et al.*, "Accelerator Physics Model of Expected Beam Loss Along the SNS Accelerator Facility During Normal Operation", *Proceedings of EPAC 2002*, Paris, France, *http://accelconf.web.cern.ch/AccelConf/e02/PAPERS/THPLE011.pdf*.

Experience with the production of a 1.3 MW proton beam in a cyclotron-based facility

Mike Seidel, Joachim Grillenberger, Anton Mezger
Paul Scherrer Institut
Switzerland

Abstract

PSI operates a cyclotron-based high-intensity proton accelerator that produces a 590 MeV beam with the primary purpose to drive meson production targets and the neutron spallation source SINQ. The accelerator is undergoing a continuing upgrade programme to raise the beam intensity and to improve the operational reliability. In 2008/2009 major steps of the upgrade programme were completed and a regular operating current of 2.2 mA (1.3 MW) was established. During test runs a stable production of 2.3 mA was demonstrated. Completed and planned measures of the intensity upgrade programme are described. The main focus of the paper lies with the specific experiences gained from operating a continuous proton beam with high power. This includes control of beam losses and their scaling with beam current, control and observation of component activation in the accelerator, analysis of accelerator reliability and trip rates. The infrastructure required to operate a high-intensity accelerator as well as specialised accelerator sub-systems, such as the technical interlock systems, will be discussed.

Facility overview

The PSI high-intensity proton accelerator generates a proton beam with 590 MeV kinetic energy and presently 1.3 MW average beam power. As of today this represents the highest average beam power of any proton accelerator world wide. In practice, the performance is limited by the beam losses at the extraction of the ring cyclotron. Those relative losses have to be kept within the lower 10^{-4} range to avoid excessive activation of accelerator components in the extraction region. The PSI accelerator consists of a Cockroft-Walton pre-accelerator and a chain of two isochronous cyclotrons, the Injector II and the ring cyclotron. The beam is produced in continuous wave mode at a frequency of 50.6 MHz. The whole facility is housed in a large hall with a length of ~130 m. The high average beam power, produced in CW mode also makes the PSI accelerator concept interesting for potential ADS applications. The high-intensity proton beam is used to produce pions and muons by interaction with two graphite targets that are realised as two rotating graphite wheels [1]. The targets have thicknesses of 5 mm and 40 mm, respectively. Pions decay into muons that are transported in large aperture beam lines to the experiments. Muon beam intensities up to $5 \cdot 10^{8}$ s^{-1} are achieved per beam line [2]. Scattering of the proton beam in the second target causes a strong emittance blow-up. Further transport of the scattered beam requires collimation whereat 30% of the beam intensity is lost. The remaining beam with roughly 1 MW is then used to produce neutrons in a spallation target that is realised in the form of a matrix of lead filled Zircaloy tubes. The neutrons are moderated in volumes filled with heavy water (D_2O) surrounding the target, and then transported to the 13 instruments installed in the Swiss Spallation Neutron Source (SINQ) facility. In 2010 a pulsed source for ultra-cold neutrons (UCN) was brought into operation as well. While the whole accelerator facility was originally used for particle physics, today the focus is condensed matter physics. The research themes at PSI cover a broad range of applications involving neutron scattering experiments, muon spin spectroscopy and a few particle physics experiments. Figure 1 shows an overview of the facility.

Figure 1: Overview of the PSI high-intensity proton accelerator complex

The diameter of the ring cyclotron, taken at the outer bounds of the magnets, is roughly 15 m

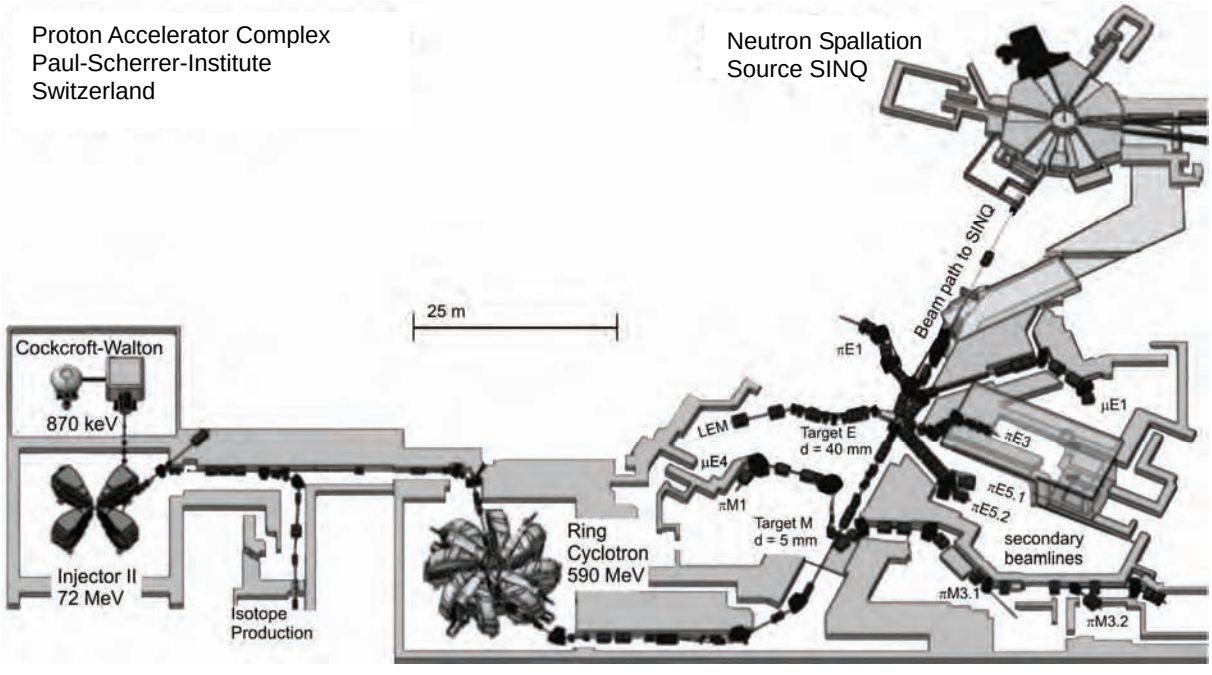

Sector cyclotrons

The cyclotron is a classic example for the concept of resonant acceleration of charged particles. The first cyclotrons were built in the 1930s by Lawrence and Livingston [3]. These first compact cyclotrons had the advantage of a simple and cheap layout and already permitted the production of a continuous beam. To overcome the lack of vertical focusing in the classical cyclotron, today's cyclotrons are realised as sector cyclotrons, a modular set-up of magnets and RF resonators. Sufficient vertical focusing is achieved by utilising two effects, the periodic variation of the bending field strength in sector magnets and intermediate gaps, and by edge focusing at magnet boundaries. Edge focusing is enhanced by introducing a spiral magnet shape. In a sector cyclotron with spiral magnets the squared vertical betatron frequency is given approximately by the relation:

$$\nu_z^2 \approx -\beta^2\gamma^2 + F\left(1 + 2\tan^2\xi\right); \qquad F = \frac{\overline{B^2} - \overline{B}^2}{\overline{B}^2} \tag{1}$$

Here F is the relative mean squared variation of the bending field along the circumference, the so-called flutter factor and ξ the spiral angle of the magnet boundaries. In order to allow continuous acceleration at constant RF frequency (revolution time), the average magnetic field increases with radius as $\frac{r}{B}\frac{\partial B}{\partial r} = \beta^2\gamma^2$. This condition of isochronicity gives rise for the negative first term in Eq. (1). Without Thomas- and edge-focusing, stable vertical orbits would not be possible. Besides such beam dynamics arguments the sector cyclotron exhibits several technical advantages, as for example the modular layout permitting the construction of large diameter cyclotrons.

Dipole magnets and RF resonators are key components of sector cyclotrons. In the PSI ring cyclotron (Figure 2) the average beam orbit varies from 2.1 m to 4.5 m, thus the magnets have to cover a wide radial area. The peak field strength is two Tesla and each of the eight magnets exhibits a weight of 250 metric tonnes. In order to fulfil the condition of isochronicity throughout the acceleration process, the magnitude of the magnetic field has to be controlled precisely. A series of 15 correction coil circuits is used to tune the field strength to the required level of precision.

Figure 2: Schematic layout and photograph of the PSI ring cyclotron

Eight spiral-shaped sector magnets, four fundamental mode resonators and one third harmonic flat-top resonator are shown, as are injection and extraction beam lines

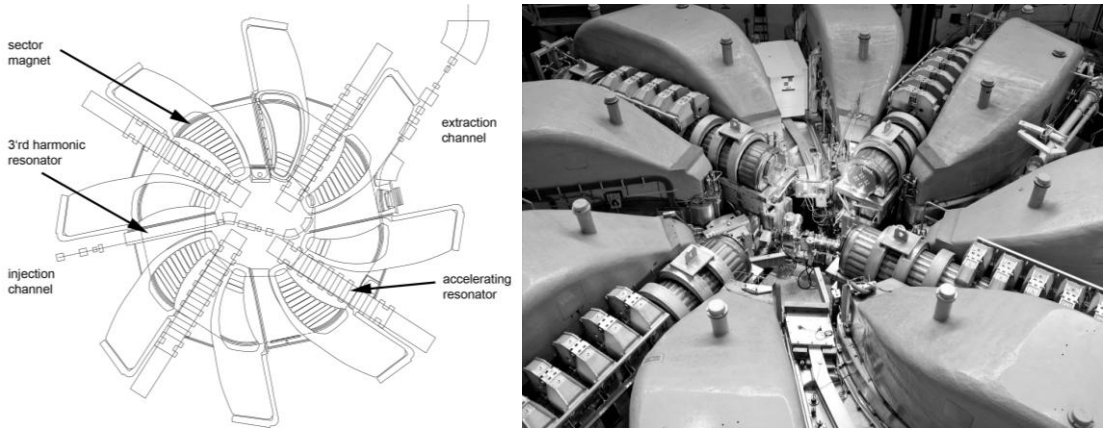

The other major cyclotron component is the specific type of resonator that is capable of covering the large radius variation. The PSI ring cyclotron has four accelerating resonators that transfer the power to the beam. The box-type resonators (see Figure 3) operate at a frequency of 50.6 MHz. A maximum of 400 kW of transferred power per cavity can be achieved within the specifications, although this number is ~285 kW at present. These copper resonators were manufactured by the French company SDMS and were installed as a replacement of the original aluminium resonators in 2006-2008. Besides the four accelerating resonators there is also a third harmonic cavity installed, a so-called flat-top resonator, to allow flattening of the sum RF voltage seen by the beam.

Figure 3: Field distribution in a cyclotron box resonator (left) and photograph of a copper resonator for the PSI ring cyclotron (right)

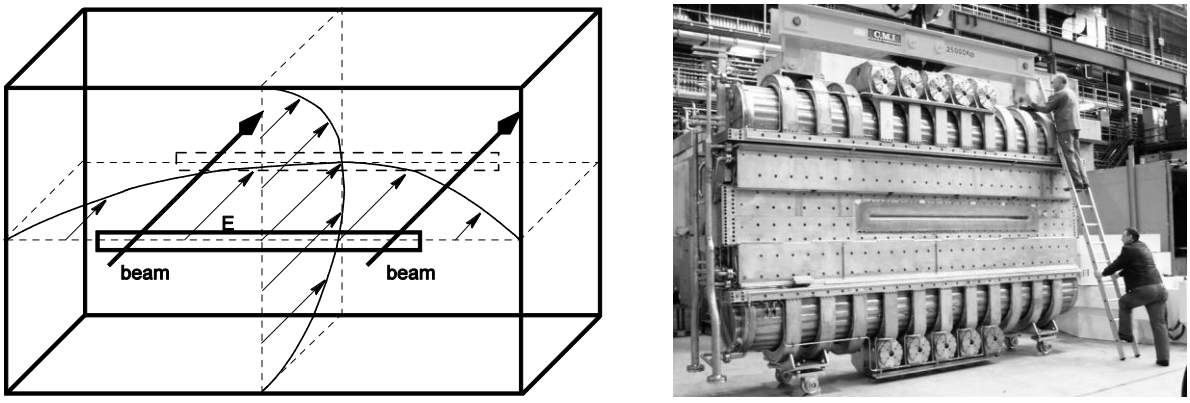

Operational experience and performance

The original PSI accelerator started operation in 1974. At that time it was expected that beam currents of the order of 100 μA could be accelerated. Since then many subsystems of the accelerator chain have been exchanged, as for example a new injector cyclotron (Injector II in 1985) or new resonators and RF systems in the ring cyclotron. The performance in terms of beam current and reliability was dramatically improved. The history of the maximum beam current is shown in Figure 4. For potential industrial applications in view of ADS the conversion efficiency of wall plug power to beam power is of interest. The entire accelerator facility consumes a total of 10 MW in order to generate the beam carrying 1.3 MW. The overall efficiency is thus 13%, but this includes many power consumers that are not needed in an optimised ADS facility. The RF system alone shows an efficiency of ~32%. In summary it may be assumed that an optimised cyclotron facility could reach an efficiency of the order of 20% with some potential for improvements.

As for many high-intensity accelerators, for the PSI cyclotrons beam losses and resulting activation also represent the performance limiting aspects. The extraction of the beam is realised with an electrostatic deflector channel that employs a series of 50 μm thick tungsten strips, charged by 140 kV against ground and placed between last and second-last turn. This device deflects the beam by 8 mrad, allowing further deflection with a magnetic septum at some distance downstream. The turn separation in this location is in the range of 15 mm. Protons in the beam tails may hit the tungsten electrode of the electrostatic element, receive a scattering angle and are lost in the extraction beam line. Vacuum chambers and magnetic elements in this beam line pile up activation. In order to allow servicing of such elements the losses have to be limited and monitored very carefully. Practical experience at PSI shows that relative losses in the order of 10^{-4} are acceptable for standard operation. The highest observed dose rate, taken at 5 cm distance from components in the extraction beam line amounts to 10 mSv/h [4].

Figure 4: History of the maximum beam current in the PSI accelerator facility

Several measures that were undertaken to upgrade the facility are marked

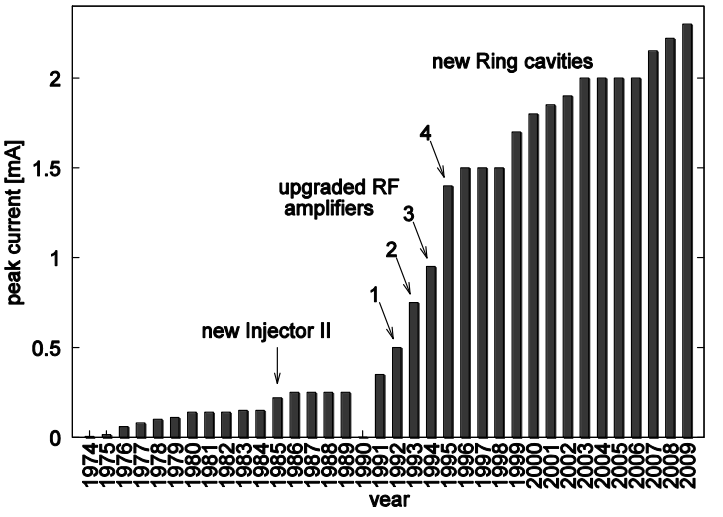

Figure 5: Radial density scan over the outer turns in the ring cyclotron

At the location of the extraction element the particle density is nearly 3 orders of magnitude lower than in the beam centre

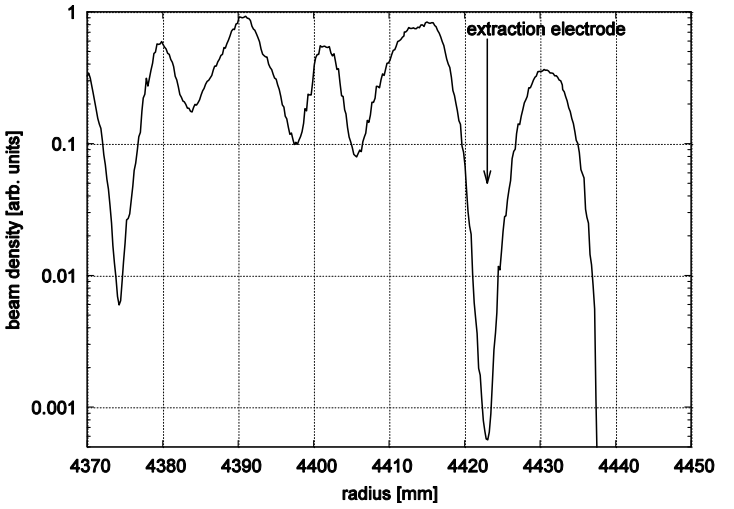

After many years of experience the handling of components in such activated areas has been optimised by the employment of many technical aids such as mobile shielding devices, shielded transport boxes or inflatable vacuum seals allowing fast dismantling of mounted components. The ultimate criterion for the activation problem in a high-intensity accelerator is finally the radiation dose the service personnel receive during standard maintenance work. In Figure 6 we show statistical data on the collective dose the involved personnel received per year from 1980 until today. Even though the total charge delivered per year was dramatically increased over the years, there is no correlation visible with the dose received by the personnel.

Another important aspect, especially in view of potential ADS applications, is the reliability of the accelerator. The many interlock systems that are necessary to operate a MW beam react very sensitively to spikes in the loss rate observed along the accelerator chain and cause beam trips. Another source for beam trips are the electrostatic injection and extraction elements that show random high voltage breakdowns, mainly because of charge up of isolator surfaces in the

Figure 6: Collective dose the service personnel received during the yearly shutdowns, together with the integrated charge delivered by the accelerator per year

While the int personnel

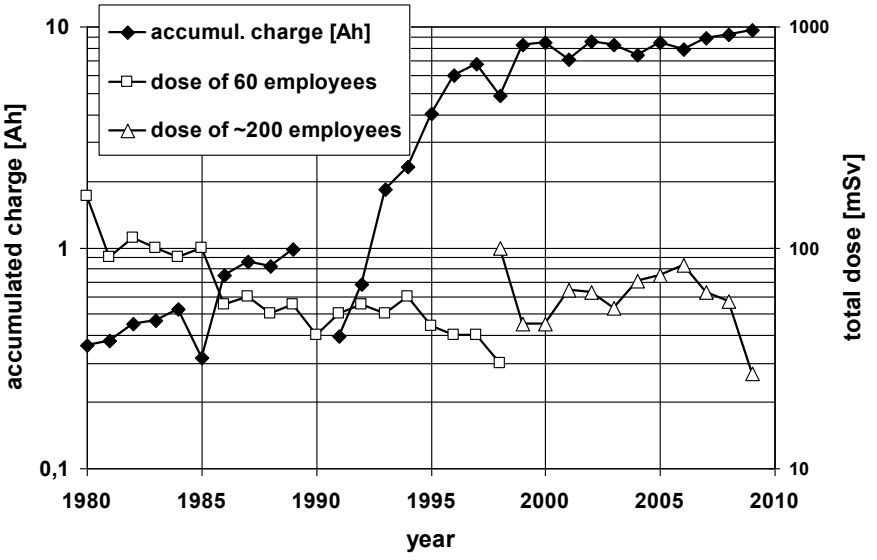

presence of the intensive proton beam. A beam trip caused by such reasons results at least in a 30-second interruption since the current has to be ramped up slowly after a trip. The ramp-up is done automatically if the interlock condition has disappeared. Typical trip rates are in the range 25.50 d^{-1}. More details on the statistics of run durations and trip durations as well as the typical causes for longer interruptions can be found in [5].

Upgrade plans and outlook

The philosophy for upgrades of this cyclotron-based facility always involved a reduction of the relative beam losses in proportion to the intensity increase, thus keeping the absolute losses constant. As described earlier, the losses occur mainly because of scattering in the extraction element of the ring cyclotron. The beam tails containing protons that may hit the tungsten stripes of the septum are generated by beam blow-up from space charge effects. The blow-up scales proportional to the time the space charge forces act, which is proportional to the number of turns needed to accelerate the beam in the cyclotron. The bunches in neighbouring turns are partially overlapping and thus one can consider the charge distribution in the cyclotron in the form of rotating sectors. The charge density in a sector is proportional to the number of turns as well, and this results in another turn number factor for the effect of the space charge forces. Finally, the turn separation at the extraction element is inversely proportional to the number of turns. With such arguments it was concluded by Joho as early as the 1980s [6] that the extraction losses would scale with the third power of the number of turns. Because of this strong scaling considerable reduction of the losses can be achieved by increasing the voltages of the accelerating resonators, i.e. by speeding up the acceleration process. The described scaling is very nicely demonstrated with the history of the maximum intensity in the PSI accelerator as a function of the number of turns. Since the accelerator was always operated at the limit of acceptable losses in the range of 100-200 W, the maximum beam intensity scaled inversely with the third power of the number of turns (Figure 7).

At present an upgrade programme is under way that employs the mentioned principle. After the exchange of the resonators in the ring cyclotron it is now planned to install new accelerating resonators in the Injector II cyclotron. At present the injector cyclotron is equipped

Figure 7: Maximum beam current as a function of the number of turns, demonstrating the scaling with the third power law

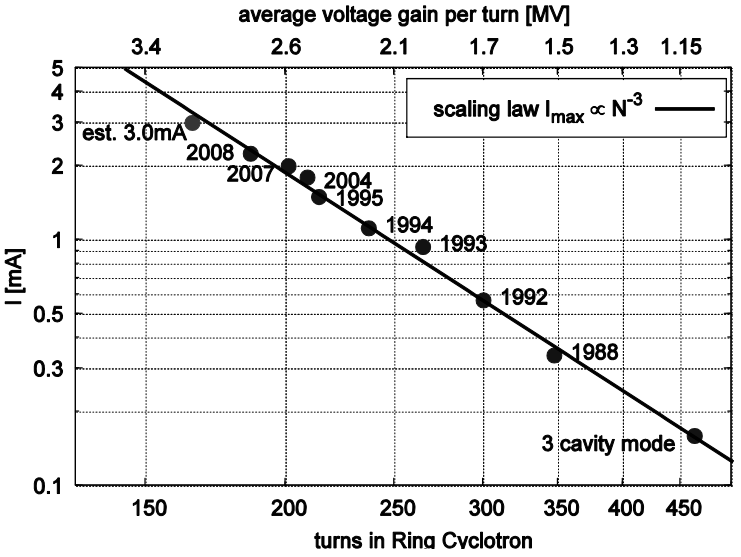

with two accelerating and two flat-top resonators. As explained below, in a new operating regime of the injector cyclotron it is now possible to replace the existing third harmonic resonators by the mentioned accelerating resonators. Only with the upgraded injector it will be possible to fully exploit the potential of the new ring cyclotron resonators.

In the PSI Injector II cyclotron it was observed that a high charge density in the proton bunches does actually not lead to further beam blow-up, but to the formation of a stable circular beam distribution in the radial/longitudinal plane. In the presence of a strong repelling force from the concentrated charge in the bunch centre, particles are accelerated away from the bunch centre. However, as soon as they gain a significant relative speed they are bent back by the dipole field of the cyclotron. The resulting path of motion has a cycloidal shape in a frame that moves with the bunch. Thus, with sufficiently high charge densities the particles rotate rapidly around the bunch centre and a bound motion is established even though the space charge force is repelling [7]. The principle of the round beam formation is illustrated in Figure 8, left, with a simple model calculation assuming a homogenous dipole field. In the PSI facility this operating regime was first observed in the Injector II cyclotron, but it should be possible in the ring cyclotron as well. The time structure measurement of the bunch distribution (Figure 8, right [8,9]) shows the observed circular bunch shape. Obviously the compact and stable circular bunch shape leads to reduced losses. In order to enhance this effect and to improve the capture efficiency an additional third harmonic buncher was installed [10] in 2007 before injection of the Injector II cyclotron. The third harmonic buncher reduces non-linearities of the standard 50 MHz buncher voltage that is used to bunch the DC beam generated in the 870 keV Cockroft-Walton pre-accelerator. Indeed a shorter beam is now observed and this opens the possibility to replace the two flat-top resonators in the Injector II cyclotron by new accelerating resonators operating at 50 MHz. A new resonator type has been designed and two copies are being manufactured at the French company SDMS. Figure 9 shows the CAD model and a photograph of the first delivered resonator. These cavities are made from aluminium, they exhibit a sector shape and the challenges of the mechanical design lie in a good cooling concept assuring frequency stability and a hydraulic tuning mechanism [11].

In the 55 m long transport line between Injector II and ring cyclotron the bunch length is considerably enlarged by the longitudinal space charge forces. In order to achieve a similar effect as in the Injector II cyclotron a tenth harmonic rebuncher [12] has been installed to counteract

Figure 8: Round beam distribution in cyclotrons

The left plot shows the trajectories of test charges within a simple model calculation, and the right plot shows round bunch configurations as they are measured on the two outer turns in the Injector II cyclotron

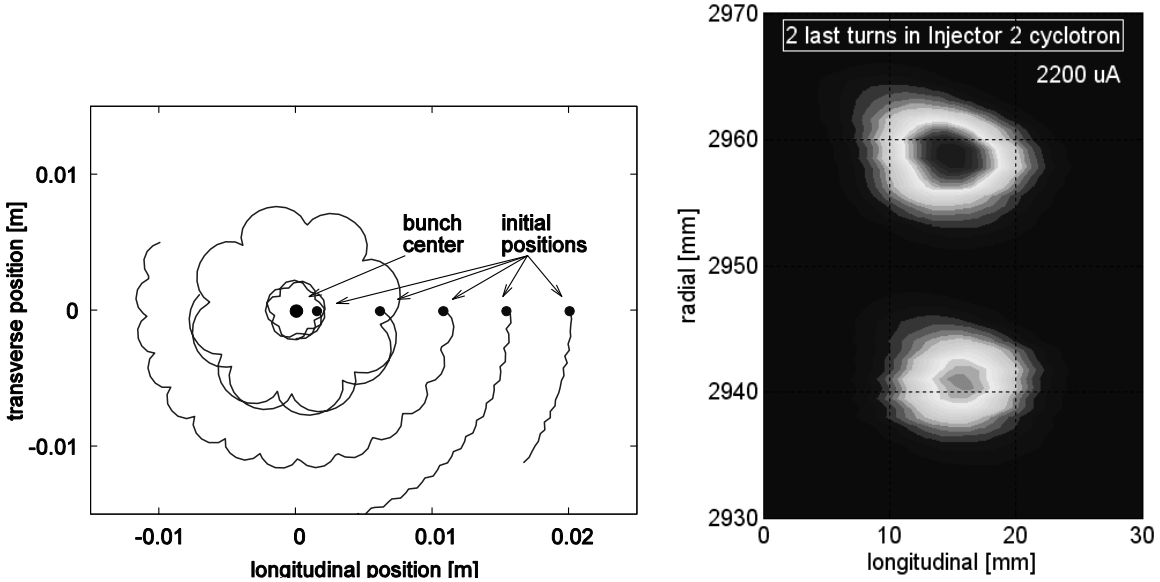

Figure 9: Photograph and CAD model of a new aluminium resonator for the Injector II cyclotron [11]

These resonators will replace the existing third harmonic flattop cavities in the cyclotron

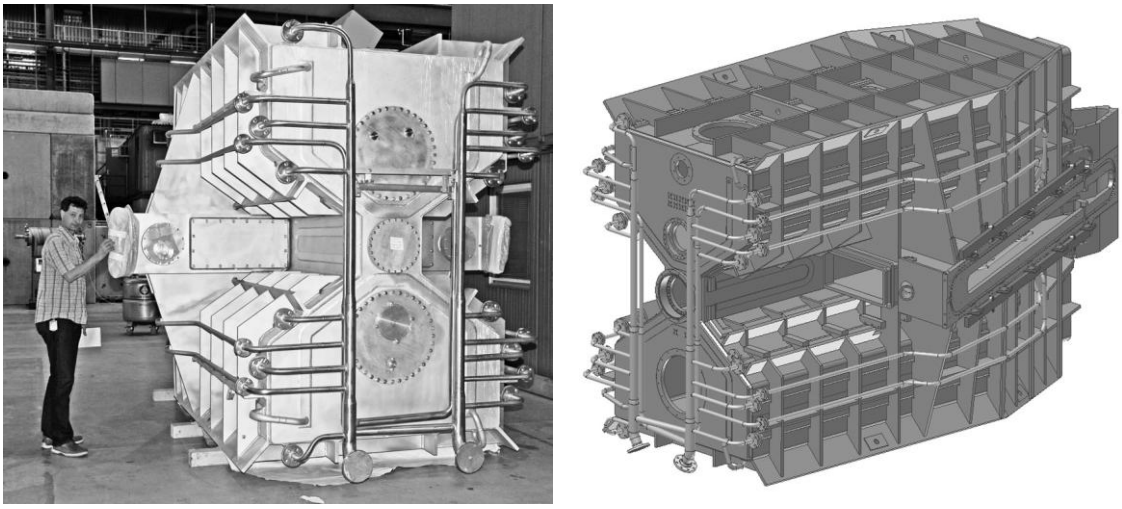

the space charge blow-up. From simulations [13] it is also expected that in the ring cyclotron the existing 150 MHz flat-top resonator can be omitted when significantly shorter bunches are injected. For successful operation of the new 500 MHz buncher a better phase control has to be established, and possibly we need a better current dependent matching of the transverse beam optics.

Another improvement project involves the installation of a new ECR source [14] that replaces the existing filament heated ion source in the spring shutdown of 2010. Although the new ion source will produce a better beam emittance, the major practical advancement consists in the better reliability. Finally, in order to reach the full beam power of 1.8 MW several absorbers behind the 40 mm graphite target (Target E) have to be redesigned.

In summary, the upgrade plans of the PSI facility [15] foresee a stepwise increase of the beam intensity to 3.0 mA. As described, the major ingredients of the upgrade path consist in higher resonator voltages in both cyclotrons and shortening of the bunch length by utilising a special tenth harmonic buncher cavity. The faster acceleration process leads to lower relative losses, permitting to increase the beam power at constant absolute losses. The installation of two new resonators in the Injector II cyclotron together with new RF amplifier chains is planned for 2013.

The resonant acceleration principle and the continuous operation mode with constant bending fields and RF frequency make the cyclotron concept a good candidate for high-intensity ion beam production. With 1.3 MW power at a beam energy of 590 MeV the PSI facility has reached a respectable performance which can still be improved to 1.8 MW by further upgrades. This is already within the useful range for experimental AD systems. For the cyclotron-based facility as well as with other accelerator concepts it will be difficult to achieve the very low trip rates of 0.01 d^{-1} that are desirable for ADS. Measures such as redundancy of vital systems and the operation of components at conservative parameters would improve the situation. In a straightforward extrapolation from the PSI facility it seems feasible to design a cyclotron accelerator that provides a 1 GeV/10 MW beam with improved reliability [16].

References

[1] Heidenreich, G., "Carbon and Beryllium Targets at PSI", *Proc. AIP*, 642, 122 (2002).

[2] Prokscha, T., *et al.*, The New μE4 Beam at PSI: A Hybrid-type Large Acceptance Channel for the Generation of a High Intensity Surface-muon Beam", *Nucl. Instr. Meth.*, A 595, 317 (2008).

[3] Lawrence, E.O., N.E. Edlefsen, "On the Production of High Speed Protons", *Science*, 72, 376 (1930).

[4] Paul Scherrer Institut (PSI), *Annual Report 2008 of the Division for Radiation Safety*, PSI AN-96-09-09, 65 (2009).

[5] Seidel, M., A. Mezger, "Performance of the PSI High Power Proton Accelerator", *Proc. of Int. Topical Meeting on Nucl. Res. Appl. and Util. of Accel.*, Vienna, Austria (2010).

[6] Joho, W., "High Intensity Problems in Cyclotrons", *Proc. 5th Int. Conf. on Cyclotrons and Their Applications*, Caen, France (1981).

[7] Chasman, C., A.J. Baltz, "Space Charge Effects in a Heavy Ion Cyclotron", *Nucl. Instr. & Meth.*, 219, 279 (1984).

[8] Dölling, R., "Measurement of the Time-structure of the 72 MeV Proton Beam in the PSI Injector-2 Cyclotron", *DIPAC2001*.

[9] Dölling, R., *New Time-structure Probes Between Injector and Ring Cyclotron*, PSI Annual Report, 15 (2004).

[10] Humbel, M., *et al.*, "Commissioning and Tuning of the New Buncher System in the 870 keV Injection Beamline", Proc. *Cyclotrons and Their Applications 2007*, Giardini Naxos, Italy, 464 (2007).

[11] Stingelin, L., M. Bopp, H. Fitze, "Development of the New 50 MHz Resonators for the PSI Injector II Cyclotron", *Cyclotrons and Their Applications*, Catania, 467 (2007).

[12] Raguin, J.Y., *et al.*, "Comparative Design Studies of a Superbuncher for the 72 MeV Injection Line of the PSI Main Cyclotron", *Proc. EPAC 04*, Lucerne, Switzerland, 1162 (2004).

[13] Yang, J.J., *et al.*, *Beam Dynamics in High Intensity Cyclotrons Including Neighboring Bunch Effects: Model, Implementation and Application*, arXiv:1003.0326v1 (2010).

[14] Schmelzbach, P.A., *et al.*, "A Compact, Permanent Magnet, ECR Ion Source for the PSI Proton Accelerator", *Proc. Cyclotrons and Their Applications 2007*, Giardini Naxos, Italy, 292 (2007).

[15] Seidel, M., P.A. Schmelzbach, "Upgrade of the PSI Cyclotron Facility to 1.8 MW", *Proc. Cyclotrons and Their Applications 2007*, Giardini Naxos, Italy, 157 (2007).

[16] Stammbach, Th., *et al.*, "The Feasibility of High Power Cyclotrons", *Nuclear Instruments and Methods in Physics Research B*, 113, 1-7 (1996).

Session III

Neutron Sources

Chair: M. Seidel

MEGAPIE spallation target: Irradiation of the first prototypical spallation target for future ADS

Ch. Latgé[1], M. Wolmuther[2], P. Agostini[3], M. Dierckx[4], C. Fazio[5], A. Guertin[6], Y. Kurata[7], G. Laffont[1], T. Song[8], K. Thomsen[2], W. Wagner[2], F. Groeschel[2], L. Zanini[2], Y. Dai[2], J. Henri[1], J. Konys[5], K. Woloshun[9]
[1]CEA Cadarache, [2]PSI Villigen, [3]ENEA Brasimone, [4]SCK•CEN Mol,
[5]FZK Karlsruhe, [6]SUBATECH Nantes, [7]JAERI, [8]KAERI, [9]DOE-LANL

Abstract

A key experiment in the accelerated-driven systems roadmap, the Megawatt Pilot Experiment (MEGAPIE) (1 MW), was initiated in 1999 in order to design and build a liquid lead-bismuth spallation target, then to operate it into the Swiss spallation neutron facility SINQ at Paul Scherrer Institute (PSI) [1]. It must be equipped to provide the largest possible amount of scientific and technical information without jeopardising its safe operation. Whereas the interest of the partner institutes is driven by the development needs of ADS, PSI interest also lies in the potential use of an LM target as a SINQ standard target providing a higher neutron flux than the current solid targets. The MEGAPIE project is supported by an international group of research institutions: PSI (Switzerland), CEA (France), FZK (Germany), CNRS (France), ENEA (Italy), SCK•CEN (Belgium), DOE (USA), JAERI (Japan), KAERI (Korea) and the European Commission.

The MEGAPIE target has been designed, manufactured, set up and fit with all the ancillary systems, on an integral test stand in Paul Scherrer Institute for off-beam tests dedicated to thermo-hydraulic and operability tests, carried out during the last months of 2005 then moved to the final implementation in the SINQ facility, with the ancillary systems, for irradiation, carried out from 14 August 2006 to 21 December 2006. The results obtained during the integral tests have shown that the target was well designed for a safe operation and allowed to validate the main procedures related to fill and drain, steady-state operation and transients due to beam trips.

The start-up procedure has been developed, and the operating and control parameters have been defined.

The irradiation allowed obtaining very important results, particularly showing the very good operational behaviour of the target, the heat exchanger and the electro-magnetic pumps. Moreover a lot of results in the thermal-hydraulic and neutronics fields as well as gas analysis have been gathered and contributed to validate the design studies and the models in that field.

The target has been cut into slices in order to prepare the samples for the future post-irradiation examinations.

The successful behaviour of the target during irradiation and the results to come concerning irradiated materials will provide ADS community with a unique, relevant design and operational feedback, paving the way to the development of high-power spallation targets for a future powerful ADS, having the industrial capability of transmuting large amounts of nuclear wastes.

The MEGAPIE project

A key experiment in the accelerated-driven systems roadmap, the Megawatt Pilot Experiment (MEGAPIE) (1 MW) was initiated in 1999 in order to design and build a liquid lead-bismuth spallation target, then to operate it into the Swiss spallation neutron source facility SINQ at Paul Scherrer Institute (PSI) [1]. It must be equipped to provide the largest possible amount of scientific and technical information without jeopardising its safe operation. Whereas the interest of the partner institutes is driven by the development needs of ADS, PSI interest also lies in the potential use of a LM target as a SINQ standard target providing a higher neutron flux than the current solid targets.

The MEGAPIE project is supported by an international group of research institutions: PSI (Switzerland), CEA (France), FZK (Germany), CNRS (France), ENEA (Italy), SCK•CEN (Belgium), DOE (USA), JAERI (Japan), KAERI (Korea) and the European Commission.

Many studies supporting design, carried out by the project partners, addressed specific critical issues in the fields of nuclear physics, materials, thermal-hydraulics, mass and heat transfer, structure mechanics and liquid metal technology, using analytical, numerical and experimental approaches.

Moreover, it was necessary to perform safety and reliability assessments in order to demonstrate the integrity and operability of the target; and thus to develop the licensing process. To reach this goal, the design had mainly to consider the structural integrity of the target for normal operating conditions, transient situations and hypothetical accidents, and the capability to evacuate the deposited heat with the heat exchanger and the electromagnetic pump system.

The design studies of the target were performed by CNRS, CEA, PSI and IPUL, with the support of all the organisations involved in the project; the main components of the target were manufactured in France by the ATEA Company and sub-contractors, and in Latvia (EM pumps), then assembled in France. The ancillary systems were designed and manufactured in Italy (Ansaldo, Criotec) and Switzerland (PSI). The main constraint was first to design a completely different concept of target in the same geometry of the current spallation targets used at PSI. The second was to develop and integrate two main prototypical systems: a specific heat removal system and an electromagnetic pump system for the hot heavy liquid metal in a very limited volume. The third imperative was to design a 9Cr martensitic steel (T91) beam window capable of reaching the assigned life duration. The reasons for the choice of lead-bismuth eutectic (Pb44.5%-Bi55.5%) and of T91 (0.1C, 0.32Si, 0.43Mn, 8.73Cr, <0.01W, 0.99Mo, 0.19V, 0.031Nb, 0.029N, 0.24Ni) for the beam window, which is the most critical component of the target, were outlined in Ref. [2].

A sketch of the target and its main characteristics is shown in Figure 1. It is designed to accept a proton current of 1.74 mA, although the probable current in 2005 may not exceed 1.4 mA. The 650 kW thermal energy deposited in the LBE in the bottom part of the target is removed by forced upward circulation by the main inline electromagnetic pump through a 12-pin heat exchanger (THX). The heat is evacuated from the THX via an intermediate diathermic oil and an intermediate water cooling loop to the PSI cooling system. The cooled LBE then flows down in the outer annulus (4 l/sec). The beam entrance window, welded to the lower liquid metal container, including the beam window, both manufactured with T91 ferritic/martensitic steel, is especially cooled by a cold LBE jet extracted at the THX outlet and pumped by a second EM pump (0.35 l/sec) through a small diameter pipe down to the beam window. A main flow guide tube separates the hot LBE upflow from the cold downflow in the outer annulus: it is equipped with a number of thermocouples to monitor the temperature field in the spallation zone. Attached to the top of the tube is the electromagnetic pump system, designed by IPUL, consisting of the concentrically arranged bypass pump and the in-line main pump on top of it. Both pumps are equipped with electromagnetic flow meters. The pump system is surrounded by the THX, designed by CEA, and

Figure 1: MEGAPIE target

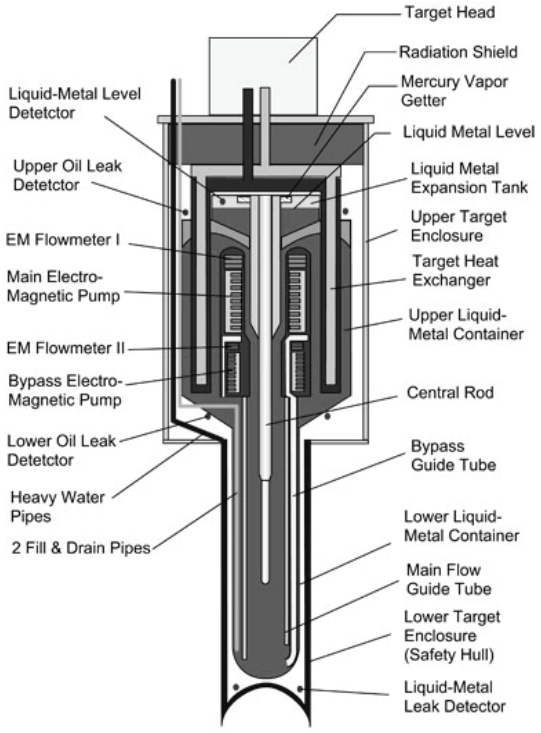

consisting of 12 pins concentrically arranged and 1.20 m long, where the lead-bismuth eutectic is cooled by diathermic oil Diphyl THT. The heat is removed from the THX by an intermediate oil loop designed by Ansaldo. An intermediate water cooling loop designed and built by PSI then evacuates the heat from the oil loop. This concept eliminates any interaction of LBE with cooling water. A central rod is inserted inside the main flow guide tube carrying a 22 kW heater and neutron detectors, provided by CEA. The lower liquid metal container, the flange of the guide tube and the heat exchanger constitute the boundary for the LBE, called the hot part. The second boundary is formed by three components, which are separated from the inner part by a gas space filled with either 0.5 bar He. The gas will stay enclosed during the experiment and only the pressure will be monitored. The components include:

- The lower target enclosure, a double-walled, D_2O cooled hull made of $AlMg_3$. The containments of the current targets are made of the same material and experience on its radiation performance exists up to about 10 dpa. The enclosure is designed to contain the LBE in case of a number of hypothetical accidents which could lead to the breach of the inner container. The enclosure is flanged to the upper target enclosure.
- The upper target enclosure, formed by a stainless steel tube. This tube is welded to the target head.
- The target head consisting of the main flange, which positions the target on the support flange of the central tube of the SINQ facility, and the crane hook. All supplies to the target and instrumentation lines are fed through the target head.

The last component is the target top shielding, which connects the hot part to the target head. The LBE-containing part of the target is thus suspended from the target head and allowed to expand with the temperature. The components also contain tungsten to shield the target head area from the intense radiation of the LBE and the noble gases and volatiles collected in the gas expansion tank. The main characteristics of the target are displayed in Table 1.

Table 1: Main characteristics of MEGAPIE target

Beam energy	575 MeV	**Deposited heat**	650 kW
Beam current	1.74 mA (design)	**Cold temperature**	230-240°C
Length	5.35.m	**Hot temperature**	380°C
LBE volume	About 82 l	**Design temperature**	400°C
Weight	About 1.5 t	**Operating pressure**	0-3.2 bar
Wetted surface	About 8 m^2	**Design pressure**	16 bar
Gas expansion volume	About 2 l	**Total flow rate**	4 l/s
Insulation gas	0.5 bar He	**Bypass flow rate**	0.25 l/s

For the target operation it was necessary to design, manufacture and connect to the target's various ancillary systems: heat removal, cover gas, insulation gas, LBE fill and drain, beam line adaptations,… The description of these ancillary systems has been reported in [3].

After manufacturing in France, the target was shipped to PSI in May 2005. In order to demonstrate the target characteristics and safe operability prior to irradiation in 2006, the target was installed, fit with all the ancillary systems (which had already been commissioned) and tested out-of beam. Then the target was equipped with some complementary systems necessary for the irradiation period: insertion of neutron flux detector, LBE leak detector close to the window and new systems were installed to watch for correct proton scattering in target and proper beam transport. The target was then installed in SINQ, then connected to ancillary systems: fill and drain, heat removal, cover gas, isolation gas,… The target was irradiated from 17 August 2006 to 22 December 2006, to obtain neutron performances, to confirm material performances and to demonstrate the ability to operate a liquid metal target under relevant conditions. During the irradiation phase, numerous operating parameters were monitored, including pressure, fluid flow rates and temperatures. Moreover, experimental measurements of neutron fluxes at various positions of the facility, and of gas production were carried out. After operation, the target was disconnected and sealed up with blind flanges, stored for several months, transferred to SWILAG hot laboratories, using a steel container, cut with band saw in 19 slices which were transported to the hot lab at PSI. The extraction of sample material for post-irradiation examination is being prepared, prior to distribution among the project partners. The remaining target pieces were conditioned in a steel cylinder in a KC-T12 concrete container.

Main feedback from MEGAPIE-related studies and operation

Seven phases of the MEGAPIE project are considered; six of them have already been carried out, providing operational feedback from experiments or studies performed within these phases:

- basic studies in support of the design, i.e. studies related to corrosion, lead-bismuth freezing and consequences, lead-bismuth water interaction, etc.;
- feedback from manufacturing;
- studies carried out during integral tests phase, before irradiation phase, including a full-scale leak test;
- implementation of the target and ancillary systems in SINQ;
- irradiation phase;
- decommissioning operations;
- post-irradiation examinations.

This last phase is under preparation, but has not yet been performed.

Basic studies

The main relevant design issues were focalised:

- on the structural integrity of the target in order to keep all active material confined inside the target for both normal operating conditions and hypothetical accidents;
- on performances of the heat exchanger to evacuate the deposited heat;
- on performances of the EM pump system;
- on the freezing properties of the LBE and the behaviour of the spallation products;
- on the integrity and coolability of the window.

These and other relevant issues streamlined the activities performed within the scientific design support by all the project partners.

Design support was organised in different sections: neutronics, materials, thermal-hydraulics, structure mechanics, mass and heat transfer, liquid metal technology and reliability assessment. The most important challenge was to develop a coherent activity between these different sections and to converge towards recommendations to the design team.

As an example among many studies, it was demonstrated that the lead-bismuth eutectic expansion could be mitigated if the cooling rate was kept as low as 0.02°C/min from the solidification point to 60°C, thanks to a better understanding of the LBE recrystallisation process.

Figure 2: LBE recrystallisation

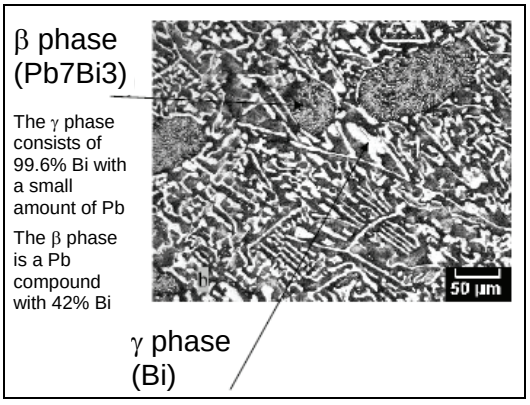

Note: Image courtesy of ENEA.

The evaporation behaviour of Po and other elements from liquid Pb-Bi was investigated, thanks to experiments carried out the CERN ISOLDE facility: it was demonstrated that below 600°C the polonium remains in LBE.

In the same manner, material behaviour was investigated in the framework of the LISOR programme.

Target manufacturing

The main feedback (from the ATEA Company) was the solutions found to solve difficulties for manufacturing due to a variety of materials: 316L, T91, tungsten,… complex geometry,... The local co-operation established among the main designer (Subatech), quality assurance (PSI) and manufacturer was essential.The Institute of Physics (IPUL) in Latvia designed and validated the pump concept by testing a prototype and manufacturing the two pumps.

A main relevant issue was the development and assessment of suitable joining and welding technologies of the selected materials for target in different geometries (e.g. window, tubes of heat exchanger,...). Joining and welding procedures were qualified for various configurations, including preparation, welding and control. Specification and welding procedure for metallic materials were approved by a pre-production welding test. Control was based on non-destructive examination of fusion welds, a radiographic testing of welded joints and also visual examination.

Integral tests phase

Single components, such as the electromagnetic pump system, the beam entrance window and the cooling pin of the heat exchanger, were first built as prototypes and tested in order to assess their performances. The target and its ancillary systems were integrated and tested out-of-beam in the so-called MEGAPIE Integral Test Stand (MITS). The objectives of the MITS experiments were to first integrate all systems, to check their functionality by simulating normal operating conditions and transients (e.g. beam trips, beam interruptions, loss of coolant) postulated for the MEGAPIE target in SINQ. The results of the single component tests were combined with the results obtained at the MITS to assess the overall target performance.

The integral tests consisted of the following main tests:

- filling of the target with lead-bismuth eutectic;
- checking the operability of the main components of the target;
- checking and calibration of the instrumentation (mainly flow meters);
- carrying out the thermal-hydraulic tests with a heater to simulate heat deposition;
- performing transients for qualification of heat removal and control systems.

The final conclusion of the integral tests and associated studies was that the overall system will be able to adequately remove the anticipated 600 kW heating of the SINQ proton beam, and the control system was able to mitigate the transient controlled trips occurring during operation. This was confirmed by calculations performed with RELAP-V.

Similar to the integral tests performed with the target, a full scale leak test (FSLT) was performed at Paul Scherrer Institut with the goal to validate both the design of the lower target enclosure (LTE) under worst case leak conditions, and the leak detector system (Figure 3), implemented in the lower part of the LTE.

Figure 3: Leak detector system

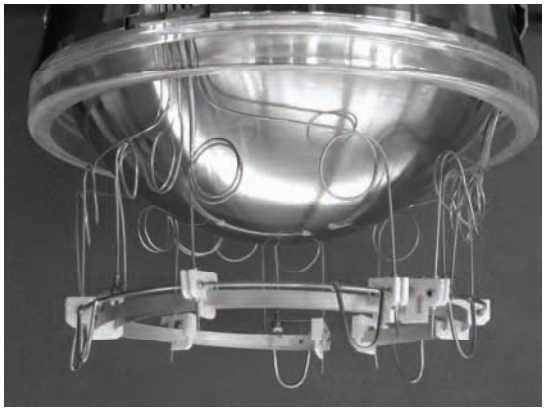

Complementary to the FSLT, within the framework of the general safety assessment, the potential consequences of three simultaneous failures of the target shells were investigated

independently with the MATTINA and SIMMER codes, able to model the hypothetical interaction between lead-bismuth alloy and D_2O, inducing water vaporisation and target pressurisation (target can withstand $P < 30$ bar). The accidental sequence was evaluated, vapour explosion was excluded and the structure integrity was demonstrated, the maximum pressure being maintained largely below 30 bar [5].

In support of the future post-test analysis phase after irradiation, the KILOPIE experimental programme was carried out by PSI and FZK to validate the heat transfer coefficient at the window and more generally to characterise the LBE behaviour [8]. In addition, large eddy scale simulations were performed by CEA to analyse the instabilities; different approvals for dedicated sub-steps of the dismantling of the LBE target have to be obtained close to the window. The objectives of these simulations with the CEA TRIO-U-VEF parallelised code were to assess the level of temperature and velocity fluctuations near the window, to gain a more "realistic vision" of the actual flow behaviour and to know qualitatively the variations of the temperature signals in real or virtual thermocouples, and consequently to give realistic data for thermo-mechanical studies aiming to demonstrate the integrity of the T91 window.

Implementation of the target and ancillary systems in SINQ

Prior to the irradiation phase, a neutron flux detector provided by CEA was inserted. The electrical cabling and other connections were installed in the target head (Figure 4). The LBE leak detector was then installed, prior to the final welding of the lower target enclosure, with a qualified procedure. The LTE tightness was checked by X-ray and pressure and leak test. The target was then installed in SINQ, then connected to ancillary systems: fill and drain, heat removal system, cover gas system, isolation gas system,…

Figure 4: Target in SINQ

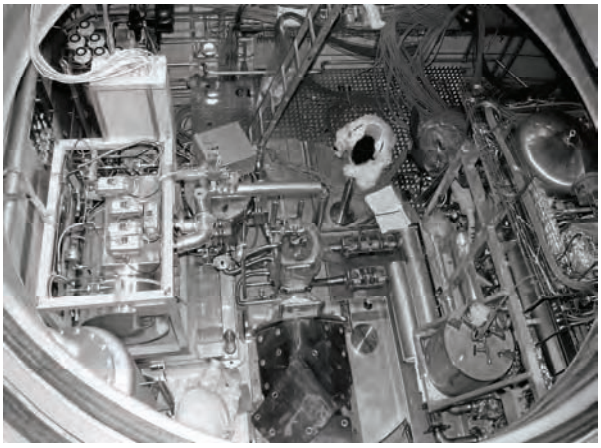

The beam has to be controlled to avoid any damage to the window: for the MEGAPIE target, due to the specific risks induced by the position of the window (bottom of the target) and the choice of a liquid lead-bismuth alloy, four new systems have been installed to watch for correct scattering in target and proper beam transport, in order to fulfil the requirement of the beam being switched off within 100 ms if 10% of the protons bypass the target. One of the new systems is the so-called VIMOS: glowing of a mesh implemented in the beam duct is monitored via special optical measurement chain and software.

In order to fulfil the requirement of 1 mSv criterion for the public, in case of an incidental release, some measures for reduction of the source term were decided and carried out:

- better sealing of the buildings over and below the target (TKE and STK), when installed in SINQ;
- inertisation system provided by MESSER was provided to prevent inflammation by the thermal oil under the most extreme conditions: the "LowOx" system reduces the oxygen content to < 13% (layout value: 11%) by nitrogen injection;
- connecting the TKE with the cooling plant in order to reduce the possible activity concentration in air;
- upgrade of the ventilation system (earthquake resistant stand-alone exhaust equipment) and of the filter systems (both with activated carbon and particle filters).

Close to the target, a ventilation system was also updated to locally control the temperature.

This phase was essential: it was mandatory to satisfy the safety requirements, taking into account the specific constraints of a liquid metal target, i.e. large inventory of spallation products and its consequences on the confinement definition, filters,…, risk of fire due to oil (even if this coolant option could be replaced by another one, more adapted to the application).

Irradiation phase

The target was irradiated from 17 August 2006 to 22 December 2006, to obtain neutron performances, to confirm material performances and to demonstrate the ability to operate a liquid metal target under relevant conditions. A specific procedure for start-up was prepared and implemented by the PSI operation team. During the irradiation phase, numerous operating parameters were monitored, including pressure, fluid flow rates and temperatures. Moreover, experimental measurements of neutron fluxes at various positions of the facility, and of gas production were carried out.

The main results obtained were the follows. The strategy defined by PSI to operate the target, delineating three main operational modes (isolation case, hot stand-by case and beam operation case), was validated, showing that it was possible to operate such a liquid target with the general principles of a solid reference one. If during the beam operation status, an anomaly in the signals is detected, the beam is switched off and the target will go into "hot stand-by case" or into "isolation case" if a critical problem is detected. If during the "hot stand-by" case, it is not possible to maintain the selected operational conditions, the target goes into "isolation case".

During the entire MEGAPIE irradiation experiment the target served as the source for the neutron scattering programme at PSI, respecting the required availability of neutrons: full power at >95% of the schedules operation time [continuous (51 MHz) 590 MeV proton beam hitting the target expected to reach routinely an average current around 1 350 μA, corresponding to a beam power ~0.80 MW]. Thus, PSI was able to satisfy researchers during this period with the MEGAPIE target.

During the operation period, mainly due to the SINQ proton beam, the system suffered:

- ~5 500 beam trips (< 60 s);
- ~ 570 beam interrupts (< 8 hrs);
- ~ 6 600 total beam transitions.

The target behaviour was excellent both during stable operation and transients due to beam trips. The temperature distributions and transients were as expected, very close to predictions. The electromagnetic pumps (EMP) operated stably and reliably, without any indication of degradation thus far. On the contrary, the performance and accuracy of the electromagnetic flow meters (EMF) were low; difficulties were mainly induced by the proximity to EMP (leakage of magnetic flux) and by T transients due to immersion in LBE (> 10°C/s). There is a strong necessity to work on the optimisation of flow meters for targets or other integrated systems (EMP + EMF).

For the main MEGAPIE ancillary systems directly connected to the target, i.e. heat removal system (HRS), cover gas system (CGS) and insulation gas system (IGS), the operating feedback was positive in general.

A further lesson was to care for redundancy of vital sensors in such a complex system [7]: one pressure transducer inside the enclosure controlling and recording the plenum gas pressure failed, most likely due to radiation damage, although qualified for radiation resistance up to a total gamma-dose of 1 MGy. Switching to the remaining redundancy solved the problem at that time, but after that no redundancy remained. Thus, there is a high necessity to develop a reliable strategy to qualify the instrumentation (scientific-operational-safety related) and to define the level of redundancy required.

Another important feedback was the necessity to upgrade the gas sampling system, indispensable to control the inventory before venting.

In the insulation gas system (IGS), designed as closed volume, the pressure, expected to rema constant during target operation and only reacting to temperature variations, in fact increased by ~5 mbar/h. Thorough analysis gave evidence that oil from the HRS was leaking into the IGS volume, decomposed by radiolysis during beam operation. This event was confirmed by the observation of residues in the window, during the decommissioning phase.

The experience with the safety devices implemented to monitor the proton flux from SINQ was very positive. The VIMOS camera was replaced and worked satisfactorily; the Stripe LBE leak detector was satisfactory, but the TC LBE leak detector was considered the most sensitive beam diagnostic.

Neutron flux measurements were performed in various places with different methods [4]: measurements at beam lines or inside D_2O tank (activation foils, Bonner spheres,… measurement of neutron flux inside the target using micro-fission chambers (Figure 5), measurement of delayed neutrons (DN) in the upper part of the target (neutron detector based on ^3He counter). All these measurements provided a large data set in order to characterise the performances of the target.

Figure 5: Micro fission chamber

Gas measurement by gamma spectroscopy following the beginning of irradiation has led to the determination of the main radioactive isotopes released by the LBE. Comparison with calculations performed with several validated codes supplied important volatile elements' release rate estimation in a spallation target. The induced database is relevant for safety and radioprotection.

In addition, calculations with MCNPX, FLUKA and SNT codes coupled with evolution codes have been performed in order to increase the knowledge of spallation target behaviour. Such calculations provided important information on structural material (container, window) and LBE activation just following the end of irradiation and at different cooling times. Such a data set was

fundamental for the post-analysis of MEGAPIE as well as the decommissioning phase, to support the licensing process and to obtain the different approvals for dedicated sub-steps of the dismantling of the LBE target.

A comparison between measurements (fluxes in n/cm^2/s/mA) and calculations using MCNPX and FLUKA has shown that the gain in terms of neutron flux was around 80% in comparison with a solid metal target, greatly exceeding expectations.

Decommissioning operations [6]

After the irradiation phase, the cooling circuits and gas volumes were emptied, rinsed and dried, the target was disconnected and sealed up with blind flanges, then it was stored for several months. After about one year and a half, the target was transferred to SWILAG Hot Laboratories, thanks to a dedicated container, (TC1)manufactured by Skoda. The target was then cut with a band saw (provided by Behringer, Germany) (Figure 7), into 19 slices (+ 2 extra parts). This critical operation was successfully carried out, thanks to the prior validation phase: the band was tested in several cold campaigns in and outside of ZWILAG, using a dummy target with appropriated working procedures (Q-plans). The feedback from this step is very essential with regards decommissioning of this highly contaminated LBE component. About 8 (weight) % of the target was transported to the hot lab at PSI, using a steel container (Figure 6) made of two concentric parts (inner contamination protection and shielding), in order to prepare the samples of material for post-irradiation examinations, which will be carried out by CEA, CNRS, ENEA, FZK, JAEA, LANL-DOE, PSI and SCK. The remaining target pieces (92%) were conditioned in a steel cylinder in a KC-T12 concrete container (TC2), manufactured by Skoda, for storage and disposal. This procedure has been approved by the National Co-operative for the Disposal of Radioactive Waste (NAGRA).

Post-irradiation examinations

The objectives of the post-irradiation examinations (PIE) are to understand: microstructural, mechanical and chemical changes in the structural materials in the target induced by irradiation and LBE corrosion, and also the production, distribution and release of the spallation and corrosion products in the LBE.

Figure 6: TC1 container for target transportation

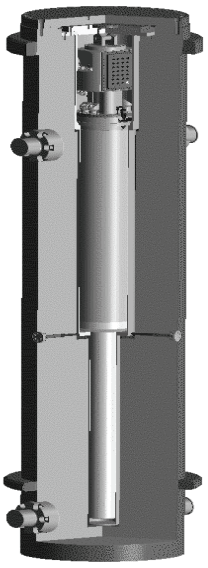

Figure 7: Cutting of the dummy target during the cold test campaign in ZWILAG in 2008

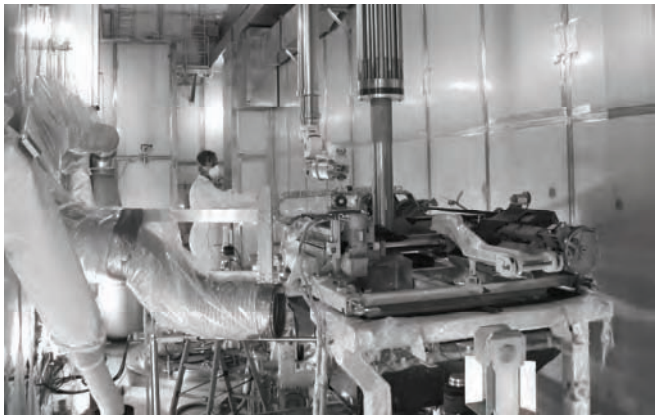

The LBE samples will be taken from the different parts of the target with the main goal to characterise the production, distribution and release of the spallation and corrosion products in the LBE. These samples will be analysed by gamma spectroscopy. Radiochemical separation will be done to study non-gamma-emitting radioisotopes with different techniques. The goal of this survey is to create a validation basis for nuclear reaction models used for the design of MEGAPIE. This information is not only of interest to the scientific community, but is also requested by the Swiss authorities in order to review the quality of the theoretical predictions for the declaration of waste from the accelerator facilities at PSI.

After the LBE sampling phase, the structural material will be separated from the LBE. This will be done by heating the sample pieces in a special oven to a temperature of 200°C (the LBE melting point is around 125°C).

The molten LBE will be collected in a shielded tank below the oven and disposed with the whole oven at the end of the sample-taking process. It is expected that a thin layer of LBE will stick on the surface facing the LBE. Therefore, tests have been conducted using specially prepared samples with a layer of ~20 μm of LBE on them. They have been cut in the EDM machine, which is going to be used to cut samples from the structural material of MEGAPIE, to study the influence of molten LBE on the EDM cutting process.

Hundreds of samples will be manufactured from the different structural parts of MEGAPIE. Some of these samples will be analysed by PSI, while the rest of the sample material is going to be distributed amongst the international partners of the MEGAPIE initiative: CEA, CNRS, ENEA, FZK, JAEA, LANL-DOE, PSI and SCK.

In more detail, the main objectives are to characterise microstructural, mechanical and chemical changes in the structural materials in the target induced by irradiation and LBE corrosion. The following analysis will be performed:

- non-destructive-tests (NDT), i.e. ultrasonic analysis of the thickness change at the beam window;
- microstructural, mechanical and surface analyses of the beam window, internal structures;
- surface analyses on EMP tube.

Conclusions

Within the framework of the Megawatt Pilot Experiment (MEGAPIE) (1 MW), initiated in 1999 in order to design and build a liquid lead-bismuth spallation target, then to operate it at the Swiss spallation neutron facility SINQ at Paul Scherrer Institute (PSI), many studies have been carried

out by the project partners, which addressed specific critical issues in the fields of neutronics, materials, thermal-hydraulics, mass and heat transfer, structure mechanics and liquid metal technology. Such undertakings have been performed employing analytical, numerical and experimental means.

The already-performed steps, conceptual and engineering design, manufacturing and assembly, safety and reliability assessment, thermo-hydraulic off-beam tests, irradiation phase, dismantling has brought already to ADS community a unique, relevant design and operational feedback to the development of accelerated-driven systems, option for the transmutation of minor actinides. The licensing process, facing the different issues, was also essential. This programme is also to a greater extent an essential contribution for the development of a Gen-IV lead fast reactor option and the feedback of some studies dedicated to the LBE and structural material behaviour is also relevant for the evaluation of an alternative coolant for intermediate loops of sodium fast reactors.

Acknowledgements

The authors warmly thank the Paul Scherrer Institute for the full involvement of its operational teams and also all the support teams from all organisations of the MEGAPIE initiative during the previous phases and also for the preparation of the upcoming post-irradiation examinations.

References

[1] Bauer, G.S., M. Salvatores, G. Heusener, "MEGAPIE, a 1 MW Pilot Experiment for a Liquid Metal Spallation Target", *J. Nuclear Mat.*, 296, 17-35 (2001).

[2] Latgé, C., F. Groeschel, "MEGAPIE Target: A Relevant Demonstration for a Liquid Metal Spallation Target", *GLOBAL 2005*, Tsukuba, Japan, 9-13 October (2005).

[3] Latgé, C., F. Groeschel, "MEGAPIE Spallation Target: Irradiation of the First Prototypical Spallation Target for Future ADS", *GLOBAL 2007*, Boise, ID, USA, 9-13 September (2007).

[4] Latgé, C., F. Groeschel, "Design Implementation and Preliminary Tests of the First Prototypical Spallation Target for Future ADS", *Conference IEMPT*, Nîmes, France, September (2006).

[5] Cadiou, Th., C. Latgé, "Analysis of the Consequences of a Common Failure of the MEGAPIE Target Container and Safety Hull", *NURETH 12*, Pittsburgh, PA, USA, 30 September-4 October (2007).

[6] Strinning, A., M. Wohlmuther, "Handling, Dismantling and Disposal Concept of the Irradiated MEGAPIE Liquid Metal Target", *ACCAPP'07*, Pocatello, ID, USA, 29 July-2 August 2007, p. 621 (2007).

[7] Wagner, W., M. Seidel, E. Morenzoni, *et al.* "PSI Status 2008 – Developments at the 590 MeV Proton Accelerator Facility", *Nucl. Instrum. & Methods*, 600, p. 5 (2009).

[8] Leung, W., J. Patorski, "CFD Simulation of Warm Jet Thermograph Study on the MEGAPIE Target", *ICANS 8*, Dongguan, China, 25-29 April (2007).

PSI experience with high-power target design and operation

Werner Wagner, Hajo Heyck, Daniela Kiselev,
Knud Thomsen, Michael Wohlmuther, Luca Zanini
Paul Scherrer Institut
Villigen PSI, Switzerland

Abstract

The PSI/SINQ solid target, with its development and upgrades during 12 years of source operation, can be rated as an instructive example for stationary high-power solid target design. SINQ is a continuous 1 MW class research spallation neutron source, driven by PSI's 590 MeV proton accelerator which routinely delivers 2.2 mA of proton beam (of which SINQ receives 1.5 mA). For the future, a programme is initiated to push the accelerator power by another ~40%, ultimately to 3 mA (2 mA for SINQ), i.e. distinctly beyond 1 MW.

Since start-up in 1997, the target of SINQ has been upgraded in several steps, from solid Zircaloy rods to instrumented lead rods clad in stainless steel tubes. More recently, further improvements for the solid target have been elaborated and scrutinised by MC simulations, aiming at the utmost possible neutron yield from this target concept. Since April 2009 an improved version of the solid target has been in operation, with a 40% increase in neutron yield compared to its predecessor, and 119% compared to the start-up target, falling only some 15% behind the liquid metal target of MEGAPIE.

Introduction

The principle of the accelerator-driven system (ADS) as potential option for transmutation strategies is the combination of an accelerator-driven neutron source and a subcritical fission core. One of the key issues of an ADS system is the sufficiently high primary neutron production by the spallation reaction in the neutron target. This requires on one hand a driving accelerator of multi-MW power, and on the other hand a target which sustains the immense power load with regard to thermo-mechanical stability and radiation damage. Regarding the target material for efficient neutron production, heavy metals yield the highest fluxes. Preferred choices are tungsten, favoured for its high thermal stability and high density, or lead, favoured for its low neutron absorption. Uranium with its booster property by fission neutrons would be a perfect candidate material if not hampered by reasons of thermo-mechanical stability. Heavy liquid metals, like mercury or lead alloys, are well suited for high-yield neutron production, as well. Liquid metals do not suffer from structural damage by radiation, and serve themselves as the primary cooling medium. The drawback is the need of a reliable confinement fighting wall materials' degradation by liquid metal embrittlement and the radiation damage.

The PSI/SINQ solid target with its development and upgrades during 12 years of source operation can be rated as an instructive example for stationary solid target design. SINQ is a continuous 1 MW class research spallation neutron source driven by the PSI 590 MeV/51 MHz proton accelerator. In terms of beam power it was, by a large margin, for many years the most powerful spallation neutron source in operation world wide (meanwhile only surpassed by the SNS which reached 1 MW for a short period). As a consequence, target load levels prevail in SINQ which were beyond the realm of existing experience. Therefore PSI always fostered combined efforts in the development of the facility, focusing on the spallation target as such, and on materials research for high-dose radiation environments.

The SINQ solid target – developments for a continuous neutron source

In contrast to other spallation neutron sources the target of SINQ is hit by the proton beam from below. In shape and external dimension, the target is a slim, about 5 m high cylindrical structure, 20 cm in diameter in the lower half, housing the spallation reaction zone at the bottom, and 40 cm in the upper part. The very first design of the SINQ target reaction zone consisted of an array of solid Zircaloy rods (Figure 1). Two solid Zircaloy targets were operated in SINQ between 1997 and 1999. The rods were 10.75 mm in diameter and were packed hexagonal with a pitch of 12.75 mm, *i.e.* the minimum width of the water flow path between the rods was 2 mm. The SINQ targets are contained in a double-walled aluminium shroud with a hemispherical beam entrance window, the so-called safety hull. Two heavy water loops actively cooled the Zircaloy rod array as well as the beam entrance window.

As a special feature, most of the SINQ targets carried rods filled with miniaturised samples of different materials, metals, steels and ceramics, for studying radiation damage effects induced by high-energy protons and spallation neutrons. This so-called SINQ Target Irradiation Programme (STIP) [1-3] was initiated in 1998 as an international collaboration, and is as strong as ever.

Due to the relatively low Z of the Zircaloy target material the neutron yield was not optimal. Heavy metals with low absorption cross-sections, for instance lead or bismuth, would be more suitable target materials. However, these materials have to be contained in some cladding to ensure structural rigidity as well as to prevent corrosion by the cooling water. To enhance the neutron yield in comparison to the first SINQ target the follow-up target Mark 3 was made of lead rods contained in austenitic stainless steel 316L tubes. This design was nicknamed the "cannelloni" target.

One target of this type, Target 4, is shown in Figure 2. This target finally received a time integrated proton charge of 10.06 Ah with peak dose levels of about 22 dpa in the 316L tubes.

Figure 1: Zircaloy rod array of the first SINQ spallation target, equipped with thermocouples and test specimen rods of the STIP programme

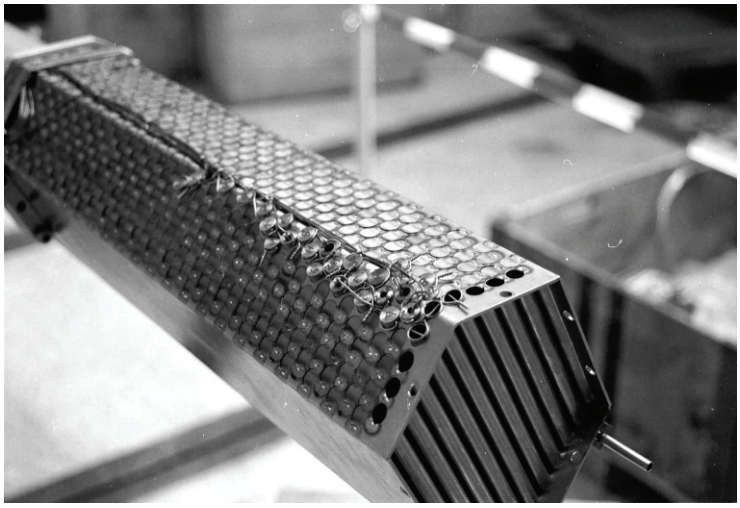

Figure 2: The steel-clad rod array of SINQ Target 4 (Mark 3)

Left: A sketch showing the positions of the STIP specimen rods in the lower part of the target. Right: A photo of the "cannelloni" target consisting of a frame holding the lead-filled target and STIP rods as well as thermocouple wires.

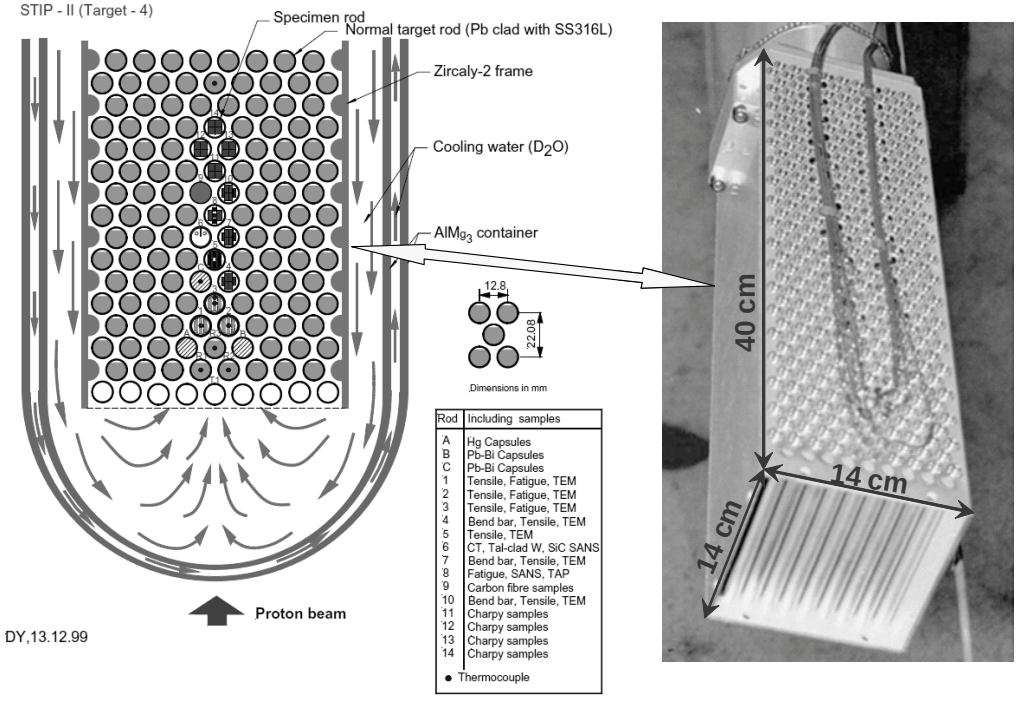

One option for improving the SINQ solid lead/steel cannelloni target was the replacement of the steel cladding by Zircaloy (Zr) tubes. Due to the lower neutron absorption of Zr compared to steel, along with a higher spallation neutron yield in the heavier Zr, this replacement promised a gain in total neutron yield of 10-15% [4]. One open question was the possible embrittlement of Zr by hydrogen produced as spallation product (Zr-hydride formation). This potential drawback was ruled out by a test experiment performed with Target 5 of SINQ (operated in 2004/2005); in this case, three rows of Zr-clad rods were implemented at both peripheral sides of the reaction zone,

and four individual test tubes in the centre (Figure 3, left). After two years of service and more than 10 Ah of proton charge received, all the Zr-clad tubes were found to be in excellent shape. Visual inspection (Figure 3, right) and neutron radiography did not show any indication of damage or degradation. Metallographic investigation of three test tubes confirmed an undamaged, homogeneous bulk structure, covered by an about 30 μm thick layer of most likely oxide or hydride at the outside (Figure 4).

Figure 3: Rod array of SINQ Target 5 (left); visual inspection of one of the four central Zr-clad rods after two years of irradiation in the SINQ target (right)

In the figure on the left, the Zr-clad rods are clearly distinguished (flat covers) from the steel-clad ones – three peripheral rows and an assembly of four rods in the centre (encircled)

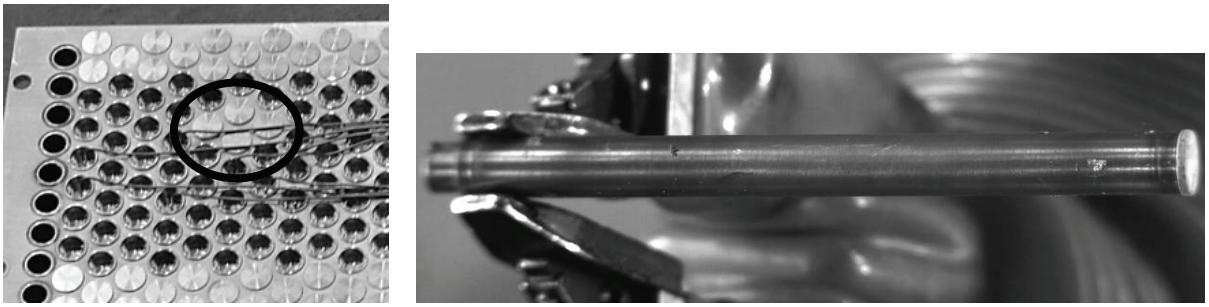

Figure 4: Typical metallographic observation from a polished cross-section of the Zr-cladding tube wall (thickness 750 μm) after two years irradiation in SINQ (left); higher magnification of the square marked on the left [5]

The figure on the left shows an undamaged, homogenous bulk structure; the figure on the right distinguishes the about 30 micron thick layer of mostly likely oxide or hydride at the outer tube surface

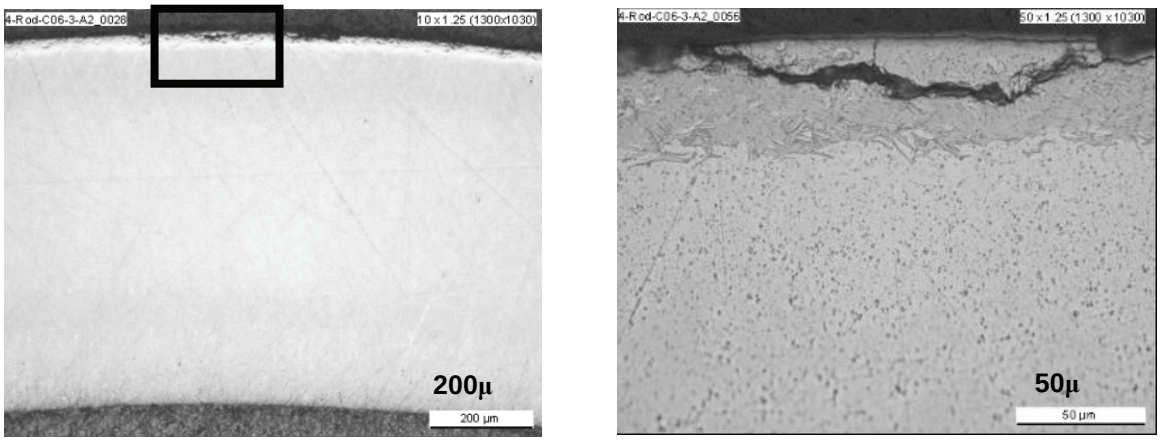

Besides the normal beam exposure the tubes sustained two severe beam excursions (unintentionally focused beam) in October 2004 and December 2005. While the nominal peak current density on the SINQ target currently lies at about 35 μA/cm^2, during the incident of October 2004 the centre of the target was exposed to 70 μA/cm^2 for 8 hours. The beam footprint diagnostic system VIMOS [6,7] did well monitor the beam focusing, however at that point in time during its first test phase it was not connected to any actuator. Therefore it took until the next morning to become aware of the situation and to correct it. Although the beam excursions caused severe damage in two of the central steel-clad rods, the Zircaloy rods did not suffer any damage or degradation, and thus it can be concluded that such a high current density seems to be possible for extended periods of time. Temperatures inside central target rods rose to more than 800°C, while the average beam current was at its nominal value, as shown in Figure 5.

Figure 5: Beam current and target temperature recordings during the unintended beam concentration of October 2004

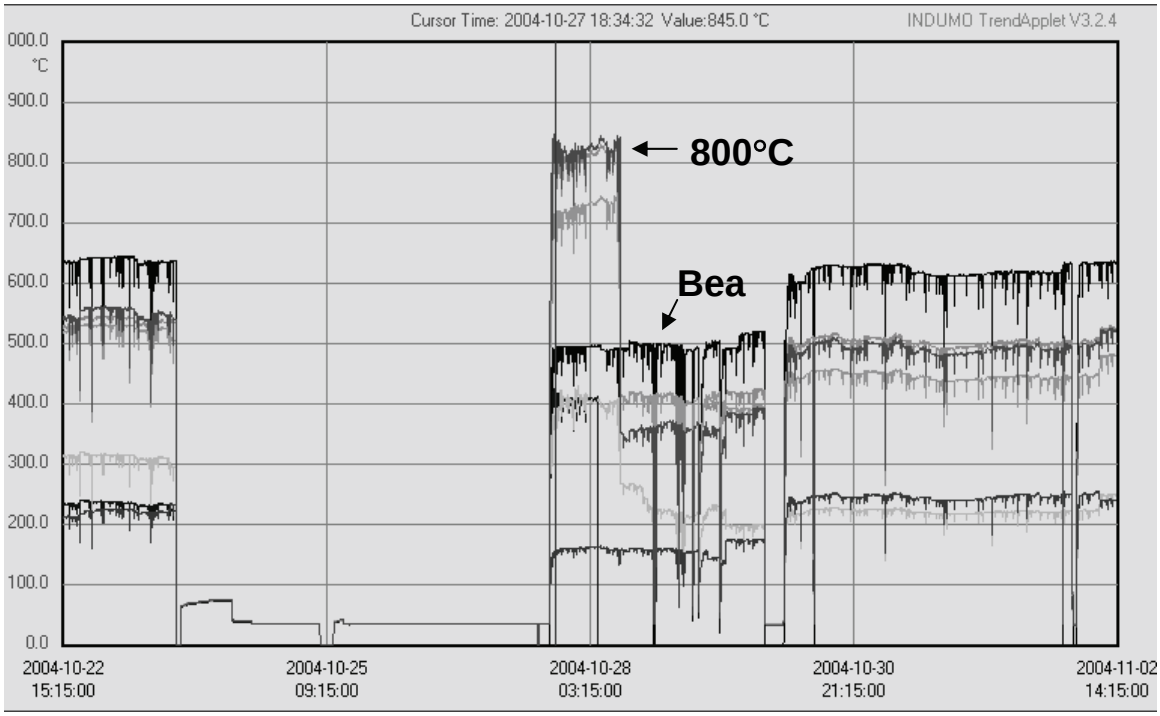

The proven robustness of the Zr-cladding in a harsh radiation environment cemented the decision to completely replace the steel cladding by Zr-tubes in a subsequent target (Target 6). After the target operation had started in April 2007, neutron flux measurements gave evidence of a neutron yield increase between 10 and 13%, very close to predictions from particle transport calculations with MCNPX.

The solid targets were replaced by the liquid metal target MEGAPIE that was irradiated in 2006 to demonstrate the feasibility of a MW liquid metal target. One of the results from the experiment was an increase in the neutron flux at the beam lines of about 80% with respect to Target 6, irradiated in 2004-2005, and of about 60% with respect to Target 7 (with all-Zircaloy rods), irradiated after MEGAPIE [9]. In an attempt to bridge the gap between the neutronic performances of solid and liquid metal based targets, a task group was formed with the goal to improve the design of the solid target.

The following possible improvements were identified: closer packing of the rods, a circular cannelloni support structure replacing the square-shaped frame, lead reflectors (blankets) in the cooling water gap around the cannelloni structure, inversion of the hemispherical beam entrance window of the safety hull to minimise the energy loss of the protons before entering the cannelloni part of the target, and minimisation of the STIP sample rods. For an optimised combination, simulations predicted improvements in useful neutron flux of 35 to 40%, the already-achieved increase from Zr-cladding not included.

The so-modified Target 7 started operation in early 2009. Figure 6 shows the design drawings of this target, highlighting the new main features. Figure 7 shows photos of the target reaction zone, without and with the lead reflector, ready for the safety shroud to be mounted before being inserted into SINQ. Flux measurements at two beam ports, one for thermal and the other one for cold neutrons, nicely confirmed the calculated flux increase by 40% on average.

Figure 6: Design drawing of SINQ Target 7, highlighting the new main features: circular geometry, the lead blanket/reflector and the inverted calotte

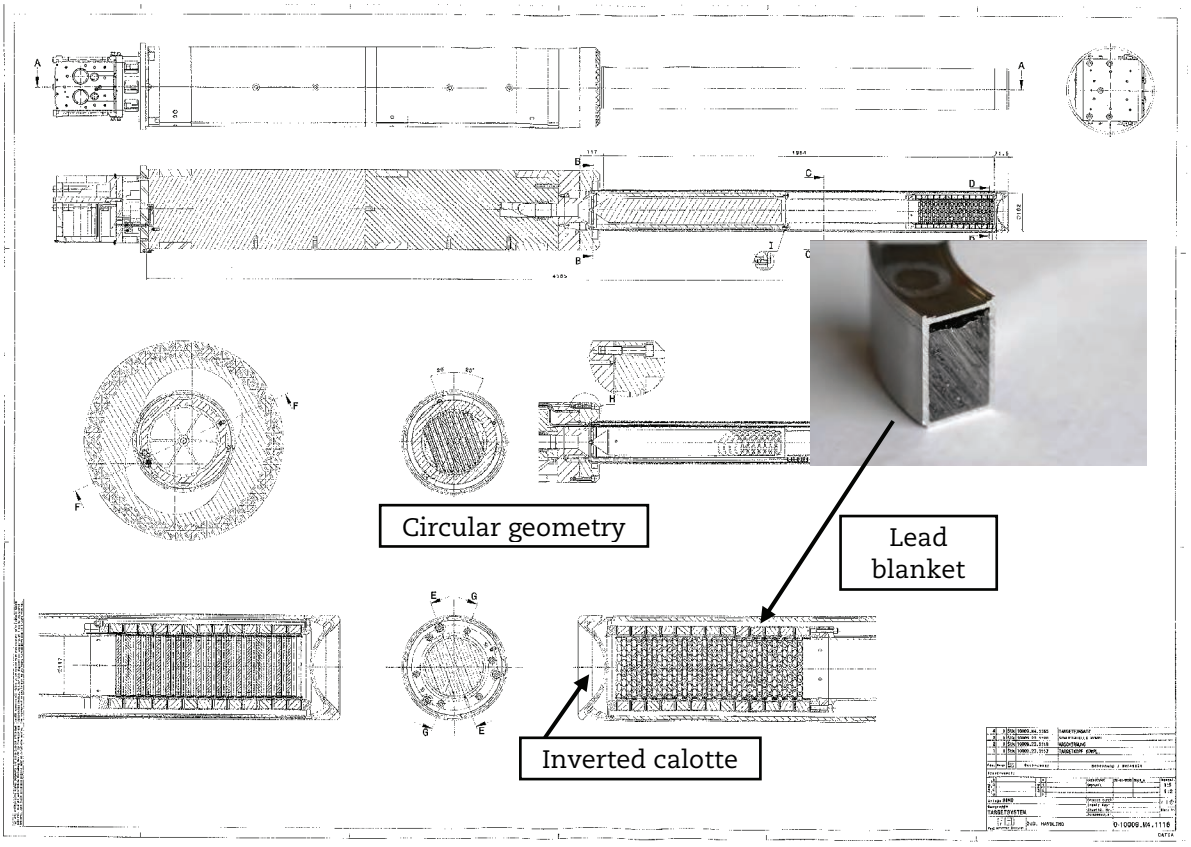

Figure 7: SINQ Target 7, without (left) and with the lead-containing reflector rings (right), ready for getting the safety shroud mounted

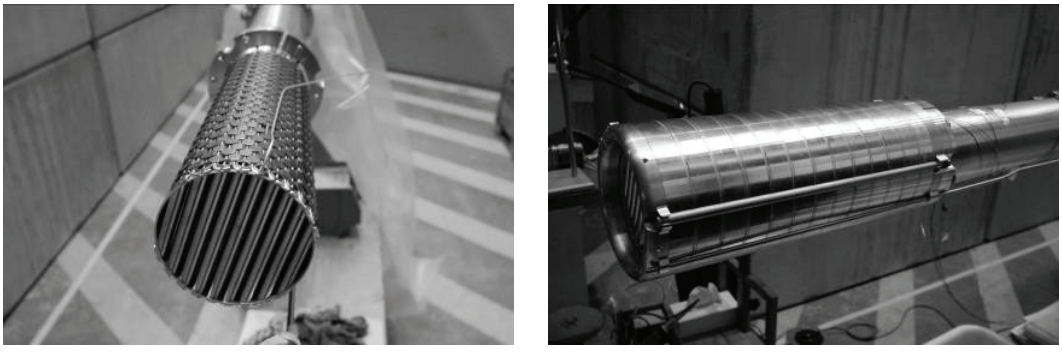

Figure 8 illustrates the complete history of SINQ target operation since the start-up in 1997. The bar chart shows the relative neutron production in comparison to the yearly accumulated proton charge. The corresponding numbers give the relative neutron yield compared to the day-one solid Zircaloy target (labelled 1.00). For Target 7 in 2009 this value is 2.19, which means a relative gain in primary neutron yield of 119% normalised to the same proton beam power. Only MEGAPIE, the lead-bismuth eutectic liquid metal experimental target operated at SINQ in 2006, surpassed this value by about 15%. For a report on the MEGAPIE spallation target experience we refer to Ch. Latgé, *et al.* [8].

Figure 8: History of yearly accumulated proton charge and related neutron yield

The numbers in the top row indicate the availability of SINQ (for most years >98%)

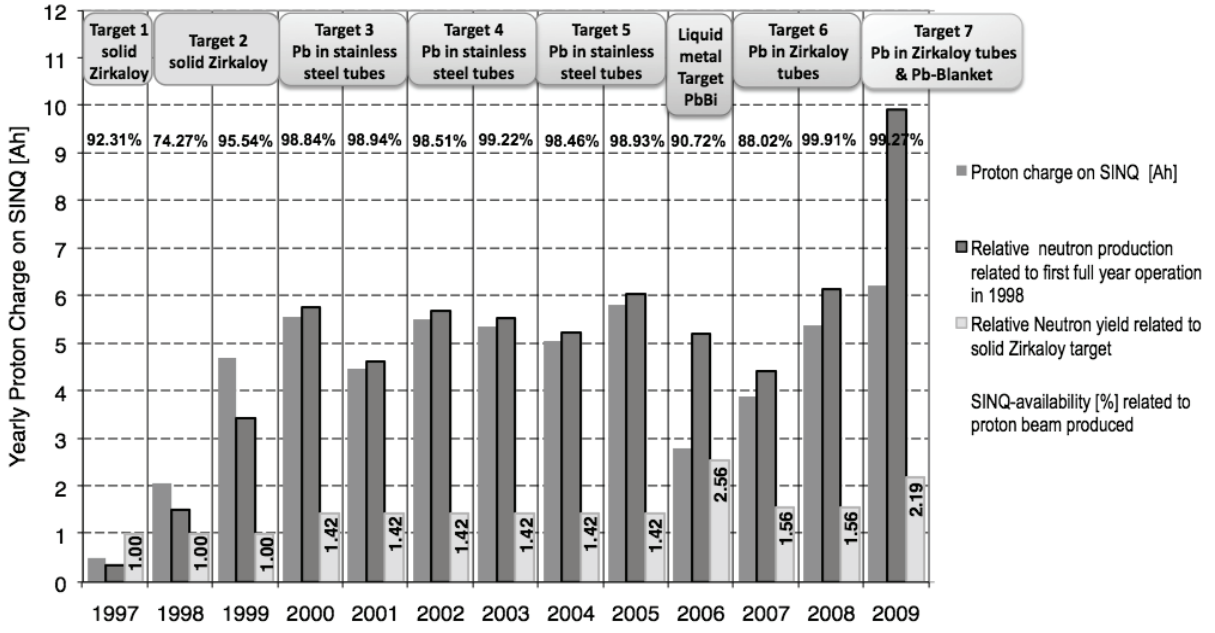

Figure 9: Results obtained for systematic variation of the beam footprint, showing almost 10% variation in neutron fluxes between the widest and most narrow beam footprints investigated

The beam current was very constant during the whole campaign at 1 000 μA

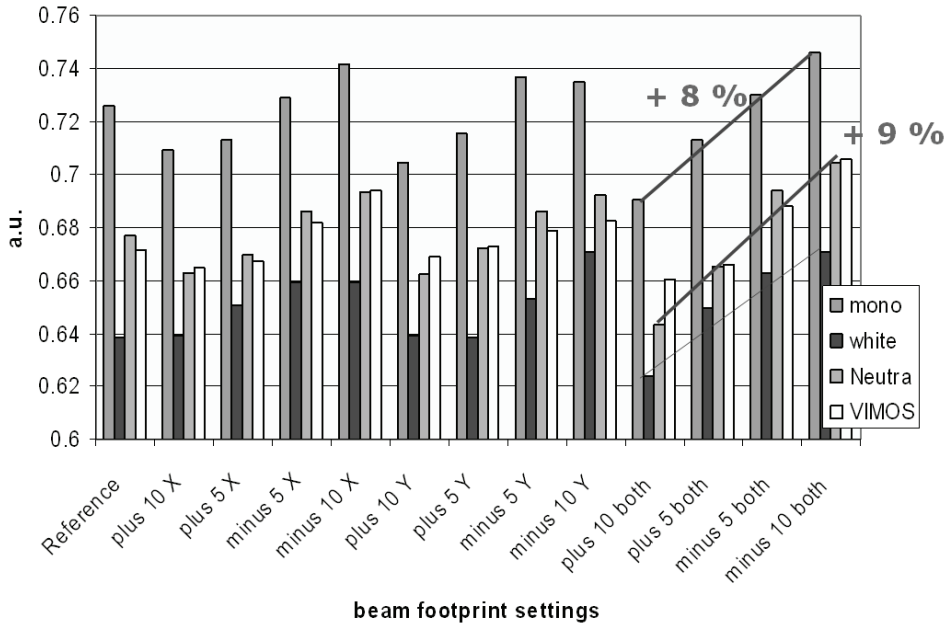

Prompted by the gain in neutron production at SINQ with the MEGAPIE liquid metal target a systematic investigation of the impact of variations in beam geometry has been started. Unexpectedly, experimental results demonstrate significant flux increases at instruments when reducing the extension of the proton beam footprint compared to the standard settings. Figure 9

shows the results obtained for systematic variation of the beam footprint. Starting from reference conditions the beam was first widened (e.g. 10% in x-dimension) and then narrowed, for x and y directions separately and finally, in both extensions simultaneously. Almost 10% variation in neutron fluxes was observed between the widest and most narrow beam footprints investigated. The beam current was very constant at 1 000 μA during the whole campaign. Initial numerical simulations reproduce the general tendency; more detailed calculations are ongoing.

Summary

The improvements of the SINQ solid target from the first, solid Zircaloy rod target to Target 7 accumulate to a total increase in useful primary neutron flux by a factor of 2.19. Only MEGAPIE, the lead-bismuth eutectic liquid metal experimental target operated at SINQ in 2006 surpassed this value by about 15%. This gap could be further decreased by optimising the present target design, or by considering different design concepts. For instance, one could reduce the thickness of the Zircaloy tubes from 0.75 mm to 0.5 mm, in order to increase the amount of lead and the neutronic performance.

In total, together with a proton beam current upgrade by a factor of 1.75 since the start-up of SINQ the users benefit from a factor ≈4 of higher neutron flux at the instruments.

References

[1] Dai, Y., G.S. Bauer, "Status of the First SINQ Irradiation Experiment, STIP-I", *J. Nucl. Mater.*, 296, 43 (2001).

[2] Dai, Y., *et al.*, *J. Nucl. Mater.*, 343, 33 (2005).

[3] Wagner, W., *et al.*, *Journal of Nuclear Materials*, 361, 274 (2007).

[4] Bauer, G.S., A. Dementyev, E. Lehmann, "Target Options for SINQ – A Neutronic Assessment", *Proceedings ICANS XIV*, ANL-98/33, 703 (1998).

[5] Urech, A., D. Gavillet, PSI-Report TM-43-07-05 (2007).

[6] Thomsen, K., "VIMOS, Near-target Beam Diagnostics for MEGAPIE", *Nucl. Instruments and Methods*, A 575, 347-352 (2007).

[7] Thomsen, K., "Advanced On-target Beam Monitoring for Spallation Sources", *Nucl. Instruments and Methods*, A 600, 38-40 (2009).

[8] Latgé, Ch., *et al.*, "MEGAPIE Spallation Target: Irradiation of the First Prototypical Spallation Target for Future ADS", these proceedings.

[9] Zanini, L., *et al.*, "Neutronic Performance of the MEGAPIE Target", *8th International Topical Meeting on Nuclear Applications and Utilization of Accelerators (ACCAPP'07)*, American Nuclear Society, LaGrange Park, Illinois 60526, 493 (2007).

EURISOL compact liquid metal converter target: Representative prototype design and tests

R.Ž. Milenković[1], K. Samec[1], S. Dementjevs[1], A. Kalt[1], C. Kharoua[3], E. Platacis[2], A. Zik[2], A. Flerov[2], L. Blumenfeld[3], F. Barbagallo[1], K. Thomsen[1], E. Manfrin[1], Y. Kadi[3]
[1]Paul Scherrer Institut (PSI), Villigen, Switzerland; [2]Institute of Physics (IPUL), University of Latvia, Riga, Latvia; [3]European Organization for Nuclear Research (CERN), Geneva, Switzerland

Abstract

The development of a high-power neutron converter target for the European Isotope Separation On-line (EURISOL) project, supported by the European Union within the context of the 6th Framework Programme for research development, included a design and test of a novel and as yet untried concept for a liquid metal target. The design of the liquid metal converter target with heat deposition densities of 8 kW/cm3 was completed using the latest version of commercial computational fluid dynamics (CFD) and finite element methods (FEM) codes. The design, which included cusp window and flow vanes, has been proposed to enhance the ability to cool the beam entrance window (BEW).

In order to test and examine structural-hydraulic behaviour of the EURISOL neutron converter target mock-up, two tests of the mock-up, named METEX 1 and METEX 2 (Mercury Target Experiment 1 and 2), were conducted by PSI team in co-operation with the Institute of Physics of the University of Latvia (IPUL) and the European Organization for Nuclear Research (CERN).

The current paper presents the overall design concept as well as engineering test data, which thoroughly confirmed the predicted performance.

Introduction

The EURISOL Design Study [1] aims to develop a European Isotope-Separation-On-line (ISOL) facility, in which a compact 4 MW liquid metal converter target is surrounded by separate uranium carbide fission targets where rare isotopes may be formed. The design of the converter target is based on ongoing liquid metal target development at PSI and draws on a substantial knowledge base gained from over 10 years in the field of liquid metal technology. The design team at PSI was faced with the challenge of an order of magnitude increase in heat deposition compared to the Megawatt Pilot Experiment (MEGAPIE). Thus, the EURISOL neutron source features a specially optimised cusp beam window and flow vanes. The main concept was validated by a successful test on the mercury loop of the Institute of Physics of the University of Latvia (IPUL).

Conceptual layout of the facility and the converter target design

EURISOL aims for the production of radioactive ion beams (RIB) using a converter target surrounded by six uranium fission targets [1,2]. The RIB beams are extracted from the secondary fission targets (Figure 1). A 1 GeV/4 MW proton beam is hitting the converter target; according to Monte Carlo particle transport simulations performed with Fluctuating Kaskades (FLUKA) at CERN heat deposition at densities of up to 8 kW/cm^3 can be released in the converter target. Therefore, the converter target designed at PSI is cooled by a forced, coaxial mercury flow in order to ensure the structural integrity of the beam entrance window and the target container.

Figure 1: Conceptual layout of the facility (picture taken from [1])

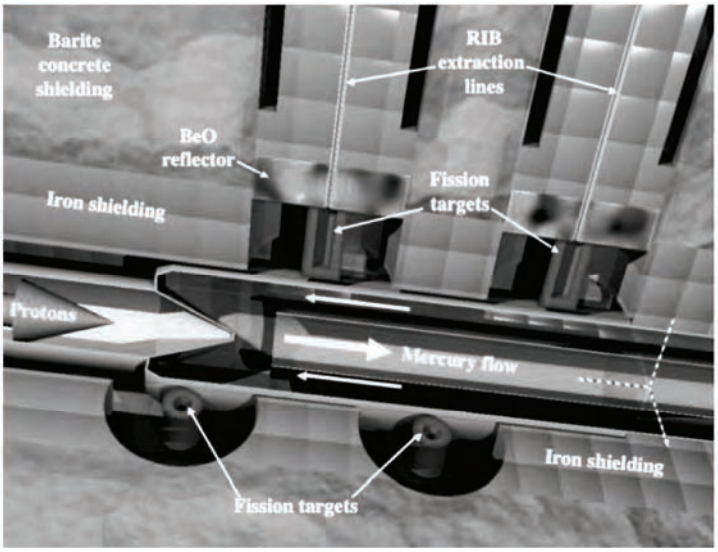

Target design: CFD and FEM computational studies

Initial conceptual studies of the whole facility performed at CERN [1] showed that the maximum heat deposited into the target material reaches 8 kW/cm^3 for the best-estimate steady-state beam footprint [3]. The heat deposition calculations were performed with the Monte Carlo particle transport code FLUKA at CERN. The radial heat deposition density profiles were fitted for a beam width of 1.5 cm and gave a 2.3 MW total power deposited into the target. Early on in the development, mercury was chosen as the target material. Mercury is liquid at room temperatures, but boils at a low temperature of 457°C at 5 bar statistic pressure, which is the reference pressure

chosen for the EURISOL loop. The material selected for the hull and overall structure of the target was T91 steel as it was used for the lower section of MEGAPIE target. These basic design parameters were taken into account for initial design iterations. Extensive thermal-hydraulics studies resulted in the design of the EURISOL converter target illustrated below. Figure 2 shows the internal structure of the target; the proton beam penetrates into the liquid metal through the conical cusp window. The target fluid reverses at the beam entrance window and exits the target downstream of the main guide tube. The main features of the design are the beam entrance window (BEW) shaped as inverted conical cusp, the flow reverser i.e. flow vanes at the target beam entrance window and near the guide tube, and the inlet section, where cold liquid metal enters the target. The design was optimised [3-5] using a number of 2-D and 3-D calculations at a constant mass flow rate of 171 kg/s, assuming uniform velocity distribution at the inlet of the beam window. To check this assumption before the subsequent hydraulic test, hydraulic calculations on flow development at the inlet section were made using the CFD code CFX 11.0.

Figure 2: Cross-section of the EURISOL converter target

1 – proton beam; 2 – flow vanes; 3 – beam entrance window (BEW); 4 – guide tube (GT); 5 – liquid metal hull (LMH); 6 – frame

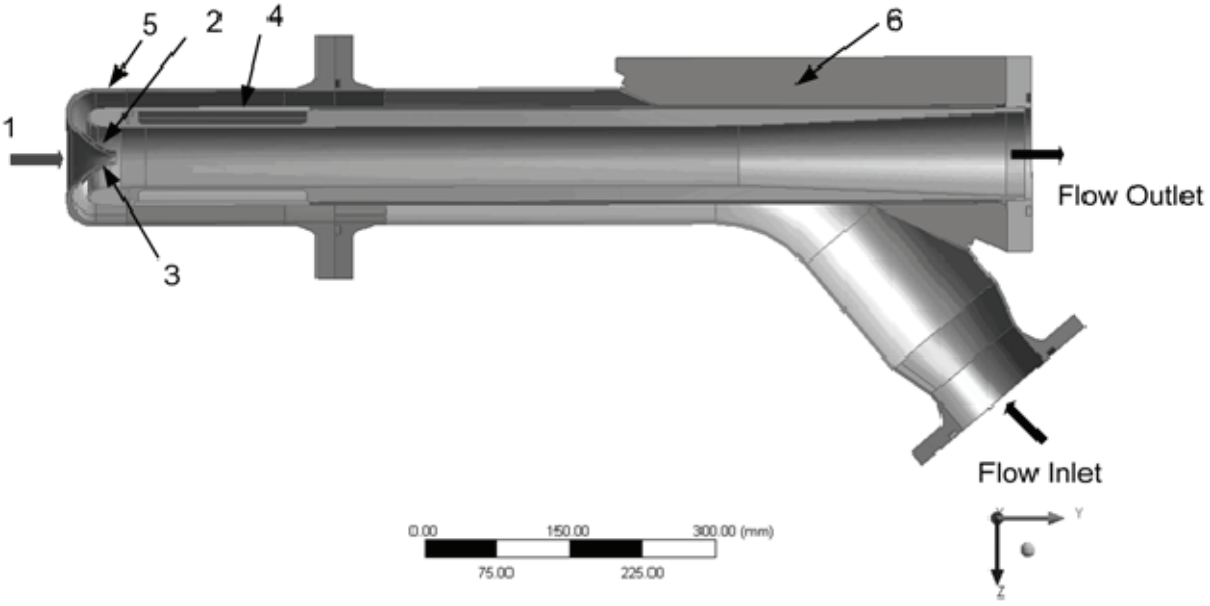

Cusp window

The cusp window or beam entrance window (Figure 3) is an essential part of the target. The proton beam penetrates the target at centre of the cusp window exactly where the flow has been reversed by 180°. Therefore, the inverted conically shaped cusp serves to reverse the liquid metal flow coming through the annulus and to direct it through the main guide tube toward the heat exchanger, thus carrying away the heat deposited by the beam in the target material whilst wetting and cooling the beam entrance window. The flow structures, which are developed inside this region of the target, affect the structural behaviour of the target and therefore the safe operation of the target. The total flow rate and the static pressure in the system were determined iteratively, taking into account various geometrical parameters such as the wall thickness distribution, the opening angle and the curvature of the cusp window, with the objective that the window temperature and the thermal stresses remain within safe limits.

Figure 3: Design of the beam entrance window (a) and flow vanes (b)

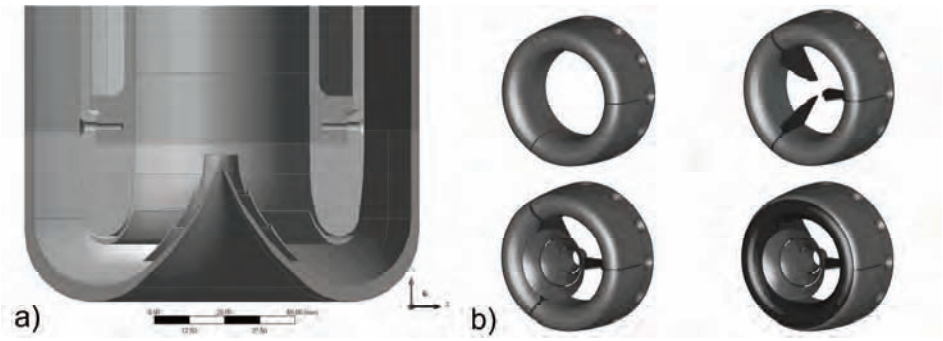

Flow vanes

In order to stabilise the flow close to the forward end of the guide tube and at the apex of the window, specially designed flow vanes [Figure 3(b)] were developed. The flow vanes, which are included for the first time in a design of the target system, function in a manner similar to fowler slats on aircraft wings. Even though large eddy simulation (LES) calculations showed that the initial objective to direct and accelerate the flow to the surface of the beam entrance window was achieved, areas of concern existed with regard to flow-induced vibrations and cavitation phenomena. An example of the instantaneous velocity field obtained by LES is shown in Figure 4. Sources of instabilities, which may cause structural resonance, are clearly marked by arrows and capital letters.

Figure 4: LES calculation showing an instantaneous velocity field

Large eddy structures and sources of instabilities are marked by arrows and capital letters

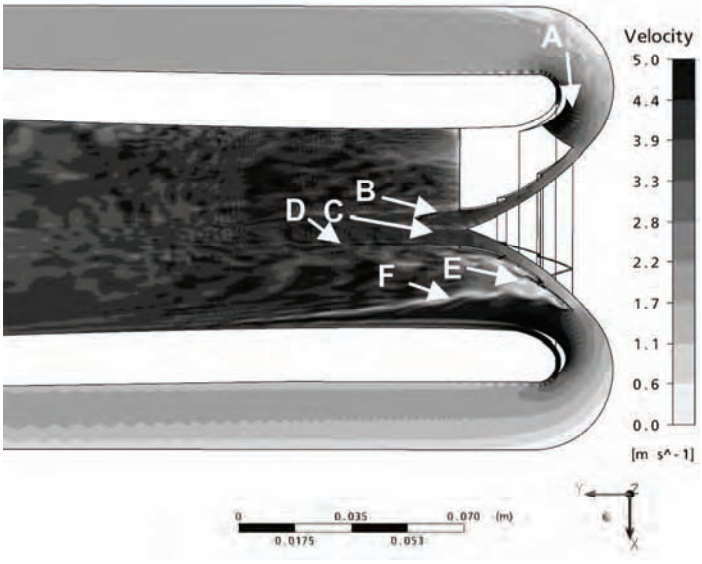

The effects of the flow vanes on the overall resonance of the target structure were investigated by the one-way coupled frequency response analysis. Specifically, the structural model (Figure 5, left) was run in a sine sweep mode with an excitation load frequency range between 10 and 150 Hz by using the amplitudes of the spatial pressure distribution extracted from the LES calculations. The hull tip displacement obtained from such analysis (Figure 5, right) showed the existence of resonance frequencies between 35 and 50 Hz, though the energy content

Figure 5: FEM structural model (left); the hull tip displacement (right)

LES computed pressure variations at representative points are applied to the FEM structural model by extraction of modal content from Fast Fourier Transform (FFT) processing of the pressure, which, when run in a sine-sweep frequency response analysis, gives displacements on all points of the structural model

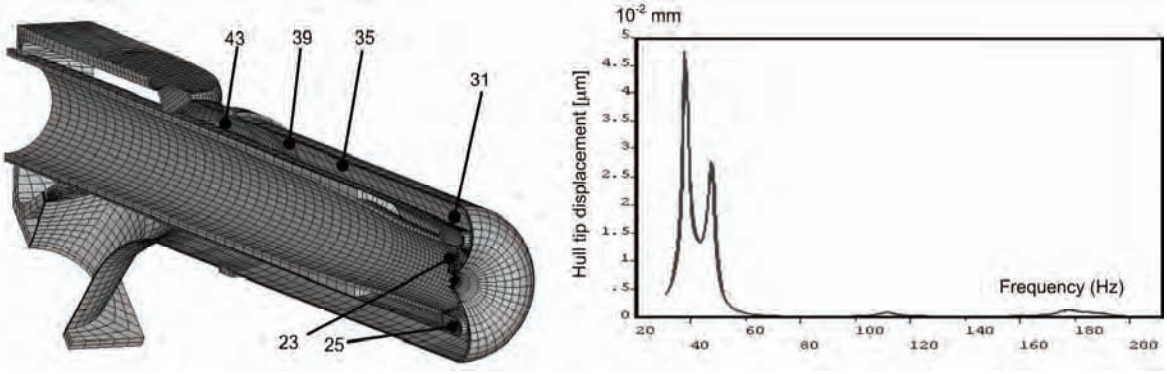

was relatively low (displacement of the hull tip was only 0.05 mm). The flow vanes are subjected to far higher dynamic loads, where load peaks are located on the welds. Due to the high stress amplitudes and frequencies the flow vanes may undergo a high-cycle fatigue [3]. In light of the prediction, adequate safety precautions were taken to guard against adverse consequences and the team was thus able to conduct the final test carefully until the rupture of the flow reverser.

The experiment and foremost results of the structural-hydraulic tests

The final configuration chosen to solve the complex cooling requirements posed at the point of entry of the beam, the so-called beam window (see Figure 3) lead PSI to test the feasibility of using the beam entrance window without and with integrated flow reverser, i.e. thin flow vanes. The main goal of experimental sessions METEX 1 and METEX 2 was to investigate the hydraulic and structural behaviour of the EURISOL target mock-up under various flow conditions and for two flow configurations as mentioned above, to provide experimental data for code validation and to test various sensors and remote monitoring techniques which are to be used for accurate predictions of the system health during real target operation.

The manufacture and design of the flow vanes were a major challenge and their weakness resulted in a partial detachment of the flow vane structure (Figure 6), which impacted the hull. The instrumentation used to monitor the status of the target picked up the resulting signals (Figure 7). More details can be found in [11].

Experimental installation

All tests were conducted at the IPUL mercury loop (Figure 8), which has DN100 piping assembled in a vertical plane on a frame. The target mock-up is connected to the loop interface flanges.

During the experiments referred to here the pressure of the cover gas, the total mass flow rate, the pressure loss in the mock-up, temperatures at various locations, local static pressure, structural acceleration, strain and sound data were acquired at the most interesting locations [11]. A schematic of the experimental set-up is given in Figure 8. The maximum liquid metal flow rate achieved with the configurations without and with flow vanes was between 10 and 11 l/s. As during the pump operation up to 40 kW of thermal power is dissipated into the liquid metal, four cooling water jackets on the stainless steel piping served to remove deposited heat. The cooling water flow rate through all four heat exchangers was manually regulated. Therefore, the mercury temperature in the loop was kept in a range from 3 to 36°C. The total mass of the mock-up filled with mercury was 176 kg.

Figure 6: Photos of the ruptured flow vanes and welds

(a) Locations of the acceleration sensors connected to channels CH0 and CH1, spot welds and failure of the bottom welds; (b) and (c) detached flow vane; and (d) the gaps between blades and supporting ribs

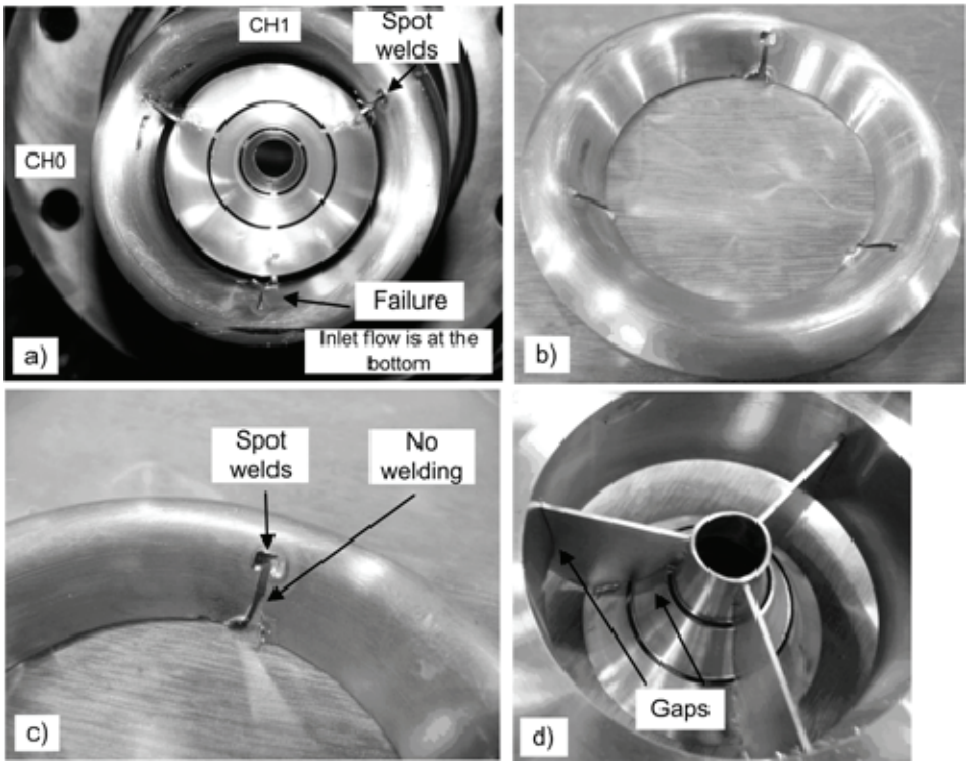

Figure 7: EURISOL target mock-up equipped with sensors was connected to the IPUL liquid metal loop (left) and flow reverser (right)

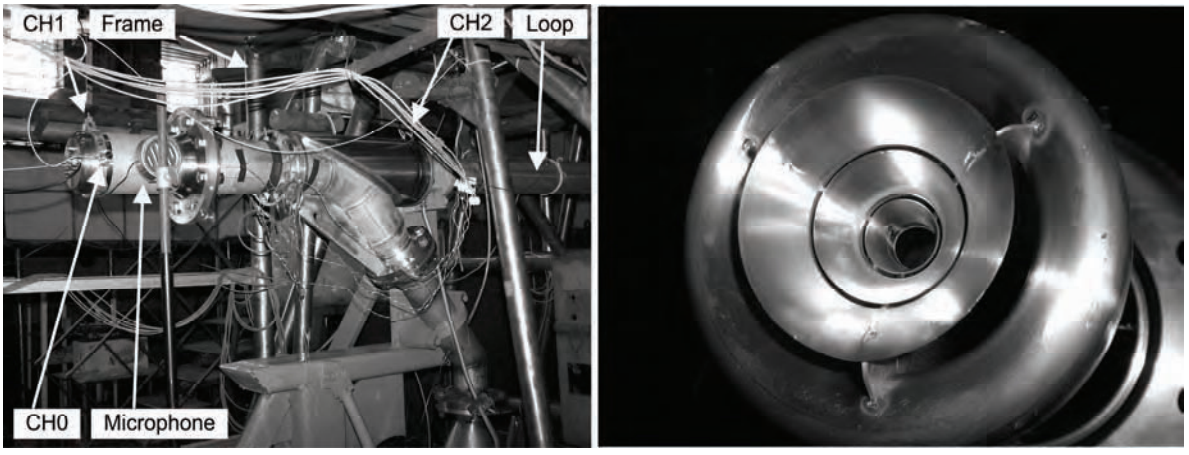

Figure 8: Experimental set-up

1 – mock-up, 2 – manometer-cover gas pressure, 3 – electromagnetic pump, 4 – flow meter, 5 – heat exchanger, 6 – expansion tank, 7 – storage tank, 8 – differential manometer-pressure loss measurement

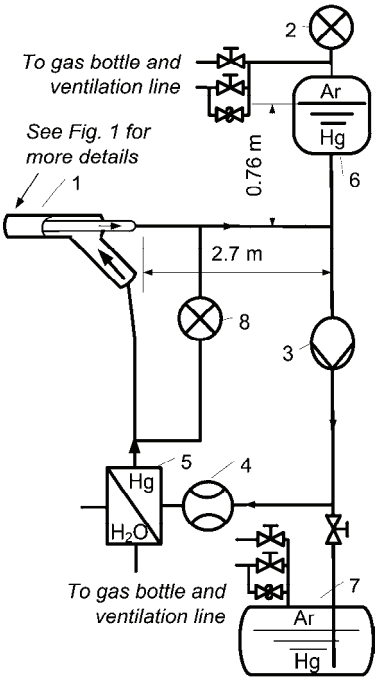

Major results

The major experimental results presented here summarise the hydraulic and structural behaviour of the target mock-up under turbulent flow conditions as well as under incipient and developed cavitation.

Pressure loss measurements

The total pressure drop in the mock-up was measured by using the differential manometer for various flow rates. In order to validate these measurements and to perform cross-checking, experimental data are compared with data taken from Ref. [9] (configuration No. 5). Experimental data include results for both configurations, without and with flow vanes (see Figure 9).

Even though the configuration analysed here ([9], configuration No. 5) does not exactly match those of our design, good agreement between the estimated and measured pressure losses was found. The experimental data were also used for calculations of the cavitation number. Figure 9 shows that some experimental data lie in the regime of incipient or of developed cavitation. These characterisations are part of complex considerations which are described in more detail in Refs. [6] and [10]. Therefore, the following conclusions are drawn:

- The pressure loss is essentially higher for the configuration with flow vanes. This conclusion is valid for flow regimes with and without cavitation.
- The cavitation effects do not influence the pressure loss measurements because the data follow the same well-established trend for regimes without cavitation. These regimes are marked with empty squares and stars in Figure 9. For comparison, calculated pressure loss due to the friction in the target mock-up is also presented in Figure 9 (open triangles).

Figure 9: Pressure loss in the target mock-up

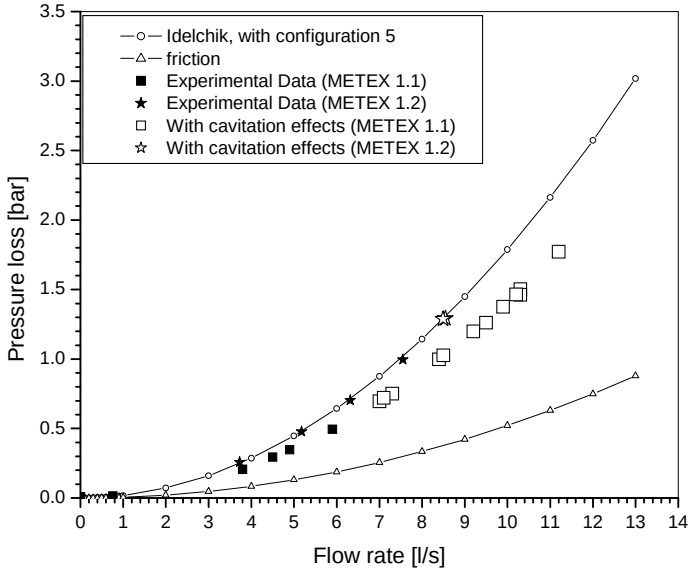

Structural acceleration measurements

As a characteristic example, the acceleration data shown in Figure 10 summarise the cause of events during transient system behaviour for the case with flow vanes before failure of the welds occurred. The pressure in the system was constant, whereas the flow rate was increased from 5 to 7.5 l/s. In the second acceleration data set (CH0 and CH1) a large peak was detected. Just twelve seconds after this event the acceleration amplitudes were increased almost threefold, which probably indicates that some spot welds were broken.

Figure 10: Acceleration data recorded before failure of the welds occurred

The data obtained from sensors are overlapping

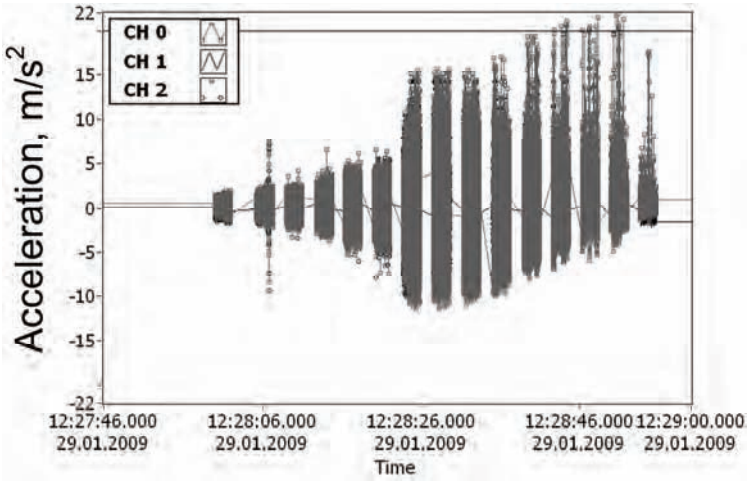

During the operation of the mock-up without flow vanes including single-phase and cavitation regimes, the structural acceleration amplitudes did not exceed the value of 2 g. This means that the simplified design worked satisfactorily, with little structural vibrations.

Strain-stress measurements

Two sets of strain gauges were set up to monitor critical locations, as shown schematically in Figure 11 (left) and indicated by the numbers 1 and 2. The Type 1 gauges were positioned at four different locations, spaced by 90° around the circumference of the tube, so as to pick up bending about either of the two main bending axes. The Type 2 gauges, which monitor the weld, were connected to a full Wheatstone bridge and measured the direct strain perpendicular to the weld.

Figure 11 (right) shows a typical output in a high flow rate regime (flow rate 8.49 l/s, outlet pressure 3.74 bar); maximum stresses around the welds at 5 MPa are well below allowable limits (65 MPa).

Figure 11: Strain gauges (left) mounted on the mock-up and stress data during operation

Flow rate 8.49 l/s, outlet pressure 3.74 bar, temperature at the mock-up outlet 27.9°C

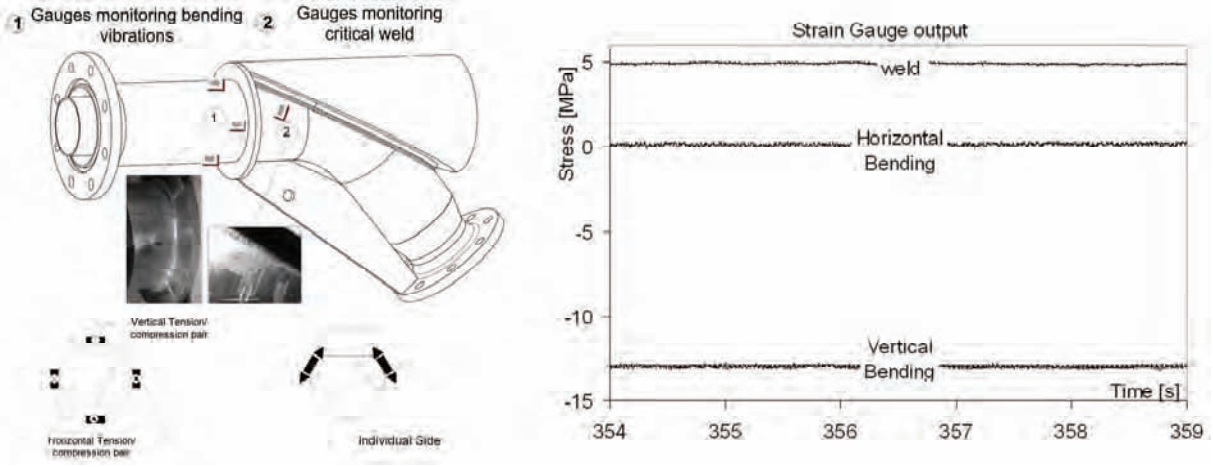

Detection of cavitation in liquid metal flows

The methodology for cavitation detection was based on an advanced analysis of the structural vibrations of the target mock-up: sound measurements, pressure measurements, strain measurements and acoustic emission measurements. Namely, various advanced time-frequency analysis methods including the Short-time Fourier Transform (STFT), in particular, the Gabor Transform (GT) and the Discrete Wavelet Analysis (DWA) were applied on data samples with specified number of points. As sound measurements are very often considered attractive since the sensors can be remotely located from the source, an example shown in Figure 12 is chosen to demonstrate real signals for flow regimes without and with developed cavitation. Even though under real operating conditions in the laboratory or at the facility various sound sources may contribute to the background noise, the knowledge of the reference pattern is essential, because any kind of abnormal system behaviour can easily be detected by simple comparison.

The noise was converted into an electric signal (voltage) and stored on the local hard disk at a rate of 22.5 kHz. The Short-time Fourier Transform was applied on sound data samples. The results are compared in Figure 12 for the configuration with flow vanes, for no flow and for developed cavitation, respectively. The spectrograms (Hanning window 64 samples, 512 frequency bins and 32 time bins) of the sound signal show the characteristics of two flow regimes in the time-frequency domain during operation of the mock-up. The flow parameters, which are given for each picture, supplement the spectrograms and characterise the selected flow regimes. For no-flow conditions a very stable 5 kHz component was captured. The source of this component is not known, but since this frequency coincides with the sampling frequency of the acceleration

Figure 12: Spectrograms of the Short-time Fourier Transform applied on sound data for configuration with flow vanes

a) For no flow conditions, b) for fully developed cavitation, when both strong audible noise and tones are detected

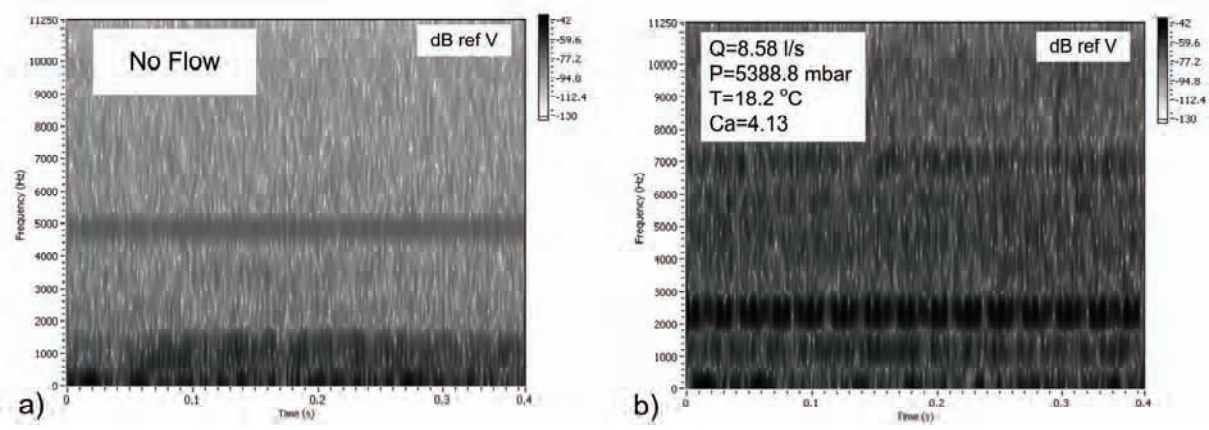

measurements, it could not be recorded in those tests. The large magnitudes of the STFT coefficients, which are spread over the full frequency domain, characterise the audible noise generated by cavitation [Figure 12(a)]. The loud tones at 1.2 and 2.5 kHz (whistling sound) can also be identified in the spectrograms [Figure 12(b)]. These resonance frequencies indicate that the mock-up with the flow vanes was operated under extreme conditions. In addition, as the flow rate was relatively high (about 8.6 l/s) and the pressure of the cover gas was low, cavitation noise is superimposed onto the whistling signal and can be identified by the larger magnitudes of the STFT coefficients. It can be concluded that the developed cavitation produces broad band noise with almost uniform power over the full frequency range (20 Hz-12 kHz).

Detection of structural resonance in liquid metal flows

The variation of total pressure loss accompanying a variation of the flow rate is presented in Figure 13(a). When the flow rate was continuously increased from 0 to 4.62 l/s, a small amplitude increase of acceleration data from both sensors suddenly occurred [Figure 13(b)]. The spectrograms [Figure 13(c)] revealed two resonance frequencies, the first one at 1 000 Hz and the second one at 1 750 Hz. The clear tones were also registered by the microphone and heard by personnel in the laboratory (the human ear can detect sounds up to 20 kHz). Usually, whistling sounds can be generated by flows through narrow gaps. As some of the gaps existed due to manufacturing inaccuracies [Figure 6(d)] and some are part of the current system design, it is not possible to distinguish the cause of this behaviour. However, the occurrence of this phenomenon is a clear indication that the design should in any case be reviewed if the work is to be pursued. Furthermore, in the course of events, which are not presented here, other strong resonance components were registered. The time-frequency analysis of the next fourth acquired data set shows various powerful resonance components [Figure 13(d)] without any change of flow rate. Such system behaviour indicates that detected spectral peaks can be caused behaviour changes suddenly. Of course this is not possible to visualise online. After termination of by cracks in welds if the system the experiment, an inspection of the flow reverser showed that the welds were broken (Figure 6).

Detection of the structural rupture

Figure 14 summarises the course of events when rupture of the flow reverser occurred. At about 12:45:17 the total pressure loss increased by about 500 mbar, whereas the flow rate dropped from 9.94 to 8.82 l/s. The sound level registered by the microphone increased almost instantaneously

Figure 13: Variation of total pressure loss accompanying a variation of the flow rate

During the flow rate increase (a), a sudden change in structural behaviour is reflected in the acceleration data (b), a slight increment in the amplitudes as indicated by the arrow. The pressure of the gas was constant (a), whereas the flow rate was increased from 0 to 4.62 l/s, then reduced and again increased. The signal power distribution in the time-frequency domain shows a change in the system behaviour after the first appearance of the resonance frequencies was detected (c). The appearance of new, strong resonance frequencies is shown in (d). They were found in the fourth data set shown in (a). Flow conditions for cases (c) and (d) are: flow rate 3.75 l/s, temperature at mock-up exit 7.1°C and pressure at the mock-up outlet 5 313 mbar.

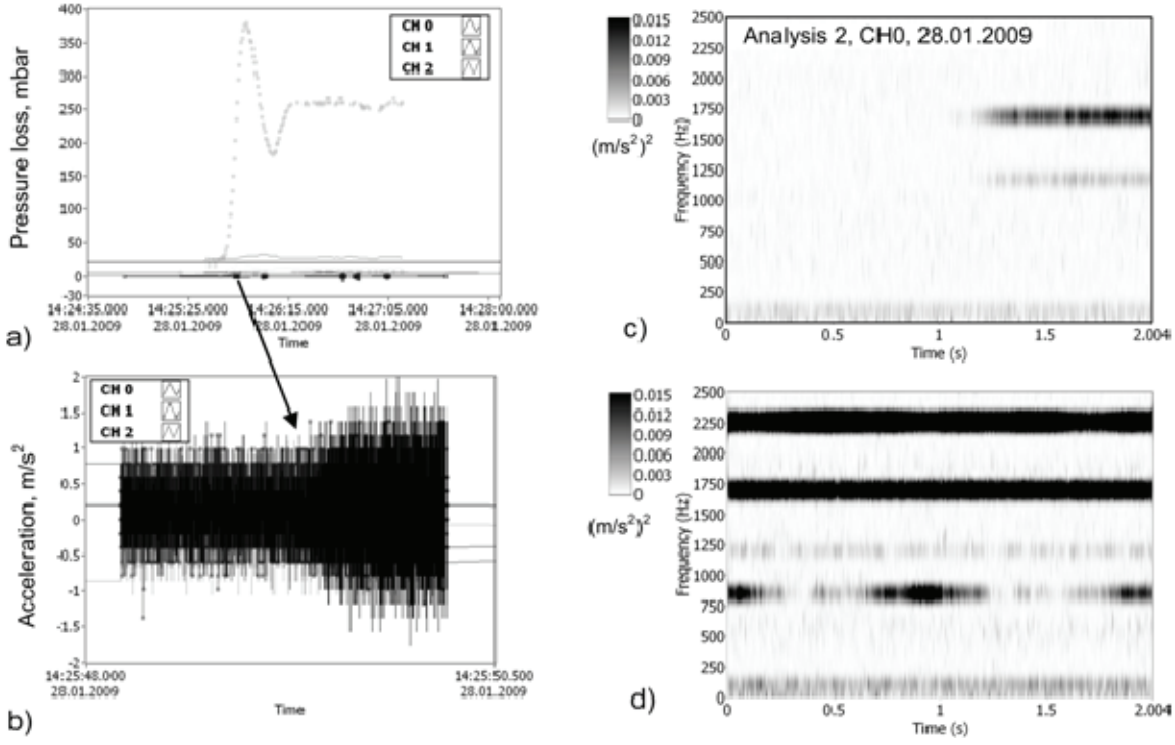

as shown in Figure 14(b). The acquisition of the sound pressure started at 12:45:00 at the sampling rate of 22.5 kHz. Five minutes after the final failure was detected, the experiment was safely terminated.

The following signals (Figure 14) are a clear indication of an unexpected event; they show the amplitude enhancement at the time when welds are assumed to have been broken and the blade separated from the supports:

- The pressure loss increased by about 500 mbar, whereas the flow rate decreased slightly [Figure 14(a)].
- Sound pressure [Figure 14(b)] results at about 12:45:00 show a sudden and huge increase of the sound level in the laboratory. The amplitude is given in V (Volts). The sampling rate was 22.5 kHz. The acquisition started at 12:45:00.
- Acceleration results [Figure 14(b)] between 12:43:00 and 12:45:00 show an increase of a factor of two during 2 minutes. During this period the flow rate was kept the same, but the pressure of the cover gas was reduced. The pressure loss remained constant. Previous results [11] showed that the regime of developed cavitation was reached for the given flow conditions at 12:43:00.Therefore, the amplitude increase is caused by developed cavitation and the contribution due to the structural resonance is hidden in the noise.
- Acceleration results [Figures 14(c) and 14(d)] at 12:45:17.177 show that acceleration amplitudes drop after weld rupture and blade detachment.

Figure 14: Signals acquired during time interval when final failure occurred

(a) Pressure loss, flow rate and pressure of the cover gas, (b) sound pressure,
(c) and (d) structural acceleration. Arrows indicate absolute time when failure occurred.

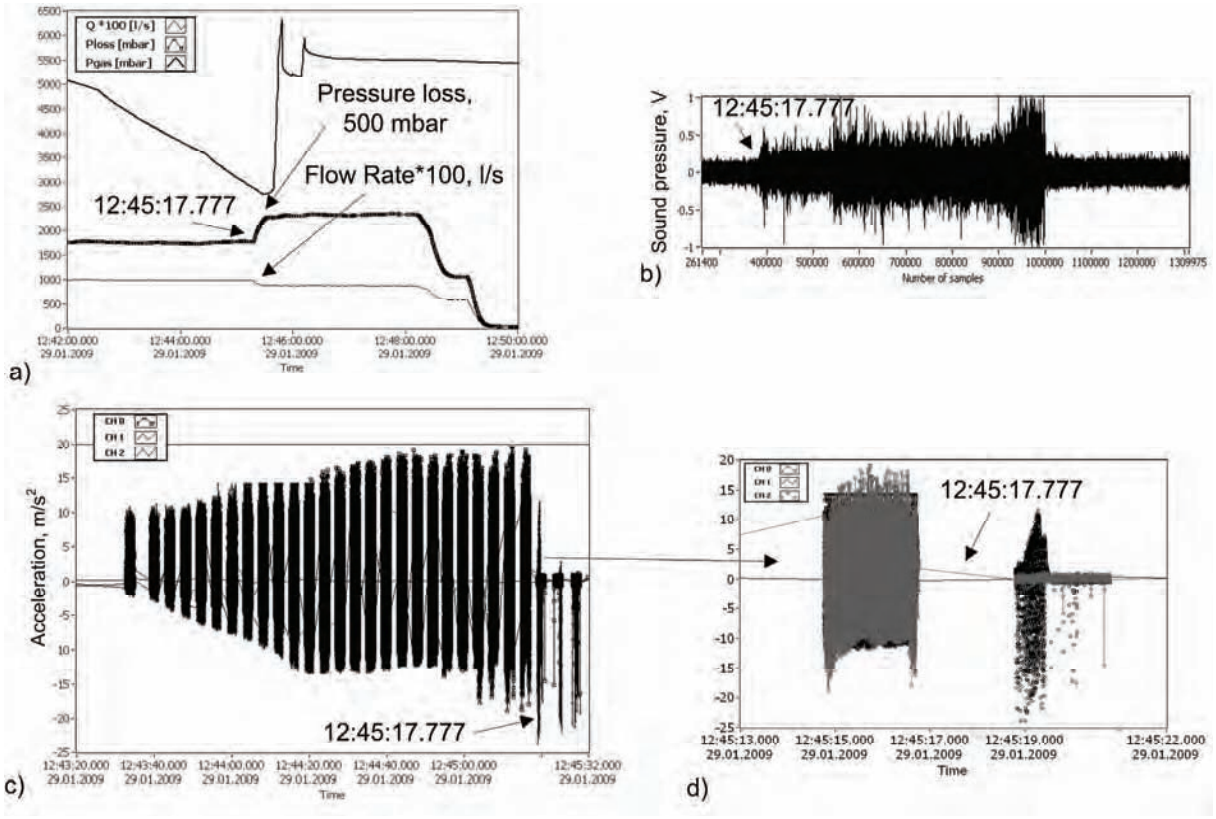

Conclusions

The most important conclusions to be drawn from these tests are as follows:

- The target has a very compact design, i.e. 15 cm in diameter, which is capable of absorbing the 2.3 MW total heat deposited in the target. The pressure loss in the target of about 2 bar is remarkably low considering the achieved 150 kg/s flow rate and peak velocities in the mercury which reach 6 m/s.
- The configuration without flow vanes worked satisfactorily and produced weak structural vibrations at 11.2 l/s (90% of the full design flow rate) with a total pressure loss lower than 2 bars. In order to suppress cavitation, sufficiently high pressure must be applied inside the target. The lower limit of the operating pressure could not be precisely estimated, but it is likely to be higher than 6 bar. The current design static pressure is set to ensure that a sufficient margin against boiling of the mercury exists when the target is under power and the liquid metal temperature reaches a peak of 290°C, which is well below the boiling point of 450°C at 5 bar. Obviously, increasing the design pressure value would benefit both margins against cavitation and boiling.
- For the design with flow vanes a flow rate of 10 l/s was reached during the final test sessions, though the design suffered from manufacturing defects. Therefore in a further design the use of flow vanes must be reconsidered and strengthened. During the first day of operation with flow vanes, moderate cavitation noise and structural accelerations with

moderate amplitudes and clear tones, were acquired. The mock-up was operated for 1 hour. During the second day, just after 25 minutes of operation at higher flow rates, a very loud crackling noise announced the failure of an internal structure (the flow vanes, welds and vane supports). Several seconds afterwards, the experiment was safely stopped. The predictions by CFD and FEM analysis were thereby confirmed and the safety monitoring systems were validated. Incipient and developed cavitation were detected by using various experimental techniques. Typical audible noise, which characterises developed cavitation was registered and recorded for a flow rate of 10 l/s and a cover gas pressure of 2 bar.

- Suppression of cavitation was made possible by raising the static pressure to over 6 bar. At high flow rates and low pressure, jet cavitation as well as flow-induced vibrations and flow-excited acoustic resonances can occur at the outlet of narrow gaps. In addition, naturally-developing instabilities can periodically be triggered and may cause blades to resonate. Having considered these aspects, as well as the structural integrity of the vanes, the design with flow vanes can be improved.
- Fast structural and sound measurements can be used for detecting and studying various flow phenomena and instabilities, such as effects of the flow turbulence on the structural vibrations, incipient and developed cavitation, vortex shedding, large coherent structures, structural resonances and the ruptures. The results of this unique and successful EURISOL mock-up test helped to validate computational results and triggered further activities regarding testing and improvement of the current design.
- The use of remote diagnostic techniques enabled accurate monitoring of the system health, including various internal or external components (some of them remote from the source). Unique data, which represent system behaviour under strong cavitating and resonating flow conditions have been generated and analysed with up-to-date post-processing techniques. Use of these techniques on-line, during operation of facilities using high-power targets under irradiation in the future, will improve system safety.

Acknowledgements

We acknowledge the financial support of the European Community under the FP6 “Research Infrastructure Action – Structuring the European Research Area” EURISOL DS project, contract No. 515768 RIDS. The EC is not liable for any use that can be made of the information contained herein.

References

[1] Blumenfeld, Y., G. Fortuna, *Final Report of the EURISOL Design Study (2005-2009)*, European Commission Contract No. 515768 RIDS, published by GANIL France, *www.eurisol.org* (2009).

[2] Blumenfeld, Y., on behalf of the EURISOL Design Study, “EURISOL Design Study: Towards an Ultimate ISOL Facility for Europe”, *Franco-Japanese Symposium: New Paradigms in Nuclear Physics*, Paris, France, 29 September-2 October (2008).

[3] Samec, K., *Design of the EURISOL Converter Target*, PSI Report TM-34-07-05 (2007).

[4] Pretet, Q., R. Milenkovic, B. Smith, *Stress Analysis of the EURISOL DS Target*, PSI Report TM-34-06-02 (2006).

[5] Ashrafi-Nik, M., *Thermo-hydraulic Optimization of the EURISOL DS Target*, PSI Report TM-34-06-0 (2006).

[6] Milenković, R., *et al.*, "Structural-hydraulic Liquid Metal Test of the EURISOL Target Mock-up", *Nuclear Instruments and Methods in Physics Research*, Section A, Vol. 607, Issue 2, pp. 279-292 (2009).

[7] Samec, K., *et al.*, "Design of a Compact High Power Neutron Source", *Nuclear Instruments and Methods in Physics Research*, Section A, Vol. 606, Issue 3, pp. 281-290 (2009).

[8] Mallat, S., *A Wavelet Tour of Signal Processing*, ISBN: 978-0-12-466606-1 (1999).

[9] Idelchik, I.D., *Handbook of Hydraulic Resistance* (1975) (in Russian).

[10] Milenković, R., *et al.*, "Wavelet Analysis of Experimental Results for Coupled Structural-hydraulic Behavior of the EURISOL Target Mock-up", *Nuclear Instruments and Methods in Physics Research*, Section A, Vol. 608, pp. 175-182 (2009).

[11] Milenković, R., *et al.*, "Detection of a Structural Impact in Liquid Metal Flow During Test Runs of the EURISOL Target Mock-up", *Nuclear Instruments and Methods in Physics Research,* Section A, Vol. 609, pp. 1-18 (2009).

The Frankfurt Neutron Source – FRANZ

O. Meusel, L.P. Chau, M. Heilmann, H. Klein, H. Podlech, U. Ratzinger, K. Volk, C. Wiesner
IAP, University Frankfurt/Main
Germany

Abstract

The Frankfurt Neutron Source will use the ^{7}Li(p,n) reaction to produce an intense neutron beam. The planned experiments require variable neutron energy between 10 and 400 keV. Hence the energy of the primary proton beam should be adjustable between 1.8 and 2.2 MeV.

The FRANZ beam line consists of two branches to allow different methods of neutron capture measurements. The compressor mode offers time-of-flight measurements in combination with a $4\pi BaF_2$ detector array. The proton beam of about 150 mA will be compressed to a 1 ns pulse with a peak current of about 9 A at a repetition rate of 250 kHz. The activation mode uses a continuous neutron flux. The primary cw proton beam with a low current up to 30 mA will be focused on the production target.

FRANZ is not only a neutron source but also a test bench for research on new accelerator and diagnostic concepts for intense ion beams. The planned proton beam properties on the target poses a challenging task of accelerator design and target development. This presentation is directed towards the ongoing construction of the neutron source and planned experiments.

Introduction

The Frankfurt neutron source FRANZ, currently under construction, is destined to be a compact accelerator-based neutron source. FRANZ comprises two experimental areas which allow different types of neutron capture measurements. The compressor mode offers time-of-flight measurements in combination with a $4\pi BaF_2$ detector array. The proton beam will be compressed to a 1 ns pulse with a peak current of about 9.6 A with a repetition rate of 250 kHz. On the other hand the activation mode uses a continuous neutron flux. Primary cw proton beams with a current up to 3 mA on solid targets and up to 30 mA on liquid metal targets are feasible as a future option.

Figure 1: Scheme of the FRANZ facility with targets and detector and irradiation and neutron shielding

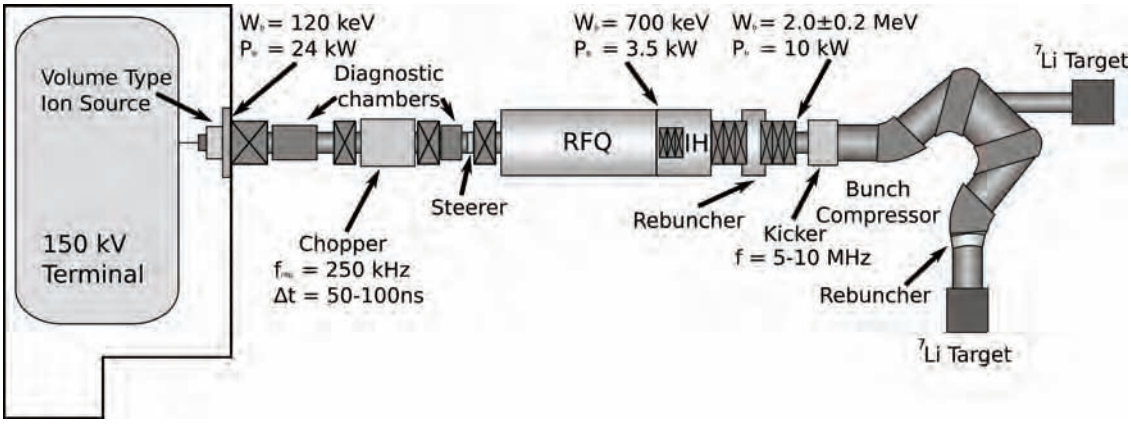

The planned accelerator front end is well suited as a test bench for new accelerator and diagnostic concepts for intense ion beams. The envisaged proton beam properties on the target lead into a challenging accelerator design to overcome the space charge forces.

Ion source

A volume type ion source was chosen for FRANZ to extract the proton beam from a hot filament driven gas discharge plasma [1]. Figure 2 shows this source type. The lifetime of the filament is limited to about one month of operation. On the other hand the plasma temperature of a gas discharge at moderate arc power is, along with the confining magnetic field, very low compared with other source types, e.g. ECR source. Therefore the beam emittance is small and gives the possibility to investigate causes of emittance growth during beam transport and acceleration along the whole linac.

For the planned beam intensities a pentode extraction system produces moderate emittance growth during the extraction and pre-acceleration phase when compared with other extraction schemes [2]. Figure 3 shows a preliminary numerical simulation of the beam extraction using the IGUN code [3] and taking into account a multi-species beam composed of approximately H^+ = 80%, $H_2^+ = H_3^+$ 10%.

LEBT section with chopper

The LEBT section consists of four solenoids for beam focusing and offers the possibility of partial space charge compensation due to residual gas ionisation. Figure 4 shows a scheme of the planned LEBT. The first and second solenoid will be used for separation of ion species and to

Figure 2: Cross-sectional view of the constructed volume-type ion source

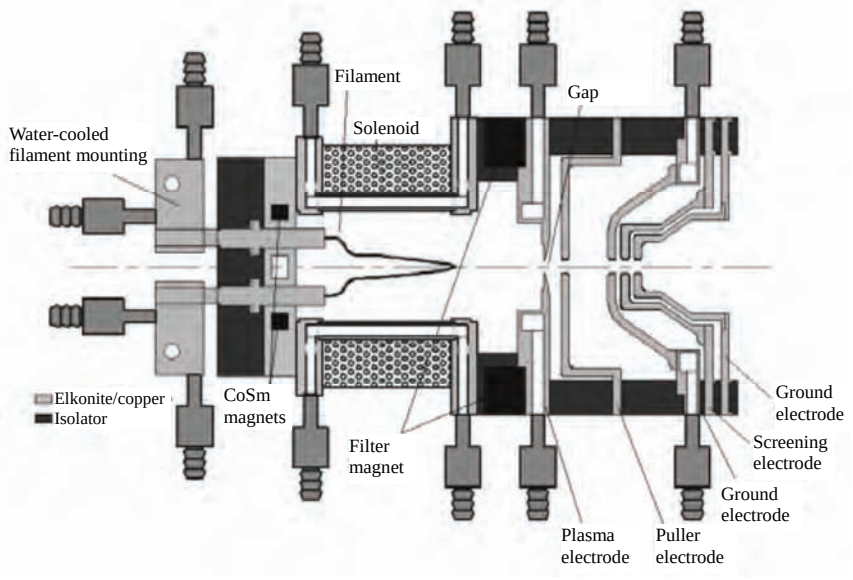

Figure 3: Illustration of a preliminary IGUN calculated beam profile along a pentode extraction system

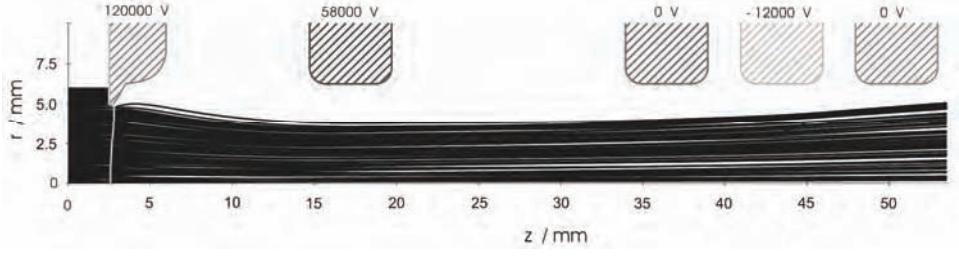

Figure 4: Scheme of the LEBT section with four solenoids and the chopper device

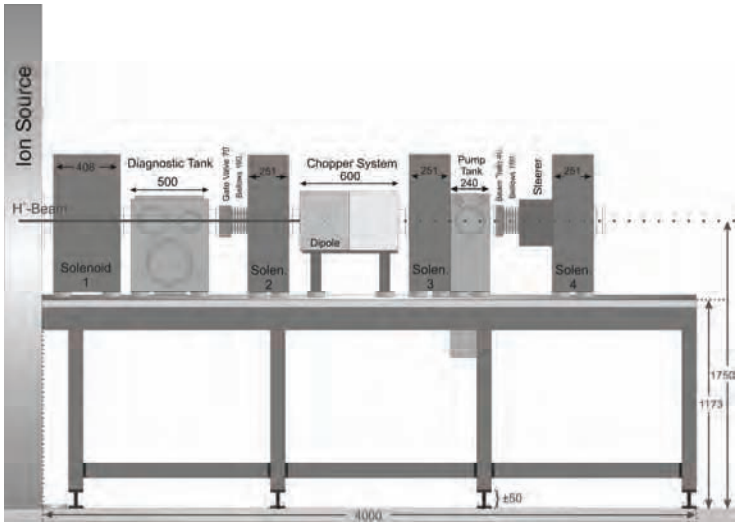

match the proton beam into the ExB chopper system. Downstream of the chopper two solenoids will focus the beam into the acceptance of the RFQ. Two pumping and diagnostic tanks will be used for several non interceptive diagnostics e.g. optical beam profile measurement and beam potential measurements using a residual gas ion energy analyser.

The chopper system consisting of a kicker and a septum magnet combined with a slit provide 100 ns proton beam pulses. Figure 5 shows the arrangement of the chopper system.

Figure 5: Schematic drawing of the ExB chopper system consisting of a fast kicker immersed in a dipole magnet and a septum magnet

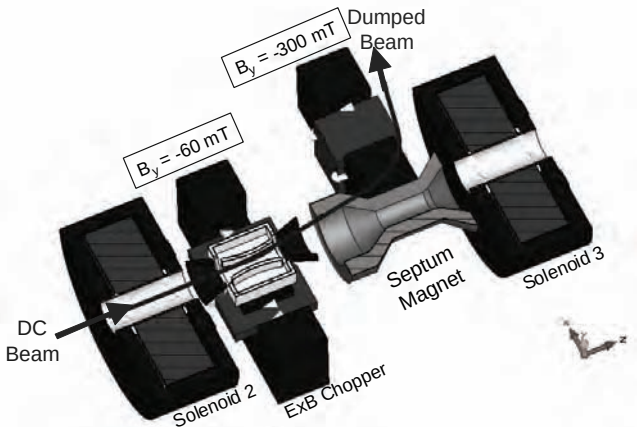

A static septum magnet provides the post-separation whereas the electric kicker deflects the beam with a repetition rate of 250 kHz and a pulse with a flat top of at least 50 ns. Comparison of electric and magnetic kicker systems using numerical simulation shows an influence of secondary electrons. The high production rate of electrons in the chopper system allows the possibility for partial space charge compensation of short beam pulses. Preliminary studies result in approximately 30% of space charge compensation with the ExB chopper system. For an electric kicker embedded in a dipole magnetic field the risk due to secondary electron production will be reduced [4]. Beam transport and chopping leads to an emittance growth by a factor of 4. It seems possible to reduce this value by further optimisation of beam transport with respect to the filling degree of the solenoids and more detailed description of space charge compensation. Pulsed beam with proton densities of $n_p = 8.2 \cdot 10^{14}$ m^{-3}, generalised perveance of $K = 3.1 \cdot 10^{3}$ and mentioned time structure will be injected into the coupled RFQ-IH DTL.

Coupled RFQ-IH DTL

In order to minimise installation costs and to use one compact common RF amplifier a coupling between the RFQ and IH-DTL is foreseen [5]. Figure 6 shows a cross-sectional view of the coupled accelerator stages. Both of the cavities can also be used separately. The RFQ is 1.75 m long and needs an input power of 150 kW [6]. Numerical simulations using the PARMTEQM [7] code show a beam transmission efficiency of 95% with acceptable emittance growth at the design current I = 200 mA for an electrode voltage of about 75 kV. Output energy of the RFQ will be 0.7 MeV. The IH-DTL will boost the proton beam to reach its final beam energy of 2 MeV. The power consumption of the IH cavity is in a range of about 65 kW to establish a gap voltage of 300 kV. Due to the bunching of the RFQ the incoming proton beam will be compressed longitudinally. The average bunch current increases up to 1.2 A and the resulting compression ratio is $\eta = 6$. At beam energy of 2 MeV downstream of the accelerator stages the proton density is $n_p = 8.2 \cdot 10^{14}$ m^{-3} and the space charge forces expressed by the generalised perveance decreases by about $K = 2.7 \cdot 10^{-4}$.

Figure 6: Scheme of the coupled RFQ and IH cavity

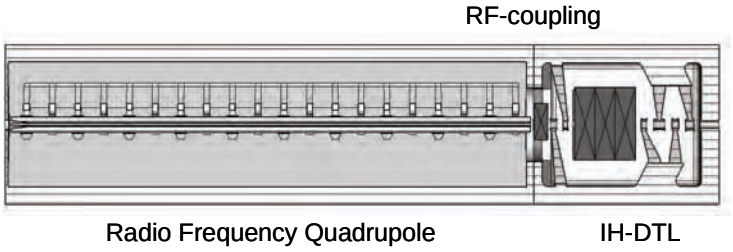

Bunch compressor

By applying the bunch compressor concept of the Mobley type [8] for high current beams a split magnetic dipole array that includes edge focusing was chosen [9]. The periodic deflection by the RF kicker at the entrance of the bending system guides up to nine bunches on different paths to the final focus, where the neutron production target is located. As shown in Figure 7, two rebuncher cavities are needed to focus the beam longitudinally.

Figure 7: Scheme of the bunch compressor

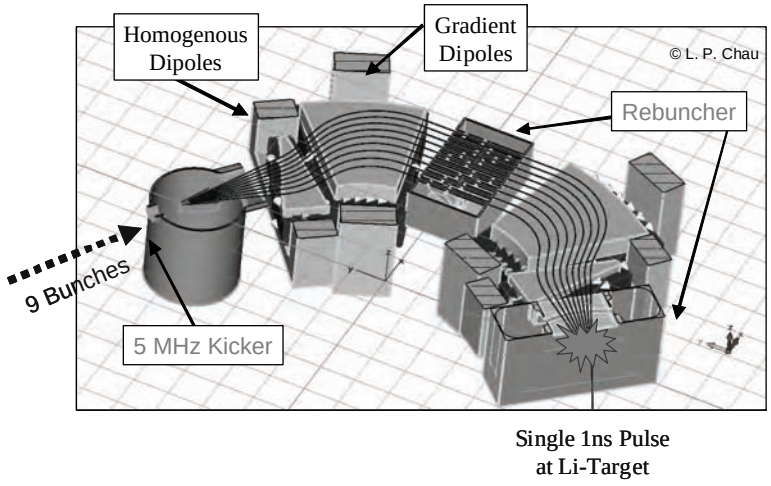

By choosing adequate parameters all nine bunches will overlap at the target and produce a 1.1 ns proton pulse with a proton density of $n_p = 8.2 \cdot 10^{14}$ m^{-3}. The compression ratio downstream of the whole proton injector is of $\eta = 48$.

Target and detector

A possible neutron production target for high beam powers of up to 4 kW, shown in Figure 8, has been investigated. It was shown that a robust solution can be obtained consisting of a copper backing 1.2 mm in thickness.

Cooling is provided by water flowing through capillaries of diameter 0.6 mm and with a spacing of 1.0 mm at a pressure of 50 bar. This concept was subject to computer simulations, which demonstrated that the moderation effect of the cooling water is acceptable and that the surface temperature at 4 kW beam power does not exceed 300°C, sufficiently low if a high temperature Li compound is used as a target material.

Figure 8: Scheme of the high-power neutron production target with cooling water connections

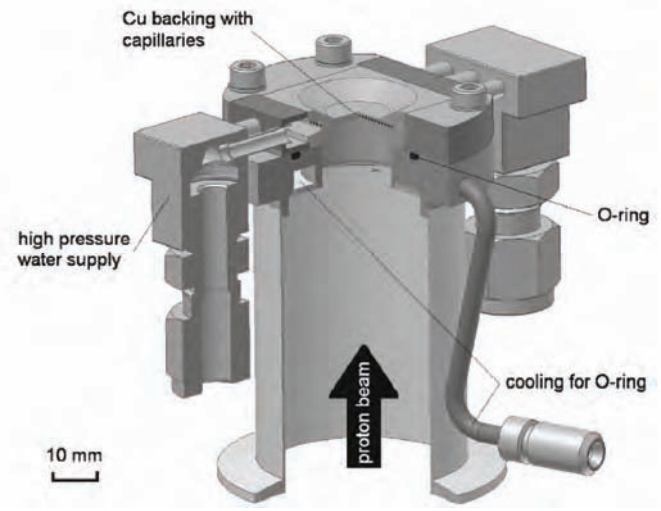

The $4\pi BaF_2$ detector array consists of 42 modules arranged on a sphere. This array was used in FZ Karlsruhe and transferred to Frankfurt University in 2008. After reassembling the detector sphere a test programme was started to evaluate the behaviour of each single module.

Conclusions

FRANZ will be a multi-purpose project. The proton linac gives an opportunity for the test and the development of new accelerator components and beam diagnostic tools. High beam current at low and medium energy range causes high space charge forces. The resulting beam behaviour, beam power and the power consumption of the accelerator are a challenge. The hardware of the proton linac of the Frankfurter neutron source FRANZ is under construction. In parallel, detailed multi-particle transport simulations show that the activation mode using a 30 mA (cw) beam will be limited by the RF power consumption, target power deposition and radiation safety. The compressor mode operation causes large beam spot size on the target. Additionally longitudinal focusing is needed to deliver bunch duration of 1 ns. Prototypes of solid ^{7}Li targets were tested at KIT Karlsruhe successfully. The high beam power demands the development of new high-power targets. First measurements for the evaluation of the $4\pi BaF_2$ were done. The estimated high neutron flux leads to a more precise measurement of neutron capture cross-sections. Both development of new accelerator concepts and estimation of nuclear data, especially neutron capture cross-sections, are needed for future accelerator-driven systems (ADS).

References

[1] Nörenberg, R., *et al.*, "Development of a High Efficiency Proton Source for the Frankfurter-Neutronen-Quelle am Stern-Gerlach-Zentrum", *Rev. Sci. Instrum.*, 79, 02B316 (2008).

[2] Hollinger, R., P. Spädtke, "Comparison of Different Extraction and Acceleration Systems for a High Intense Proton Beam for the Future Proton Linac at GSI", *Rev. Sci. Instrum.*, 75, 1656 (2004).

[3] Becker, R., W.B. Herrmannsfeldt, "IGUN: A Program for the Simulation of Positive Ion Extraction Including Magnetic Fields", *Rev. Sci. Instrum.*, 63, 2756 (1992).

[4] Wiesner, C., *et al.*, "A 250 kHz Chopper for Low Energy High Intensity Proton Beams", *Proc. Eur. Part. Acc. Conf.*, Genoa, Italy (2008).

[5] Bechtold, A., *et al.*, "A Coupled RFQ-drift Tube Combination for FRANZ", these proceedings.

[6] Zhang, C., *et al.*, "Development of a High Current Proton Linac for FRANZ", *EPAC'06*, ID: 2342-THPCH007.

[7] Los Alamos National Laboratory (LANL), *LANL Manual of RFQ Design Codes*, LANL Report No. LA-UR-96-1836 (1996).

[8] Mobley, R.C., "Proposed Method for Producing Short Intense Monoenergetic Ion Pulses", *Phys. Rev.*, 88 (2), 360-361 (1951).

[9] Chau, L.P., *et al.*, "One Nano-second Bunch Compressor for High Intense Proton Beam", *Proc. Eur. Part. Acc. Conf.*, Genoa, Italy (2008).

[10] Petrich, D., "A Neutron Production Target for FRANZ", *Nuclear Instruments and Methods in Physics Research*, A 596, 269-275 (2008).

Session IV

Subcritical Systems

Chairs: K. Tsujimoto, E.M. González-Romero, J.U. Knebel

ADS-related activities at IAEA: From accelerators, neutron sources to fuel cycle and databases

F. Mulhauser, P. Adelfang, R.M. Capote Noy, V. Inozemtsev, G. Mank, D. Ridikas, A. Stanculescu, A. Zeman
International Atomic Energy Agency
Vienna, Austria

Abstract

The ADS-related activities at the IAEA address nuclear science and nuclear energy topics, and are implemented as a joint effort between the Departments of Nuclear Sciences and Applications and Nuclear Energy. The IAEA is pursuing efforts on utilising accelerators and research reactors to support the basic and applied research, provide intense neutron sources, characterise and qualify materials of nuclear interest and concomitantly, train and qualify a highly educated nuclear workforce. At the back end of the nuclear fuel cycle, environmental concerns linked with the long half-life radioisotopes generated from nuclear fission have led to increased R&D efforts to develop a technology aimed at reducing the amount of radioactive waste through transmutation in either fast fission reactors or ADS. In the framework of the project on Technology Advances in Fast Reactors and Accelerator-driven Systems, the IAEA has implemented a number of initiatives on utilisation of plutonium and transmutation of long-lived radioactive waste, accelerator-driven systems, thorium fuel options, innovative nuclear reactors and fuel cycles, non-conventional nuclear energy systems, and fusion/fission hybrids. This paper gives an overview of IAEA's accelerator-related activities in nuclear science for materials development, and partitioning and transmutation of nuclear waste.

Introduction

Accelerators and research reactors can provide some of the best analytical techniques and applications in a diverse range of fields such as materials science, environmental science, cultural heritage and the biosciences. The effective utilisation of research reactors and accelerators is being promoted through participation in knowledge-building activities, the development and application of innovative nuclear science, and the development of new generation nuclear energy systems. These areas offer a broad spectrum of activities for development, and new applications for accelerators and accelerator-based techniques.

This report describes the latest developments as supported by the IAEA in the field of low-energy accelerators, especially the use for cultural heritage, for medium-energy accelerators and their use for the effective production of neutrons, as well as the research reactors' issues and trends. The new requirements on structural materials for fission and fusion reactors request the use of both accelerators and research reactors including new modelling efforts. The main emphasis of the work of the IAEA is on sharing and disseminating knowledge followed by training and education. In the field of education the IAEA is working together with the Abdus Salam International Centre of Theoretical Physics (ICTP), Trieste, Italy. The IAEA has Co-ordinated Research Projects (CRP) on this topic, but would like to increase its efforts, as requested by the member states.

Structural materials

Nuclear power systems, whether based on fission, fusion, fusion-fission hybrids or driven by spallation reactions (ADS), require the use of structural alloys that can serve in very strenuous environments for decades without failure. In addition to exposure to high temperatures and corrosive environments, these alloys must withstand a high level of constant internal bombardment by neutrons, charged particles and energetic photons. In addition to the deposition of thermal energy this bombardment causes most importantly the displacement of atoms from their lattice site, producing vacancies and interstitial atoms, both of which are highly (but differently) mobile, and which can both contribute to extensive microstructural and microchemical alteration of the alloy [1].

Normally, the fast reactors with closed fuel cycles are the primary candidates for next generation nuclear power plants, and it is expected that most of the reactors will be operated at higher neutron fluxes compared to those in light water reactors by one order of magnitude. From this point of view, core components are subjected to much higher rates of atomic displacement and microstructural-microchemical evolution. Additionally, fast reactors will operate at higher temperatures, leading to a greater tendency toward microstructural-microchemical alteration, phase instability and dimensional changes. For effective power generation critical structural components should be stable against radiation degradation to ~650°C for optimum performance in any coolant or neutron flux-spectra. This stability of structural materials should be maintained long enough that the fuel reaches the maximum burn-up consistent with neutronic and economic requirements. Since the microstructural-microchemical processes are driven primarily by atomic displacement it is traditional practice to define the exposure dose in terms of "displacements per atom" or dpa. An exposure of 20 dpa means that on the average, each atom in the alloy has been displaced twenty times from a lattice site. For effective utilisation of the fuel to reach maximum burn-up, for instance, fuel cladding alloys must reach exposure doses significantly greater than 100 dpa, however for most fast reactor applications, 200-250 dpa would be required as indicated in Figure 1. Otherwise the lifetime of a fuel pin or a fuel assembly would be determined by the radiation-degraded integrity of the structural containment and not by its burn-up potential. Unfortunately, the R&D community today faces a critical lack of irradiation capacities of material test reactors (MTR). To reach 100-200 dpa in the few currently functioning test reactors operating

Figure 1: Growing operational requirements for present and future nuclear systems

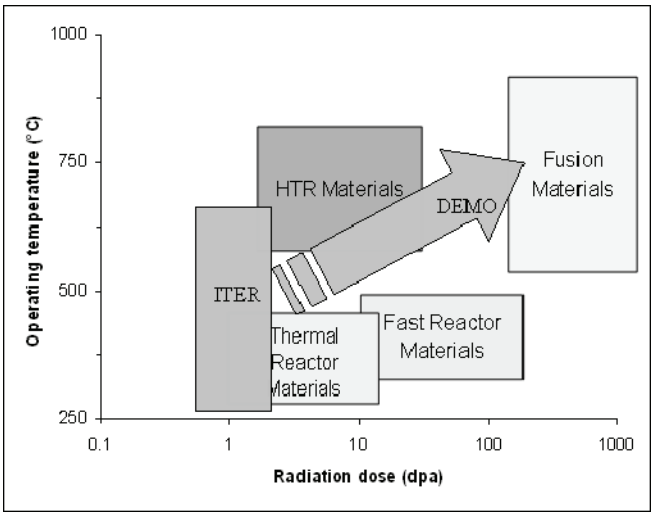

at ~10 dpa/year (e.g. BOR-60, ATR, HFIR) requires a very large amount of stable operation and funding for 10-20 years, an unrealistic expectation given that even the currently operating reactors have decommissioning dates within this time period and nuclear budgets are often rather uncertain and volatile, both in the long and short term. With the recent final shutdown of the French Phénix reactor and the temporary shutdown of Joyo (Japan) today there is only one powerful fast reactor operational (BN-600) to produce ~40 dpa/year and only a few testing facilities with fast neutron spectra but rather limited experimental capabilities. For various reasons these reactors will most likely not be easily employed for testing suitable to the research effort at the necessary scale.

In view of these circumstances, the IAEA initiated a CRP on "Accelerator Simulation and Theoretical Modelling of Radiation Damage" which deals with several issues related to the proton and ion beam irradiation in order to achieve very high radiation damage. This particular project aims to facilitate following issues: *i)* better understanding of radiation effects and mechanisms of material damage and basic physics of accelerator irradiation under specific conditions; *ii)* improvement of knowledge and data for the present and new generation of structural materials; *iii)* contribution to developmental of theoretical models for radiation degradation mechanism; *iv)* fostering of advanced and innovative technologies by support of round robin testing, collaboration and networking. Extensive theoretical and experimental studies are being carried out among participating laboratories form Belgium, China, the European Commission, France, India, Japan, Korea, Kazakhstan, Poland, Russia, Spain, Switzerland, Slovakia, Ukraine and the United States.

The ongoing project should extend understanding of the basic physics of accelerator irradiation under operational conditions in fission reactors, and through synergy with other nuclear concepts such as fusion and spallation systems. That goal will bridge from micro- to macroscopic behaviour of materials through modelling validated by specific detailed experiments. Special emphasis is placed on the following phenomena [2]: *i)* primary damage, cascade and sub-cascade formation; *ii)* irradiation-activated kinetic processes; *iii)* void and gaseous swelling, including He+H synergisms; *iv)* phase stability and self-organisation under irradiation; *v)* irradiation effects on mechanical properties; *vi)* corrosion processes under irradiation; *vii)* role of impurities (e.g. transmutation, fabrication).

Preliminary achievements show that ferritic or ferritic-martensitic alloys strengthed by dispersion hardening with very small insoluble nano-oxides of Al, Y and other solute elements, are primary candidates for key structural components. This type of modification, designated as

oxide-dispersion strengthening (ODS), not only maintains alloy strength at much higher temperatures, but also appears to contribute to additional resistance to swelling at lower temperatures. However, these ODS alloys are often rather difficult to manufacture and their development is still very much in the R&D phase. In order to develop and optimise such alloys, however, irradiation tests must be conducted on the alloys at very high doses to confirm that they are indeed stable under irradiation. This brings forward the major impediment to the R&D effort [3].

Improved production and utilisation of short pulsed, cold neutrons at low-medium energy spallation neutron sources

The scientific and technological problems being addressed using neutron beams are becoming increasingly large and complex, to the extent that research reactors alone will not be able to cater to all the requirements. They will need to be complemented by neutron beams from spallation neutron sources, where the extremely high peak neutron fluxes and specific time structure of the pulsed neutron beam opens up numerous new experimental opportunities. The IAEA has initiated a CRP to investigate how high-end technologies from the flagship neutron sources can be cost-effectively adapted to lesser powered neutron sources, while assuring best experimental conditions for users in both the developing nations and industrially developed member states. The scope of the CRP covers the following topics: *i)* increase of potential usage of beam lines by contributing to improve mini-focusing small angle neutron scattering (SANS); *ii)* improvement of spallation source by development of cryogenic moderators; *iii)* enhanced capability for strain determination by improving data extraction and evaluation from high resolution energy-dispersive transmission measurements.

The demonstration of a working "mini-focusing SANS" instrument provides an opportunity to have a qualitative impact on this technique in terms of both its general availability world wide and the ease with which the technique might be introduced to a new facility. Energy-dispersive transmission measurements can provide a wealth of important data on a wide variety of materials and it is possible to perform these measurements at relatively weak sources. Development of these techniques therefore offers an opportunity for national-scale neutron sources to have significant impact on local industry, but realising this potential will require significant development of the technique. Two groups (Argentina and Japan) have made significant progress in this arena. Parallel development of analysis software will facilitate the eventual validation of both.

The neutron moderator lies at the heart of all neutron scattering experiments, but the development of new moderator concepts has been inhibited by the lack of available computer models and corresponding data libraries of candidate materials at the desired temperatures, and a significant part of the CRP activity is devoted to the development of new models. This will include the collection of appropriate data for validating the models as well as the computational work itself. Strong collaboration led by Argentina is taking place between Japan, India, the United States and Russian Federation groups. New moderators will be developed for the facilities of at least three of the participating groups thereby providing a significant boost to the capabilities of those facilities. The optimisation of designs for target/moderator/reflector assemblies at small scale accelerator-driven neutron sources (ADNS) is expected to be different from those for larger scale spallation sources or research reactors. One of the activities in the CRP will directly address this issue. Simulations of the performance of a low-energy Li-target based system are being completed with significant detail. Experimental verification of the predicted performance of the re-entrant hole mesitylene moderator should be completed. A list identifying those materials for which we have both reasonable kernels and adequate spectral data should be produced as a first step toward providing a catalogue of evaluated neutron kernels. This will require communication among the groups from Argentina, Japan, Russia and the United States.

Research reactor issues and trends

Research reactors (RR) have played and continue to play an important role within several fields of basic science, in the development of nuclear science and technology, in the valuable generation of radioisotopes and other products for various applications, in support of nuclear power programmes, including the development of human resources and skills. For nuclear research and technology development to continue to prosper, RR must be safely and reliably operated, efficiently utilised, refurbished when necessary, provided with adequate non-proliferating fuel cycle services and safely decommissioned at the end of life. From more than 670 RR (including critical and subcritical facilities) constructed around the world, in February 2010, 234 were still operating, while 11 were under the status of "temporary shutdown" [4]. Russia has the highest number of operational RR (48), followed by the United States (41), China (15), Japan (13), France (11) and Germany (10). The RR are distributed over 56 member states (MS), including 40 developing countries. Of the RR that are no longer operating, some are planned to resume operation in the future, some are undergoing decommissioning or waiting to be decommissioned, and others are in an extended shutdown state with no clear future plans.

Nowadays the decreasing fleet of these facilities faces a number of critical issues and important challenges such as underutilisation, inexistent or inappropriate strategic business plans, ageing and needs for modernisation/refurbishment, presence of fresh or spent HEU fuel, unavailability of qualified high-density LEU fuels, accumulation of spent nuclear fuel, advanced decommissioning planning and implementation stages, and, in some cases, safety and security issues. In addition to this non-exhaustive list of challenges are the plans to build new RR by MS without no or little experience in this domain. In response to these challenges, the IAEA is taking action and designing activities to tackle these issues (see e.g. [5] and references therein) and make sure that promotion, support and assistance to MS in the development and uninterrupted operation of strong, dynamic, sustainable, safe and secure RR dedicated to peaceful uses of atomic energy and nuclear techniques is preserved.

IAEA research reactor database

The IAEA Department of Nuclear Science and Applications (NA) and the Department of Nuclear Energy (NE) jointly manage a Research Reactor and Spent Fuel Database (RRDB) [5]. This database serves to promote the capabilities of individual facilities as well as to help IAEA internal and external stakeholders plan and develop programmatic activities in response to the expressed needs of individual MS. The complete IAEA RRDB contains information on both operational, planned, shutdown and decommissioned RR. It is prepared from the data provided by RR administrators of the MS through annual questionnaires. While every attempt is made to keep the RRDB current, the IAEA makes no guaranties, either express or implied, concerning the accuracy, completeness, reliability or suitability of the information. Therefore, national RR data providers or individual RR managers are asked to inform the RRDB Project Officers of any updates or corrections needed.

For the promotion and support and the peaceful, efficient and sustainable uses of RR, the IAEA has recently developed a dedicated Operational RR Database (ORRDB) [6], a specific output of the IAEA computerised RRDB [4]. The table of contents for this new ORRDB is shown in Figure 2. It contains only the information related to the operational RR facilities and classifies them into three major categories according to: *i)* geographical location; *ii)* reactor characteristics/ features; *iii)* reactor utilisation and applications. Thanks to the pre-designed classification filters, some useful statistical information can easily be found relevant to all operational RR, including lists of the facilities providing specific applications, i.e. products and services such as isotope production, activation analysis, teaching and training, etc. In addition, the ORRDB includes all detailed technical information reports of the individual facilities. Finally, although the ORRDB is available on Internet [6], it can also operate off-line and occupies less than 10 MB of disk space.

Figure 2: Table of contents of the dedicated Operational RR Database (ORRDB) [3]

This new utilisation and application-driven ORRDB provides IAEA MS with a resource to assist efforts in developing strategies for capacity building, effective utilisation and management of RR on a national, regional and international basis. It also contains somewhat "sensitive" information like the utilisation rates of both individual RR as well as country-averaged statistics. It is expected that this new ORRDB, in addition to standard book-keeping, should help in enhanced and more efficient utilisation of RR in MS for many practical applications, facilitate co-operation between different RR centres, and promote networking both for RR host and non-host MS. The responsible Project Officer would appreciate all MS' input concerning how this new tool could be further improved to achieve targeted objectives.

Use of LEU in accelerator-driven subcritical systems

The subcritical assembly alone or in combination with an external neutron source (ADS) contains nuclear fuel. In principle, HEU or LEU can be used for the subcritical assembly fuel. At a Technical Meeting held in Vienna from 10-12 October 2005 and attended by 15 experts from 13 member states, it was recommended that a CRP or an international collaborative work on the use of LEU in ADS systems be organised. In November 2006, with financial support from the United States DOE-GTRI, the IAEA organised a Technical Meeting with the purpose of establishing a working plan for the proposed collaborative work intended to study the feasibility of using LEU in ADS systems. Seven facilities were included in the working plan: Yalina-Thermal (Belarus); Yalina-Booster (Belarus), with three possible configurations; Kharkov Facility (Ukraine); ADS IPEN/MB-01 (Brazil), with two possible configurations; RC-1 TRIGA Casaccia (Italy); H5B (Serbia), and AHWR (India). For each facility the participants defined their area of interest and proposed a number of supporting activities. The work methodology adopted consists in carrying out benchmark studies on the use of LEU in ADS systems within the scope of the collaborative work as described above. Organisations in developing countries work under specific IAEA contracts entailing some financial support, while institutions in industrialised countries contribute their work at no cost to the IAEA.

The second Technical Meeting of the collaborative work was held on 12-16 November 2007, in Rome, and was attended by 40 experts from 18 member states. At the meeting, participants provided technical presentations describing the research activities carried out during 2007,

discussed results obtained and established the work plan for 2008. There was broad consensus that results obtained so far show encouraging perspectives for the use of LEU in ADS systems. It was recommended to extend the collaborative work, originally meant to finish by end 2008, to end 2009. Additional funds to cover this extension have been provided by US-DOE-GTRI. The third and last Technical Meeting is planned to be held in Mumbai, India in February 2010.

The output of this collaborative effort will be in the form of an IAEA technical document with the summary of the results of the work done, and a description of the results achieved by each participating organisation. It will also identify open issues for future R&D activities, and indicate a possible role for the Agency in the subject. It is expected that such a document would be a driving force to consider utilisation of LEU in all future ADS designs. For example, a new subcritical assembly under construction in Jordan will use uranium enriched only up to 3.5%.

Accelerator-driven systems (ADS)

There are four major challenges facing the long-term development of nuclear energy as a part of the world's energy mix: improvement of the economic competitiveness, meeting increasingly stringent safety requirements, adhering to the criteria of sustainable development and public acceptability.

While not involving the large quantities of gaseous products and toxic solid wastes associated with fossil fuels, radioactive waste disposal is today's dominant public acceptance issue. One of the primary reasons that are cited is the long life of many of the radioisotopes generated from fission. This concern has led to increased R&D efforts to develop a technology aimed at reducing the amount of long-lived radioactive waste through transmutation in fission reactors or ADS. In recent years, in various countries and at an international level, more and more studies have been carried out on advanced and innovative waste management strategies (i.e. actinide separation and utilisation/elimination). With regard to collaborative R&D, the IAEA has completed the CRP on "Studies of Advanced Reactor Technology Options for Effective Incineration of Radioactive Waste" [7], and has an ongoing CRP (2005-2009) on "Analytical and Experimental Benchmark Analyses of Accelerator Driven Systems (ADS)" [8].

The first CRP concentrated on the assessment of the dynamic behaviour of various transmutation systems. The reactor systems investigated included critical reactors, subcritical accelerator-driven systems with heavy liquid metal and gas cooling, critical molten salt systems, and hybrid fusion/fission systems. For all reactor systems fertile and fertile-free fuel options have been investigated. A major effort of the CRP consisted in the benchmarking of steady-state core configurations and performing transient/accident simulations. The results of the CRP show that for steady-state analyses the neutronic tools in each domain are advanced enough to provide good agreement. This holds for both mechanistic SN and Monte Carlo codes. Larger spreads in the results are generally caused by the different nuclear data libraries used. These deviations may not only be caused by the minor actinide data but also by data of other constituents, e.g. the treatment of matrix material in inert fuels and the fission products. Transient calculations have been performed for all transmutation systems but the gas-cooled ADS. Very different code systems were employed from point-kinetics to space-time kinetics, and also different levels in the sophistication of the thermal-hydraulics modelling. The benchmarking leads to the conclusion that different level code systems are currently needed to cover all the timescales of the different systems and transients. The very detailed codes have difficulties in their running times, for instance in the case of a long-lasting loss of heat sink accidents, while the less detailed codes naturally neglect important phenomena. A need for an intermediate class of codes becomes obvious. With one exception (ADS with fertile-free fuel), the benchmarking has exclusively been performed in the range of transients and accidents without core disruption.

The objective of the second CRP is to improve the understanding of the physics of the coupling of external neutron sources with subcritical cores. The CRP participants are performing

computational and experimental benchmarking for ADS and non-spallation neutron source driven subcritical systems. In the first stage, the CRP comprises the following benchmark exercises: YALINA Booster (SOSNY, Minsk, Belarus); Kyoto University Critical Assembly (KUCA); Pre-TRADE (ENEA, Italy); FEAT and TARC (both CERN); ADS kinetics analytical benchmarks; actinide cross-sections; spallation targets; and ADS performance.

In collaboration with the International Centre for Theoretical Physics (ICTP), the IAEA convened in 2008-2009 the "Advanced Workshop on Model Codes for Spallation Reactions" [9], the "Workshop on Nuclear Reaction Data for Advanced Reactor Technologies", and the school on "Physics, Technology and Applications of Innovative Fast Neutron Systems". Two major international conferences related to the scope of this paper were organised by the IAEA in 2009: the "Topical Meeting on Nuclear Research Applications and Utilisation of Accelerators, AccApp'09" (in collaboration with the ANS, Vienna, 4-8 May 2009), see below for details; and the conference on "Fast Reactors and Related Fuel Cycles: Challenges and Opportunities (FR09)", hosted by JAEA in Kyoto, 7-11 December 2009.

Nuclear data library for ADS

The utilisation of ADS for power generation and the transmutation of actinide and fission product waste require well-defined cross-section libraries suitable for their transport calculations. The groups involved in ADS analysis have expressed their nuclear data requirements in conferences and topical meetings. These needs include additional nuclear data measurements, theoretical data based on nuclear models, and cross-section libraries suitable for transport calculations.

More specifically, the generation of a test library for a number of code systems used in the analysis of ADS was discussed during an IAEA Technical Meeting entitled "Application Libraries for ADS and Transmutation", held in Vienna on 15-17 December 2004 [10]. Participants recommended the generation of a test library of limited scope for Monte Carlo as well as deterministic transport codes used in the analysis of ADS. This library should also be applicable to criticality calculations of new reactor designs.

The preparation of the ADS nuclear data library was undertaken in 2005 by the IAEA Nuclear Data Section (NDS) in the form of ADS-1.0 [11]. This test library has now been fully updated in 2008 as ADS-2.0, and the data files are available to users at *www-nds.iaea.org/ads* and also on CD-ROM upon request. Sources of the evaluated nuclear data files were the ENDF/B-VII.0 library [12], the JENDL/AC actinoid files [13] and the IAEA-NDS project for W isotopes [14]. Processing was carried out using NJOY-99.259 [15] with local updates at IAEA-NDS. The resulting files are available in ACE format for MCNP [16] and in MATXS format and GENDF format for multi-group transport calculations by deterministic transport codes used in the analysis of ADS. This resulting data package can also be applied to criticality calculations for new reactor designs, particularly for high-temperature systems (core materials up to 1 800 K). ADS-2.0 is freely available from the IAEA Nuclear Data Section, and is readily accessible on the web site: *www-nds.iaea.org/ads*.

IAEA benchmark of spallation models

Spallation reactions are nuclear reactions which play an important role over a wide domain of applications ranging from neutron sources for condensed matter and material studies, transmutation of nuclear waste and rare isotope production to astrophysics, simulation of detector set-ups in nuclear and particle physics experiments, and radiation protection near accelerators or in space. The simulation tools developed for these domains use nuclear model codes to compute the production yields and characteristics of all the particles and nuclei generated in these reactions. The codes are generally Monte Carlo implementations of Intra-Nuclear Cascade or Quantum Molecular Dynamics models followed by de-excitation (principally evaporation/ fission) models.

The IAEA has recently organised several expert meetings on model codes for spallation reactions. The experts have discussed in depth the physics bases and ingredients of the different models in order to understand their strengths and weaknesses. Since it is of great importance to validate on selected experimental data the abilities of the various codes to predict reliably the different quantities relevant for applications, it has been agreed to organise an international benchmark of the different models developed by different groups in the world. The specifications of the benchmark, including the set of selected experimental data to be compared to models, have been fixed for the use of the experts. The benchmark was organised under the auspices of IAEA.

The benchmark is restricted to nucleon-induced reactions on nuclei from carbon to uranium. Although, in principle, intranuclear cascade models are based on physics assumptions not valid below a hundred of MeV, it has been decided to have comparisons to data mostly above 100 MeV but with a few sets at low incident energies. The reason is that, in many cases, simulation code users perform calculations in which the models are used down to 20 MeV, at least for certain isotopes. This happens in particular because: *i)* 20-150 MeV libraries are not available for all isotopes; *ii)* when using libraries below 150 MeV residue production can be calculated only through activation libraries not available or not totally reliable in the whole energy range for all isotopes; *iii)* the use of libraries does not allow taking into account correlations between particles. The goal of the benchmark is to test the physics models either presently used or which could be used in the future in high-energy transport codes to compute the production yields and properties of particles and nuclei emitted in a fundamental spallation interaction. Therefore, only comparisons with elementary experimental data on thin targets are being considered.

The last expert meeting on model codes for spallation reactions was organised by CEA Saclay. This "Second Advanced Workshop on Model Codes for Spallation Reactions" followed the first one held at ICTP two years ago. During the previous workshop it had been agreed to organise an international benchmark on the different models developed by different groups in the world and the specifications of this benchmark, including the set of selected experimental data to be compared to models, have been fixed. Within these two years experimental data have been collected and uploaded on a web site dedicated to this benchmark. Calculation results from participants have been received. Tools to draw all these results have been developed and about ten thousands graphs (figures and deviation factors) are available to help with the benchmark analysis. The codes have been compared with respect to neutron production and neutron multiplicity, light charged particles, pion production, residue, and excitation function. The codes compared are: cem03-02, cem03-03, cascade-04, phits-jam, phits-bertini, phits-jqmd, isabel-smm, isabel-gemini++, geant4-bertini, geant4-binary, cascade-asf, incl4.5-abla07, incl4.5-smm, isabel-abla07, incl45-gemini++, cascade-x, and mcnpx-bert. Results will be presented at the conference ND2010 [17] and ICANS XIX [18].

Database of Ion Beam, Neutron Beam and Synchrotron Light Facilities in the World

The Database of Ion Beam, Neutron Beam (non-RR) and Synchrotron Light Facilities in the World contains technical information on accelerator and nuclear radiation facilities used for applied research and analytical services in IAEA member states. The database is compiled using information publicly available from IAEA databases, research institutes in MS, and accelerator manufacturers. The IAEA makes no warranties, either express or implied, concerning the accuracy, completeness, reliability or suitability of the information. The database organises the accelerator and nuclear radiation facilities into three categories: low-energy electrostatic (ion beam) accelerators, spallation neutron sources and synchrotron light sources. Included are geographical maps of the global distribution of these facilities and as well as individual entries in MS. The database is available on-line [19].

There are 9 entries for spallation neutron sources, distributed over 5 MS, and 38 entries for synchrotron light sources, distributed over 20 MS. This database contains 163 low-energy

electrostatic accelerators distributed over 50 MS. The history of development of low-energy electrostatic accelerators has spanned over 50 years, producing machine technologies which can be categorised by physical design (single-ended or tandem) and by voltage generation method, either mechanical charging (belt or pelletron chain) or cascade generator. The wide variety of machine technologies in use today, both modern and old, is better categorised by the accelerator manufacturers' terminologies, which are widely used by the scientific community: *i)* EN-FN-MP-UD are large machines built during the 1960s-1980s. Model EN (rated terminal voltage of 5 MV), FN (7.5 MV), MP (10 MV), UD (> 10 MV, vertical tandem); *ii)* Pelletron®; *iii)* Single-ended (includes KN, Singletron™ and other single-ended designs); *iv)* Tandetron™.

The IAEA plays an important role in helping to establish sound frameworks for the efficient, safe and secure use of nuclear technologies, and to develop the capabilities and infrastructure of interested MS to manage their own programmes devoted to nuclear and radiological applications. This database provides MS with a resource to assist efforts in developing strategies for capacity building, and effective utilisation and management of research facilities on a national, regional and international basis through possible coalitions, networks and shared-user facilities.

Exchange of information

The International Topical Meeting on Nuclear Research Applications and Utilisation of Accelerators took place on 4-8 May 2009, at IAEA headquarters Vienna, Austria. The conference was organised by the IAEA in co-operation with the American Nuclear Society (ANS). The main objectives of the conference as stated in the announcement were to promote exchange of information among IAEA member states' representatives/delegates and to discuss new trends in: *i)* accelerator applications including nuclear materials research; *ii)* ADS; *iii)* accelerator technology. In total about 233 submissions were accepted for presentation as oral or poster only. The majority of presentations (about half of the submitted abstracts) were related to accelerator applications and materials research. About a quarter each of the presentations were related to accelerator technology and ADS. About 216 experts and 23 observers from 50 countries and 4 international organisations participated in the conference. Seventy-one (71) participants came from 28 developing countries. In total 159 oral presentations were given and 145 posters displayed during the five-day conference. Four social events took place. The proceedings are published in the IAEA conference series as a CD-ROM [20]. The IAEA co-operated with the conference series of the ANS, know as AccApp. This conference series has a 12-year tradition and its main emphasis is on ADS, spallation, applications and technology.

The conference was also aimed at enhancing research collaboration between the different member states. It should promote education on topics related to the conference and emphasising the potential of accelerator based technology for solving a wide variety of societal issues. In order to fulfil this objective the scientific secretaries organised six satellite meetings, with participation of specialised experts on specific themes of interest. The topics of the satellite meetings were: *i)* European Fast Neutron Transmutation Reactor Projects (MYRRHA/XT-ADS); *ii)* Neutron Based Techniques for the Detection of Illicit Materials and Explosives; *iii)* Nuclear Spallation Reactions; *iv)* Application of Electron Accelerators: Prospects and Challenges; *v)* Particle Accelerators in Analytical and Educational Applications; *vi)* Applications of Synchrotron Radiation in Natural and Applied Sciences. Besides scientific presentations the satellite meetings offered the possibility for plenum and round table discussions. Thus specific requests by experts from member states could be taken into account and discussed. In total seven round table discussions took place during the meeting. The structure of the satellite meetings was different depending on the topic, ranging from mostly presentations to satellite meetings featuring discussions on scientific or educational issues.

ADS main achievements were presented during the main conference and intensively discussed during the satellite meeting. The studies and progress achieved demonstrated that

sufficient intensity is reachable under improved beam stability and reliability. A major milestone as discussed during the conference is the successful MEGAPIE irradiation experiment in Switzerland. The device is now under detailed investigation. The MYRRHA/XT-ADS is the most advanced ADS programme. Important ADS experimental efforts are under way in Belarus (YALINA Booster), Belgium (GUINEVERE), Japan (FFAG-KUCA, Phase 2 of J-PARC), China (Venus), India (coupling experiments), Korea (SNU), and the United States (revive studies).

"Accelerators are fundamental to research, training and education. They are particularly valuable in understanding the basic structure of materials, in improving materials and in testing new materials," said W. Burkart, Deputy Director General. The main part of the conference was dedicated to this topic and summarised under the application sessions. Innovative papers included proposals on irradiation experiments utilising accelerator facilities. The summary speaker noted that accelerators are at the moment the only one possible choice in the absence of high flux neutron irradiation facility to investigate materials for future nuclear reactors. In basic research investigations of advanced materials are quite important, as presented during the conference. A presentation on industrial accelerators showed the economic importance of accelerators: about 500 ion implanters are sold per year; the electron beam business is estimated to be 50 billion US$/year for different irradiated products. The sales of accelerators is about 1.8 billion US$/year, increasing about 10% every year. Table 1 displays the amount of industrial accelerators and their economic impact related to sales of facilities (no medical irradiation accelerators are included).

Table 1: Industrial accelerators

Application	Total (2007)	System sold/yr	Sales/yr [$M]	System price [$M]
Ion implantation	~9 500	500	1 400	1.5-5.0
Electron beam modifications	~4 500	100	150	0.5-2.5
Electron beam and X-ray irradiators	~2 000	75	130	0.2-8.0
Ion beam analysis (including AMS)	~200	25	30	0.4-1.5
Radioisotope production (including PET)	~550	50	70	1.0-30
High-energy X-ray inspection	~650	100	70	0.3-2.0
Neutron generators (including sealed tubes)	~1 000	50	30	0.1-3.0
Total	18 400	900	1 780	

Conclusions

The ADS-related activities at the IAEA address nuclear science and nuclear energy topics, and are implemented as a joint effort between the Departments of Nuclear Sciences and Applications and Nuclear Energy. They concern properties of structural materials, improved production of neutron, utilisation of RR, benchmark analysis of ADS, utilisation of LEU in ADS, applications of accelerators, production of related databases and exchange of information at conferences.

References

[1] International Atomic Energy Agency (IAEA), *IAEA Co-ordinated Research Project Technical Specification*, CRP 1488, Vienna, Austria (2008).

[2] IAEA, *IAEA 1st RCM Report – Working Material*, CRP 1488, Vienna, Austria (2008).

[3] IAEA, *IAEA CM Report – Working Material*, CS-39073, *14-ICFRM*, Sapporo, Japan (2009).

[4] IAEA, *The IAEA Research Reactor Database (RRDB)*, February (2010).

[5] IAEA, *IAEA Project D2.01: Enhanced Utilisation and Applications of Research Reactors*, February (2010).

[6] *Operational RR Database (ORRDB)*, February (2010).

[7] IAEA, *Advanced Reactor Technology Options for Utilization and Transmutation of Actinides in Spent Nuclear Fuel*, IAEA-TECDOC-1626 (2009).

[8] Abánades, A., G. Aliberti, *et al.*, "IAEA Co-ordinated Research Project (CRP) on 'Analytical and Experimental Benchmark Analyses of Accelerator Driven Systems'", *PHYSOR 2008*, Interlaken, Switzerland, 14-19 September (2008).

[9] *Joint ICTP-IAEA Advanced Workshop on Model Codes for Spallation Reactions*, International Nuclear Data Committee Report, INDC(NDS)-0530, August (2008).

[10] Stanculescu, A., A. Trkov, "Application Libraries for ADS and Transmutation", IAEA Headquarters, Vienna, Austria, 15-17 December 2004, INDC (NDS)-469, IAEA, Vienna (2004).

[11] Lopez Aldama, D., A. Trkov, *ADS-v1: A Test Application Library for ADS Systems*, INDC(NDS)-474, IAEA, Vienna (2005).

[12] Chadwick, M.B., *et al.*, "ENDF/B-VII.0: Next Generation Evaluated Nuclear Data Library for Nuclear Science and Technology", *Nucl. Data Sheets*, 107, 2931-3060 (2006); ENDF/B-VII: *www.nndc.bnl.gov/exfor/endf00.htm*.

[13] Iwamoto, O., *et al.*, "Development of JENDL Actinoid File", *PHYSOR 2008*, Interlaken, Switzerland, 14-19 September (2008), *www.ndc.jaea.go.jp/ftpnd/jendl/jendl-ac-2008.html*.

[14] Trkov, A., *et al.*, "Evaluation of Tungsten Nuclear Reaction Data with Covariances", *Nucl. Data Sheets*, 109, 2905-2909 (2008), *www-nds.iaea.org/wolfram/wolfram.htmlx*.

[15] MacFarlane, R.E., D.M. Muir, *NJOY-99.0: Code System for Producing Pointwise and Multigroup Neutron and Photon Cross Sections from ENDF/B Data*, PSR-480, Los Alamos National Laboratory (2000).

[16] Briesmeister, J.F., *MCNP – A General Monte Carlo N-particle Transport Code, Version 4C*, LA-13709-M, Los Alamos National Laboratory (2000).

[17] Leray, S., *et al.*, "Results from the IAEA Benchmark of Spallation Models", *Int. Conference on Nuclear Data for Science and Technology (ND2010)*, Jeju Island, Korea, 26-30 April (2010).

[18] Khnadaker, M.U., *et al.*, "Codes and Data for Spallation Sources, Benchmark of Nuclear Spallation Models", *International Collaboration on Advanced Neutron Sources (ICANS XIX)*, Grindelwald, Switzerland, 8-12 March (2010).

[19] *Ion and Neutron Beam Accelerator Data Base*, February (2010).

[20] *Proceedings of the International Topical Meeting on Nuclear Research Applications and Utilization of Accelerators*, Vienna, Austria, ISBN 978-92-0-150410-4, STI/PUB/1433; IAEA, Vienna, Austria (2010), *www-pub.iaea.org/MTCD/publications/PDF/P1433_CD/datasets/foreword.html*.

The designs of an experimental ADS facility (XT-ADS) and of a European Industrial Transmutation Demonstrator (EFIT)

Luigi Mansani, Marco Reale
Ansaldo Nucleare, Italy

Carlo Artioli
ENEA, Italy

Didier De Bruyn
SCK•CEN, Belgium

Abstract

Within the EURATOM 6th Framework Programme, the EUROTRANS Integrated Project, funded by the European Community, is expected to provide a significant contribution to the demonstration of the industrial transmutation through the accelerator-driven system route. The goal will be reached through the realisation of a detailed design for an experimental facility of 50-100 MW_{th} power which shows the technical feasibility of an ADS (XT-ADS), and the development of a conceptual design of a generic European transmutation demonstrator (European Facility for Industrial Transmutation – EFIT) to be realised in the long term. EFIT is conceived to fission at best minor actinides while producing electric energy exactly from their fissions. The SCK•CEN has offered and the EUROTRANS partners have accepted to use the MYRRHA design as a starting basis for the XT-ADS design. Instead of starting from a blank page, this allowed optimising an existing design towards the needs of XT-ADS within the limits of safety requirements. EFIT is designed on the basis of the experience acquired in the previous PDS-XADS project, and it is fuelled with minor actinides (U-free fuel). In EFIT the use of pure lead instead of LBE as the primary coolant, the higher power density and primary temperatures are the features for compactness and efficient energy generation. In the present paper, the general configurations of the EFIT and XT-ADS primary system as well as their cores are presented.

Introduction

The implementation of partitioning and transmutation of a large part of the high-level nuclear wastes in Europe requires the demonstration of the feasibility of several installations at an "engineering" level. This is the general objective of the integrated project EUROTRANS (European Research Programme for the Transmutation of High-level Nuclear Waste in an Accelerator-driven System). The overall EUROTRANS integrated project had the goal to demonstrate the possibility of nuclear waste transmutation/burning in accelerator-driven systems (ADS) at industrial scale. In particular the domain DESIGN was tasked with providing the pre-design of the European Transmutation Demonstrator (ETD) able to achieve such a goal. The focus during this FP6 European Commission partially funded programme is on a Pb-cooled ADS for the European Facility on Industrial Scale Transmuter (EFIT) with a back-up solution based on a He-cooled ADS in continuity with the PDS-XADS FP5 project. As an intermediate step towards this industrial-scale prototype, an experimental transmuter based on the ADS concept (XT-ADS) able to demonstrate both the feasibility of the ADS concept and to accumulate experience when using dedicated fuel subassemblies or dedicated pins within a MOX fuel core has also been studied. The possibility of irradiating these dedicated subassemblies under conditions representative of the EFIT (after both concepts have been pre-designed) would then be one of the major tasks of this XT-ADS.

The two machines (XT-ADS and EFIT) have been designed in a consistent manner, lending more credibility to the potential licensing of these plants. As part of this objective, synergies between both designs have been identified with their respective particular objectives in mind. The XT-ADS design has been proceeding with margins taking into account the uncertainties associated regarding what is known of material boundary limits. The EFIT design has been proceeding with a similar approach, though with material boundary limits defined without uncertainties given the expected time of the construction of the plant, i.e. 25 years. These constraints were defined at the start of the project, anticipating future R&D results.

The EFIT design

EFIT [1-3] will be deployed within a nuclear park in which it will produce part of the electricity. In order to limit the burden of such a plant EFIT should produce electricity with rather good efficiency. This leads to operate the primary coolant cycle with rather high output temperature. The lead coolant offers such a possibility with three orders lower bismuth activation than LBE. With the lead coolant inlet and outlet temperatures of respectively 400°C and 480°C, a thermal efficiency of ~40% can be reached with the superheated vapour secondary circuit. This thermal efficiency should also take into account electricity required by pumps. The primary circuit is designed for effective natural circulation, i.e. relatively low pressure losses. The core pressure drop is one of the constraints limiting plant efficiency, and thus should be limited to low values. Other considerations associated with decay heat removal in transient events and elevation of the plant favour a pressure drop below 1 bar.

The corrosion resistance of the structural material is very much linked to thermal-hydraulic conditions, especially to the temperature level and to the coolant velocity. Long-term operation of the existing T91 cladding in Pb-flow is limited to 500°C under oxygen control conditions and to the average channel speed to 2.0 m/s. However, using T91 cladding with the current limitation would make the margin to the coolant outlet temperature rather small and hence the possibility of increasing the power density rather small. The upper temperature limit for long-term operation of the T91 cladding is set at 550°C with the help of an aluminium coating (GESA technology).

EFIT main systems

The configuration of the primary system is pool-type. The pool concept allows containing all the primary coolant within the reactor vessel, thus eliminating all problems related to out-of-vessel

transport of the primary coolant. The pool design has important beneficial features, including a simple low temperature boundary containing all primary coolant, the large thermal capacity of the coolant in the primary vessel, a minimum of components and structures operating at the core outlet temperature. The primary coolant is molten lead characterised by high melting. The operating temperatures are 400°C at core inlet (to have sufficient margin from the risk of lead freezing) and 480°C at core outlet. The core outlet temperature is chosen taking into account, on the one hand, the corrosion risk of structures in molten lead environment that increases with temperature and, on the other hand, considering that the outlet temperature cannot be too low because the associated increase of coolant flow rate would bring about unacceptable erosion of the structures. The proposed operating temperatures are, hence, a compromise between corrosion/erosion protection and performance. The speed of the primary coolant is kept low (less than 2 m/s) to limit the erosion. Wherever this cannot be complied with, e.g. at the tip of the propeller blades, the relative speed is kept lower than 10 m/s and appropriate construction materials are selected for qualification. Protection of structural steel against corrosion is ensured, in general, by controlled activity of oxygen dissolved in the melt and additional coating for the hotter structures.

Reactor vessel and internal structure

The reactor vessel is a welded structure without nozzles, made of a cylindrical shell with hemispherical bottom head and top Y-piece, both branches of which terminate with a flange. The conical, outer branch is flanged to, and hangs from, the annular support anchored to the civil structure of the reactor cavity, whereas the inner branch supports the reactor roof. All welds can be accessed for in-service inspection by means of remotely-operated vehicles. An innovative cylindrical inner vessel, hung from the roof, separates the core region and the above core volume from the steam generators region. The core diagrid is fixed on the bottom of inner vessel. A cylindrical structure, welded inside on the vessel bottom head, is a radial restraint for inner vessel and core

Steam generator and primary pump subassembly (SG-PP_SA)

The SG-PP_SA is an integral part of the primary loop, i.e. from pump suction to steam generator outlet. It is made of two steam generator units (SGU) and one primary pump (PP) arranged between the SGU, all included in a casing supported by, and hung from, the reactor vessel roof. It is designed to carry out both functions of hot coolant circulation and power heat transfer. The casing cross-section is arranged in the annular space between cylindrical inner vessel and reactor vessel. It is immersed in the cold pool. The only connection with the reactor internals is by the suction pipe of the PP that is engaged in the piston seal at the upper end of the elbow welded to the inner vessel. Thus, the whole subassembly can be easily put in and out of the reactor vessel with relatively short handling time. The lead coolant flow path is illustrated by arrows in Figure 1. The hot lead is pumped into the enclosed pool above the PP and SGU and driven shell-side downwards across the SGU helical-tube bundles into the cold pool. The steam generator unit is a contra-flow heat exchanger, whose size is 52 MW, giving eight units per station to achieve the nominal thermal power of EFIT (= 416 MW). The SGU is a vertical unit with an inner and an outer shell. The primary coolant flows downwards shell-side through the annulus between inner and outer shell. The tube bundle is made of helical tubes put on the annulus between the shells. The total length of tubes is less than the current maximum length of commercially available tubes (= 28 m). Therefore the tube bundle can be fabricated without welds in the tubes. The tube ID of 14.2 mm allows the visual inspection of the inner surface. The primary pump is to operate at 480°C and to supply the coolant at a rate of 8 625 kg/s. Its most important part is the impeller, the circumferential speed of which reaches 9 m/s.

Figure 1: EFIT primary system

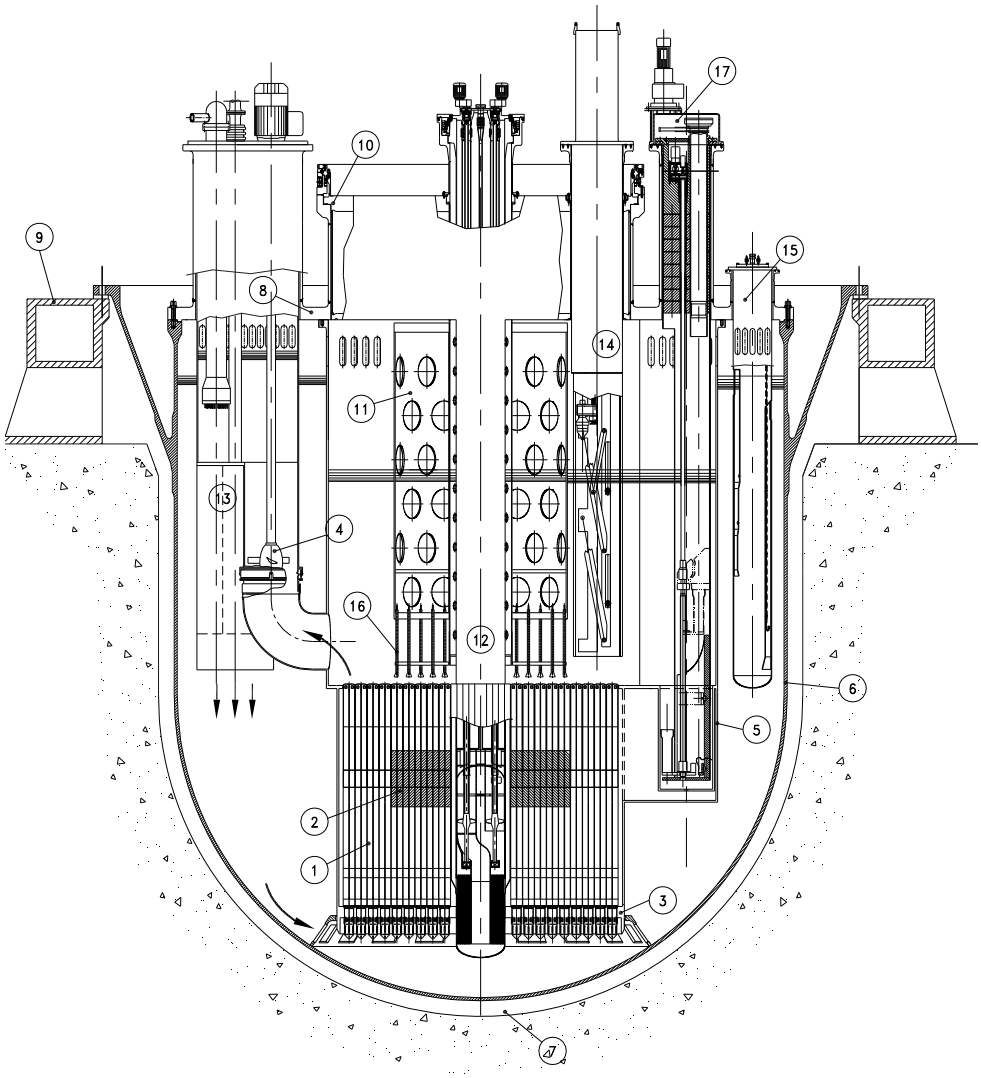

The target unit

The coupling of the accelerator to the subcritical core takes place via the target unit. This has been designed as a removable component, because its service life is anticipated to be shorter than the reactor lifetime, owing to the intense irradiation and local high thermal stresses. The target unit is a slim component of cylindrical form, positioned co-axially with the reactor vessel and hung from the reactor roof. Because it also serves as inner radial restraint of the core, the outline of its outer shell fits the inner outline of the core. Its main component parts are the proton beam pipe, the heat exchanger and the two axial flow pumps arranged in series in the vertical legs of the loop upstream and downstream the horizontal target region.

In-vessel fuel handling system

The in-vessel fuel handling system provides the means to transfer the absorber assemblies from their storage positions in the outer rows of the diagrid (reactor in operating conditions) to the inner rows location (reactor in shutdown conditions), and to transfer the core assemblies to and from all in-vessel positions. Functionally, this system consists of the rotating plug, the extendable above core structure, the transfer machine (pantograph type) and the rotor lift machine. Access to any core position is achieved by rotation of both rotating plug and transfer machine.

Decay heat removal systems

Three systems contribute to the DHR function in EFIT: the non-safety-grade water/steam system, the safety-related DHR N1 (isolation condenser) system and the DHR N2 [direct reactor cooling (DRC)] system. Following reactor shutdown, the non-safety-grade water/steam system is used for the normal decay heat removal. In case of unavailability of the water/steam system, the DHR N1 system is called upon and in the unlikely event of unavailability of the first two systems the DHR N2 passively starts to evacuate the DHR.

Isolation condenser

The "isolation condenser" system was designed by Ansaldo Nucleare in 1992 as part of the co-operation for the development of the SBWR design and it was tested in Italy by SIET (ENEA) under full scale SBWR conditions. The same arrangement has been proposed for EFIT. The inlet piping of the system is attached to the main steam line. Steam is then routed to a vertical condenser immersed in a pool and the outlet of the condenser is connected to the feedwater line. Under normal operation the isolation valve below the condenser is closed, the condenser is full of water and no heat exchange takes place. In case of emergency conditions, after feedwater line and steam line isolation, the isolation condenser is called to operate by opening the condenser isolation valve. The water stored in the system is injected into the steam generator and the steam condensation process starts. The system is composed of four identical loops (three out of four loops are sufficient to perform the DHR function). A scheme of the isolation condenser is shown in Figure 2. A hot storage tank located below the isolation valve is used to provide additional water mass in case of isolation valve leakage and to limit the thermal shock to the steam generators at system start-up. Safety relief valves located on the steam line are used to limit the system pressure to 150 bars. Condenser pools are sized to provide a three-day grace period.

DRC system

The DRC system is composed of four identical loops (three out of four loops are sufficient to perform the DHR function), one of which is shown in Figure 3. The main components of the loop are a molten lead-diathermic oil heat exchanger (DHX) and an air-diathermic oil vapour condenser (AVC) with stack chimney. During normal operation the oil boiling temperature is maintained at the cold plenum temperature (400°C) by pressurising the system with inert gas. In case of an emergency condition, lead starts to enter the DHX at higher temperature, with a natural circulation flow rate, and oil starts to vaporise massively, pushing and confining the inert gas into the gas storage tank. Hence the oil vapour can condense in the AVC. The DRC system is always in operation and during normal operation it evacuates the heat losses between the hot and cold plenum to maintain the vessel temperature at the cold plenum value.

EFIT core

As matter of fact, the significant parameter to measure the burning capability for an ADS is the balance result expressed in kg (of fissioned MA)/TWh. The yield in energy/fission corresponds to some 42 kg of fissioned heavy nuclei/TWh. The "optimum" MA burning capability implies that all the fissions occur on the MA, directly or indirectly. Therefore the balances of the two components

Figure 2: Isolation condenser system

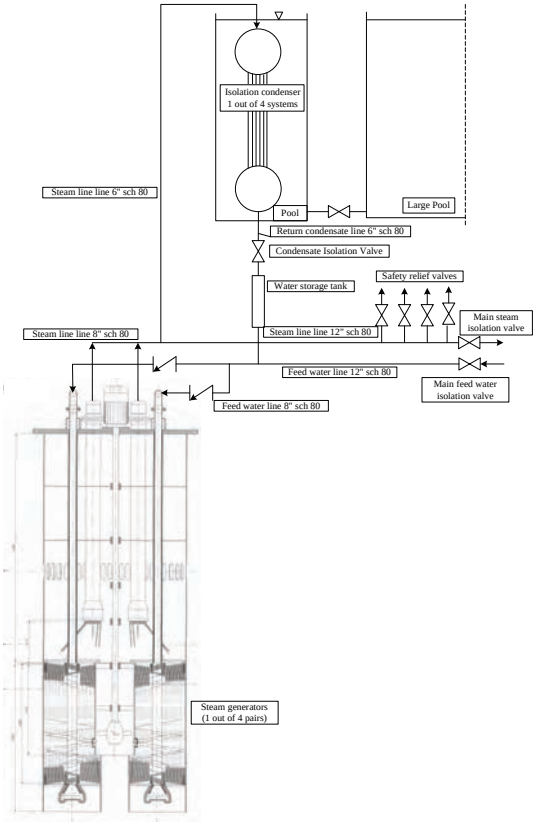

Figure 3: Direct reactor cooling system

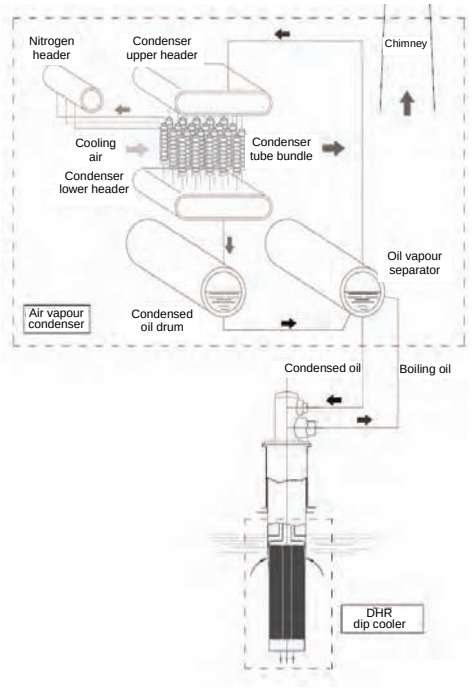

TECHNOLOGY AND COMPONENTS OF ACCELERATOR-DRIVEN SYSTEMS, ISBN 978-92-64-11727-3, © OECD 2011

of the fuel (apart the matrix) Pu and MA must be respectively 0 kg/TWh$_{th}$ and -42 kg/TWh$_{th}$ (the 42-0 concept), in any case their algebraic sum always being -42 kg/TWh$_{th}$ (Figure 4). This optimised splitting of the total balance between Pu and MA depends on their ratio in the fuel, once the spectrum ruling all the cross-sections is defined; no matter the core geometrical and power figures and other core data. The EFIT core neutronic design has been based on this concept and the related approach. By a guess spectrum, a suitable enrichment to get the 42-0 balances has been calculated and found Pu/(Pu+MA) = 45.7%. Keeping this result constant, the core has been designed for the other neutronic and thermal-hydraulic parameters. Figure 5 shows the logical flow chart of the design. It is worth observing how in this approach the starting point is the enrichment, while the core size appears as the last output. Tuning of a desired core power becomes possible by acting on core parameters, except the enrichment ruling directly the goal. On the other hand, any change of a significant component such as coolant fluid or matrix, implies a different spectrum and therefore a consequently different enrichment.

Figure 4: Balances of the two components of the fuel, MA and Pu

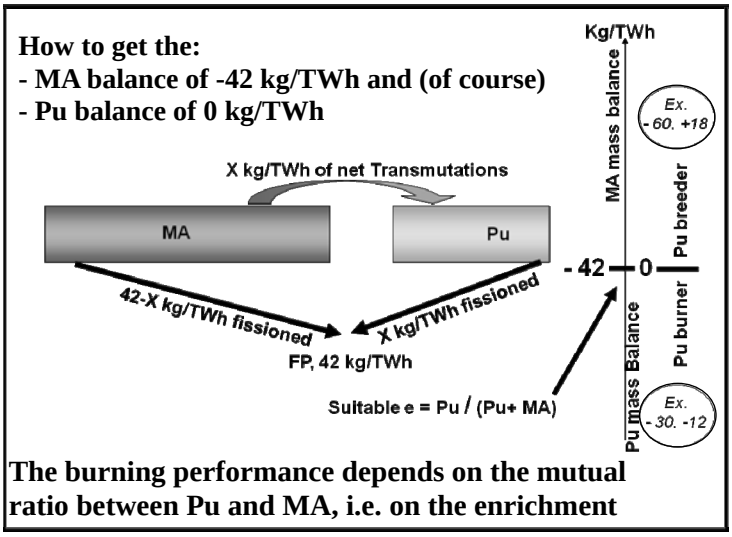

Figure 5: Logical flow chart of the core design

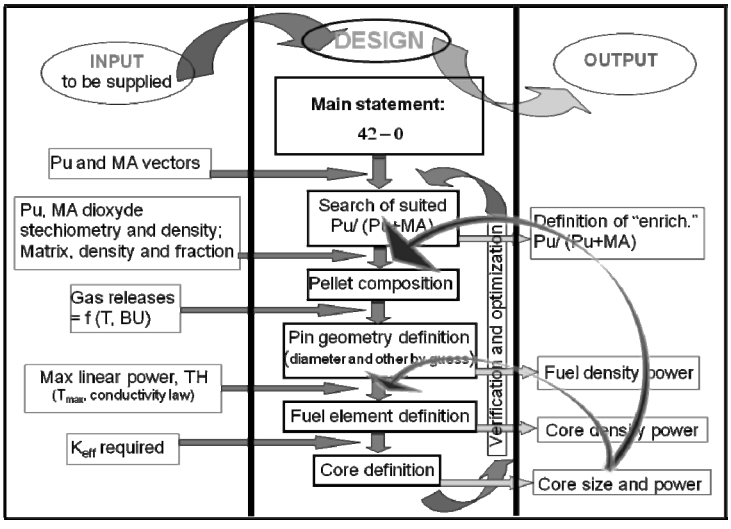

As not negligible consequence of the constant content of Pu along the cycle, as major contributor to the reactivity, even the reactivity shows a moderate swing (some 200 pcm/year), which accounts for a very high accelerator load factor. For the 385 MW_{th} EFIT, the required current results not higher than 14 mA of 800 MeV protons. A real optimisation of the core power size has not been done at this stage, therefore a core power of some 400 MW_{th} has been chosen as reference. Figure 6 shows, as the most important result for a core devoted to MA burning, the evolution of the MA and the Pu along the cycle. It is clear that the MA linearly decreases alongside the release of the energy, while the content of Pu is kept constant. Discrepancies between the aimed 42-0 and the actual result (-40.17/-1.74) mean that a very easy feedback, refinement is required the updating the enrichment, without any variation on the core design.

Figure 6: Evolution of the MA and the Pu along the cycle

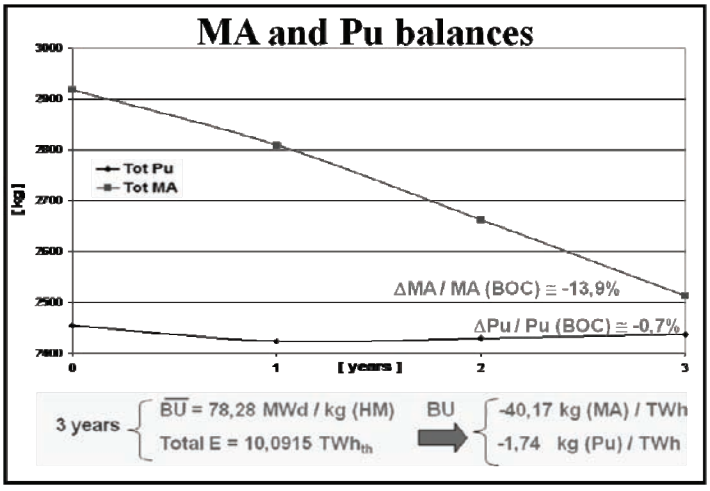

EFIT feedback from safety

The results of the safety analyses demonstrate that the Pb-cooled EFIT plant is a very robust design ascribable to the unique combination of inherent and plant design features, which, for example are: the favourable thermo-physical properties and the high thermal inertia associated with the coolant Pb; the excellent natural convection characteristics of the plant design; adopting a modest linear power rating assuring that temperatures of the innovative MgO-MA-based fuel are below the upper temperature limits (namely 1 380°C under nominal conditions and 1 500°C under accident conditions, as experiments have indicated that this fuel may loose its mechanical integrity at temperatures above 1 500°C); a modest ^{210}Po accumulation. Somewhat less favourable characteristics of the Pb as coolant are: the high melting point of Pb requiring that the primary system is always operated at temperatures assuring a safety margin from the freezing point; the high corrosion rate of the flowing lead on steel metal surfaces (this requires that all sensitive components, within the primary system and in the core region, are always covered by either a protective oxide layer or by some other protective layer such as aluminium – GESA treatment); negative impact of steam generator tube ruptures leading to potentially rapid vaporisation of water (potential primary system over-pressurisation and positive reactivity insertion); the response of the plant to earthquakes (structural integrity of the plant system are mitigated by adopting seismic isolators but potential reactivity insertions due to core compaction have to be anticipated).

The combination of the favourable features of lead as a coolant assures that the integral core damage frequency is very low (most likely significantly below < 10^{-5}/reactor year), and that the core and primary system temperatures for almost all transient scenarios are below the

temperature limits. There were only very few transients in which the core conditions could approach clad melting and/or release of radioactivity (e.g. the almost complete blockage of a subassembly without accelerator trip). In general, however, the safety analysis performed for the EFIT-Pb design demonstrates the very forgiving nature of this plant design under most adverse transient conditions. With the exception of the fuel assembly blockage transient, most unprotected transients allow a sufficient grace time (~30 minutes) before manual corrective actions are required. This plant behaviour is almost unique when compared to most other critical reactor plant designs in that these designs exhibit significantly smaller grace times under similar transient conditions. By this standard, EFIT-Pb must be judged to be a very "safe" reactor design in accordance with its mission of using a large inventory of unique minor actinide transmutation fuel with its associated large in-core actinide radionuclide inventory.

The XT-ADS design

XT-ADS main systems

The XT-ADS is a pool-type reactor, cooled by lead-bismuth eutectic (LBE). Different arrangements of the primary system for XT-ADS have been compared and it appeared that an evolution of the MYRRHA "Draft-2" [4] primary system was the more viable arrangement [5]. A liquid metal was selected as a coolant due to the desired high fast flux and the high power density. The low LBE melting temperature (around 125°C) allows the primary system to work at rather low temperatures which is an interesting approach to limit the corrosion issue onto metallic materials. The nominal core outlet temperature is around 400°C and the LBE core inlet temperature is 300°C. The pool-type solution is of interest because it benefits from the thermal inertia provided by the large coolant volume. The pool system also enables to contain all the primary coolant within the main vessel, in which the primary components (pumps, heat exchanger, fuel handling tools, experimental rigs, etc.) are inserted by the top. In order to maintain a greater flexibility for loading experimental devices and because of the presence of the spallation source, the loading of fuel assemblies is foreseen to be from underneath. The primary system is designed to evacuate a power of 70 MW_{th}.

The spallation loop is off centred located from the core. The requirement of high flux levels leads to design a compact core and the central hole in the core to house the spallation target has to be limited dimensions (around 100 mm). Thus, the spallation loop (i.e. loop achieving the circulation of LBE used as spallation target) is located at the core periphery; it is connected to the central beam tube and spallation target by two horizontal tubes, one passing above and the other below the core. The spallation loop contains a feed tank, a circulation pump, a heat exchanger and an auxiliary system for the control of oxygen contents and the required instrumentation. A windowless target design is retained, i.e. without a physical separation between the accelerator beam line vacuum and the LBE used as liquid target window. An advantage of this solution is that it enables high beam currents needed for industrial transmutation.

In the reactor main vessel (around 6 m diameter), the hot and cold pools are separated by a cylindrical inner vessel. LBE circulates by means of two mechanical pumps and the power generated by the core is removed by four (2 × 2) LBE/water/steam primary heat exchangers (PHX). The maximum LBE velocity in the primary circuit is 2 m/s in order to limit erosion under control onto metallic materials of all internals except the pump impeller. The two pumps are axial flow pumps which operate at 300°C and supply a total flow rate of 7 000 kg/s. Each pump runs the LBE from the hot pool at the level of the PHX outlet window and passes it to the cold plenum. Ongoing research programmes are dedicated to find an appropriate material or coating for the pump impeller, resistant to LBE velocities up to 10 m/s. The four PHX are gathered in two circuits, each including two PHX and one pump. The PHX is a one-tube-pass vertical evaporator which works in natural circulation on the water side. The elevation of the heat exchanger with regard to the core has been designed to achieve natural circulation capabilities. The lower edge of the

Figure 7: XT-ADS reactor assembly

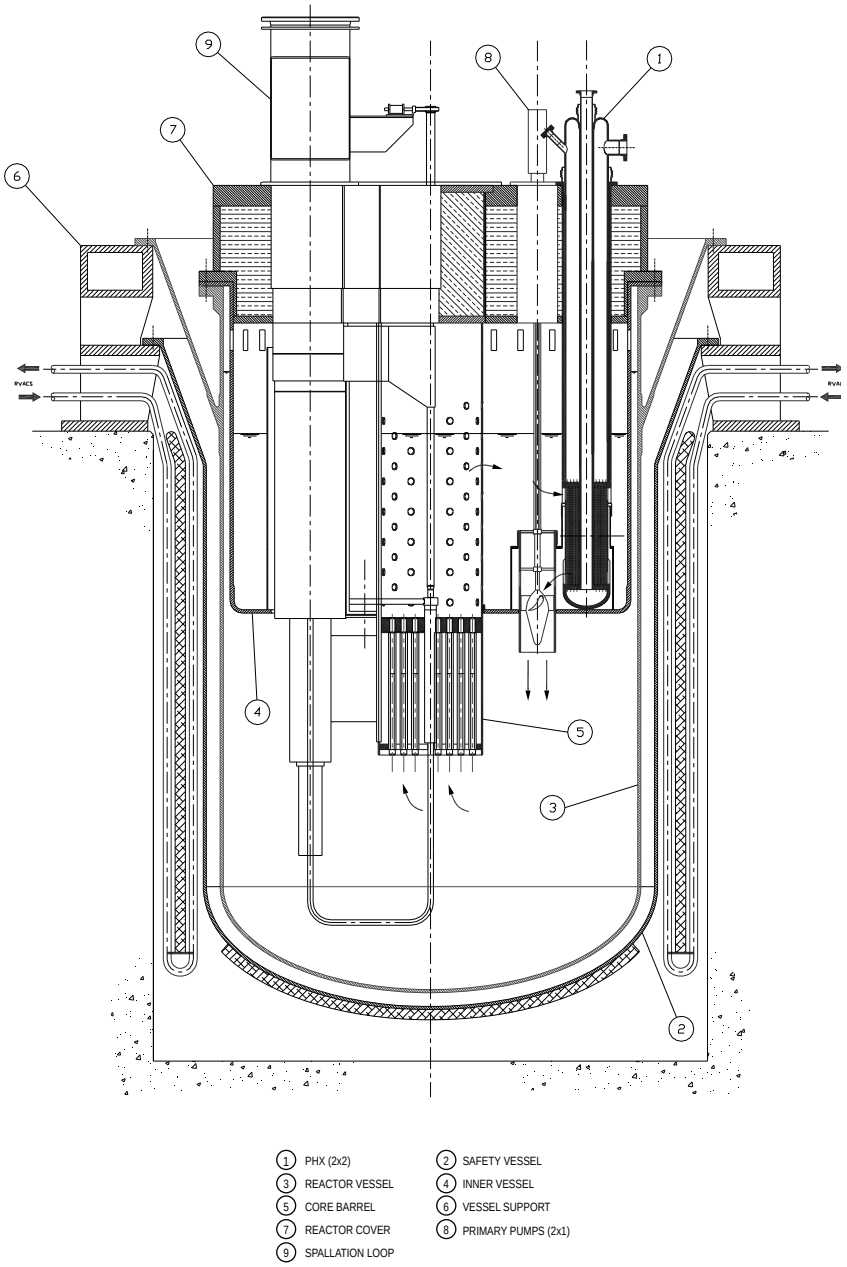

PHX inlet window remains immersed in LBE in case of a reactor vessel leakage, to ensure the primary coolant circulation and the core cooling. The PHX is designed with the double-wall water pipes. This design aims at reducing the risk of a massive water leakage in the primary system. To meet the same goal, the PHX elliptical bottom head is reinforced. In each circuit, saturated water enters and goes out as a steam water mixture. The mixture then goes in a steam separator. The steam rising from the separator is condensed into an air condenser and the water comes back to the PHX tubes.

Two systems are provided for removing decay heat providing diversity and redundancy. For normal reactor shutdown, the decay heat removal function is ensured by the secondary cooling system using the primary LBE/water steam heat exchanger and two independent loops. In case

of unavailability of the secondary cooling system, the safety grade reactor vault cooling system (RVACS) is used. The RVACS is placed between the guard vessel and the concrete wall.

XT-ADS core

The reference core of XT-ADS consists of 72 fuel assemblies surrounding the spallation target which is housed in the equivalent of three hexagonal positions (see Figure 8). To address the requirement for XT-ADS to be a flexible irradiation facility, eight positions have been selected to house in-pile positions (IPS). These eight positions differ from the other positions by the fact that there are penetrations foreseen in the cover lid to be able to access these positions more easily. This allows for a design of an in-pile position of a loop-type where irradiations can be performed under different conditions (temperature, pressure, coolant) than in the normal core positions.

Figure 8: XT-ADS core cross-section

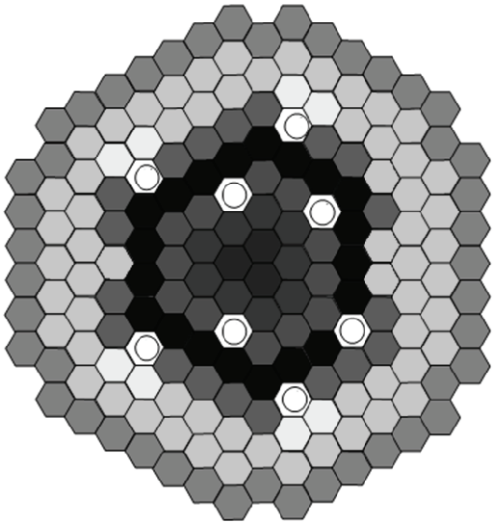

Compared to the MYRRHA Draft-2 design, both fuel pin and fuel assembly have been modified. The fuel pellet is now of the annular type and consists of MOX of 35 wt.% Pu. The plutonium vector is coming from the reprocessing of the current generation PWR spent fuel with an initial enrichment of 4.5% in ^{235}U. The gas plenum of the pin has been increased to be able to cope with the pressure build-up caused by a 100% fission gas release during a ULOF accident. This increased the size of the fuel pin to 1 400 mm. The fuel pin pitch has also been increased to reduce the pressure drop over the core. The fuel assembly wrapper thickness has also been increased. Consequently, the fuel assemblies have become slightly larger (93.2 mm flat-to-flat). The inter-wrapper spacing has also been increased to 3 mm, resulting in a fuel assembly pitch of 96.2 mm. The core power has been fixed to 57 MW_{th} as a reference value. For a 600 MeV proton beam, this requires about 2.3 mA of proton current. This core reaches total neutron fluxes of 3.3 10^{15} n/(cm^2.s) and fast (> 0.75 MeV) neutron fluxes of 0.7 10^{15} n/(cm^2.s). Different aspects of this core have characterised and quantified. A reactivity balance has been established, taking into account different feedback effects. The (neutronically) optimal position of the target free surface level has been established.

The proton and neutron damage (dpa and He production) induced on the fuel cladding and spallation target structures have been estimated. The neutron-induced damage on the core barrel and core support plate has also been quantified. To better protect the core barrel, two extra rings of hexagons have been included in the core (as compared to the MYRRHA Draft-2) in which the outer one has been filled with steel pins to better shield from impinging neutrons. All these values can be used by the design engineers to estimate the lifetime of these components.

Finally, a proposal for core shuffling has been set-up: a five-step shuffling scheme. Using this five-step shuffle, on average the core loses about 1 200 pcm per 90 full power days. Irradiation capabilities have been estimated in IPS using preliminary designs for a material irradiation IPS and a fuel pin irradiation IPS. These estimates show that the XT-ADS core can deliver 17 dpa per year to steel samples while fuel cladding dpa can go up to 30 dpa.

XT-ADS feedback from safety

The XT-ADS design is based on safety requirements which are consistent with modern European safety framework developed for European fast reactors and advanced European light water reactors defined within the European Utility Requirements (EUR). The safety objectives are achieved through the application of the defence-in-depth principle which consists in the implementation of an appropriate set of successive provisions to ensure protection against hazards and in particular radiological ones. Although the definitive criteria for assessing the consequences of the design base condition (DBC) and design extended condition (DEC) events are the radiological ones, physical limits are defined which can be more easily applied to the design process. These design criteria are related to the loadings on the structures resulting from the initiating events (e.g. temperature, pressure, stress, mechanical damage, corrosion). They concern in particular the components achieving safety functions, such as: the fuel and clad; the structural integrity of the equipment performing core support function (e.g. reactor vessel); the confinement barriers and the components necessary for removing the decay heat.

A preliminary safety analysis has been performed both for DBC and DEC events. The results of the safety analyses demonstrated that during DBC events the peak fuel and clad temperatures are, respectively, below 1 580°C and 500°C which are lower than the limits. One of the safety objectives of the XT-ADS is to accommodate in case of a DEC event such as the unprotected loss of flow transient (unprotected means that the proton beam shutdown is postulated not to have occurred) for at least 30 minutes without any significant number of clad failures. The results of the safety analyses demonstrated that during this event the peak fuel temperature remains below 1 740°C. The cladding temperature increases up to 840°C. Fuel clad failure time is ~1 hour taking into account the fission gas release rate of 100%. Assuming a more realistic fission gas release rate of ~50% the clad failure time increases from 1 hour to 2.4 hours. Based on these preliminary results, the current LBE-cooled XT-ADS design seems adequate. Attention needs to be paid however to the operational control of the oxygen content in the LBE coolant in order to control chemical fouling and the build-up of the oxide layer.

EFIT and XT-ADS common and diverging characteristics

EFIT and XT-ADS are two machines conceived for the same goal in a different time frame. The XT-ADS should be as much as possible serve as a technological test bench of the main components of EFIT (Pb). Nevertheless divergence in the choices of components or parameters of the two machines to be designed is allowed. This divergence is even necessary as the time scales of realisation of the two facilities are different.

EFIT and XT-ADS have some common characteristics such as:

- the accelerator (superconducting linac CW modular accelerator; proton beam injection from the vessel top; windowless target type; high reliability and availability – spurious beam trip < 5/y and continuous operation for beam interruptions < 1 s; 200 μs holes for subcriticality measurements);
- the core structure (fuel pin spacer, wrapper-type and hexagonal fuel assembly; subcritical by design in all operating, accidental and abnormal conditions; no control rods);

- the reactor vessel (primary system integrated in the vessel, all components removable from the top for ISI);
- maintenance and replacement;
- primary coolant circulation is forced in normal conditions and is natural in decay heat removal conditions;
- the reactor vessel structural material AISI 316L steel;
- hung vessel and similar vessel support (EFIT has horizontal anti-seismic supports; XT-ADS benefits of Mol soil);
- the fuel handling (both machines rely on remote handling);
- the heavy liquid metal technology (HLM technology experimental results are in principle applicable to LBE and lead).

Some other options differ between EFIT and XT-ADS, such as:

- the accelerator proton energy (XT-ADS 600 MeV and 3 mA; EFIT 800 MeV and 20 mA);
- the spallation target [XT-ADS – LBE confluent flow, off-centred; EFIT – lead perpendicular (horizontal) flow, centred];
- the fuel type and the power density (XT-ADS – MOX; 700 W/cm^3; EFIT – U-free: (Pu, AM)O_2 + MgO or Mo matrix; 450 ÷ 650 W/cm^3);
- the primary coolant and operating temperature (XT-ADS – LBE, inlet T 300°C, outlet T 400°C; EFIT – lead, inlet T 400°C, outlet T 480°C);
- the fuel core loading (XT-ADS – from bottom with horizontal fixed handling arm machine; EFIT – from top with extendible handling arm machine);
- the secondary system (XT-ADS – low pressure boiling water; EFIT – superheated water cycle and electricity production);
- the decay heat removal systems (XT-ADS – System 1 portion of secondary system in natural circulation and System 2 RVACS fully passive; EFIT – System 1 isolation condenser on secondary system and System 2 deep cooler in the reactor vessel fully passive).

Conclusions

The two machines (XT-ADS and EFIT) have been designed in a consistent manner, lending more credibility to the potential licensing of these plants and with sufficient details to allow definition of the critical issues as regards design, safety and associated technological and basic R&D needs. The different designs fit rather well with the technical objectives fixed at the beginning of the project in consistency with the European Roadmap on ADS development.

Acknowledgements

The XT-ADS and EFIT design work has been performed under the Integrated Project EUROTRANS (Ref. FI6W-CT-2004-516520) co-funded by the European Union in its 6th Framework Programme. Acknowledgment is also due to all the colleagues of the participating institutes for their contributions to many different topics.

References

[1] Barbensi, A., *et al.*, "EFIT: The European Facility for Industrial Transmutation of Minor Actinides", *AccApp'07 Conference*, Pocatello, Idaho, 30 July-2 August 2007, pp. 885-892 (2007).

[2] Artioli, C., *et al.*, "Optimization of the Minor Actinides Transmutation in ADS: the European Facility for Industrial Transmutation EFIT-Pb Concept", *AccApp'07 Conference*, Pocatello, Idaho, 30 July-2 August 2007, pp. 560-567 (2007).

[3] Artioli, C., "Minor Actinides Burning in the 42-0 Concept: The EU 'EFIT' (European Facility for Industrial Transmutation) ADS", *International Conference on Peaceful Uses of Atomic Energy*, New Delhi, 29 September-1 October (2009).

[4] Aït Abderrahim, H., P. D'hondt, D. De Bruyn, "MYRRHA, a New Fast Spectrum Facility", *Seminar on Fission*, Corsendonck Priorij, 18-21 September 2007, Proceedings April 2008, World Scientific, ISBN 978-981-279-105-4, pp. 207-221 (2008).

[5] De Bruyn, D., *et al.*, "From MYRRHA to XT-ADS: The Design Evolution of an Experimental ADS System", *AccApp'07 Conference*, Pocatello, Idaho, 30 July 30-2 August 2007, pp. 848-854 (2007).

XT-ADS windowless spallation target design and corresponding R&D topics

A. Guertin, N. Thiollière, A. Cadiou, J.M. Buhour, O. Batrak
Laboratoire SUBATECH, CNRS/IN2P3-EMN-Université, Nantes, France

M. Dierckx, J. Heyse, K. Rosseel, P. Schuurmans, K. Van Tichelen
SCK•CEN, Mol, Belgium

R. Stieglitz, A. Batta, A. Class
Forschungszentrum Karlsruhe, Karlsruhe, Germany

F. Roelofs, V.R. Gopala
NRG Petten, Petten, Netherlands

H. Jeanmart
UCL, Louvain-la-Neuve, Belgium

V. Moreau
CRS4, Pula, Italy

Abstract

The objective of the European 6th Framework Programme Integrated Project (IP) EUROTRANS (European Research Programme for the Transmutation of High-level Nuclear Waste in an Accelerator-driven System) is to demonstrate the feasibility of transmutation of high-level nuclear waste using subcritical accelerator-driven systems (ADS). In the framework of the IP EUROTRANS, which started in April 2005, the XT-ADS (Experimental Demonstration of Transmutation in an Accelerator-driven System) reference design with lead-bismuth eutectic (LBE) cooling is developed in a detailed manner amongst others to prove the feasibility of a windowless spallation target. Studies have been done making maximum use of the existing work for defining the needed complementary work in terms of design, thermal-hydraulics or neutronic and nuclear assessment. In this document the present status of the design of a windowless spallation target for the XT-ADS and the status of corresponding R&D topics are discussed.

Introduction

The Integrated Project EUROTRANS within the ongoing EURATOM 6th European Commission Framework Programme is devoted to the study of the transmutation of high-level waste. The work is focused on transmutation in an accelerator-driven system.

The XT-ADS is to be built and tested in the near future. The machine should fulfil three objectives:

- demonstrate the ADS concept (coupling of accelerator, spallation target and subcritical core) and its operability;
- demonstrate the transmutation of a sizeable amount of waste;
- provide an irradiation facility for the testing of different EFIT (European Facility for Industrial Transmutation) components (samples, fuel pin, fuel assembly,…).

At the heart of the XT-ADS is the spallation target which provides the primary neutrons that are multiplied in the surrounding subcritical nuclear core. The design of this spallation target is the key issue of the Work Package 1.4 of EUROTRANS. The MYRRHA spallation target module has served as the starting point for the target design of the XT-ADS [1].

After the definition of the design boundary conditions, the general layout of the spallation target loop is presented. Then the different design support studies that have been performed are described. In the last section some conclusions are formulated.

Spallation target boundary conditions

The XT-ADS spallation target system has been designed to be compatible with a remote handling scheme envisaged for the entire XT-ADS. The full loop can be removed from the main vessel after unloading of the core. All active elements are placed in a separate sub-unit which allows servicing of these parts without removal of the spallation loop. The closed outer housing allows regular (yearly) replacement of the spallation target zone that will be required because of radiation-induced embrittlement.

The main characteristics have been defined to obtain a flexible testing facility. Very compact target geometry has been settled upon so as to achieve sufficiently high neutron flux levels ($\phi_{Tot} \approx 3.10^{15}$ n/cm².s). The target space is created by removing three of the hexagonal fuel assemblies in the centre of the core [2] as is shown in Figures 1(a) and 1(b).

Figure 1: Centre of the core

Three assemblies in the centre of the core are removed to make room for the spallation module (dimensions in mm) (a); hatched area indicates the space available for the LBE feeder line, the inner circle indicates the space available for the proton beam (b).

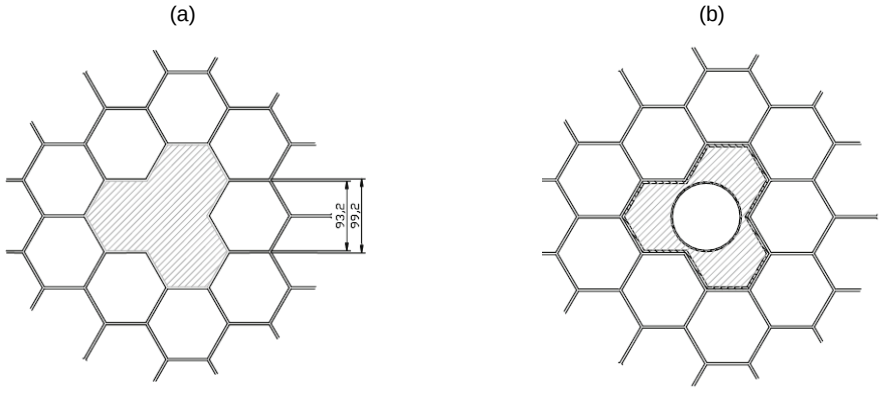

The needed high-power proton beam, several hundreds of MeV at few mA (600 MeV and 3 mA in the reference design), is delivered by an accelerator. For the accelerator part of the system, we opt for a linac solution. The main reason for that choice is the improvement of beam reliability at such levels of proton energy. The beam ingress is foreseen from the top of the vessel. One of the major reasons for that choice is strongly related to the choice made for the target unit interface. The interface being windowless, interlinking the core with an off-axis housing for all active components, beam ingress from the bottom becomes simply unfeasible (having a penetration in the reactor vessel is of course unsuitable).

In Figures 2(a) and 2(b), the global geometrical boundary conditions of the XT-ADS spallation loop and its interference with the core are shown.

Figure 2: XT-ADS spallation loop

Global geometrical boundary conditions (outer dimensions) (a); general view (upper part) and interference of the spallation loop with the core (lower part) (b)

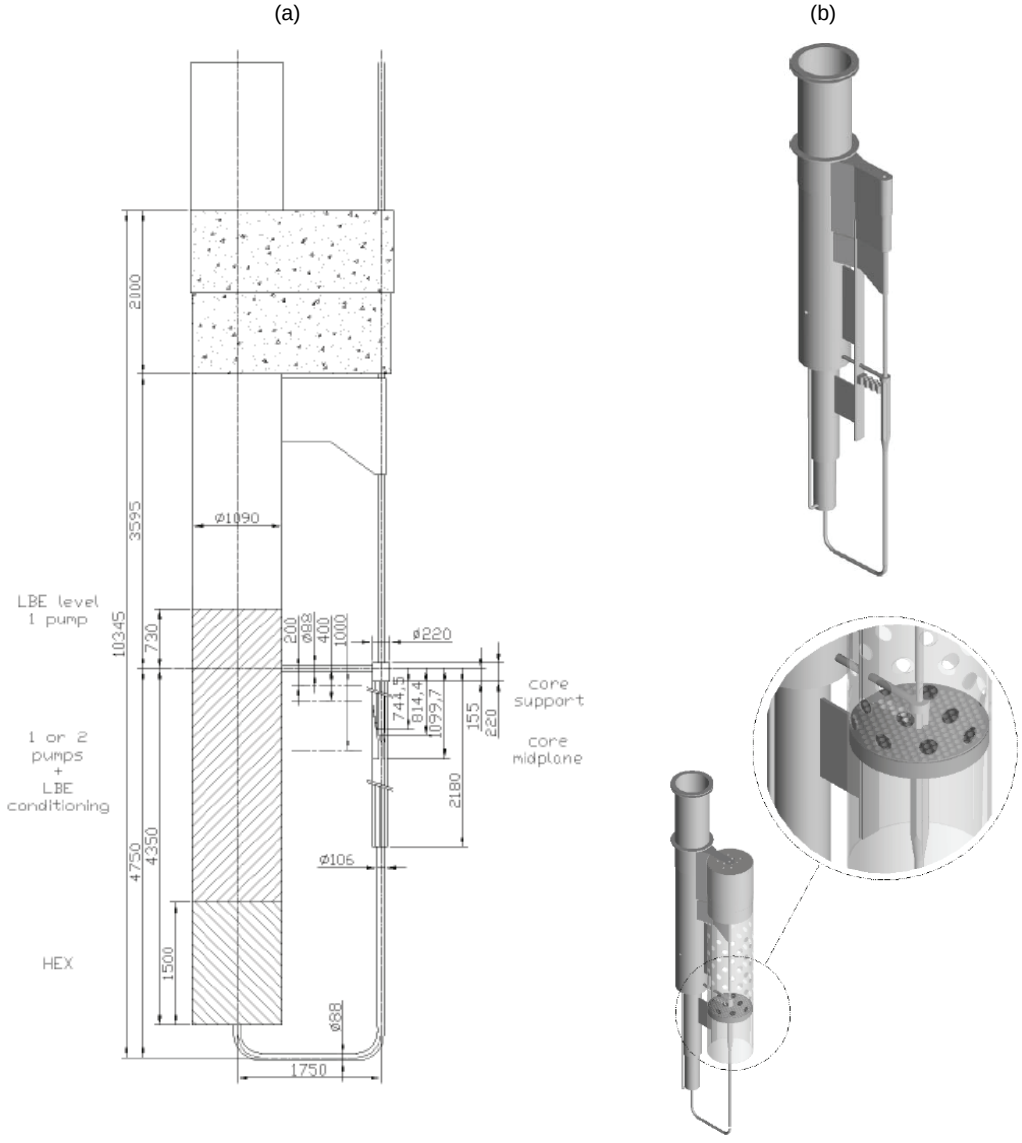

This reliability requirement is essentially related to the number of allowable beam trips, because, frequently repeated, they can significantly damage the reactor structures, the target or the fuel, and also decrease the plant availability. Therefore, beam trips in excess of one second duration should not occur more frequently than five per year.

The total power level of the XT-ADS will be ranging between 50 and 70 MW_{th}.

A replacement of the spallation target, within the envisaged lifetime of the XT-ADS, is unavoidable. This operation should not be required too often. The spallation target unit should be able to survive operation within the ADS system for a sufficient amount of time (roughly one year).

The limited space available in the core and the high proton current lead to very high proton beam densities in the range of 150 $\mu A/cm^2$. No structural material is expected to withstand these conditions at elevated temperatures during a reasonable lifetime of the spallation target. That is why the spallation target is being designed without a hot window between the target area and the vacuum of the beam line.

Spallation loop layout

The off-axis design of the spallation loop (Figure 3) leaves the top and bottom of the subcritical core accessible for fuel manipulations and the installation of irradiation experiments [3]. In addition the main part of the spallation loop is moved away from the high radiation zone which is beneficial for its lifetime.

Figure 3: Spallation target (left); schematics of the spallation loop (right)

General layout showing how the spallation target is split up in a centre and an off-centre part and how the two parts are connected; hatched areas indicate LBE coolant (left), and LBE spallation material (right)

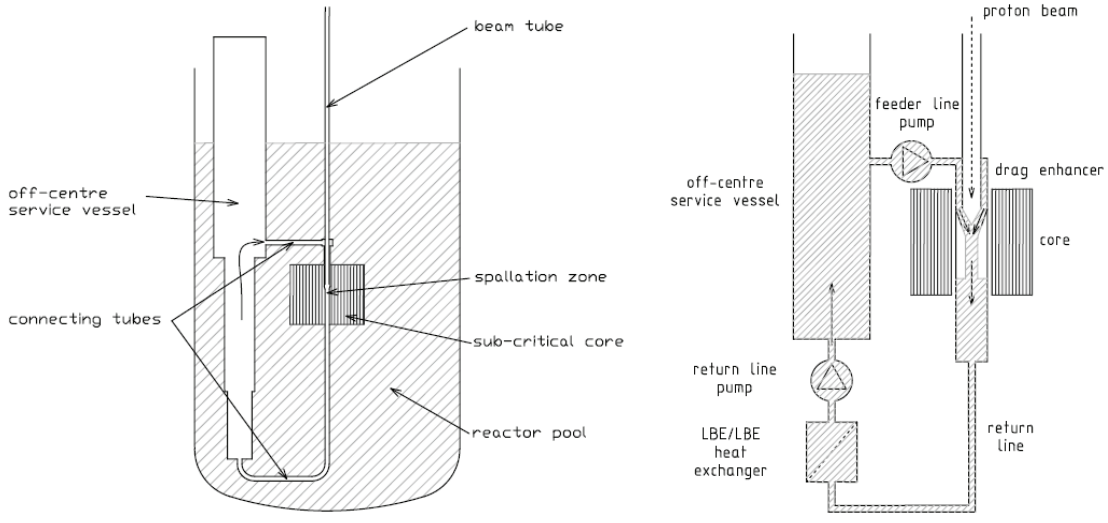

Free surface and recirculation zone

The limited space to implement the target is responsible for the choice of a vertical confluent flow as formation mechanism for the target free surface. The liquid LBE is fed to the target nozzle via a vertical three-lobed annular pipe to optimise the use of the available space in the core. The target nozzle itself is designed to ensure a stable free surface flow.

A firm control over the size of the recirculation zone, formed in the centre of the target free surface, is essential.

When the recirculation zone is too small, LBE droplets are ejected from the LBE confluent zone, which may cause metal evaporation when hit by the beam. If the recirculation zone is too large, it will be directly heated by the proton beam causing the temperatures to increase very rapidlym which would also lead to excessive evaporation of LBE and other volatiles.

LBE as coolant and target material

The use of LBE as a core coolant allows lower working temperatures than foreseen in the lead-cooled EFIT. Liquid LBE is also used for a target material, as forced convection cooling is required due to the thermal energy deposited by the proton beam, both circuits are separated.

In order to limit LBE evaporation and corrosion of structural materials in the target loop, the maximal temperature allowed in the target is set at about 430°C. The lower limit of the LBE flow rate is determined by this value. Because the spallation target material is cooled against the main vessel coolant, the lowest achievable temperature during normal operation of 330°C is mainly determined by the inlet temperature of the core, 300°C.

Pumping options

The free surface level is particularly difficult to maintain under the dynamic changes caused by beam trips and during the start-up/shutdown procedures. In order to cope with these dynamics, an extra free surface is created just below the target zone. This extra free surface will act as a buffer, stabilising the target format process. The main pump lifts the LBE that has passed the heat exchanger to the level of the second free surface. From here, the LBE flows through the feeder line to the target nozzle by gravity.

The vertical flow in the feeder line just above the target is equipped with a drag-enhancing structure, exceeding the minimum drag of 1 bar/m necessary to compensate for the hydrostatic pressure, so as to prevent the LBE tearing apart in the feeder line and reaching the target zone in free fall.

Several options still exist as concerns the pumping strategy of the spallation loop [4]. One choice is one pump in the return line and one smaller pump in the feeder line. The feeder pump is only required to compensate for changes in friction losses in the feeder line. If these changes in friction losses prove to be acceptable or if they can be compensated for another way it may be possible to completely remove the feeder pump from the design. This would decrease the complexity of the system, thus making it not only cheaper and easier to produce but also more reliable.

Due to lack of experimental validation, in particular for the pressure loss, it was proposed to opt for the conservative option of having two pumps in the spallation loop: one big main pump in the return line; one small pump in the feeder line will be used to counteract erosion/corrosion effects.

Vacuum system

The vacuum system has two essential functions. The pressure directly above the spallation target should be below the 10^{-3}-10^{-4} mbar range to guarantee compatibility with the vacuum of the proton beam line and to avoid plasma formation caused by the interaction between the rest gas above the target and the proton beam. The confinement of volatile radioactive spallation products – the vacuum system – is equipped with a closed back-end composed of sorption and getter pumps from which they can be batch-wise removed.

The large second free LBE surface in the servicing vessel (Figure 3), directly underneath the main vacuum pumps, minimises emanation of spallation products into the proton beam line.

Design support studies

MHD pump definition

A sizing of a 13 l/s – 4 bar EMP, for the return line, has been done by R. Stieglitz in [5]. Within this report the general electromagnetic pump design requirements are described as well as the principle design of the MHD pump acting as a long-term regulator in the return line. Based on design requirements the pump is designed, the nominal operating point of the pump is calculated together with the efficiency and other electromagnetic parameters relevant for the following power balance of the pump.

This pump could be designed and technically realised as a cylindrical electromagnetic pump with overall dimensions of 0.6 m in diameter and 2 m in length (see Figure 4).

Figure 4: Design sketch of the biggest MHD pump in the spallation target loop

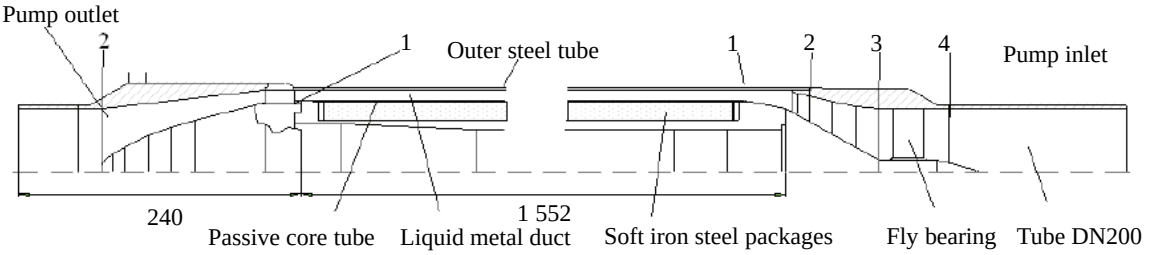

A 4 bar EMP is able to deliver the maximally needed pressure head in a one pump scenario under transient conditions. In case of a two-pump scenario, this maximal pressure head can be distributed in a nominal pressure head of 2.5 bar for the return pump and a transient head of 1.5 bar for the feeder pump. In this case, we estimate that the return pump may be designed and technically realised with overall dimensions $\varnothing$ 0.4 × 1 m. It can be noticed that the feeding pump is smaller due to the fact that the driving pressure is even lower.

Target nozzle

Water flow mock-up experiments performed at the Université Catholique de Louvain (UCL) have shown that a more stable flow is achieved if some detachment of the LBE flow is allowed. Further experiments with LBE at the KALLA laboratory of the Forschungszentrum Karsruhe (FzK) are planned to confirm the observations made in the water loop.

The feasibility of a target nozzle that explicitly forces flow detachment is studied. Two principally different nozzle layouts are studied (Figure 5). They are different by the fact that in the left nozzle the LBE flow is designed to be in contact with the walls at all times, while the right nozzle is designed to have the LBE flow separate from the walls and form a free falling jet.

Due to its inherent stability the nozzle with flow detachment is chosen to be the reference design for further target development [2].

At this stage, the current hydraulic design of the target area of the XT-ADS spallation loop is shown in Figure 6(a).

Several iterations were needed to develop the current design version number v0.10LBE. The main revision number remains zero, to indicate that some improvements might still be required based on experimental verification. This layout has been chosen to be the reference design for numerical and experimental investigations. The detailed study of the three-feeder option [Figure 6(b)] for the LBE downcomer, which has the advantage that optimal use is made of the available space in the ADS core, is not in the scope of the project.

Figure 5: Two different nozzle principles

Without flow detachment (left), with flow detachment (right)

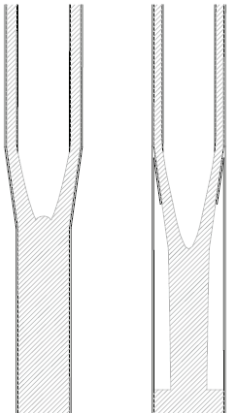

Figure 6: The XT-ADS nozzle design called v0.10LBE

Schematic layout of the nozzle design (a); going from a three-feeder configuration towards an axi-symmetric design for optimisation of target formation process (b)

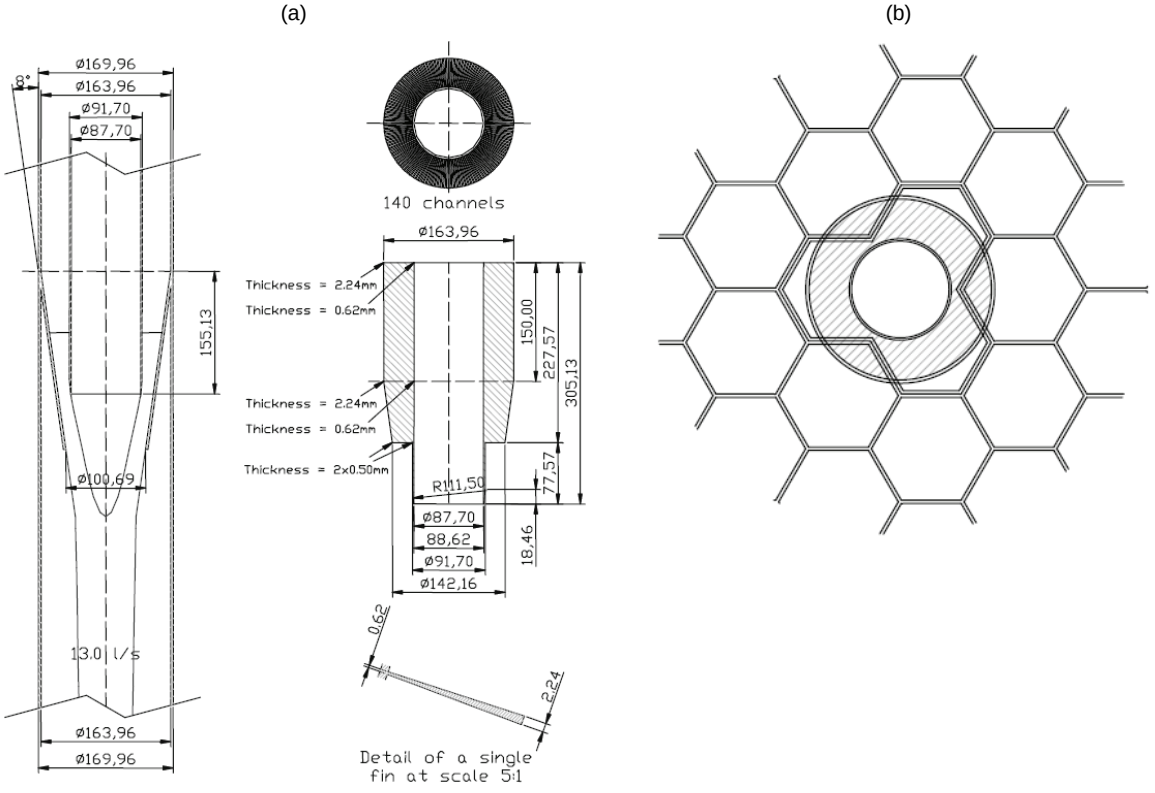

Heat deposition

The proton beam will be swept around the central recirculation zone of the target, in order to avoid overheating and thus evaporation of this central recirculation zone. Given a certain beam shape and sweep profile, Monte Carlo codes like MCNPX can calculate the heat deposition inside the target.

The heat deposition profile of a 600 MeV proton pencil beam, Gaussian beam (σ = 4 mm) and swept Gaussian beam (circular sweep with 22 mm radius, σ = 4 mm) have been calculated [6] using MCNPX. The results are shown in Figure 7. This last configuration is compatible with the latest design of the XT-ADS target nozzle.

Figure 7: Linear (left) and logarithmic (right) heat deposition profile of a 600 MeV Gaussian beam with σ = 4 mm that is swept around a circle with 22 mm radius

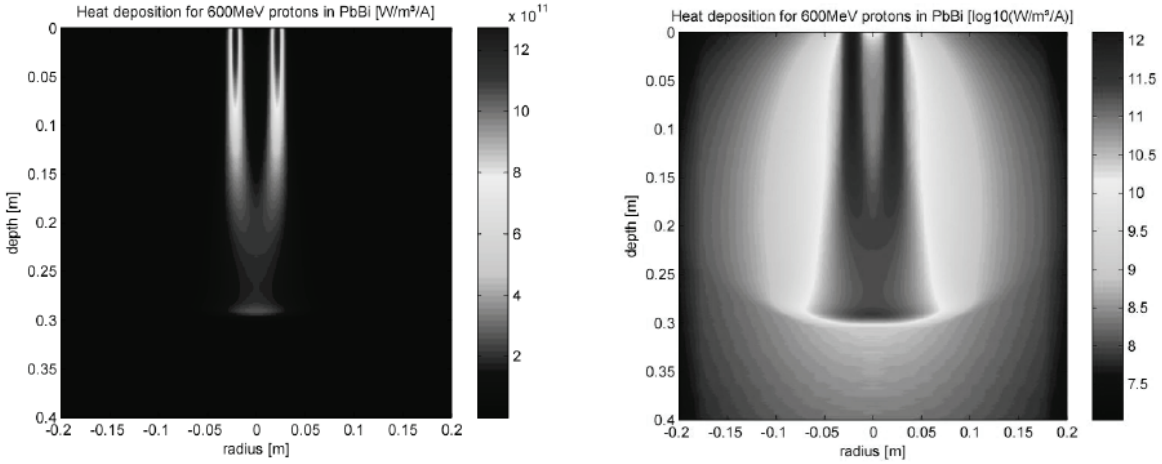

The linear heat deposition profile indicates that most of the heat is generated at the top of the target zone (Figure 8). At 27 cm there is a sudden rise in the linear heat deposition corresponding to the Bragg peak expected from theory. Integrating the linear heat deposition profile results in the total heat deposition in the target: 4.16 10^8 W/A. As such, 69% of the total beam power is converted into heat inside the target. For 3.0 mA beam intensity, the heat deposited corresponds to roughly 125 MW.

Figure 8: Linear heat deposition profile for a 600 MeV proton beam

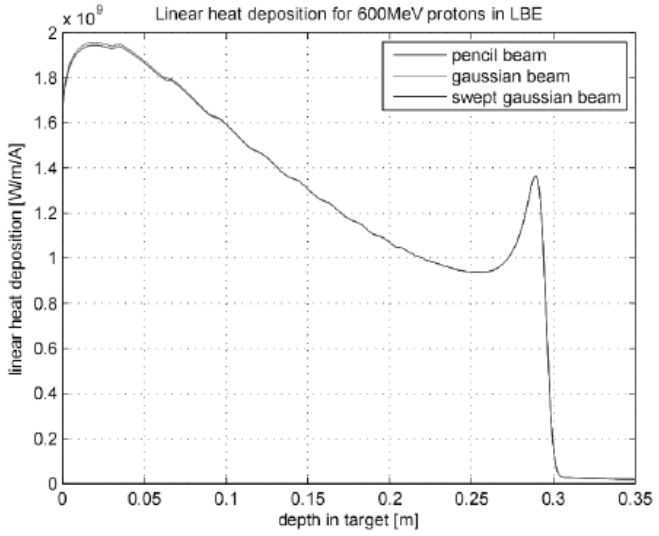

Nuclear and neutronic assessment of the target has also been perfomed using MCNPX. The studies mainly focused on proton and neutron flux, spallation vector and evaluation of dpa in structural material [7].

Thermal-hydraulics

The current hydraulic design of the spallation target area is the result of a lengthy design process accompanied by a set of full scale experiments. An experimental campaign has started for the improvement and validation of the developed numerical models. Measurement techniques are also developed for thermal-hydraulics experiments and for operational techniques in the XT-ADS. The focus is on local fluid velocity measurement, integral contactless flow meters, and free surface level sensors.

For the spallation target, particular attention has been paid to the characterisation of the free surface flow, flow detachment, study of the three-feeder option and development of measurement techniques for HLM flows [8].

Since no experiment can demonstrate the ability to transport the deposited heat in a windowless spallation target adequately, validated numerical methods are required. For this purpose, computational fluid dynamics (CFD) simulation methods are the most appropriate. This requires sufficiently accurate free surface modelling, predicting a unique (sharp) interface between LBE and beam vacuum in combination with adequate turbulence modelling. In the European 5th Framework Programme project ASCHLIM [9], it was demonstrated that sufficiently accurate CFD modelling of such free surface targets was not possible with the state-of-the-art methods available at that time. Within the EUROTRANS project, the development of CFD methods for the simulation of the removal of deposited heat in the LBE windowless target has progressed substantially [10].

A series of computations has led to a fundamental understanding of the free target flow and the proposed design. Comparison of numerical simulations with a water experiment [11] is shown in Figure 9.

Figure 9: Comparison of numerical simulations with a water experiment [11]

Predicted water volume fraction (WVF) (dark grey is water, black is vapour) (left); observed free surface in the water loop experiments (centre); comparison of numerical and experimental results, the dark lines indicate the expected LBE flow profile, light grey lines highlight the experimentally observed free surface (right)

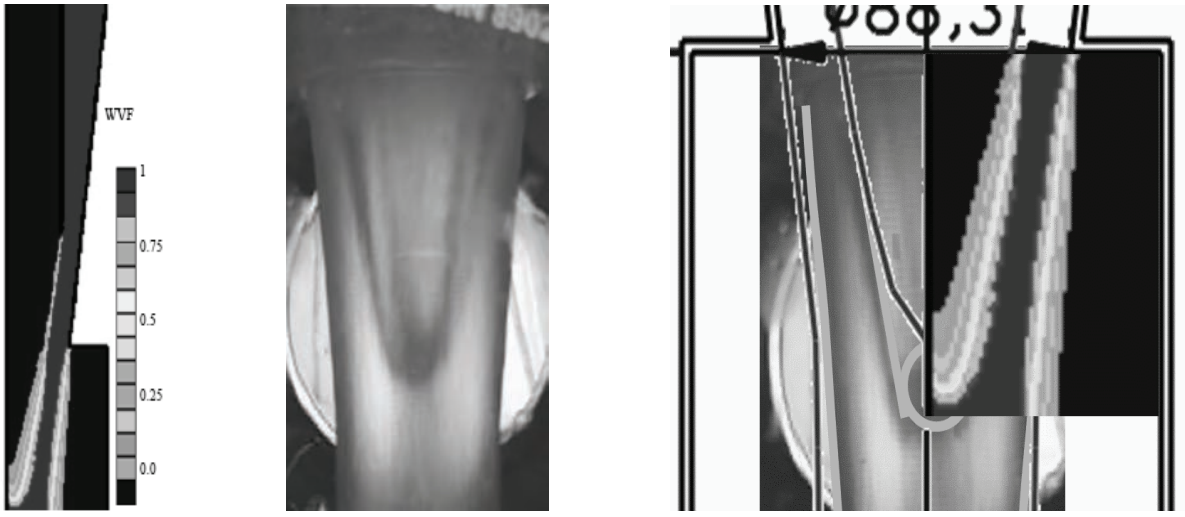

The cavitation model of the commercial code STAR-CD in conjunction with a high resolution interface capturing technique has been employed to compute the flow in the XT-ADS windowless target and related experiments. The numerical scheme is capable to compute the free surface flow in the target and the experiments and can be used in design optimisation and parametric studies. A HLM experiment demonstrating the feasibility of stable flow in the HLM windowless target is currently installed in KALLA [12].

Beam target interaction

The purpose of the study performed by NRG is to determine whether the heating from the proton beam results in an expansion wave/pressure wave through the system resulting in LBE splashing after impact of the beam. Splashing could be an issue and is studied numerically. Although results are promising, no firm conclusions can be made at this stage.

Safety analysis

A detailed analysis of the spallation loop behaviour during operational and accidental transients using a system code is mandatory. It allows assessing in detail whether the current loop layout can accommodate these transients or whether design measures need to be taken to improve the loop response. The simulations (start-up transient, main pump failure, loss of heat sink,…) were performed within the VELLA I^3 Project of the European Commission's 6th Framework Programme using a version of the RELAP5/Mod.3.3 code purposely modified to account for LBE properties and behaviour. The conclusions of the study can be found in [13]. At this stage, even if the correctness of the approach for the exact simulation of the free surface levels still needs further investigation and confirmation, no showstoppers were found.

Conclusions

This paper gives the reference design boundary conditions and the general layout of the XT-ADS spallation target loop. The different design support studies that have been performed within the framework of the IP EUROTRANS DM1 DESIGN are summarised. In this design support studies, no showstopper was identified. These include the spallation target zone and spallation loop thermal-hydraulics, system dynamics, beam impact studies, neutronic and safety analyses.

Acknowledgements

The DM1 DESIGN work has been performed under the Integrated Project EUROTRANS (Ref. FI6W-CT-2004-516520) co-funded by the European Union in its 6th Framework Programme. Acknowledgment is also due to all the colleagues of the participating institutes for their contributions to many different topics.

References

[1] Aït Abderrahim, H., P. D'hondt, D. De Bruyn, "MYRRHA, a New Fast Spectrum Facility", *Seminar on Fission*, Corsendonck Priorij, 18-21 September 2007, Proceedings April 2008, World Scientific, ISBN 978-981-279-105-4, pp. 207-221 (2008).

[2] Dierckx, M., *Target Area Design Options for the XT-ADS Spallation Loop*, SCK•CEN Report R4649 (2009).

[3] Reale, M., *Description and Functional Sizing of Main Components of the Reference Design of XT-ADS*, EUROTRANS Deliverable D.1.27 – D.1.28 (2009).

[4] Dierckx, M., *XT-ADS Spallation Loop Operation and Pumping Options*, SCK•CEN Report R4666 (2009).

[5] Stieglitz, R., *MHD-pump for the XT-ADS Design*, KIT (2009).

[6] Dierckx, M., *Heat Deposition Profile in the XT-ADS Target*, SCK•CEN Report R4567 (2008).

[7] Van den Eynde, G., *XT-ADS Core Summary Report*, EUROTRANS Deliverable D.1.56 (2009).

[8] Roelofs, F., B. de Jager, A. Class, *et al.*, "European Research on HLM Thermal-hydraulics for ADS Applications", *Journal of Nuclear Materials*, 376, 401-404 (2008).

[9] Arien, B., *et al.*, *Assessment of Computational Fluid Dynamic Codes for Heavy Liquid Metals-ASCHLIM*, EC Contract FIKW-CT-2001-80121-Final Rep. (2004).

[10] Batta, A., A.G. Class, H. Jeanmart, "Comparative Experimental and Numerical Analysis of the Hydraulic Behaviour of Free-surface Flow in the Water Experiment of the XT-ADS Windowless Spallation Target", *Proceedings of ICAPP'10*, San Diego, CA,USA, forthcoming (2010), paper-Id 10342.

[11] Batta, A., *et al.*, "Hydraulic Design of the Windowless XT-ADS Spallation Target", *HeLiMeRT in Europe*, SCK•CEN, Mol, Belgium, 20-22 April (2009).

[12] Class, A.G., A. Batta, "XT-ADS Windowless Target: High Resolution Interface Capturing Simulations", these proceedings.

[13] Forgione, N., *et al.*, *MYRRHA Spallation Target Loop: RELAP 5 Simulation*, VELLA Deliverable, European Commission (2009).

Investigation of safety for accelerator-driven system

Takanori Sugawara, Kenji Nishihara, Kazufumi Tsujimoto, Yuji Kurata, Hiroyuki Oigawa
Japan Atomic Energy Agency, Japan

Abstract

It is supposed that the accelerator-driven system (ADS) is safer than other critical systems such as fast reactors since the ADS is driven by an external neutron source in the subcritical state. In this study, the possibility of a core disruptive accident (CDA) for the ADS is investigated by detailed safety analyses. Safety analyses for unprotected transient over power (UTOP) and unprotected loss of flow (ULOF) are carried out using the SIMMER-III code.

The calculation results show that the maximum temperatures of the nitride fuel and the clad tube (316SS) in the accidents are lower than their melting points (2 780°C and 1 400°C, respectively). For example, the maximum temperature of the fuel has reached about 1 800°C and that of the cladding tube reached 1 100°C in ULOF. It is, therefore, concluded that there are hardly possibilities of CDA for the ADS. It has also been found by Level 1 PSA that the frequency of those accidents would be exceedingly small. Although the creep rupture of the cladding tube might happen in beam over power (BOP), which is a kind of UTOP, and ULOF, it is concluded that the possibility of CDA or a re-criticality accident in an ADS is unlikely.

Introduction

An accelerator-driven system (ADS) has been studied to transmute minor actinides (MA) included in the high-level waste (HLW) to reduce the burden for the geological disposal of the HLW. The Japan Atomic Energy Agency (JAEA) has investigated a lead-bismuth eutectic (LBE) cooled ADS [1]. A high-intensity proton accelerator with 1.5 GeV beam energy and a subcritical core with 800 MW thermal power are designed to transmute 250 kg MA per year in the system. Figure 1 and Table 1 present a conceptual diagram and the main parameters of the ADS, respectively.

Figure 1: Conceptual diagram of ADS

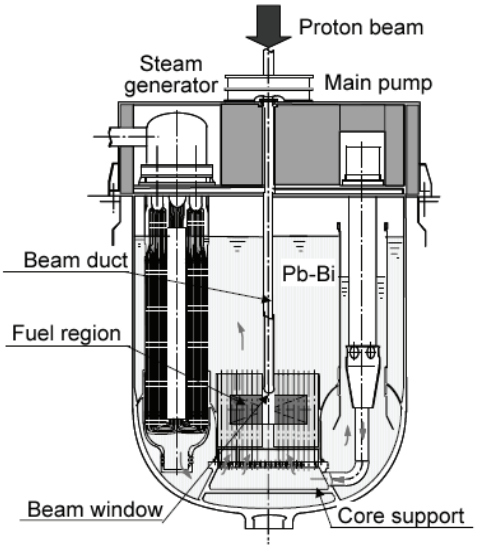

Table 1: Main parameters of ADS

Plant	Thermal power	800 MWt
	Coolant	LBE
	Inlet temperature	300°C
	Coolant velocity	2.0 m/sec
	Upper limitation of k_{eff}	0.97
	Operation period	600 EFPD*
Fuel assembly	Type	Ductless and hexagonal
	No. of fuel assemblies	84
	Pitch	233.9 mm
	Width	232.9 mm
	No. of fuel pins per assembly	391
	No. of tie rods per assembly	6
Fuel	Composition	(MA+Pu)N+ZrN
	Pu enrichment (inner/outer)	15.1/21.3 wt.%
	ZrN ratio (inner/outer)	49.7/49.7 wt.%
	Theoretical density	90%
	Smear density	85%
	Pin outer diameter	7.65 mm
	Thickness of cladding tube	0.5 mm
	Pin pitch	11.48 mm
	Active height	1 000 mm

* Effective full power days.

It is considered that the ADS is safer than conventional critical reactors since the operation of the ADS is able to be stopped by the shutdown of the accelerator. It is also supposed that the possibility of a core disruptive accident (CDA) for the ADS is lower than that for conventional critical reactors. JAEA has performed some dynamics calculations for the accident with a simple calculation model. However, systematic investigations for CDA had not been performed.

As the systematic investigations of CDA for the ADS, this study performed an investigation of abnormal events and detailed safety analyses. The investigation for abnormal events was carried out by Level 1 probabilistic safety assessment (PSA). The safety analysis was performed by the SIMMER-III code developed by JAEA [2]. Through these investigations, this study shows that the possibility of CDA for the ADS is very low.

Investigation for abnormal events

Level 1 PSA was used to quantify the frequency of an abnormal event. The frequency was analysed by the initiating event and the mitigation function. The initiating event is an abnormal event in an intended plant. The mitigation function is a function to ease the abnormal event and to prevent a severe accident. The initiating events used in this study are summarised in Table 2.

Table 2: Initiating event and its frequency

Event	Frequency [/reactor · year]*3
Beam over power	1e-1*1
Beam window breakage	1e-1*1
Failure of primary coolant control system*2	3e-2
Breakage of primary coolant boundary*2	1e-6
Primary coolant pump trip*2	7e-2
Recirculation pump trip*2	7e-2
Loss of flow for water supply*2	3e-1
Breakage of heat exchanger tube*2	7e-3
Loss of external power*2	5e-2

*1: Assumption.

*2: Based on the investigation for the fast reactor [3].

*3: 1e-1 means 1×10^{-1}.

The initiating events were selected based on the investigation of Level 1 PSA for the fast reactor [3]. The frequencies for those events were also referred from Ref. [3]. As for the inherent events for the ADS, “beam over power” and “beam window breakage” were assumed from the viewpoint of the severe accident. The frequencies of these two events were assumed to be 0.1 [/reactor · year]. Since there is no knowledge for these two events, relatively high frequencies were assumed in this study.

The mitigation functions shown in Table 3 were supposed. This table also presents the unreliability, which means a probability to fail its function. The unreliability of the mitigation function was quantified by the SQD (semi-quantitative semi-deterministic) method which gives a frequency based on a classification; safety/normal system, passive/active system (Table 4). For example, the guard vessel is a system to prevent a leakage of coolant from the reactor vessel. This is the passive/safety system and its unreliability was assumed 1×10^{-4} from Table 4. Since the emergency power, which is the active/safety system, is supposed to be prepared two systems in the ADS, its unreliability was $(10^{-2})^2 = 1 \times 10^{-4}$. For the scram signal, the unreliability was calculated considering a circuit configuration of “2 out of 4”.

Table 3: Mitigation function and its unreliability

Mitigation function	Unreliability [/demand]*2
Scram signal	4e-8
Proton beam shutdown	1e-6
Primary coolant pump trip	1e-2
Turbine bypass	1e-2
Guard vessel	1e-4
Start-up of PRACS*1	1e-6
Emergency power	1e-4

*1: Primary reactor auxiliary cooling system.

*2: 1e-1 means 1×10^{-1}.

Table 4: Unreliability for each system

Unreliability [/demand]	10^{-4}	10^{-3}	10^{-2}	10^{-1}
Passive/safety system	x			
Passive/normal system		x		
Active/safety system			x	
Active/normal system				x

Based on these initiating events and the mitigation functions, the frequencies of the abnormal events were calculated. The results were sorted into "design basis accident" (DBA) and "beyond design basis accident" (BDBA). DBA is the accident to estimate the design or to determine the design condition. BDBA is the accident exceeding DBA and its frequency is much lower than that for DBA. A criteria, 1×10^{-6} [/reactor · year] employed in the feasibility study of the fast reactor [4] was used to determine DBA or BDBA. An event with a frequency larger than 1×10^{-6} [/reactor · year] was designated DBA.

Table 5 summarises DBA of the ADS. As the result, only two cases became DBA. The first one was unprotected transient over power (UTOP) caused by the beam window breakage and the failure of the scram signal. In this case, positive reactivity would be inserted with the failure of the shutdown. The second one was protected loss of heat sink (PLOHS) caused by the loss of external power and the failure of the emergency power. In this case, loss of heat sink would occur with the success of the shutdown. To respond to these DBA by the design, a multiplexing of each mitigation function is supposed. It is also required to revise the frequency of the beam window breakage.

Table 5: Frequency of DBA

Case	Initiating event	Scram signal	Proton beam shutdown	Primary coolant pump trip	Turbine bypass	Guard vessel	Start-up of PRACS	Emergency power	Frequency [/reactor · year]
UTOP*1	Beam window breakage	x							2e-5
PLOHS*2	Loss of external power							x	5e-6

*1: Unprotected transient over power.

*2: Protected loss of heat sink.

From the viewpoint of CDA, it is not necessary to assume PLOHS since the ADS succeeds in the shutdown. A provisional estimation with a simple model for PLOHS indicated that the LBE

temperature hardly increased during several decades. For beam window breakage (BWB), it is supposed that LBE flows into a beam duct which is a vacuum region to transport protons. This phenomenon will introduce a positive reactivity insertion by a decrease of neutron leakage but the external neutron source in the core region will decrease. Although it was considered BWB would not induce CDA, a detailed calculation was performed by the SIMMER-III code since this was one of the typical accidents for the ADS.

The discussion for BDBA from the viewpoint of CDA was also performed and beam over power (BOP) and unprotected loss of flow (ULOF) were supposed to have a possibility to induce CDA. For BOP, it was assumed that a reactor power would increase with a change of proton beam intensity. It introduces an increase of a cladding tube temperature and its failure. For ULOF, the increase of the cladding tube temperature was also expected, and Ref. [5] reported that ULOF was one of the severest accidents for ADS. Though the frequencies of these two accidents were exceedingly smaller than DBA, detailed calculations were also carried out to confirm the possibility of CDA.

Calculation conditions

Calculation code

The SIMMER-III code was employed for the safety analysis. The SIMMER-III code is an advanced safety analysis code, which has been developed to investigate postulated core disruptive accidents in fast reactors. The SIMMER-III code is a two-dimensional three-velocity field, multi-phase, multi-component, Eulerian fluid dynamics codes coupled with a structure model and a space-, time- and energy-dependent neutron kinetics model. The latest version of the SIMMER-III code is available to analyse the LBE-cooled ADS by adding features to treat the external neutron source, the subcritical state and properties for the LBE [6].

Calculation model

The RZ calculation model shown in Figure 2 was used in the safety analysis. Parameters shown in Table 1 were employed in this investigation. The proton beam from the superconducting linac (SC-Linac) is induced to the LBE spallation target through the beam duct from the top of the ADS. The LBE spallation target is separated by the partition wall to avoid the cross-flow from the core to the target region since ductless assemblies are employed in this system. The core consists of 84 fuel assemblies that are divided into four zones. The innermost zone is designated as the first zone, the next is the second zone and so on. These zones were used in the investigation of a multi-zoned ADS in Ref. [7], and in this study a two-zoned model which has two different plutonium enrichments was employed.

In Ref. [7], it was found that the power distribution in the second end of cycle (EOC) was the severest state since the subcriticality in second EOC was the largest (k_{eff} = 0.944) during the ADS operation. Figure 3 presents the changes of the effective multiplication factor and the maximum temperature at the surface of the cladding tube by burn-up. This figure indicates that the temperature condition at the second EOC is the severest. Based on this result, a neutronic calculation model in the second EOC state was employed as the severest case.

Calculation case

For BWB, two calculation cases were performed to consider a change of the external neutron source. Since the SIMMER-III code is unable to treat a dynamic change of the external neutron source, calculations with or without the external neutron source at the beam window breakage were carried out. It was considered that an actual event would become between these results.

Figure 2: RZ calculation model

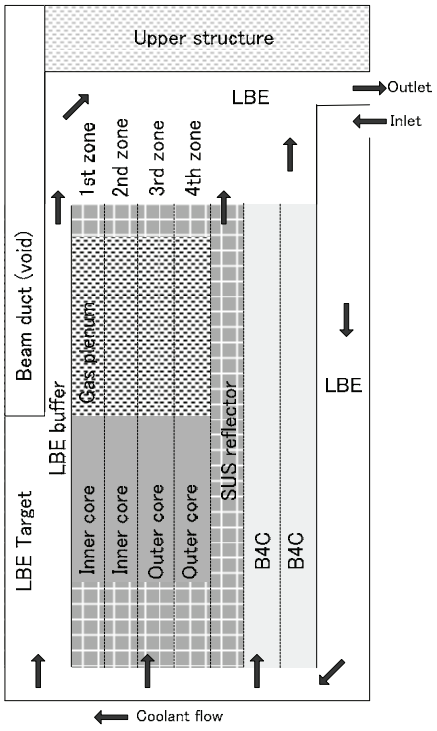

Figure 3: Changes of effective multiplication factor and maximum temperature at the surface of the cladding tube by burn-up [7]

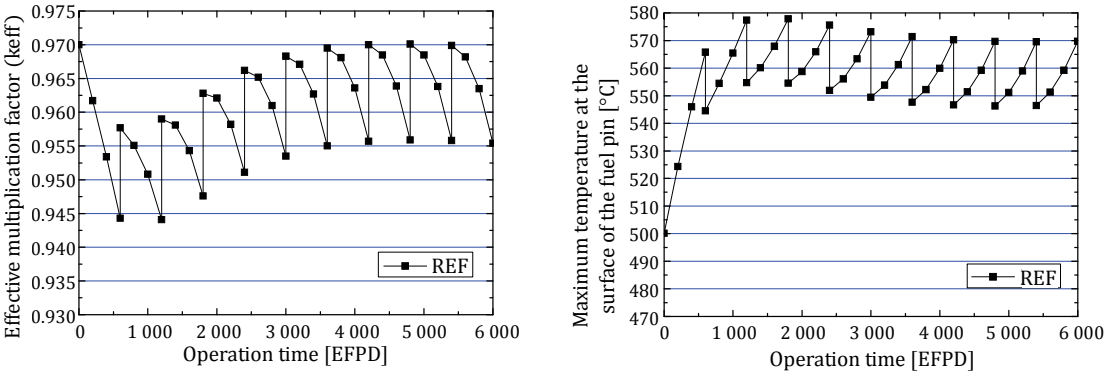

For BOP, a transient with doubled intensity of the external neutron source was analysed as the beam current was changed from 10.2 to 20.3 mA during the burn-up cycle shown in Figure 3.

For ULOF, a transient with the external neutron source without a pump driving force was performed. The coast-down of the pump was assumed to be from 0 to 15 sec.

Calculation results

Beam window breakage (BWB)

Figure 4 illustrates the change of LBE at the beam window breakage. In this figure, t = 25 sec corresponds to the time of the beam window breakage. A part at Radial = 1, Axial = 23-45 shown in Figure 4 corresponds to the beam duct (vacuum). About one second after the breakage

Figure 4: Change of LBE at beam window breakage

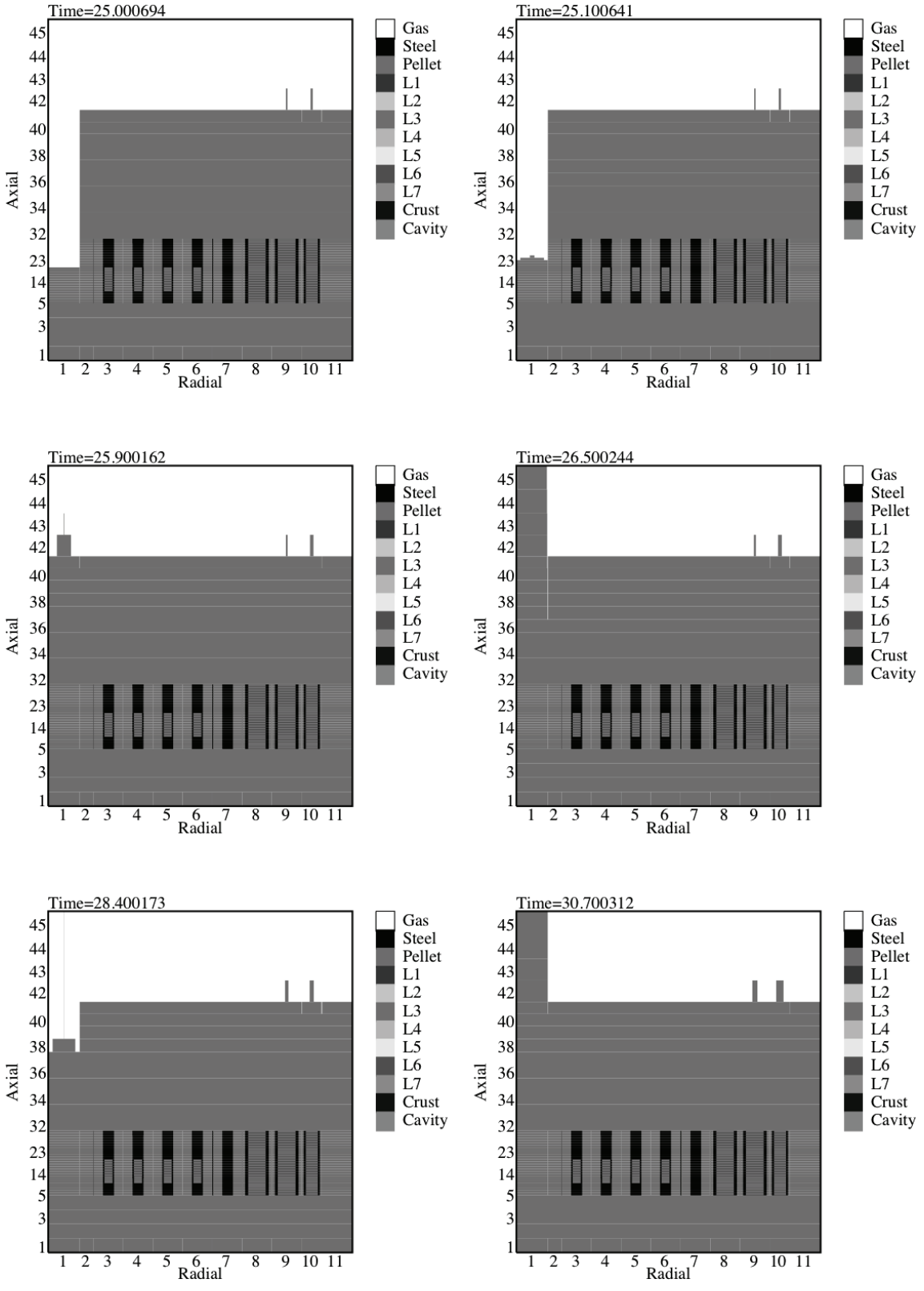

(t = 25.9 sec in Figure 4), a LBE level in the beam duct reached a level in the reactor vessel and the LBE level reached a top of the calculation model at 1.5 sec (t = 26.5 in Figure 4). Then, the LBE level decreased (t = 28.4 sec in Figure 4) and reached the top again (t = 30.7 sec in Figure 4). It was found that the LBE flowed into the beam duct and the LBE level vibrated and converged on the LBE level in the reactor vessel. This result means that the external neutron source will move up and an effective source in the core will decrease.

Figure 5 presents the temperature changes of the fuel and the cladding tube in BWB with the external neutron source. These data are the temperatures for the assembly in the nearest position from the target region and the position z = 3.65 [m] in Figure 5 (left) means the maximum fuel temperature. From these results, it was confirmed that the temperatures slightly increased by the insertion of a positive reactivity due to a decrease of neutron leakage by BWB. However, these changes were very small and there was no possibility of CDA by BWB.

Figure 5: Temperature changes of fuel and cladding tube in BWB (with neutron source)

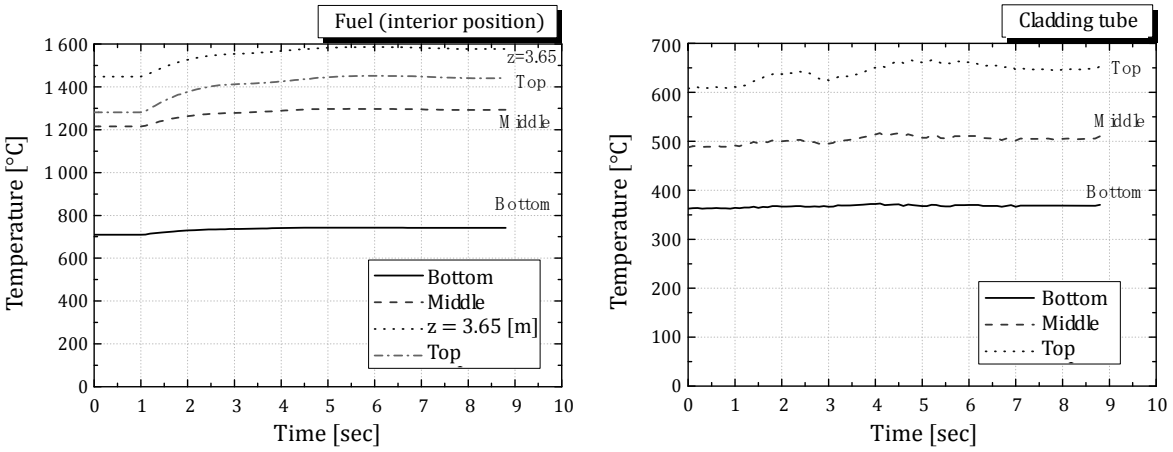

Figure 6 shows the temperature changes of the fuel and the cladding tube in BWB without the external neutron source. The transient is almost the same as a transient at the ADS shutdown. From Figures 5 and 6, it was confirmed that BWB was not a sufficiently severe accident to induce CDA.

Figure 6: Temperature changes of fuel and cladding tube in BWB (without neutron source)

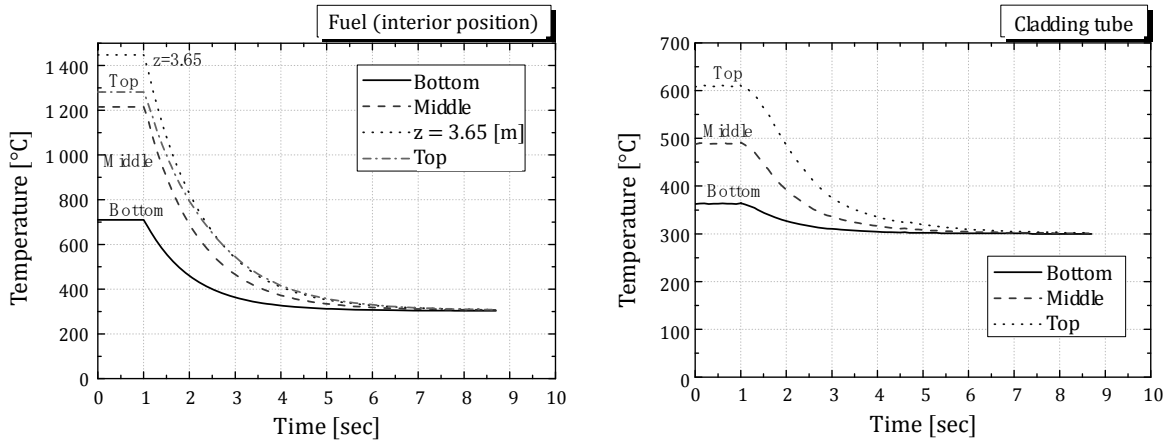

Beam over power (BOP)

The changes of the fuel and cladding tube temperature in BOP are shown in Figure 7. By the doubled intensity of the external neutron source, the maximum temperature of the fuel was about 2 500°C and that of the cladding tube was about 900°C. From these results, it was found that there was little possibility of a pin failure with the doubled intensity of the external neutron source since the melting points of the nitride fuel and the fuel pin (SS316) are 2 780°C and 1 400°C, respectively. However, it was considered that there was a possibility of the creep rupture of the cladding tube.

Figure 7: Temperature changes of fuel and cladding tube in BOP

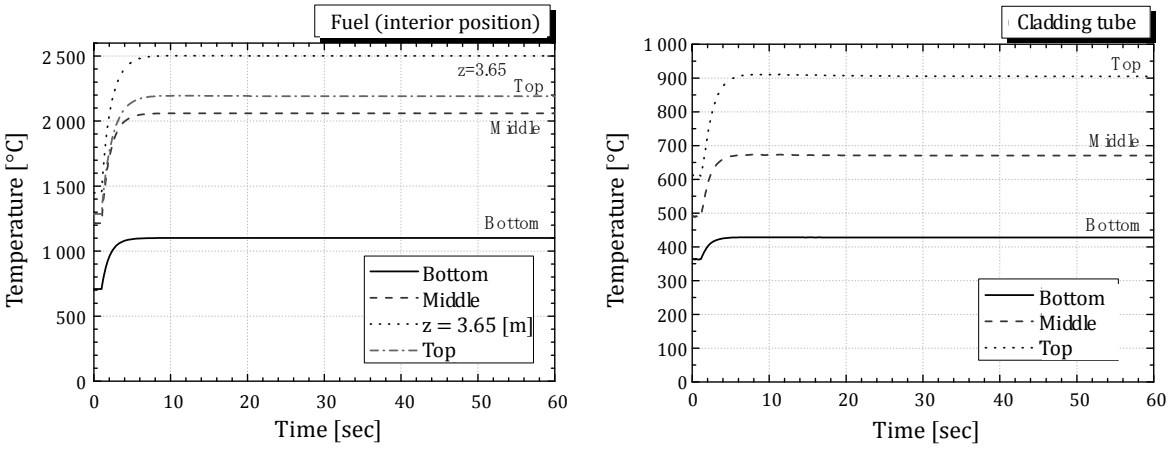

Unprotected loss of flow (ULOF)

The changes of the power and the flow rate in ULOF are shown in Figure 8. The power was increased by about 2% at 15 sec and slightly decreased. Figure 9 shows the fuel and cladding tube temperature changes. The maximum temperature of the fuel reached about 1 800°C and that of the cladding tube reached 1 100°C. These analysis results indicated that there was very little possibility of CDA in ULOF since both the fuel and the cladding tube temperatures were lower than their melting points. On the other hand, the possibility of the creep rupture of the cladding tube was also considered.

Figure 8: Power and flow rate changes for ULOF

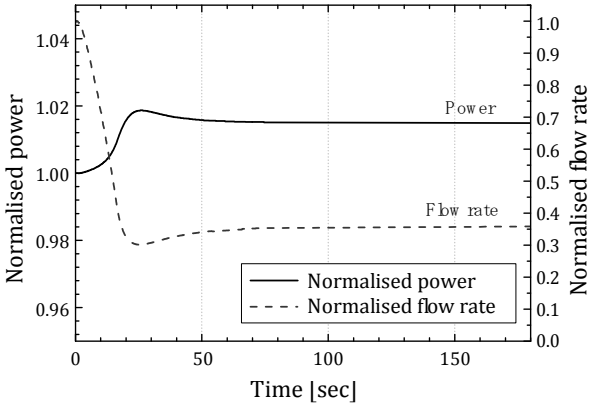

Figure 9: Temperature changes of fuel and cladding tube in ULOF

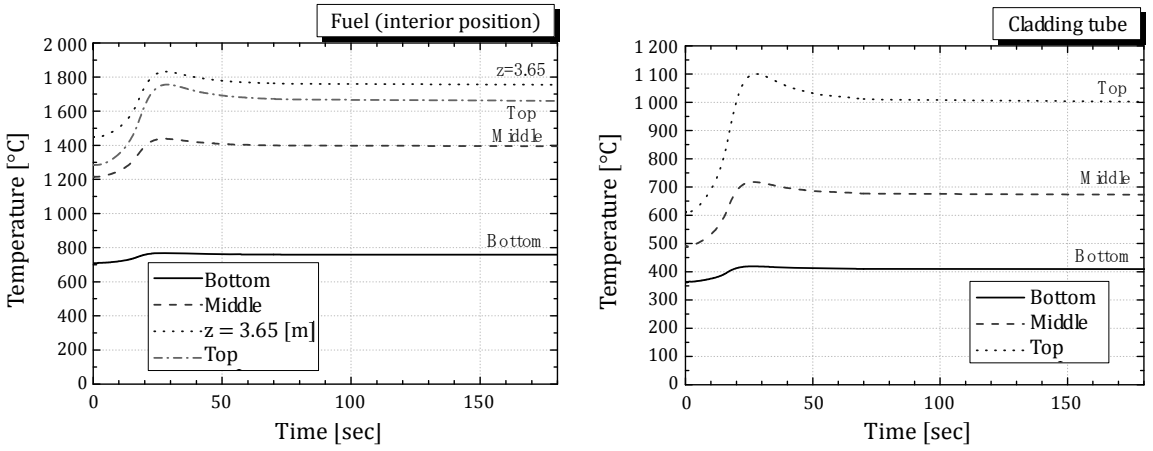

Conclusion

The systematic investigations of CDA for the ADS were performed by using Level 1 PSA and the SIMMER-III code. In the investigation by Level 1 PSA, it was found that two cases, UTOP-BWB and PLOHS became DBA for the ADS designed by JAEA. Based on these results, BWB was analysed by the SIMMER-III code. The safety analyses for BOP and ULOF were also carried out although these cases were BDBA. This was because it was guessed that the possibilities of CDA in both BOP and ULOF were larger than other accidents.

These safety analysis results indicated that there was very little possibility of CDA in the ADS. It was also confirmed that there was no possibility of CDA by BWB since the LBE flowed into the beam duct and the external neutron source in the core region decreased. On the other hand, it was supposed that there was a possibility of the creep rupture of the cladding tube in both BOP and ULOF.

Although there is a possibility of the creep rupture of the cladding tube in BOP and ULOF, these are BDBA and these frequencies are very low ($<1 \times 10^{-6}$ [/reactor · year]). Through these investigations, it is concluded that the ADS has very little possibility of CDA or a re-criticality accident.

Acknowledgements

The authors would like to express their great thanks to Dr. T. Suzuki of JAEA for his helpful advice and comments concerning the SIMMER-III analysis.

References

[1] Tsujimoto, K., *et al.*, "Neutronics Design for Lead-bismuth Cooled Accelerator-driven System for Transmutation of Minor Actinide", *J. Nucl. Sci. and Technol.*, 41 [1], 21-36 (2004).

[2] Tobita, Y., Sa. Kondo, H. Yamano, *et al.*, "The Development of SIMMER-III, an Advanced Computer Program for LMFR Safety Analysis, and its Application to Sodium Experiments", *Nuclear Technol.*, 153, pp. 245-255 (2006).

[3] Hioki, K., K. Kurisaka, T. Mihara, *Level 1 PSA on Large Fast Breeder Reactor*, PNC TN9410 93-134 (1993) [in Japanese].

[4] Japan Atomic Energy Agency (JAEA), *Feasibility Study on Commercialized Fast Reactor Cycle Systems – (1) Fast Reactor Plant Systems*, JAEA-Research 2006-042, JAEA (2006) [in Japanese].

[5] Suzuki, T., *et al.*, "Transient Analyses for Accelerator Driven System PDS-XADS Using the Extended SIMMER-III Code", *Nuclear Engineering and Design*, 235, pp. 2594-2611 (2005).

[6] Maschek, W., *et al.*, "SIMMER-III, a Code for Analyzing Transients and Accidents in ADS", *Proc. of Topical Meeting on AccApp'00*, Washington, DC, USA (2000).

[7] Nishihara, K., *et al.*, "Neutronics Design of Accelerator-driven System for Power Flattening and Beam Current Reduction", *J. Nucl. Sci. and Technol.*, 45, 8, 812-822 (2008).

Optimisation of the EFIT fuel design

Vitaly Sobolev, Wim Uyttenhove
Studiecentrum voor Kernenergie•Centre d'Étude de l'Énergie Nucléaire (SCK•CEN), Belgium

Werner Maschek, Andrei Rineiski, Xue-Nong Chen
Karlsruher Institut für Technologie (KIT), Germany

Jan Wallenius, Andrei Fokau
Kungliga Tekniska Högskolan (KTH), Sweden

Fabienne Delage
Commissariat à l'énergie atomique (CEA), France

Abstract

The minor actinides (MA) accumulated in the spent nuclear fuel of LWR are considered as very hazardous nuclear waste. One of potential options of their neutralisation is a transmutation in accelerator-driven systems (ADS). In the framework of the integrated project EUROTRANS (the 6th Framework Programme of EURATOM) the European Facility for Industrial Transmutation (EFIT) of MA is being developed. One of the most important issues in this project is design and optimisation of the fuel dedicated to MA transmutation. Two composite fuel candidates: cercer with MgO-matrix and cermet with Mo-matrix, both with (Pu,Np,Am,Cm)O_{2-x} fuel particles, were selected for detailed study and optimisation. In the adopted strategy of MA burning it was postulated that the Pu balance has to be close to zero by the end of fuel residence time. In order to fulfil this requirement, the composition of both candidates, the fuel element design and the cycle duration in EFIT with thermal power of 400-600 MW were optimised. An option to use natural molybdenum as a matrix in the cermet fuel was also analysed, with the aim to reduce fuel costs.

Introduction

Plutonium (Pu) and the minor actinides (MA), such as neptunium (Np), americium (Am) and curium (Cm), accumulated in the spent nuclear fuel of LWR are very hazardous components of long-life nuclear waste. Different options are considered in different countries to manage them. One of promising solutions is to use Pu in the form of Pu-U mixed-oxide fuel (MOX) in power reactors and to burn MA in the dedicated second strata subcritical accelerator-driven systems (ADS) or critical reactors.

In the European Integrated Project (IP) EUROTRANS (European Research Programme for the Transmutation of High-level Nuclear Waste in ADS), performed in the 6th Framework Programme of EURATOM, the conceptual design of the European Facility for Industrial Transmutation (EFIT) of MA is being developed [1].

The design and optimisation of the fuel dedicated to MA transmutation in EFIT are extremely important issues. Three potential strategies of Pu and MA burning were considered at the beginning: to burn both Pu and MA, to burn only MA keeping the Pu amount about constant, to transmute MA breeding Pu. Finally, the second option was chosen that allows reaching high burn-up of fuel and long-term operation of the core with reasonable changes of reactivity and power peaking factors.

Based on analysis of different fuel candidates performed at an earlier stage of the IP EUROTRANS in Domain AFTRA (Advanced Fuels for Transmutation Systems), two composite fuel systems: cercer with MgO-matrix and cermet with Mo-matrix, both with $(Pu,Np,Am,Cm)O_{2-x}$ fuel particles, were selected for detailed study and optimisation [2].

The Pu/MA ratio, the fuel element design and the cycle duration in EFIT with thermal power of 400-600 MW were optimised to obtain a Pu balance close to zero and a MA burning rate close to 42 kg TW_{th}^{-1} d^{-1} after an operation cycle from three to five years. It was also shown that the effect of the storage time on the spent fuel composition is important [3].

An option to use the natural molybdenum as a matrix in the cermet fuel was also analysed, with the aim to reduce fuel costs.

EFIT reference cores

Different variants of possible simplified reference cores of EFIT were considered in the AFTRA domain for fuel studies before the final selection was made. Two core configurations were chosen: a single-zone core for sensitivity studies, fuel optimisation and selection and a three-zone core with different fuel fraction in each zone to ensure more uniform power distribution in the radial direction and to be a prototype core for final calculations. Both variants are based on the reference mechanical design of EFIT [5] proposed in the Domain DESIGN of IP EUROTRANS to avoid jeopardising the EFIT design deviations in the AFTRA and DESIGN Domains.

The configuration of the single-zone reference core selected for parametric calculations is presented in Figure 1. A central hole for the spallation target block is composed by the withdrawal of 19 fuel assemblies from the central region. The core consists of six rings of fuel assemblies (FA), surrounded by two rings of reflector/absorber assemblies. The core is contained within a cylindrical core barrel with a wall thickness of 30 mm. For the calculations performed here, it is postulated that in the radial and axial directions the core is covered by a layer of 500 mm of liquid lead (Pb) contained within a reactor vessel. Models of the fuel assembly and a fuel element used in these calculations are presented in Figure 1. More detailed information is given in [4].

A three-zone reference core differs from that presented in Figure 1 only by subdivision of the active zone into three sub-zones: inner, middle and outer. The volume fuel fractions (fuel/matrix ratio or fuel pellet diameter) in the zones are chosen to ensure more uniform power distribution

Figure 1: Radial schematics of one-zone EFIT core model and axial schematics of FA and FE

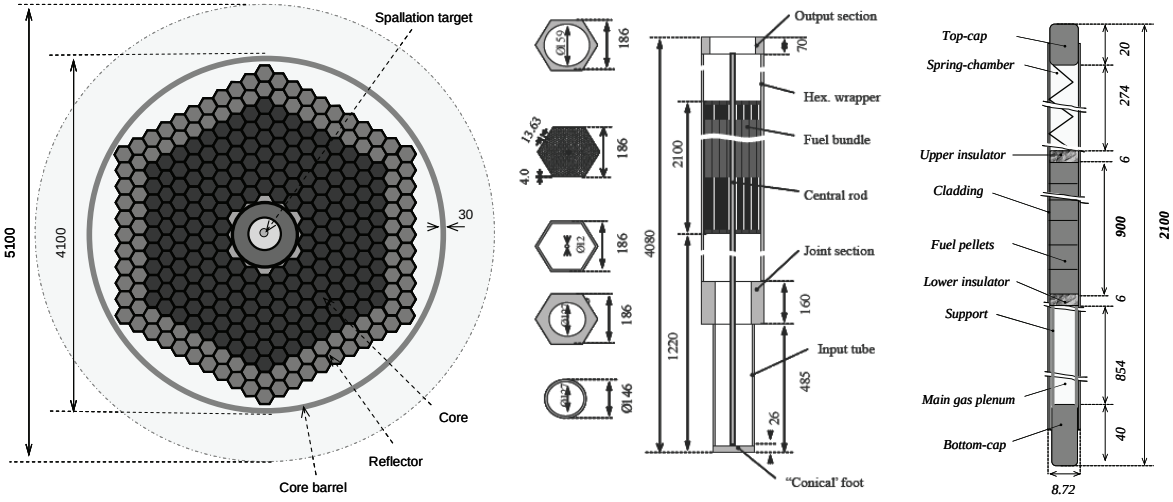

in the radial direction, keeping the initial neutron multiplication factor close to ~0.97. Two core variants: cercer and cermet, are presented in Figure 2. Fuel and reflector assemblies have the same geometric sizes in all variants, as required by the EFIT reference design [5]. The active fuel height is 900 mm.

Figure 2: Radial schematics of two three-zone EFIT cores with cercer (a) [5] and cermet (b) [3] fuels

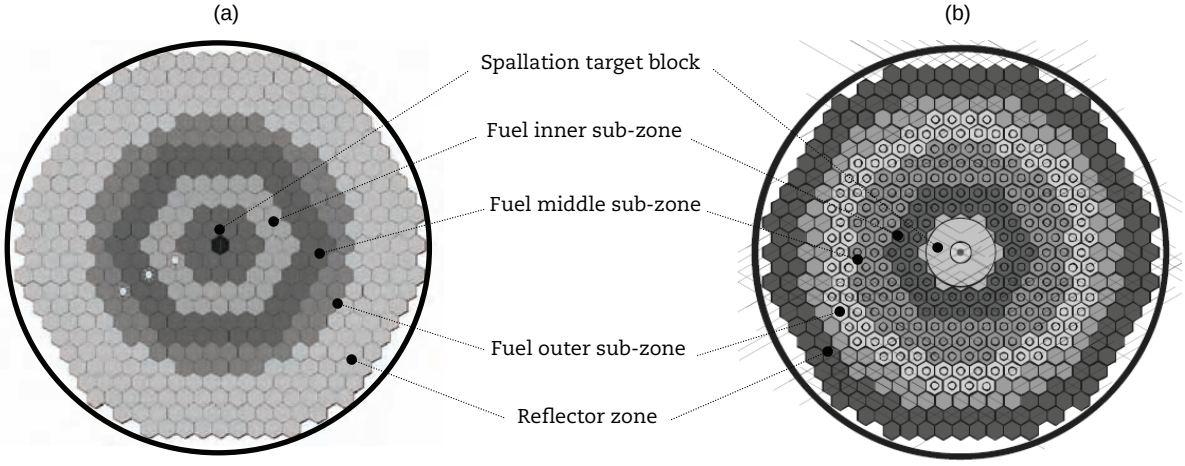

To flatten the radial distribution of power in an EFIT core a three-zone design with the variable matrix fraction was used in the EFIT with the cermet core [3]. In the cercer case both approaches were applied, the variable matrix fraction and the variable pin diameter [5].

Liquid lead (Pb) with natural isotopic composition is used as a coolant with the input temperature 400°C and the output temperature of 480°C. About 10^{-6} wt.% oxygen is dissolved in Pb, in order to assure the formation of the oxide protective layer on the outer surface of the cladding; this is neglected in neutron physics calculations.

Composite fuel

In the AFTRA domain it was assumed that the cermet pellets are made of the metallic light Mo-matrix containing uniformly distributed ceramic fuel particles with a mean diameter of 0.1 mm. The composition of the cercer pellets differs only in the matrix material: MgO ceramics are used in the place of Mo.

The selected elemental and isotopic composition and density of the cercer and cermet composites and of structure material used in the calculations are reproduced from [4]. Analysis performed in the framework of IP EUROTRANS showed that for the EFIT cores loaded with cercer fuel the optimum Pu content in fuel particles should be 43-46% of the initial heavy metal (ihma) in order to respect a requirement of non-production/consumption of supplementary Pu [6]. At the first stage the same value was adopted for cermet fuel.

The material of the fuel particles is the solid solution of $(Pu_{0.4570}Np_{0.0211}Am_{0.4986}Cm_{0.0233})O_{1.88}$. The isotopic vectors of Pu, Np, Am and Cm agreed upon in IP EUROTRANS [7] are presented in Table 1. It was assumed that all fuel particles are of 90% of the theoretical density (TD).

The Mo-matrix is made of either natural Mo or of Mo enriched in the light Mo isotopes with low neutron absorption cross-section; the Mo isotopic composition for these two cases is presented in Table 1 [8,9]. This last material of 96% TD is mentioned hereafter as "light Mo". The ceramic MgO-matrix is of 90% TD. The natural isotopic composition is adopted for both elements O and Mg.

Table 1: Isotopic composition of fuel in cercer and cermet core of EFIT

Material or element	Isotopic vector (at.%)
Fuel material	
$^{238}Pu/^{239}Pu/^{240}Pu/^{241}Pu/^{242}Pu/^{244}Pu$	3.7371/46.4457/34.1213/3.8447/11.8500/0.001
$^{241}Am/^{242m}Am/^{243}Am$	82.2387/0.2763/17.4850
$^{243}Cm/^{244}Cm/^{245}Cm/^{246}Cm/^{247}Cm/^{248}Cm$	1.5407/69.8470/26.5109/2.0600/0.0390/0.0024
Matrix material	
MgO: Mg and O	Natural Mg and O
Mo: $^{92}Mo/^{94}Mo/^{95}Mo/^{96}Mo/^{97}Mo/^{98}Mo/^{100}Mo$	
Natural	14.84/9.25/15.92/16.68/9.56/24.13/9.63
Light	86.69/8.35/3.70/1.04/0.13/0.08/0.01

The fuel pin cladding and fuel assembly structures are made of ferritic-martensitic steel T91; the typical simplified composition [10] is presented in Table 2.

Table 2: Assumed elemental composition of FMS T91 (wt.%)

	Cr	Mo	V	Nb	Mn	Si	Ni	C	Fe
T91	9.0	1.00	0.2	0.1	0.5	0.4	0.4	0.1	Balance

The fuel rod free space is filled in with the natural helium (He); the He initial pressure was assumed to be of p_{He} = 0.2 MPa at T = 300 K.

Computational tools

At SCK•CEN, cercer and cermet cores of EFIT were modelled with MCNPX [11,12] (version 2.5.0 and higher) and the Monte Carlo burn-up code system ALEPH [13,14], employing the ZZ ALEPH-LIB-JEFF3.1 [15,16], a continuous energy multi-temperature nuclear data library created at

SCK•CEN for the ALEPH code. Consistency tests have been carried out between the versions of MCNPX used during the calculations, and no difference in the results could be identified with regard to the code version.

The Monte Carlo codes [11,12,17] and nuclear data from the JEFF-3.1 evaluation [18] were also employed by KTH.

At FZK two computation options were employed: *i)* the SIMMER-III coupled neutronic and fluid-dynamics code [19]; *ii)* the DANTSYS neutron transport code [20]. The TRAIN code [21] was applied for burn-up calculations. For both FZK options, 2-D RZ homogeneous calculation models were employed.

Results

Single-zone variants of the EFIT core were used in DM3 AFTRA to study the effects of the matrix type, of the Pu fraction in heavy metal (HM) and of the geometrical parameters of the fuel pin, on the core reactivity swing and MA transmutation efficiency.

Effect of matrix on reactivity

The single-zone core with the same fuel geometry and the matrix fraction of 50 vol.% in fuel pellets were used for both cercer and cermet in order to study only the matrix effect. The variation in the main neutronic and burn-up performances during operation time of about five years was modelled in order to determine the effect of the matrix on the core reactivity swing and efficiency of MA incineration.

The main results of neutronic calculations performed at the start of operation are presented in Table 3; the number of assemblies in the core needed to obtain the desired value of the neutron multiplication factor k_{eff} close to 0.97, the calculated values of k_{eff}, the neutron multiplication factor k_s taking into account the presence of the spallation source, the source importance factor ϕ^*, the absolute neutron multiplication factor of the core with source MF and the proton beam current I_p, need to obtain the core power of 400 MW. The following formulae were used to calculate ϕ^*, MF and I_p:

$$\phi^* = \frac{k_s\left(1-k_{eff}\right)}{k_{eff}\left(1-k_s\right)} \qquad MF = \frac{1}{1-k_s} \qquad P_{core} = I_p \cdot Y_{sp}\frac{MF}{\nu}\cdot E_f$$

where Y_{sp} is the neutron yield of the spallation source per incident proton, ν is the mean neutron yield per fission and E_f is the fission energy deposited in the core.

From Table 3 it can be seen that the neutron multiplication factors of the one-zone cermet core with the fuel matrix made of the natural Mo is significantly lower than those of the equivalent reference one-zone cercer core, resulting in an almost four times higher proton beam current needed to obtain the core thermal power of 400 MW. This is mainly due to a high neutron absorption cross-section of ^{95}Mo and heavier isotopes of Mo. Taking into account that the core diameter is limited, it was proposed to use "light" Mo (enriched in ^{92}Mo) for the cermet matrix (see Table 1; this material is produced at laboratory scale [9]). This allowed to significantly increase the neutron multiplication factor of the cermet core (column 2 of Table 3) and to obtain about the same neutron parameters as those of the reference cercer core but with a fewer number of fuel assemblies (180 instead of 198).

The core power form factor in both one-zone cores is higher than the value of ~1.3 targeted for an industrial prototype, therefore a three-zone core design was proposed for both EFIT variants. In the case of the cercer core different matrix fractions were used in three zones to flatten the radial power distribution; the thicker (but the same in all three zones) fuel rods were adopted to

Table 3: Effect of matrix on the neutron multiplication in the single-zone cercer and cermet core of EFIT-400 (AFTRA); Pu content in HM is 45.7 at.%, clad thickness is 0.6 mm

	Cermet			Cercer	
Column no.	1	2	3	4	5
Number active sub-zones	1	1	3	1	3
Matrix material	**Natural Mo**	**Light Mo**	**Light Mo**	**MgO**	**MgO**
Number of assemblies: inner sub-zone middle sub-zone outer sub-zone	198	180	216 42 90 84	198	180 42 66 72
Matrix volume fraction (%) inner sub-zone middle sub-zone outer sub-zone	50	50	 65 57 50	50	 57 50 50
Fuel rod/pellet diameters (mm): inner sub-zone middle sub-zone outer sub-zone	8.72/7.2	8.72/7.2	 9.52/8.0 9.52/8.0 9.52/8.0	8.72/7.2	 8.62/7.1 8.62/7.1 9.52/8.0
Core power radial form-factor	–	1.61	1.32	1.57	1.39
k_{eff}	0.91401	0.97528	0.97975	0.97274	0.97373
k_s	0.86366	0.9596	0.95480	0.95864	0.94622
Source importance (ϕ^*)	0.5960	0.6020	0.4366	0.6495	0.4747
Source multiplication factor (*MF*)	6.33	23.75	22.12	23.18	18.59
Proton beam current (mA) (to obtain P_{core} = 400 MW_{th})	41.0	10.9	12.6	11.2	15.2

compensate for the reduction of the fuel fraction in the pellets of the inner and middle zones (see column 3 of Table 3). In the three-zone cermet core the matrix fraction was reduced only in the inner zone, and this reduction was compensated for by increasing the fuel pellet diameter only in the outer zone (see column 5 of Table 3). Thus the core power form factor was reduced to 1.32 for the cermet core and to 1.39 for the cercer core; on the other side, the needed proton beam current increased respectively from 10.9 mA up to 12.6 mA and from 11.2 up to 15.2.

The simulation of the long-term behaviour of two single-zone variants of the EFIT-400 core with the basic cercer and cermet fuels described above indicates that they exhibit a very different variation of the neutron multiplication factor with burn-up (Figure 3).

During the first two to three years of operation the value of k_s for the cercer core monotonically increases from 0.9587 to about 0.97. Then k_s starts to decrease and after five years of continuous operation at power 400 $MW_{(th)}$ reaches $k_s \approx 0.961$, which is close to its value at start of life. The neutron multiplication factor for the cermet core (with the light Mo matrix) constantly decreases and in five years of the nominal operation reduces to 0.911.

The higher reactivity loss with burn-up in the cermet core, compared to the cercer core, can be explained by a difference in their neutron spectra. The spectrum is harder in the cermet core, resulting in an insufficient reproduction of plutonium at the given Pu/MA ratio (~46/54). The Pu is mainly provided by a three-stage nuclear reaction starting with a neutron capture by Am followed by β-decay producing Cm, and then α-decay of Cm yielding Pu [22]. In order to increase the amount of Pu production in the cermet fuel, the fraction of Am in fuel particles should be increased (i.e. Pu/Am ratio should be reduced). It was therefore proposed to consider a cermet fuel with a lower than 46% Pu content in HM (taking into account that the initial Np/Am/Cm ratio and the actinide isotopic vectors are fixed by design [7]).

An option to use natural molybdenum in the cermet fuel was also analysed using the single-zone EFIT (AFTRA) core models, aiming at the reduction of costs of the fuel itself and of the fuel cycle. The replacement of the enriched Mo by the natural Mo in the cermet fuel significantly

Figure 3: Reactivity evolution of the cercer and cermet cores of EFIT-400 (AFTRA) during long-term operation

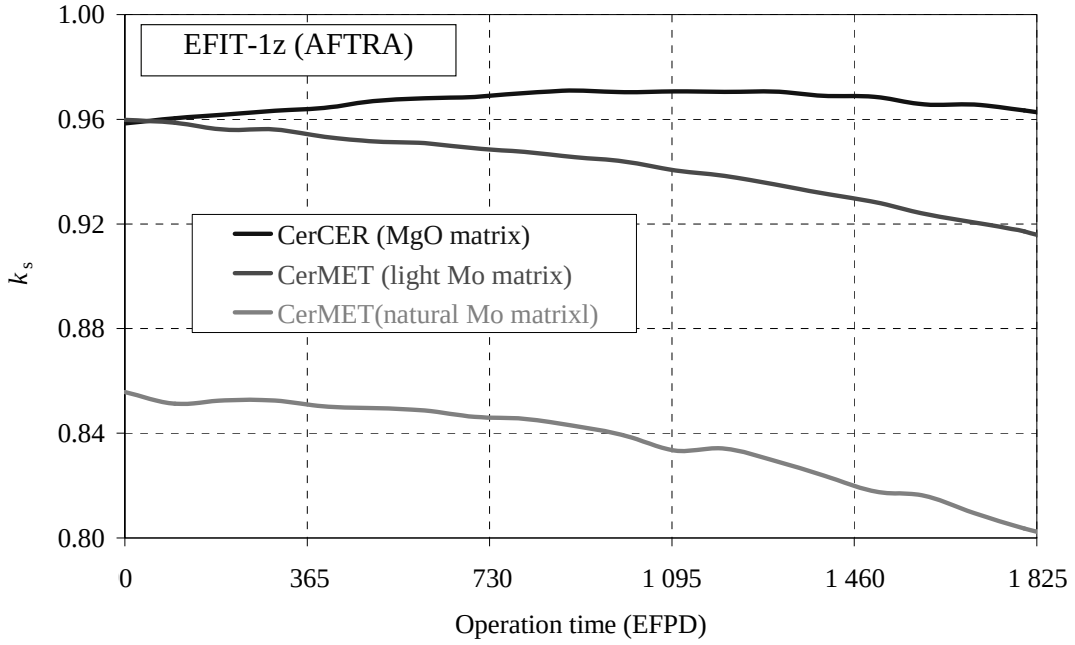

reduces the core initial reactivity level (from $k_s \approx 0.96$ to $k_s \approx 0.86$ – Table 3). However, the magnitude of the reactivity swing and its time dependence during long-term operation is almost the same as in the case of the Mo matrix enriched in the light isotopes (Figure 3).

Correlation between evolution of the core power form-factor and the reactivity

The power form factor of a subcritical core increases with decreasing core neutron multiplication factor (k_{eff} or k_s). This effect at the beginning of the fuel life in a cermet core was demonstrated in [7]. Figure 4 presents the evolution of k_s and the radial power form-factor (K_R) with operation time for both cercer and cermet one-zone cores considered in the previous section.

It can be seen that a change in k_s strongly affects K_R. In both cores the general tendency is that K_R increases with the reduction of k_s and vice versa, however, their quantitative changes are different. In the cercer core the maximum value of $K_R = 1.586$ is at the start of life. In the cermet core K_R increases with time with decreasing k_s; its value increases from 1.608 at start-up to about 1.83 after five years (1 825 d) of nominal operation. This effect produces a permanent increase in the linear power of the hottest cermet fuel rods with the operation time that can result in increased temperatures of fuel, cladding and coolant in the hottest fuel assemblies.

Effect of matrix on Pu burn-up and MA transmutation

The Pu and MA mass change in the above-considered cercer and cermet single zone cores of EFIT with the operation time is presented in Figure 5. Their evolution is very similar in both cases: while the amount of Pu and Am, and to a lesser extent Np, decreases with time, the amount of Cm increases.

After five years of operation of the cercer core the amount of Pu in it was reduced for 3.3% (82.9 kg), the amount of Np decreased for 19.9% (23.2 kg), the mass of Am for 27.6% (773 kg) and the mass of Cm increased for 95.7% (127 kg). Similar values for the cermet core are as follows: 5.3% (136 kg) Pu, 18.4% (21.4 kg) Np, and 27.0% (755 kg) Am disappeared and 88.3% (117 kg) Cm was produced. In both cores Cm is mainly generated due to the transmutation of Am caused by

Figure 4: Correlation between the evolution of the core radial power factor and the reactivity in the cercer and cermet EFIT cores

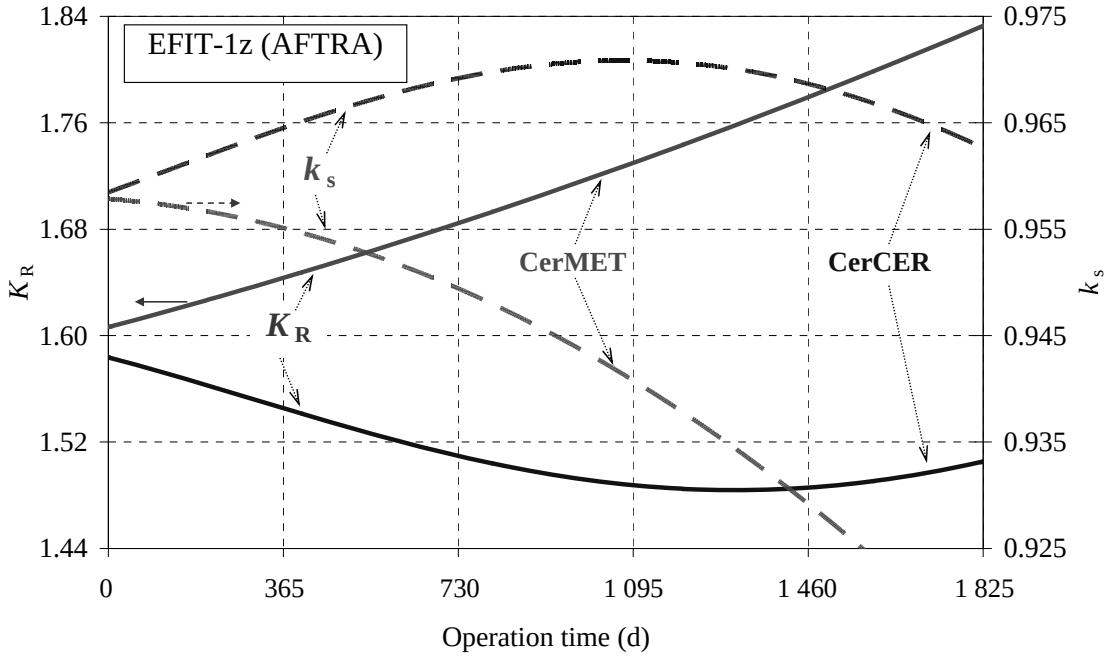

Figure 5: The change in Pu and MA mass in the cercer and cermet cores of EFIT

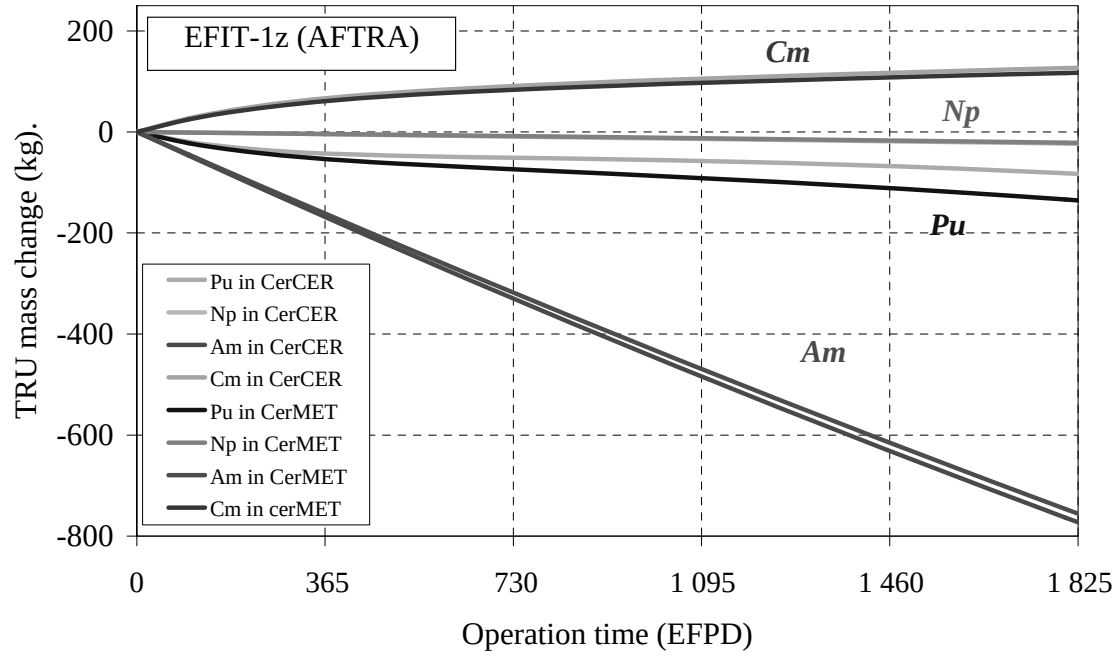

the radiative capture of neutrons followed by β decay. The net MA disappearance of 669 kg in the cercer core and 660 kg in the cermet core and the average burn-ups of 13.4% and 14.2% of the initial heavy metal atoms respectively are achieved after five years of nominal operation.

In both cases, cercer and cermet, the energetic efficiency of the MA transmutation at the beginning of life is about twice as low as the targeted value of 42 $kg_{(MA)}/TWh_{(th)}$ (see Figure 6). At the

Figure 6: Evolution of the energetic efficiency of Pu and MA burning in the cercer and cermet during long-term operation

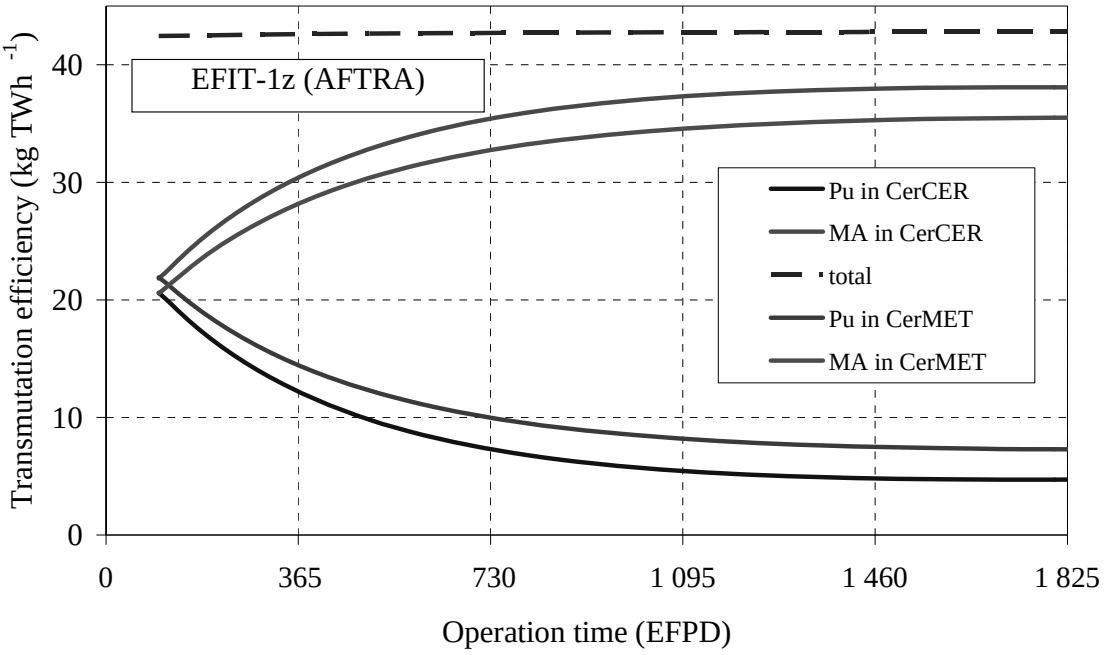

start of operation, the value of the energetic efficiency of the MA transmutation is close to the energetic efficiency of Pu consumption. For both cercer and cermet, the MA transmutation efficiency increases with the operation time, but at a slightly higher rate in the cercer core. After five years of operation it reaches 38.1 $kg_{(MA)}/TWh_{(th)}$ in the cercer core and 35.5 $kg_{(MA)}/TWh_{(th)}$ in the cermet core. During this period the efficiency of the Pu consumption reduces with time due to the Pu reproduction by the nuclear reactions starting with neutron capture by Am.

Effect of Pu-to-MA ratio on reactivity swing

In order to study the effect of varying Pu content on the core reactivity swing and on the efficiency of MA incineration, three fuel cases were considered: with 35, 40 and 46 wt.% Pu in HM; in all cases cermet fuel with the light Mo matrix was used. The active fuel length was fitted in the range of 90-130 cm in order to have comparable values of k_s in all three cases. The fuel power density in a core was chosen the same as in the reference cercer case. Figure 7 shows the evolution of k_s as a function of the operation time. The reactivity swing is strongly positive in the case of the fuel with 35 wt.% Pu in HM. In the case of 40 wt.% Pu the reactivity swing over five years is also positive but rather small in magnitude and the maximum variation of the reactivity during the operation time is close to that of the reference cercer core. In the case of 46% Pu in HM, the reactivity swing is strongly negative. Thus, from the point of view of the reactivity swing, the optimum Pu content in HM of the cermet fuel is close to 40 wt.%.

Effect of Pu/MA ratio on Pu and MA transmutation

The change in the Pu and MA mass in the single-zone EFIT core loaded with cermet fuels containing 35, 40 and 46 wt.% Pu in HM is presented in Figure 8. In the case of 35 wt.% Pu, the reproduction of Pu during the second year of operation becomes larger than its consumption; 3.7% of Pu is accumulated and 24.2% of MA is incinerated on average by the end of the fifth year. In the core containing cermet with 40 wt.% Pu in HM the Pu balance is slightly negative: -1.25% Pu at the end of operation.

Figure 7: Reactivity evolution of the cermet cores with 35, 40 and 46% Pu in HM at a constant power density

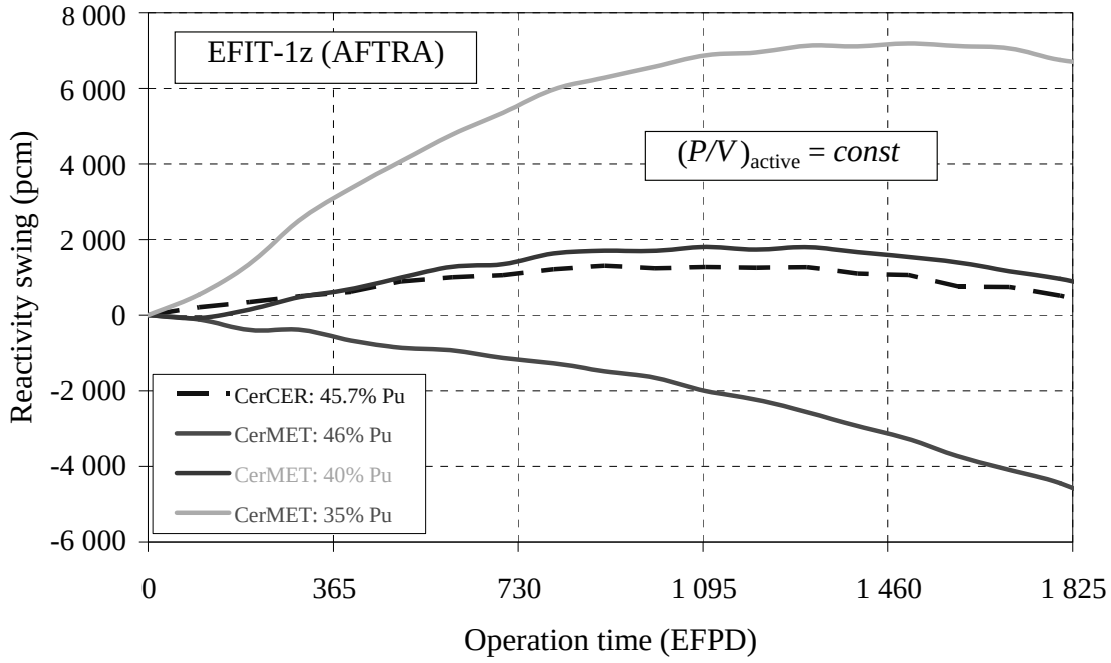

Figure 8: Change in the Pu and MA mass in the EFIT core loaded with cermet fuels containing 35, 40 and 46 wt.% Pu in HM

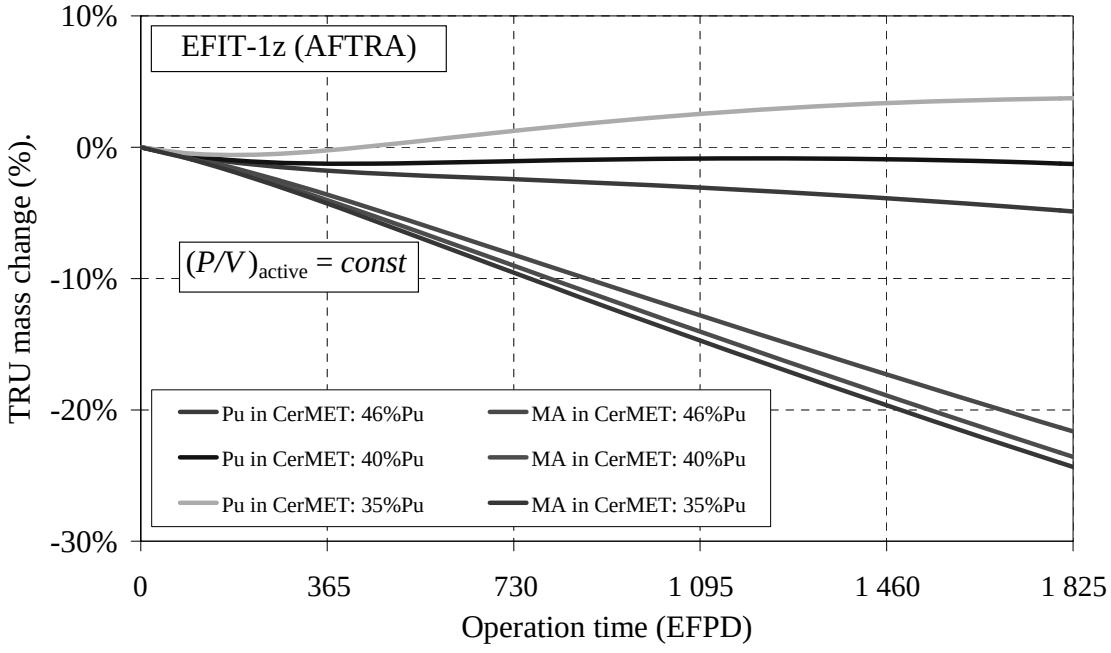

The energetic efficiency of the MA and Pu transmutation as a function of the operation time for the above-mentioned three cermet cases is presented in Figure 9. The maximal consumption (46.7 $kg_{(MA)}/TWh_{(th)}$ after five years) is in the case of 35 wt.% Pu. However, the production of Pu reaches 3.9 $kg_{(MA)}/TWh_{(th)}$. The case with 40 wt.% Pu in HM is almost optimal from the point of

Figure 9: Evolution of the energetic efficiency of Pu and MA burning in the EFIT core loaded with cermet fuels containing 35, 40 and 46 wt.% Pu in HM

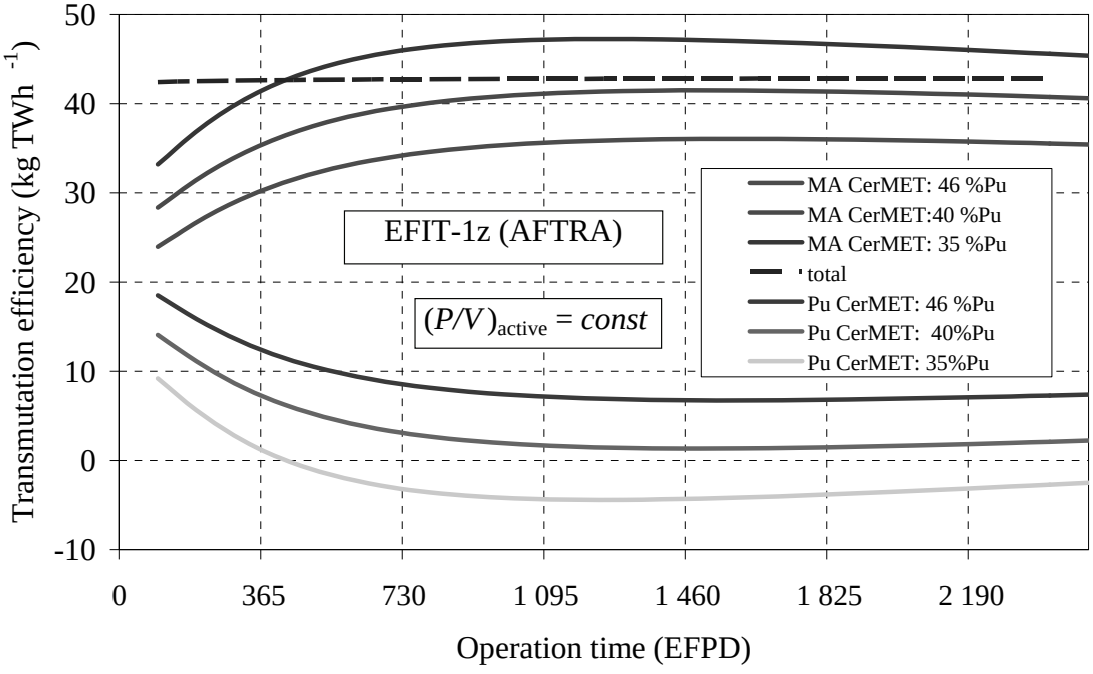

view of the adopted strategy (to have a Pu balance close to zero and the efficiency of MA transmutation close to 42 $kg_{(MA)}/TWh_{(th)}$) among the three considered cases. After five years of operation the Pu balance is -1.25% and the energetic efficiency of the MA transmutation is 41.4 $kg_{(MA)}/TWh_{(th)}$.

These results demonstrate that the "optimum" content of the plutonium in the cermet fuel of EFIT from the point of view of the minimum reactivity swing, the power form factor and Pu balance is close to 40% Pu in HM, depending on the cycle duration. However, in order to reach the targeted value of k_s ~ 0.96 at the start of cycle the amount of fuel in the core must be increased.

Quasi-optimised cermet case

After determination of the optimal Pu/MA ratio for the cermet fuel particles, the cermet fuel rod design for the single zone EFIT was slightly modified without jeopardising the EFIT core reference design: the fuel pellet diameter was increased up to 7.80 mm in order to increase the amount of fuel in the core needed to obtain the aimed value of k_s ~ 0.96. The inner and outer diameters of the cladding were increased to 8.12 mm and 9.32 mm, respectively. No changes in the fuel assembly geometrical sizes were made. The evolutions of k_s, K_R and the efficiency of MA and Pu consumption in this cermet core are presented in Figures 10-12.

Figure 10 shows that, for the given quasi-optimised cermet fuel composition and fuel power density, the optimal residence time is about four years (from the point of view of the reactivity variation), i.e. one year shorter that for the cercer reference core. The variation of the radial power form factor of the cermet core loaded with the fuel containing 40 wt.% Pu in HM, and its correlation with k_s, is also illustrated in this figure. One can see that the K_R behaviour is very similar to that of the cercer core: the maximum value of K_R is observed at the start of life.

Figure 10: Correlation of the radial power form factor with reactivity in the EFIT-400 core loaded with the cermet fuel containing pellets of 7.8 mm diameter and 40 wt.% Pu in HM

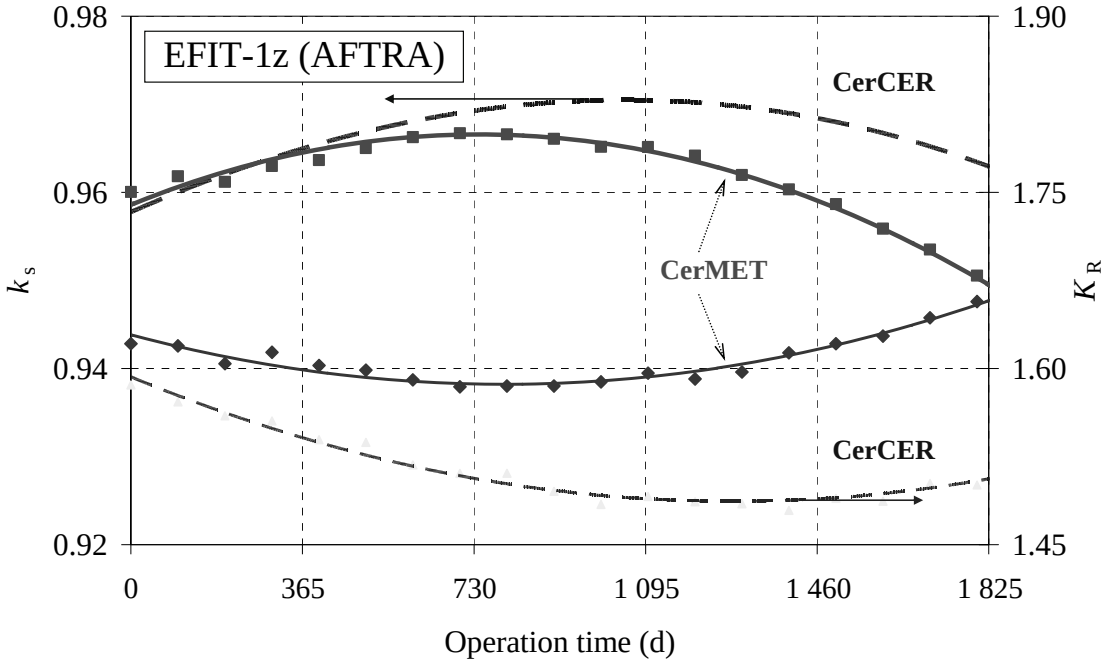

Figure 11: Change in the Pu and MA mass in the EFIT core loaded with cermet fuel containing pellets of 7.8 mm diameter and 40 wt.% Pu in HM

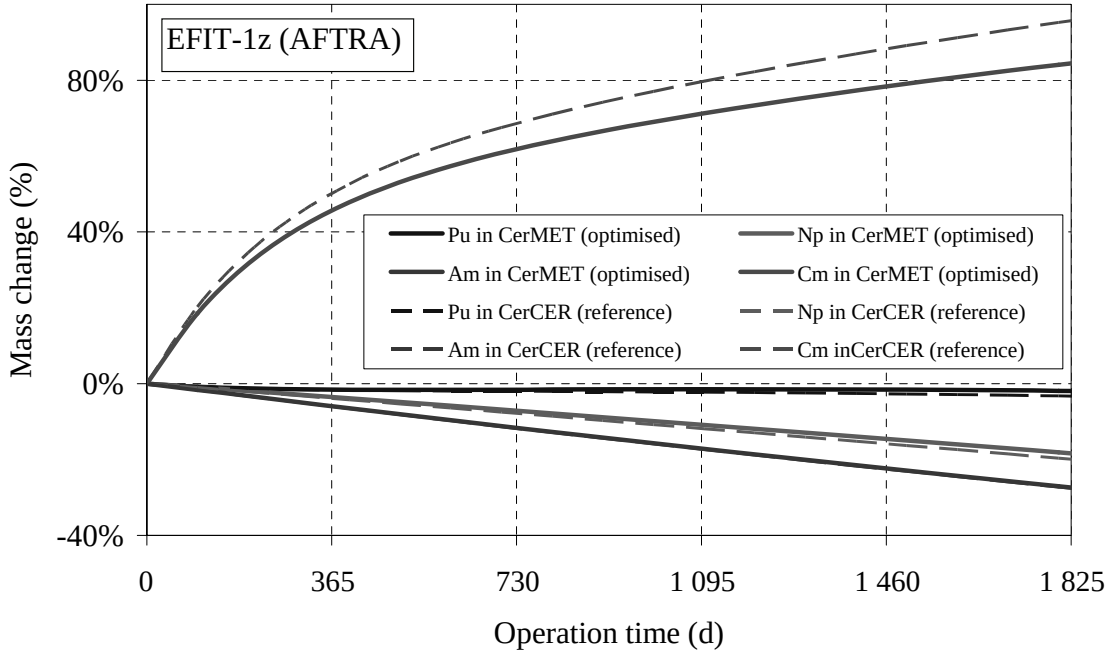

Figure 12: Evolution of the energetic efficiency of Pu and MA transmutation in the single-zone core of EFIT loaded with cermet fuel pellets of 7.8 mm diameter and 40 wt.% Pu in HM

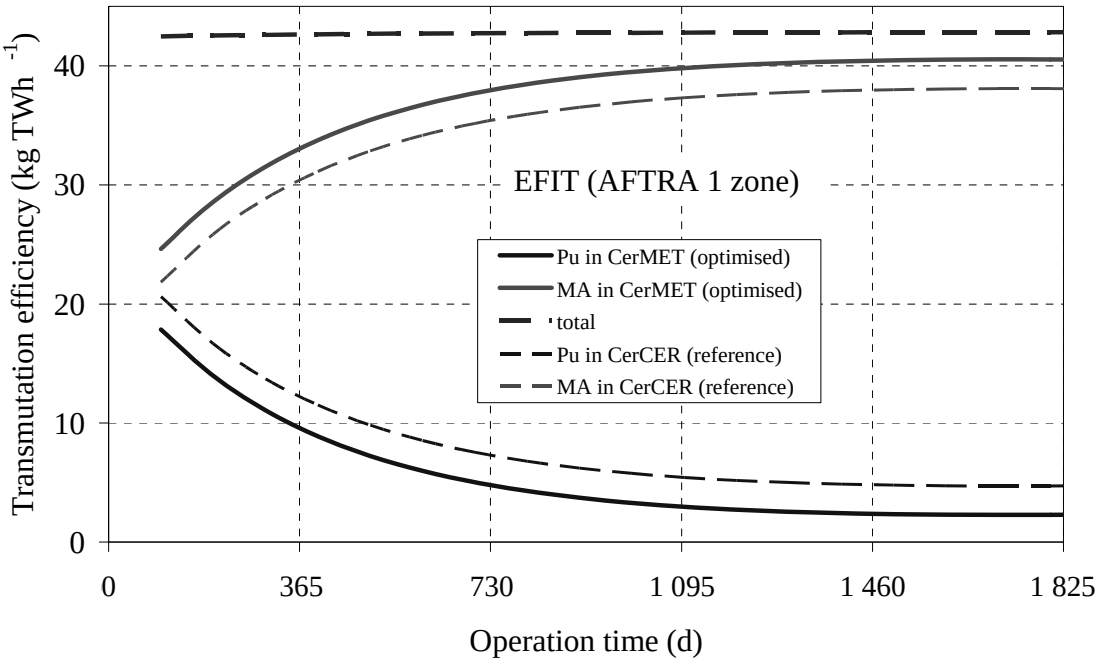

Moreover, more Cm is generated in the cercer core (Figure 11), and the efficiency of MA incineration and the Pu balance of the core with this cermet fuel after four years is higher than for the reference cercer core (see Figure 12). Further optimisation of the Pu content and the pellet diameter can be performed to better adapt the fuel design to the EFIT specifications on the Pu burn-up and MA transmutation.

About the same results were obtained for an EFIT core loaded with cermet fuel containing the same fuel particles (40 wt.% Pu in HM) in the natural Mo matrix. However, the active length of the core was increased almost by a factor of 2 to obtain k_s close to 0.96 [3].

Discussion

The results presented above on EFIT fuel optimisation were obtained with a single zone variant of the core. Supplementary modelling showed that all results obtained for these cores can be extended with minor corrections to three-zone cores.

Due to a lower Pu/MA ratio, the optimised cermet core requires more fuel than the reference cercer core. So as to avoid jeopardising the thermo-hydraulic performance of the core, a variant of the fuel assembly design with a smaller number of thicker cermet fuel pins was proposed and analysed at KIT [3,7]. It was shown that with this option, all earlier problems experienced in EFIT pertaining to cermet fuel can be overcome. Increasing the pin diameter is possible due to significantly higher thermal conductivity of cermet as compared with the cercer composite.

The main disadvantage of the larger cores is a lower efficiency of the spallation neutron source. To bypass this difficulty, a more dense fuel and less absorbing light matrices should be considered. A compact EFIT core with dense nitride fuel, lead-bismuth eutectic coolant (with about 200°C lower melting temperature than Pb) and a 15-15 Ti type austenitic steel for the fuel cladding was proposed and analysed by KTH [25]. Due to the good neutron economy of nitride fuel, the EFIT active zone was reduced and the proton source efficiency was increased. Additionally, it was shown that two times lower coolant void worth compared to the reference

core can be obtained. The most important problems concerning the nitride fuel (that have yet to be resolved) are difficulties related to fabrication of MA-based inert matrix nitride fuels with densities higher than 85% TD and its instability under irradiation [2]. At the moment nitride fuel can be considered only as a potential variant for applications far in the future, once the difficulties mentioned above have been solved.

Conclusions

Neutronic analysis of the EFIT cores with composite cercer (MgO matrix) and cermet (light Mo matrix) fuels selected in IP EUROTRANS for MA transmutation was performed with the objective to optimise the performance of the cermet core. The effects of matrix and Pu fraction variations on the reactivity swing and MA transmutation efficiency in the EFIT core were analysed under nominal operation conditions for a cycle length up to five years. An optimised cermet fuel composition option was proposed with lower Pu/MA ratio (~40 wt.% Pu in HM in the place of ~46 wt.%), in order to reduce the reactivity swing and to optimise the energetic efficiency of Pu and MA transmutation. The reduction of the core reactivity related to the reduction of the Pu content in HM was compensated for by slightly thicker fuel pins. It was demonstrated that this optimised variant of the EFIT cermet core has slightly better transmutation performance compared to that of the reference cercer core.

Finally, it can be concluded that both fuels – cercer and cermet with light Mo matrix – are capable of satisfying the main neutronic design criteria of EFIT at normal operation and of achieving the acceptable neutronic and MA transmutation performances. Nitride fuel can be considered as a potential variant for the distant future.

Acknowledgements

This work was performed in the framework of IP EUROTRANS of the 6th EURATOM Framework Programme with the financial support of the European Commission, the Belgian Nuclear Research Centre SCK•CEN, Karlsruhe Institute for Technology (Germany) and the Royal Institute of Technology KTH (Sweden).

References

[1] *Integrated Project EUROTRANS, Annex 1 – Description of Work*, Contract No. FI6W-CT-2004-516520, EURATOM FP6, March (2005).

[2] Wallenius, J., *et al.*, *Selection of the Preliminary Fuel Candidate for DM1*, Deliverable D3.7, FP6 IP EUROTRANS, Contract No. FI6W-CT-2004-516520, EURATOM FP6, February (2006).

[3] Rineiski, A., *et al.*, *Comparison of the Neutronic Performances of the ETD Reference Core Loaded with the Selected TRU-fuels from BOL to EOL*, Deliverable D3.3, FP6 IP EUROTRANS, Contract No. FI6W-CT-2004-516520, EURATOM FP6, March (2010).

[4] Sobolev, V., *et al.*, *Neutronic Performances of EFIT-400 (AFTRA) Reference Cores at the Beginning of Operation*, Intermediate Technical Report, Deliverable D3.2, EURATOM FP6, IP EUROTRANS, Contract No. FI6W-CT-2004-516520, August (2007).

[5] Corsini, G., M. Petrazzini, *Main Components Functional Sizing of EFIT*, Deliverable D1.24, FP6 IP EUROTRANS, Contract No. FI6W-CT-2004-516520, EURATOM FP6, November (2006).

[6] Artioli, C., *Specification for the EFIT Core and Fuel Element*, Deliverable D1.6, FP6 IP EUROTRANS, Contract No. FI6W-CT-2004-516520, EURATOM FP6, November (2006).

[7] Rimpault, G., *et al.*, *Definition of the Detailed Missions of both the Pb-Bi Cooled XT-ADS and Pb Cooled EFIT and its Gas Back-up Option*, Deliverable D1.1, FP6 IP EUROTRANS, Contract No. FI6W-CT-2004-516520, EURATOM FP6, December (2005).

[8] Commission on Atomic Weights and Isotopic Abundances, report for the International Union of Pure and Applied Chemistry in: *Isotopic Compositions of the Elements 1989, Pure and Applied Chemistry* (1998).

[9] F. Klaassen, private communication.

[10] Haarmann, K., *et al.*, *The T91/P91 Book*, Vallourec & Mannesmann Tubes (1999).

[11] Pelowitz, D.B., *MCNPX, Version 2.6.a, Extensions*, Tech. Rep. LA-UR-05_8225, Los Alamos National Laboratory, USA (2005).

[12] Pelowitz, D.B., *MCNPX Version 2.5.0. User's Manual*, Tech. Rep. LA-CP-05-0369, Los Alamos National Laboratory, USA (2005).

[13] Haeck, W., B. Verboomen, "An Optimum Approach to Monte Carlo Burn-up", *Nucl. Sci. and Engineer.*, 156, 180-196 (2007).

[14] Haeck, W., *et al.*, "ALEPH – A Monte Carlo Burn-up Code", *12th International Conference on Emerging Nuclear Energy Systems (ICENES 2005)*, Brussels, Belgium, 21-26 August (2005).

[15] Haeck, W., B. Verboomen, *Verification and Validation of a Multi-temperature JEFF-3.1 Library for MCNP(X)*, JEF/DOC-1099, November (2005).

[16] Haeck, W., B. Verboomen, *NEA-1745 ZZ ALEPH-LIB-JEFF3.1, MCNP Neutron Cross-section Library Based on JEFF-3.1*, *www.nea.fr/abs/html/nea-1745.html* (2006).

[17] Cetnar, J., W. Gudowski, J. Wallenius, "MCB: A Continuous Energy Monte Carlo Burn-up Simulation Code", *Proc. 5th OECD/NEA Information Exchange Meeting on Actinide and Fission Product Partitioning and Transmutation*, Mol, Belgium, 25-27 November 1998, OECD/NEA, Paris (1999), pp. 523-532.

[18] Nuclear Energy Agency (NEA), *The JEFF-3.1 Nuclear Data Library. JEFF Report 21*, NEA No. 6190, OECD/NEA, Paris (2006).

[19] Kondo, Sa., *et al.*, *SIMMER-III: A Computer Program for LMFR Core Disruptive Accident Analysis*, JNC TN9400 2001-002, Japan Nuclear Cycle Development Institute (2001).

[20] Alcouffe, R.E., *et al.*, *DANTSYS: A Diffusion Accelerated Neutral Particle Transport Code System*, LA-12969-M, Los Alamos National Laboratory, USA (1995).

[21] Rineiski, A., "Decay Heat Production in a TRU Burner", *Progress in Nucl. Ener.*, 50, 377-381 (2008).

[22] Chen, X-N., *et al.*, "Parametric Studies of an EFIT Core with Cermet Fuel", *10th OECD Nuclear Energy Agency Information Exchange Meeting on Actinide and Fission Product Partitioning and Transmutation*, Mito, Japan, 6-10 October 2008, OECD/NEA, Paris (2010).

[23] Haeck, W., *et al.*, *J. Nucl. Mater.*, 352, 295-290 (2006).

[24] Chen, X-N., *et al.*, "Design and Safety Studies of an EFIT Core with Cermet Fuel", these proceedings.

[25] Fokau, A., *et al.*, "A Source Efficient ADS for Minor Actinides Burning", *Annals of Nucl. Energ.*, 37, 540-545 (2010).

Design and safety studies of an EFIT core with cermet fuel

Xue-Nong Chen[1], **Werner Maschek**[1], **Ping Liu**[1], **Andrei Rineiski**[1], **Shisheng Wang**[1], **Claudia Matzerath Boccaccini**[1], **Vitaly Sobolev**[2], **Gérald Rimpault**[3]
[1]Karlsruhe Institute of Technology (KIT), Institute for Nuclear and Energy Technologies (IKET), Karlsruhe, Germany; [2]Studiecentrum voor Kernenergie-Centre d'Étude de l'Énergie Nucléaire (SCK•CEN) Mol, Belgium; [3]Commissariat à l'énergie atomique (CEA), Cadarache Center, DER/SPRC, Laboratory of Core Development Studies, Saint Paul-lez-Durance, France

Abstract

Within the framework of the EUROTRANS programme, a European Facility for Industrial Transmutation (EFIT) is under development. This paper deals with the design and safety analyses of an EFIT core with Mo matrix-based cermet fuel. A three-zone core design was developed, which satisfies the EFIT general and specific requirements. The fuel/matrix ratio in each zone is determined for a suitable subcritical level at a k_{eff} of about 0.97 and a total power peaking factor around 1.5.

The Pu/MA ratio determines the transmutation rate and the burn-up characteristics. The initial reference value is taken as Pu/MA = 46/54 at.%. Then it is reduced down to 35/65 at.% so as to optimise the reactivity swing and the MA transmutation efficiency. The effect of reduced Pu/MA ratio on the reactivity needs to be compensated for by increasing the fuel volume fraction, which can be realised by reducing the pin number per SA and increasing the pin diameter. It is shown that the original coolant/clad thermal-hydraulic conditions can be preserved, as the pin number is reduced and the fuel volume is increased. A good transmutation efficiency and an almost zero reactivity swing have been achieved by a 61-pin arrangement with Pu/MA = 35/65 at.%.

Based on the preliminary core design, the following parametric safety studies are performed: i) impact of subcriticality on the power shape and the clad temperature in the ULOF case; ii) impact of pressure drop on ULOF. It is shown that there is an optimal point at $k_{eff} = 0.98$, where the power peaking factor and the clad temperature under the ULOF condition are minimal. The pressure drop variation shows that the core is also able to survive the ULOF under quite high pressure drop conditions.

Introduction

The European Facility for Industrial Transmutation (EFIT) is a conceptual design of an accelerator-driven transmuter (ADT) at an industrial scale. A key issue of the R&D work is the choice of an adequate fuel to be used in such an ADT. Within the EUROTRANS programme, especially in the AFTRA domain, various fuel forms have been assessed and cercer and cermet fuels, specifically the Mo and MgO matrices, have finally been selected and were under closer investigation. The final recommendation on fuels by AFTRA gave a ranking of these fuels based on a number of criteria. The composite cermet fuel $(Pu_{0.5},Am_{0.5})O_{2-x}$ – Mo (with the isotope ^{92}Mo comprising 93% of the molybdenum) has been recommended as the primary candidate for the EFIT. This cermet fuel fulfils adopted criteria for fabrication and reprocessing, and provides excellent safety margins. Disadvantages include the cost for enrichment of ^{92}Mo and a lower specific transmutation rate of minor actinides. The composite cercer fuel $(Pu,MA)O_{2-x}$ – MgO has therefore been recommended as a back-up solution as it may offer a higher consumption rate of minor actinides for a same Pu/MA ratio, and can be manufactured for a lower unit cost.

In the current investigation we concentrate on an EFIT with cermet fuel. A three-zone core design was carried out, which satisfies the EFIT general and specific requirements and especially fits into the overall Ansaldo plant design for the EFIT [1]. According to the optimisation of the minor actinides (MA) transmutation, a so-called "0-42 approach" can be achieved by optimising the Pu/MA ratio, where Pu and MA are burned at rates of ~0 and ~42 kg/TWhth, respectively [2]. Therefore the Pu/MA ratio was initially fixed at 46/54 at.% for the current cermet reference core design and the transient analyses, which is close to the optimised value 45.7/54.3 for the cercer core [2]. The fuel/matrix volume ratios are used for flattening the radial power profile with an upper limit of the fuel content of 50 vol.%. The number of subassemblies (SA) and the associated fuel/matrix ratios in three zones are determined by the plant design, for a targeted subcritical level at k_{eff} about 0.97 and a required total peaking factor around 1.5.

A study of the transmutation efficiency is made by changing the Pu/MA ratio. Generally reducing the Pu/MA ratio is favourable to the MA transmutation efficiency. But this leads to a lower subcriticality k_{eff}. To compensate for this effect, more fuel is needed in the core, where the Pu content has to be rather constant in order to maintain k_{eff} at a certain level. On the other hand the good thermal conductivity of the cermet fuel makes the fuel temperature less of a constraint, therefore allowing for thicker pins in the design. Simply increasing the pin diameter, however, will deteriorate the thermal-hydraulic performance. An optimal solution is to reduce the pin number per SA and to enlarge the pin diameter in order to obtain more fuel and an equivalent thermal-hydraulic performance. Burn-up calculations are performed by an FZK code TRAIN [3] for Pu/MA = 46/54, 40/60 and 35/65. Promising results are obtained.

The preliminary core design has been analysed with SIMMER parametrically for variation of subcriticality under operating conditions and unprotected loss of flow (ULOF) conditions and for variation of pressure drop in the ULOF case. Because of the high fuel thermal conductivity, the fuel temperature is not a concern in all of the cases investigated, but the clad temperature is generally the constraint in the core design. The variation of subcriticality shows that there is an optimal point at k_{eff} = 0.98 in this three-zone arrangement, where the power peaking factor and the clad temperature under the ULOF condition are minimal. The variation of the pressure drop shows that the core can survive a ULOF under a quite high pressure drop condition. It is concluded that the core has been designed, examined and optimised by possible parameter variations from the viewpoints of safety and transmutation.

Design of EFIT cermet core

The ADT has a subcritical core. Protons from an accelerator hit a central lead target. As the result of a spallation process, neutrons will be supplied to the core. The heat removal in the pool design

is established via forced convection flow through eight steam generators. In the past, various preliminary core design proposals were investigated in the AFTRA domain. The results have been reported in [4,5]. The current cermet three-zone core design is adapted to the most recent EFIT overall plant design by [1,2]. The cermet fuel has a high thermal conductivity and the restriction on the power density and the fuel temperature as for cercer fuel can be relaxed. This means a larger pin diameter can be chosen. To flatten the radial power profiles the "variable matrix technique" is applied. The cross-plane of the current three-zone core and the SA/pin design are schematically depicted in Figure 1. Geometric SA/pin data are given in Table 1.

Figure 1: Cross-plane of current AFTRA three-zone core and its SA and cermet fuel pin arrangement

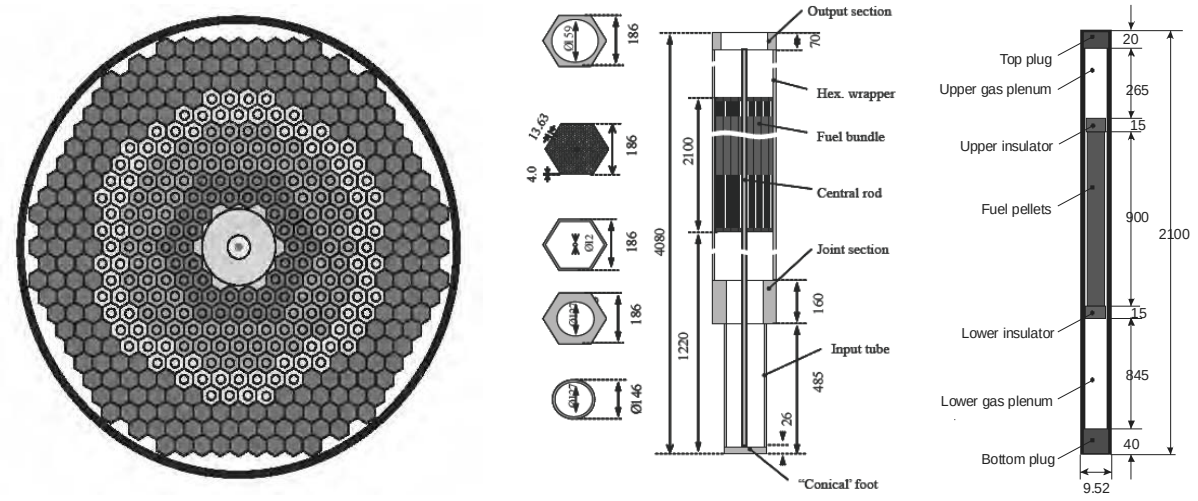

Table 1: SA and pin geometrical data

Parameter	Cercer-EFIT inner/middle zone	Cermet-EFIT	Parameter	Cercer-EFIT inner/middle zone	Cermet-EFIT
Fuel SA pitch	191 mm	191 mm	Fuel pins per SA	168	168
Wrapper inner width	178 mm	178 mm	Fuel pin pitch	13.63 mm	13.54 mm
Wrapper thickness	4.0 mm	4.0 mm	Fuel pin diameter	8.62 mm	9.52 mm
Active core height	900 mm	900 mm	Cladding thickness	0.6 mm	0.6 mm
Fuel SA number	182	216	Fuel pellet diameter	7.10 mm	8.00 mm

The main core and safety parameters are given in Table 2. The minor actinide vector of the fuel is typical for MOX fuel reprocessed 30 years after irradiation [6]. Because of the MA load, the safety parameters deteriorate: small β_{eff}, no Doppler effect and a significant coolant void worth (about +7 300 pcm). A whole core voiding has a very low probability. However a partial core voiding and reactivity addition could be triggered, e.g. by a pin failure with helium fission gas release. The calculated void worth distribution is shown in Figure 2.

Cermet fuel pellet fabrication and its thermal property measurements have been carried out in AFTRA [7]. The calibrated thermal conductivities for this three-zone design are presented in Figure 3. A T91-cladding creep test was recently carried out by CIEMAT experiments [8]. From these data one can extrapolate in a first guess the creep temperature limits for various fission gas pressures by the so-called Larson-Miller parameter, e.g. [9] for EFIT pins. The obtained creep temperature limits are shown in Table 3. Recent results [10] suggest more pessimistic data and lower limits, but have not taken into account in the current study.

Table 2: Thermal-hydraulic and neutronic parameters

Parameter	Value	Parameter	Value
Nominal thermal power	400 MW	Zone and total fuel assemblies	42 + 98 + 84 = 216
Average linear power	122 W/cm	Fuel/matrix volume ratio in three zones	35:65, 43:57, 50:50
Av. fuel volumetric power	244 W/cm^3	Pu/MA ratio	46/54 at.%
k_{eff}	0.97336	Effective beta	168.6 pcm
Void worth	7 335 pcm	Doppler constant	-68 pcm
Inlet coolant temperature	673 K	Outlet coolant temperature	753 K
Average coolant velocity	0.885 m/s	Overall pressure drop	1.1 bar (ref. value)
Axial peaking factor	1.174	Radial peaking factor	1.230
Peak pin factor	1.075	Total peaking factor	1.552

Figure 2: Void worth distribution

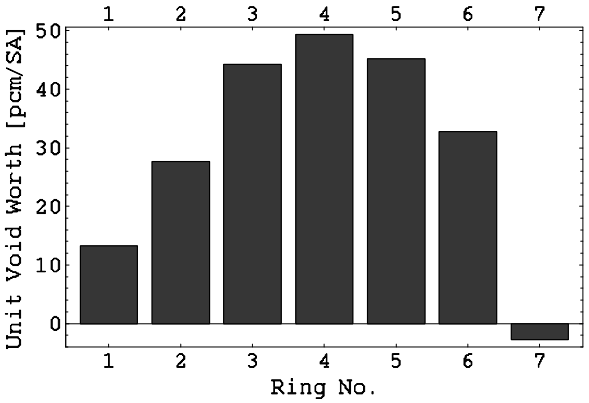

Table 3: Creep failure temperature limits in K for cermet T91 steel pin

Failure time / Gas pressure	0.1 s	1 s	10 s	2 min	30 min	10 h
1 MPa	1 342.58	1 279.97	1 222.94	1 166.83	1 111.27	1 055.66
5 MPa	1 315.21	1 253.87	1 198.00	1 143.04	1 088.61	1 034.14
10 MPa	1 281.77	1 222.00	1 167.55	1 113.99	1 060.94	1 007.85

Design and safety parametric studies

Burn-up calculations

It was shown and discussed in the past that MgO matrix (cercer) fuel is slightly better than the Mo matrix (cermet) fuel in the aspect of transmutation in the case of the same pin/SA geometry and same Pu/MA ratio [2,12]. However, the much higher thermal conductivity of cermet fuel makes a core design with thicker pins so suitable that the transmutation efficiency is improved.

A simply increase of the pin size without changing the pin number can reduce Pu/MA ratio and can consequently improve the transmutation efficiency only to some extent, because the thermal-hydraulic performance worsens in this case, e.g. the clad temperature is significantly increased, especially in the ULOF case. Therefore this is not an optimal solution. But if the pin number per SA is reduced, more fuel can be obtained without deteriorating the thermal-hydraulic/elastic performance.

Two variations of pin number are considered:

- Variation 1: To keep the coolant area, the clad thickness and the pin gap unchanged.
- Variation 2: To keep the coolant flow rate and the pressure drop unchanged and the clad thickness and the pin gap are increased proportionally to the pin diameter.

Variation 1 is straightforward. The pin diameter and the fuel volume fraction are given in Table 4. As the pin number is reduced, the pressure drop coefficient becomes smaller and therefore the thermal-hydraulic performance becomes better. But the clad/fuel thermal elastic performance becomes obviously worse. Variation 2 is not as explicit as Variation 1, but it provides truly equivalent thermal-hydraulic/elastic conditions. The constant pressure drop and flow rate conditions provide a relationship between the coolant area and the hydraulic diameter, from which the pin diameter is determined. The results are shown in Table 5. Fortunately, for a certain pin number, both variations yield roughly the same fuel volume fraction. Therefore the neutronic burn-up calculations can be performed for just one variation and the results are approximately valid for the other as well.

Table 4: Pin number Variation 1 – coolant area, clad thickness and pin gap are unchanged

Pin number per SA	Pin diameter	Hydr. diameter	Clad thickness	Gap	Fuel diameter	Fuel volume fraction
168+1 (12 mm)	9.52 mm	10.82 mm	0.6 mm	0.16 mm	8.00 mm	26.73%
127	11.00 mm	12.28 mm	0.6 mm	0.16 mm	9.48 mm	28.38%
91	13.00 mm	14.19 mm	0.6 mm	0.16 mm	11.48 mm	29.79%
61	15.87 mm	16.80 mm	0.6 mm	0.16 mm	14.35 mm	31.24%
61* out zone	16.87 mm	15.97 mm	0.6 mm	0.16 mm	15.35 mm	35.74%

Table 5: Pin number Variation 2 – coolant flow rate and pressure drop are unchanged, clad thickness and pin gap are proportional to the pin diameter

Pin number per SA	Pin diameter	Eff. hydr. diameter	Clad thickness	Gap	Fuel diameter	Fuel volume fraction
169	9.520 mm	10.87 mm	0.6 mm	0.16 mm	8.00 mm	26.88%
127	11.274 mm	11.54 mm	0.71056 mm	0.18948 mm	9.47 mm	28.34%
91	13.695 mm	12.39 mm	0.86312 mm	0.23016 mm	11.51 mm	29.96%
61	17.233 mm	13.48 mm	1.08613 mm	0.28964 mm	14.48 mm	31.80%

Burn-up calculations are performed by applying the TRAIN code [3] with nuclear data JEFF-3.1 for Variation 1. The results are shown in Table 6. Thus the reactivity swing and the transmutation efficiency can be improved by reducing the Pu/MA ratio. To maintain the same k_{eff}, almost the same Pu mass is needed. This cannot be fully realised in the case of 61 pins. Therefore we have to use even thicker pins in the outer zone to compensate for the fuel shortage.

For the original Pu/MA = 46/54 the 400 MW core has quite a large reactivity loss of 2 324 pcm after a three-year operation. Its Pu and MA consumption rates are 5.71 and 37.96 kg/TWhth, respectively. For the optimised Pu/MA = 35/65 the reactivity loss is almost zero and the Pu and MA consumption rates are -7.22 and 51.08 kg/TWhth, respectively. This means that the cermet fuel disadvantage of low transmutation efficiency can be completely overcome by using thicker pins and a lower Pu/MA ratio.

Table 6: Burn-up calculation results of pin number Variation 1

Pin number per SA	168 + 1	91	61	61 + thicker pins in outer zone
Pu/MA atom ratio over all	46/54	40/60	35/65	35/65
Power	400 MW	400 MW	400 MW	400 MW
Fuel vol. fraction in the core/the outer zone	26.73%	29.79%	31.24%	31.24%/35.75%
k_{eff} initial	0.9820	0.9724	0.9428	0.9667
k_{eff} after three years	0.9593	0.9625	0.9455	0.9660
Pu initial mass	3 055 kg	2 966 kg	2 726 kg	2 899 kg
MA initial mass	3 610 kg	4 479 kg	5 056 kg	5 377 kg
Pu consumption [kg/TWhth]	5.71	-1.06	-7.95	-7.22
U consumption [kg/TWhth]	-0.48	-0.49	-0.50	-0.51
Am consumption [kg/TWhth]	46.80	54.72	63.40	62.40
Cm consumption [kg/TWhth]	-9.70	-10.70	-12.27	-11.76
Np consumption [kg/TWhth]	0.86	0.96	0.60	0.44
MA consumption [kg/TWhth]	37.96	44.98	51.73	51.08

Effect of subcritical level on the radial peaking factor

The steady-state equilibrium can be calculated by the SIMMER code [11]. The current three-zone arrangement with the suitable fuel/matrix ratios makes the radial temperature profiles quite flat and the total peaking factor less than 1.6.

The peaking factors, especially the radial peaking factor, are strongly dependent on the subcritical level, i.e. k_{eff}. In order to investigate its influence, we fix the zone arrangement and the fuel/matrix ratios, but artificially change the macroscopic neutron generation cross-section to get the desired parametric k_{eff}. The results are presented with the radial power profiles at the core mid-plane in the left plot of Figure 3 and the total peaking factors in the right plot of Figure 3. It is well known that the peaking factor decreases as k_{eff} increases to approach one. What is shown here is that if k_{eff} is sufficiently close to one, e.g. larger than 0.98, the peaking factor stays almost constant and the peak fuel temperatures moves radially from the inner zone to the middle zone. The k_{eff} is chosen in the design for certain operational and safety reasons, but the findings here give some insight concerning the core behaviour under transient or accidental conditions, in case of a reactivity insertion. The main motivation of the study was to assess the pin failure propagation potential in the core regions with the high void worth under accidental reactivity increase conditions.

Figure 3: The radial power profiles at the core mid-plane (left) and the total peaking factors vs. k_{eff} (right)

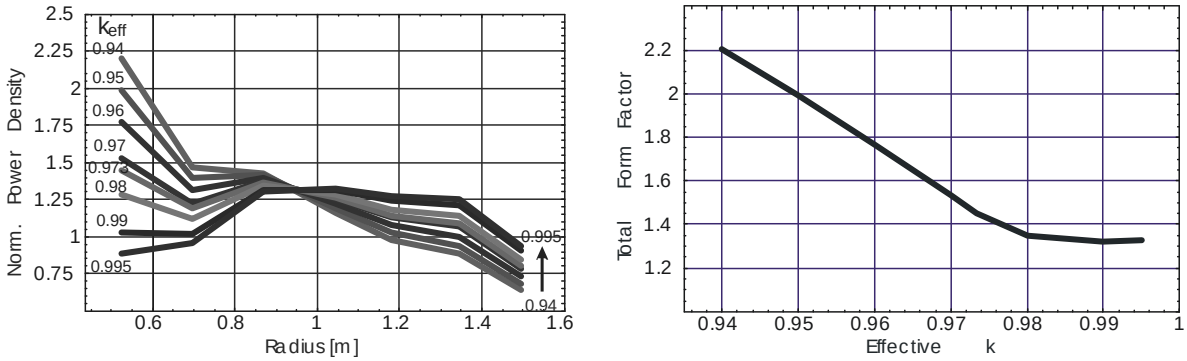

ULOF calculations

Unprotected loss of flow (ULOF) is taken as a typical accident for assessing the core safety behaviour. Favourably the core should survive this transient. As the liquid lead has good natural convection properties, after the primary coolant pump coasts down, the natural convection takes over the cooling function at a certain reduced mass flow rate. The remaining mass flow rate depends mainly on the pressure drop in the primary loop, the coolant temperature difference between the core outlet and inlet and the height of the steam generating units (SGU). The last two have been already fixed in the EFIT design, e.g. the SGU height (from core mid-plane to SGU mid-plane) is 3.7 m and the nominal temperature rise through the core is 80 K. The total pressure drop given in the Ansaldo design [1] was under discussion for a long time and therefore parametric studies have been performed to optimise the pressure drop via design of the primary pump, the steam generating units, the subassembly in- and outlets and the grid spacers in the core. To study the pressure drop influence a range of parametric values has been investigated for the total pressure drop (from 0.64 bar to 1.6 bar under operational conditions). Due to the positive coolant feedback, the power increases about 1.6-2.6% during the ULOF transient for pressure drops varying from 0.64 to 1.6 bar.

In the ULOF case, the power increase is small and the fuel temperature is not a problem. Therefore only the maximal clad temperature and the maximal coolant velocity for various pressure drops are shown in Figure 4. We see that the maximal clad temperature will stabilise after the pump coast down at 960 K in the case of 0.64 bar pressure drop and at 1 050 K in the case of 1.6 bar. The former temperature value is well below the clad safety margin and the latter value means that the pin may withstand more than half an hour without clad creep failure under a high pin gas pressure of 5 MPa, assumed as the pressure limit in the plenum (see Table 3).

Figure 4: The maximal clad temperature and coolant velocity transients for difference drops for a slow pump stop process

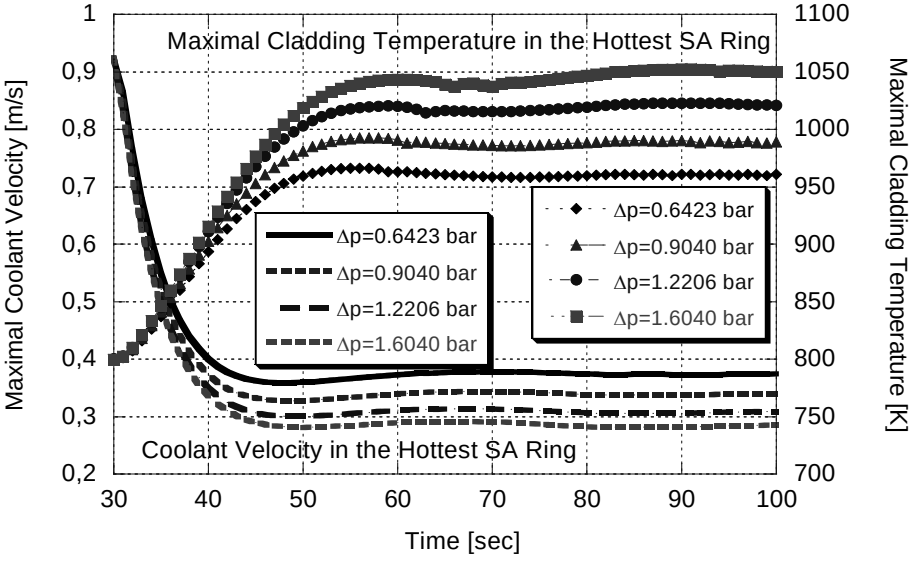

Another issue here is to investigate the influence of the subcriticality level on ULOF results. In Figure 5 the maximal clad temperature vs. k_{eff} curves are shown for the ULOF at the condition of 0.64 bar pressure drop. The maximal clad temperature has a minimum at about $k_{eff} = 0.98$. Due to the increasing peaking factor the clad temperature increases as k_{eff} decreases. Since the positive coolant feedback becomes more significant as k_{eff} approaches unity, the clad temperature will also increase as k_{eff} increases.

Figure 5: Maximal clad temperatures at steady state (lower) and in the ULOF case (upper) at the 0.64 bar pressure drop condition

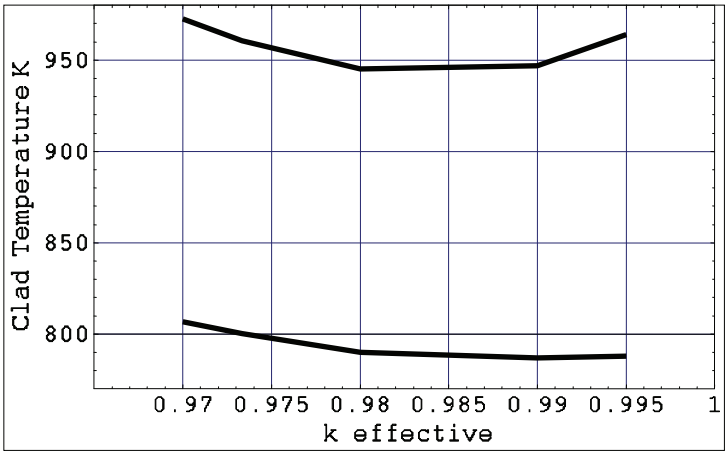

Conclusions

The conclusions of the present study are summarised as follows:

- An EFIT core with Mo matrix-based cermet fuel has been developed fulfilling the required operational and safety criteria.
- The Pu/MA ratio has been optimised for better transmutation efficiency and an almost zero reactivity swing in a three-year operation. Because the fuel temperature is not a constraint for the current design due to the high thermal conductivity of cermet fuel, the pin number reduction together with the increase in pin diameter provides an equivalent thermal-hydraulic condition, where more fuel in the core, consequently a lower Pu/MA ratio, can be realised. A cermet core can be designed with a similarly good transmutation efficiency and limited reactivity swing as a cercer core. As the fuel safety margins for cermet are very high, one could also increase the power density of the core under the condition that the clad safety limits are not violated under transient conditions.
- Parametric safety studies show there is an optimal point for the radial peaking factor and the clad temperature in the ULOF case at $k_{eff} = 0.98$.
- The cermet EFIT core can survive a ULOF transient, even under high pressure drop conditions, i.e. without short time pin creep failures.

Acknowledgements

The authors appreciate the effort and support of all the scientists and institutions involved in IP EUROTRANS, as well as the financial support of the European Commission through contract No. FI6W-CT-2004-516520.

References

[1] Mansani, L., *et al.*, *Main Components Functional Sizing of EFIT*, Deliverable D1.24, 6th Framework Programme, EUROTRANS, DM1 DESIGN (2007).

[2] Sarotto, M., C. Artioli, V. Peluso, *Preliminary Neutronic Analysis of the Three Zone EFIT-MgO/Pb Core*, EUROTRANS-DM1-WP.1.2-Task 1.2.4, FPN-P9EH-002 (2007).

[3] Rineiski, A., "Decay Heat Production in a TRU Burner", *Progress in Nuclear Energy*, 50, 377-381 (2008).

[4] Maschek, W., *et al.*, "First Results of Safety Analyses for ADTs with Cercer and Cermet Fuels Within the EUROTRANS-AFTRA Program", *Actinide and Fission Product Partitioning and Transmutation, 9th Information Exchange Meeting*, Nîmes, France, 25-29 September 2006, OECD/NEA, Paris (2007).

[5] Maschek, W., *et al.*, "Accelerator Driven Systems for Transmutation: Fuel Development, Design and Safety", *Progress in Nuclear Energy*, 50, 333-340 (2008).

[6] Sobolev, V., *et al.*, *Neutronic Performances of EFIT-400 (AFTRA) Reference Cores at the Beginning of Operation*, Deliverable D3.2, 6th Framework Programme, EUROTRANS, DM3 AFTRA (2007).

[7] Staicu, D., *et al.*, *Measurement of Thermophysical Properties of the Inert Matrix Fuels (Zr,Pu,Am) O_2 + Mo, (Pu,Am) O_2 + Mo, ($Pu_{0.2}$,$Am_{0.8}$) O_2 + MgO and ($Pu_{0.5}$,$Am_{0.5}$) O_2 + MgO*, Deliverable D3.40b, 6th Framework Programme, EUROTRANS, DM3 AFTRA (2006).

[8] Schikorr, M., D. Struwe, *Temperature Limits for XT-ADS Clad Material T91*, EUROTRANS: DM1 WP1.5 Safety Meeting, Lyon, 10-11 October (2006).

[9] Liu, P., *et al.*, "ULOF and Unprotected Blockage Accident Analyses of the 400MWth Class EFIT Accelerator Driven Transmuter with the SIMMER-III Code", *NURETH-13*, Japan (2009).

[10] Fazio, C., "Progress in Structural Materials for Transmutation Devices", *Euratom PARTRA Cluster Meeting*, FZK, Karlsruhe, Germany, February 25-26 (2008).

[11] Maschek, W., *et al.*, "SIMMER-III and SIMMER-IV Safety Code Development for Reactors with Transmutation Capability", *M&C 2005*, Avignon, France (2005).

[12] Rimpault, G., *Caracterisation neutronique de l'avant-projet de coeur de systeme sous-critique Pb-EFIT*, CEA Report, SPEC/LEDC/09-402 (2009).

Fuel rod performance analysis for the Italian LBE-XADS: A comparison of two different cladding materials

Federico Agosti, Pietro Botazzoli, Valentino Di Marcello, Lelio Luzzi, Giovanni Pastore
Department of Energy – Enrico Fermi Center for Nuclear Studies (CeSNEF)
Politecnico di Milano
Milan, Italy

Abstract

In this paper, fuel rod performance analyses are presented for the Italian 80 MW_{th} XADS (Experimental Accelerator-driven System). This subcritical system is cooled by lead-bismuth eutectic (LBE), which rises on average from 300°C to 400°C at the core exit, and is fuelled with UO_2-PuO_2 mixed-oxides. Both the ferritic-martensitic T91 and the austenitic AISI 316L steels have been considered as cladding materials, and the overall fuel rod behaviour has been simulated under normal operation conditions from the beginning to the end of life. In order to point out some critical issues related to the two steels, thermo-mechanical analyses have also been accomplished at extended burn-up. Moreover, a sensitivity study has allowed evaluating the role of some significant aspects on fuel rod performance. Calculations have been carried out by means of the TRANSURANUS code, which has been recently adapted for modelling the behaviour of T91 and AISI 316L in an LBE environment (with in situ oxide layer protection), and three different coolant channels representative of the XADS core have been considered. For the demanding operating conditions of the hot channel (HC), analysis has indicated that corrosion effects would significantly degrade the entire thermo-mechanical performance of fuel rods without the adoption of appropriate protective coatings. The HC fuel rod with T91 cladding exhibits a better performance with respect to the AISI 316L rod in terms of swelling strain, maximum fuel temperature, fission gas release and inner pressure, but the resistance of T91 to radiation embrittlement and creep requires further investigation, especially under closed gap conditions [fuel cladding mechanical interaction (FCMI)].

Introduction

Innovative concepts of nuclear reactors often involve quite demanding operating conditions, such as extended exposure to neutron irradiation, high temperatures and corrosive environment, offering challenges to engineers and designers on structural and cladding materials selection. Among the next generation reactors, systems cooled by heavy liquid metals (HLM) are proposed, such as the lead fast reactors (LFR), acknowledged in the scope of the Generation IV International Forum [1], and the accelerator-driven systems (ADS) [2], which are cooled by lead or LBE and are conceived for the purpose of nuclear waste incineration. Historically, the primary material for fast reactor fuel claddings was AISI 316L stainless steel, which successfully operated in the sodium-cooled Superphénix reactor. Ferritic-martensitic steels such as T91 (modified 9Cr-1Mo) are considered nowadays for in-core applications in HLM fast reactors, mainly due to their excellent irradiation resistance to void swelling compared to austenitic stainless steels [3]. However, few studies have been accomplished up to now for assessing the in-reactor performance of T91, such that uncertainties exist on its behaviour under irradiation (e.g. embrittlement, swelling, creep) [4].

In this paper, analyses of fuel rod performance are presented for the Italian 80 MW_{th} XADS [2], for which a complete, consistent design is available [5]. This subcritical system is cooled by LBE, which rises on average from 300°C to 400°C at the core exit, and is fuelled with UO_2-PuO_2 mixed-oxides. The in-reactor performance of T91 and AISI 316L claddings is analysed and compared in terms of the overall fuel rod behaviour. Simulations have been carried out, from the beginning to the end of life, under normal operation conditions and with *in situ* oxide layer protection [6] against corrosion. Extension of the irradiation time has also been taken into account, and the thermo-mechanical fuel rod behaviour has been investigated focusing on the fuel-cladding gap evolution. This analysis may give some indications for other HLM fast reactors, such as the lead-cooled European Lead-cooled System (ELSY) [7] and European Facility for Industrial Transmutation (EFIT) [8], which employ the T91 steel as cladding material. For a better assessment of critical issues potentially affecting the fuel rod performance in HLM-cooled nuclear systems, a sensitivity analysis has been carried out by investigating some modelling aspects on which uncertainties exist. In particular, different correlations for heat transfer to LBE, a different treatment of the AISI 316L swelling, as well as the effect of the adoption of protective coatings compared to *in situ* oxide layer protection, have been considered.

Since the fuel rod behaviour is determined by the synergy of several phenomena (heat transfer to the coolant, creep, swelling and corrosion of the cladding, relocation, densification and swelling of the fuel, fission gas release, etc.), a fuel rod analysis can be adequately accomplished by means of integral performance codes [9]. In the present work, calculations have been carried out by means of the integral code TRANSURANUS [10], which has recently been extended to the modelling of the behaviour of T91 and AISI 316L steels in LBE environment [11,12]. The results of the analyses are presented for three different coolant channels representative of the XADS core.

Modelling

The Italian 80 MW_{th} XADS basically consists of a subcritical core reactor coupled to an accelerator of a proton beam, which is injected into a LBE target located inside the core, producing the external neutron source needed to sustain the neutron balance via spallation reactions [2]. The core is made up of 120 fuel subassemblies, each one containing 90 fuel rods, gridded in a triangular lattice bundle. The fuel assemblies have a hexagonal lattice and surround the inner cavity foreseen for the spallation target [Figure 1(a)]. In the following, close reference is made to design data reported by Ansaldo in [5], where a complete description of the Italian LBE-XADS can be found.

Figure 1: Horizontal core section (a) and analysed coolant channels (b,c,d) of the Italian 80 MW_{th} XADS

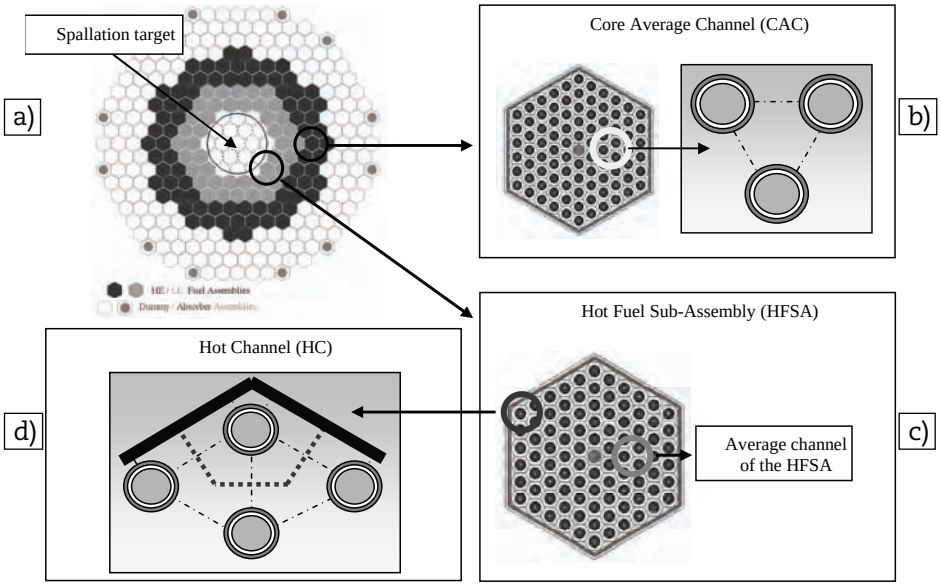

Thermal-hydraulics modelling

Three different coolant channels of the XADS have been identified by means of a preliminary thermal-hydraulic analysis [13]: the core average channel (CAC), the average channel of the hot fuel sub-assembly (HFSA) and the hot channel (HC).

The CAC [Figure 1(b)] is defined as the channel placed in a generic subassembly, which is representative of the core average thermal-hydraulic conditions, while the HFSA [Figure 1(c)] is representative of the average conditions of the hot fuel subassembly. The HC [Figure 1(d)] is characterised by the highest linear heat rate and coolant outlet temperature, and consequently by the highest cladding temperatures. It is placed in the HFSA and is representative of the most critical conditions achieved in the core (i.e. in the corner fuel rod nearest to the LBE target unit). The main thermal-hydraulic parameters of the three considered channels are presented in Table 1. It is noteworthy that the linear heat rate produced by the HFSA and the HC increases from the beginning of life (BOL) to the end of life (EOL), which corresponds to 900 EFPD (equivalent full power days) [5].

Table 1: Main thermal-hydraulic parameters of CAC, HFSA and HC

	CAC	HFSA		HC	
		BOL	*EOL*	*BOL*	*EOL*
Average linear heat rate [kW/m]	8.5	10.7	11.3	11.8	12.7
LBE mass flow rate* [kg/s]	0.30	0.30		0.45	
LBE outlet temperature [°C]	400	427	435	490	505

* Data refer to the channel area highlighted by dashed lines in Figures 1(b) and 1(d).

As concerns evaluation of the heat transfer from the cladding surface to the coolant, several correlations for liquid metals are available in literature, specific for different fluids and geometries (rod bundle, single tube), with significant differences (even a factor of 2.5 for LBE-XADS conditions) in the calculation of the Nusselt number [12,14]. The importance of the convective heat transfer coefficient is not only because of its influence on fuel rod temperatures, but also in

view of the coupling between thermo-mechanical and chemical phenomena, to which the cladding material is subjected in reactor. In this work, the correlation reported in [15] (referred to as Kirillov-Stromquist) has been adopted. For the demanding conditions and the particular geometry of the HC, a sensitivity study has been performed in order to assess the impact of differences among heat transfer correlations on fuel rod performance analysis. To this purpose, the correlations reported in [16] (Ibragimov-Subbotin-Ushakov) and [17] (Subbotin, *et al.*), which are more and less conservative than Kirillov-Stromquist, respectively, have been chosen.

Fuel rod modelling

The performance analysis of a fuel rod during the life in-reactor must take into account a very large number of mechanical, chemical, thermal and nuclear effects, and their interactions, so that *integral* performance codes are required to adequately carry out simulations of the fuel rod behaviour. In the present work, the TRANSURANUS code (v1m1j09 version) [18] has been employed, which is a well-known and qualified tool for the thermal and mechanical analysis of various fuel rod types. TRANSURANUS is available for the analysis of fuel rods with AISI 316L steel and has recently been extended for the modelling of T91 steel [11,12]. As concerns cladding corrosion, simple correlations (based on Tedmon's model [19]) for the behaviour of T91 and AISI 316L in flowing LBE under oxygen control have been embodied in TRANSURANUS [11,12], and have been adopted in the present analyses. In addition, a preliminary modelling of fuel rods provided by FeCrAlY coating by means of GESA technique [6,20] has been attempted[1]. As concerns thermo-mechanics, the effects of radiation embrittlement in LBE [4,24] are not accounted for.

Fuel rod geometrical parameters are resumed in Table 2. The fuel comprises an 870 mm long stack of mixed-oxide (UO_2 and PuO_2) annular pellets, with nominal smear density of 95% TD and 21.8% of Pu enrichment in the inner zone (HC and HFSA) and 28.2% in the outer zone of the core (CAC). On both ends of the fuel stack, a 15 mm thick layer of depleted uranium oxide serves as thermal shielding. As far as boundary conditions are concerned, inlet temperature and mass flow rate of the coolant are imposed according to the data reported in Table 1. The fuel rod has been geometrically represented in TRANSURANUS by 14 axial slices, corresponding to the values of fast neutron flux and linear heat rate (LHR) evaluated in Ref. [13], where axial cosine profiles have been conservatively assumed. The calculations have been accomplished from BOL to the EOL, over the design lifetime of 900 EFPD, to which a burn-up of 22-32 MWd/kgHM corresponds (depending on the considered channel).

Table 2: Fuel rod geometrical parameters from Ref. [5]

Outer cladding diameter	8.5 mm
Cladding thickness	0.565 mm
Fuel pellet outer diameter	7.14 mm
Fuel pellet inner diameter	1.8 mm
Fuel active length	870 mm
Helium fill gas pressure	0.1 MPa
Upper plenum length	162 mm
Lower plenum length	150 mm
Pin pitch	13.41 mm
Wrapper to pin cluster gap	2.5 mm

1. FeCrAlY coating has been simply modelled as an additive thermal resistance on the cladding outer surface, and no oxide layer has been assumed to grow up. A coating thickness of 40 μm [21,22] has been conservatively assumed, with thermal conductivity of 15 W/(m·K) [23].

Since increasing the irradiation time leads to an enhancement of all phenomena related to burn-up and fast neutron fluence, with a consequent worsening of the overall fuel rod performance, a time extension of 50% till 1 350 EFPD (referred to as EXL and corresponding to a burn-up of 33-48 MWd/kgHM[2]) has been taken into account. The analysis of performance over the extended life has allowed to better evaluate the differences between the two considered steels in terms of the fuel rod behaviour, and to point out some problems to deal with.

Results and discussion

In this paragraph, a critical comparison between fuel rods with T91 and AISI 316L claddings is proposed in terms of the overall rod behaviour, and some critical issues of fuel rod performance are individuated. To this purpose, indicative design limits have been established for the Italian 80 MW_{th} XADS as a guide for the discussion of the results. These limits are based on indications made for the advanced liquid metal-cooled reactor (ALMR) reported in Ref. [25], and are briefly resumed in Table 3. Moreover, the maximum inner cladding temperature and oxide layer thickness are two additional important parameters, which are discussed through this paragraph, since they are connected to the cladding creep resistance and to the stability of the protective oxide layer, respectively.

Table 3: Main design limits

Fuel centreline temperature	< melting temperature
Outer cladding temperature[3] (*in situ* oxide layer protection)	< 550°C
Cladding thermal creep strain	< 1%
Cladding swelling strain	< 5%
Cladding total strain (swelling excepted)	< 3%

CAC and HFSA channels

The CAC fuel rod of the XADS does not show any critical issue in terms of performance, also at EXL conditions. It can be considered as a "cold" rod, mainly due to the low linear heat rate and temperature of the coolant in comparison with other HLM fast reactors [7,8]. The main results of the analyses are reported in Table 4. It is noteworthy that the maximum swelling strain of AISI 316L is low at EOL, since the fast neutron fluence falls near the threshold value for the onset of steady-state swelling [18].

Table 4: Main results of the analyses of the CAC fuel rod with T91 and AISI 316L claddings

CAC	T91		AISI 316L	
	EOL	EXL	EOL	EXL
Maximum fuel temperature [°C]	852	882	865	905
Maximum outer cladding temperature [°C]	431	431	426	426
Maximum inner cladding temperature [°C]	438	438	436	436
Maximum swelling strain [%]	0.14	0.20	0.09	0.32
Maximum total strain (swelling excepted) [%]	0.50	0.50	0.80	0.80
FGR [%]	0.15	0.22	0.15	0.22

2. For each analysed channel, the LHR and fast neutron flux profiles at EOL have been maintained throughout the extended life.
3. Throughout the paper, outer cladding temperature refers to the metal-oxide interface.

Under HFSA conditions, the AISI 316L cladding exhibits a higher swelling strain compared to T91 (Table 5). At EXL, the different swelling response of AISI 316L results in fuel-cladding gap widening and thermal conductance degradation that leads to higher fuel temperatures and fission gas release (FGR) through a retroactive mechanism (so-called "thermal feedback"). However, the performance analyses of the HFSA rod do not indicate any critical issue for both steels, also in terms of creep strain[4].

Table 5: Main results of the analyses of the HFSA fuel rod with T91 and AISI 316L claddings

HFSA	T91		AISI 316L	
	EOL	EXL	EOL	EXL
Maximum fuel temperature [°C]	1 049	1 119	1 109	1 661
Maximum outer cladding temperature [°C]	484	486	471	471
Maximum inner cladding temperature [°C]	493	495	484	483
Maximum swelling strain [%]	0.18	0.28	0.55	1.51
Maximum total strain (swelling excepted) [%]	0.57	0.59	0.89	0.97
FGR [%]	0.20	0.18	0.42	49

Hot channel

Some critical situations are individuated in the HC fuel rod. A comparison between the results obtained with the two considered steels is presented in Figures 2 and 3. The outer cladding temperature in the axial peak position [Figure 2(a)] reaches values above 550°C at the EOL for both T91 and AISI 316L (582°C and 551°C, respectively). Experiments indicate that around 550°C both these steels suffer from severe corrosion in LBE, so the analyses suggest that the adoption of adequate protective coatings (e.g. via aluminisation) is necessary [6,19,20,22]. The higher temperature of T91 cladding with respect to AISI 316L is due to the development of a thicker low-conductivity[5] oxide layer (53 μm vs. 4 μm are calculated in axial peak position at the EOL) that, besides being potentially unstable ("spalling off"), constitutes an additional thermal resistance between the cladding and the coolant.

Figure 2: Comparison between T91 and AISI 316L fuel rod performance in the HC

(a) Axial profile of outer cladding temperature; (b) Radial temperature profile at LHR axial peak position

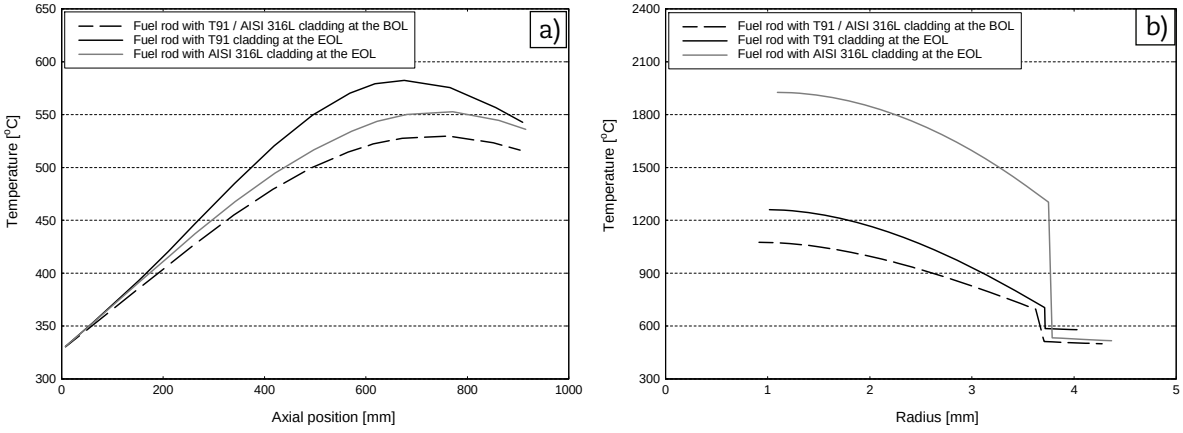

4. For brevity, creep analyses are not detailed here.
5. A value of 1 W/(m·K) has been assumed for the oxide thermal conductivity [26].

The T91 cladding allows an ample margin with respect to the fuel melting temperature [Figure 2(b)], while thermal feedback occurs in the AISI 316L rod, leading to a maximum fuel temperature of 1 940°C at EOL (and 2 140°C at EXL, not shown). Consequently, higher values of FGR (even about 82% at EXL) and inner rod pressure are recognised with AISI 316L cladding [Figure 3(a)]. As shown in Figure 3(b), the fuel rod with AISI 316L cladding maintains an "open gap" geometry throughout the irradiation history (due to swelling response and the arising of thermal feedback), while gap closure occurs at extended burn-up in the T91 rod, which is a favourable condition for the heat transfer. However, the fuel cladding mechanical interaction (FCMI) causes the onset of contact pressure and consequently a sudden increase of cladding stress [Figure 3(b)], which can be a concern in terms of resistance of T91 to creep.

Figure 3: Comparison between T91 and AISI 316L fuel rod performance in the HC

(a) FGR and inner rod pressure; (b) fuel-cladding gap width, contact pressure and Von Mises stress at LHR axial peak position

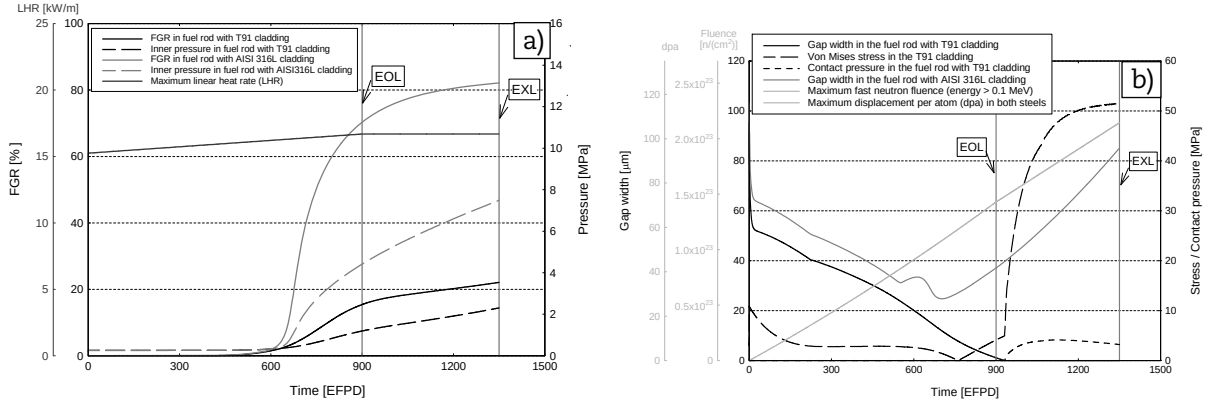

A sensitivity study has been carried out using a swelling model for AISI 316L based on Ref. [27] (referred to as the "Waltar model") instead of the TRANSURANUS model [18]. Results (Figure 4) show swelling strains beyond the design limit of 5% at EXL when using the Waltar model, which involves a higher swelling rate with respect to the TRANSURANUS model. It is worth noting that cladding temperature fall near the peak of steady-state swelling rate of AISI 316L (that is around 540-560°C [18,27]).

Figure 4: HC fuel rod with AISI 316L – axial profile of swelling strain in the cladding

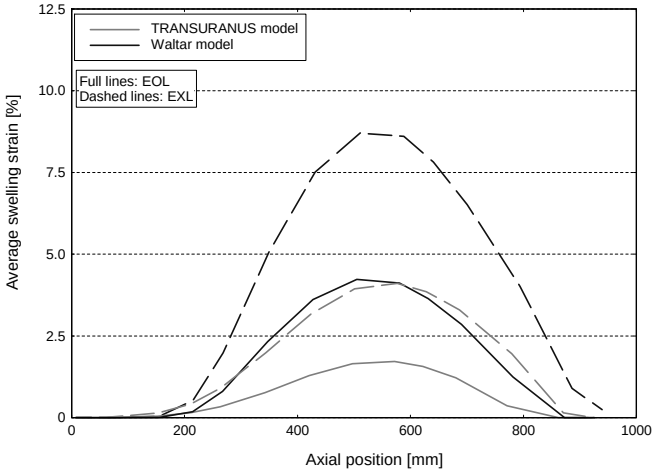

The sensitivity analysis of the HC fuel rod with T91, in terms of different correlations for the Nusselt number, has pointed out the importance of uncertainties in the calculation of the convective heat transfer. Actually, differences up to about 60°C in the evaluated outer cladding temperature can be achieved [Figure 5(a)], with relevant consequences on the overall rod behaviour. Lower cladding temperatures (around 540°C at both EOL and EXL) are calculated if the Subbotin, *et al.* correlation is employed. However, a likely unstable oxide layer (about 40 μm thick) develops, suggesting that *in situ* protection is unsatisfactory, independently of uncertainties in the evaluation of heat transfer. The analysis with the conservative Ibragimov-Subbotin-Ushakov correlation shows that cladding temperatures around 600°C may be reached at extended burn-up [Figure 5(a)]. A preliminary calculation, based on the Larson-Miller parameter, of the thermal creep rupture time [12] has predicted cladding failure due to creep before EXL in this case, because of the synergy between high temperature and stress due to FCMI. Actually, in the presence of contact pressure, cladding stresses severely increase as a consequence of the strong reduction in cladding section due to heavy oxidation. Hence corrosion, which causes both increase of temperature (due to thermal resistance of the oxide layer) and wall thinning, degrades the whole thermo-mechanical performance of the cladding. Preliminary calculations have been carried out for the T91 rod considering FeCrAlY coating protection, which allows lower cladding temperatures [Figure 5(b)] and no reduction in cladding section with respect to *in situ* oxide layer protection. In the analysed cases, thermal creep rupture has not occurred. This result gives further confirmation of the need of suitable coatings for the purpose of employing the T91 steel as cladding material in HLM reactors. However, high inner temperatures (up to 570°C, depending on heat transfer correlation) have been recognised even for coated cladding, so that thermal creep resistance of T91 may be a delicate issue, especially if FCMI conditions are achieved. Finally, the outcomes of the above sensitivity study point out the importance of the heat transfer coefficient evaluation, which results to strongly influence the thermo-mechanical performance of the cladding. Therefore, further investigation would be useful to better assess the problem of heat transfer to HLM.

Figure 5: HC fuel rod with T91: outer cladding temperature as a function of time at the axial peak position with (a) *in situ* oxide layer protection and (b) FeCrAlY coating protection[6]

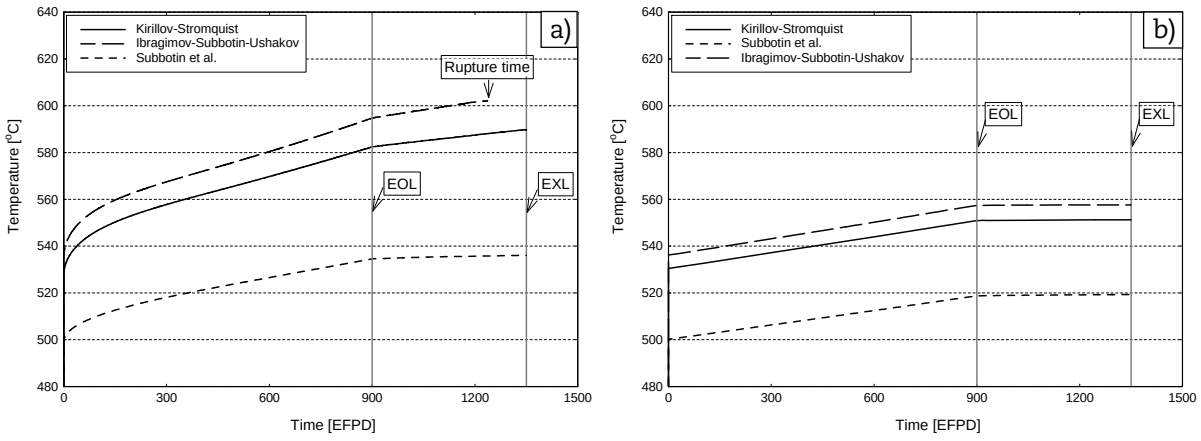

Conclusions

In this paper, analyses of fuel rod performance were presented for the Italian 80 MW_{th} LBE-XADS. Both the austenitic AISI 316L and the ferritic-martensitic T91 steels were considered as cladding materials. Calculations were carried out by means of the TRANSURANUS code over the design

6. In Figure 5(b), outer cladding temperature refers to the metal-coating interface.

lifetime of 900 EFPD, considering three different coolant channels of the XADS core under normal operation conditions. Simulations were performed also at extended burn-up, with the aim of pointing out some critical situations to which the considered cladding steels may be subjected. It was found that in the CAC and the HFSA the fuel rod behaviour does not exhibit any critical issue for both steels. The HC conditions resulted demanding (particularly at extended burn-up), and significant differences were found between the two steels in terms of fuel rod performance (maximum fuel temperature, FGR, cladding stress state and permanent strain). Actually, the fuel rod with T91 behaves as a "closing-gap" rod, due to the lower swelling of this steel, while the AISI 316L rod maintains an "open-gap" geometry and is subjected to a severe *thermal feedback*. For both steels, high outer cladding temperatures were found in the HC, so the adoption of adequate protective coatings (e.g. via aluminisation) is necessary in order to avoid heavy oxidation/dissolution.

A sensitivity study was carried out in order to evaluate the role of some critical aspects on fuel rod performance in the HC conditions. The following main conclusions can be drawn:

- In the AISI 316L cladding, strain beyond the design limit may occur at extended burn-up, depending on the swelling model. This is the main weak point of this steel in the particular conditions of the HC, since the cladding temperature falls within the peak of the swelling steady-state rate.
- The T91 cladding may be subjected to rupture due to thermal creep at extended burn-up, as a consequence of the synergy between high cladding temperatures (due to development of a thick, low-conductivity oxide layer) and high stresses (due to FCMI and the reduction in cladding section caused by oxidation). To this purpose, the sensitivity study highlighted the importance of the uncertainties on the convective heat transfer with HLM.
- The adoption of a protective coating leads to several advantages in terms of cladding performance, but tests simulating the in-reactor behaviour are needed to better qualify the coating adequacy.

All things considered, the T91 steel is confirmed to be a promising material for the future employment in HLM-cooled nuclear reactors. However, further investigation is required as regards the creep resistance under FCMI conditions and the behaviour under irradiation (e.g. embrittlement, integrity of coating) of the aluminised T91, so that a more reliable modelling can be afforded by means of *integral* fuel rod performance codes.

Acknowledgements

The authors wish to thank the TRANSURANUS Developers Team at ITU (European Commission, Joint Research Centre, Institute for Transuranium Elements, Karlsruhe, Germany), the Nuclear Fission Division at ENEA (Italian National Agency for New Technologies, Energy and Sustainable Economic Development, Bologna, Italy) and Mr. Michele Devita (Politecnico di Milano).

References

[1] US DOE Nuclear Energy Research Advisory Committee and the Generation IV International Forum, *A Technology Roadmap for Generation IV Nuclear Energy Systems*, GIF-002-00, December (2002).

[2] Cinotti, L., B. Giraud, H.A. Abderrahim, "The Experimental Accelerator Driven System (XADS) Designs in the EURATOM 5th Framework Programme", *J. Nucl. Mater.,* 335, 148-155 (2004).

[3] Garner, F.A., M.B. Toloczko, B.H. Sencer, "Comparison of Swelling and Irradiation Creep Behavior of FCC-austenitic and BCC-ferritic/martensitic Alloys at High Neutron Exposure", *J. Nucl. Mater.,* 276, 123-142 (2000).

[4] Klueh, R.L., A.T. Nelson, "Ferritic/martensitic Steels for Next-generation Reactors", *J. Nucl. Mater.*, 371, 37-52 (2007).

[5] Ansaldo, *XADS Pb-Bi Cooled Experimental Accelerator Driven System – Reference Configuration*, Summary Report ANSALDO ADS 1 SIFX 0500, Ansaldo Nuclear Division (2001).

[6] Nuclear Energy Agency (NEA), *Handbook on Lead-bismuth Eutectic Alloy and Lead Properties, Materials Compatibility, Thermal-Hydraulics and Technologies,* Technical Report NEA No. 6195, OECD/NEA (2007).

[7] Sobolev, V., E. Malambu, H. Aït Abderrahim, "Design of a Fuel Element for a Lead-cooled Fast Reactor", *J. Nucl. Mater.*, 385, 392-399 (2009).

[8] Meloni, P., G. Bandini, M. Polidori, "T/H and Transient Analyses to Confirm EFIT Preliminary Design", *J. Nucl. Mater.*, 376, 405-408 (2008).

[9] Aybar, H.S., P. Ortego, "A Review of Fuel Performance Codes", *Prog. Nucl. Energy*, 46 (2), 127-141 (2005).

[10] Lassmann, K., "TRANSURANUS: A Fuel Rod Analysis Code Ready for Use", *J. Nucl. Mater.*, 188, 295-302 (1992).

[11] Botazzoli, P., *et al.*, "Extension of the TRANSURANUS Code to the Fuel Rod Performance Analysis of LBE-cooled Nuclear Reactors", *Radiat. Eff. Defect. S.*, 164 (5-6), 330-335 (2009).

[12] Agosti, F., *et al.*, *Extension of the TRANSURANUS Code to the Analysis of Cladding Materials for Liquid Metal Cooled Fast Reactors: A Preliminary Approach*, Technical Report CESNEF-IN-11-2009, pp. 1-168, Department of Energy, Nuclear Engineering Division, Politecnico di Milano, November (2009).

[13] Agosti, F., *The Italian LBE-XADS: Fuel Rod Performance with Two Different Cladding Materials*, Nuclear Engineering – Master's Thesis, Politecnico di Milano, Milan (2007).

[14] Pfrang, W., D. Struwe, *Assessment of Correlations for Heat Transfer to the Coolant for Heavy Liquid Metal Cooled Core Designs*, Technical Report FZKA 7352, Karlsruhe (2007).

[15] Cheng, X., N-i. Tak, "Investigation on Turbulent Heat Transfer to Lead-bismuth Eutectic Flows in Circular Tubes for Nuclear Applications", *Nucl. Eng. Des.* 236, 385-393 (2006).

[16] Ibragimov, M., V.I. Subbotin, P.A. Ushakov, "Investigation of Heat Transfer in the Turbulent Flow of Liquid Metals in Tubes", *Atomnaya Energiya*, 8 (1), 54-56 (1960).

[17] Subbotin, V.I., *et al.*, "Heat Transfer in Elements of Reactors with a Liquid Metal Coolant", *Proceedings of the 3rd International Conference on Peaceful Use of Nuclear Energy*, New York, Vol. 8, pp. 192-200 (1965).

[18] Lassmann, K., *et al.*, *TRANSURANUS Handbook*, ©1975-2009, Institute for Transuranium Elements, Karlsruhe, Germany (2009).

[19] Zhang, J., "A Review of Steel Corrosion by Liquid Lead and Lead-bismuth", *Corros. Sci.*, 51, 1207-1227 (2009).

[20] Heinzel, A., M. Kondo, M. Takahashi, "Corrosion of Steels with Surface Treatment and Al-alloying by GESA Exposed in Lead-bismuth", *J. Nucl. Mater.*, 350, 264-270 (2006).

[21] Del Giacco, M., *Structural Materials for ADS Development: Experimental Investigation of some Aspects of LBE Corrosion*, Materials Engineering – Master's Thesis, Politecnico di Milano, Milan (2009).

[22] Weisenburger, A., *et al.*, "T91 Cladding Tubes with and Without Modified FeCrAlY Coatings Exposed in LBE at Different Flow, Stress and Temperature Conditions", *J. Nucl. Mater.*, 376, 274-281 (2008).

[23] Andersen, O., *et al.*, "Advanced Porous Structures made from Intermetallic and Superalloy Fibers", *Proceedings of the 1st International Conference on Materials Processing for Properties and Performance*, Singapore, 1-3 August (2002).

[24] Van den Bosch, J., *et al.*, "TWIN ASTIR: First Tensile Results of T91 and 316L Steel After Neutron Irradiation in Contact with Liquid Lead-bismuth Eutectic", *J. Nucl. Mater.*, forthcoming, doi:10.1016/j.jnucmat.2009.10.012.

[25] NEA, *Fuels and Materials for Transmutation: A Status Report*, NEA No. 5419, OECD/NEA, Paris (2005).

[26] Müller, G., "Liquid Metal Corrosion and Corrosion Protection", *Topical Day on Compatibility of Structural Materials with Heavy Liquid Metals*, SCK•CEN, Mol, 29 April (2008).

[27] Waltar, A.E., A.B. Reynolds, *Fast Breeder Reactors*, Chapter 11, p. 430, Pergamon Press, New York (1981).

Isotope equilibrium in fast thorium reactors

David J. Coates, Geoffrey T. Parks
Department of Engineering, University of Cambridge
Cambridge, United Kingdom

Abstract

The development of accelerator-driven subcritical reactors operating with pure and enriched thorium fuel mixtures has been heralded as delivering a new era in sustainable nuclear power production. Many benefits have been claimed for these systems, particularly with respect to their ability to consume existing plutonium stockpiles and their inability to breed additional plutonium. Although these characteristics can be achieved under specific operating conditions, such descriptions obscure the true nature of the actinide generation and incineration mechanisms taking place. This paper examines the operation of fast thorium reactors in terms of actinide evolution and equilibrium. The fundamental mechanisms that affect nuclide evolution are demonstrated and the freedoms and constraints bounding this process are shown. These principles are demonstrated through the development of a simple lumped model, the use of which allows the steady-state actinide populations and their transient evolution within a homogeneous reactor to be predicted. Fast reactors operating with a 100% thorium fuel source are shown to generate plutonium and to offer no advantage over enriched thorium fuel in terms of actinide generation in longer-term operation.

Introduction

The prospect of developing an accelerator-driven system (ADS) is receiving increasing attention, with its potential to address public concerns about safety and waste through subcritical operation in a fast neutron spectrum. The use of thorium fuel has also been receiving attention as a means of reducing the production of long-lived actinides in both thermal and fast reactors.

There is a widespread belief that thorium-fuelled ADS reactors do not produce plutonium. A number of publications have contributed to this confusion including: COSMOS magazine, "no plutonium is bred in the reactor" [1]; IAEA-TECDOC-1450, "(Th, Pu)O_2 fuel is more attractive, as compared to (U,Pu)O_2, since plutonium is not bred in the former" [2]; the Thorenco LLC website, "The advantages of the thorium fuel cycle are that it does not produce plutonium…" [3]; IAEA-TECDOC-1319, "Examination of claimed advantages, (a) producing no plutonium, this is true of the pure thorium cycle" [4]; *power-technology.com*, "The fuel cycle can also be proliferation resistant, stopping a reactor from producing nuclear weapons-usable plutonium" [5].

This paper examines the evolution of actinides within fast thorium-fuelled ADS reactors against the backdrop of the claimed benefits of the technology, particularly in terms of plutonium production. Actinide production is described from the perspective of steady-state equilibrium and this principle is demonstrated through the creation of a "lumped" homogeneous reactor model to calculate the relative abundance of actinides within the reactor at steady-state conditions. The reactor, despite having an initial fuel load of pure thorium, is shown to generate plutonium as part of the nuclide balance.

A transient model is developed to demonstrate the mechanisms taking place inside a fast thorium reactor as a function of time and is validated against previously published data. The transient code is used to demonstrate the lowest possible outcomes for actinide growth as a function of time that can be achieved through irradiation and, as such, provides a graphical representation of the nuclide positions which can be occupied by enrichment isotopes. It is shown that over a sufficiently long period of operation all nuclides reach the same equilibrium positions regardless of the starting conditions.

Thus, although under particular sets of circumstances the statements highlighted above can be true, they are misleading; they do not fully convey the true nature of the actinide generation and incineration mechanisms taking place in fast thorium reactors.

Actinide equilibrium and evolution within fast reactors

The rate of change of a nuclide population within a reactor is a function of natural decay and neutron interactions [fission, capture and (n,2n)]. Additionally the rate at which the atoms of a particular nuclide are lost is a function of the number of such atoms present. The rate at which such atoms are produced is influenced by the abundance of other related isotopes within the reactor. The relative abundance of a given nuclide will increase or decrease in value until equilibrium is achieved between the mechanisms for its production and destruction. At this point the nuclide will be in steady-state equilibrium for a given neutron flux value. Figure 1 presents an example of actinide evolution in an 86% thorium 14% "dirty" plutonium lead-cooled energy amplifier, showing the growth of ^{233}U and the reduction in plutonium isotopes over the first 250 $GWdt^{-1}$ of burn-up. The evolution of actinides within the energy amplifier will be equivalent to that in a fast ADS or other fast critical reactor. Over short periods of operation, over a few fuel cycles or a single "once-through" fuel load, steady-state conditions are not achieved. In such circumstances it is possible to assume incorrectly that specific nuclides within the reactor inventory are continuously consumed or generated.

In the example shown in Figure 1 all the plutonium nuclides are falling in abundance. In this case one possible, but incorrect, conclusion would be to assume that this elimination process will

Figure 1: Generation of ^{233}U and burning of Pu isotopes in a lead-cooled energy amplifier [6]

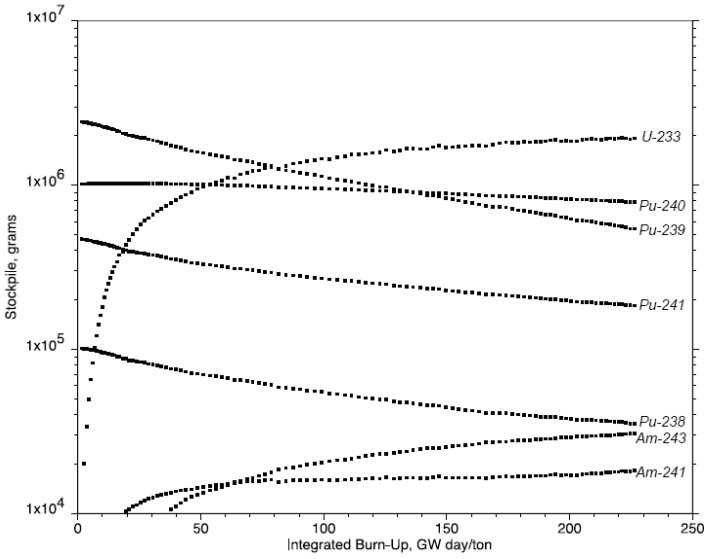

continue until a zero plutonium inventory is achieved. In fact, for all the nuclides shown in Figure 1 the changes in population are as a result of the difference between the abundance of the given nuclide and its steady-state equilibrium value. In the case of ^{233}U the increase is achieved by loading the reactor with a quantity below its equilibrium position, and for the plutonium isotopes the decreases result from initial populations above their equilibrium positions. By making adjustments to the starting values of these nuclides it is possible to achieve a plutonium breeder and a ^{233}U burner, or to have both plutonium and ^{233}U breeding or burning concurrently. Hence, it is inappropriate to describe fast reactors as either generators or burners of any particular nuclide; rather they are a means by which nuclides can be generated or burned towards their equilibrium levels within the reactor.

Steady-state reactor model

The principle of nuclide equilibrium within a fast thorium reactor can be demonstrated using a simple "lumped" reactor model ignoring spatial effects. For this purpose, a series of differential equations were established describing the rates of change of each of 33 nuclides within the reactor model. The specific isotopes included in the model are shown in Figure 2. The factors affecting the rates of change described within the model include various forms of decay and neutron interactions: (n,γ), (n,f) and (n,2n). The equations are arranged to enable solutions to be found for the 33 isotopes therein and also to enable subsequent alterations to the neutron flux value without the need to make significant alterations to the model.

The equations derived to describe the rates of change of the isotopes within the model are all of the form of Eq. (1):

$$\frac{dIs_N}{dt} = Is_N \Phi \left[-\sum_i \sigma_{i_{IsN}} - \frac{\sum_j \lambda_{j_{IsN}}}{\Phi} \right] + \sum_k \sigma_{k_{ItMk}} It_{Mk} \Phi + \sum_l \lambda_{l_{ItMl}} It_{Ml} \qquad (1)$$

where Is_N is abundance of the isotope in question; Φ is the neutron flux level; $\sigma_{i_{IsN}}$ is the microscopic cross-section for an interaction of type i, where i could be c for (n,γ) capture, *f* for fission, or *n,2n*; $\lambda_{j_{IsN}}$ is the decay constant for decay mechanism *j* for isotope Is_N, where *j* could be

Figure 2: Relative abundance of nuclides within the fast reactor model for a neutron flux of 5×10^{15} cm^{-2}s^{-1}

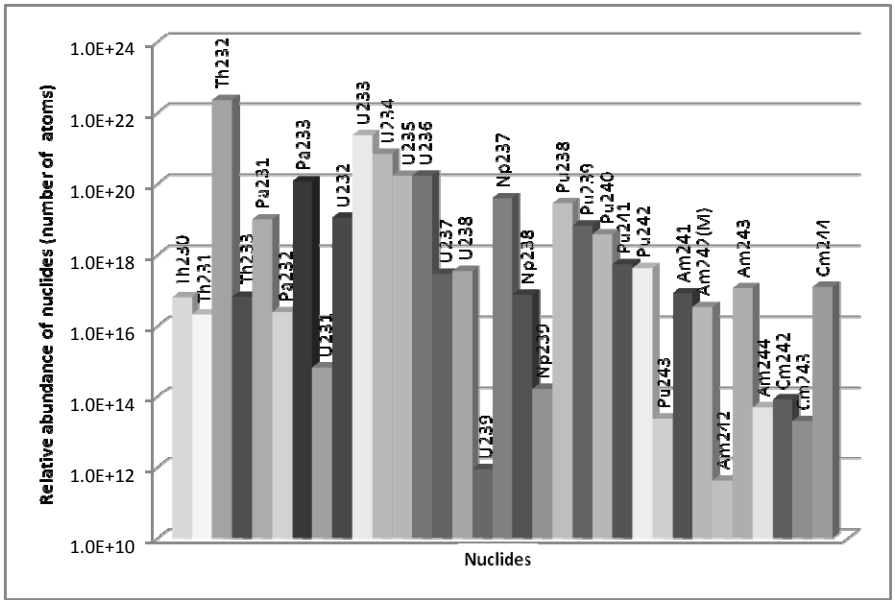

α for alpha decay, β^- for beta decay, ε for electron capture, *IT* for metastable decay [$Am(M)_{242}$ only], *SF* for spontaneous fission, *Ne* for neon decay (some U isotopes only), or Si + Mg for Si and Mg decay (^{238}Pu only); It_{Mk} is the abundance of the isotope from which Is_N is created by interaction *k*, where *k* could be *c* or *n*,2*n*; and It_{Ml} is the abundance of the isotope from which Is_N is created by decay mechanism *l*, where *l* could be α, β^-, ε or *IT*. Table 1 presents a key to this nomenclature.

Table 1: Key to nomenclature

Symbol	Description	Symbol	Description
σ_f	Microscopic cross-section for fission (n,f)	$\sigma_{n,2n}$	Microscopic cross-section for (n,2n)
σ_c	Microscopic cross-section for capture (n,γ)	λ_ε	Decay constant (electron capture fraction)
Φ	Neutron flux	Th_{232}	Atom population of isotope
λ_α	Decay constant (alpha fraction)	λ_{SF}	Decay constant (spontaneous fission fraction)

Thus, for example:

$$\frac{dTh_{232}}{dt} = Th_{232}\Phi\left[-\sigma_{f_{Th232}} - \sigma_{c_{Th232}} - \sigma_{n,2n_{Th232}} - \frac{\left(\lambda_{\alpha_{Th232}} + \lambda_{SF_{Th232}}\right)}{\Phi}\right] + \sigma_{c_{Th231}} Th_{231}\Phi + \lambda_{\alpha_{U236}} U_{236} + \lambda_{\varepsilon_{Pa232}} Pa_{232} \quad (2)$$

Any reactor physics code that models the nuclide evolution within the core will, of course, use and solve equations such as these. The ORIGEN-S code [7], which computes time-dependent concentrations and source terms for large numbers of isotopes simultaneously being generated or eliminated by these mechanisms, uses equations of this form. Space limitations preclude the inclusion of the averaged cross-sections and decay data used in the model. However, the data are available from the authors upon request.

At steady state, equilibrium is achieved between the relative abundances of each of the nuclides within the reactor. At this point the rate of change of the population of each nuclide is zero, of course, and it therefore follows that for the purposes of the model the left-hand side of

each instance of Eq. (1) can be set to zero to represent these conditions. It should then be possible to find the equilibrium populations. However, in order to represent the periodic refuelling with ^{232}Th, Eq. (2) was, in effect, suppressed, and instead an equilibrium ^{232}Th population defined. The ^{232}Th population density adopted was taken to be the number of thorium atoms present in a 1 cm^3 volume of ThO_2, namely 2.28×10^{22}, assuming a ThO_2 density of 10 gcm^{-3} [8]. In order to find solutions for the equilibrium nuclide populations, $\underline{N}_\infty$, the 33 equations [with Eq. (2) replaced by: $Th_{232} = 2.28 \times 10^{22}$ cm^{-3}] were mapped to a 33×33 matrix, $\underline{\underline{M}}$, representing the 33 nuclides and 33 equations, and a 33×1 vector, $\underline{S}$, of the corresponding steady-state left-hand side values (32 zeros and 2.28×10^{22}), giving:

$$\underline{S} = \underline{\underline{M}}\underline{N}_\infty \tag{3}$$

The resulting matrix and vector were input into the MATLAB 7.6 software package, and the equilibrium nuclide populations $\underline{N}_\infty = \underline{\underline{M}}^{-1}\underline{S}$ found using the matrix inversion facility. A neutron flux of 5×10^{15} cm^{-2}s^{-1} was selected for this calculation, taken from CERN 95-53(ET) [9].

Steady-state model results

The populations for nuclides within a fast thorium reactor that are established in steady-state conditions, as predicted by the model, are shown in Figure 2. Actinides are generated right across the range of isotopes included within the model. Plutonium, americium and curium are generated despite the reactor operating from a 100% thorium fuel source. The relative abundances of the nuclides shown represent their steady-state equilibrium positions and, as such, they identify the levels towards which nuclides will evolve during irradiation. These relative abundances represent the transition points for initial fuel compositions above or below which subsequent population growth or reduction will result.

Transient model for fast reactors

A transient model was developed using the equations and cross-section and decay data previously developed for the steady-state model. The transient model uses the fourth-order Runge-Kutta method to numerically integrate the equations and was coded using MATLAB. In order to assess the relative accuracy of the transient model a comparison with an established code was necessary. This was done using results produced using the Energy Amplifier Monte Carlo (EA-MC) code which was developed at CERN for the purpose of modelling ADS reactor performance [10]. An analysis published in [11] shows the operation of a lead-cooled ADS with a 76% thorium, 20% plutonium, 2% americium, 1.3% neptunium, 0.04% curium initial fuel load. The calculated growth and decline of the nuclide populations in terms of combined isotopes for particular elements are shown in Figure 3. An appropriate means of comparison between the two codes was established by adopting a neutron flux value which produced the equivalent reduction in ^{232}Th over the same five-year period of operation. The actinide populations predicted by the transient model are shown in Figure 4.

The results in Figure 4 are in good agreement with Figure 3 for ^{232}Th, uranium, plutonium, americium and neptunium. The growth curve for curium produced by the transient model predicts a similar total quantity of curium over a five-year period, although with a slower initial growth rate. The differences in the results can be attributed to the fact that the transient model assumes a uniform flux throughout the reactor, whereas the simulations from [11] were based on full, three-dimensional modelling of the core. Variations in the flux profile will favour the generation of particular isotopes over others within the same reactor. Differences in the values of cross-sections used may also contribute to the discrepancies observed. Our transient model is a one-group model, while EA-MC can simulate multiple neutron energy groups.

Figure 3: Actinide populations versus burn-up in an ADS thorium reactor [11]

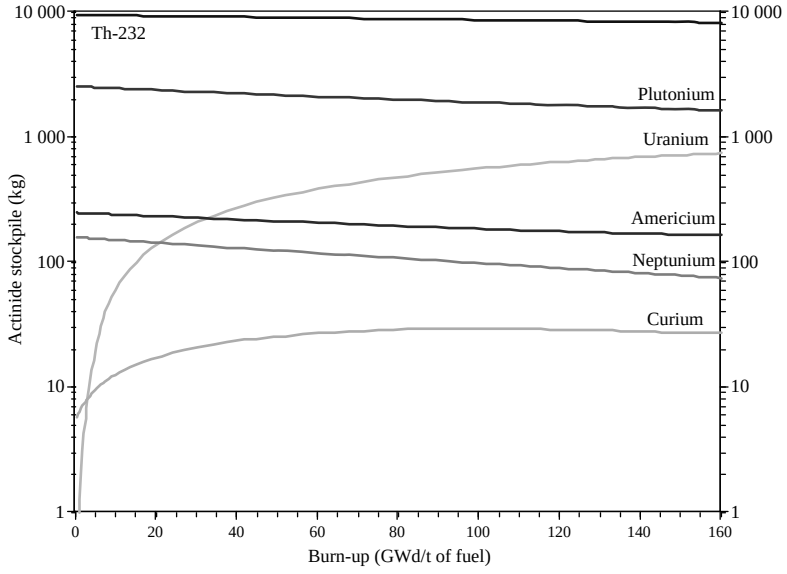

Figure 4: Transient model predictions of actinide populations versus time in an ADS thorium reactor

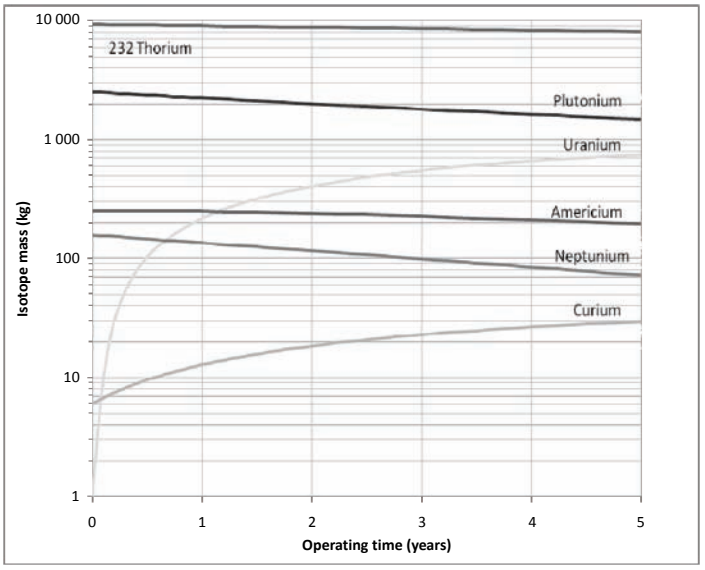

Despite the inevitable differences, which result from the simplifying assumptions adopted, the results of the two codes are within a reasonable level of agreement, given that the purpose of the transient model is to demonstrate to first-order accuracy the principles of actinide evolution and equilibrium within a fast reactor.

Actinide evolution within enriched thorium reactors

To examine in more detail the possible evolution characteristics of different isotopes, the nuclide composition of a 15% plutonium-enriched fast thorium reactor was simulated over an extended period of operation of 120 years. In order to model the effect of refuelling, every 10 years the atom population of ^{232}Th was "topped up" to replace the ^{232}Th lost during irradiation. The ^{232}Th population was in each case re-set to a value of 2.28×10^{22} cm^{-3}, this being the assumed starting

population for a 100% thorium reactor. The refuelling regime included full reprocessing of all actinides and assumed no losses, thus the nuclide populations of all isotopes other than ^{232}Th remained unaffected directly by the 10-yearly interventions. A constant neutron flux of 5×10^{15} cm^{-2}s^{-1} was assumed. The resulting profiles for the evolution of the plutonium isotopes are shown in Figure 5.

Figure 5: Changes to the quantities of plutonium isotopes over 120 years' operation for a 15% enriched thorium/plutonium reactor

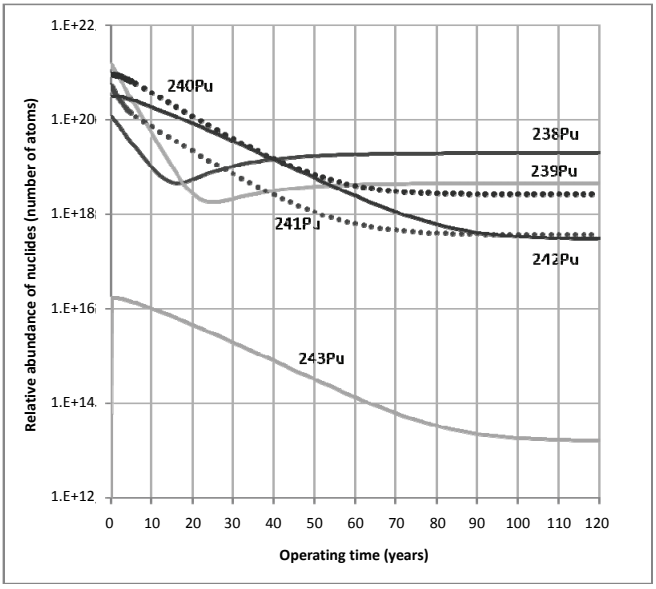

Three patterns of evolution emerge for the plutonium isotopes. In the case of ^{240}Pu, ^{241}Pu and ^{242}Pu the abundances decrease monotonically from the initial enrichment levels until steady-state equilibrium is reached. The decrease is a result of the initial enrichment values being higher than the steady-state equilibrium values; the decrease demonstrates the subsequent adjustment necessary to achieve steady-state equilibrium.

A different pattern emerges for ^{243}Pu (which was absent from the initial enrichment composition). It displays a very rapid increase in its abundance followed by a decrease until steady-state equilibrium is achieved. The initial increase is a result of the initial enrichment value of ^{243}Pu being below its short-term transient equilibrium value relative to the other lighter plutonium enrichment isotopes. The abundance of ^{243}Pu is then maintained in proportion to the lighter plutonium isotopes and falls in value until the long-term steady-state equilibrium positions are reached by all the plutonium isotopes.

The third pattern is shown by ^{238}Pu and ^{239}Pu. This involves an initial decrease in abundance followed by an increase. This is explained in more detail in the next section.

The dominance of isotopes generated by the ^{232}Th neutron reaction and decay pathways

The initial fall in value for the isotopes ^{238}Pu and ^{239}Pu, shown in Figure 5, is a result of enrichment values being above the long-term equilibrium values, and, as such, the early behaviour reflects that of ^{240}Pu, ^{241}Pu and ^{242}Pu. However, unlike the effect seen for the other enrichment isotopes, the initial decrease is followed by a subsequent increase. This change of direction results from the more rapid rate of decrease than is initially experienced by the ^{238}Pu and ^{239}Pu isotopes; this causes them to intercept the dominant ^{232}Th nuclide growth path on its upward curve. This effect can be seen in Figure 6 which shows the evolution curves resulting from 100% ^{232}Th and

Figure 6: Plutonium isotope growth/decline patterns for 15% plutonium enrichment and 100% thorium reactor configurations

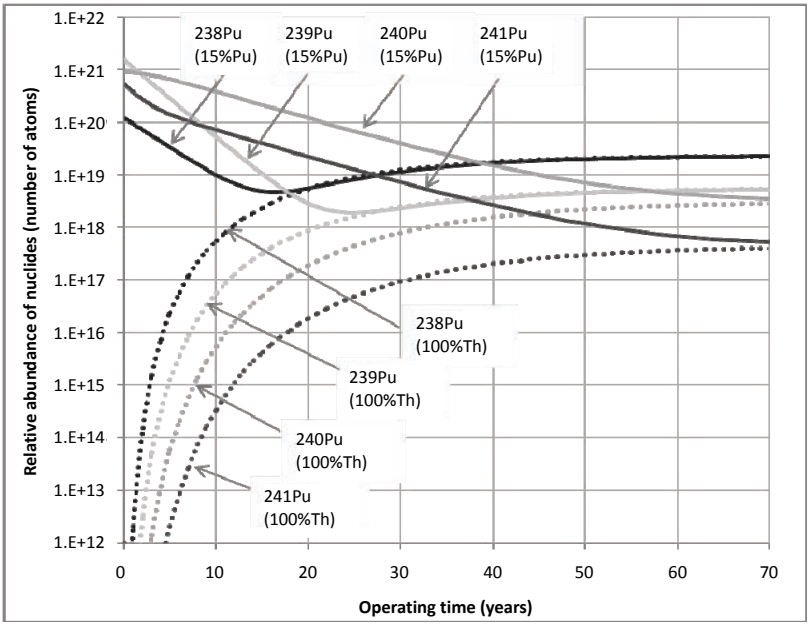

15% plutonium enriched scenarios. In the cases of ^{240}Pu and ^{241}Pu the intercept takes place after the 100% thorium profile has, in effect, reached steady-state equilibrium, and consequently there is no obvious change in the evolution pattern for these isotopes. For ^{238}Pu and ^{239}Pu the change from decline to growth clearly occurs at the point at which the trajectories intersect with the 100% thorium curves; from this point onwards the minimum values that can be achieved as a result of irradiation are dictated by the ^{232}Th production route.

Every nuclide within the reactor has a unique ^{232}Th evolution growth profile associated with it. These growth profiles represent the lowest possible nuclide abundance that can be achieved through irradiation; enrichment isotopes with initial compositions above the ^{232}Th profile cannot cross below it. It is possible to achieve a nuclide abundance below the ^{232}Th profile by physically removing irradiated fuel and replacing it with a new fuel batch with particular isotopes absent or reduced in quantity.

The 100% thorium curve does not represent a limit on the maximum possible nuclide growth that can be achieved. With the addition of enrichment isotopes it is possible to exceed the ^{232}Th profile through the creation of short-term, transient equilibrium positions; this effect was previously demonstrated in Figure 5 where the plutonium enrichment caused the ^{243}Pu level to significantly exceed its steady-state value. Without repeated enrichment the enhanced growth positions of such nuclides will ultimately return to their long-term equilibrium levels.

Conclusions

Fast reactor systems when operated over extended durations ultimately achieve a balanced equilibrium between the relative abundances of the isotopes generated. By viewing reactor operation in terms of nuclide equilibrium balance, a more appropriate picture emerges of the movements over time of the isotope abundances. This enables a more accurate description of reactor performance in terms of actinide generation or removal to be provided.

The equilibrium nuclide populations within a reactor are functions of natural decay and neutron interactions and, as has been shown, it is possible to create a simple, lumped model

predicting their variation from differential equations which describe the factors governing the rates of change of individual nuclide levels. It is straightforward to solve these equations for the steady-state case to determine the equilibrium values of the relative abundance of the isotopes.

For a fast thorium reactor to achieve nuclide equilibrium in practice a period of operation in excess of 100 years would be necessary with an associated series of recycling and refuelling operations. In order to predict the evolution of actinide isotope concentrations with time, the differential equations of the lumped model can be integrated using a standard fourth-order Runge-Kutta method. The predictions of this transient model are in reasonable agreement with the results produced by much more sophisticated reactor physics codes, giving confidence that the model can be used for its intended purposes: to demonstrate to first-order accuracy the principles of actinide evolution and equilibrium within a fast reactor and to allow the identification of trends within the nuclide transformations.

When a thorium fuel platform is adopted the underlying growth of nuclides generated from the thorium provides a baseline describing the lowest levels of actinide abundances which can be achieved over any given time period. The addition of enrichment isotopes can produce accelerated growth of other associated nuclides in excess of that produced via the thorium reaction route, as such actinides establish a position relative to the abundance of the enrichment isotopes. If the enrichment operation is finite (i.e. it is not repeated throughout the reactor lifetime) the ultimate levels of abundance achieved within the reactor for all isotopes will be those for the 100% thorium scenario.

References

[1] Dean, T., "New Age Nuclear", *COSMOS Magazine*, *8* (2006), *www.cosmosmagazine.com/node/348/*, accessed 6 December 2009.

[2] International Atomic Energy Agency (IAEA), *Thorium Fuel Cycle – Potential Benefits and Challenges*, IAEA-TECDOC-1450, IAEA, Vienna (2005).

[3] Thorenco LLC, *Thorium: The Preferred Nuclear Fuel of the Future* (2009), *www.thorenco.com/index.html*, accessed 6 December 2009.

[4] Wilson, P.D., K.F. Ainsworth, "Potential Advantages and Drawbacks of the Thorium Fuel Cycle in Relation to Current Practice: A BNFL View", In: *Thorium Fuel Utilization: Options and Trends*, IAEA-TECDOC-1319, 305–315, IAEA, Vienna (2002).

[5] Beedie, M., "Thorium: Cleaner Nuclear Power?", power-technology.com website (2007). *www.power-technology.com/features/feature1141/*, accessed 6 December 2009.

[6] Rubbia, C., *et al*., *Conceptual Design of a Fast Neutron Operated High Power Energy Amplifier*, CERN/AT/95-44 (ET), European Organisation for Nuclear Research (1995).

[7] Hermann, O.W., R.M. Westfall, *ORIGEN-S: Scale System Module to Calculate Fuel Depletion, Actinide Transmutation, Fission Product Buildup and Decay, and Associated Radiation Source Terms*, ORNL/NUREG/CSD-2/V2/R6, ORNL, Oak Ridge, TN (1998).

[8] Etherington, H., *Nuclear Engineering Handbook*, 1st Ed., McGraw-Hill Education, New York (1958).

[9] Rubbia, C., *et al.*, *A Realistic Plutonium Elimination Scheme with Fast Energy Amplifiers and Thorium-plutonium Fuel*, CERN/AT/95-53 (ET), European Organisation for Nuclear Research (1995).

[10] Kadi, Y., "The EA-MC Monte Carlo Code Package", *Proc. 5th Int. Meeting SARE-5*, Paris, France, 17-18 July (2000).

[11] Herrera-Martínez, A., *Transmutation of Nuclear Waste in Accelerator-driven Systems*, PhD Thesis, University of Cambridge (2004).

Subcritical minor actinide reduction through transmutation – SMART

Richard L. Sheffield, Eric J. Pitcher
Los Alamos National Laboratory
United States

Abstract

Nearly all issues related to risks to future generations arising from long-term disposal of spent nuclear fuel are primarily attributable to transuranic elements and long-lived fission products, approximately 2% of its content. The transuranic elements of concern are plutonium, neptunium, americium and curium, which are produced by neutron captures in uranium fuel. Long-lived (>100 000-year half-life) isotopes of iodine and technetium are also created by nuclear fission of uranium. If we can reduce or otherwise securely handle this 2% of the spent fuel, the toxic nature of the remaining spent fuel after a few centuries of cooling is below that of the natural uranium ore that was originally mined for nuclear fuel. We propose an interim solution called "Subcritical Minor Actinide Reduction through Transmutation" (SMART). Our proposed interim solution is to dispose spent fuel using a combination of approaches depending on the lifetime of the radioactive isotope. Long-lived fissile isotopes like ^{239}Pu and ^{235}U can be stored with ^{238}U and ^{237}Np for fabrication into nuclear fuel at a future date. The short-lived fission products can be stored in man-made containers until they safely decay to low radiotoxicity levels. The long-lived fission products can either be vitrified and buried or transmuted. That leaves addressing the intermediate-lived isotopes, mainly americium. The Am can be transmuted using an accelerator. Since it is envisioned that the government would be responsible for constructing the accelerator burners, the number of accelerator systems must be kept to an absolute minimum. This approach results in a design having only an Am feedstock to the transmuter. The goals of SMART are: i) to use an accelerator to transmute the intermediate-lived actinide, americium, thus eliminating Am impact on the packing density and long-term radiotoxicity in the repository design; ii) preserve the energy-rich component of spent fuel for future use; iii) reduce proliferation risk. Most of the remaining wastes have half-lives of a few hundred years and can be safely stored in man-made containment structures (casks or glass).

Introduction

A key roadblock to development of additional nuclear power capacity is the concern over management of nuclear waste. Nuclear waste is predominantly comprised of used fuel discharged from operating nuclear reactors. The 104 operating US light water reactors (LWR), that currently produce about 20% of the US electricity or more than 70% of the US emission-free electricity, and, given the life extension of present plants, will create about 120 000 tonnes of such spent fuel over the course of their lifetimes. World wide, more than 250 000 tonnes of spent fuel from reactors currently operating will require disposal. The toxicity of the spent fuel, mainly due to ionising radiation, will affect future generations for quite some time. The large quantity and its long-lived toxicity present significant challenges in waste management.

The US employs a "once-through" nuclear fuel cycle. Concerns about an ever-expanding "plutonium economy" and the associated proliferation concerns in other countries led the US to the once-through fuel cycle. Also, the low price for uranium ore over the last several decades has made the once-through cycle economical. However, long-term nuclear waste disposal remains to be addressed. Under any scenario, at some point in time either short-term or long-term geologic repository(ies), Figure 1, must be made available to receive the reactor waste. In the US, spent nuclear fuel is presently stored in buildings on reactor sites, with the expectation that it was to be sent to the proposed Yucca Mountain repository once the repository receives regulatory approval to accept high-level waste. Recently a change in government opinion has led to a determination that the financial or political cost of Yucca Mountain may not be acceptable, which has revived the question of what is the best course of action for spent nuclear fuel.

Figure 1: Unprocessed spent fuel containing materials that need isolation from environment for greater than 10 000 years requires a geologic repository

This type of repository uses geologic characteristics to isolate wastes after containers and barriers fail. For geologic repositories, groundwater transport is a key issue, and climate change and population shifts add uncertainty to the long-term isolation design basis. However, if the plutonium and minor actinides are removed, the requirements change in that the toxicity falls below natural uranium ore within a few centuries. Current man-made containers are capable of providing more than 300 years of isolation.

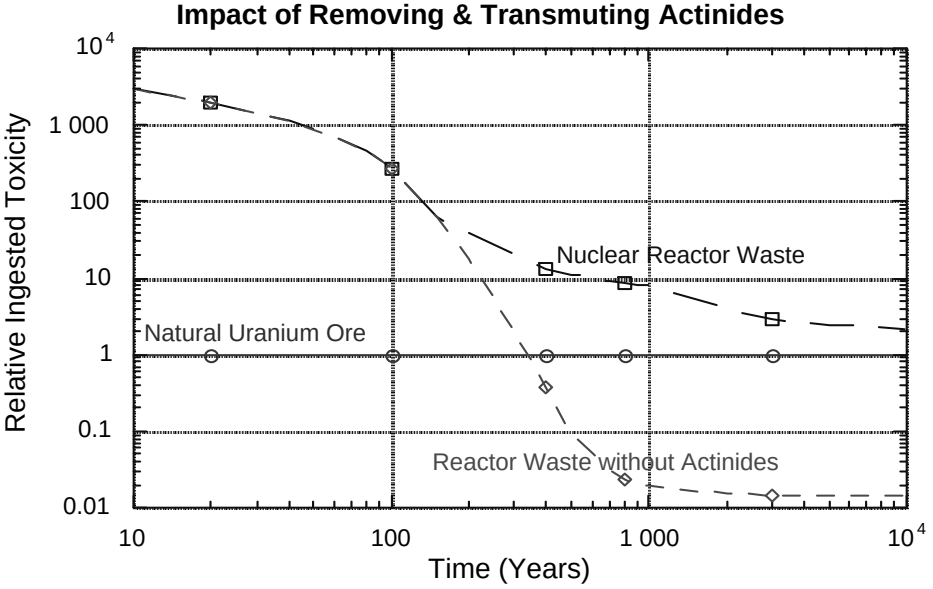

Nuclear fuel seems ideally suited for recycling. Only a small fraction of the available energy in the fuel is extracted on a single pass and the majority of the "problem wastes" could be burned in fast neutron spectrum reactors. Most of the remaining wastes have half-lives of a few hundred

years and can be safely stored in man-made containment structures (casks or glass). The very small amount of remaining long-lived waste could be safely stored in a small geologic repository. The problem for the next 100 years is that a sufficient number of fast reactors will not be built by industry to burn their own waste and the LWR waste from existing and new reactors. Thus an interim solution is required to transition to a fast reactor economy.

An interim solution is to dispose spent fuel using a combination of approaches depending on the lifetime of the radioactive isotope. Long-lived fissile isotopes like ^{239}Pu and ^{235}U can be stored with ^{238}U and ^{237}Np for fabrication into nuclear fuel at a future date. The short-lived fission products can be stored in man-made containers until they safely decay to low radiotoxicity levels. The long-lived fission products can be vitrified and buried. A number of projects have looked at transmuters with only minor actinide loading [1]. We have put forward a proposal called Subcritical Minor Actinide Reduction through Transmutation (SMART). The goals of SMART are: *i)* to significantly reduce the impacts due to the intermediate-lived actinide, americium, on the packing density and long-term radiotoxicity in the repository design; *ii)* preserve the energy-rich component of spent fuel for future use; *iii)* reduce proliferation risk. Storage is limited by the heat from radioactive decay in the short term (<500 years). Long-term storage is limited by container failure and the potential spread of radiotoxic isotopes. Isotopic contributions to the decay heat are shown in Figure 2.

Figure 2: Dominant decay heat contributors in spent PWR fuel irradiated to 50 GWd/MTHM [2]

The goal is to eliminate components of the nuclear waste stream that account for the majority of the heat load and toxicity over the 300 to 10 000 year time frame. The circled isotopes are the major contributors to the decay heat in this time frame. If these isotopes are removed then: the thick line shows the decay heat of the remaining waste; the light grey dashed line shows the time at which the surface temperature of the waste container is below the boiling point of water; and the dark grey dashed line gives the time at which the waste radiotoxicity is below Class C nuclear waste.

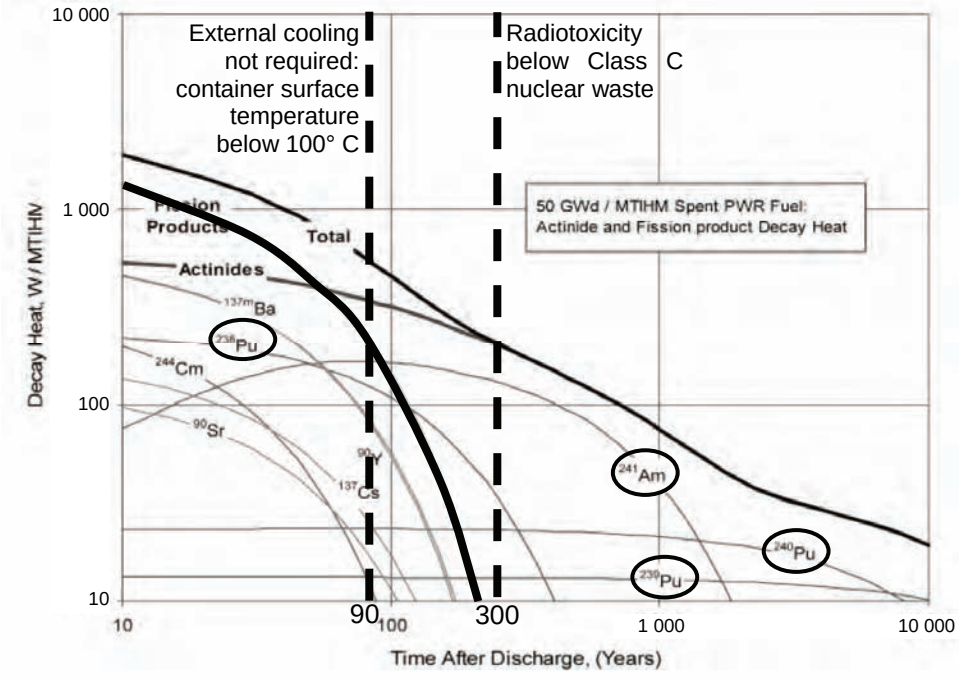

Americium can most efficiently be eliminated through nuclear transmutation using fast neutrons. One fast neutron production method is by a high-energy proton beam generating spallation neutrons. These spallation neutrons can drive a subcritical core to transmute the long-lived Am isotopes to shorter-lived fission products, and these products are disposed of in

short-term repositories. The Am feedstock is assumed to be from spent fuel that has set for 50 years after removal from the reactor. At 50 years, 97% of the ^{241}Pu has decayed to ^{241}Am. The remaining un-decayed 3% of ^{241}Pu can be sent for long-term storage with the other Pu isotopes without significantly impacting the overall properties (internal heating, neutron source, etc.) of the stored material.

Accelerator-based transmutation

Fast-neutron-based transmutation is composed of three major technology elements: separations, fuels and waste forms, and a fast neutron source coupled with a transmuter. A well-designed accelerator-driven transmuter would operate in a subcritical mode, and with limited excess reactivity such that the transmuter cannot reach criticality under any design basis accident [3]. For this type of transmuter, the fission rate is directly proportional to the source neutron production rate. The flexibility enabled by subcritical operation has several advantages:

- It can drive systems with low fissile content (Th or MA) or high burden of non-fissile materials.
- Unlike critical reactors, it can safely operate with fuel having a relatively low delayed neutron fraction.
- It can compensate for large uncertainties in initial reactivity or burn-up reactivity swings by varying the source rate, which for an accelerator-driven system is proportional to the beam current.

Accelerator technology

The power of the accelerator is determined by the design of the subcritical multiplier. For example, for a subcritical blanket fission power of 3 GW and with the multiplier k_{eff} in a range of 0.95 to 0.98, the proton beam power ranges from 55 MW to 21 MW and a beam current swing of 37 mA to 14 mA, assuming a beam energy of 1.5 GeV. Either starting out with a lower k_{eff} or going to deeper burn, again resulting in a lower k_{eff}, would require an increase in the accelerator current. Given fixed beam energy, the accelerator capital cost is determined in large part by the average current. Designing an accelerator for a large current swing requires a very high beam current that is used for only part of the transmutation cycle. This application is best served by a continuous wave machine, either linac or cyclotron. Cyclotrons could potentially deliver up to 10 MW of beam power (10 mA at 1 000 MeV). Linacs are limited to about 100 mA per front end system, with funnelling used to double the current. Either type could serve to drive a subcritical transmuter.

Since this transmuter system will be a production system, a factor of 1.5 to 2 overhead margin is typically built into the performance specification to assure high operational reliability and long life. So the maximum operational currents are 5 to 8 mA for cyclotrons and 50 to 75 mA for linacs. In this paper we are looking at accelerator systems that could drive plants of several GW thermal power and have currents up to 40 mA, and so the accelerator technology covered in this article will be limited to linac systems.

Economy of scale generally favours going to the highest average power from a single accelerator. Note that the beam may impinge on a single target in a core, be split into separate targets in a single core or be directed to multiple cores. Of course, with the consideration of multiple targets, multiple accelerators may provide system redundancy and improved reliability, but at added cost. Beam parameters consistent with the above operating numbers were demonstrated to be feasible under the Accelerator Production of Tritium (APT) [4,5] programme (Figure 3).

Figure 3: The accelerator preliminary design is based on the technologies developed for the APT programme. The superconducting linac reduces cost and improves performance and reliability (i.e. beam continuity).

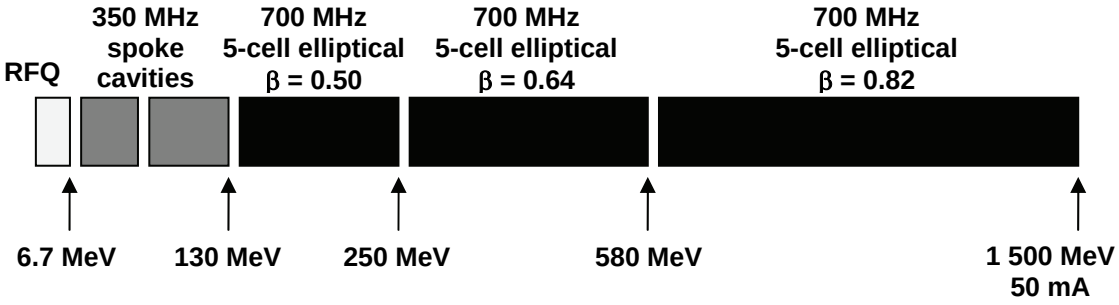

The linac requirements follow from other sub-system requirements, but more thorough studies are required to determine the full sets of requirements. For example, beam interrupts longer than 1 second might negatively impact the subcritical multiplier. The engineering challenges need to be fully scoped out for the safe, controlled coupling of an accelerator to a subcritical reactor through a spallation target. System control and safe operation will demand the understanding and resolution of the potentially complex behaviour of this coupled accelerator/target/reactor system.

A SCRF linac has been chosen for the linac because, compared to linacs using traditional room temperature (RT) copper technology, SCRF linacs are more power efficient and expected to have higher reliability. The SCRF linac will employ independently controlled RF modules with redundancy, allowing the less than 300 ms adjustment of RF phases and amplitudes of RF modules to compensate for faults of individual cavities, klystrons or focusing magnets. The SCRF cavities will have larger bore radius that relaxes alignment and steering tolerances, as well as reducing beam loss. Thermal transient has been a major cause of out-of-lock trips in RT linacs. Operating at a stable cryogenic temperature, SCRF linacs are expected to have a significantly reduced number of such trips.

The expected cost of an accelerator based transmuter system compared to a reactor is expected to be <30%. As will be seen later, we estimate that just three transmuters can support the entire existing fleet of US LWR. So if the incremental cost to the present electrical rate is based on the addition of three transmuter plants (that do not produce any power), the incremental cost to the electrical rate of the 104 LWR should be just a 2 to 5%, not including reprocessing costs. Not including reprocessing costs is fair if the US decides that the new fuel cycle going forward will be a closed cycle and reprocessing will be an inherent feature; the additional cost for reprocessing for the accelerator transmuter system would be incremental. Since operation of the transmuter is expected to generate an excess of 8 GWth/year, converting that power into a useable energy source is highly advantageous to help recover the facility capital and operating costs.

- Consideration should still be given to converting the generated energy to another form useful for national consumption:
  - One option is to sell the excess power to the grid:
    - Based on recent experience with superconducting accelerator technology, the design of highly fault-tolerant accelerators is a reasonable expectation [6].
    - Storing power with the use of the above-mentioned power storage devices could provide the electricity to run through faults if they can store sufficient electricity to provide steady power to the grid through the longest of expected interruptions. The practicality of running through the range of possible interruptions requires a more detailed design effort.

  - Another option is to convert the power into another energy form:
    - Charles Forsberg has proposed that biomass be converted to greenhouse-gas-neutral liquid fuels [7]. The conversion of biomass-to-liquid fuels is energy intensive but the transmuter can produce the significant amount of heat, electricity and hydrogen required for the processing of biomass-to-liquid fuels. The overall process has a comparable efficiency to electrical production, but the end result can be carried away in tankers. If the accelerator operation is deemed too unreliable for the electrical grid, then converting biomass into fuel for a net-zero carbon footprint would seem to be not only a good option, but the preferred option.
- Other than intermittent operation affecting the quality of the power produced by the transmuter, transients will affect the lifetime of components in the transmuter assembly:
  - The effect of transients on materials and fuels was evaluated at LANL for the proposed Material Test Station [8]:
    - The studies show no significant deleterious effects for core clad or structural materia for the expected accelerator interruptions.
    - Similar studies also show no concern for fuels.

Subcritical minor actinide reduction through transmutation – SMART

SMART was developed at Los Alamos National Laboratory to support the existing US LWR economy, preserve the energy-rich component of nuclear waste as a future energy resource, and provide a long-term strategy enabling the continuation and growth of nuclear power in the US.

The basic concept of SMART was discussed in the introduction of this paper. SMART is to extract and store the Pu, U and Np together in interim storage facilities for future fabrication into fuel, vitrify and store the short-lived in interim storage facilities, vitrify and store the long-lived fission products in small geologic repositories along with small amounts of other residual high-level waste, and burn the Am in an accelerator-driven transmuter.

The reasons for burning only the Am are economic and technical. From an economic standpoint, no incentive exists for the large scale deployment of accelerator-based facilities by private industry, and so any facility whose primary function is to deal with burning nuclear waste will probably be government owned and operated by a government contractor. This implies a scenario that uses the minimal number of facilities to support the waste mission. The number of facilities depends in large part on what mixture of actinides the facility is to burn. A reactor of fixed size is ultimately limited by the thermal heat generated from burning its nuclear fuel. A 3 GW thermal (GWth) reactor burns about 1 metric tonne (MT) of fuel each year. A subcritical transmuter also burns fuel, but the composition of the fuel is not limited by the same safety considerations as a critical reactor. The equilibrium feed for an Am burner is 100% Am. SMART (Figure 4) is focused on transmuting the one element that has the greatest impact on nuclear waste management.

The major technical reasons, the high radiotoxicity and long half-life, for concentrating on Am was given in the introduction, but other related aspects give concern for storing Am as a future fuel component:

- Am and its daughter nuclides are difficult to handle because of their high decay heat and radioactivity.
- The vapour pressure of americium limits fuel pellet fabrication temperatures.
- In fast reactor accident scenarios the americium could boil out of the fuel and thus present a more difficult safety case.

Figure 4: The SMART concept

Spent LWR fuel is sent to a reprocessing centre where the short-lived fission products are vitrified and sent to storage. The Pu, U and Np are sent to another storage facility for the possible fabrication into fuel. After transmuter start-up with an initial feed of Am and Pu, the only feedstock is Am. In equilibrium, an excess of Pu is generated from the Am transmutation chain. This Pu supplies the required fertile fuel component for maintaining k_{eff} and the excess goes back into the separations facility and ends up in the Pu, U, Np storage.

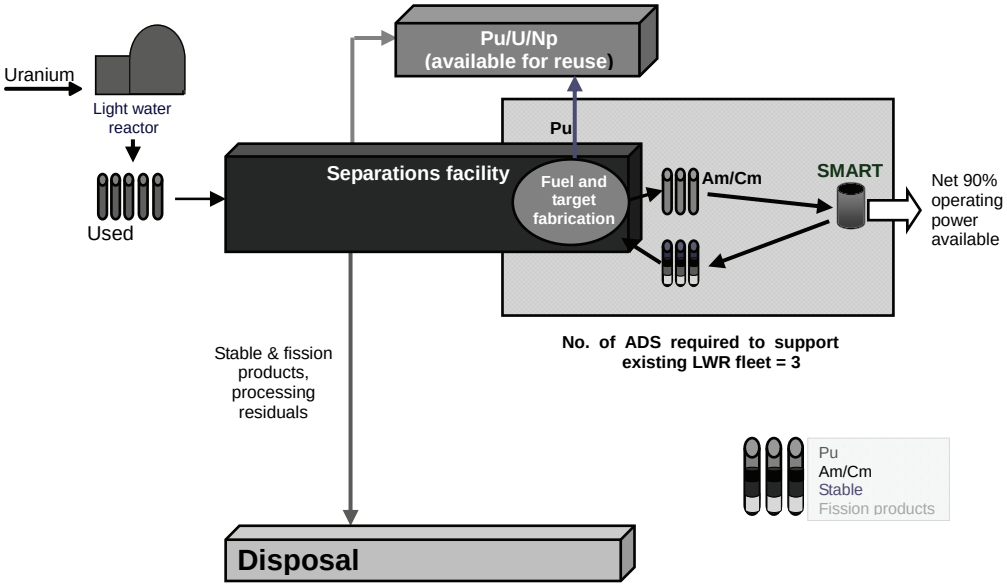

Separating out and storing the Np, U and Pu for future use has several advantages:

- Neptunium has similar chemical properties to uranium and plutonium and shows good compatibility not only in nitride fuel but also in oxide fuel.
- Processing criticality issues are mitigated since the Pu is not separated out.
- U/Pu/Np ratios are 98.7:1.2:0.1, making this a very unattractive material for diversion since the fertile elements are heavily diluted.
- ^{240}Pu (0.3% of U, Np, Pu at 50 years) has an easily detectable neutron signature adding in diversion detection [9].

Flow sheets for this transmuter can be based on advances to PUREX reprocessing. The initial separation of an Am/Cm product stream from reprocessing does not appear to be the major technical challenge from a chemistry/materials view point. However, the following could be problem areas:

- Target manufacture if Cm is a component of that fuel target.
- Dissolution of that target after irradiation for recycle of actinides.
- A recycle option needs to be considered that does not involve aqueous separations, for instance, a molten salt recycle.

A fuel form optimised for the proposed Am transmuter needs to be developed. Although some effort has been undertaken for heavily Am-loaded fuels [10], each type of transmuter requires its own fuel form depending on the isotopic composition of its radionuclides and the reprocessing flow sheets.

More effort is needed to fully develop the SMART concept, specifically:

- design an optimised subcritical reactor core and associated refuelling methodology;
- develop a tailored flow sheet for Am, U, Pu and Np separation;
- determine the optimal fuel form for an Am burner;
- develop fair cost comparison to other fuel cycles.

Summary

A significant impact on nuclear waste treatment can be made by conversion of the 0.24% non-fissile fraction of the commercial spent fuel that requires long-term isolation into materials that are primarily stable or short-lived. The use of an accelerator adds flexibility in burning these "difficult" fuels and is the missing link in integrated waste transmutation systems. Most likely the LWR waste will be the government's problem – this is consistent with an accelerator collocated with a government reprocessing facility with the following objectives:

- reducing isolation requirements to fit the lifetime of man-made containers and barriers;
- reducing incentives and consequences of intrusions into repositories;
- improving prospects for waste storage and nuclear technologies;
- improving fuel utilisation;
- reducing proliferation risk.

The major challenges concerning accelerator-driven transmuters are related to fuel forms and separations; the accelerator is based on demonstrated technologies.

Production of electricity or converting the energy to other forms is optional but would pay for the facility and associated operational costs. Since only two to three transmuters are required for the present LWR fleet then the incremental electrical cost should be a few per cent, neglecting the other components needed to close the nuclear fuel cycle (e.g. reprocessing and hot fuel fabrication). If reprocessing is funded separately as part of a new nuclear fuel cycle, then the facility will more than pay for itself. Over the next three decades a reasonable expectation is that:

- Accelerator faults can be reduced to an acceptable level through technology improvements.
- High-capacity energy storage systems will see significant improvements driven by alternative energy sources, such as solar and wind.

References

[1] Artiolia, C., *et al.*, "Minor Actinide Transmutation in ADS: the EFIT Core Design", *International Conference on the Physics of Reactors. Nuclear Power: A Sustainable Resource*, Interlaken, Switzerland, 14-19 September (2008). See also T. Sasa, *et al.*, "Actinide Reformer Concept", *Progress in Nuclear Energy*, 50, pp. 353-358 (2008). See also A. Zrodnikov, *et al.*, "Nuclear Waste Burner for Minor Actinides Elimination", *Progress in Nuclear Energy*, Vol. 47, No. 1-4, pp. 339-346 (2005).

[2] Wigeland, Roald, Figure 1 from *Nuclear Technology*, Vol. 154, p. 95, April (2006).

[3] Rimpault, Gérald, "Safety Coefficients and Subcriticality Levels EFIT and XT-ADS", *EUROTRANS DM1 Safety Meeting*, FZK, RFA, 27-28 November (2008).

[4] Lisowski, P.W., "Accelerator Production of Tritium Program", *Proceedings of the 17th Particle Accelerator Conference (PAC-97)*, Vancouver, BC, Canada, 12-16 May, Vol. 3, pp. 3780-3784 (1998).

[5] Schneider, J.D., *et al.*, "Low-energy Demonstration Accelerator (LEDA) Test Results and Plans", *Proceedings of the IEEE Particle Accelerator Conference*, Chicago, IL, USA, 18-22 June, Vol. 5, pp. 3296-3298 (2001).

[6] Campisi, I.E., *et al.*, "Operation of the Superconducting Linac at the Spallation Neutron Source", *AIP Conference Proceedings* [0094-243X], Vol. 985, Issue 1, pp. 1586-1593 (2008).

[7] Forsberg, C.W., "Meeting U.S. Liquid Transport Fuel Needs with a Nuclear Hydrogen Biomass System", Volume 34, Issue 9, pp. 4227-4236 (2009).

[8] Pitcher, E., *et al.*, "Progress on the Materials Test Station", *Proc. of the Int. Conf. on the Physics of Reactors (PHYSOR08)*, Interlaken, Switzerland (2008), log 574.

[9] Belayev, S.T., *et al.*, "The Use of Helicopter-borne Neutron Detectors to Detect Nuclear Warheads in the USSR-US Black Sea Experiment", *Science and Global Security*, 1, No. 3-4 (1990).

[10] Maschek, W., *et al.*, "Accelerator Driven Systems for Transmutation: Fuel Development, Design and Safety", *Progress in Nuclear Energy*, 50, pp. 333-340 (2008).

A source-efficient ADS for minor actinide burning

Andrei Fokau, Youpeng Zhang, Janne Wallenius
Royal Institute of Technology, Division of Reactor Physics, AlbaNova University Center
Stockholm, Sweden

Shinya Ishida
Tokyo Institute of Technology, Dept. of Nuclear Engineering, Sekimoto Laboratory
Tokyo, Japan

Abstract

External source efficiency of three fuel options for the European Facility for Industrial Transmutation (EFIT) has been studied based on the reference EFIT core design developed within the Integrated Project EUROTRANS. We show that the neutron economy of fuel, influencing the EFIT core size, has strong impact on the external source efficiency. Thus, the nitride fuel with ZrN base, featuring excellent neutron economy, allows designing more compact core than that with composite oxide fuels based on MgO and Mo matrix. This significantly boosts the external source efficiency and reduces the coolant void worth. Additionally, adoption of the austenitic steel 15/15Ti as clad material and lead-bismuth eutectic as coolant allows to reduce the fuel pin pitch and therefore the coolant volume fraction in the core, making the neutron energy spectrum faster and consequently increasing minor actinide fission probabilities.

Introduction

Accelerator-driven systems (ADS) may help to stabilise radiotoxic inventory of high-level nuclear waste (HLW) by efficient multi-recycling of minor actinides (MA) separated from spent nuclear fuel (SNF) [1,2]. Taking into account neutronic, chemical and safety factors, two composite oxide fuel options have been selected within the FUTURE project [3,4] of the 5th Framework Programme (FP) of EURATOM. Both fuels are actinide sesquioxide $(Pu,Np,Am,Cm)O_{2-x}$ dispersed in a matrix material, which is MgO for ceramic-ceramic (cercer) fuel and Mo for ceramic-metallic (cermet) fuel. Properties of these composite oxide fuels have been investigated in detail within the EUROTRANS project [5], in which the MgO-based fuel has been selected for the reference design of the European Facility for Industrial Transmutation (EFIT) [6]. On the other hand, nitride fuel, featuring good neutron economy and good thermal conductivity [7], has been rejected by the FUTURE project due to the lack of experience in fabricating americium-containing nitride fuels and has been separately studied within the 6th FP CONFIRM project [8].

Recent success in the fabrication of (Np,Pu,Am,Cm)N compounds [9,10] and good results of (Pu,Zr)N irradiation [11-13] motivate considering nitride fuels for early implementation of ADS technology. A design for an 800 MW_{th} ADS with nitride fuel had been proposed [14] and was further optimised [15,16] by JAEA. The optimised core driven by 1.5 GeV proton source (10.5-15.6 mA) features an energy gain of 35-50 and demonstrates high external source efficiency.

In this paper, we present results of neutronic and burn-up studies of the EFIT core loaded with cercer, cermet and nitride fuel. The nitride core has been designed to reach high source efficiency, while the composition of cermet and nitride fuels has been optimised for reducing the reactivity swing.

EFIT core models

Table 1 gives parameters of models used for neutronic and burn-up simulation. The reference design and fuel composition of the EFIT-MgO/Pb core [6] were used for the cercer core model. The dimensions of fuel assemblies and fuel pins of the cermet [17,18] and nitride [19] cores correspond to the outer zone of EFIT-MgO/Pb, however, the fuel pin pitch in the cercer core is set to 13.54 mm, and the fuel pin pitch in the nitride core is decreased to 12 mm in order to allow the placement of 216 fuel pins. The three-zone loading schemes are presented in Figure 1. The good neutron economy of the nitride fuel and the dense fuel pin packing allow a lower mass of fissionable material in the nitride core and a smaller number of fuel assemblies (78 FA) compared to the reference core (180 FA). On the contrary, the worse neutron economy of the cermet fuel (due to the neutron absorption by molybdenum) requires more fuel assemblies (216 FA), since the matrix fraction must be above 50 vol.% to ensure continuous matrix phase and therefore a good thermal conductivity.

The composition of actinide vectors is given in Table 2, together with the assumed vector for enriched molybdenum used for cermet fuel. Nitrogen in the nitride fuel is enriched up to 100% of ^{15}N. The ratio between fuel and matrix (or diluent material) was obtained for each zone in order to minimise radial power peaking factor and to achieve subcriticality of the reference core (k_{eff} = 0.97).

Since Ti-modified austenitic steels have a considerably higher creep rupture strength than ferritic-martensitic steels [20], allowing clad temperatures of up to 1 200 K during transients, adoption of the austenitic steel 15/15Ti as clad material allows us to safely reduce the fuel pin pitch from 1.36 cm (in average) to 1.20 cm. It makes it possible to fit one extra fuel pin row in the fuel assembly geometry, so that the number of fuel pins per assembly is increased from 168 to 216. Safety of the new core design was confirmed by a full set of transient analyses [21].

Table 1: Parameters of EFIT models used for simulation

Values for the JAEA design (see "OPT" in [16]) are given for comparison

Model parameter	Cercer	Cermet	Nitride	JAEA [16]
Core power, MW_{th}	384	488	201	800
k_{eff} at BOL	0.97	0.97	0.97	0.97
Cycle length, EFPD	1 095	1 095	1 095	600
Average specific power, MW/t_{HM}	71.5	71.5	71.5	115.1[d)]
Average linear power rating, kW/m	14.1	15.0	13.3	24.4
Fuel mass, $tonne_{HM}$	5.4	6.8	2.8	6.95[d)]
Fuel assemblies	180	216	78	84
Target area, SA	19	19	7	7
Target radius, cm	39	39	22	27
Proton energy, GeV	0.8	0.8	0.8	1.5
FA pitch, mm	191	191	191	239.9
Fuel pins per FA	168	168	216	391
Active height, m	0.9	0.9	0.9	1.0
Fuel pin pitch, mm	13.63/13.54[a)]	13.54	12.0	11.48
Fuel pin diameter, mm	8.62/9.52[a)]	9.52	9.52	7.65
Pin pitch to diameter ratio	1.58/1.42[a)]	1.42	1.26	1.50
Cladding thickness, mm	0.6	0.6	0.6	0.5
Gas gap, mm	0.16	0.16	0.16	n/a
Fuel form	AnO_{2-x}	AnO_{2-x}	AnN	AnN
Matrix/diluent	MgO	Mo[b)]	ZrN	ZrN
Average matrix fraction, vol.%	51.5	54.8	71.8	40.9[c,d)]
Pu/(Pu+MA) ratio, at.%	45.9	42.0	43.5	29.2[c,d)]
Cladding material	T91	T91	15/15Ti	T91
Coolant and target material	Pb	Pb	LBE	LBE
Coolant inlet temperature, K	673	651	583	573
Coolant outlet temperature, K	753	753	753	n/a
Coolant temperature increase, K	80	102	170	n/a

a) When two values are specified, the first value is for the inner and middle zones, and the second value is for the outer zone.

b) Enriched molybdenum vector.

c) The value corresponds to the BOL.

d) Approximately (estimated value).

Figure 1: Loading scheme of cercer (180 FA), cermet (216 FA) and nitride (78 FA) cores

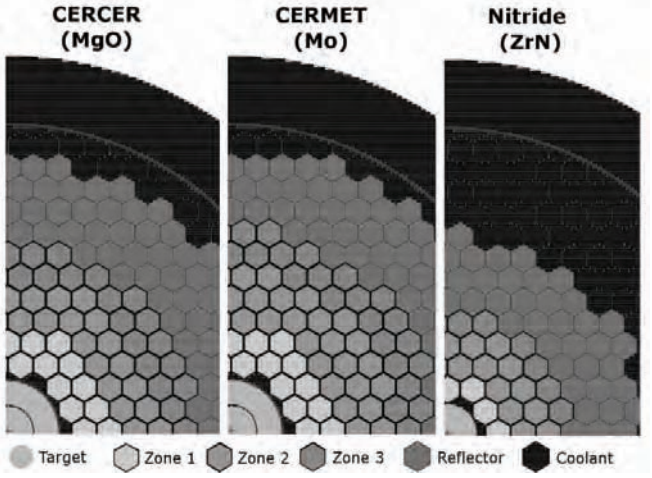

Table 2: Actinide vectors used for core simulation [18] and assumed molybdenum vector

Pu	**238**	**239**	**240**	**241**	**242**	**244**
at.%	3.7	46.4	34.1	3.8	11.9	1.2e-3
Cm	**243**	**244**	**245**	**246**	**247**	**248**
at.%	1.5	69.8	26.5	2.1	4.0e-2	2.3e-3
Am	**241**	**242m**	**243**			
at.%	82.2	0.3	17.5			
Mo	**92**	**94**	**95**	**96**		
at.%	92.9	6.1	1.0	0.1		
MA	**Np**	**Am**	**Cm**			
at.%	3.9	91.8	4.3			

Modelling tools

A number of simulations were performed in order to obtain the neutronic and burn-up characteristics of the models. An irradiation period of three years was used, which corresponds to the maximum allowable radiation damage of the most exposed fuel pin (150 dpa) [22]. The Monte Carlo codes MCNPX2.7a [23] and MCB2 [24], and the JEFF-3.1.1 data library [25] were used in the simulations. Neither Doppler broadening nor gamma heating treatment was applied for the cross-section library.

A neutron source created by 800 MeV protons has been prepared by means of MCNPX with the LA150 data library [26] invoking the CEM03 model [27]. According to standard procedure, all neutrons leaking to the core from the spallation target (i.e. the source neutrons) were recorded to a surface source file. The MCB code was then applied for both burn-up and neutron transport calculations, using only neutrons with energy below 20 MeV from the source file.

In order to estimate the effect of the discarded high-energy neutrons at the beginning of life (BOL), we have compared the number of fissions per proton calculated by the two-step approach with MCB, to those obtained by the direct calculation by MCNPX. As shown in Table 3, the source efficiency of the nitride core is 20.5% higher when the high-energy neutrons are considered. In order to take this effect into account, the correction factors listed in Table 4 have been applied to affected parameters, such as neutron source efficiency, φ^* [28], and proton source efficiency, ψ^* [29].

Table 3: Impact of high-energy source neutrons on source efficiency at BOL

Core model	Target radius, cm	Fraction of source neutrons above 20 MeV, %	Number of fissions per source proton	
			MCNPX and MCB	MCNPX only
Nitride	22	2.8	165	199 (+20.5%)
Cercer	39	1.5	112	128 (+14.1%)
Cermet	39	1.5	91	98 (+8.1%)

Table 4: Correction factors used to take into account effect of high-energy source neutrons

Correction for	Nitride	Cercer	Cermet
Proton source efficiency	1.205	1.141	1.081
Number of source neutrons per proton	1.028	1.015	1.015
Neutron source efficiency	1.173	1.125	1.065

Results of modelling and optimisation

As shown in Table 5, the smaller core size and smaller target area of the nitride core result in a 80% higher proton source efficiency, while the cermet core is 18% less source efficient than the cercer core. The smaller core power and higher source efficiency lower the demand on proton current by 67%. Using the definition of source neutrons given above and applying the correction factors discussed earlier, the neutron source efficiency for the nitride core becomes 0.95, or 76% higher than that of the cercer core. As a result of the smaller target, the source neutron energy is higher for the nitride core providing higher fission probabilities and higher number of secondary neutrons produced by (n,xn) reactions [30,31]. Finally, our calculations show that the energy gain of the nitride core is 53, assuming average fission energy release of 215 MeV per fission, including capture and decay heat. Note that due to the reactivity swing of the composite oxide cores, the values of their energy gain tend to worsen during fuel burn-up. The JAEA design [16] provides significantly higher proton source efficiency than EFIT cores because of an almost doubled proton energy. However, due to the large reactivity swing (taking into account the shorter cycle length), the energy gain drops to about 35 at the end of the second cycle. It should be noted that the proton source efficiency of the EFIT cores may also decrease during the equilibrium cycle, and therefore need to be studied.

Table 5: Model parameters related to the external source efficiency at the BOL

	Cercer	Cermet	Nitride	JAEA*
Target radius, cm	39	39	22	27
Proton energy, GeV	0.8	0.8	0.8	1.5
Average energy of source neutrons, MeV	2.0	2.0	3.1	n/a
Proton source efficiency	11.0	9.0	19.8	36.2
Neutron source efficiency	0.54	0.45	0.95	n/a
Number of fissions per proton	128	98	199	354
Required proton current, mA	14.4	23.6	4.8	10.5
Proton beam power, MW	11.5	18.9	3.8	15.8
Energy gain	34	27	53	51

* Approximately (estimated values).

Reactivity swing (change of the reactivity during fuel burn-up) was studied by analysing swings of the effective multiplication factor without source, k_{eff}, and the effective multiplication factor with source, k_s [32]. A significant difference between the swing of k_{eff}, and the swing of k_s is obtained for the composite oxide fuels (see Table 6 and Figure 2). However, this difference is negligible for the nitride fuel due to the neutron source efficiency being close to unity. Moreover, both k_{eff} and k_s of the nitride core have very low swings during three years of operation from the BOL.

Table 6: Reactivity swing for the first irradiation cycle of three years

	Cercer	Cermet	Nitride
k_{eff} swing, pcm	709	165	234
k_s swing, pcm	1 665	977	228
Ratio $\frac{k_{eff}\ \text{swing}}{k_s\ \text{swing}}$	2.4	5.9	1.0
Proton current swing, mA	4.8	4.0	0.3

Figure 2: Evolution of multiplication factors during burn-up

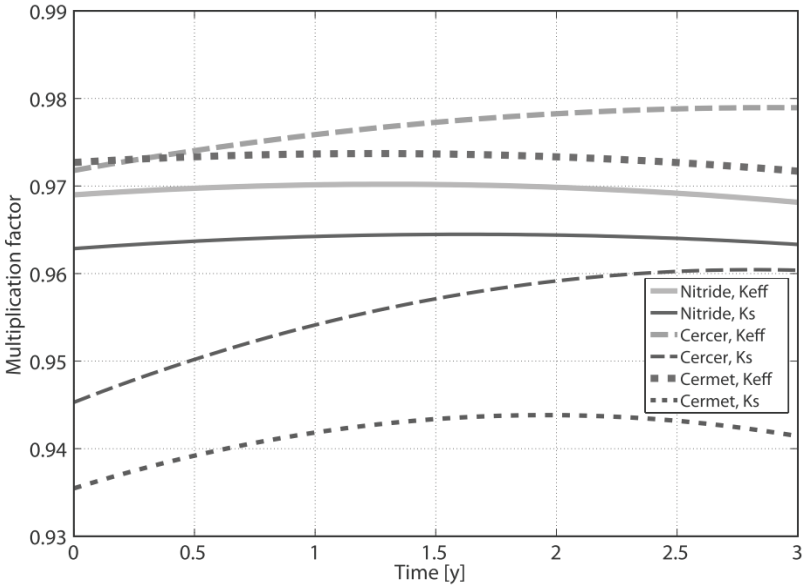

Coolant void worth is calculated as the difference between k_{eff} with normal core conditions and k_{eff} of the core with the coolant removed around the fuel and between the fuel assemblies in the active zone. As seen in Table 7, the smaller core size and smaller coolant volume fraction contribute to a two times smaller coolant void worth of the nitride core compared to the reference cercer core. In addition, a noticeable decrease (14-18%) of the void worth during three years of irradiation is obtained for all cores as a result of americium burn-up. The large amount of americium and strong dependence of its fission probability on the neutron spectrum [33] make Am to be the major contributor to the coolant void worth. The decrease of the void worth may allow increasing k_{eff} of the cores by 200-300 pcm per year, improving economy of ADS operation. This can be implemented by a positive reactivity swing of matching value.

Table 7: Coolant void worth

	Cercer	Cermet	Nitride
Void worth at BOL, pcm	7 077	6 244	3 504
Void worth at EOC, pcm	6 037	5 384	2 877
Void worth change, pcm	1 040	859	627
Void worth change, %	-15	-14	-18
Coolant volume fraction in the core, %	58	54	43
Voided coolant volume, m^3	3.0	3.3	1.0
Fuel mass, tonne HM	5.4	6.8	2.8
Am weight fraction change, %	-6.9	-6.6	-4.2

While the relative burn-up of minor actinides (MA, namely Np, Am and Cm) and all actinides in total (An) is similar for all cores (see Table 8), the absolute burn-up is essentially proportional to the total core power. It must be noted that even if relative burning of minor actinides is higher for the cercer core, the value may change when the reactivity swing is optimised to approach zero. *Vice versa*, if to adjust the nitride fuel composition for a higher fraction of MA to be transmuted, the reactivity swing will be consequently shifted away from the current minimal value. By the EOC, a burn-up of 78.3 GWd/t (or 8.3% FIMA after three years of cooling) is achieved for all fuels. Evolution of Pu inventory during three years of operation and 10 years of cooling is presented in Figure 3. As one can see, the lowest Pu mass at the end of cycle (EOC) is followed by

a significant build-up of Pu isotopes due to decay of Cm (Table 9, Figure 3) with the maximum value being reached in about three years of cooling. If this maximum value is desired to be equal to the initial Pu mass, i.e. if ADS is used for burning MA and keeping Pu for fast reactors, then one needs to tune the Pu/MA ratio with the consequences discussed above.

Table 8: Burn-up characteristics after three years of operation and three years of cooling

	Cercer	Cermet	Nitride
Total burn-up, GWd/t	78.3	78.3	78.3
Relative burn-up, % FIMA	-8.3	-8.3	-8.3
Relative mass change of Pu, %	-0.9	-0.3	-1.0
Relative mass change of MA, %	-14.7	-13.9	-14.2
Absolute mass change of An, kg	-439	-548	-232
Specific mass change of An, kg/TWh	-43.5	-42.8	-43.9
Specific mass change of An, kg/GWy	-381	-375	-385

Table 9: Actinide inventory in tonnes

	Pu, t		Am, t		Cm, t	
	BOC	EOC	BOC	EOC	BOC	EOC
Nitride core	1.22	1.18	1.46	1.22	0.07	0.12
Cercer core	2.46	2.39	2.68	2.22	0.13	0.23
Cermet core	2.86	2.78	3.65	3.05	0.17	0.29

Figure 3: Mass change of Pu and Cm

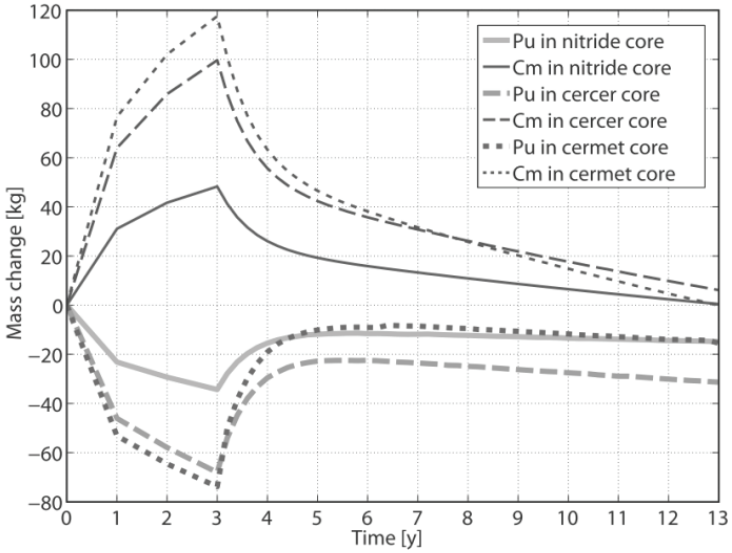

Conclusions

Neutronic and burn-up parameters of EFIT core with three fuel options (cercer, cermet and nitride) were presented in this paper. It was shown that the reactivity swing of the cermet core (EFIT-Mo/Pb) is minimised if the plutonium fraction in fissionable material is set to 42 at.% for the specific power of 71.5 MW/t_{HM}. Because of the worse neutron economy of cermet fuel, the EFIT-Mo/Pb core requires a larger amount of fuel and therefore larger core size, which decreases the efficiency of external source.

A compact EFIT core with nitride fuel (EFIT-N/PbBi) has been designed, based on the geometry of the EFIT-MgO/Pb core. It is shown that the good neutron economy of nitride fuel allows reducing the core size and therefore the total reactor power, while keeping the specific power constant, which then permits reduction of the spallation target radius. The smaller EFIT-N/PbBi core and smaller spallation target area result in a significant increase of the proton source efficiency (by 80% as compared to the cercer core) and the neutron source efficiency (up to 0.95). Consequently, the proton current demand and the proton beam power decrease by 67%, which then decreases the heat deposit into the target and the load of the target heat removal. Additionally, much lower swings are achieved for both k_{eff} and k_s of the nitride core during the first cycle, providing conditions for safe and economical reactor operation. However, a reactivity swing optimisation for the nitride and cermet cores should also be performed for the equilibrium cycle.

Replacement of the ferritic steel T91 by the austenitic steel 15/15Ti in the EFIT-N/PbBi core allows reducing the pin pitch safely, which contributes to a reduction of coolant void worth by more than a factor of two. Decrease of the void worth by 200-300 pcm per year may allow a positive reactivity swing of a corresponding magnitude. The high matrix fraction (66-78 vol.%) of the nitride fuel in the EFIT-N/PbBi core leads not only to good thermal conductivity, but also allows space for future design optimisation.

Despite the good characteristics of the nitride core, its low total power, the need in enrichment of nitrogen in ^{15}N, and stability issues of the nitride fuel may decrease attractiveness of the proposed design. All three EFIT fuel candidates need further analysis before the optimal choice can be made based on their manufacturability, neutronic parameters, in-core behaviour and economical efficiency.

Acknowledgements

This work was financially supported by SKB AB (the Swedish Nuclear Fuel and Waste Management Company), and the European Commission in the framework of the Integrated Project EUROTRANS.

References

[1] Salvatores, M., *et al.*, "Fuel Cycle Synergies and Regional Scenarios", *Actinide and Fission Product Partitioning and Transmutation, 10th Information Exchange Meeting*, 6-10 October 2008 Mito, Japan, OECD/NEA, Paris (2010).

[2] Salvatores, M., "Physics Features Comparison of TRU Burners: Fusion/Fission Hybrids, Accelerator-driven Systems and Low Conversion Ratio Critical Fast Reactors", *Annals of Nuclear Energy*, 36, 1653-1662 (2009).

[3] Pillon, S., J. Wallenius, "Oxide and Nitride TRU Fuels: Lessons Drawn from the CONFIRM and FUTURE Projects of the 5th European Framework Program", *Nuclear Science and Engineering*, 153, 245-252 (2006).

[4] Pillon, S., *et al.*, "The European FUTURE Programme", *GLOBAL 2003: Atoms for Prosperity: Updating Eisenhowers Global Vision for Nuclear Energy*, New Orleans, LA, USA (2003).

[5] Maschek, W., *et al.*, "Accelerator Driven Systems for Transmutation: Fuel Development, Design and Safety", *Progress in Nuclear Energy*, 50, 333-340 (2008).

[6] Artioli, C., *et al.*, *Specification for the EFIT Core and Fuel Element*, IP EUROTRANS (2008).

[7] Wallenius, J., S. Pillon, L. Zaboudko, "Fuels for Accelerator-driven Systems", *Nuclear Instruments and Methods in Physics Research, Section A: Accelerators, Spectrometers, Detectors and Associated Equipment*, 562, 625-629 (2006).

[8] Wallenius, J., *CONFIRM: Collaboration on Nitride Fuel Irradiation and Modeling*, CONFIRM Project, Contract FIKW-CT-2000-00096 (2009).

[9] Arai, Y., *et al.*, "Development of Nitride Fuel and Pyrochemical Process for Transmutation of Minor Actinides", *Actinide and Fission Product Partitioning and Transmutation, 10th Information Exchange Meeting*, Mito, Japan, 6-10 October 2008, OECD/NEA, Paris (2010).

[10] Minato, K., *et al.*, "Thermochemical and Thermophysical Properties of Minor Actinide Compounds", *Journal of Nuclear Materials*, 389, 23-28 (2009).

[11] Arai, Y., M. Akabori, K. Minato, "JAEA's Activities on Nitride Fuel Research for MA Transmutation", *Actinide and Fission Product Partitioning and Transmutation, 9th Information Exchange Meeting*, Nîmes, France, 26-28 September 2006, OECD/NEA, Paris (2007).

[12] Golovanov, V.N., F.N. Kryukov, S.V. Kuzmin, *et al.*, "Results of Post-irradiation Examinations of Nitride and Inertmatrices Fuels Irradiated in BOR-60 Reactor", *Working Material of an IAEA Technical Meeting*, Obninsk, Russia, 21-23 November 2005, IAEA, Vienna, Austria, (2006), pp. 740-778.

[13] Hilton, B., D. Porter, S. Hayes, "Post-irradiation Examination of AFCI Nitride and Oxide Transmutation Fuels at 8 at.%", *Transactions of the American Nuclear Society* (2006) pp. 777-779.

[14] Tsujimoto, K., *et al.*, "Neutronics Design for Lead-bismuth Cooled Accelerator-driven System for Transmutation of Minor Actinide", *Journal of Nuclear Science and Technology*, 41, 21-36 (2004).

[15] Saito, S., *et al.*, "Design Optimization of ADS Plant Proposed by JAERI", *Nuclear Instruments and Methods in Physics Research, Section A: Accelerators, Spectrometers, Detectors and Associated Equipment*, 562, 646-649 (2006).

[16] Nishihara, K., *et al.*, "Neutronics Design of Accelerator-driven System for Power Flattening and Beam Current Reduction", *Journal of Nuclear Science and Technology*, 45, 812-822 (2008).

[17] Maschek, W., *et al.*, "Design, Safety and Fuel Developments for the EFIT Accelerator Driven System with cercer and cermet Cores", *Actinide and Fission Product Partitioning and Transmutation, 10th Information Exchange Meeting*, Mito, Japan, 6-10 October 2008, OECD/NEA, Paris (2010).

[18] Sobolev, V., *et al.*, *Neutronic Performances of EFIT-400 (AFTRA) Reference Cores at the Beginning of Operation*, Deliverable 3.2, IP EUROTRANS (2007).

[19] Fokau, A., *et al.*, "A Source Efficient ADS for Minor Actinides Burning", *Annals of Nuclear Energy*, forthcoming (2010).

[20] Cannon, N.S., F.H. Huang, M.L. Hamilton, "Transient and Static Mechanical Properties of {D9} Fuel Pin Cladding and Duct Material Irradiated to High Fluence", *ASTM Special Technical Publication*, 1071-1082 (1992).

[21] Zhang, Y., A. Fokau, J. Wallenius, "Safety Analysis of a Compact ADS with Nitride Fuel", forthcoming (2010).

[22] Henry, J., "Structural and Cladding Materials for Gen-IV Sodium Cooled Reactors", *MATGEN-IV.2 Winter School*, Jukkasjärvi, Sweden (2009).

[23] Pelowitz, D.B., *et al.*, *MCNPX 2.7.A Extensions*, Los Alamos National Laboratory (2008).

[24] Cetnar, J., W. Gudowski, J. Wallenius, "MCB: A Continuous Energy Monte Carlo Burn-up Simulation Code", *Actinide and Fission Product Partitioning and Transmutation, 5th Information Exchange Meeting*, Mol, Belgium, 25-27 November 1998, OECD/NEA, Paris (1998).

[25] Nuclear Energy Agency (NEA), *The JEFF-3.1 Nuclear Data Library*, OECD/NEA, Paris (2006).

[26] Chadwick, M., *et al.*, "Nuclear Data for Accelerator-driven Systems", *Progress in Nuclear Energy*, 38, 179-219 (2001).

[27] Mashnik, S., *et al.*, "CEM03 and LAQGSM03 – New Modeling Tools for Nuclear Applications", *Journal of Physics: Conference Series*, 41, 340-351 (2006).

[28] Salvatores, M., *et al.*, The Potential of Accelerator-driven Systems for Transmutation or Power Production Using Thorium or Uranium Fuel Cycles", *Nuclear Science and Engineering*, 126, 333-340 (1997).

[29] Seltborg, P., *et al.*, "Definition and Application of Proton Source Efficiency in Accelerator-driven Systems", *Nuclear Science and Engineering*, 145, 390-399 (2003).

[30] Seltborg, P., R. Jacqmin, "Spallation Neutron Source Effects in a Sub-critical System", *Proc. Int. Topical Mtg. Accelerator Applications/Accelerator Driven Transmutation Technology Applications (AccApp/ADTTA'01)*, Reno, NV, USA (2001).

[31] Yang, W.S., *et al.*, "Effects of Buffer Thickness on ATW Blanket Performances", *Proc. Int. Topical Mtg. Accelerator Applications/Accelerator Driven Transmutation Technology Applications (AccApp/ADTTA'01)*, Reno, NV, USA (2001).

[32] Dulla, S., *et al.*, "Effects of Neutron Source Characteristics in Direct and Adjoint Problems for Subcritical Systems", *International Journal of Nuclear Energy Science and Technology*, 2, 361-377 (2006).

[33] Tuček, K., J. Wallenius, W. Gudowski, "Coolant Void Worth in Fast Breeder Reactors and Accelerator-driven Transuranium and Minor-actinide Burners", *Annals of Nuclear Energy*, 31, 1783-1801 (2004).

Annex 1: Scientific Advisory Committee

Chair

Joachim U. Knebel (*KIT, Germany*)

Scientific Secretary

Yong-Joon Choi (*OECD/NEA*)

Committee Members

Pierre J. D'hondt (*SCK•CEN, Belgium*)

Alex Müeller (*CNRS, France*)

Dominique Warin (*CEA, France*)

Horst Klein (*University of Frankfurt, Germany*)

Concetta Fazio (*KIT, Germany*)

Minoru Takahashi (*TIT, Japan*)

Jonghwa Chang (*KAERI, Republic of Korea*)

Mike Seidel (*PSI, Switzerland*)

John Galambos (*ORNL, United States*)

Richard Sheffield (*LANL, United States*)

Yousry Gohar (*ANL, United States*)

Annex 2: List of participants

Belgium

AIT ABDERRAHIM, Hamid
Director of Institute
Advanced Nuclear Systems
SCK•CEN
200 Boeretang
B-2400 Mol
Tel: +32 (0)14 332277
Fax: +32 (0)14 321529
Eml: haitabde@sckcen.be

ANGULO-PEREZ, Carmen
Avenue Ariane 7
B-1200 Brussels
Tel:
Fax:
Eml: carmen.angulo@gdfsuez.com

DE BRUYN, Didier
SCK•CEN
Boeretang 200
B-2400 Mol
Tel: +3214333409
Fax: +3214321336
Eml: didier.de.bruyn@sckcen.be

GIOT, Michel
Université Catholique de Louvain
Unité Thermodynamique (TERM)
Place du Levant, 2
B-1348 Louvain-La-Neuve
Tel: +32 10 47 22 10
Fax: +32 10 45 26 92
Eml: michel.giot@uclouvain.be

UYTTENHOVE, Wim
SCK•CEN
Boeretang 200
B-2400 Mol
Tel: +32 14332186
Fax: +32 14321529
Eml: wim.uyttenhove@sckcen.be

VANDEPLASSCHE, Dirk
IBA
Chemin du Cyclotron 3
B-1348 Louvain-la-Neuve
Tel: +32 (10) 475849
Fax: +32 (10) 475847
Eml: dvandepl@sckcen.be

Bulgaria

IVANOV, Ivaylo
72 Tzarigradsko chaussee, Blvd.
BG-1784 Sofia
Tel: +359 2 979 5497
Fax: +359 2 975 3619
Eml: ivanov@inrne.bas.bg

Canada

JACKSON, David
McMaster University
Dept. of Engineering Physics
1280 Main Street West
Hamilton, Ontario, L8S 4L7
Tel: +1 905 525 9140 ext. 24651
Fax: +1 905 529 1975
Eml: jacksond@mcmaster.ca

Czech Republic

SUCHOPAR, Martin
Academy of Sciences of Czech Republic
Borského 663/4
15200 Prague 5

Tel: +420737148103
Fax:
Eml: suchopar@ujf.cas.cz

France

BEAUCHAMP, François
Nuclear Energy Division
CEA Cadarache
DTN/STPA/LTTS
Bât. 201
F-13108 Saint-Paul-lez-durance

Tel:
Fax:
Eml: francois.beauchamp@cea.fr

BIARROTTE, Jean-Luc
IPN Orsay
F-91406 Orsay Cedex

Tel: +33 1 69 15 79 30
Fax:
Eml: biarrott@ipno.in2p3.fr

BOULY, Frederic
IPNO/CNRS
15 rue Georges CLEMENCEAU
F-91406 Orsay

Tel: +33 1 69 15 65 31
Fax: +33 1 69 15 77 35
Eml: bouly@ipno.in2p3.fr

CLAVEL, Jean-Baptiste
Laboratoire SUBATECH
UMR 6457
4 rue Alfred Kastler
La Chantrerie BP 20722
F-44307 Nantes Cedex 3

Tel: +33 2 51 85 84 63
Fax:
Eml: jean-baptiste.clavel@subatech.in2p3.fr

COUROUAU, Jean-Louis
CEA/DEN/DPC/SCCME
CEA Saclay
F-91191 Gif-sur-Yvette Cedex

Tel: +33 1 6908 1643
Fax:
Eml: jean-louis.courouau@cea.fr

DELAGE, Fabienne
CEA Cadarache
BP01
DEC/SESC/LC2I
Bât. 315
F-13108 Saint-Paul-lez-Durance

Tel: +33 4 42 25 61 82
Fax:
Eml: fabienne.delage@cea.fr

GRANGET, Gilbert
CEN Cadarache
Bât. 212
F-13108 Saint-Paul-lez-Durance

Tel: +33 4 42 25 75 91
Fax: +33 4 42 25 70 25
Eml: gilbert.granget@cea.fr

GUERTIN, Arnaud
Laboratoire SUBATECH – Bureau H117
CNRS/IN2P3
École des Mines – Université de Nantes
4, rue Alfred Kastler
F-44307 Nantes

Tel: +33 251858464
Fax: +33 251858424
Eml: arnaud.guertin@subatech.in2p3.fr

LATGE, Christian
Research Director
CEA Cadarache
F-13108 Saint-Paul-lez-Durance
Tel: +33 4 42 25 44 71
Fax: +33 4 42 25 48 68
Eml: christian.latge@cea.fr

MORIER, Olivier
CEA
F-13108 Saint-Paul-lez-Durance
Tel:
Fax:
Eml: olivier.morier@cea.fr

MUELLER, Alex
Department Head
R&D Accelerators/Exotic Beams
Institut de Physique Nucléaire
Bât. 106, 15, rue G. Clemenceau
F-91406 Orsay Cedex
Tel: +33 01 69 15 62 40
Fax: +33 01 69 15 77 35
Eml: mueller@ipno.in2p3.fr

SALVATORES, Massimo
CEA Cadarache
DEN/Dir Bât. 101
F-13108 Saint-Paul-lez-Durance
Tel: +33 4 4225 3365
Fax: +33 4 4225 4142
Eml: massimo.salvatores@cea.fr

THIOLLIERE, Nicolas
Laboratoire SUBATECH
École des Mines de Nantes
4, rue Alfred Kastler
F-44307 Nantes Cedex 03
Tel: +33 2 51 85 86 42
Fax:
Eml: nicolas.thiolliere@subatech.in2p3.fr

VOGT, Jean-Bernard
Université de Lille 1
Cité Scientifique
F-59650 Villeneuve d'Ascq
Tel: +33 3 20 43 40 35
Fax: +33 3 20 33 61 48
Eml: jean-bernard.vogt@univ-lille1.fr

WOAYE HUNE, Anthony
AREVA-NP
10 rue J. Récamier
F-69003 Lyon
Tel: +33 4 72 74 73 92
Fax:
Eml: antony.woayehune@areva.com

Germany

BATTA, Abdalla
IKET FZK
Hermann von Helmholtz Platz 1
D-76344 Eggenstein-Leopoldshafen
Tel: +49 7247 82-2464
Fax: +49 7247 82-4837
Eml: abdalla.batta@iket.fzk.de

BAURICHTER, Arnd
Corp. Techn.
Mozartstrasse 57
D-91054 Erlangen
Tel: +491735293114
Fax:
Eml: arnd.baurichter@siemens.com

CHEN, Xue-Nong
KIT
Inst. for Nuclear and Energy Technologies
Hermann-von-Helmholtz-Platz 1
D-76344 Eggenstein-Leopoldshafen
Tel: +49 7247 82 5985
Fax: +49 7247 82 3824
Eml: xue-nong.chen@iket.fzk.de

CLASS, Andreas G.
Karlsruhe Institute of Technology
Institute for Nuclear
and Energy Technologies
Postfach 3640
D-76021 Karlsruhe, Germany
Tel: +49 7247 823487
Fax: +49 7247 824837
Eml: andreas.class@kit.edu

CURA, Harald
Guenther-Scharowsky-Str. 1
D-91058 Erlangen
Tel: +49-9131-7-34032
Fax: +49-9131-7-20240
Eml: harald.cura@siemens.com

D'ANDREA, Danilo
Karlsruhe Institute of Technology
Hermann-von-Helmholtz-Platz 1
D-76344 Leopoldshafen-Eggenstein
Tel: +49 7247 822967
Fax:
Eml: danilo.dandrea@iket.fzk.de

DEL GIACCO, Mattia
Hermann-von-Helmholtz-Platz 1
D-76344 Eggenstein-Leopoldshafen
Tel: ++497247828475
Fax: ++497247822823
Eml: mattia.delgiacco@ihm.fzk.de

FAZIO, Concetta
KIT – Nuclear Safety Research Programme
Hermann-von-Helmholtz Platz 1
D-76344 Eggenstein-Leopoldshafen
Tel: +49 7247 82 5517
Fax: +49 7247 82 5508
Eml: concetta.fazio@kit.edu

FRITZ, Peter
Chairman
Kompetenzverband Kerntechnik
FZ Karlsruhe GMBH
Hermann-von-Helmholtz Platz 1
D-76344 Eggenstein-Leopoldshafen
Tel: +49 7247 822013
Fax: +49 7247 822196
Eml: peter.fritz@kit.edu

GABRIELLI, Fabrizio
Karlsruhe Institute of Technology
Hermann-von-Helmholtz Platz 1
D-76344 Eggenstein-Leopoldshafen
Tel: +49 7247 82 2491
Fax: +49 7247 82 3824
Eml: fabrizio.gabrielli@kit.edu

GORDEEV, Sergej
Karlsruhe Institute of Technology
Institute for Nuclear
and Energy Technologies
P.O. Box 3640
D-76021 Karlsruhe
Tel: +49 7247 82 3464
Fax:
Eml: gordeev@iket.fzk.de

KETTLER, John
Forschungszentrum Jülich
Institute for Energy Research (IEF-6)
Postfach 1913
D-52425 Jülich
Tel:
Fax:
Eml: j.kettler@fz-juelich.de

KLEIN, Horst
Director of Institute
Institut für Angewandte Physik
Johann Wolfgang Goethe-University
Robert-Mayer-Str. 2-4
D-60054 Frankfurt am Main
Tel: +49 (69) 798 23489
Fax: +49 (69) 798 285 10
Eml: horst.klein@iap.uni-frankfurt.de

KNEBEL, Joachim U.
Head of Programme Nuklear
Karlsruhe Institute of Technology
Postfach 3640, D-76021 Karlsruhe
Tel: +49 7247 82 5510
Fax: +49 7247 82 5508
Eml: joachim.knebel@kit.edu

KRIVENTSEV, Vladimir
Karlsruhe Institute of Technology
Postfach 3640
D-76021 Karlsruhe
Tel:
Fax:
Eml: vladimir.kriventsev@kit.edu

LITFIN, Karsten
Karlsruhe Institute of Technology
Institute for Nuclear
and Energy Technologies
Postfach 3640
D-76021 Karlsruhe
Tel: +49 7247 82 4407
Fax: +49 7247 82 4837
Eml: litfin@kit.edu

MASCHEK, Werner
Forschungszentrum Karlsruhe GmbH
Hermann-von-Helmholtz Platz 1
D-76344 Eggenstein-Leopoldshafen
Tel: +49 (72) 47 82 26 48
Fax: +49 (72) 47 82 48 74
Eml: werner.maschek@iket.fzk.de

MATZERATH BOCCACINI, Claudia
Karlsruhe Institute of Technology KIT
Postfach 3640
D-76021 Karlsruhe
Tel:
Fax:
Eml: claudia.matzerath@kit.edu

MERCATALI, Luigi
Karlsruhe Institut Für Technologie
Institute für Reaktorsicherheit (IRS)
Hermann-von-Helmholtz Platz 1
D-76344 Eggenstein-Leopoldshafen
Tel: +49 7247 82 2751
Fax: +49 7247 82 3718
Eml: luigi.mercatali@kit.edu

MEUSEL, Oliver
Max-von-Laue-Strasse 1
D-630438 Frankfurt am Main
Tel: +49 ++49 69 798 47450
Fax: +49 ++49 69 798 47407
Eml: o.meusel@iap.uni-frankfurt.de

MOORMANN, Rainer
Forschungszentrum Jülich
GmbH – ESS-FZJ
D-52425 Jülich
Tel: +49 2461 614 644
Fax: +49 2461 618 255
Eml: r.moormann@fz-juelich.de

MUELLER, Georg
Forschungszentrum Karlsruhe (FZK)/IHM
P.O. Box 3640
D-76021 Karlsruhe
Tel: +49 72 47 82 46 69
Fax: +49 72 47 82 22 56
Eml: georg.mueller@kit.edu

PELLINI, Donella
Karlsruhe Institute of Technology
IKET
P.O. Box 3640
D-76021 Karlsruhe
Tel: +49 7247 82 2490
Fax: +49 7247 82 3824
Eml: donella.pellini@iket.fzk.de

PICHO, Oxana
Institut für Materialforschung III
Hermann-von-Helmholtz Platz 1, Bau 695
D-76344 Eggenstein-Leopoldshafen
Tel:
Fax:
Eml: oxana.picho@kit.edu

PODLECH, Holger
IAP
Max-von-Laue-Str. 1
D-60438 Frankfurt
Tel: +49 69 798 47453
Fax:
Eml: h.podlech@iap.uni-frankfurt.de

RINEISKI, Andrei
Institut für Kern- und Energietechnik
Forschungszentrum Karlsruhe
FZK/IKET, B. 421
D-76344 Eggenstein-Leopoldshafen
Tel: +49 7247 82 4695
Fax: +49 7247 82 3824
Eml: andrei.rineiski@kit.edu

SCHIKORR, Michael
Institute for Reactor Safety
Forschungszentrum Karlsruhe
Tel: +49 7247 82 - 2963
Fax: +49 7247 82 - 7963
Eml: michael.schikorr@kit.edu

SCHITTHELM, Oliver
Forschungszentrum Jülich GmbH
IEF-6
Leo Brandt Strasse
D-52428 Jülich
Tel: +49 02461 611751
Fax:
Eml: o.schitthelm@fz-juelich.de

SVED, John
NSD-Fusion GmbH
Steller Strasse 61A
D-27755 Delmenhorst
Tel: +49 4221 973 9351
Fax: +49 4221 973 9352
Eml: john.sved@nsd-fusion.com

TIEDE, Rudolf
IAP
Max-von-Laue-Str. 1
D-60438 Frankfurt
Tel:
Fax:
Eml: tiede@iap-frankfurt.de

TRAVLEEV, Anton
Forschungszentrum Karlsruhe, INR/FZK
Hermann-von-Helmholtz Platz 1
D-76344 Eggenstein-Leopoldshafen
Tel: +49-7247-82-4147
Fax:
Eml: travleev@inr.fzk.de

TROMM, Th. Walter
Deputy Head
Nuclear Safety Research (Nuklear)
KIT – PF 3640
D-76021 Karlsruhe
Tel: +49 7247 82 5509
Fax: +49 7247 82 5508
Eml: walter.tromm@kit.edu

VOGEL, Hanspeter
Friedrich-Ebert-Strasse 1
D-51429 Bergisch Gladbach
Tel: +492204842583
Fax: +492204842599
Eml: heidi.lohmar@research-instruments.de

WEINRICH, Udo
Planckstrasse 1
D-64291 Darmstadt
Tel:
Fax:
Eml: u.weinrich@gsi.de

WEISENBURGER, Alfons
IHM Forschungszentrum Karlsruhe
Hermann-von-Helmholtz Platz 1
D-76344 Eggenstein-Leopoldshafen
Tel: +497247826238
Fax: +497247822256
Eml: alfons.weisenburger@ihm.fzk.de

WETZEL, Thomas
Karlsruhe Institute of Technology
Institut für Thermische Verfahrenstechnik
D-76128 Karlsruhe
Tel:
Fax:
Eml: thomas.wetzel@tvt.uka.de

YURECHKO, Mariya
Forschungszentrum Karlsruhe GmbH
Hermann-von-Helmholz Platz 1
D-76344 Eggenstein-Leopoldshafen
Tel: +49 7247 82 3263
Fax: +49 7247 82 3956
Eml: mariya.yurechko@imf.fzk.de

ZHANG, Chuan
Tel:
Fax:
Eml: zhang@iap.uni-frankfurt.de

Greece

FRAGOPOULOU, Marianthi
Aristotle University
University of Thessaloniki
School of Physics
Nuclear and Elementary Particle Division
541.24 Thessaloniki
Tel: +302310998082
Fax:
Eml: fragom@auth.gr

Italy

BOTAZZOLI, Pietro
Politecnico di Milano
Department of Energy
Enrico Fermi Center for Nuclear Studies
via Ponzio 34/3
I-20133 Milano
Tel: +39 02 2399 6333
Fax: +39 02 2399 6309
Eml: pietro.botazzoli@mail.polimi.it

CARTA, Mario
ENEA C.R. Casaccia
FPN-FISION S.P. 101
via Anguillarese, 301
I-00123 S. Maria di Galeria, Roma
Tel: +39 06 3048 3183
Fax: +39 06 3048 6308
Eml: mario.carta@enea.it

MANSANI, Luigi
Ansaldo Nuclear
Corso Perrone, 25
I-16161 Genova
Tel: +39 10 655 8078
Fax: +39 10 655 8078
Eml: luigi.mansani@ann.ansaldo.it

MILAZZO, Paolo Maria
via Valerio, 2
Trieste
Tel:
Fax:
Eml: paolo.milazzo@ts.infn.it

MONTI, Stefano
ENEA – Fusion, Fission
and Nuclear Technology Dept.
via Martiri di Monte Sole, 4
I-40129 Bologna
Tel: +39 051 6098 462
Fax: +39 051 6098 785
Eml: stefano.monti@enea.it

NAPOLITANO, Marco
Dip. de Scienze Fisiche
Univ. “Federico II” & INFN
Complesso Univ. Monte Sant’Angelo
via Cintia
I-80126 Napoli
Tel: +39 081 676129
Fax: +39 081 676346
Eml: marco.napolitano@na.infn.it

PISACCHE, Fabrizio
ENEA
Tel:
Fax:
Eml: fabrizio.pisacche@enea.it

POLIDORI, Massimiliano
ENEA
via Martiri di Monte Sale, 4
I-40129 Bologna
Tel: +39 051 6098 419
Fax:
Eml: massimiliano.polidori@enea.it

RENIERI, Alberto
Capo Dipartimento Fusione, Tecnologie
e Presidio Nucleare
ENEA FPN Centro Ricerche Frascati
via Enrico Fermi, 45
I-00044 Frascati (Roma)
Tel: +39 06 94005445
Fax: +39 06 94005770
Eml: alberto.renieri@enea.it

TARANTINO, Mariano
ENEA
Brasimone
I-40032 Camugnano (Bologna)
Tel: +39 534 801 262
Fax:
Eml: mariano.tarantino@enea.it

Japan

LIM, Jae-Yong
Assistant Professor
Kyoto University
Research Reactor Institute
Asashiro-nishi
Kumatori-cho, Sennan-gun
Tel: +81 72 451 2389
Fax: +81 72 451 2603
Eml: limjy@rri.kyoto-u.ac.jp

NISHIHARA, Kenji
Nuclear Transmutation Technology Group
Nuclear Sci. and Eng. Directorate
Japan Atomic Energy Agency
Tokai-mura, Naka-gun, Ibaraki-ken, 319-11
Tel: +81 29 282 5289
Fax: +81 29 282 5901
Eml: nishihara.kenji@jaea.go.jp

OBAYASHI, Hironari
JAEA
2-4, Shirane, Shirakata,
Tokai-mura, Ibaraki-ken
Tel: +81 29 282 6256
Fax: +81 29 282 5901
Eml: obayashi.hironari@jaea.go.jp

SAITO, Shigeru
Transmutation Section
J-PARC Center
Japan Atomic Energy Agency
2-4 Shirane Shirakata, Tokai-mura
Naka-gun, Ibaraki 319-1195
Tel: +81 29 282 5058
Fax: +81 29 282 5671
Eml: saito.shigeru@jaea.go.jp

SUGAWARA, Takanori
JAEA
Shirakata Shirane 2-4
Ibaraki
Tel: +81 29 282 6436
Fax:
Eml: sugawara.takanori@jaea.go.jp

TAKEI, Hayanori
Japan Atomic Energy Agency
Tokai-mura, Naka-gun
Ibaraki-ken 319-1195
Tel: +81 29 282 6948
Fax: +81 29 282 5671
Eml: takei.hayanori@jaea.go.jp

TSUJIMOTO, Kazufumi
J-PARC Center
Japan Atomic Energy Agency
2-4 Shirakata-Shirane, Tokai-mura
Ibaraki, 319-1195
Tel: +81 29 282 6436
Fax: +81 29 282 5671
Eml: tsujimoto.kazufumi@jaea.go.jp

YOSHIDA, Hiroyuki
Japan Atomic Energy Agency
2-4, Shirakata, Tokai, Naka
Ibaraki, 319-1195
Tel: +81 29 282 5275
Fax: +81 29 282 6427
Eml: yoshida.hiroyuki@jaea.go.jp

Poland

GAJDA, Pawel
AGH – University of Science
and Technology
ul. Mickiewicza 30
30-059 Krakow
Tel: +48 502613383
Fax:
Eml: pawel.gajda@data.pl

Portugal

VAZ, Pedro
Instituto Tecnologico e Nuclear
Estrada Nacional 10
P-2686-953 Sacavém
Tel: +351 21 994 62 30
Fax: +351 21 994 19 95
Eml: pedrovaz@itn.pt

Russian Federation

KHORASANOV, Georgy
IPPE
1 Bondarenko Square,
Obninsk, Kaluga Region
249033
Tel: +7484399 85 05
Fax:
Eml: khorasan@ippe.ru

Spain

GONZALEZ-ROMERO, Enrique
Director of the Nuclear Fission Division
Department of Energy of CIEMAT
Avenida Complutense, 22
ES-28040 Madrid
Tel: +34 91 346 6120
Fax: +34 91 346 6576
Eml: enrique.gonzalez@ciemat.es

VILLAMARIN, David
CIEMAT
Avda. Complutense, 22. Edf. 17
ES-28040 Madrid
Tel: +34 913466731
Fax: +34 913466576
Eml: david.villamarin@ciemat.es

Sweden

FOKAU, Andrei
The Royal Institute of Technology (KTH)
AlbaNova University Centre
SE-106 91 Stockholm
Tel: +46 8 5537 8204
Fax: +46 8 5537 8216
Eml: andrei.fokau@neutron.kth.se

SIMUTKIN, Vasily
Department of Neutron Research
Uppsala University
Box 525
SE-751 20 Uppsala
Tel: +46 184712631
Fax: +46184713853
Eml: vasily.simutkin@tsl.uu.se

WALLENIUS, Janne
Associate Professor and Head of Division
Reactor Physics
Royal Institute of Technology (KTH)
AlbaNova University Centre
SE-106 91 Stockholm
Tel: +46-8-5537 8200
Fax: +46-8-5537 8216
Eml: janne@neutron.kth.se

WALLIN, Gustav
Uppsala University
Institution for Fysik and Astronomi
Box 516
SE-751 20 Uppsala
Tel: +46 739139621
Fax: +46 184715999
Eml: gustav.wallin@fysast.uu.se

Switzerland

HEINITZ, Stephan
Paul Scherrer Institute
CH-5232 Villigen
Tel: +41 56 310 2407
Fax:
Eml: stephan.heinitz@psi.ch

MILENKOVIC, Rade
Paul Scherrer Institute
CH-5232 Villigen PSI
Tel: +41563104453
Fax:
Eml: rade.milenkovic@psi.ch

SEIDEL, Mike
Paul Scherrer Institute
CH-5232 Villigen PSI
Tel: +41 563103378
Fax:
Eml:mike.seidel@psi.ch

STRINNING, Ake
Paul Scherrer Institute
CH-5232 Villigen PSI
Tel:
Fax:
Eml: ake.strinning@psi.ch

WAGNER, Werner
Paul Scherrer Institute
Spallation Source Division, ASQ
CH-5232 Villigen PSI
Tel: +41 56 310 2517
Fax: +41 56 310 3131
Eml: werner.wagner@psi.ch

ZANINI, Luca
Paul Scherrer Institut
ODGA/112
CH-5232 Villigen PSI
Tel: +41 56 310 5255
Fax: +41 56 310 3131
Eml: luca.zanini@psi.ch

Turkey

ATAK, Haluk
Hacettepe University,
Department of Nuclear Energy Engineering
06800 Beytepe, Ankara
Tel: +90 3122977300
Fax: +90 3122992122
Eml: ha@hacettepe.edu.tr

GURDAL, Samil Osman
Department of Nuclear Engineering
Hacettepe University
06800 Beytepe, Ankara
Tel:
Fax:
Eml: samil.gurdal@gmail.com

United Kingdom

ASHWORTH, Roger
Phoenix House
3 Surtees Way
Surtees Business Pary
Stockton-on-Tees
TS18 3HR
Tel: +441642334061
Fax:
Eml: roger.ashworth@akersolutions.com

COATES, David
University of Cambridge
3 Grassington Green
Ingleby Barwick
Stockton-on-Tees
Tel: +44 7503 616049
Fax:
Eml: djc75@cam.ac.uk

FULLER, Colin
AKER Solutions E&C Ltd
Tel:
Fax:
Eml: colin.fuller@akersolutions.com

STEER, Steven
University of Cambridge,
Department of Engineering
Trumpington Street
Cambridge CB2 1PZ
Tel: +44 1223 748575
Fax: +44 1223 332662
Eml: sjs218@cam.ac.uk

VILA NOVA GONCALVES, Leonardo
University of Cambridge
Department of Engineering
Trumpington Street
Cambridge CB2 1PZ
Tel:
Fax:
Eml: lvng2@cam.ac.uk

United States of America

KIM, SANG-HO
1 Bethel Valley Rd
P.O. Box 2008
Oak Ridge, TN 37831
Tel: +1-865-386-1094
Fax:
Eml: kimsh@ornl.gov

MCINTYRE, Peter
Texas A&M
Dept. of Physics
College Station, TX 77843
Tel: +1 979 255 5531
Fax: +1 979 845 2590
Eml: mcintyre@physics.tamu.edu

SHEFFIELD, Richard
Los Alamos National Laboratory
LANSCE-DO, MS H851
Los Alamos, New Mexico 87545
Tel: +1 505 667 1237
Fax: +1 505 667 7443
Eml:sheff@lanl.gov

International organisations

MULHAUSER, Françoise
International Atomic Energy Agency
Vienna International Center
A-1400 Vienna, Austria
Tel: +43 1 2600 21753
Fax:
Eml: f.muelhauser@iaea.org

CHOI, Yong-Joon
OECD Nuclear Energy Agency
12 boulevard des Iles
F-92130 Issy-les-Moulineaux

Tel: +33 145241091
Fax: +33 145241128
Eml: yongjoon.choi@oecd.org

RUBBIA, Carlo
Chairman ETWG
CERN
SL Division
CH-1211 Geneva 23

Tel: +41 22 767 2282
Fax: +41 22 767 7960
Eml: carlo.rubbia@cern.ch

SALMIERI, Delia
CERN
1211 Geneva 23

Tel:
Fax:
Eml: delia.salmieri@cern.ch

NEA PUBLICATIONS AND INFORMATION

Printed material

The NEA produces a large selection of printed material, part of which is on sale, and part of which is distributed free of charge. The full catalogue of publications is available online at www.oecd-nea.org/pub.

Internet and electronic products

In addition to basic information on the Agency and its work programme, the **NEA website** offers free downloads of hundreds of technical and policy-oriented reports.

For full access to all print and electronic products, see the OECD/NEA **Nuclear Energy iLibrary** at www.oecd.org/bookshop?16121s1.

An **NEA monthly electronic bulletin** is distributed free of charge to subscribers, providing updates of new results, events and publications. Sign up at www.oecd-nea.org/bulletin/.

You can also visit us on **Facebook** at: www.facebook.com/OECDNuclearEnergyAgency.

OECD PUBLISHING, 2 rue André-Pascal, 75775 PARIS CEDEX 16
ISBN 978-92-64-11727-3

Technology and Components of Accelerator-driven Systems

The accelerator-driven system (ADS) is a potential transmutation system option as part of partitioning and transmutation strategies for radioactive waste in advanced nuclear fuel cycles. These proceedings contain all the technical papers presented at the workshop on Technology and Components of Accelerator-driven Systems held on 15-17 March 2010 in Karlsruhe, Germany. The workshop provided experts with a forum to present and discuss state-of-the-art developments in the field of ADS and neutron sources. It included a special session on the EUROTRANS as well as four technical sessions covering current ADS experiments and test facilities, accelerators, neutron sources and subcritical systems.

(66 2011 01 1 P) € 90
ISBN 978-92-64-11727-3

www.oecd-nea.org
www.oecdbookshop.org

9 789264 117273